PB88-173257

REPORT NO.
UCB/EERC-87/08
JULY 1987

EARTHQUAKE ENGINEERING RESEARCH CENTER

UNDRAINED CYCLIC TRIAXIAL TESTING OF GRAVELS—THE EFFECT OF MEMBRANE COMPLIANCE

by

MARK D. EVANS
H. BOLTON SEED

A report on research sponsored by
the National Science Foundation

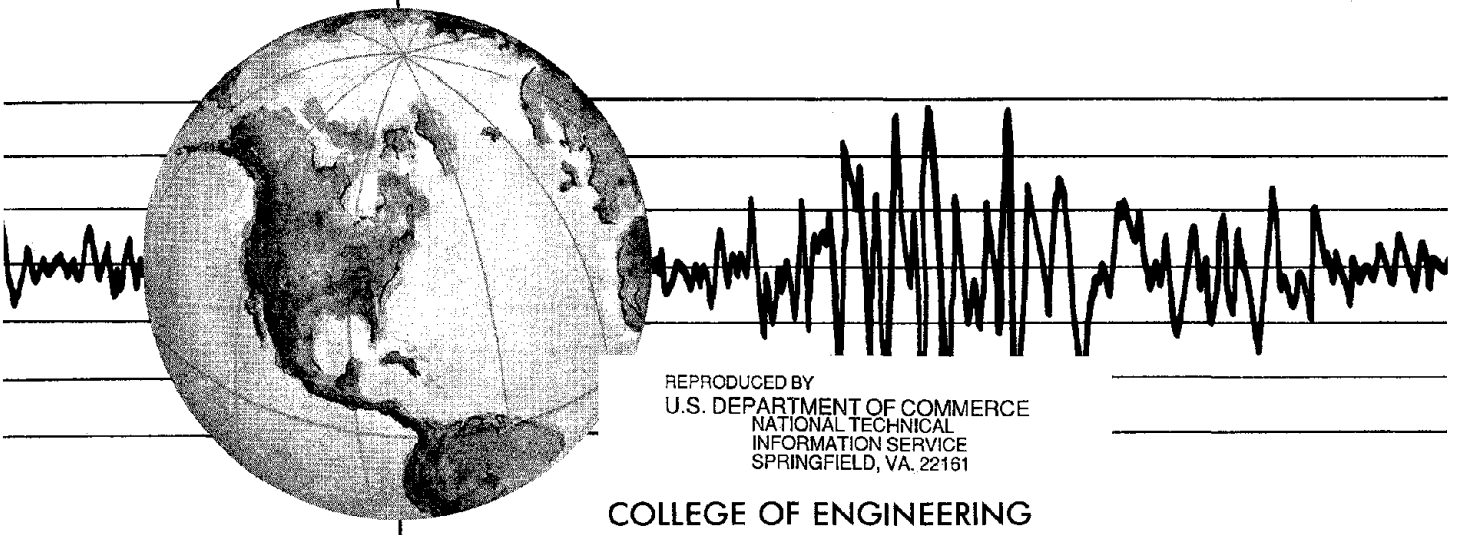

COLLEGE OF ENGINEERING

UNIVERSITY OF CALIFORNIA · Berkeley, California

For sale by the National Technical Information Service, National Bureau of Standards, U. S. Department of Commerce, Springfield, Virginia 22151.

See back of report for up to date listing of EERC reports.

50272-101

REPORT DOCUMENTATION PAGE	1. REPORT NO. NSF/ENG-87035	2.	3. Recipient's Accession No. PB88-173257

4. Title and Subtitle
Undrained Cyclic Triaxial Testing of Gravels-- The Effect of Membrane Compliance

5. Report Date
July 1987

6.

7. Author(s)
Mark D. Evans and H. Bolton Seed

8. Performing Organization Rept. No.
UCB/EERC-87/08

9. Performing Organization Name and Address
Earthquake Engineering Research Center
University of California
1301 South 46th Street
Richmond, California 94804

10. Project/Task/Work Unit No.

11. Contract(C) or Grant(G) No.
(C)
(G) MSM-8311985

12. Sponsoring Organization Name and Address
National Science Foundation
1800 G. Street, N.W.
Washington, D.C. 20550

13. Type of Report & Period Covered

14.

15. Supplementary Notes

16. Abstract (Limit: 200 words)

This research attempted to define the magnitude of the effect of membrane penetration and compliance on the undrained cyclic loading resistance of various gravels so that this factor can be taken into account in assessing the undrained strength loss which could occur in gravelly soils.

A comparative study is made between the results of tests performed on gravel specimens tested in a conventional compliant system and comparable gravel specimens tested in a specially prepared non-compliant or low-compliance system. Special test conditions, including isotropic and anisotropic consolidation, the use of various numbers and thicknesses of confining membranes, and construction of a thin annular sand shell around the outside of the gravel specimens, were imposed on several test groups to investigate their effects on the relationships between the cyclic loading resistance curves and the pore pressure ratio curves for sluiced and unsluiced gravel specimens.

Membrane penetration volume changes during hydrostatic rebound seem to be the key to determining the severity of the effects of membrane compliance that may occur. It is tentatively suggested that the effects of membrane compliance may be estimated by comparing membrane penetration volume changes with the values measured in this study and computing a proportional value of membrane compliance correction.

17. Document Analysis a. Descriptors

membrane penetration
membrane compliance
isotropic consolidation
anisotropic consolidation
hydrostatic rebound
sluiced gravel
unsluiced gravel

b. Identifiers/Open-Ended Terms

c. COSATI Field/Group

18. Availability Statement:	19. Security Class (This Report)	21. No. of Pages
Release unlimited	Unclassified	437
	20. Security Class (This Page) Unclassified	22. Price A19 38.95

(See ANSI-Z39.18) See Instructions on Reverse

OPTIONAL FORM 272 (4-77)
(Formerly NTIS-35)
Department of Commerce

EARTHQUAKE ENGINEERING RESEARCH CENTER

UNDRAINED CYCLIC TRIAXIAL TESTING OF GRAVELS - THE EFFECT OF MEMBRANE COMPLIANCE

by

Mark D. Evans

H. Bolton Seed

Report No. UCB/EERC-87/08

July 1987

A report on research sponsored by
the National Science Foundation

College of Engineering
University of California
Berkeley, California

TABLE OF CONTENTS

Acknowledgements

This investigation was supported by Grant No. MSM-8311985 from the National Science Foundation. The support of the Foundation for this research is greatly appreciated.

LIST OF FIGURES

List of Figures (continued)

List of Figures (continued)

List of Figures (continued)

List of Figures (continued)

List of Figures (continued)

List of Figures (continued)

List of Figures (continued)

List of Figures (continued)

List of Figures (continued)

List of Figures (continued)

List of Figures (continued)

List of Figures (continued)

List of Figures (continued)

List of Figures (continued)

LIST OF TABLES

List of Tables (continued)

List of Tables (continued)

CHAPTER 1

INTRODUCTION

The problem of liquefaction of sands has been well established by a myriad of investigators over the years (Seed and Lee, 1966; Lee and Seed, 1967; Seed, 1979; Castro, 1969, 1975; Casagrande, 1975; and others). While specific terminology, methods of sample testing and design applications may not be universally accepted, there seems to be general agreement that loose, clean, cohesionless sand will develop excess pore pressures and may undergo extreme strength loss and large deformations if subjected to a sufficient level of undrained (cyclic or monotonic) loading.

Gravels on the other hand, are not generally considered as being liquefiable for a number of reasons:

(1) The hydraulic conductivity of gravel is often sufficiently high that drainage can easily occur and an undrained situation may never occur in the field.

(2) There is no substantial body of conclusive case histories in which gravels have liquefied.

(3) No field tests are currently in use to aid in determining the undrained, cyclic behavior of gravels or to correlate field data with laboratory test results (such as the use of standard penetration testing for sands).

(4) Little cyclic laboratory testing has been performed which would provide evidence of the liquefaction behavior of gravels.

(5) Membrane compliance plays a significant role in inhibiting liquefaction in undrained, cyclic triaxial tests performed on gravels

and there is currently no satisfactory method for accounting for this phenomenon. Thus, the noncompliant cyclic loading resistance of gravels is not easily determined.

Each of the above points will be discussed in the following paragraphs:

(1) The hydraulic conductivity of gravel is often sufficiently high that drainage can easily occur and an undrained situation may never occur in the field.

Gravels are indeed likely to be free-draining in ideal cases but drainage may be impeded under particular situations. For example, a gravel formation may be bounded by comparatively impermeable silty material which renders the gravel layer undrained. Such formations may occur naturally in an abandoned river channel or an alluvial fan deposit where deposits of gravel and finer material may be interlayered, or by silt deposition on the upstream face of a gravel or rockfill dam. Also, some gravel formations may be so extensive (very large dams for example) that excess pore pressure may not dissipate rapidly enough, thus momentarily rendering the mass undrained.

Alternatively, drainage may also be impeded where a sand and gravel mixture is involved. Such composite materials will have a significantly reduced hydraulic conductivity as compared to that of relatively clean gravels alone. Consider for example the use of rockfill which had been sluiced with sand in the construction of the Malpaso Canyon Dam in Peru (Park, 1939) or the Aswan High Dam (Abu-Wafa, Hanna Labib; 1970, 1971; Hassouna et al., 1970; High and Aswan Dams Authority, 1969). The upstream

portion of the 255 foot high Malpaso Canyon Dam was constructed of derrick-laid rocks while the downstream portion consists of dumped rockfill as shown in Figure 1.1. Both sections of the dam were sluiced with sand and fine gravel in order to increase the mass of the dam and to reduce settlement, however, dissipation of any excess pore pressure that may have been generated in the event of an earthquake, would have been significantly impeded. In the Aswan High Dam, large quantities of dumped rockfill were sluiced with sand, as shown in Figure 1.2, in order to avoid the need to construct a filter blanket. The hydraulic conductivity of the resulting sand-rockfill mixture was not significantly different from that of the sand alone, about 3×10^{-3} cm/sec. Thus, if excess pore pressures were generated in such structures, during an earthquake for example, the rate of pore pressure dissipation would be significantly reduced due to the presence of the sand in the gravel voids.

(2) There is no substantial body of conclusive case histories where gravels have liquefied.

It is certainly true that the abundance of case histories involving liquefaction of sands does not exist for gravels. There are a few noteworthy cases, however, as discussed by Harder and Seed (1986) where liquefaction of gravels has occurred. These cases include:

(a) The liquefaction of a gravelly-sand alluvial fan deposit in the 1948 Fukui earthquake (Ishihara, 1985).

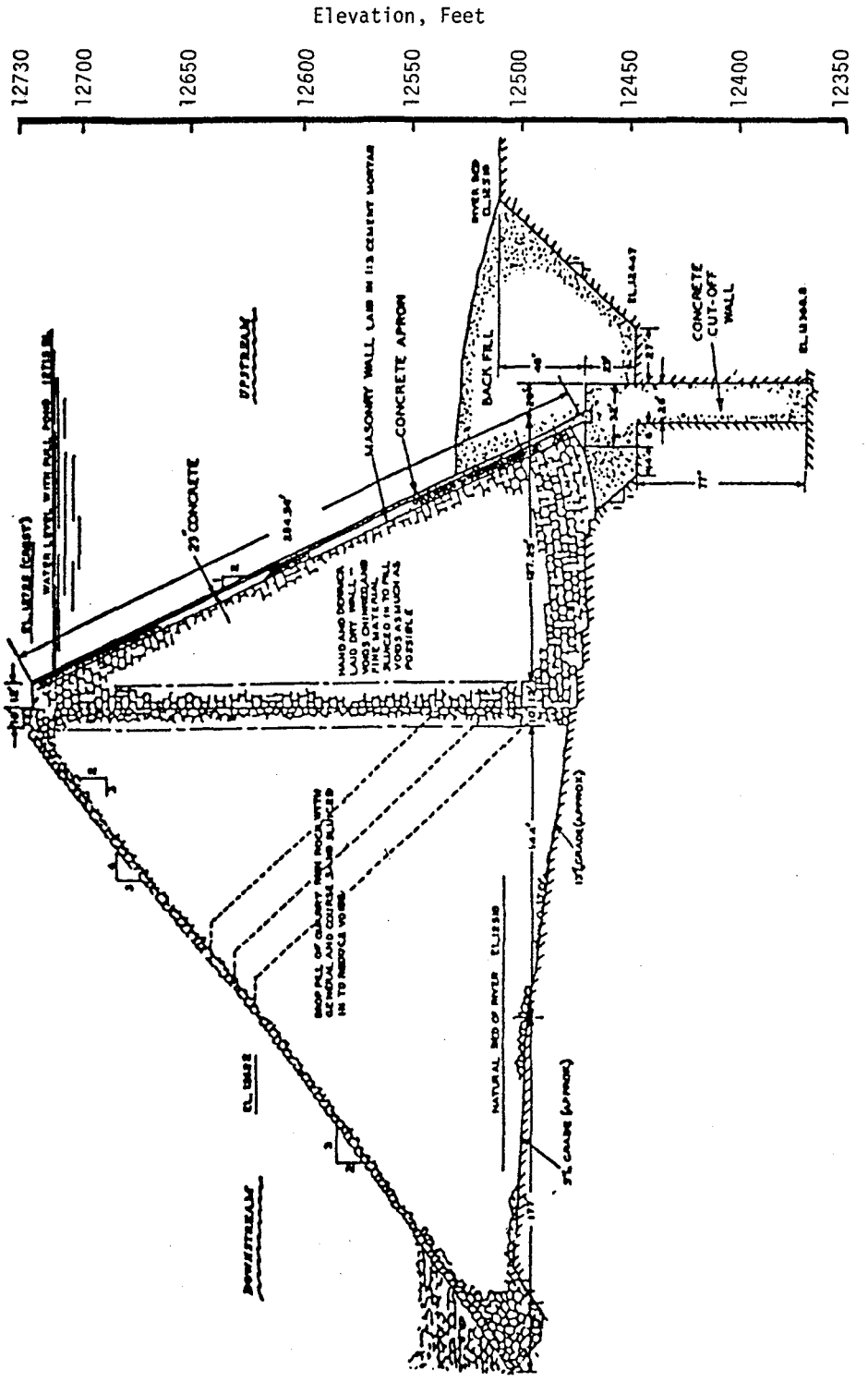

Figure 1.1 Cross Section of the Malpaso Canyon Dam (after Park, 1939)

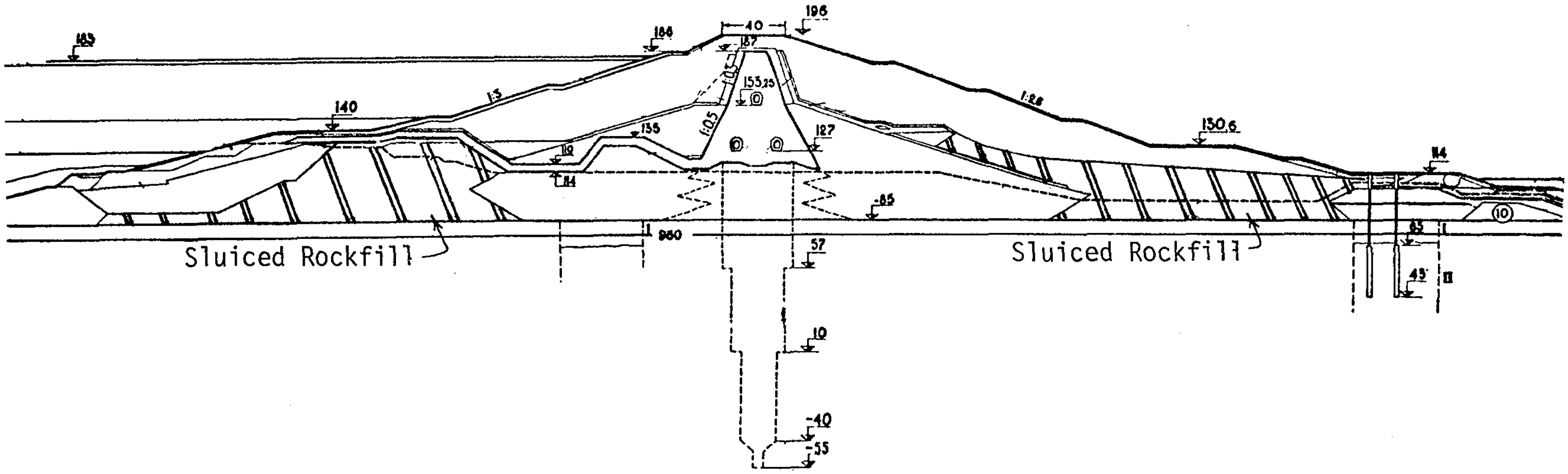

Figure 1.2 Cross Section of the Aswan High Dam at Station 16+50 - Zones of Sluiced Rockfill Are Shown Cross-Hatched (after High and Aswan Dams Authority, 1969)

(b) The flow slide at Valdez in an alluvial fan containing large zones of gravelly sand and sandy gravel in the 1964 Alaska Earthquake (Coulter and Migliaccio, 1966).

(c) The slide in the upstream gravelly sand shell of Shimen Dam in the 1975 Haicheng Earthquake (Wang, 1984) shown in Figure 1.3. This is a 46 meter high central clay core dam with "relatively loose" gravelly sand shells. Moments after the M 7.3 earthquake, an eyewitness reported air bubbles rising to the surface of the reservoir over the upstream slope, thus, indicating that an upward flow of water (and air) had occurred in the shell material, presumably as a result of liquefaction. Eighty minutes later, a slide scarp appeared just above the reservoir water surface. The time delay between the earthquake occurrence and the appearance of the slide scarp indicated either that (1) a progressive slide had taken place or that (2) excess pore pressure redistribution within the slope led to a gradual strength reduction eventually causing a slide to occur. The grain size distribution for the gravelly sand shell material is shown in Figure 1.4.

(d) The slide in the upstream sandy gravel slope protection layer of Baihe Dam in the 1974 Tangshan Earthquake (Tamura and Lin, 1983; Wang, 1984) shown in Figure 1.5. This is a 66 meter high inclined core dam with a sandy gravel slope protection layer having a maximum thickness of about 7.5 meters. The slope protection layer shows evidence of having liquefied during the main earthquake shock (M=7.8, Intensity=VI) causing a major slide in the upstream slope involving 150,000 cubic meters of material.

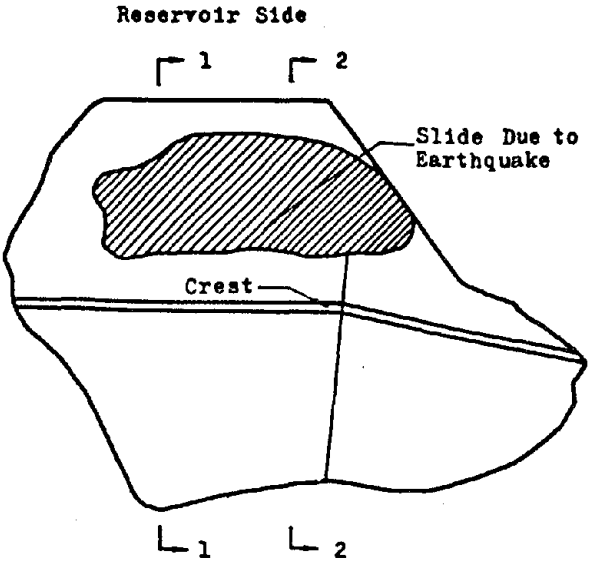

(a) Plan

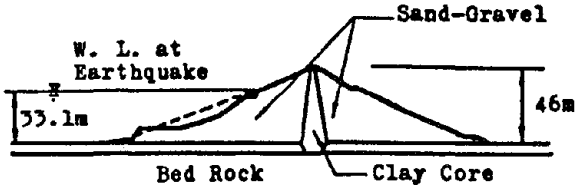

1-1

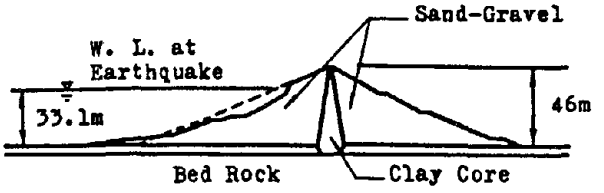

2-2

(b) Cross Sections

Figure 1.3 Slide in the Upstream Shell of the Shimen Dam - (a) Plan View (b) Cross Section (after Wang, 1984)

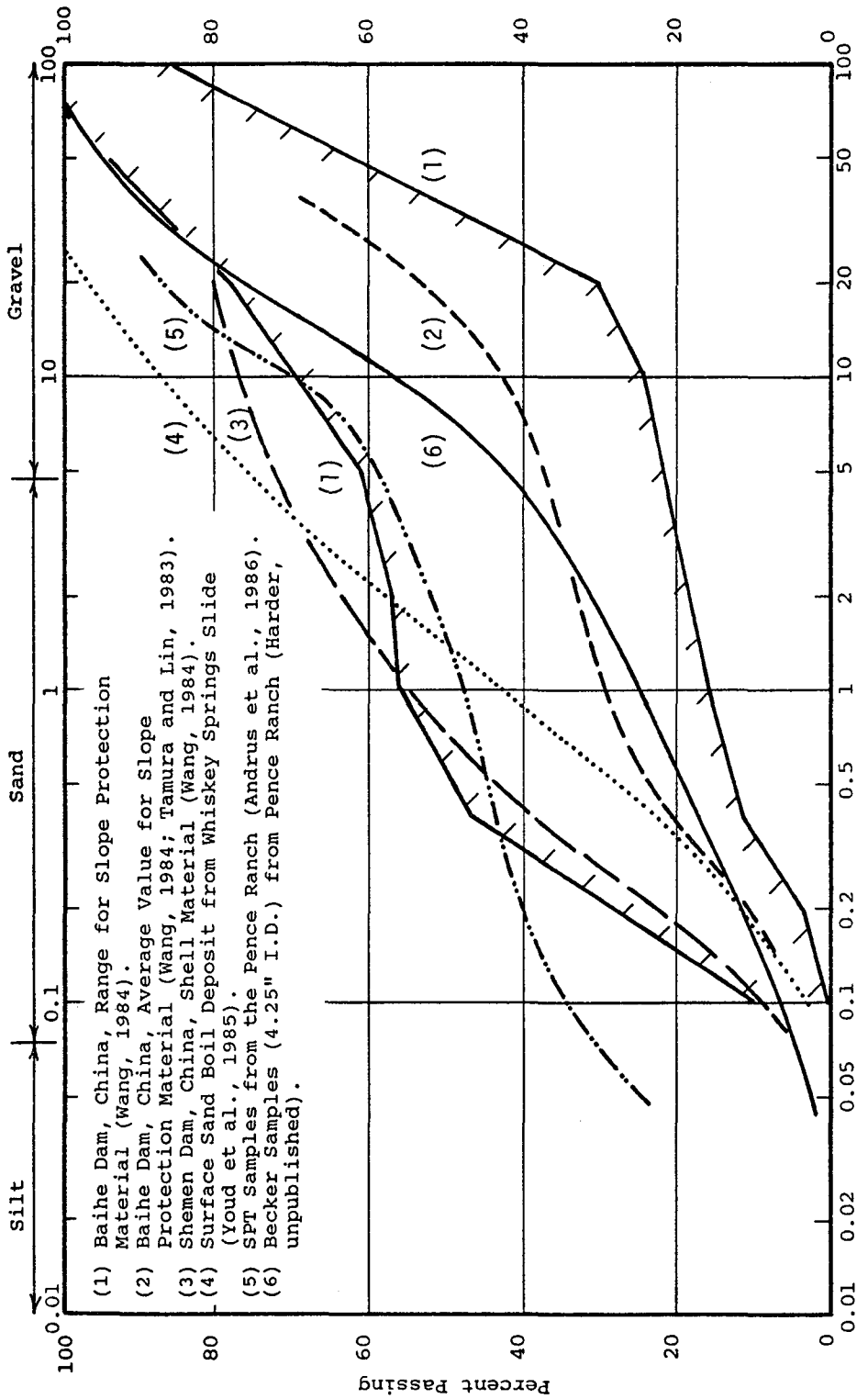

Figure 1.4 Grain Size Distributions of Liquefied Gravels and Gravelly-Sand Deposits

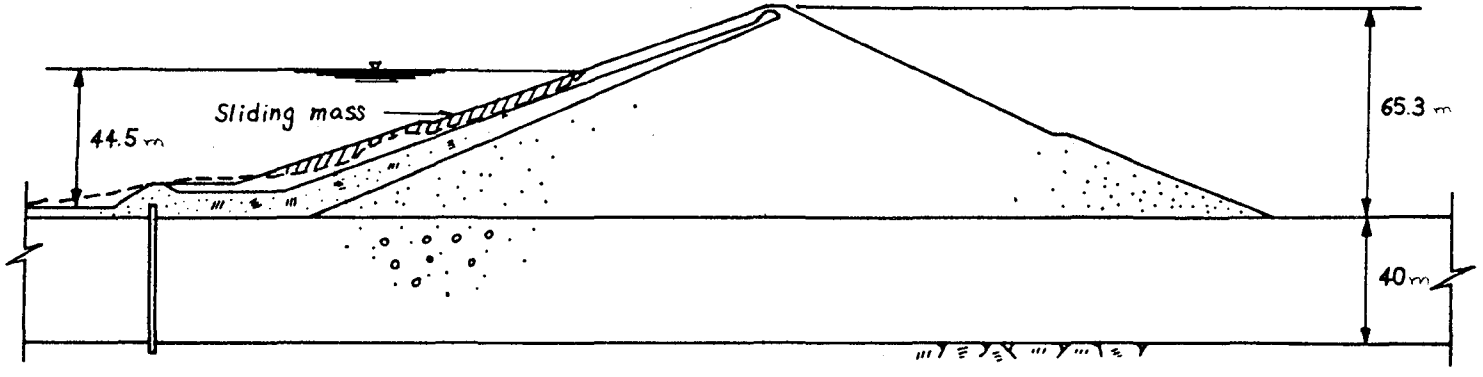

Figure 1.5 Upstream Slide in the Baihe Dam (after Tamura and Lin, 1983).

The top of the slide scarp approximately paralleled the reservoir water surface and extended as deep as the sloping clay core in some places. Some of the slide material traveled "hundreds of meters" upstream from the upstream toe indicating that a flow slide had developed. However, the bulk of the slide material was deposited within 70 meters of the upstream toe.

This dam was originally designed to withstand an Intensity VIII earthquake and the results of a reevaluation before the Tangshan Earthquake occurred had indicated that the dam was still safe for the design earthquake level. Wang reported the following material properties for the gravelly shell material:

Dry density = 2.11 t/m^3,

Permeability = 10^{-3} to 10^{-4} cm/sec, and

Effective friction angle = 40°.

A grain size distribution for the sandy gravel slope protection material is shown in Figure 1.4.

(e) The liquefaction of gravelly soils at the Pence Ranch, and in sloping ground causing the Whiskey Springs Slide, during the 1983 Mount Borah Earthquake (Youd, et al., 1985; Andrus, et al., 1986). Grain size distributions for these materials are also shown in Figure 1.4. Curve (4) in this figure was obtained from a surface sand boil deposit on the Pence Ranch. It may be seen that particles up to one inch in diameter are present in this material which was "washed" up to the surface from the liquefied deposit. Since only the finer portion of a deposit is likely to be carried to the ground surface when liquefaction occurs, it is reasonable to assume that coarser particles existed

in the liquefied deposit. Grain size curves (5) and (6) show material obtained by SPT sampling (1.375" I.D.) and Becker Drill soundings (4.25" I.D.), respectively, in what was believed to be a liquefied deposit below another nearby sand boil. Particles up to three inches in diameter are present in this layer.

Clearly, liquefaction related failures have occurred in gravelly soils and thus a suitable method for accurately analyzing the liquefaction potential of these deposits must be determined.

(3) No field tests are currently in use to aid in determining the undrained, cyclic behavior of gravels or to correlate field data with laboratory test results (such as the use of standard penetration testing for sands).

Until recently, it was true that there was no applicable field test for determining the cyclic strength properties of gravels or rockfill materials in-situ. The field density test and static strength parameters (internal friction angle, compressibility, and strength) were the only parameters which could be determined with reasonable accuracy to give the engineer some information for design evaluations. Beside being tedious and requiring large scale laboratory and field equipment for tests on coarse gravels and rockfills, these tests supply insufficient information about the undrained, cyclic behavior of such materials.

SPT and CPT tests are of little use when large particles, in excess of about one inch, are present in a significant quantity. Thus, there has been no convenient method to correlate

the actual performance of gravel deposits during earthquake loadings with measurable in-situ gravel properties.

Recently, a new penetration test applicable for use in gravels has been developed (Harder and Seed, 1986). A Becker Hammer is used to drive a large diameter closed end bit into the deposit. Bit sizes range from 5.5 to 9.0 inches O.D. Comparison of SPT and Becker Hammer tests in sands show excellent agreement when appropriately interpreted. This test bodes well for the future development of a data base for liquefied gravel sites. Once it becomes available, such data will provide a basis for guiding engineers in the design and evaluation of gravelly sites or earth structures.

(4) Little cyclic laboratory testing has been performed which would provide evidence of the liquefaction behavior of gravels.

This is comparatively true since cyclic laboratory testing of coarse gravels requires large scale equipment which is available at only a few laboratories in the world. The large monetary expense required for installation and upkeep of such equipment and its general unavailability has resulted in very little research being done in the area of gravel liquefaction. However, research conducted at the University of California, Berkeley rockfill testing facility has shed some light on the performance of gravels and rockfill materials under undrained, cyclic loading conditions (Wong, 1971; Wong et al., 1974; Banerjee et al., 1979). Undrained cyclic triaxial tests performed on 12 inch diameter gravel specimens as part of this study have developed pore pressure ratios of 100% and have

developed over 10% double amplitude strain during the application of just a few cycles of loading. This indicates that undrained liquefaction of gravels can occur in laboratory tests and, since gravelly soils have liquefied in the field, must be considered in the design of earth structures.

(5) Membrane compliance plays a significant role in inhibiting liquefaction in undrained, cyclic triaxial tests performed on gravels, yet there is currently no satisfactory method for accounting for this phenomenon. Thus, the noncompliant cyclic loading resistance of gravels is not easily determined.

Investigators who have studied membrane penetration and compliance (see Chapter 4) have accurately explained these phenomena and their effect on the results of various laboratory tests. However, the magnitude of the effect on the cyclic stress ratio causing liquefaction or on the shape of the pore pressure development curves for undrained, cyclic tests performed on gravels is not well understood.

The purpose of the research described in this report is to attempt to define the magnitude of the effect of membrane penetration and compliance on the undrained cyclic loading resistance of various gravels in order that this factor can be taken into account in assessing the undrained strength loss which could occur in gravelly soils.

CHAPTER 2

USE OF THE CYCLIC TRIAXIAL TEST IN LIQUEFACTION ANALYSIS

Earthquake-Induced Stresses

Conventional liquefaction analysis involves a comparison of (1) the earthquake induced dynamic shear stresses in a soil deposit and (2) the stresses required to cause liquefaction of the soils, as determined by laboratory or field tests (Seed and Idriss, 1971; Seed and Peacock, 1971; Castro, 1975; Seed et al., 1976). Seed and Idriss (1971) used the simplified relationship:

$$\tau_{av\text{-}induced} \simeq 0.65 \times \gamma h/g \times a_{max} \times r_d;$$

for determining the average induced shear stresses for level-ground conditions. In this relationship:

$\tau_{av\text{-}induced}$ is the average earthquake induced shear stress;

a_{max} is the maximum earthquake acceleration; and

r_d is a depth reduction factor to account for the deformability of the soil mass with depth.

Alternatively, more sophisticated dynamic response analyses using computer programs like SHAKE or FLUSH may be used to determine the earthquake-induced shear stresses.

The number of significant stress cycles, N_c, to which the soil mass can be expected to be subjected varies with the earthquake magnitude. Representative numbers of cycles suggested by Seed and Idriss (1982) are as follows:

Earthquake Magnitude, M	Number of Significant Stress Cycles, N_c
5.25	2 - 3
6	5

6.75	10
7.5	15
8.5	26

The next step in the analysis is to determine if the induced stress level and the number of stress cycles are sufficient to cause liquefaction of the soil mass in the field. This may be determined through the use of case studies (Seed et al., 1983, 1984; Yoshimi and Tokimatsu, 1983) or by performing laboratory tests on representative soil samples (Seed and Idriss, 1971; Ishihara, 1985). Since laboratory tests provide a potential basis for such evaluations for gravelly soils, the use of cyclic load triaxial compression tests is discussed below.

The Undrained, Cyclic Triaxial Test

Ideally, high quality, undisturbed samples from the soil layer of interest or representative samples of deposits or fills should be obtained for cyclic testing. Specimens may also be reconstituted in the laboratory, although such specimens may not appropriately represent the actual condition of the deposit in the field (Seed and Peacock, 1971; Mulilis et al., 1975, 1977; Mori et al., 1977; Singh et al., 1979). Having obtained appropriate samples, the samples are installed in the triaxial cell and subjected to lateral and axial stresses representative of the effective stresses which exist in-situ, as shown in Figure 2.1. The consolidated sample is then subjected to a cyclic deviator stress, σ_d, under undrained loading conditions, until the sample liquefies. Typically, several test specimens are subjected to various cyclic stress levels in order to define a relationship between

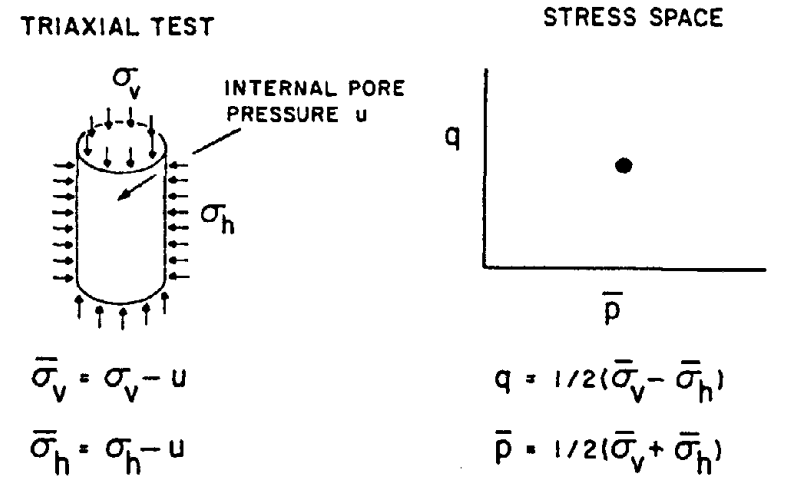

(b)

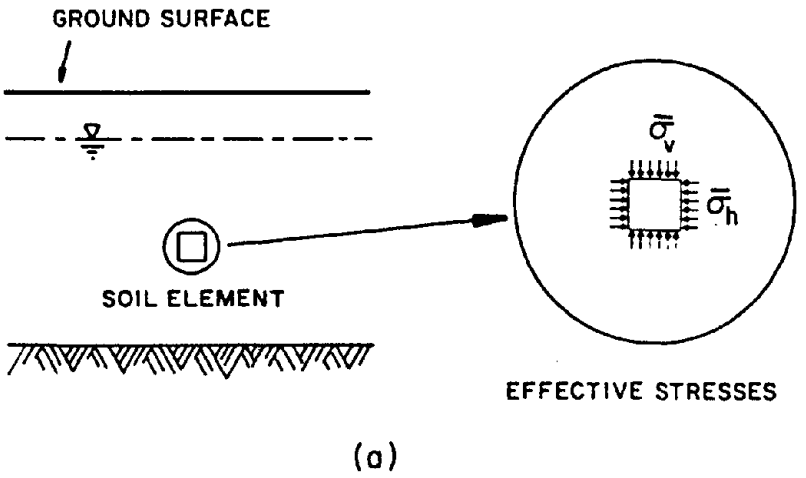

(a)

Figure 2.1 Illustration of the State of Stress in a Soil Element - (a) in the Ground and (b) in the Triaxial Test (after the Committee on Earthquake Engineering, 1985)

cyclic stress ratio, $\sigma_d/2\sigma_{3c}$, and number of cycles required to cause liquefaction, N_ℓ.

A typical relationship determined by laboratory tests performed on sand specimens is shown in Figure 2.2. The use of such results to evaluate the liquefaction potential of a granular soil deposit is discussed in the following sections.

Sand Deposits

Suppose that the critical zone of a sand deposit, in terms of liquefaction potential, extends from a depth of about 15 to 25 feet below the ground surface as shown in Figure 2.3.

Given the following parameters:

Earthquake Magnitude = 6.5,

$N_c = 10$,

$a_{max} = 0.16$ g,

$\gamma_d = 115$ pcf, and

$K_o = 0.4$;

analysis may be performed for the conditions at a representative depth of 20 feet below the ground surface.

At this depth, $\sigma_o \simeq 20 \times 115 = 2300$ psf,

$\sigma_o' \simeq 4 \times 115 + 16 \times 52.5 = 1300$ psf,

$r_d \simeq 0.95$,

and the earthquake induced cyclic stress ratio is;

$$\tau_{av}/\sigma_o' \simeq 0.65 \times a_{max}/g \times \sigma_o/\sigma_o' \times r_d;$$

$$\simeq 0.65 \times 0.16 \times 2300/1300 \times 0.95$$

$$\simeq 0.175.$$

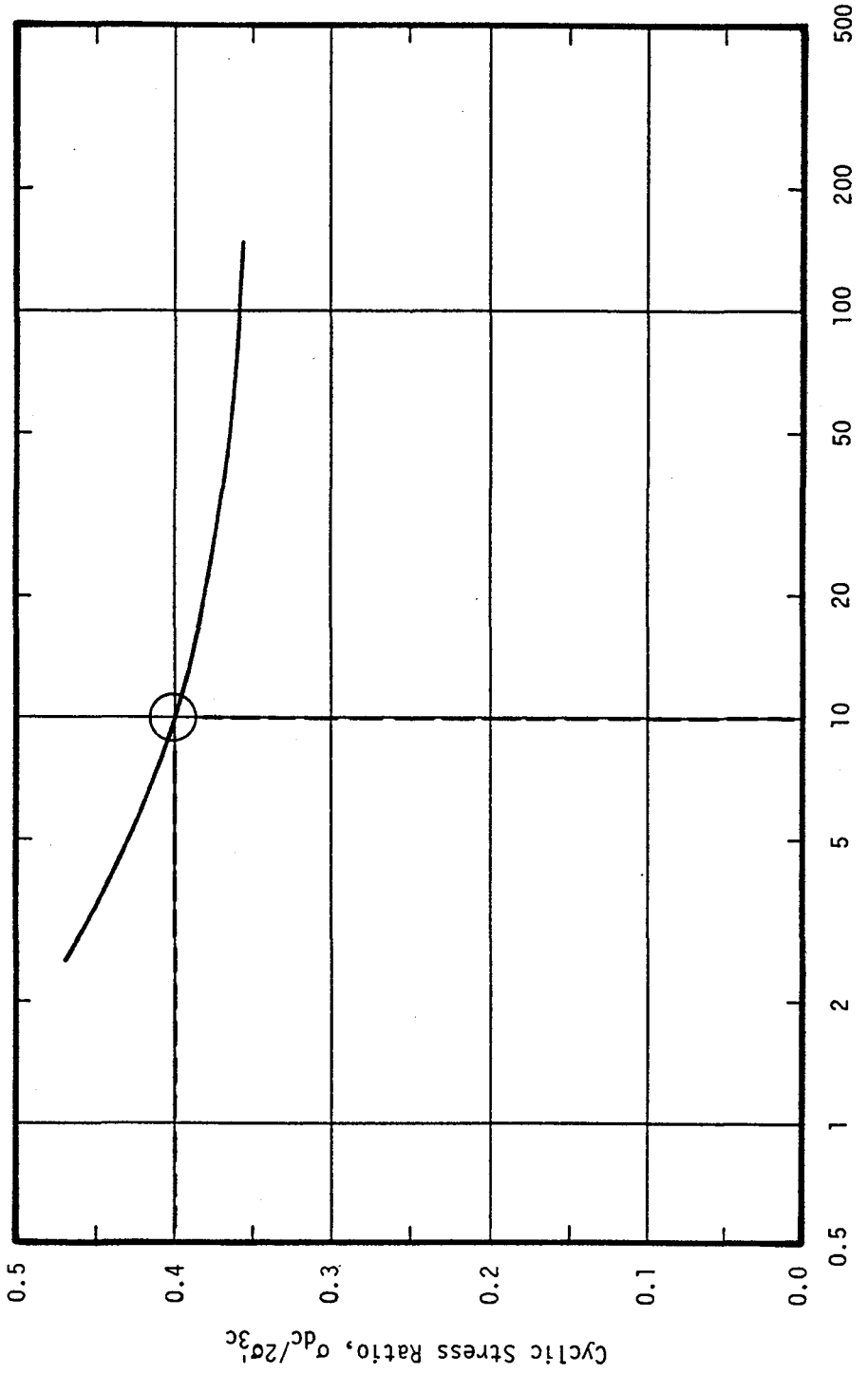

Figure 2.2 Typical Relationship Between Cyclic Stress Ratio and Number of Stress Cycles Causing Liquefaction For Sand Specimens

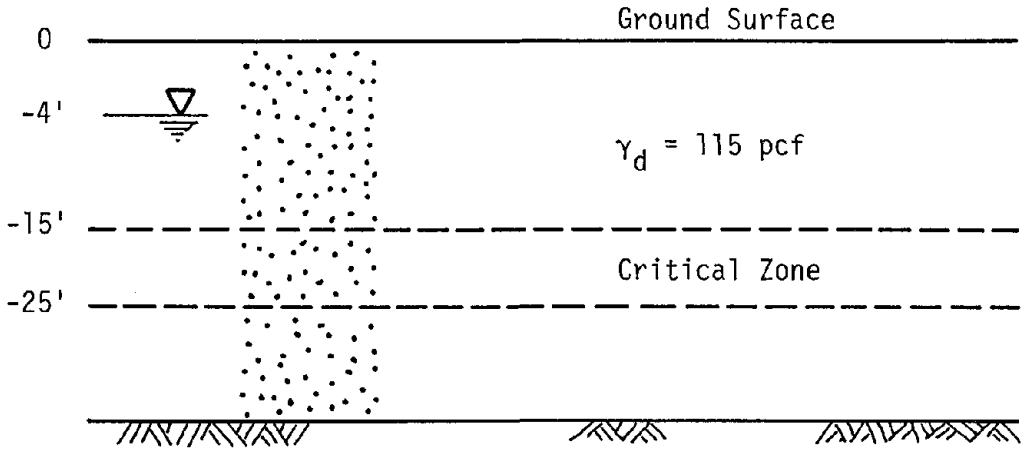

(a)

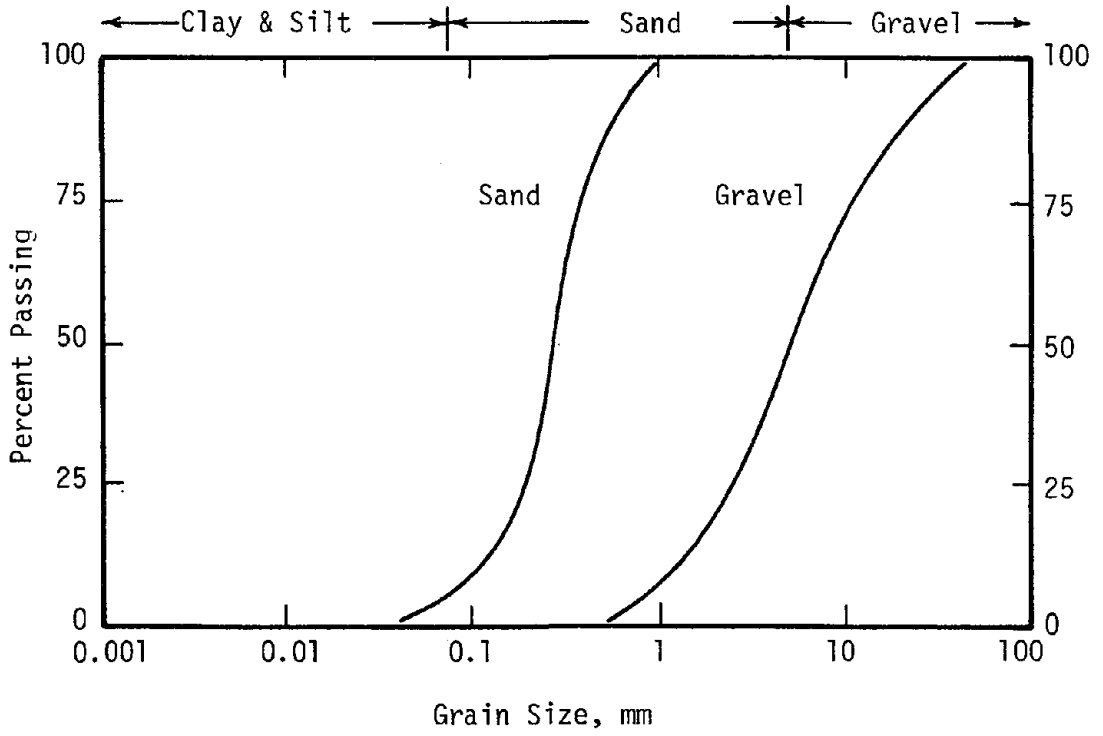

(b)

Figure 2.3 Soil Profile and Grain Size Distributions for Liquefaction Illustration

Thus, soil elements at this depth can be expected to be subjected to about 10 cycles of stress at an average cyclic stress ratio of about 0.18.

Suppose that a cyclic laboratory test program has been performed on representative samples from the sand deposit under investigation and the relationship shown in Figure 2.2 was determined. These results show that a stress ratio of 0.40 is required to cause liquefaction in 10 stress cycles in the cyclic triaxial test. This value of stress ratio must be corrected to account for imperfect modeling of the in-situ stress conditions in the triaxial test as shown in Figure 2.4. Seed (1979) and DeAlba et al.(1976), proposed using the following relationship to account for the difference in the laboratory and field stress conditions.

$$[\tau_h/\sigma_v']_{\ell\text{-field}} \simeq C_r \times [\sigma_{dc}/2\sigma_a]_{\ell\text{-triaxial}},$$

where, $C_r \simeq 0.57$ for $K_o = 0.4$,

and $C_r \simeq 0.9$ to 1 for $K_o = 1$.

Thus the stress ratio which can be expected to cause liquefaction in the field can be calculated as follows:

$$\tau_h/\sigma_v' \simeq 0.57 \times 0.40 \simeq 0.23.$$

This value is greater than that expected to occur in the field. Thus it may be concluded that the deposit is safe against liquefaction for the design earthquake, with a stress ratio factor of safety of $0.23/0.17 = 1.35$.

Gravel Deposits

In order to explore how a gravel deposit might behave in a similar study, let us assume that all of the information used for the

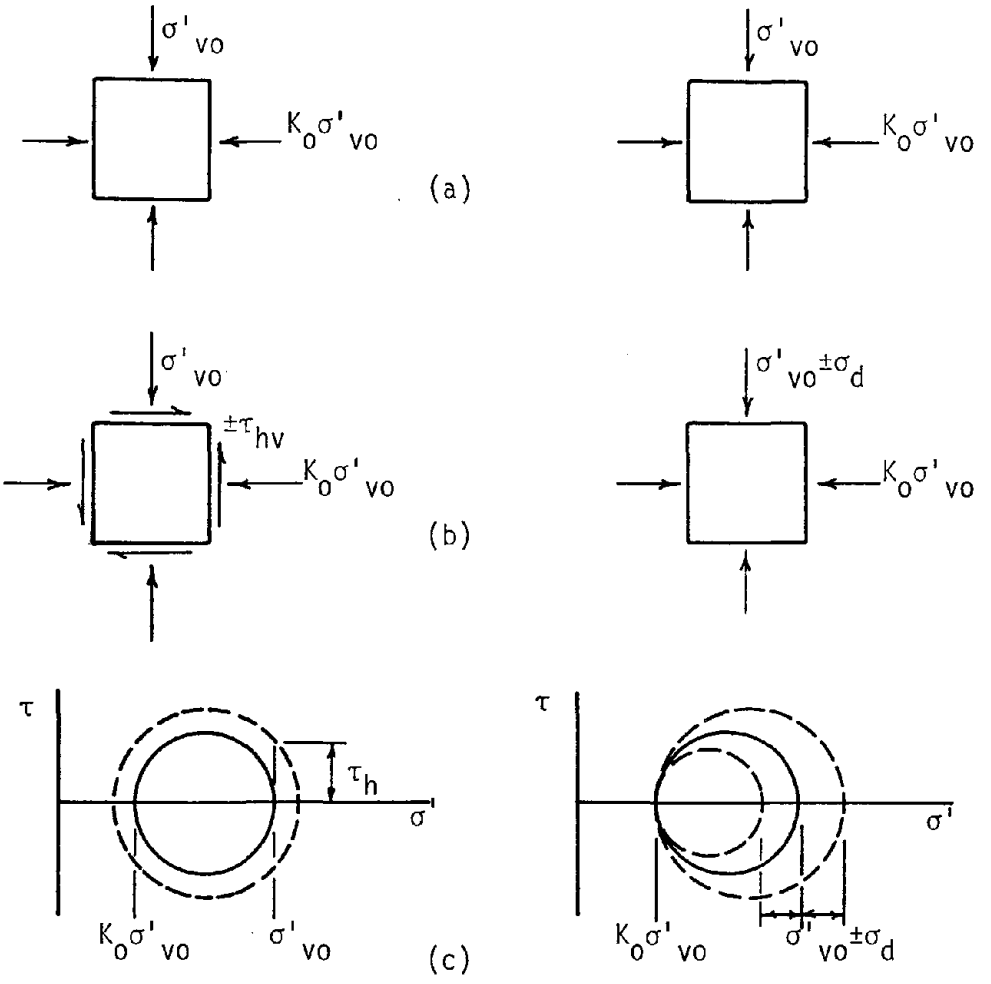

In-situ or Simple Shear Triaxial Test

Figure 2.4 Illustration of The Imperfect Modeling of In-situ Stress Conditions in the Triaxial Test - (a) Static Stress Conditions, (b) Superimposed Dynamic Stresses, and (c) Mohr Circle Representation

sand deposit analysis also applies for the gravel deposit, as shown in Figure 2.3. Since the geometry of the site, the earthquake parameters, and the soil properties are all unchanged (except for the grain size distribution), the expected earthquake induced cyclic stress ratio is again about 0.18.

Laboratory specimens may have been obtained either by freezing a sample of the soil deposit in-situ and thawing it after it had been trimmed and installed in the triaxial chamber (Singh et al., 1982), or by reconstituting samples in the laboratory. The latter method requires that considerable judgment be exercised in order to accurately model the characteristics of the in-situ soil deposit which influence its cyclic loading resistance. These characteristics have been identified as relative density, particle structure, cementation that develops with age, and the seismic history of the deposit (Seed et al., 1975, 1977). Scalping or modeling techniques (Donaghe and Townsend, 1976; Siddiqi 1984) may be used to reduce the required size of the triaxial specimen in some cases. Otherwise, a 12 inch diameter specimen would probably be required in order to maintain a ratio of specimen diameter to maximum particle size of at least six for well-graded soils and up to eight for uniform soils (Holtz and Gibbs, 1956; Leslie, 1963).

Let us assume, however, that suitable gravel specimens were obtained or properly reconstituted, tested in the laboratory, and that the relationship between cyclic stress ratio and number of cycles to liquefaction shown previously in Figure 2.2 was again determined. Since the gravel deposit was found to have the same earthquake-induced stresses, the same expected number of earthquake stress cycles, and

the same laboratory-determined cyclic loading resistance as the sand deposit, it might well be considered reasonable to conclude that the gravel deposit is also safe against liquefaction. However, this conclusion fails to consider the effect of membrane compliance on the triaxial test results.

Membrane compliance artificially inhibits excess pore pressure development in an undrained triaxial test as will be discussed in the following chapter. It is a phenomenon that occurs only in laboratory tests and it leads to erroneously higher values of the cyclic stress ratio required to cause liquefaction in a given number of cycles than would actually be required in the field. Thus, it leads to an unconservative assessment of the cyclic strength of the deposit unless a correction is made.

Application of a membrane compliance correction factor, C_m, (where $C_m \leq 1$) to the results of the triaxial tests would result in a more accurate assessment of the true in-situ cyclic strength of the gravel deposit. However, there is little basis for assessing the magnitude of the required correction factor. Values of C_m ranging from 1.0 to about 0.60 have been proposed. If it is assumed that C_m=1.0, then it would be concluded that the gravel deposit will not liquefy during the design earthquake. On the other hand, a membrane compliance correction factor of, C_m=0.65, would lead to a value of cyclic loading resistance equal to 0.57 x (0.65 x 0.40) $\simeq$ 0.15 and thus the value of the shear stress ratio which will cause liquefaction in the field is less than the shear stress ratio which is expected to be induced by the design earthquake. Consequently, the gravel deposit would be expected

to liquefy if the design earthquake occurs, with a stress ratio factor of safety of 0.15/0.18 = 0.83.

This example clearly shows that quantification of the magnitude of the membrane compliance correction factor, C_m, to be applied to the results of cyclic triaxial tests on gravels, is an important step in assessing the liquefaction potential of gravelly sites and earth structures. The issue of membrane compliance will be discussed in more detail in the next chapter and a method for assessing the magnitude of a membrane compliance correction factor will be presented and explored later in this report.

CHAPTER 3

MEMBRANE PENETRATION AND COMPLIANCE IN THE TRIAXIAL TEST

Introduction

The terms "membrane penetration" and "membrane compliance" are often used interchangeably yet they have different causes and effects on triaxial test results. Membrane penetration into peripheral sample voids occurs during an increase in confining pressure in a drained test. The only effect of this phenomenon is to cause volume change measurements to be greater than would otherwise occur. Membrane penetration has no effect on the drained test strength parameters, unless area and other corrections are made using the inaccurate volume change data. Membrane compliance, on the other hand, results from a change in the effective confining pressure during an undrained test. The effect in this case is to inhibit pore pressure changes (increases or decreases) that would have occurred in a noncompliant system. Both of these phenomena are discussed in more detail in the following pages.

Membrane Penetration

Membrane penetration is the intrusion of the confining membrane into the peripheral voids of a test specimen; it is caused by a deformation of the membrane due to increased confining pressure in a drained system as shown in Figure 3.1. This is a reversible process and both directions (penetration or rebound) affect only volume change measurements during drained loading or unloading in the horizontal, typically minor principle stress, direction. Axial loading or unloading will not significantly affect membrane penetration. This

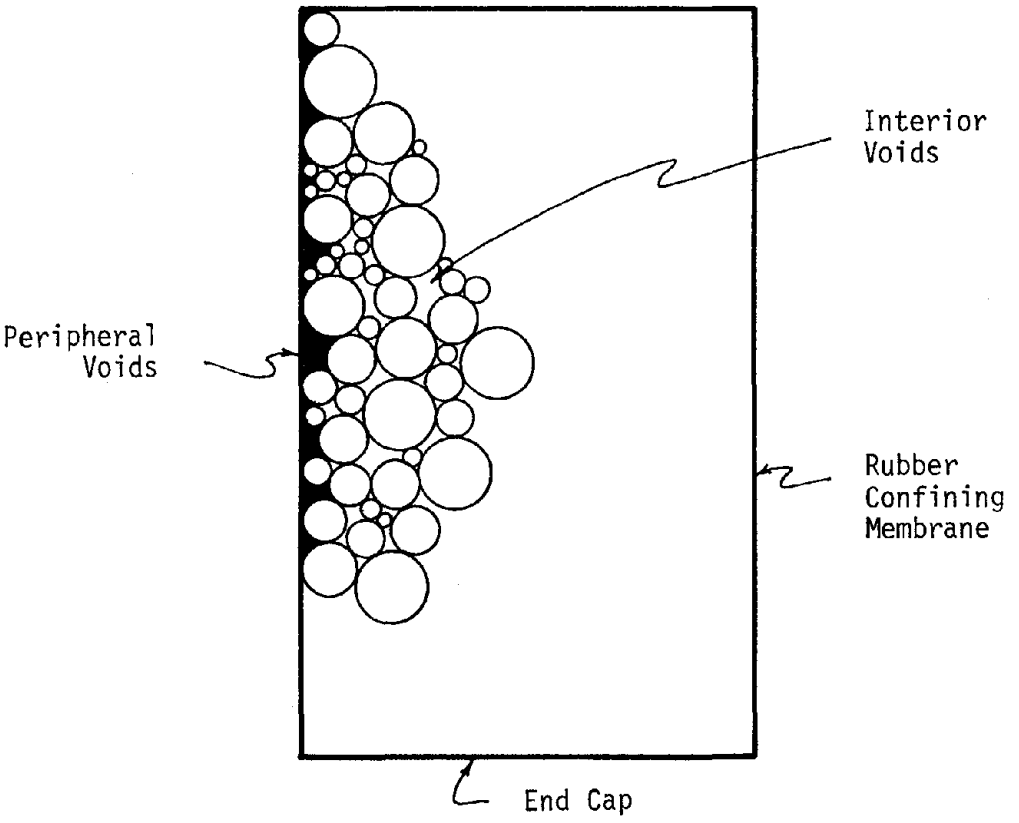

Figure 3.1 Illustration of Triaxial Specimen Peripheral Voids (shaded) and Interior Void

process of membrane penetration or rebound has no direct effect on any static or dynamic parameter measurement other than volume change. However, membrane penetration can, in some cases, lead to the more serious problem of membrane compliance.

When a triaxial specimen is set up for testing, the membrane is initially stretched flat over the surface of the specimen, bridging the peripheral sample voids before any initial effective confining pressure is applied as shown in Figure 3.2. As the effective confining pressure is increased, the membrane will penetrate into these voids. Additional penetration occurs with each subsequent effective pressure increase until no more penetration is possible and the ultimate membrane penetration occurs.

The degree of penetration that occurs at any time is a function of the effective confining pressure, the membrane thickness and modulus, and the peripheral pore sizes. For any given test specimen, the membrane parameters and specimen void sizes are essentially fixed so that the only variable during a test may be the effective confining pressure. Thus, the amount of membrane penetration that occurs is uniquely related to the effective confining pressure for a given set of test constraints. In fact, it is the only quantity that determines the amount of membrane penetration that occurs. When confining pressure is applied to a specimen that is susceptible to membrane penetration, stresses are built-up and stored in the membrane with each increase in confining pressure. A portion of the stored energy is released when the effective confining pressure is reduced. It is this stored energy that causes the membrane to rebound when the effective confining pressure is reduced. This behavior becomes quite significant when

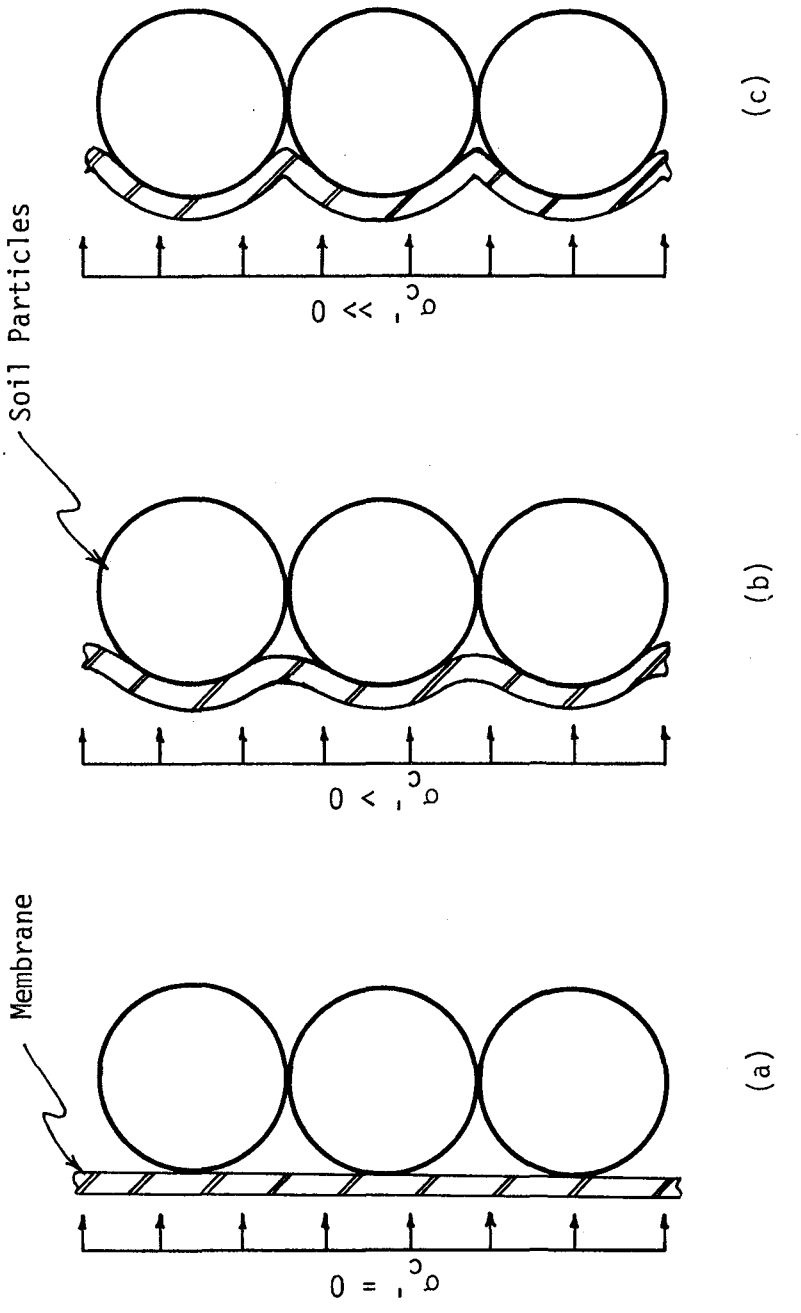

Figure 3.2 Membrane Penetration into Peripheral Voids with Increasing Effective Confining Pressure - (a) No Membrane Penetration, (b) Intermediate Membrane Penetration, and (c) Ultimate Membrane Penetration

dealing with membrane compliance in undrained tests and will be discussed in the following section.

Membrane penetration can only occur when the peripheral voids are sufficiently large with respect to the thickness of the confining membrane. Fine grained soils, such as very fine sands, silts, and clays are not susceptible to membrane penetration when typical thickness membranes, about 0.3 mm, are used. Kiekbusch and Schuppener (1977) did measure some volume change due to membrane penetration in consolidation-type tests on silts using a rubber membrane on the upper loading surface. However, it is doubtful that such minute volume changes would have any practical effect on the results of triaxial tests. Consequently, it is only the coarser grained soils that experience significant membrane penetration effects.

Membrane penetration may only occur during a drained triaxial test when the effective confining pressure changes. The resulting volume changes have approximately the same value for both loading and unloading; thus, positive volume changes (contraction) due to increased effective confining pressure and increased membrane penetration will be approximately equal in magnitude to negative volume changes (expansion) due to reduced effective confining pressure and decreased membrane penetration.

The effect of membrane penetration is to exaggerate volume changes. During consolidation, volume changes are measured due to the combination of skeletal contraction as well as membrane penetration into the sample voids. The amount of volumetric strain due to membrane penetration, ε_{vm}, may be estimated by first calculating the true

skeletal volumetric strain, ε_{vs}, and subtracting it from the total measured volumetric strain, ε_{vt}:

i.e. $$\varepsilon_{vm} = \varepsilon_{vt} - \varepsilon_{vs}.$$

Skeletal volumetric strain can be determined by assuming that the specimen consolidates isotropically so that volumetric strain equals three times the measured axial strain, ε_a, as originally suggested by Newland and Allely (1957):

$$\varepsilon_{vs} = 3\varepsilon_a.$$

However, El-Sohby and Andrawes (1972) suggested that a better estimate may be obtained by using the above formula along with volumetric rebound curves rather than consolidation curves for most granular soils. Alternatively, a more precise determination can be made by measuring both axial and radial deformations with the use of girth gages (Banerjee et al., 1979) or some other appropriate measuring system.

Consolidated sample areas and volumes should be determined using values corrected for membrane penetration especially for medium to coarse sands and gravels. The author conducted isotropic triaxial consolidation tests on 2.8 inch diameter specimens of loose, clean, uniform fine gravel, D_{50}=6.5 mm, using one ordinary membrane. The amount of volumetric strain that occurred due to membrane penetration in these tests was about 25 times the value attributable to skeletal contraction alone as is presented in Chapter 9. Isotropic rebound of these same samples produced a similar result.

Extended periods under sustained loads produces a small amount of temporary plastic deformation in the rubber membrane. The amount of volume change due to this effect is not recoverable in a short period

of time. Consequently, total volumetric strain calculated from consolidation curves will be greater than that calculated from rebound curves for the same change in confining pressure, especially as the period of time under sustained loading is increased. This effect is particularly pronounced when systems of multiple membranes are used as will be discussed in more detail in Chapter 9.

The same properties of rubber membranes that make them desirable for testing purposes (i.e., thin, elastic, and low modulus of elasticity), also make them more susceptible to membrane penetration. A thicker, stiffer material would penetrate less into peripheral voids under the same confining pressure and a plastic material would not rebound after penetration had occurred. However, such materials would introduce very large errors in the measured strength of the test specimen and thus would be undesirable.

Membrane penetration, in and of itself, is not generally a problem but it can lead to other complications that are associated with a change in the degree of membrane penetration that might occur during undrained testing. This is what is known as "membrane compliance".

Membrane Compliance

Membrane compliance is a phenomenon involving a change in the degree of membrane penetration which occurs because of a change in the effective confining pressure that is due to a volume change tendency of the soil mass during undrained shear loading (cyclic or monotonic). This is also a reversible process but it affects pore pressure values and thus static or dynamic strength parameters. Membrane compliance tends to inhibit the normal development of conditions which would

otherwise have occurred in a noncompliant system. A contractive soil under undrained, static shear loading, for example, would develop reduced excess pore pressure and thus appear stronger than would be the case in a noncompliant system. A dilative soil, on the other hand, would experience less of a pore pressure reduction and thus appear weaker than would otherwise be the case. Therefore, membrane compliance leads to an unconservative strength assessment in soil that loses strength, and an overconservative strength assessment in a soil that gains strength during shear loading.

It is important to note that while some granular soils may dilate and gain strength during undrained, monotonic loading, the same soils may contract and lose strength if subjected to a sufficiently high level of undrained, cyclic loading as shown in Figure 3.3. Thus, membrane compliance effects may result in either overestimation or underestimation of undrained strengths as determined from monotonic loading conditions. However, membrane compliance effects will invariably result in an overconservative assessment of the undrained, cyclic loading resistance. Table 3.1 summarizes the effects of membrane compliance on soils at different initial test states.

Membrane compliance causes erroneous pore pressure changes because it permits the specimen pore fluid to redistribute during undrained testing. In order to better understand how membrane compliance affects pore pressure changes, it is first necessary to examine the process by which cyclic loading can reduce the strength of a granular soil in a saturated, undrained, noncompliant system. This loading may be due to earthquakes, blasting, construction vibrations, or loading in laboratory testing apparatus.

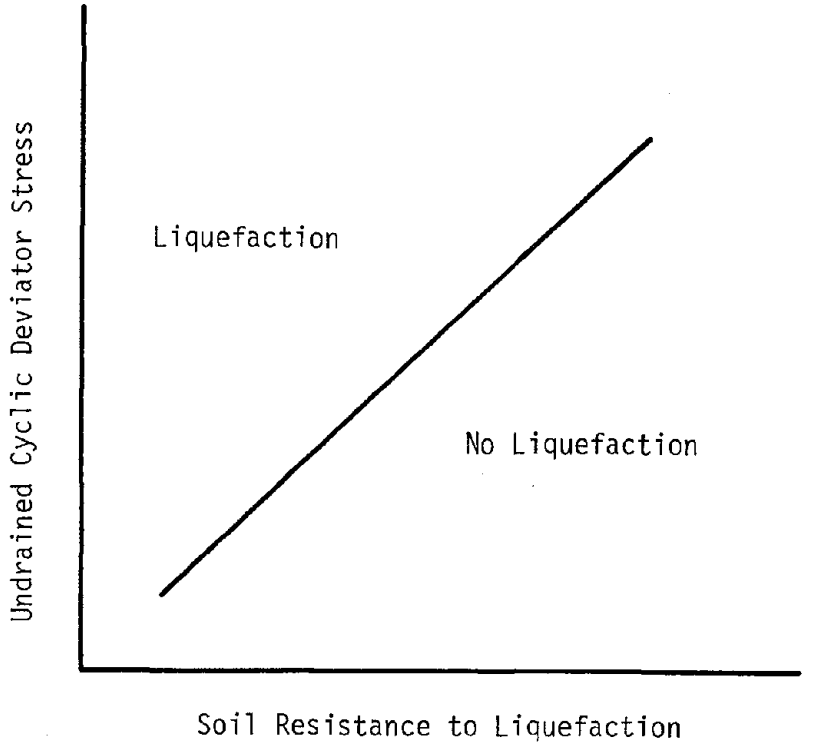

Figure 3.3 Qualitative Relationship Between Soil Resistance to Liquefaction and Undrained, Cyclic Deviator Stress Causing Liquefaction - (Note similarity to penetration resistance vs. cyclic stress ratio causing liquefaction proposed by Seed and Peacock, 1971)

Table 3.1 SUMMARY OF MEMBRANE COMPLIANCE EFFECTS

Noncompliant system

Conditions: 1) Contractive Soil	2) Critical e	3) Dilative Soil
u increases	u constant	u decreases
σ_3' decreases	σ_3' constant	σ_3' increases
∴ strength loss during shear	∴ strength constant during shear	∴ strength gain during shear

Compliant system

Conditions: 1) Contractive Soil	2) Critical e	3) Dilative Soil
u increases but not as much as above	u constant	u decreases but not as much as above
σ_3' decreases but not as much as above	σ_3' constant	σ_3' increases but not as much as above
∴ strength loss during shear but not as much as above	∴ strength constant during shear	∴ strength gain during shear but not as much as above

Result of Membrane Compliance:

strength loss is inhibited- leads to an unconservative, high assessment of the in-situ (non-compliant) strength	no effect	strength gain is inhibited- leads to an overconservative, low assessment of the in-situ (non-compliant) strength

Note: Cyclic loading will typically result in a contractive condition as described earlier in this chapter. Monotonic loading, on the other hand, may result in any of the three conditions described above depending on the soil state and the test conditions.

When a soil element is subjected to cyclic loading under a constant total confining pressure, stresses at grain contacts are increased to a level above the previous static condition. This increased stress, if sufficiently high, can cause particle breakage at grain contacts together with particle rearrangement due to sliding or rotation. As a few particles are moved from their previous stable arrangement, stresses are further increased on nearby particle contacts causing additional crushing, translation, or rotation. As this process progresses, the particles no longer form a stable, continuous structure and the new structure is not strong enough to support the applied confining pressure. If the specimen were drained, the grain structure would contract until it became stable and continuous once again. However, if it can not contract because the system is undrained, the excess confining pressure that the soil structure can no longer support is transferred to the pore fluid phase of the specimen thus increasing the pore pressure. Transfer of some portion of the confining pressure to the pore fluid phase will unload the solid particle phase and tend to cause it to rebound elastically. Again, since the system is undrained, the particle structure can not expand but this tendency to expand will result in a decrease in the pore water pressure. The initial increase in pore pressure due to grain shifting and the subsequent decrease in pore pressure due to elastic rebound happen simultaneously and result in a net pore pressure increase.

At the start of each new load cycle, the effective confining pressure is lower than at the start of the previous cycle. If the cyclic loading is continued, the process of grain rearrangement and pore pressure build-up will also continue until the effective confining

pressure is reduced to zero (initial liquefaction) and/or large strains develop in the sample.

Membrane compliance affects this process of pore pressure build-up in the following way. As the pore pressure increases (due to particles shifting) the effective pressure is reduced, thus unloading the membrane and causing it to relax and move out of the void space as shown in Figure 3.4. It is the effective confining pressure across the membrane which causes the membrane to penetrate into the peripheral voids. When the value of effective confining pressure is reduced, energy stored in the membrane during distortion will be released and this will result in a tendency for the membrane to relax and move out of the void space. As this occurs, water migrates to the zones previously occupied by the penetrated membrane. Since no volume change can occur within the membrane, the outward flow of pore water from the interior sample void spaces to the peripheral void spaces must be accompanied by a consolidation of the grain structure. The amount of structural volume change that occurs is equal to the sum of all the recoverable membrane penetration volume over the range of effective confining pressure experienced as shown in Figure 3.5. The drainage of interior voids causes a structural volume change resulting in consolidation of the specimen. The combined effect of reduced pore pressure build up and effective consolidation of the grain structure is to indicate a higher undrained cyclic strength than truly exists in a noncompliant system.

Many investigators seem to have been confused by the redistribution of pore fluid and have incorrectly concluded that membrane compliance causes a volume change within the system. This is

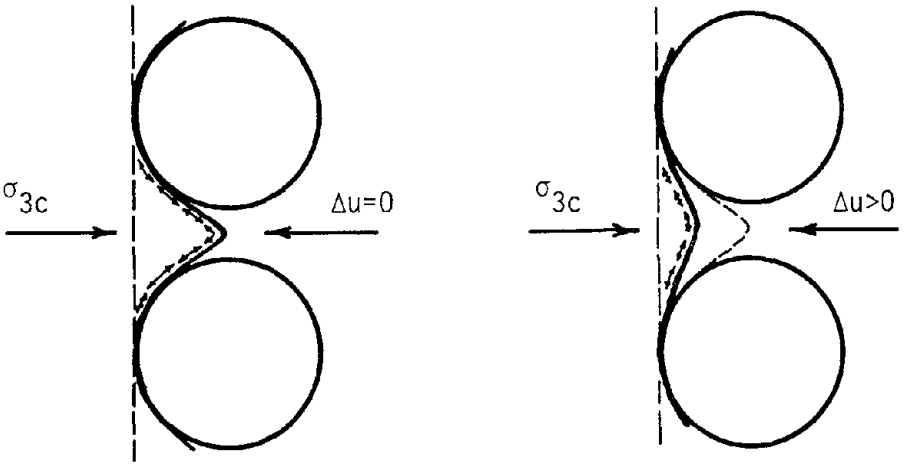

(a) Stress condition just before cyclic loading - tensile stresses are stored in the membrane

(b) Excess pore pressure development as a result of cyclic loading - σ_3' is reduced and stored stresses are released as membrane rebounds.

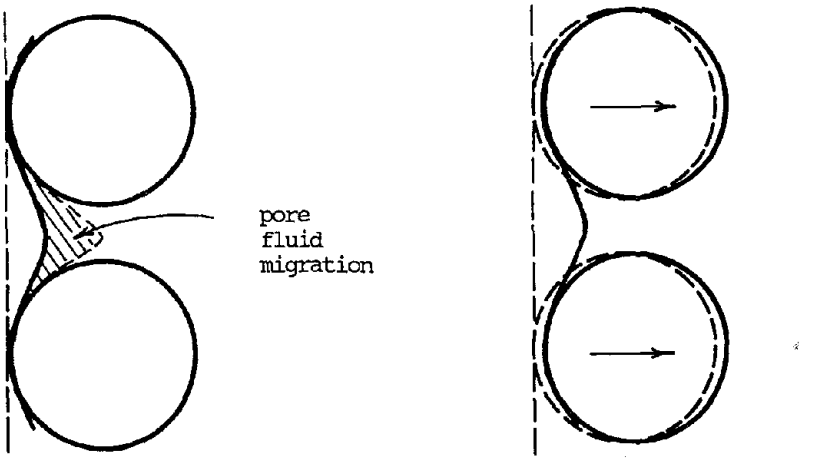

(c) Pore fluid is drawn to membrane penetration site as membrane rebounds, causing partial drainage of the interior voids

(d) Pore fluid redistribution from interior to peripheral voids causes consolidation of the grain structure to balance migration of fluid mass.

Figure 3.4 Membrane Compliance Effects Resulting in Partial Drainage of the Interior Voids During Undrained, Cyclic Triaxial Loading

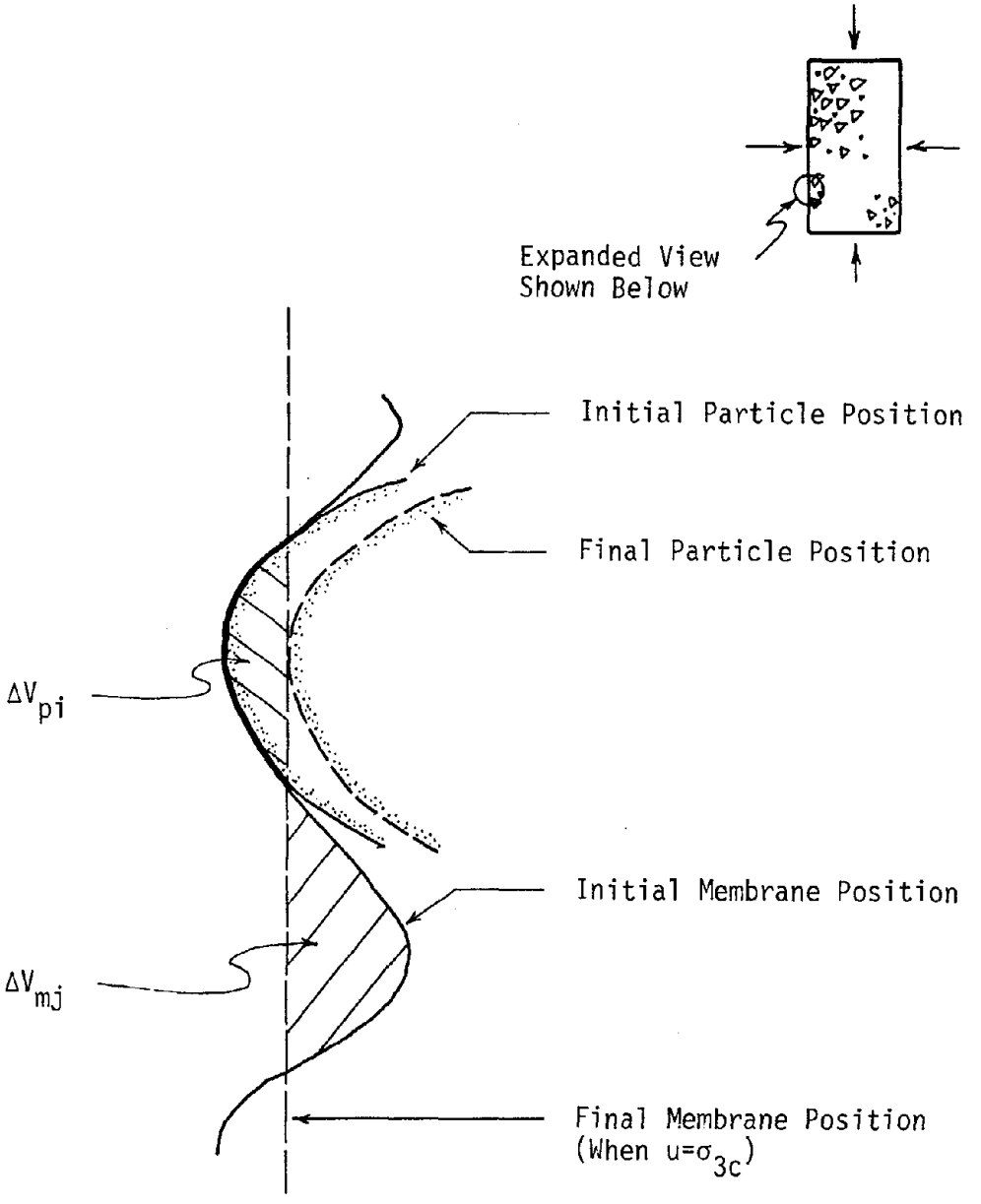

$$\Sigma_i \Delta V_{pi} = \Sigma_i \Delta V_{mj}$$

Where: $\Sigma_i \Delta V_{pi}$ = Total Volumetric Compression of the Particle Structure,

$\Sigma_i \Delta V_{mj}$ = Total Volume of Redistributed Pore Fluid Due to Membrane Compliance.

Figure 3.5 Illustration of Particle Structure Compression and Pore Fluid Redistribution Caused by Membrane Compliance

not possible from a purely physical point of view. No volume change can occur within the sealed system bounded by the confining membrane and the end platens. A saturated (S=100%) triaxial soil specimen is composed of soil grains forming a continuous particulate structure with the void space filled with water. The top and bottom ends of the specimen are confined by end caps and a thin rubber membrane envelopes the sides of the specimen and it is sealed at the end caps. The material confined within the membrane and end caps (soil particles and water) is essentially incompressible over a typical range of confining pressure. Thus, no change in volume can occur within the confines of the end caps and the confining membrane, and stress redistribution must occur in order to comply with this constraint.

CHAPTER 4

REVIEW OF PREVIOUS INVESTIGATIONS INTO MEMBRANE PENETRATION AND MEMBRANE COMPLIANCE EFFECTS

Introduction

Over the last 30 years, many investigators have explored the phenomena known as membrane penetration and membrane compliance and attempted to account for their effects on triaxial test results. A great many experimental and theoretical corrections for these phenomena have been developed and used with varying degrees of success. This chapter provides a review of most of the studies related to these subjects. A list of the previous investigators is presented in Table 4.1.

Review of Previous Investigations

Newland and Allely (1957)

The effects of membrane penetration on the results of triaxial compression tests were first noted by Newland and Allely in 1957. They performed axial load tests on specimens of lead shot to determine if the difference between peak and residual strength could be accounted for by the energy required to cause volumetric expansion during shear. During the course of the testing program, they noted that the membrane was in contact only with the outer edges of the particles comprising the sample and that the membrane spanned across the voids between particles. They called this phenomenon "membrane misfit". They also noted that during various stages of shear and hydrostatic compression, the membrane would penetrate into the peripheral voids to varying degrees. During reloading, small strains would result in a sudden

Table 4.1 LIST OF PREVIOUS INVESTIGATORS OF MEMBRANE PENETRATION AND MEMBRANE COMPLIANCE EFFECTS

Investigator(s)	Year
Newland and Allely	1957
Newland and Allely	1959
Roscoe, Schofield and Thurairajah	1963
El-Sohby	1964
Holubec	1966
Steinbach	1967
Chan	1972
El-Sohby and Andrawes	1972
Pickering	1973
Frydman, Zeitlen and Alpan	1973
Raju and Sadasivan	1974
Wong, Seed and Chan	1975
DeAlba, Chan and Seed	1975
Lade and Hernandez	1977
Kiekbusch and Schuppener	1977
Martin, Finn and Seed	1978
Chan	1978
Banerjee	1979
Raju and Venkataramana	1980
Ramana and Raju	1981
Chan	1982
Ramana and Raju	1982
Wu and Chang	1982
Baldi and Nova	1983
Torres	1983
Vaid and Negussey	1984

volume expansion due to frictional release of the membrane. They concluded that this alternate penetration and expansion of the membrane could result in erroneous volume change measurements, and thus they attempted to quantify this effect. Hydrostatic compression tests were performed in which axial deformation and total volumetric deformation, (V_t), were measured. Newland and Allely assumed that the sample would deform isotropically so that:

$$\varepsilon_{volumetric} = 3\varepsilon_{axial},$$

and from this equation, the volumetric strain due to membrane penetration, (ε_{vm}), could be computed as :

$$\varepsilon_{vm} = \varepsilon_{vt} - \varepsilon_{vs}$$

where ε_{vt} = total volumetric strain, and

ε_{vs} = skeletal volumetric strain.

Newland and Allely (1959)

Newland and Allely continued their investigations of membrane penetration effects by performing "simulated" undrained triaxial compression tests. In these tests, constant pore volume was maintained by adjusting the cell pressure as required thereby simulating an undrained condition. They noted that the amount of membrane penetration increased with increasing effective confining pressure. Thus as the skeleton expands, membrane penetration increases along with increasing effective confining pressure as shown in Figure 4.1. A plot of the change in volume attributed to membrane penetration versus effective confining pressure was generated as shown in Figure 4.2. The effect of the membrane penetration, they observed, is to considerably reduce the value of effective confining pressure at failure. They

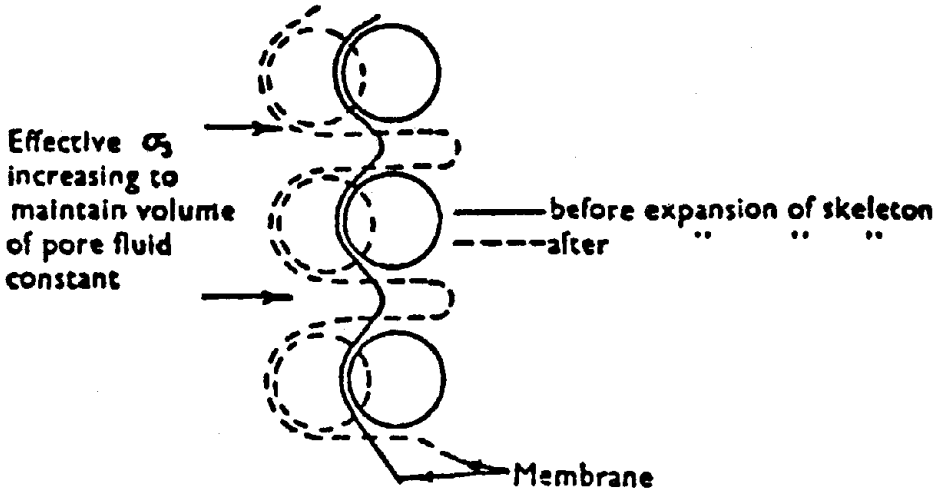

Figure 4.1 Increased Membrane Penetration with Increasing Effective Pressure (after Newland and Allely, 1959)

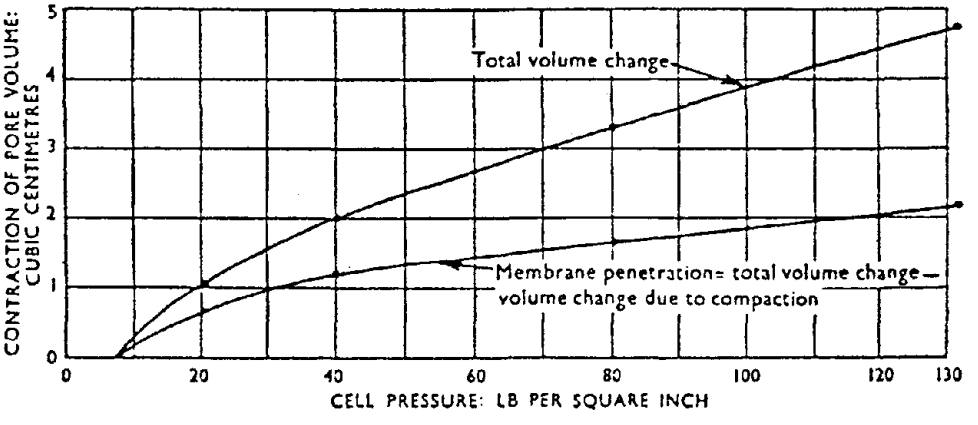

Figure 4.2 Volume Changes Due to a Change in Effective Pressure (after Newland and Allely, 1959)

concluded that this effect could be reduced by (1) using thicker membranes and (2) testing samples with larger dimensions.

These early studies by Newland and Allely provided an accurate assessment of the phenomenon known as membrane penetration. Their work laid the groundwork for future investigations into this subject.

Roscoe, Schofield and Thurairajah (1963)

Roscoe, Schofield and Thurairajah introduced the dummy rod method for quantifying volumetric strains due to membrane penetration. In this method, several triaxial test specimens of sand, 3 inches high by 1-1/2 inches in diameter, were constructed, each with a full height cylindrical brass rod placed coaxially within it. Rod diameters varied from 1/4 inch to 1-3/8 inches.. It was assumed that the volumetric strain due to membrane penetration would be the same for all tests. However, the total volumetric strain, caused by soil skeleton compression and membrane penetration, would decrease with increasing rod diameter and decreasing soil volume. Thus, extrapolation to a rod diameter equal to the sample diameter, or zero soil volume, would indicate the value of volume change attributable only to membrane penetration. Figure 4.3 shows a typical plot generated for a constant soil state and an increase in cell pressure from 5 psi to 100 psi for several dummy rod diameters. Extrapolation to the specimen diameter of 1-1/2 inches in this figure, indicates a value of membrane penetration volume change equal to 0.92 cc. Assuming that a specimen height to diameter ratio of 2.5 exists, this value of membrane penetration volume change represents a volumetric strain of about 0.9%. It may be seen from Figure 4.3 that the value of volume change due to membrane penetration accounts for about 65% of the total measured volume change

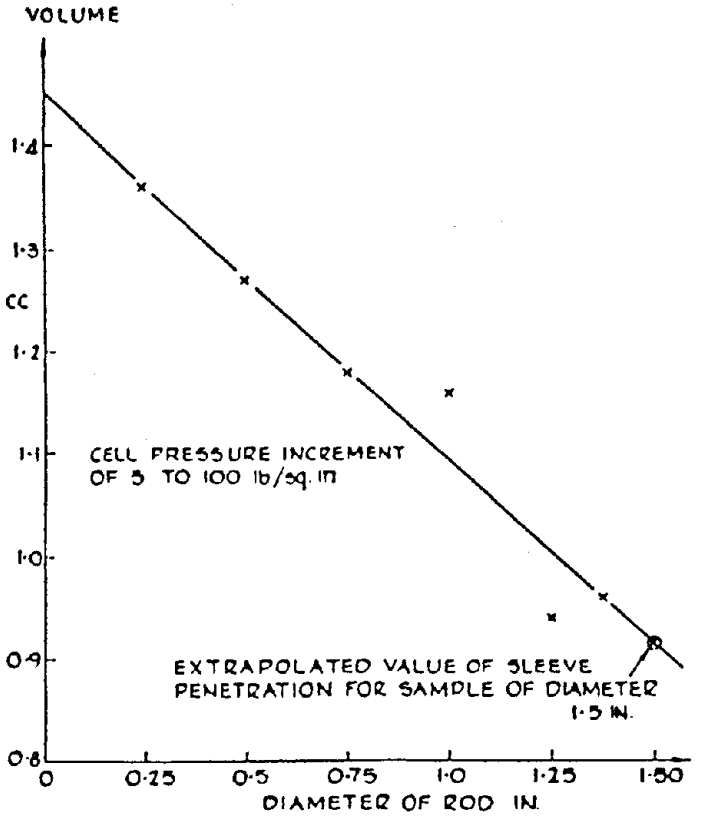

Figure 4.3 Volume of Water Expelled from Triaxial Specimens of Sand with Coaxial Cylindrical Rod Inclusions (after Roscoe et al., 1963)

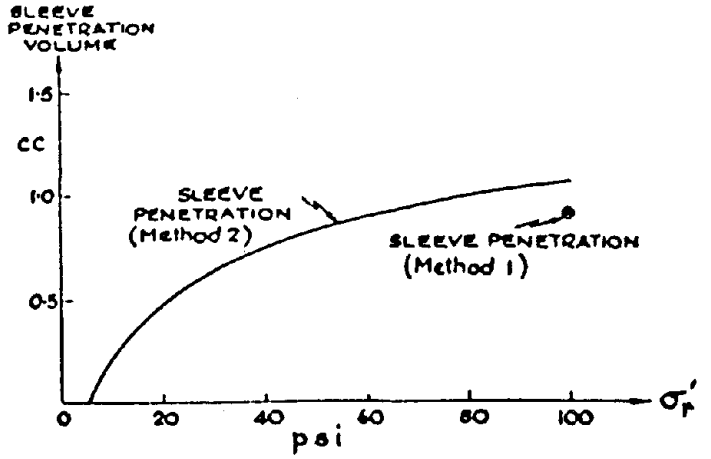

Figure 4.4 Membrane (Sleeve) Penetration Volume Change Comparison for Two Proposed Methods (after Roscoe et al., 1963)

in specimens where no dummy rod was used. These results were obtained from tests performed on sand specimens. It would be expected that the effect of membrane penetration on the results of similar studies performed on gravelly soil specimens might be much greater.

Roscoe et al. (1963) also further investigated the method of isotropic compression introduced by Newland and Allely. In these studies, the sample was again assumed to deform isotropically so that volumetric strains were computed as three times the axial strain, and tests were performed on specimens of rounded Leighton Buzzard Sand at relative densities of 43% and 100%. The tests were repeated for membrane thicknesses of 0.02, 0.01, and 0.005 inches and the total measured volumetric strain was found to be about 5 times that of the skeleton strain alone. For all membrane thicknesses, however, the volume changes due to membrane penetration were within ±5% of the mean indicating that membrane thickness may not be as significant as suggested by Newland and Allely.

Both methods, the dummy-rod and the isotropic consolidation methods, were used to evaluate the volume changes due to membrane penetration for specimens constructed of uniform glass beads (D_{50}=1 mm), and good agreement was found between the two sets of results. However, it was concluded that the second method, which assumes isotropic deformation, probably provided the better results since the brass rods may interfere with the particle structure. Comparison of the results obtained by these two methods are shown in Figure 4.4. Note that Roscoe et al. used the word "sleeve" for what is commonly referred to as a "membrane".

El-Sohby (1964)

El-Sohby suggested that sand samples may not deform isotropically even when subjected to isotropic stresses and, for this reason, he thought that the Roscoe et al. dummy rod method may be a more reliable way of determining membrane penetration volume changes.

Holubec (1966)

Holubec also suggested that sand specimens may strain anisotropically and thus true skeletal strains should be determined by measuring both axial and radial deformations.

Steinbach (1967)

Steinbach performed tests on 18 different gradations of sands with various mean particle sizes. He assumed that the specimens would deform isotropically under hydrostatic consolidation so that soil skeleton volumetric strain could be determined by measuring the axial strain only. Membrane penetration was determined by subtracting skeletal volumetric strain from the measured total volumetric strain. He found that the membrane penetration effect for well graded soils was similar to that for uniform soils with the same mean grain diameter, and he proposed a relationship expressing volume change due to membrane penetration in terms of D_{50}. However, this study was conducted only on sands and thus it is not readily apparent that the proposed relationship based on D_{50} will also apply to gravelly soils.

Chan (1972)

Chan developed a special membrane for testing rockfill at high confining pressures, as shown in Figure 4.5. During this investigation, he experimented with covering the surface of the sample

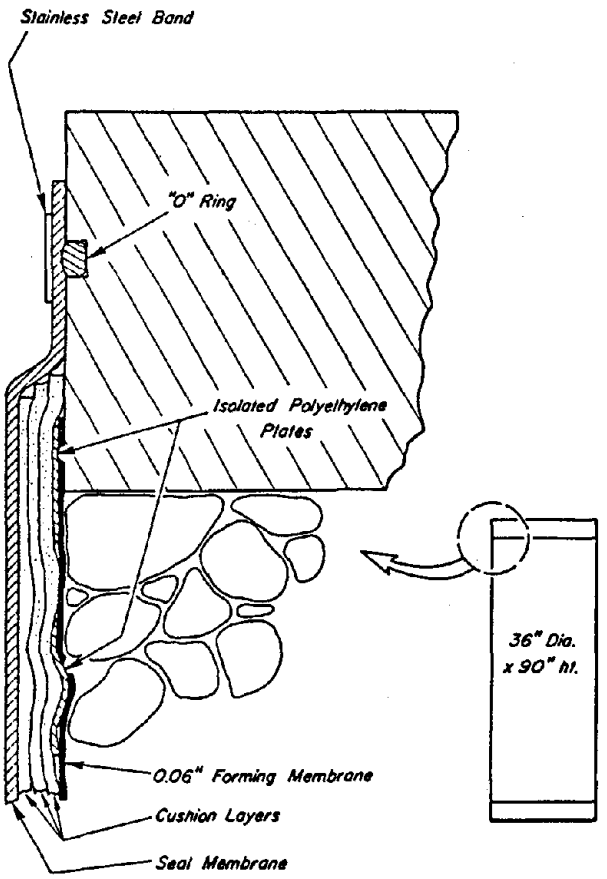

Figure 4.5 Special Membrane Developed for Testing Rockfills (after Chan, 1972)

with square plates of high density polyethylene to prevent membrane rupture. This procedure would also be useful for reducing membrane penetration, since the plates would bridge over the surface interstices. However, the plates deformed plastically over the surface irregularities of the sample when significant confining pressures were applied, thus forming a stiff, rigid shell for which substantial stress corrections would be required.

El-Sohby and Andrawes (1972)

El-Sohby and Andrawes performed hydrostatic compression tests on loose and dense sand specimens. They divided the specimen deformation into elastic (recoverable) and sliding (non-recoverable) components. For dense sands, they found that most of the deformation was elastic and the material behaved isotropically as shown in Figures 4.6 & 4.7 respectively. For loose samples, on the other hand, the sliding component of deformation was much larger, resulting in values of radial strains which were significantly larger than those for axial strains. Thus, it was concluded that loose sands could not be assumed to behave isotropically.

Pickering (1973)

Pickering considered the problem of membrane penetration (and system compliance) in cyclic simple shear tests on saturated sands. He proposed the use of the equivalent drained constant-volume liquefaction test to overcome system compliance problems associated with undrained tests. In this procedure, dry sand samples are kept at constant volume by locking the vertical load ram in place to maintain constant height. Reductions in the values of vertical stress which occur during loading reflect the reductions in vertical effective pressure that would occur

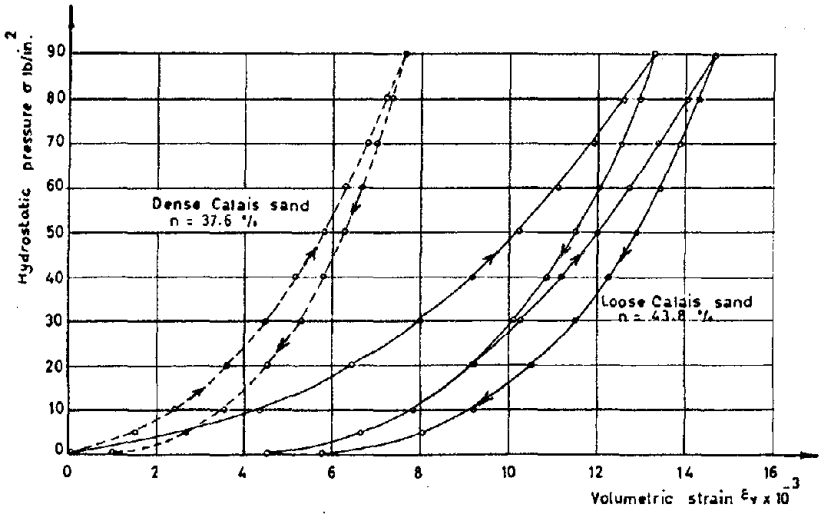

Figure 4.6 Relationship Between Applied Hydrostatic Pressure and Volumetric Strain for Cycles of Loading and Unloading on Specimens of Loose and Dense Sand (after El-Sohby and Andrawes, 1972)

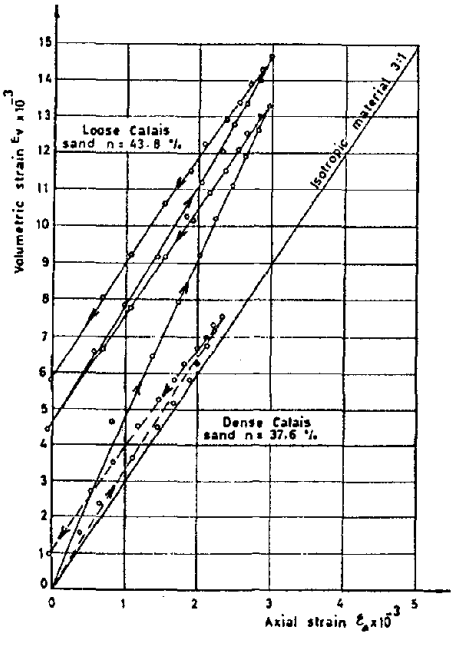

Figure 4.7 Relationship Between Volumetric Strain and Axial Strain for Cycles of Loading and Unloading for Specimens of Loose and Dense Sand (after El-Sohby and Andrawes, 1972)

due to a pore pressure increase in undrained tests performed on saturated samples. Comparative studies between the results from typical undrained cyclic simple shear tests and Pickering's modified equivalent drained cyclic simple shear test yielded a compliance reduction factor value, C_R, of about 25% in order to model the results expected from true, noncompliant test systems. That is, the results from cyclic simple shear tests performed in compliant systems should be reduced by about 25%. This study introduced the first attempt to move beyond simply understanding the problem of membrane compliance and to quantify the effect of membrane compliance on the results of undrained, cyclic load tests.

Frydman, Zeitlen and Alpan (1973)

Frydman, Zeitlen and Alpan noted that volume change measurements may be made on water entering or leaving either the sample or the triaxial chamber, provided that corrections are made for expansion of the chamber due to an increase in confining pressure. These investigators reviewed previous studies and concluded that particle size was the major factor influencing membrane penetration effects for a given change in cell pressure. Particle shape, size distribution and sample density were thought to have only minor effects. Hydrostatic compression tests were performed on specimens composed of three different sizes of uniformly graded glass beads. Both loose and dense packings of full specimens and hollow cylindrical specimens were tested. Test results for material A, for which D_{50}=0.18 mm, are shown in Figure 4.8. The hollow cylinder apparatus used in this study was based on a design by Proctor, shown in Figure 4.9, for which, instead of a metal cylindrical inclusion, a cylindrical cavity was formed

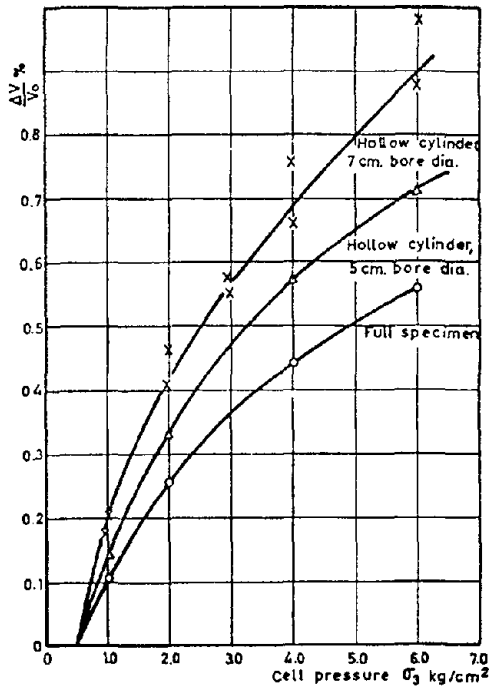

Figure 4.8 Measured Volumetric Strain vs. Chamber Pressure Under Hydrostatic Loading Conditions (after Frydman et al.,1973)

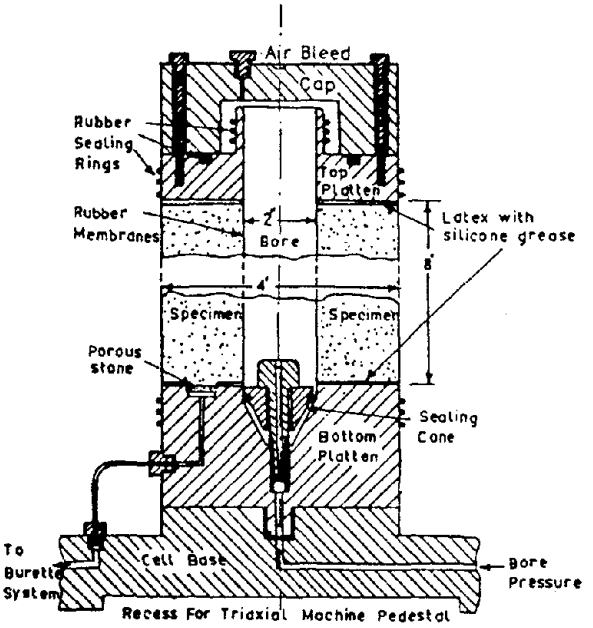

Figure 4.9 Cross Section of Hollow Cylinder Device Proposed by Proctor (after Frydman et al.,1973)

within the specimen, with a separate membrane, so that it could be pressurized to the same pressure as that in the cell.

Tests were performed on full samples (no hollow space) and samples with two different size hollow cylinders. The test results were plotted in terms of $\Delta V/V_o$ versus A_m/V_o where V_o = initial sample volume and A_m = membrane surface area. The resulting linear plot intercepted the ordinate at the true volumetric strain with a slope equal to the membrane penetration volume per unit area, as shown in Figure 4.10.

Plots of unit membrane penetration $\Delta V_m/A_m$ versus log chamber pressure showed that there was little difference in membrane penetration effects for cycles of either loading or unloading or for dense or loose packings. The greatest differences arose from the three different materials (based on the mean grain diameter) used in the study, as shown in Figure 4.11.

A numerical relationship between the slope of the membrane penetration curve, S, and the particle size diameter, d (notation used by Frydman et al. for D_{50}), was developed from the results of this study and the work of others. The resulting relationship, shown in Figure 4.12, is expressed by the equation:

$$S = 0.014 \log d - 0.001$$

This equation is applicable for standard thickness latex rubber membranes, about 0.03 centimeters thick, as used by Frydman et al.

This study established that particle diameter does indeed contribute more significantly to membrane penetration than does the state of the specimen. An equation is suggested for computing the slope of the unit membrane penetration curve for a range of grain

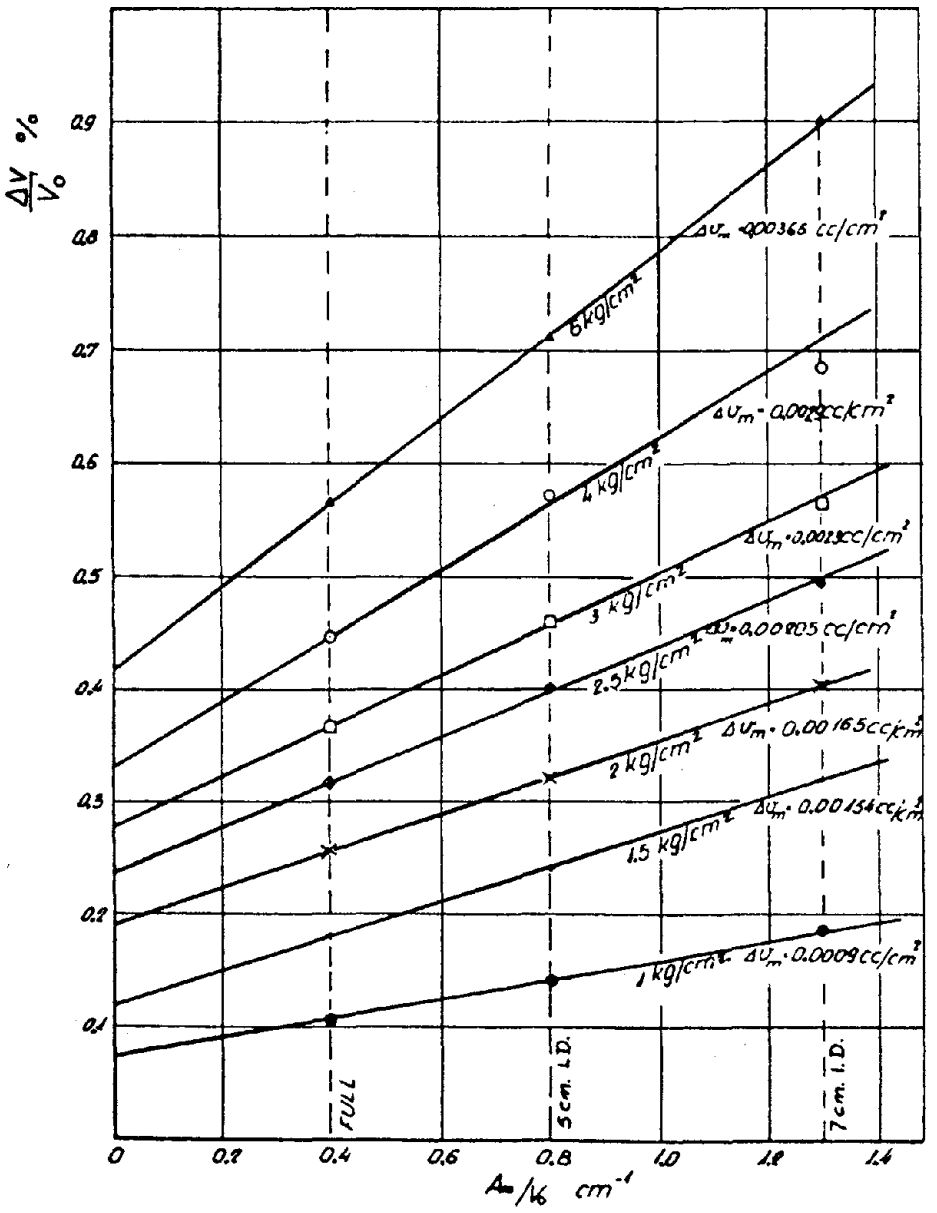

Figure 4.10 Measured Volumetric Strain vs. Normalized Membrane Area, A_m/V_o, Under Hydrostatic Loading Conditions (after Frydman et al., 1973)

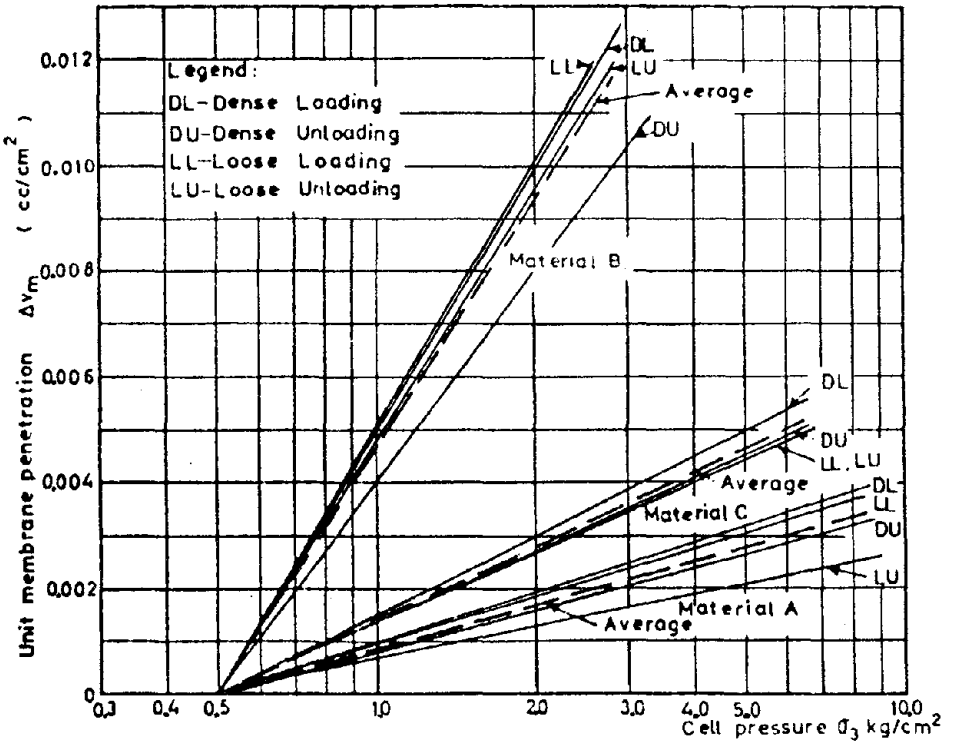

Figure 4.11 Unit Membrane Penetration vs. Chamber Pressure for Three Soils Tested in Both Loose and Dense States (after Frydman et al., 1973)

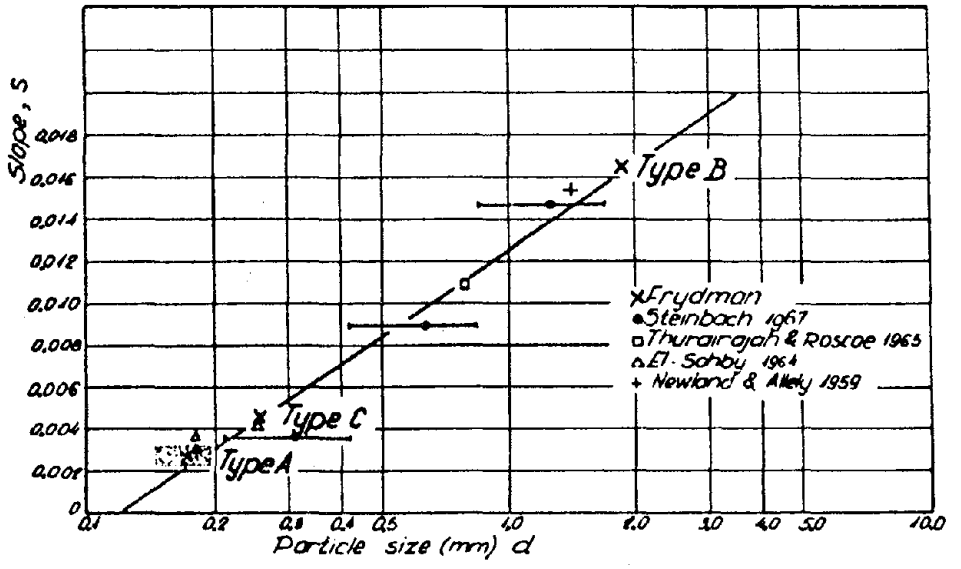

Figure 4.12 Relationship Between Particle Size and the Slope of the Membrane Penetration Curve (after Frydman et al., 1973)

sizes. However, it has not been determined whether this proposed relationship is applicable to specimens composed of gravel-size particles. Furthermore, the effect of the membrane penetration volume change on the results of triaxial compression tests still remains to be determined.

Raju and Sadasivan (1974)

Raju and Sadasivan identified four major factors controlling the effect of membrane penetration volume changes: (1) the change in effective confining pressure, (2) the specimen pore characteristics at the soil/membrane interface, (3) the dimensions and characteristics of the membrane and (4) the surface area of the soil/membrane interface. These investigators suggested two areas in which the dummy rod method proposed by Roscoe et al. could be improved. First, the use of a flexible, annular top cap was proposed in order to induce a more uniform, isotropic stress state in the sample. Second, a nonlinear relationship was proposed to exist between the total volume change and the rod diameter as opposed to the linear relationship between these parameters proposed by Roscoe et al. Raju and Sadasivan noted that the volume compressibility of the soil is independent of the dummy rod diameter and used this information to illustrate the nonlinear relationship between total volume change, ΔV_t, and dummy rod diameter, d, so that:

$$\begin{aligned}\Delta V_t &= \Delta V_m + \Delta V_s \\ &= \Delta V_m + \varepsilon_{vs} \times V_o \\ &= \Delta V_m + \varepsilon_{vs}[(\pi D^2 h/4) - (\pi d^2 h/4)] \\ &= \Delta V_m + \varepsilon_{vs}(D^2 - d^2) \times \pi h/4\end{aligned}$$

therefore, $\underline{\Delta V_t = A - B \times d^2}$.

Where: $A = \Delta V_m + \varepsilon_{vs}(\pi D^2 h/4)$,

$B = \varepsilon_{vs}(\pi h/4)$,

m = membrane,

s = soil skeleton,

and D = sample diameter.

A linear relationship was found to exist, however, between the total measured volume change and the volume of the soil specimen (or rod volume) as shown in Figure 4.13. Note the break in the curves that occurs for specimens with rigid top caps between specimens with and without dummy rod inclusions. There is no corresponding break in the data curves generated for specimens with flexible top caps indicating that the rigid top caps interfere with isotropic compression of the specimen in tests with dummy rod inclusions. Comparison of volume change measurements for samples having full rigid and flexible annular top caps as shown in Figure 4.14, indicates that rigid caps yielded lower volume change measurements and thus result in membrane penetration volume changes that were as much as 30% higher than those for tests in which flexible top caps were used. Thus, using flexible top caps may result in a more accurate assessment of the membrane penetration volume changes which occur in isotropic compression tests when employing the dummy rod method.

Wong, Seed and Chan (1975)

Wong, Seed and Chan performed cyclic loading tests on 2.8 inch and 12 inch diameter samples of Monterey Sand to investigate the effect of sample size on cyclic stress ratios causing soil liquefaction. Figure 4.15 shows that the cyclic deviator stresses required to cause initial liquefaction in any given number of cycles is

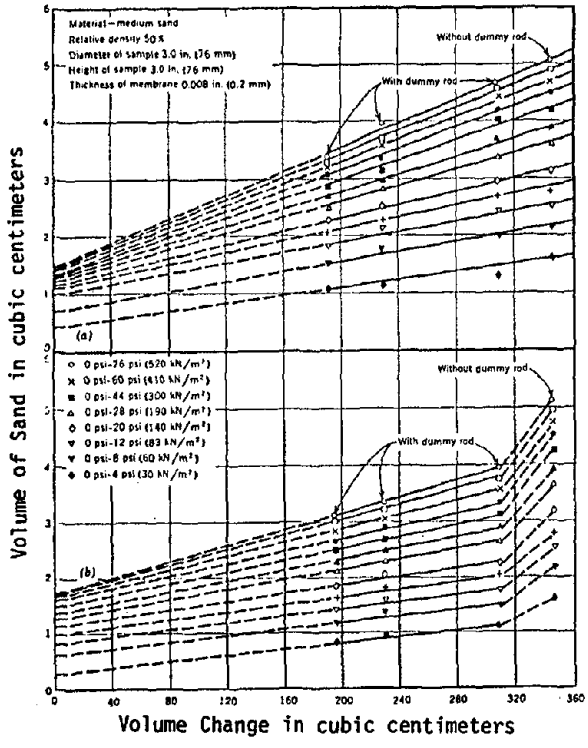

Figure 4.13 Total Volume Changes vs. Volume of the Sand Specimens Subjected to Various Confining Pressures for Flexible and Rigid Top Caps (after Raju and Sadasivan, 1974)

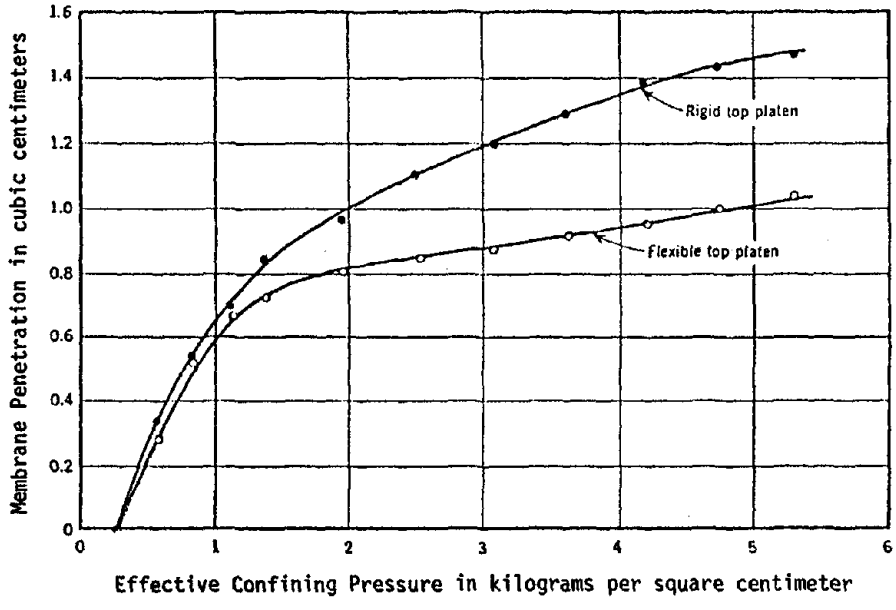

Figure 4.14 Comparison of Membrane Penetration Volume Change for Flexible and Rigid Top Caps (after Raju and Sadasivan, 1974)

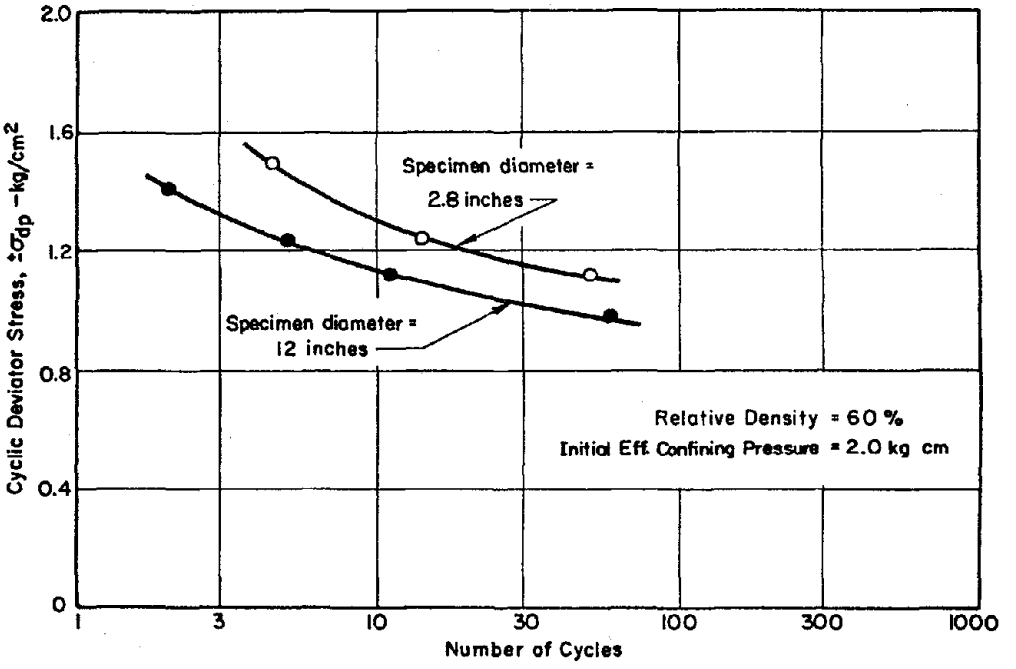

Figure 4.15 Cyclic Deviator Stress Causing Liquefaction in 2.8" and 12" Diameter Specimens of Sand (after Wong et al., 1975)

about 10% lower for the 12 inch diameter samples than for the 2.8 inch diameter samples. This difference was attributed largely to the decreasing effect of membrane penetration as sample size increases. Pore pressures built up faster in specimens with reduced membrane compliance and thus, a condition of initial liquefaction ($r_u \simeq 100\%$) was reached in fewer cycles for a given applied cyclic stress ratio. In 12 inch diameter cyclic tests performed on a well-graded gravelly soil from the Oroville Dam, these investigators elected to use a thick membrane in order to minimize the effects of membrane compliance. It may be recalled that Newland and Allely (1959) originally suggested the use of (1) thicker membranes and (2) larger specimens to reduce the effects of membrane penetration and compliance. However, Roscoe et al. (1963) had concluded from their study that membrane thickness was not a significant factor in controlling membrane penetration volume changes. Thus, the potential effects of membrane thickness on membrane penetration has not been clearly established .

DeAlba, Chan and Seed (1975)

DeAlba, Chan and Seed developed a membrane compliance correction based on an analytical model of soil behavior proposed by Martin et al. (1975). This model is based on the relationship between the volume change of dry sand subjected to cyclic shear stress and the increase in pore pressure of an equivalent saturated, undrained sand under the same stress conditions. It involves the use of relationships between shear modulus, G, and sample volumetric strain decrement, ε_{vd}, and shear strain, γ, developed from experiments performed on specimens of equivalent dry or drained soil. The liquefaction model operates as shown in Figure 4.16, by performing the following steps in each cycle:

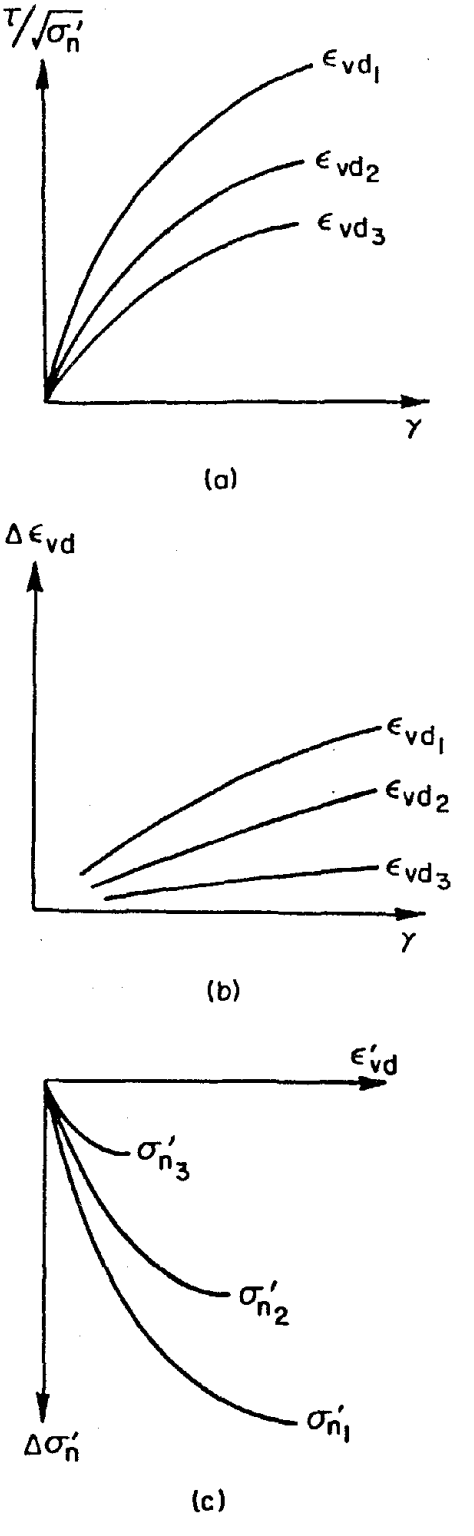

Figure 4.16 Basic Input Data for Liquefaction Model (after DeAlba et al., 1975)

(1) For a known applied shear stress, τ, normal effective stress at the end of the previous cycle, σ'_{no}, and total accumulated volume change up to the previous cycle, ε_{vd}, the value of shear strain, γ, for the cycle is determined as shown in Figure 4.16(a).

(2) For the value of γ, obtained from step (1), and for the known value of ε_{vd}, the incremental volume change for that cycle, $\Delta\varepsilon_{vd}$, is obtained from Figure 4.16(b) and added to the previous value of ε_{vd} to obtain ε'_{vd}.

(3) For the value of ε'_{vd} obtained from step (2), the value of stress release due to unloading, $\Delta U = \Delta\sigma_n'$, is obtained from Figure 4.16(c) and a new value of normal effective stress is calculated:

$$\sigma'_{nf} = \sigma'_{no} - \Delta\sigma'_n.$$

This value is then used in step (1) of the next cycle. Step (3) is where additional volume change due to compliance may be introduced, using modified rebound curves that include both material rebound and system compliance (after DeAlba et al., 1975).

Pore pressure increases, ΔU, in a saturated, undrained system may be determined based on the volume decrease of an equivalent dry soil, $\Delta\varepsilon_{vd}$, subjected to the same stress conditions such that:

$$\Delta U = \Delta\varepsilon_{vd}/[1/k_r + 1/k_m]$$

where, k_r represents the rebound modulus of the material for the appropriate stress level and boundary conditions,

and k_m is the gradient of volume change due to membrane penetration for the testing system.

This procedure was first used to determine how accurately the model predicted the results of undrained, compliant shake table tests performed by DeAlba. Input parameters were modified until reasonable agreement with the actual test data was obtained, as shown in Figure

4.17. A second program run was made to simulate the results of an ideal, noncompliant system. The ratio of τ/σ_o' computed for the ideal system was compared to the value determined from the compliant system, at the appropriate number of cycles, to determine the value of the stress ratio correction factor which would account for the effects of membrane compliance in the actual laboratory test results. The correction factors obtained are summarized in Figure 4.18. The result of this analysis for sand yielded a stress reduction factor ranging from 0.7 to 0.8 in the range of 30 stress cycles. This was considered to be a very good approximation of the results that would be obtained in an ideal, noncompliant testing system.

Volumetric strain due to membrane penetration was determined by performing rebound tests on large-scale shake table specimens of sand which were 0.125 inches and 4.0 inches in height. The results of such tests are shown in Figure 4.19. It may be noted from this figure that there is no substantial effect of a change in specimen density on the volume change measurements. It was assumed that the change in height of the specimens would not affect the value of volumetric strain due to specimen rebound. Extrapolation to zero specimen height, and thus zero membrane penetration volume change, indicates the value of volumetric strain due to membrane penetration.

This study provided a valuable assessment of a correction factor which may be applied to the results of cyclic triaxial tests to account for the effects of membrane compliance. The magnitude of the correction factor proposed in this study is similar to the value proposed by Pickering (1973). However, the ratio of the sample surface area covered by the membrane to the specimen volume is significantly

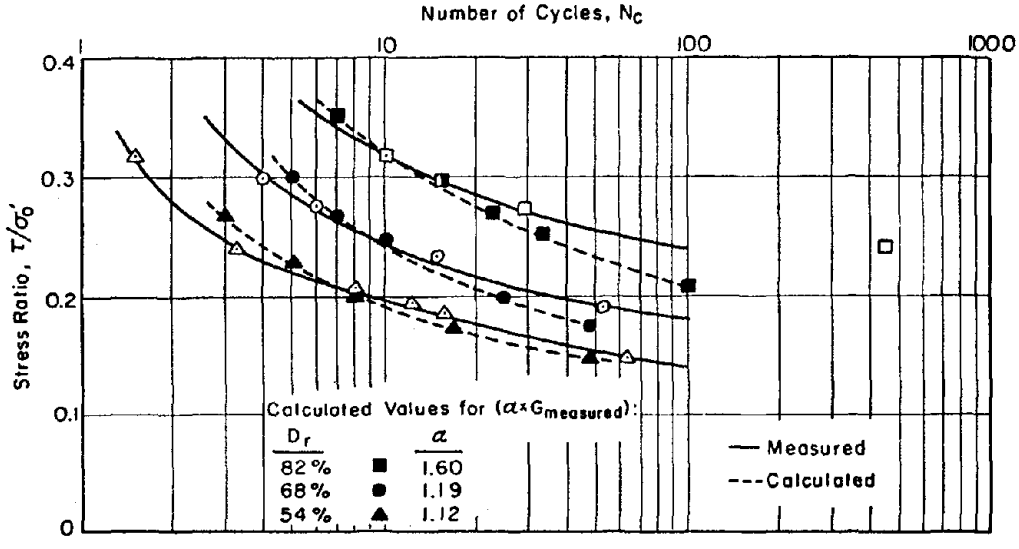

Figure 4.17 Calculated and Measured Values of Stress Ratio vs. Number of Cycles to Cause Liquefaction (after DeAlba et al., 1975)

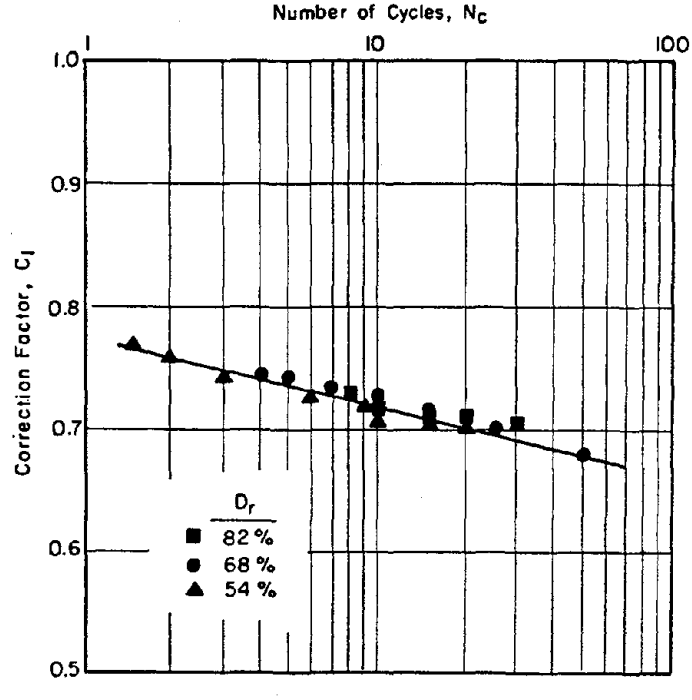

Figure 4.18 Correction Factors Generated from Martin's Soil Behavior Model (after DeAlba et al., 1975)

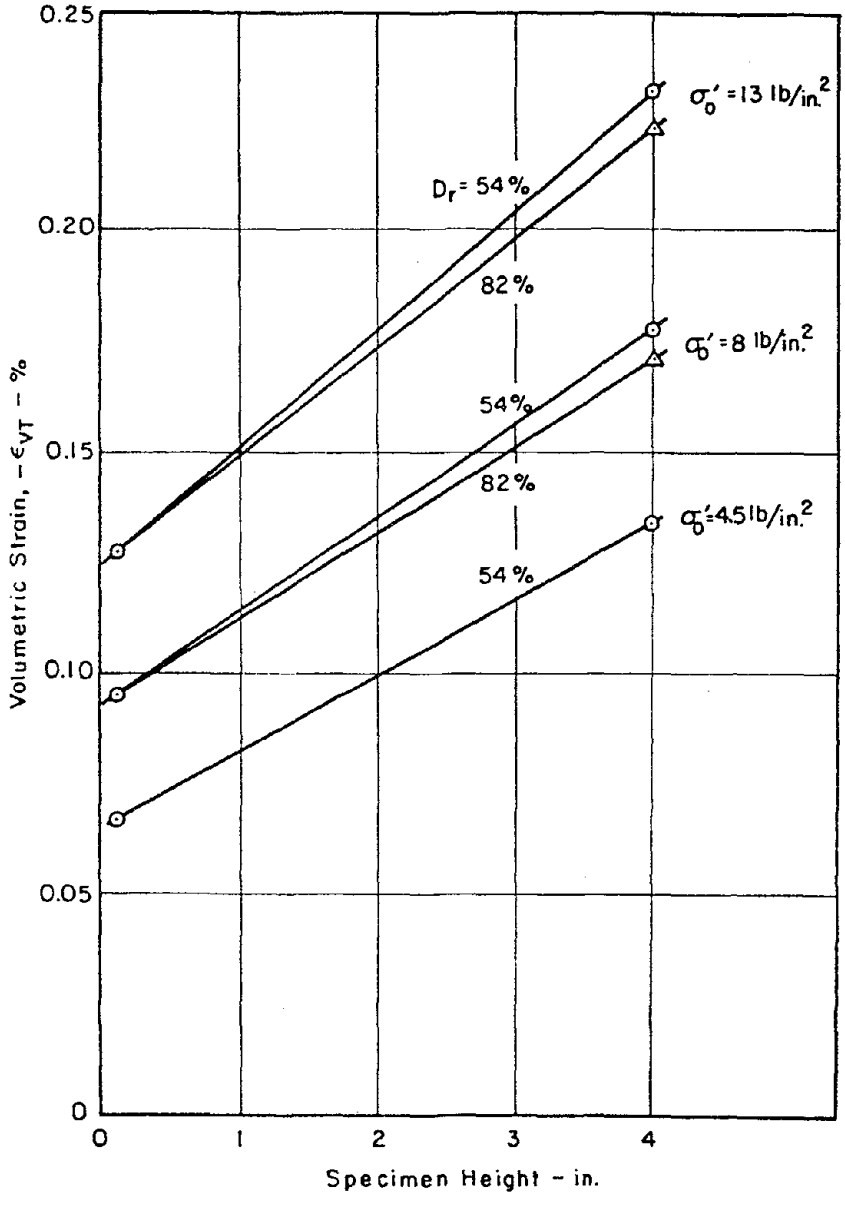

Figure 4.19 Volumetric Strain vs. Specimen Height (after DeAlba et al., 1975)

smaller in the shake table tests of this study than in the simple shear tests performed by Pickering. The area to volume ratio provides some indication of the possible severity of membrane compliance effects. It might be expected that the stress ratio correction factor would be lower for specimens with higher surface area to volume ratios.

The correction factors shown in Figure 4.18 were developed for Monterey No. 0 Sand. It might be expected that the correction factor would be much more significant for coarser diameter particles such as gravels. Further study in this area is clearly necessary to determine the true, noncompliant cyclic loading resistance of gravelly soils.

Lade and Hernandez (1977)

Lade and Hernandez identified average particle size, soil void ratio, change in effective pressure and surface area covered by the membrane as the most important factors influencing the magnitude of membrane penetration. Factors considered to have negligible effect were soil gradation, particle shape and membrane thickness (up to 0.6 mm) at low to medium confining pressures. They further stated that the effects of membrane penetration were negligible for soils with mean particle diameters less than 0.1 to 0.2 mm. The effect of membrane penetration on volume change was illustrated graphically in Figure 4.20, and the effect of sample size on the cyclic loading resistance of specimens with 1.4 inch and 2.8 inch diameters is shown in Figure 4.21.

These investigators also identified the critical confining pressure as a factor playing a major role in membrane penetration effects. They noted that volume changes during shear are more significant at confining pressures far removed from the critical confining pressure, and that for such conditions membrane penetration

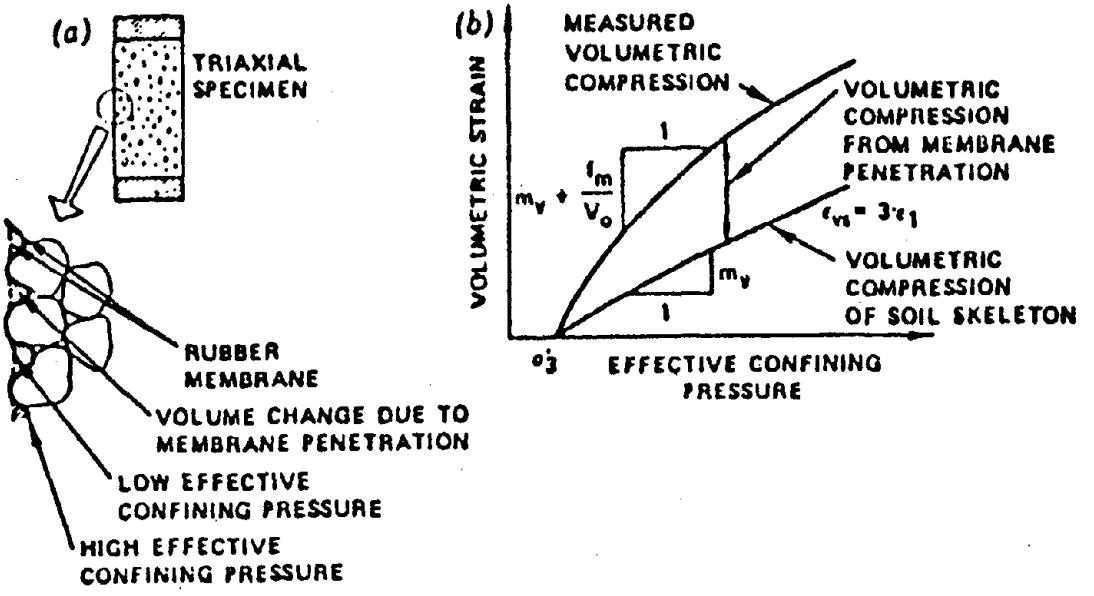

Figure 4.20 (a) Membrane Penetration in a Triaxial Specimen (b) Determination of Membrane Flexibility from the Results of Isotropic Compression Tests (after Lade and Hernandez, 1977)

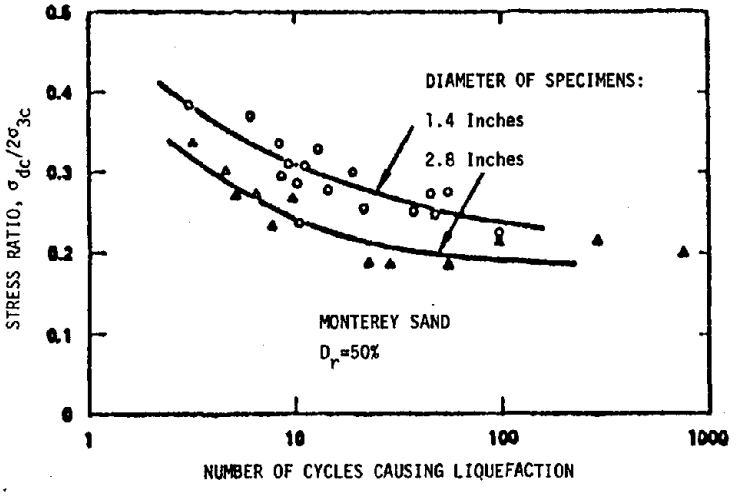

Figure 4.21 The Effect of Specimen Diameter on the Cyclic Stress Ratio Causing Liquefaction (after Lade and Hernandez, 1977)

effects are most problematic. Soils tested at an effective confining pressure greater than critical would be contractive while undergoing shear strain. The subsequent pore pressure buildup would be reduced by membrane penetration effects and the sample shear strength would appear higher than it truly is. However, for samples tested at confining pressures lower than the critical confining pressure, the samples would be dilative and the opposite effect would be observed. Pore pressure decreases would be inhibited by membrane penetration and the sample shear strength would appear lower than its true undrained value

In this study, undrained triaxial compression tests were performed on 2.8 inch diameter specimens of uniformly graded sand. In order to reduce membrane penetration effects, 1 inch x 1 inch x 0.0006 inch thick brass plates were placed over the surface of the membrane-covered sample before a second membrane was applied. These plates overlapped slightly in the vertical direction but gaps were left in the horizontal direction to reduce plate interference as the specimens strained axially. This arrangement was not intended to reduce membrane penetration completely but it did reduce membrane flexibility, f_m, to about 1/3 of that for regular membranes. Membrane flexibility was defined as the volume change of the specimen due to membrane penetration per unit change in effective confining pressure. Pore pressures developed in tests with plates were more than double those for tests without plates. However, although membrane compliance effects are reduced with this arrangement, axial loads would have to be corrected for the load carried by the plates. Thus, this method is not a completely viable alternative for performing true, noncompliant, undrained tests.

Kiekbusch and Schuppener (1977)

Kiekbusch and Schuppener concluded after reviewing the findings of previous investigators, that membrane penetration was controlled mainly by particle size. They performed one-dimensional consolidation tests on six different gradations of fine sand, silt and clay, most with mean grain diameters less than 0.15 mm. The sides and bottom of the testing apparatus were sealed except for one drainage line to measure volume change. The top of the sample was covered with a flexible membrane, the inside surface of which was first coated with a thin layer of latex rubber. The liquid rubber penetrated the surficial voids, as shown in Figure 4.22, and was allowed to harden under a small confining pressure before testing began. Surface settlements under consolidation pressures were measured using a dial gage and a small tripod with three legs resting on the surface of the specimen to obtain an average height change. The difference in volume change between that calculated from the axial deformation and that recorded from the volume change burette was attributed to membrane penetration. Control tests were set up in a similar manner except that no liquid rubber coating was applied to the membrane. Membrane penetration was reduced significantly for all materials tested with rubber coated membranes. For a fine sand, membrane penetration with a rubber coated thin membrane was only about 15% of the corresponding value found for untreated membranes.

Three different fine to medium sands were tested in the undrained triaxial test, both with and without rubber coated membranes. Pore pressures measured for samples with treated membranes were up to twice those for samples with conventional membranes. Significant differences

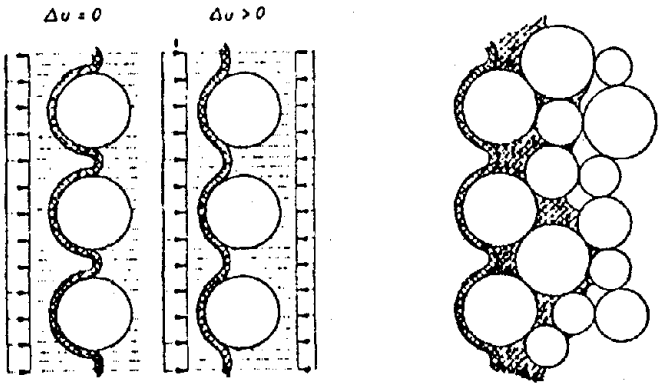

Figure 4.22 (a) Membrane Penetration Due to a Change in Pore Pressure, (b) Liquid Rubber Penetrating Surficial Voids (after Kiekbusch and Schuppener, 1977)

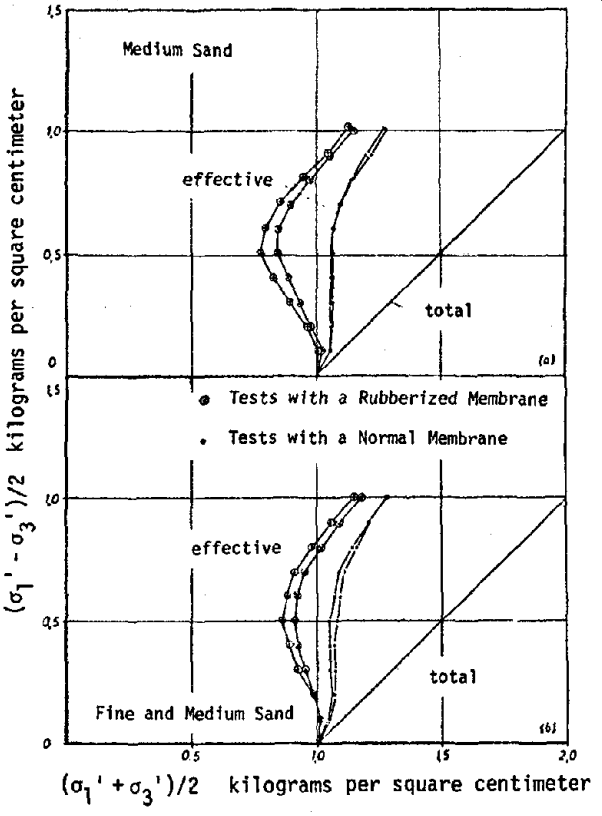

Figure 4.23 Differences in Stress Paths Determined for Specimens with and without Rubber Coated Membranes - (a) Fine Sand, (b) Fine and Medium Sand (after Kiekbusch and Schuppener, 1977)

in stress path were noted and Figure 4.23 shows that tests with normal membranes led to significant overestimates of the undrained shear strength. This investigation also confirmed that a relationship exists between mean grain diameter and membrane penetration as shown in Figure 4.24. However, the investigators concluded that no simple correction was applicable and they suggested only that the influence of membrane penetration could be significantly reduced by using rubber coated membranes in triaxial tests. Rubber coating was shown to work better with thin membranes rather than thick.

The method described previously is an effective alternative for significantly reducing the effects of membrane compliance subject to two constraints: (1) The method is only appropriate for specimens which are reconstituted inside the confining membrane; undisturbed specimens would need to be self supporting (i.e., have some cohesion) to allow a rubber coated membrane to be installed onto the specimen; (2) The method is probably not applicable to gravelly soil specimens since relatively thick rubber coatings would be required. The required rubber coating would probably be about as thick as the mean grain diameter of the soil in order to fill the peripheral voids. This may be over 1 inch thick for some 12 inch diameter specimens of gravelly soil. Construction of the specimen may prove to be difficult if not impossible without disturbing the rubber coating. Also, a large axial load correction would be involved for thick coatings of rubber.

Martin, Finn and Seed (1978)

Martin, Finn and Seed studied system compliance in the triaxial and simple shear tests. They concluded that: (1) Membrane penetration was the main contributor to system compliance in the triaxial test,

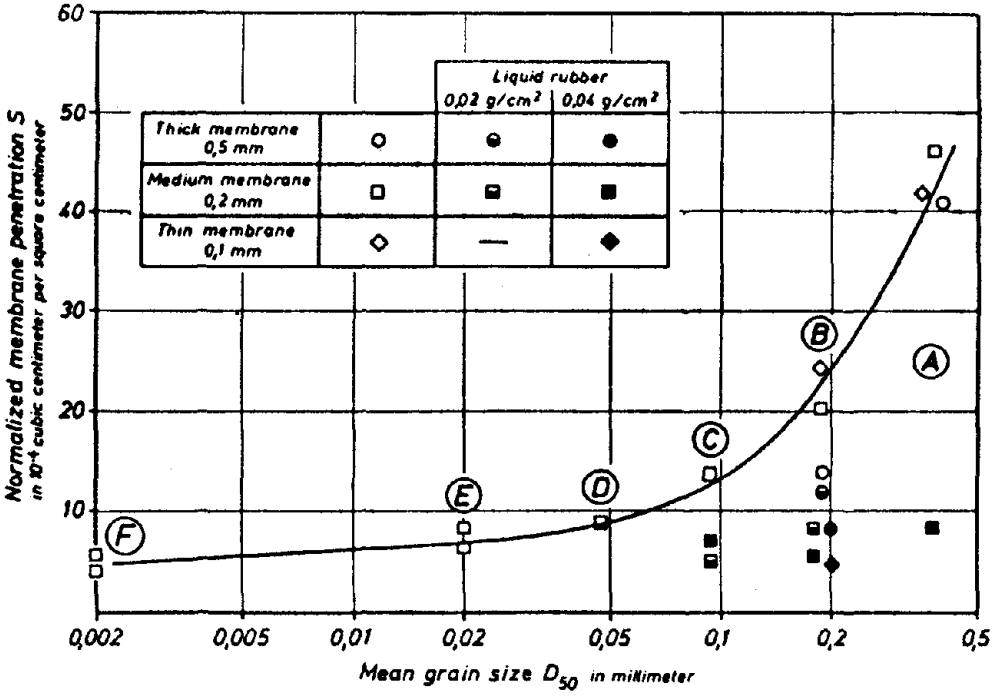

Figure 4.24 Relationship Between Membrane Penetration and Mean Grain Diameter (after Kiekbusch and Schuppener, 1977)

although a small amount was attributable to compliance in lines, valves and fittings; (2) Investigations performed by others have indicated that membrane penetration is primarily a function of particle size as characterized by the mean grain diameter, and is reasonably independent of sample density; and (3) Membrane penetration tests performed on specimens of Ottawa Sand (D_{50}=0.4 mm) indicated that membrane penetration characteristics are essentially independent of membrane thickness in the range of 0.51 to 0.051 mm.

Martin et al. also developed a theoretical stress ratio correction for cyclic simple shear tests and applied this correction to cyclic stress ratios for 1.4 inch diameter triaxial test specimens. Using data presented in Figure 4.25 for medium density sands and data published by El-Sohby (1969), the membrane compliance ratio, C_{RM} (the ratio of the average slope of the rebound curve of the sand skeleton to that of the membrane penetration volume change curve), was computed and the results are shown plotted versus D_{50} in Figure 4.26 for 1.4 inch diameter specimens requiring 30 stress cycles to develop initial liquefaction. Curves for 2.8 inch and 12 inch diameter specimens, shown in Figure 4.27, were constructed by reducing this error in proportion to the inverse of sample diameter.

Although the curves shown in Figure 4.27 were developed for only a small range of particle sizes, it was assumed that they could be extrapolated linearly into the gravel size range. The significance of these corrections was then assessed for actual cyclic triaxial test data as shown in Figure 4.28. Test data for 2.8 inch and 12 inch diameter specimens showed essentially the same results after correction for membrane compliance effects, suggesting that differences in initial

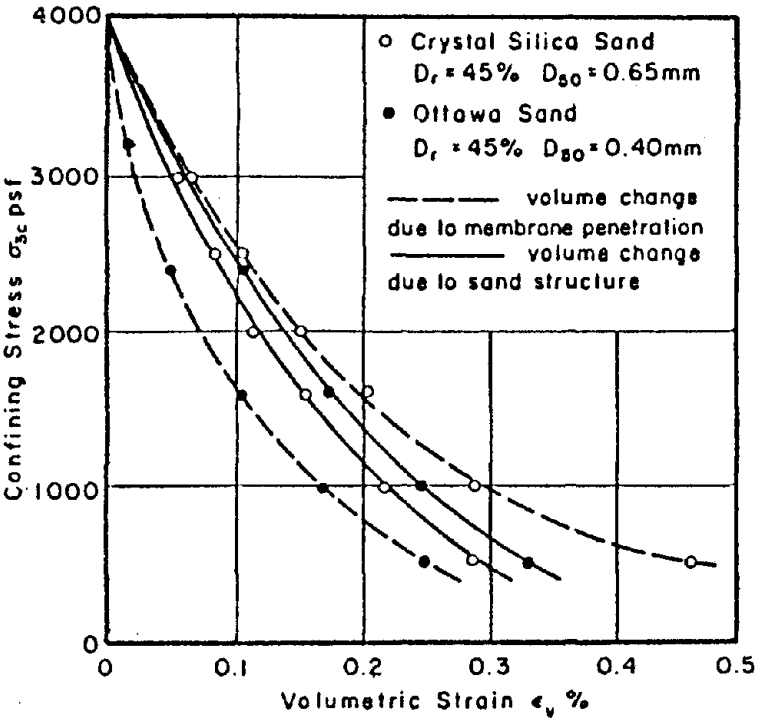

Figure 4.25 Relative Volume Changes Due to Elastic Rebound and Membrane Penetration for 1.4" Diameter Triaxial Test Specimens (afterMartin et al., 1978)

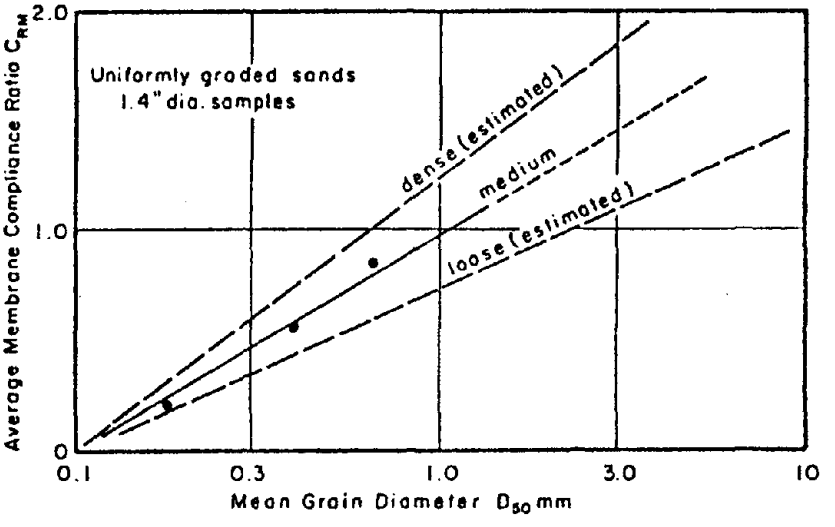

Figure 4.26 Relationship Between Membrane Compliance Ratio and Mean Grain Diameter (after Martin et al., 1978)

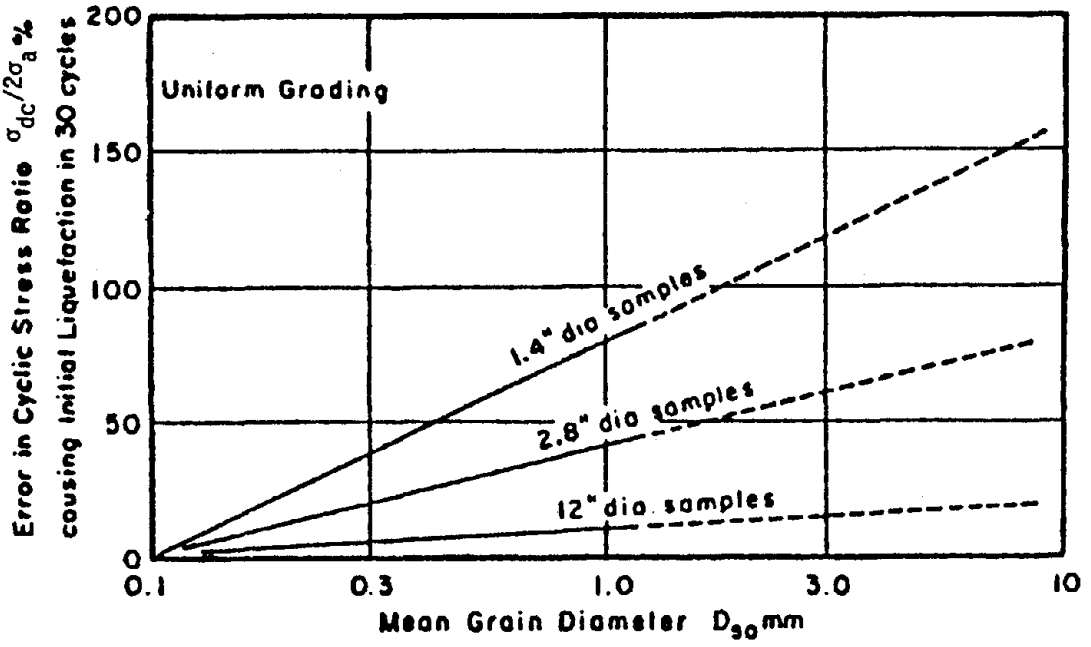

Figure 4.27 Cyclic Stress Ratio Correction vs. Mean Grain Diameter (after Martin et al., 1978)

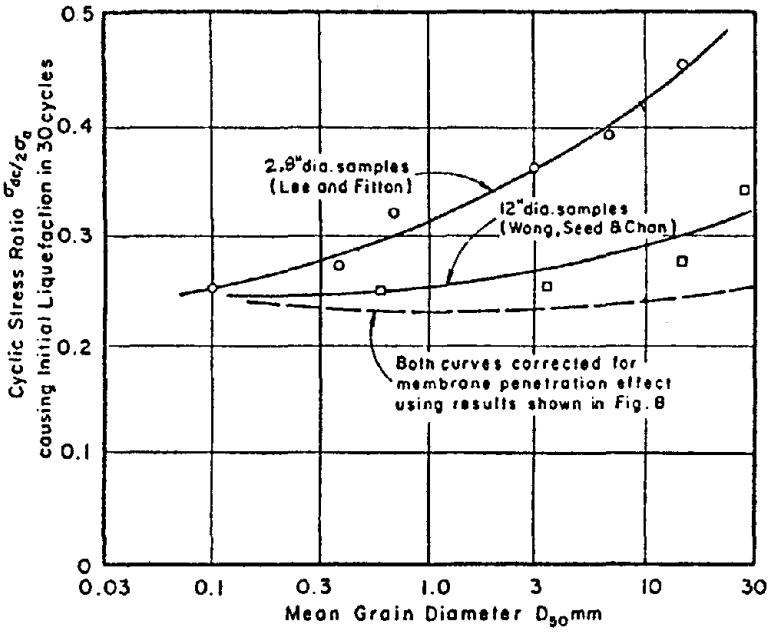

Figure 4.28 Actual and Corrected Test Results Using Figure 4.21 (after Martin et al., 1978)

liquefaction resistance for different sample sizes are primarily due to increased membrane penetration effects with decreasing sample diameter. It may also be noted that this curve suggests that membrane penetration is insignificant for values of D_{50} less than 0.1 mm. This correction was developed for uniform soils and may not apply to well-graded soils because of the less severe effects of membrane penetration in the latter due to a reduction in the size of peripheral voids. This has been illustrated experimentally by both Lee and Fitton (1968) and Wong et al. (1975).

Although no experiments were performed on gravelly soils in this study, the authors suggest that the relationships developed between C_{RM} and D_{50} may be extrapolated to coarser grained soils. Also, it may be noted from Figure 4.26 that the effects of membrane compliance are more pronounced in undrained cyclic tests performed on dense soils than on loose soils. This study was the first to call attention to the fact that although membrane penetration volume changes are similar for both loose and dense soils, the effects of membrane compliance on the results of cyclic tests is more significant for dense soils than for loose soils.

Chan (1978)

Chan performed isotropic compression tests on 36 inch diameter samples of Monterey No. 20 sand to assess the magnitude of membrane penetration volume changes. Total volume changes were measured by observing water column height changes in a burette, soil skeleton volumetric strains were computed from measured height and radius changes, and radial deformations were measured by using a system of several "girth gages" around the circumference of the sample which

utilized a horizontal LVDT to monitor changes in circumference. The roller wheels on the girth gage were of sufficient size that they would not be influenced by the surficial irregularities of the membrane caused by membrane penetration and would record only skeletal volume changes. This method of monitoring radial deformations appears to be a promising means to determine the true value of skeletal volumetric strains which are unaffected by membrane penetration.

Banerjee (1979)

Banerjee studied the effects of membrane penetration on the undrained cyclic triaxial strengths of gravels from Oroville Dam. He performed hydrostatic consolidation tests on 12 inch diameter specimens of gravel with 2 inch maximum particle size. These tests indicated that deformations were isotropic for values of effective confining pressure that were less than critical, however, for values greater than the critical confining pressure, it was found that;

$$\varepsilon_v \simeq 3.3\,\varepsilon_a.$$

Since the material was shown to behave somewhat anisotropically, it was considered desirable to measure both axial and radial deformations to determine volumetric strains. Radial deformations were measured by using a set of four girth gages with nine sets of double contact point rollers each, similar to those used by Chan (1978). Again, it was assumed that the rollers would not be affected by the indentations caused by the membrane penetration and that they would measure only skeletal volume changes. After consolidation and back pressure saturation, the back pressure was raised in order to reduce the effective confining pressure and the volume of water flowing into the sample was measured. At the same time, the height and girth gage

LVDT's were used to measure total changes in the volume of the specimen. Results from typical tests performed on specimens of Oroville Gravel and Monterey No. 0 Sand are shown in Figure 4.29. The volumetric strain due to membrane penetration, ε_{vm}, was computed as the difference between (1) the total volume change, ε_{vt}, measured from the burette and (2) the skeletal volume change, ε_{vs}, such that;

$$\varepsilon_{vm} = \varepsilon_{vt} - \varepsilon_{vs}.$$

The membrane compliance ratio, C_{RM}, defined by Martin et al. (the ratio of the average slope of the skeletal rebound curve to the average slope of the membrane penetration volume change curve) was determined for the material in this study by experimental testing, as shown in Figure 4.30, and from the chart developed by Frydman et al. shown in Figure 4.31. The error in cyclic stress ratio caused by membrane compliance effects, C_{RM}, determined in this study, is compared to results presented by Frydman et al. and by Martin et al. in Figure 4.32. The value of the stress ratio corrections for dense Oroville gravel in 12 inch diameter triaxial tests were judged to be about 10% (i.e. cyclic stress ratio obtained from lab testing should be reduced by about 10% to accurately predict actual initial liquefaction at 30 cycles) using the method proposed by Martin et al. (1978).

Similar tests were performed on a modeled gradation of gravel from the Oroville Dam in 2.8 inch diameter samples. Values of the cyclic stress ratio corrections, C_{RM}, for these samples were determined to be about 50%, indicating that the effects of membrane penetration are significantly greater for specimens of smaller diameter.

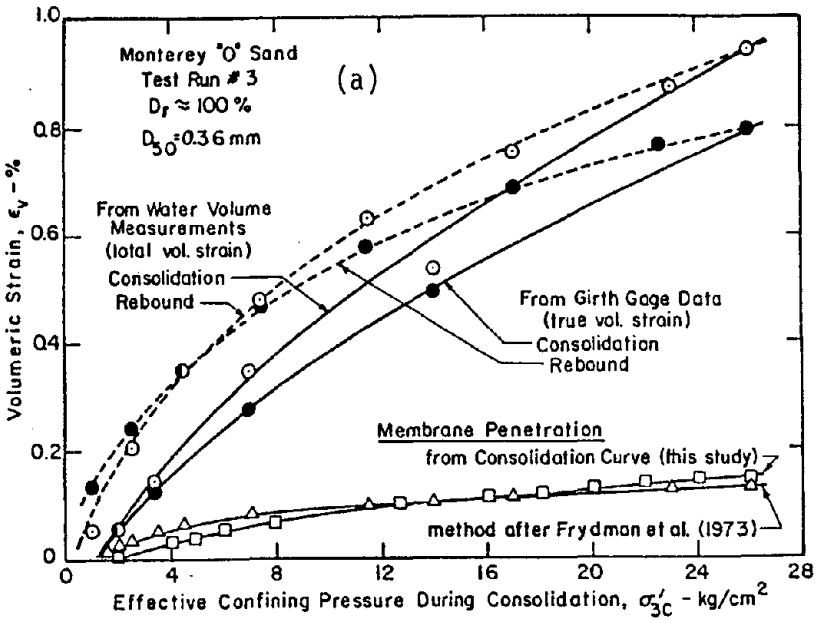

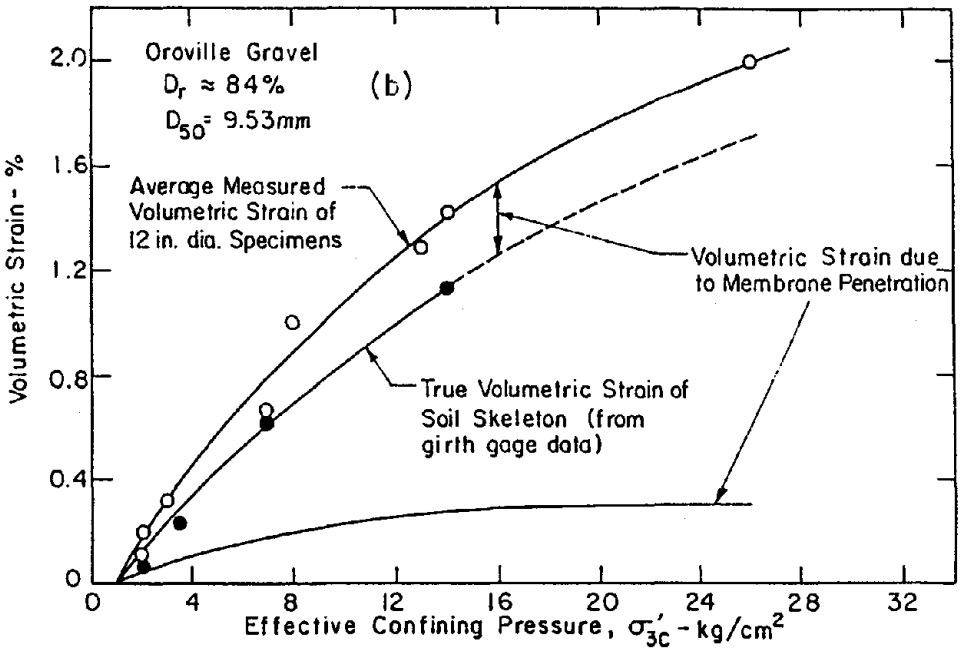

Figure 4.29 Total and Skeletal Volume Change Measurements from a Burette and Girth Gage Data - (a) Monterey No. 0 Sand (b) Oroville Gravel (after Banerjee, 1979)

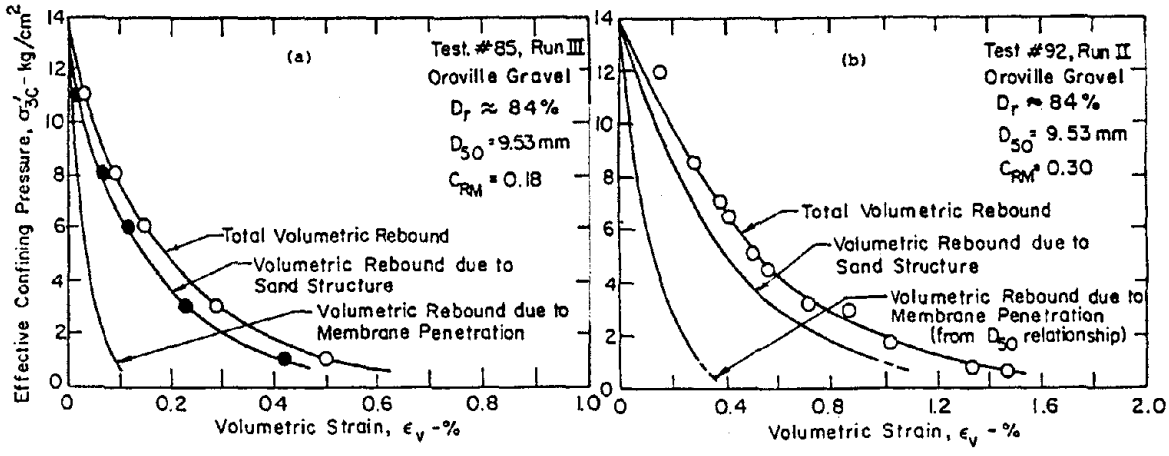

Figure 4.30 Experimental Determinations of the Membrane Compliance Ratio, C_{RM} (after Banerjee, 1979)

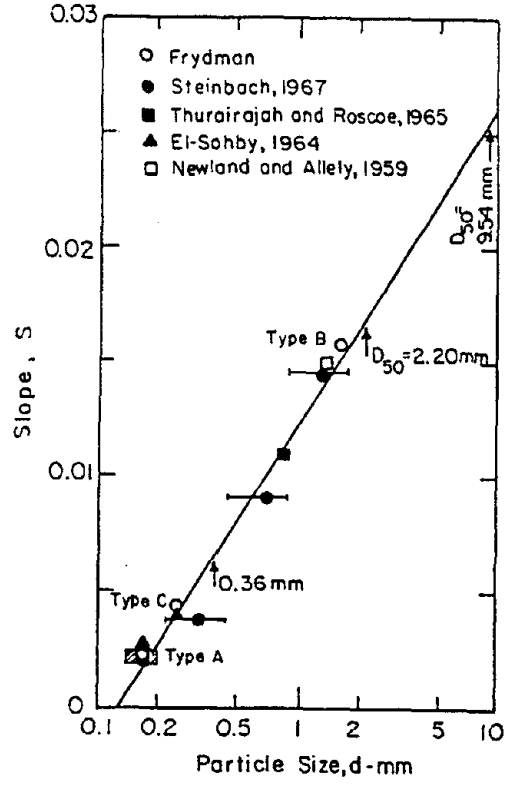

Figure 4.31 Slope of the Membrane Penetration Curves vs. Particle Size (after Banerjee, 1979)

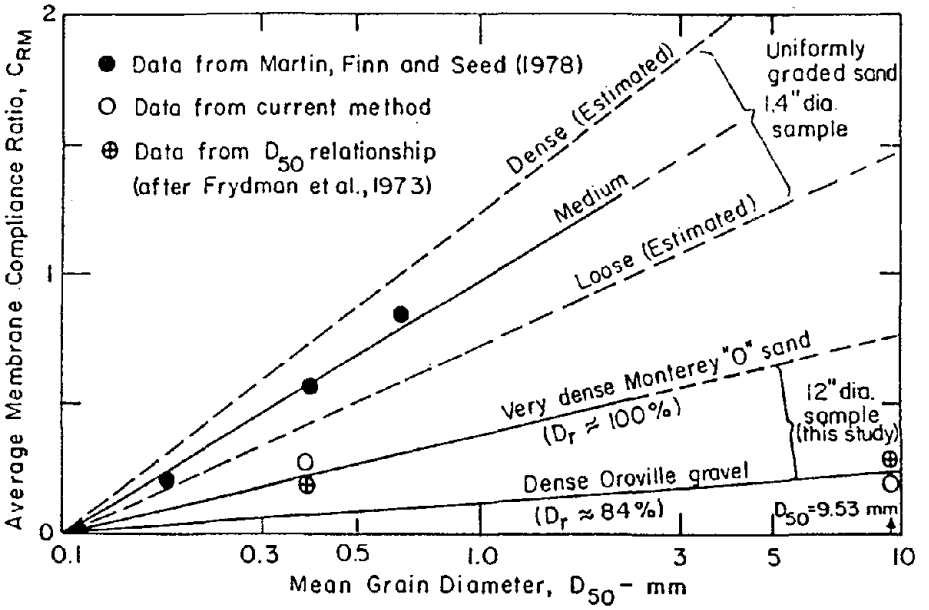

Figure 4.32 Membrane Compliance Correction Ratio, C_{RM}, Determined From This Study Compared to Data from Martin et al. (after Banerjee, 1979)

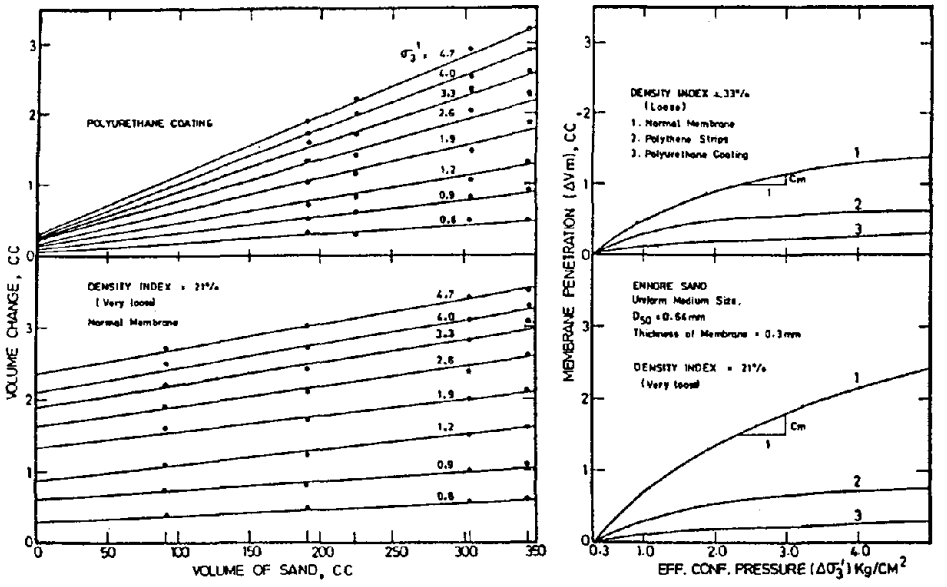

Figure 4.33 Determinations of Volume Changes Due to Membrane Penetration for Various Membrane Systems (after Raju and Venkataramana, 1980)

Raju and Venkataramana (1980)

Raju and Venkataramana investigated membrane penetration effects in the undrained triaxial test by performing isotropic compression and rebound tests on specimens composed of a uniform sand with D_{50}=0.63 mm. Three different systems of confining membranes were used in this study. In the first, greased polythene strips were attached to the inside of the rubber membrane before the sand sample was built by "raining" the sand into the sample mold. In the second, a thin film of polyurethane was spread onto the inside of the membrane after it had been installed on the sample mold and the sand was again rained into the forming mold. Both of these membrane systems, along with samples confined with ordinary membranes, were used to assess membrane penetration effects by using the modified dummy rod method described by Raju and Sadasivan (1974). After testing, the polythene strips were found to be indented by angular sand particles indicating that significant frictional forces developed between the strips and the sand particles, while the polyethylene-coated membranes visually appeared to perform well. Results from isotropic compression tests performed on very loose (D_r=21%) and loose (D_r=33%) sand specimens using the three membrane systems are shown in Figure 4.33. Note that these results indicate that there is a significant difference in the membrane penetration volume changes measured for specimens of 21% or 33% relative density when ordinary membranes are used. This finding is not in agreement with the results of previous studies which indicate that there is little difference in membrane penetration volume changes for specimens of different densities. For the sand specimens of both 21% and 33% relative density tested in this study, membrane penetration volume

changes measured using coated membrane systems were reduced to 15% to 25% of the values measured using ordinary membranes. Again, this approach seems satisfactory for fine grained soils but may not be satisfactory for gravelly soils.

Compensated undrained tests were also performed in this study in order to assess the magnitude of the pore pressures that would develop if the effects of membrane penetration could be eliminated. Volume changes due to membrane penetration for a given change in effective stress can be determined from isotropic consolidation curves such as those shown in Figure 4.33. Compensation is performed by injecting a volume of water, equivalent to the membrane penetration volume change, into the sample to correct the pore pressures for the membrane penetration effects. This volume correction further changes the effective confining pressure and thus the amount of membrane penetration volume which must, in turn, be corrected further. The process is repeated several times until a constant value of pore pressure is obtained conforming to a no volume change condition. Undrained axial loading triaxial tests were performed on specimens of loose sand and compared to the results of equivalent, compensated load tests. Pore pressures generated in compensated tests were highest, since the effect of membrane penetration was eliminated, and undrained shear strengths were correspondingly lower. This method of compensating for the effects of membrane compliance is effective but requires that the test be stopped for several minutes while the compensation is completed. This presents serious drawbacks in using the method for compliance compensation in the cyclic triaxial test as several adjustments would be required during each of the load and

unload phases of each cycle. Thus the method does not appear to be viable for cyclic tests conducted in the range of typical frequencies of about 1 Hz.

Tests performed with polyurethane-coated membranes developed the next highest pore pressures. Membrane penetration effects were not eliminated but they were reduced significantly. The axial loads carried by the polyurethane were assessed to be very low and these values were easily determined and applied to axial stresses.

Polythene strips were least effective in reducing membrane penetration effects although the reduction in membrane penetration volume change was still significant. Axial loads carried by the strips, on the other hand, were large and not easily determined. Results from axial compression tests performed on specimens of very loose sand are shown in Figure 4.34. Stress-strain curves and pore pressure development curves are compared in this figure for specimens confined by the three membrane systems as well as the results of compensated tests. The significance of these results has been previously discussed.

Ramana and Raju (1981)

Ramana and Raju further investigated the application of compensated-undrained tests for eliminating the effects of membrane penetration by testing a uniform medium sand at relative densities of 21% and 33%. Again, the effects of membrane compliance were compensated by injecting a volume of water equal to the value of the change in membrane penetration volume for a given change in effective confining pressure. The step-by-step procedure is outlined below:

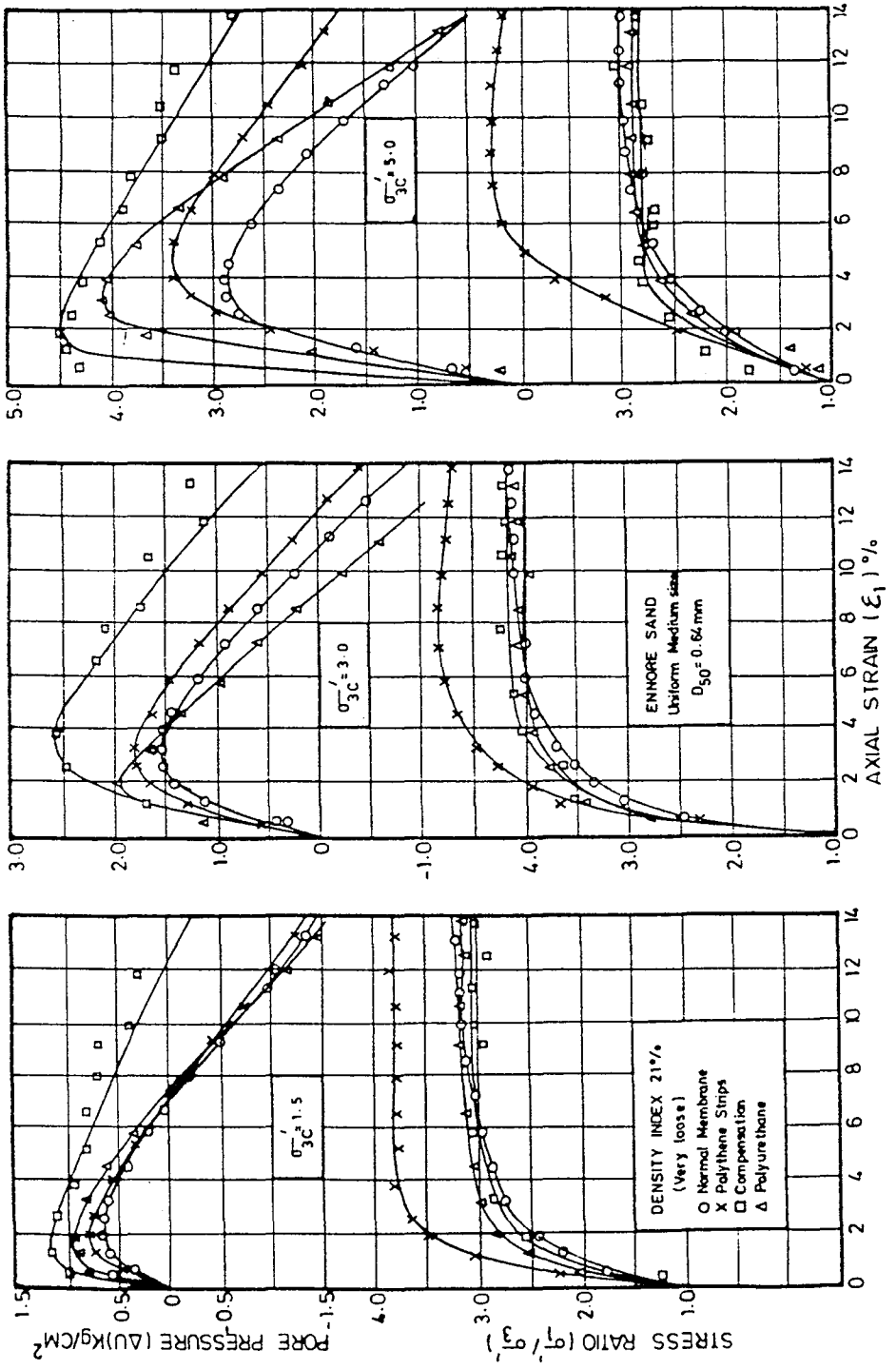

Figure 4.34 Stress-Strain and Pore Pressure Data from Undrained Tests on Very Loose Sand Illustrating the Effects of Different Membrane Systems on Membrane Compliance (after Raju and Venkataramana, 1980)

1. Define ΔV_t vs. ΔV_s using the modified dummy rod method for various changes in effective confining pressure, $\Delta\sigma_3'$, as shown in Figure 4.35.
2. Prepare a curve showing unit membrane penetration ($\Delta V_m/V_t$) for various effective confining pressures similar to that shown in Figure 4.36.
3. Prepare a curve showing membrane penetration volume vs. $\Delta\sigma_3'$as shown in Figure 4.37.
4. At various stages of an undrained test, $\Delta\sigma_3'$ is noted and the corresponding change in membrane penetration is read from curves such as that shown in Figure 4.37. A corresponding volume of water is injected into the sample causing an increase in pore pressure. This change in pressure must be further compensated and the process continued until no change in volume is required.

Cyclic load and unload tests were performed on several test specimens at 21% relative density. The pore pressure responses for compensated and uncompensated tests are shown in Figure 4.38. These tests were performed at a frequency of one cycle per minute. For compensated tests, adjustments were made at zero and peak stress values as well as at several intermediate stress values.

Compensated tests developed peak pore pressure values in significantly fewer cycles than uncompensated tests, once again illustrating that the effects of membrane penetration can lead to an overestimation of cyclic load strength. The method of compensating for membrane compliance effects may become more practical if a computer

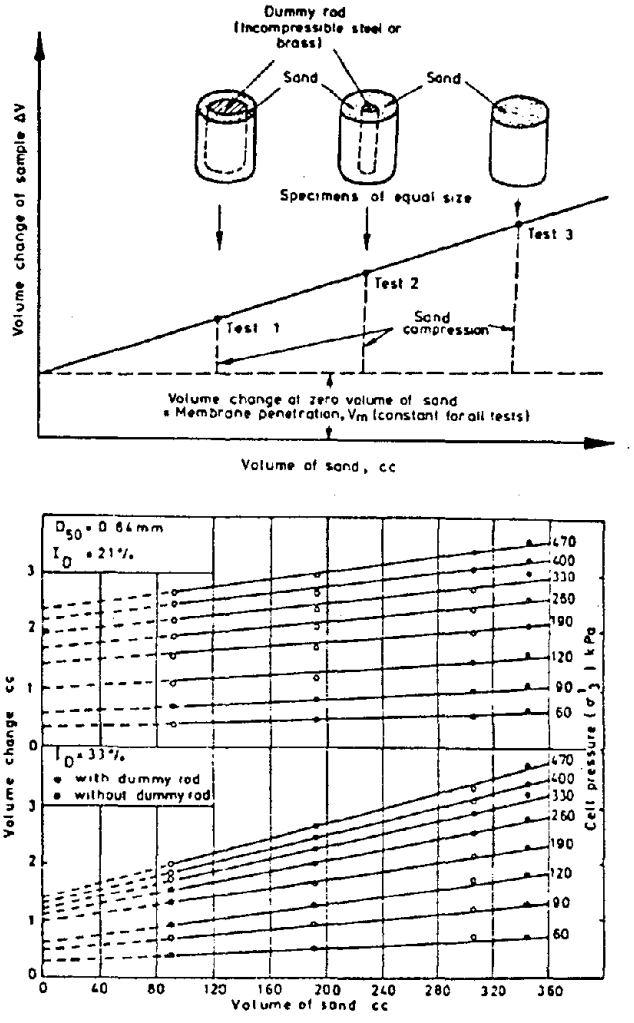

Figure 4.35 Determinations of Membrane Volume Changes vs. Effective Pressure Using the Dummy Rod Method (after Ramana and Raju, 1981)

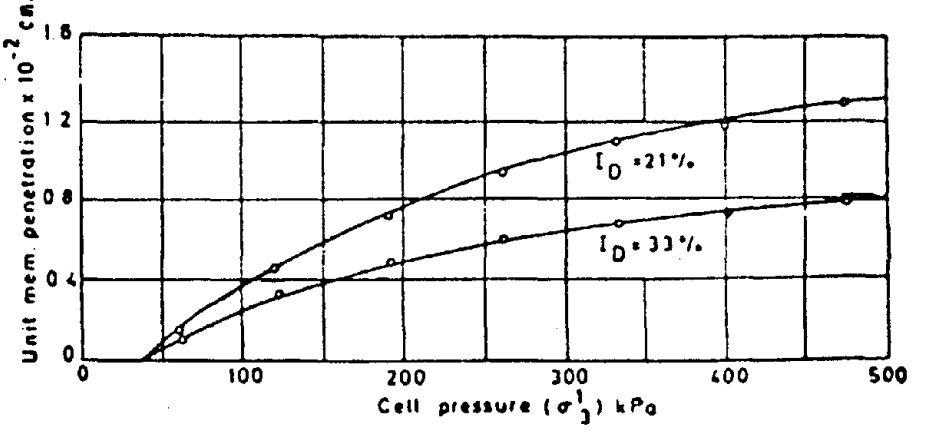

Figure 4.36 Curves of Unit Membrane Penetration vs. Cell Pressure (after Ramana and Raju, 1981)

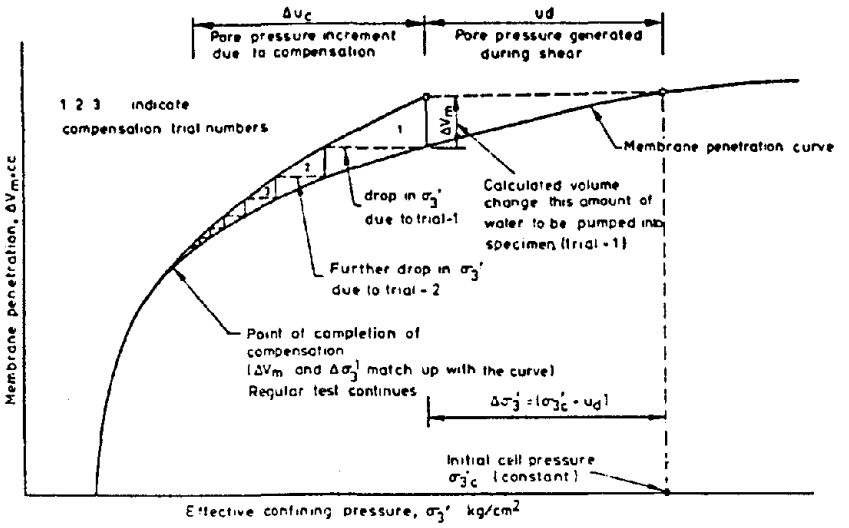

Figure 4.37 Membrane Penetration Volume Change vs. Effective Pressure Curve Used for Compensating for Membrane Compliance Effects (after Ramana and Raju, 1981)

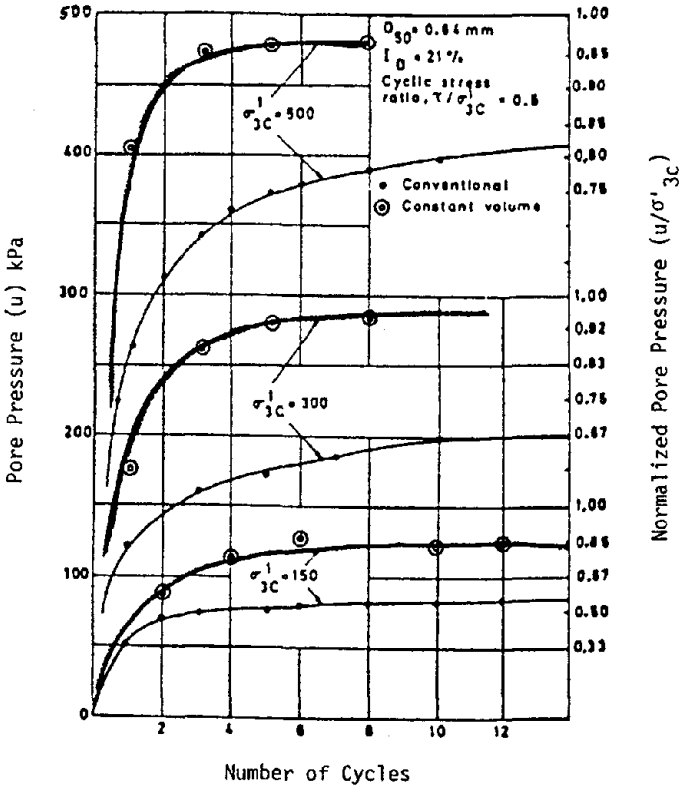

Figure 4.38 Pore Pressure Responses for Both Compensated and Uncompensated Undrained Axial Load Tests (after Ramana and Raju, 1981)

controlled system were developed so that each adjustment requires no more than a few seconds to perform.

Chan (1982)

Chan attempted to minimize the effects of membrane penetration in undrained cyclic tests on sand by applying a coating of liquid latex rubber to the outside of the membrane. 2.8 inch diameter specimens were setup on the triaxial cell base, confined with a rubber membrane, and a vacuum was applied to an internal drainage line. A uniform coating of latex rubber was then applied to the outside of the membrane in vertical sections over the entire membrane and allowed to set. During cyclic loading of specimens prepared in this way, a marked early build-up of pore pressure was noted to occur in tests with latex coated membranes as compared to those with ordinary, uncoated membranes. Typical test results showed that pore pressure ratios of 90% were developed in latex coated specimens in 1/3 to 1/2 the number of cycles required for uncoated samples. However, the effect of membrane compliance on the cyclic stress ratio required to cause liquefaction could not be accurately determined because of gross data scatter between specimens with rubber coated membranes. This is probably due to inconsistent rubber coating thicknesses from test to test because a large number of operators were involved in sample preparation. A uniform stress ratio correction was applied to account for the load carried by the rubber coating but no allowance was made for the variability of the coating thickness. This method shows some promise for future application, however, the thickness of the rubber coating first needs to be controlled. Also, this method can not eliminate all of the effects of membrane compliance since the membrane is allowed to

penetrate the specimen voids before the rubber coating is applied. Energy is stored in the deformed membrane as described in the previous chapter. A substantial thickness of rubber would be required to prevent all of the membrane penetration rebound. Thus either large axial load corrections would be required or some effects of membrane compliance would still occur.

Ramana and Raju (1982)

Ramana and Raju reviewed earlier investigations into the effects of membrane penetration and developed a numerical relationship for volumetric strain due to membrane penetration as a function of D_{50} and sample diameter, d, based on the data shown in Figure 4.39. This relationship is applicable for "standard thickness" membranes and soils with D_{50} between 0.001 and 2.0 mm

$$\varepsilon_{vm} = f \times (D_{50}/d) \times \log (\sigma_3'/\sigma_3'_i)$$

where f = 0.050 for medium soils,

0.057 for loose soils, and

0.047 for dense soils.

Values of ε_{vm} determined by this equation compared favorably with measured values of membrane penetration as shown in Figure 4.40.

Wu and Chang (1982)

Wu and Chang analyzed the stress conditions in specimens using the dummy rod method proposed by Roscoe and found that the stress conditions were anisotropic. These investigators concluded that this method is therefore not suitable for determining membrane penetration effects since it does not adequately represent the stress state of a sample subjected to actual triaxial test conditions. The modified dummy rod method suggested by Raju and Sadasivan (1974) was found to

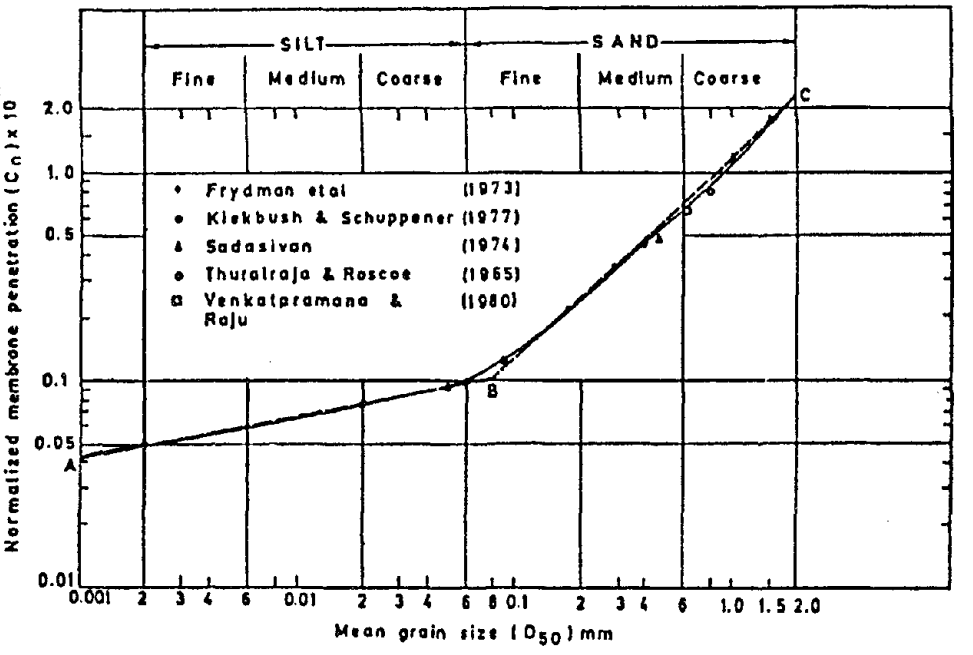

Figure 4.39 Normalized Membrane Penetration vs. Mean Grain Diameter (after Ramana and Raju, 1982)

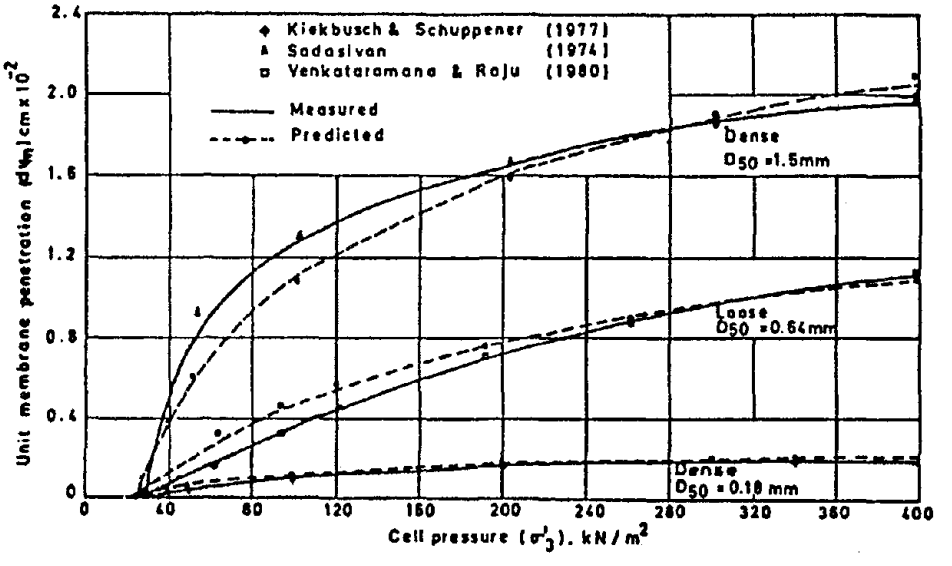

Figure 4.40 Comparison of Predicted and Measured Values of Membrane Penetration Volume Changes (after Ramana and Raju, 1982)

more closely reproduce true isotropic stress conditions in triaxial test specimens. These investigators concluded that the modified dummy rod method would most accurately predict the effects of membrane penetration. They also suggested that: (1) Volume change measurements should be made along the unload-load portion of the stress-strain curve rather than beginning with the initial load cycle; and (2) A straight line may be drawn through the hysteresis loop to estimate volume changes due to membrane penetration.

Baldi and Nova (1983)

Baldi and Nova noted that the influence of membrane penetration depends not only on the flexibility of the membrane but also on the volumetric stiffness of the soil sample. The latter factor depends upon the state of stress which exists within the test specimen and is continuously changing during an undrained test. They proposed the following equation for determining the unit membrane penetration, v_M, where $v_M = V_m/A_1$ or the ratio of volume change due to membrane penetration to the lateral area of the specimen:

$$v_M = 1/8 \times d_g \times [(\sigma_3' \times d_g)/(E_m \times t_m)]^{1/3}$$

where d_g = average grain diameter (may be estimated by D_{50}),

E_m = membrane modulus,

and t_m = membrane thickness.

This equation compares favorably with the linear relationship found by Frydman et al. as shown in Figure 4.41.

Experimental determinations to test the applicability of the proposed relationship were carried out on dense ($D_r \simeq 93\%$), 38 mm diameter specimens of a uniformly graded siliceous sand with values of C_u=1.48 and D_{50}=0.6 mm. Total and skeletal volumetric strains under

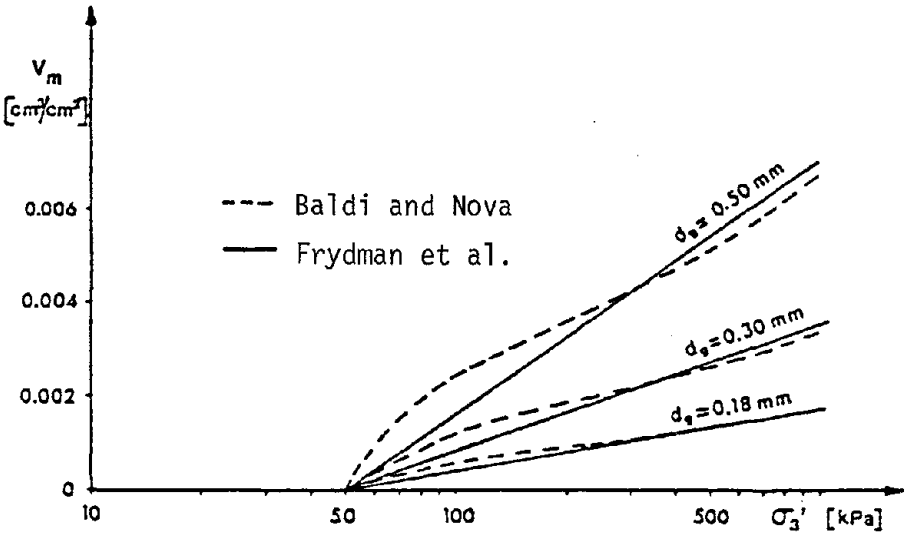

Figure 4.41 Comparison of Membrane Penetration Volume Changes Predicted by Baldi and Nova and from Frydman et al. (after Baldi and Nova, 1983)

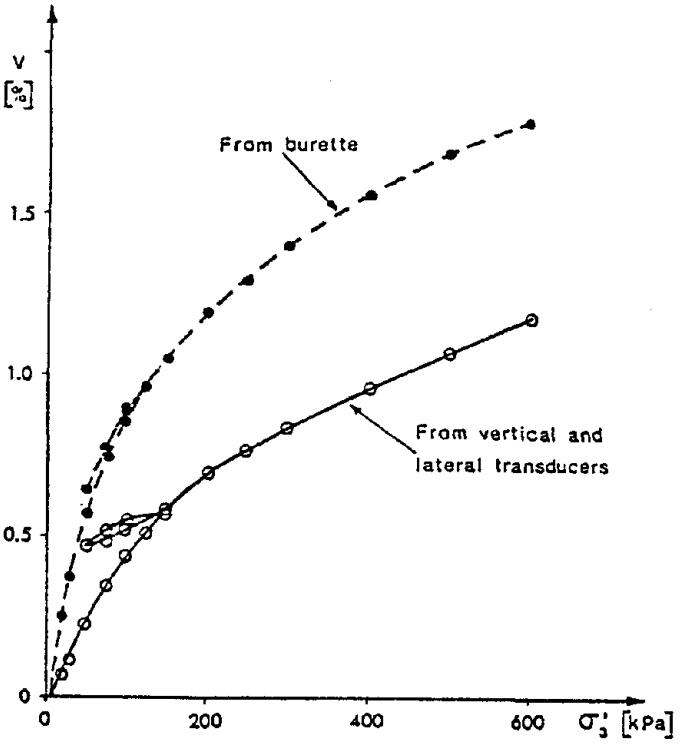

Figure 4.42 Total and Skeletal Volume Change Measurements Made to Determine the Volume Change Due to Membrane Penetration (after Baldi and Nova, 1983)

isotropic compression were measured and the results are shown in Figure 4.42. Membrane characteristics were determined to be t_m=0.3 mm and E_m=1300 kPa. The change in volume attributed to membrane penetration by experimental methods is shown in Figure 4.43 together with the values determined by the preceding equation; the results are shown to be in good agreement.

Theoretical pore pressure corrections were also developed to account for membrane flexibility and the state of stress in the specimen. Undrained, axial compression tests were performed on specimens of the sand described above, and pore pressures were recorded during the test. The theoretical values of pore pressure, corrected for the effects of membrane penetration, were determined to be twice the values measured in the compliant system.

These investigators concluded that volumetric strains due to membrane penetration decreased linearly with an increase in specimen diameter. Also, the factors with greatest influence on membrane penetration volume changes were identified as grain size (this study was conducted on uniform soils only), confining pressure, and thickness and rigidity of the membrane.

Torres (1983)

Torres attempted to reduce membrane penetration effects by coating the outside of the sample membrane with a thin layer of liquid latex rubber as suggested by Chan (1982). Cyclic triaxial tests were performed on two materials; (a) A uniform subrounded coarse sand; and (b) A well-graded slightly silty sand. Both materials were tested at relative densities of 40% and 70%, and tests were performed with and without rubber coatings. A sufficient coating of latex rubber was

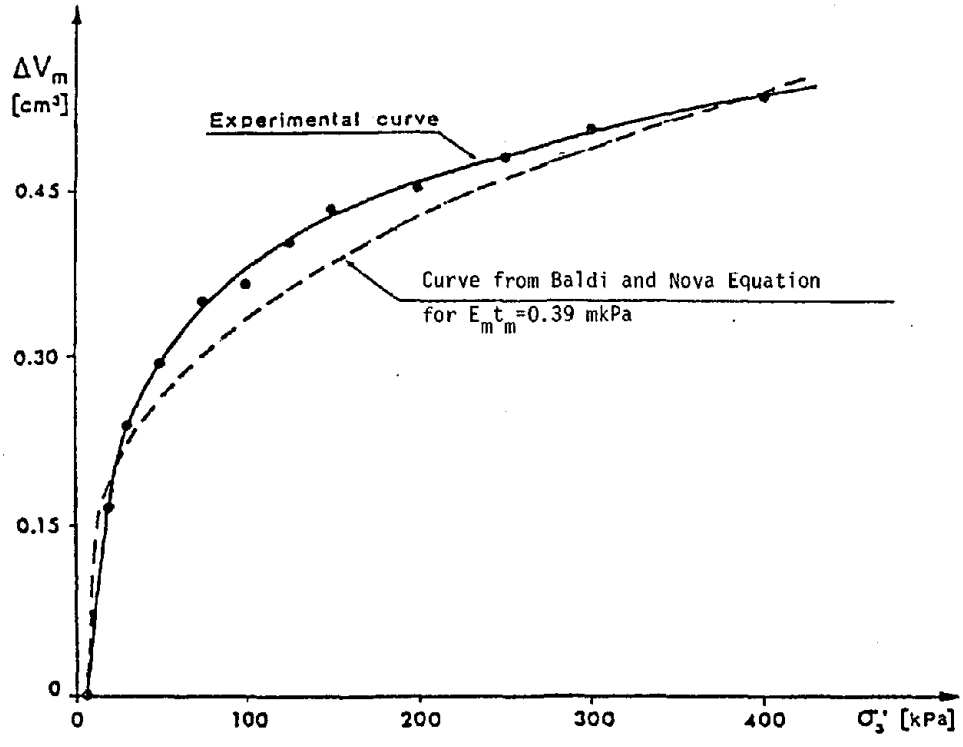

Figure 4.43 Experimental Volume Change Curve Compared with Proposed Numerical Relationship (after Baldi and Nova, 1983)

applied, with the sample under a vacuum, to just fill the surficial voids created by membrane penetration. The results of cyclic load tests performed on 2.8 inch diameter specimens indicated that the cyclic stress ratios required to cause 5% double amplitude axial strain in 30 stress cycles were reduced by about 6% to 10% when the liquid rubber coating was used. The resulting stress ratio correction factors determined by this study, were significantly lower than correction factors predicted by Martin et al. (1978), indicating that the rubber coating does not appear to account sufficiently for the effects of membrane compliance.

Volumetric strains due to membrane penetration were also determined in this study by performing isotropic consolidation tests and measuring total volume change as well as axial and radial deformations. The results of these tests are shown in Figure 4.44. Reductions in unit membrane penetration for an effective confining pressure change of 1 kg/cm^2 ranged from 73% to 91% with the use of rubber coating as shown in Table 4.2. These results show that, although membrane penetration was not eliminated, the effects on volume changes were significantly reduced.

Vaid and Negussey (1984)

Vaid and Negussey concluded that previous methods for determining membrane penetration effects involved stress condition errors and proposed two new methods for determining the value of volumetric strain due to membrane penetration. The first method stems from the fact that results from simple shear tests indicate that hydrostatic unloading is isotropically elastic. Therefore, a single hydrostatic unloading test may be performed on a triaxial specimen such that:

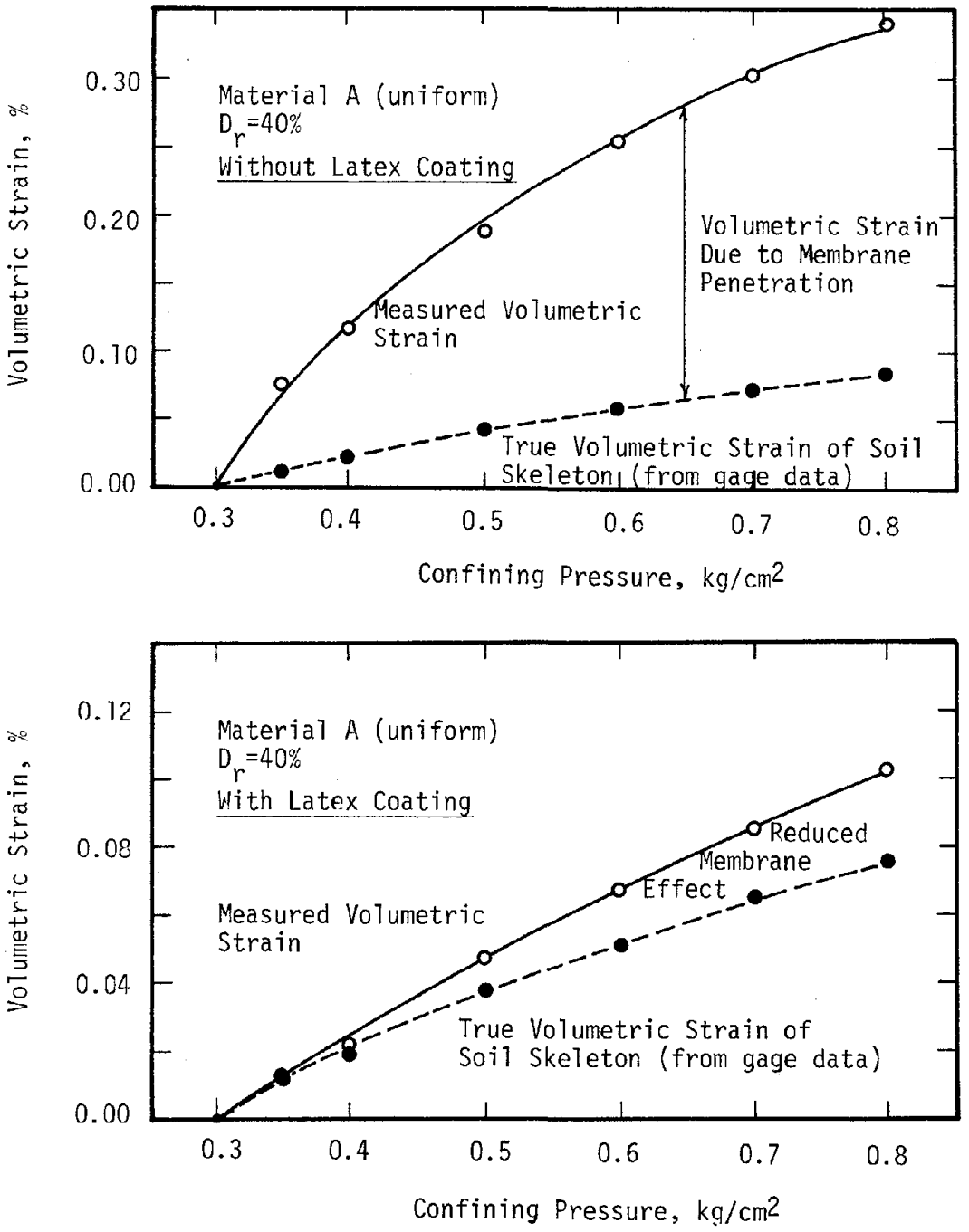

Figure 4.44 Volumetric Strain Due to Membrane Penetration for Tests with and without Latex Coated Membranes (after Torres, 1983)

MATERIAL	Dr %	MEMBRANE PENETRATION REDUCTION %
A Uniform	70%	78.7
A Uniform	40%	90.7
B Well Graded	70%	74.5
B Well Graded	40%	72.5

Table 4.2 Reductions in Membrane Penetration Volume Changes for σ_3'=1.0 kg/cm^2 with the Use of Rubber Coated Membranes (after Torres, 1983)

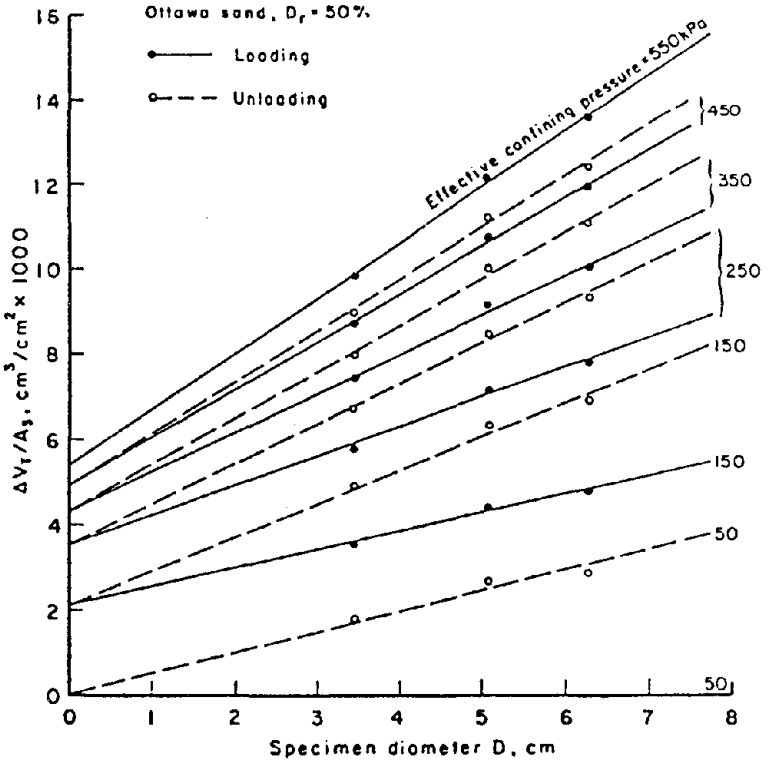

Figure 4.45 Normalized Volume Change Results from the Multiple Specimen Method (after Vaid and Negussey, 1984)

$$\varepsilon_{vu} = 3 \times \varepsilon_{au}$$

where ε_v and ε_a represent the volumetric and axial specimen strain respectively, and u indicates unloading. It may be recalled that the use of volume change data from the isotropic rebound portion of the curve was originally suggested by Wu and Chang (1982).

In the second method, hydrostatic compression or rebound tests were performed on several specimens at the same density but with different diameters, D. Then, the following linear relationship between $\Delta V_T/A_s$ and D can be used to determine the volumetric strain due to membrane penetration, ε_m:

$$\Delta V_T/A_s = (\varepsilon_v/4) \times D + \varepsilon_m.$$

where ΔV_T = the total measured volume change,

and A_s = the surface area of the specimen covered by the membrane.

Since this equation is in the form y=mx+b, the results of several tests may be plotted and the value of ε_m may be determined as the y-intercept of the resulting straight line as shown in Figure 4.45. Experimental investigations were performed in this study for specimens of Ottawa sand using the two proposed methods. It may be seen in Figure 4.45 that both unloading and loading cycles show the same value of ε_m for a given value of confining pressure. This indicates that membrane penetration effects are reversible for either an increase or decrease in effective confining pressure.

Test results for the single specimen method are shown in Figure 4.46 illustrating the use of the relationship shown above. The results of both of the proposed methods are shown in Figure 4.47 and it can be seen that they yield nearly identical results. The hypothesis that hydrostatic unloading is isotropic was confirmed by the test results

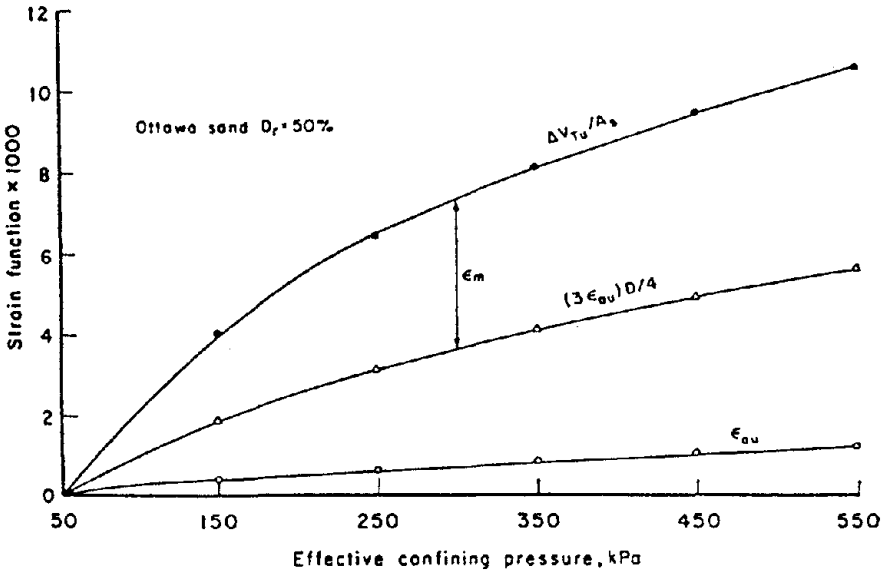

Figure 4.46 Membrane Penetration Volume Changes Determined by Hydrostatic Unloading of a Single Specimen (after Vaid and Negussey, 1984)

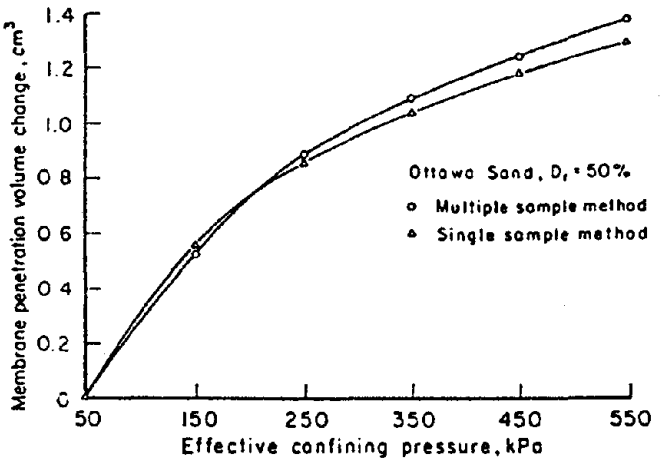

Figure 4.47 Comparison of Single and Multiple Specimen Methods for Determining Membrane Penetration Volume Changes (after Vaid and Negussey, 1984)

shown in Figure 4.48. It may be seen from this figure that the results of isotropic loading are somewhat anisotropic whereas the results of isotropic unloading are indeed isotropic. This study provides the investigator with yet another method to determine the volume changes due to membrane penetration. However, it provides no information to aid in assessing the effects of membrane compliance on the results of undrained triaxial compression tests. This latter point needs to be addressed further.

Conclusions

The objective of this investigation is to explore the effects of membrane compliance on the results of undrained, cyclic triaxial tests on gravels. After reviewing the previous studies, it became clear that much groundwork has been laid but that additional investigation into this topic was warranted because there is apparently no well accepted, conclusive method to account for membrane compliance effects. The objective of assessing the magnitude of volume changes due to membrane penetration seems to have been thoroughly addressed. Also, a fair amount of research has been directed toward assessing the effects of membrane penetration volume changes on the results of cyclic and monotonic undrained, triaxial load tests. Theoretical stress ratio corrections have been proposed as well as corrections based on tests performed on specimens of smaller grain sizes. However, both of the latter approaches require some verification of their validity for application to the results of tests performed on gravels. Ideally, membrane compliance effects should be accounted for during testing rather than applying a correction after completion of the test. A

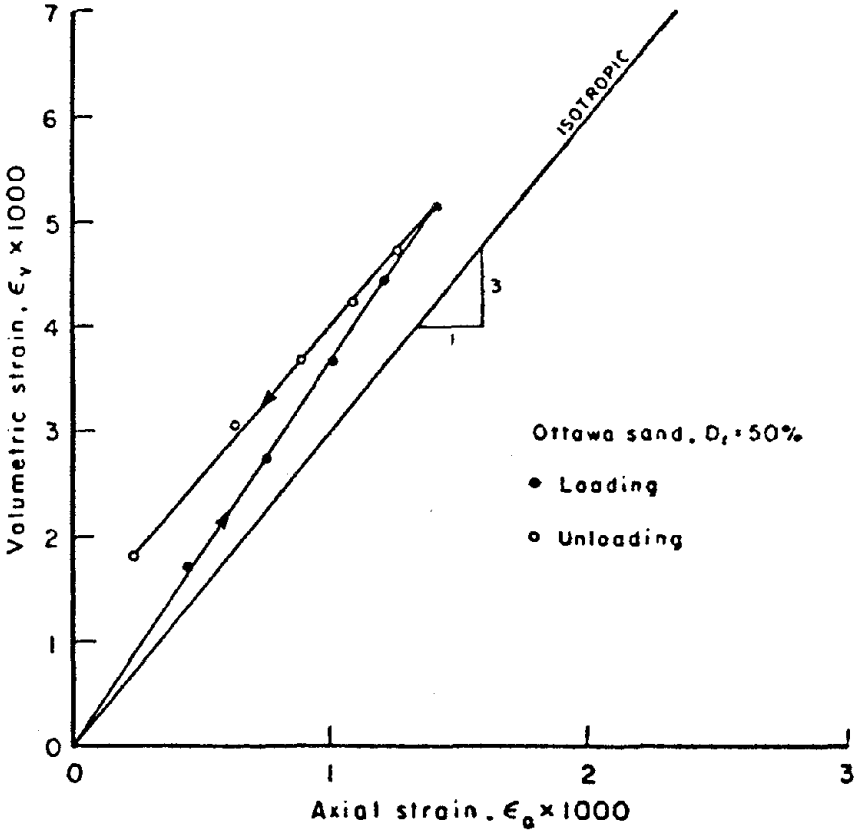

Figure 4.48 Measured Volumetric vs. Axial Strain Caused by Hydrostatic Loading and Unloading (after Vaid and Negussey, 1984)

method for performing noncompliant tests on gravel triaxial specimens will be presented and discussed in subsequent chapters of this report.

CHAPTER 5

SLUICING GRAVELS AND ROCKFILLS WITH SAND

Introduction to Research Program

After reviewing the previous investigations noted in Chapter 4, it was apparent that further research should be directed toward determining the effects of membrane compliance on the results of undrained cyclic loading tests performed on gravels. A potential method for performing such determinations was conceived after reviewing studies which described the field sluicing of rockfills with sand. Such rockfills may be found in the Malpaso Canyon Dam in Peru (Park, 1939) or the Aswan High Dam in Egypt (Abu-Wafa, Hanna Labib, 1970, 1971; Hassouna et al., 1970; High and Aswan Dams Authority, 1969) as noted previously in Chapter 1. Although sluicing was performed in these dams for reasons that were totally unrelated to membrane compliance, it seemed that gravel triaxial specimens which were sluiced with sand would have a smoother specimen/membrane contact surface, and thus experience reduced membrane penetration volume changes during consolidation. Any reduction of membrane penetration during consolidation would lead to reduced membrane compliance effects during undrained, cyclic loading. And, if these effects could be eliminated, the true, noncompliant cyclic loading resistance of gravel specimens could be accurately determined.

A preliminary research investigation was undertaken to determine if: (1) Gravel triaxial specimens could be satisfactorily sluiced with sand in the laboratory, and (2) Sluicing sand into the voids of a gravel specimen would sufficiently reduce the effects of membrane

penetration so that the noncompliant cyclic loading resistance of the gravel specimens could be accurately determined. The trial sluicing program, described in the following sections of this chapter, indicated that satisfactory sluicing could be accomplished under controlled conditions. It was noted that the outer surface of the sluiced triaxial specimens was, in fact, considerably smoother than the outer surface of the unsluiced specimens, as shown in Figures 5.1 through 5.4, leading to significantly reduced membrane penetration in the sluiced specimens.

As a result of these observations, several undrained, cyclic loading tests were performed on specimens of sluiced and unsluiced gravel. The results of these tests are shown in Figure 5.5 where it may be noted that the cyclic loading resistances of the sluiced gravel specimens are considerably lower than the cyclic loading resistances of the unsluiced gravel specimens. In fact, only about 65% of cyclic stress ratio which resulted in 5% double amplitude strain in 10 stress cycles in the unsluiced gravel specimens was required to cause a corresponding failure in the sluiced gravel specimens.

It is believed that the difference in these values of cyclic loading resistance is due primarily to the reduction of membrane compliance effects in the sluiced specimens. Sluiced gravel specimens were completely constructed in order to create the desired particle structure, and then the water in the voids was replaced with sluicing sand as will be described in Chapter 6. Thus, the individual gravel particles formed a continuous, stable load carrying structure and the voids between these particles, rather than being filled with water, were filled with sand. The presence of sand in the gravel voids may

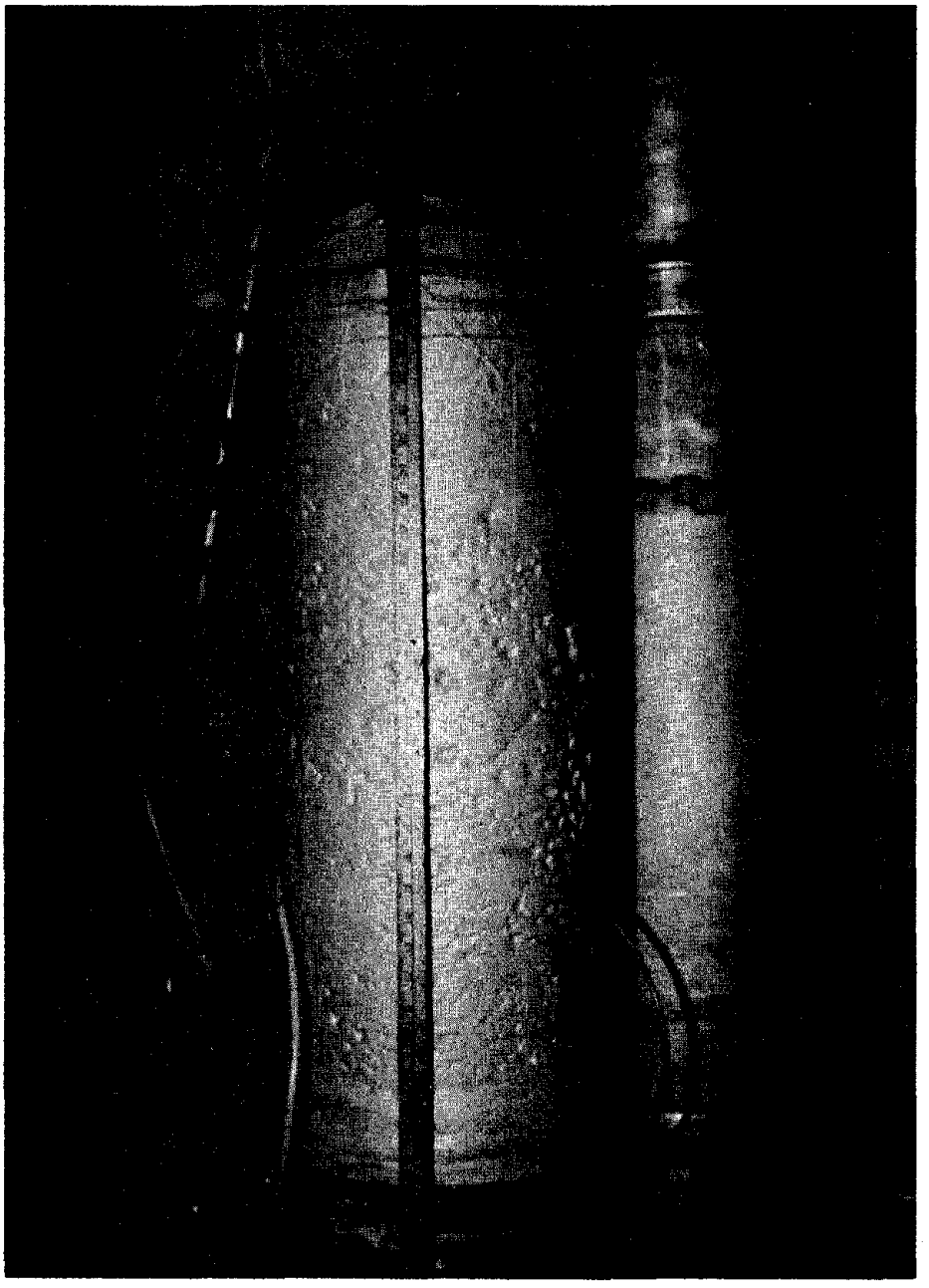

Figure 5.1 Photograph of a 12 Inch Diameter, Sluiced Gravel Specimen

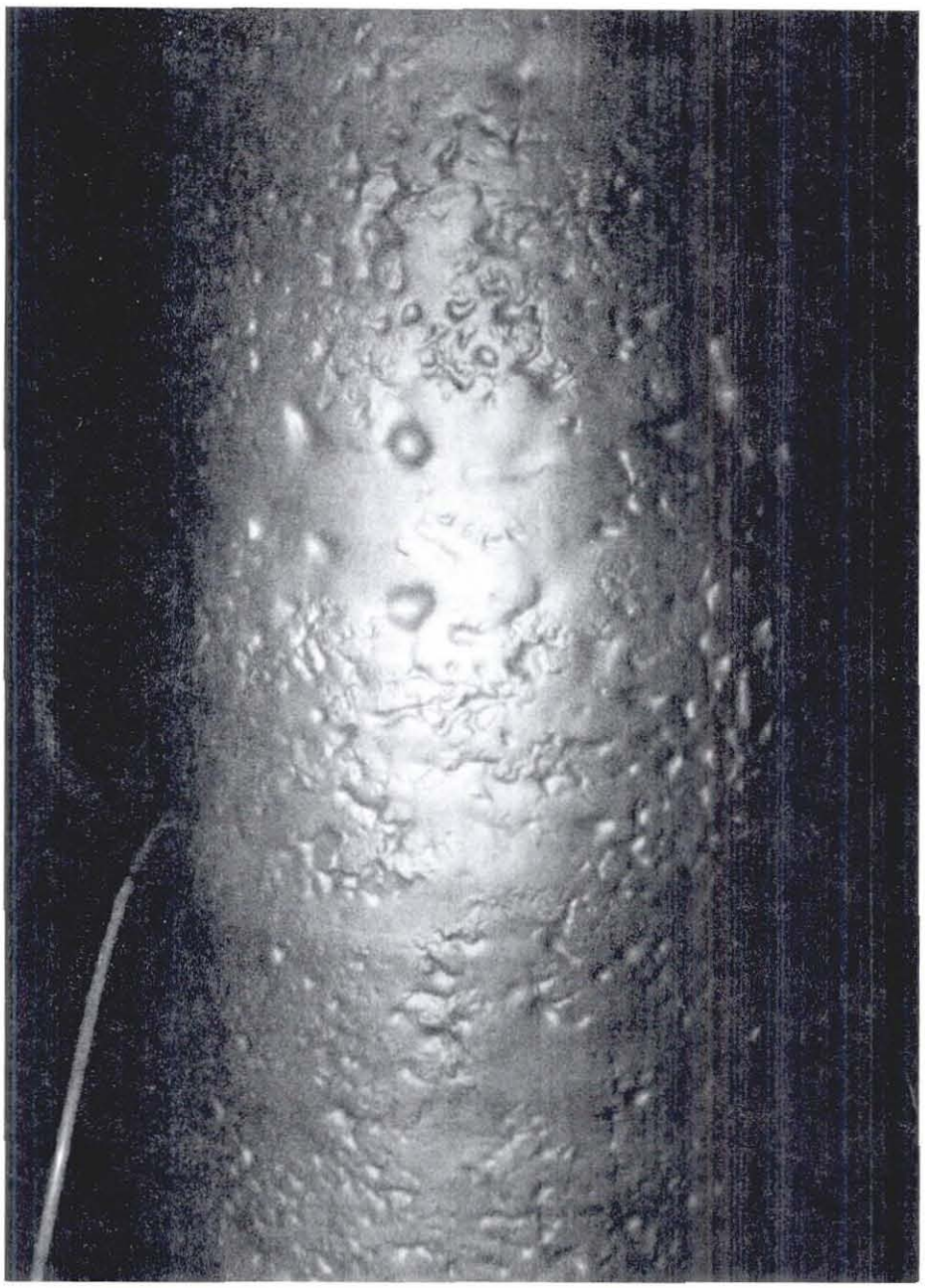

Figure 5.2 Photograph of a 12 Inch Diameter, Sluiced Gravel Specimen

Figure 5.3 Photograph of a 12 Inch Diameter, Unsluiced Gravel Specimen

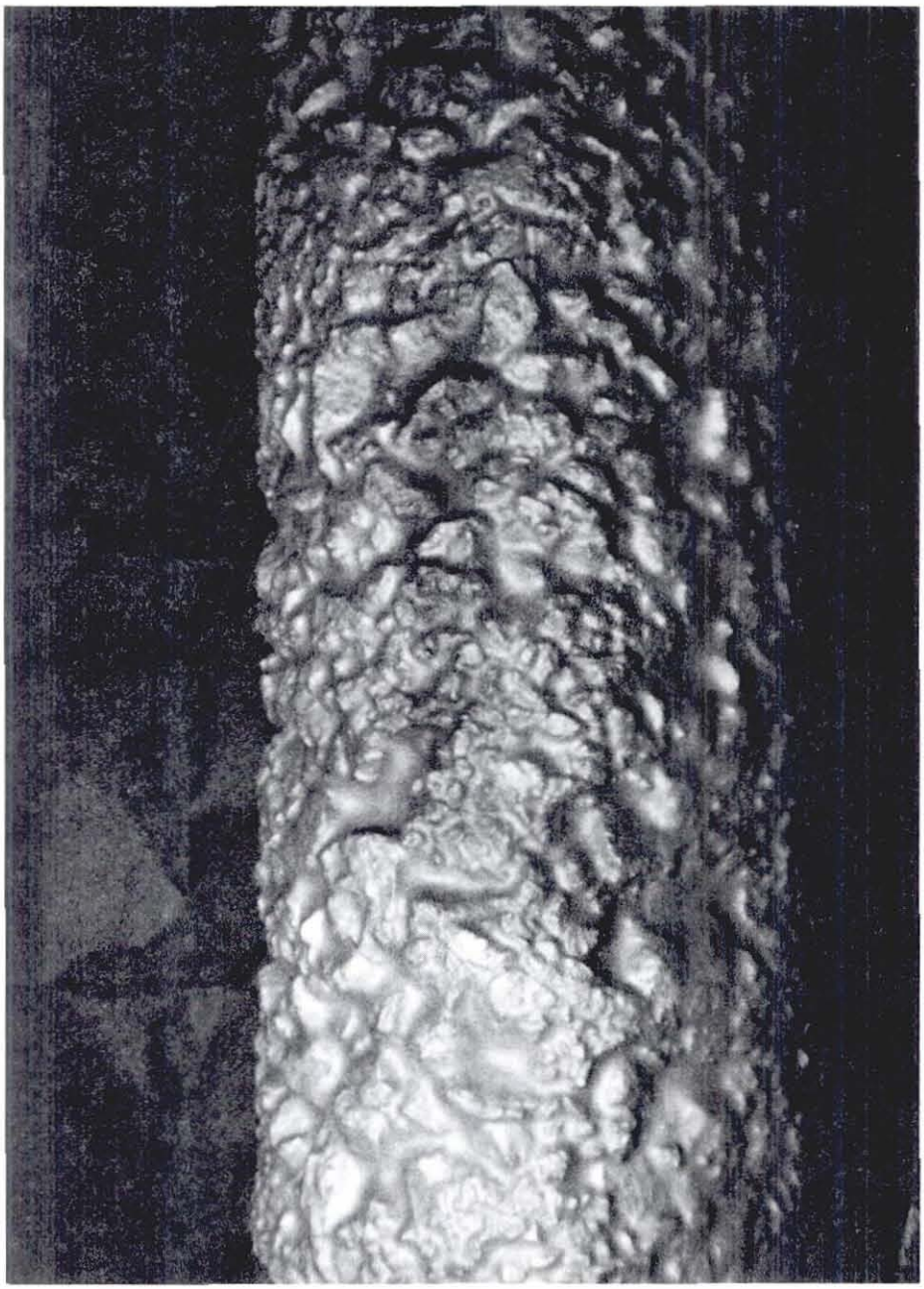

Figure 5.4 Photograph of a 12 Inch Diameter, Unsluiced Gravel Specimen

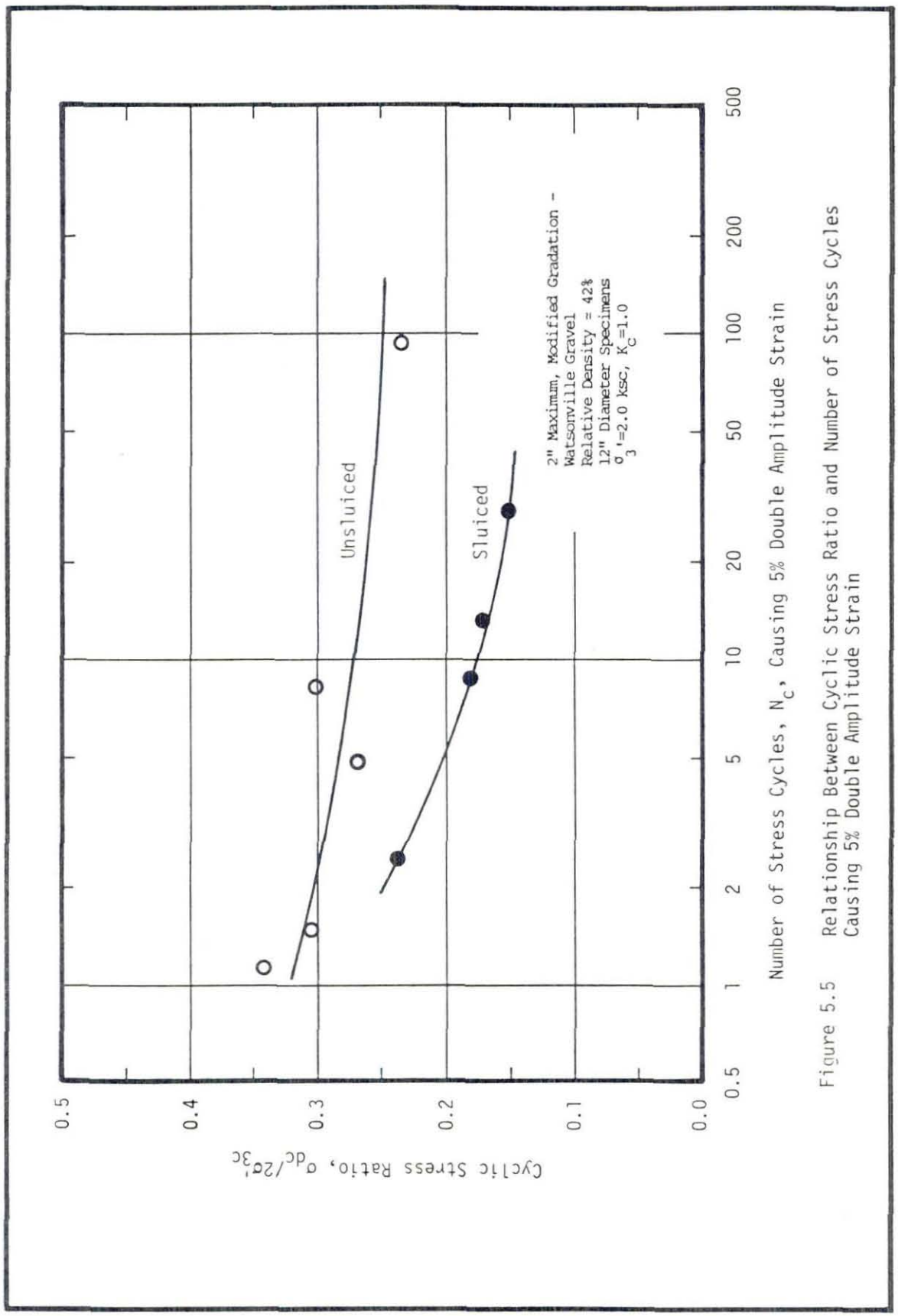

Figure 5.5 Relationship Between Cyclic Stress Ratio and Number of Stress Cycles Causing 5% Double Amplitude Strain

contribute slightly to the cyclic loading resistance of the sluiced gravel specimens by preventing rearrangement of the gravel particles. It may be recalled from the discussion in Chapter 3 that liquefaction is caused by particle rearrangement or crushing due to the applied cyclic load. If particle rearrangement or crushing is inhibited, however slightly, the effect will be to increase the cyclic loading resistance of the specimen. The sand which is sluiced into the gravel specimen voids is in a very loose condition, however, even the very loose sand has greater shearing resistance than the water (which has no shearing resistance) in the voids of the unsluiced specimens. Therefore, it is considered that the sand in the gravel voids may contribute slightly to the cyclic loading resistance of the sluiced gravel specimen if it has any direct effect on loading resistance at all. The contribution of the sand to the cyclic loading resistance of the sluiced gravel specimens was considered to be negligible and only the reduction in membrane compliance effects was considered to be significant. Additional evidence that the sluicing sand did not adversely affect the cyclic loading resistance of the gravel specimen was obtained during the testing program and is summarized in Chapter 10.

This preliminary investigation indicated that sluicing seemed to be a viable method of reducing membrane compliance effects in gravel specimens. It was decided that additional laboratory testing should be performed on sluiced specimens, but first, previous field and laboratory sluicing efforts were investigated. The early sluicing programs performed for the Malpaso Canyon Dam and the Aswan High Dam provide a basis for evaluating the sluiced triaxial specimens as

performed in this study. Thus, these studies are reviewed in the following sections. A laboratory sluicing study was then performed as part of this investigation and the results of this study are also presented in this chapter.

Malpaso Canyon Dam Rockfill Sluicing

The Malpaso Canyon Dam was constructed on the Mantaro River by the Cerro de Pasco Copper Corporation during the years 1929 to 1937. The purpose of the dam was to store and supply water for hydroelectric power generation to be used by the Oroya smelting and refining plants located downstream. The dam was constructed of derrick-placed rock in the upstream portion and dumped rockfill in the downstream portion as previously shown in Figure 1.1. A masonry wall ranging in thickness from 3 to 6 feet was constructed on the upstream face over which was applied a 23 inch thick concrete apron.

Prior to construction of the masonry wall and apron, surface voids on both faces of the dam were hand chinked with stones and then river sand and gravel were washed into the rockfill mass through any remaining openings. The purpose of sluicing sand into the dam was reported to be threefold: (1) To increase bearing and contact areas of the rock; (2) To reduce settlement of the dam; and (3) To add to the mass of the upstream derrick-laid section of the dam. The dam was sluiced with river sand and gravel by using streams of water 1-1/2 inches in diameter and having a nozzle velocity of more than 100 feet per second. No control or monitoring of the sluicing process was reported.

Aswan High Dam Rockfill Sluicing

Completed in 1970, The Aswan High Dam was constructed as a joint venture between the United Arab Republic (Egypt) and the U.S.S.R. At that time, it was the the world's largest rockfill dam with a total volume of about 42 million cubic meters and a height of about 111 meters. This is one of the few major rockfill dam to have had major portions of its dumped rockfill mass sluiced with a fine dune sand during construction (see Figure 1.2). Soviet engineers have reportedly sluiced small dams and dykes subject to 6 to 8 meters of head (Hassouna et al., 1970) but no information regarding construction of these structures was found in the literature.

Rockfill sluicing was proposed for this project in order to avoid the need to construct a filter blanket over the alluvial foundation sand deposits. By filling the rockfill voids with sand, it was judged that foundation sands would not be washed upward into the voids of the completed rockfill dam, thus, eliminating the need for a filter blanket. Construction of the filter blanket, as originally proposed, would have been particularly difficult in this instance since the filter and a large portion of the dam were to be constructed under 35 to 40 meters of water in the upstream reservoir of the old Aswan Dam. The water level in the reservoir could not be lowered significantly during construction since the stored water was vitally needed for crop irrigation. Also, construction of a separate upstream cofferdam was judged to be too expensive. Therefore, about 4 million cubic meters of crushed rock were dumped and sluiced through standing water in order to form the lower portion of the dam.

An extensive evaluation of field and laboratory rockfill sluicing was undertaken by Soviet engineers at the time of construction of the Aswan High Dam. These studies were reviewed for this research and a discussion of the findings is included in the following sections.

Field Sluicing of the Aswan High Dam

During construction of The Aswan High Dam, the sluiced rockfill mass was divided into two distinct sections: (1) Rockfill that was placed and sluiced under water; and (2) Rockfill that was placed and sluiced above water. Rockfill placement and sluicing procedures for these sections are discussed below.

In the early stages of construction, all rockfill was placed through water up to 40 meters deep. Barges with 250 and 500 ton capacity were floated into position on the reservoir and dumped to form zones or "prisms" of rockfill. Once these zones were completed, a dune sand slurry, composed of 90% water and 10% sand, was pumped to the upper surface of the rockfill and deposited there. Sand penetrated into the rockfill voids mainly by gravity, aided by a low head of 2 to 3 meters at the discharge pipe opening. Sand sluiced into the rockfill voids in this manner achieved a density of 82 to 88 pcf.

Once the dam attained a height above the reservoir water level, rockfill was trucked on to the dam and dumped using conventional earthmoving equipment. The surfaces of these sections constructed above water were prepared for sluicing by removing the upper layer of fine crushed rockmuck created by equipment traffic. A sand slurry was then washed into the rockfill by high pressure jetting. The sand sluiced into the rockfill voids above the reservoir water level in this way achieved a dry density of 85 to 88 pcf.

Grain size curves for the screened rockfill and the dune sand used for sluicing are shown in Figure 5.6. The rockfill material was excavated from quarries comprised of migmatites, medium grained pink gneiss-granite and fine granite (Hassouna et al., 1970). The dune sand consisted mainly of a light gray quartz with rare feldspar grains. Table 5.1 summarizes the properties of these materials.

The quality of sluicing that was achieved in the dam was checked by various direct and indirect methods as described below.

(1) The quantity of sand added to the rockfill was compared to the volume of the rockfill voids. Sand consumption into the rockfill mass was calculated to be about 40% of the volume of voids of the rockfill prisms with a dry density of 82 to 88 pcf (Abu-Wafa, Hanna Labib, 1970).

(2) Trenches were excavated into the sluiced rock mass for visual evaluation of the quality of sluicing accomplished and also for performing large-scale field density tests. The zones that were inspected were described as being either "well filled with sand" or "partially filled with sand" (Hassouna et al., 1970). The latter zones were flushed with water and resluiced.

(3) The in-situ coefficient of permeability was determined through drilled boreholes and test pits. This quantity was determined to range between 2.5×10^{-3} and 8×10^{-3} cm/sec (Hassouna et al., 1970).

Laboratory Sluicing Studies for the Aswan High Dam

During 1959 to 1962, two Soviet research agencies conducted laboratory and large scale sluicing experiments on modeled rockfill masses. Additional laboratory tests were also conducted by the

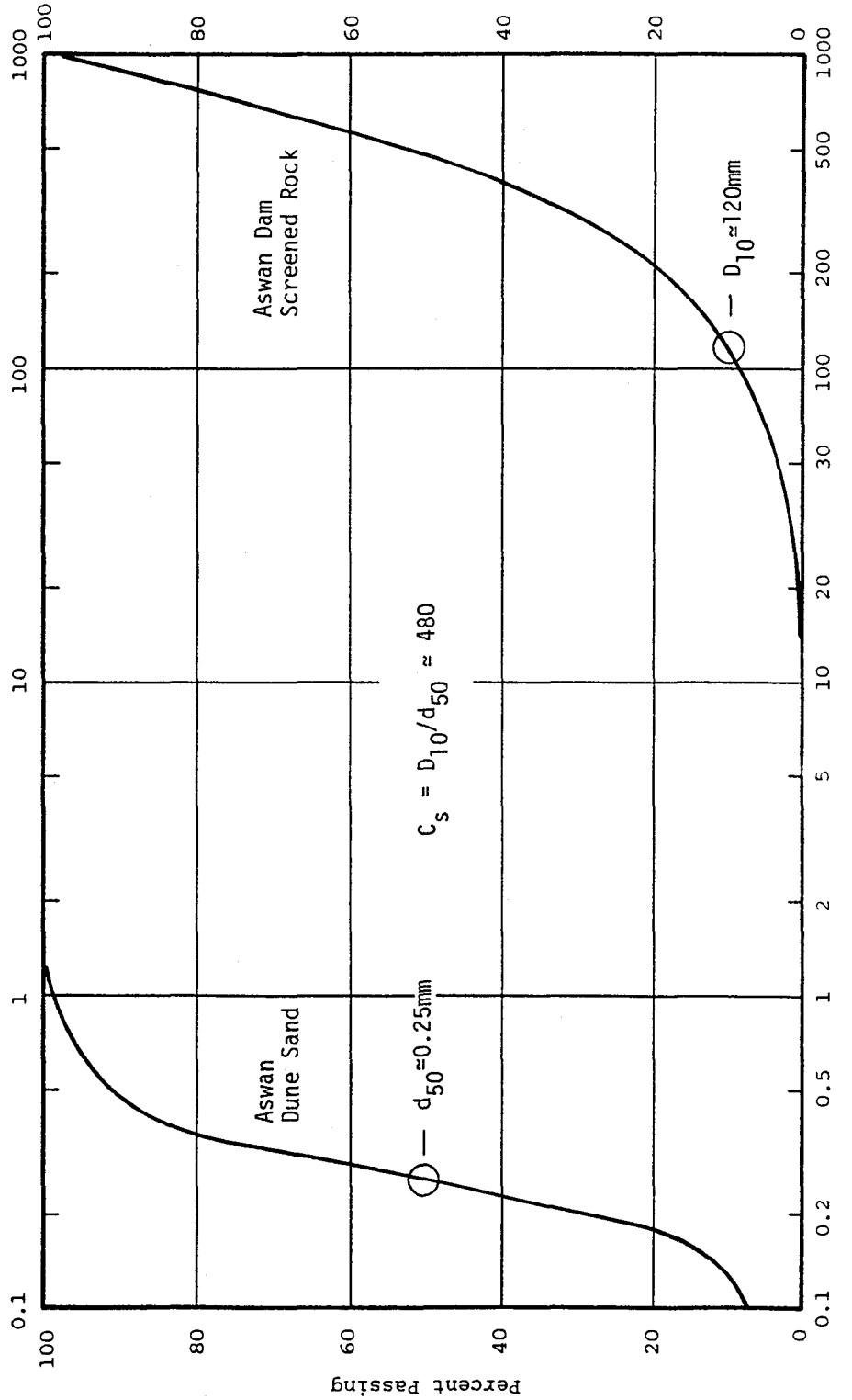

Figure 5.6 Gradation Curves for the Aswan High Dam Screened Rock and Dune Sand (Hassouna et al., 1970).

Table 5.1 SUMMARY OF ASWAN HIGH DAM SCREENED ROCK AND DUNE SAND PROPERTIES

Material Description	D_{60}	D_{50} (mm)	D_{10}	C_u	G_s	γ_{max}	γ_{min} (pcf)	$\gamma_{max}-\gamma_{min}$
Aswan Dune Sand	0.30	0.25	0.12	2.5	2.67	116-121	92-94	24-27
Aswan Screened Rock	580	485	102	4.8	-	-	-	-

Research Department of The Aswan High Dam at the dam site in 1964 and 1965. All of these tests were designed to accomplish the following goals:

(1) Select a method of delivering the sand to the rockfill;

(2) Establish an optimum gravel/sand grain size relationship which results in a well-sluiced rockfill;

(3) Evaluate the filtration stability of a sluiced rockfill;

and (4) Evaluate the degree of compaction of the sand in the rockfill voids.

Sand and screened rock similar in gradation to those used in the Aswan High Dam were used for the initial laboratory tests. Large scale model tests were conducted in a trench 16 meters wide and 100 meters long. Truckloads of screened rock were dumped into the trench to form the model rockfill. The trench was then filled with enough water to cover the rockfill and then sand was pumped to the surface of the rockfill in the form of a slurry.

The laboratory rockfill mass was sluiced with sand in the form of a slurry since it had been decided that the use of a slurry was the most practical and efficient means of delivering the sand to the rockfill in the dam. Also, an ample supply of reservoir water and dune sand was available nearby for processing to form a slurry.

Model tests were conducted with various sand concentrations in the slurry ranging from about 1% to 20%. Slurries with lower concentrations of sand produced flatter slopes with a smoother surface within the rock mass, thus, producing a higher degree of sluicing, since the sand could flow more readily into hard-to-reach voids beneath rock particles. Higher sand concentrations produced steeper and rougher sand surfaces which left more of the voids beneath particles

unfilled. However, a higher concentration of sand reduced the quantity of slurry that was required to be processed and pumped. The amount of time required to complete the sluicing operation was also reduced, thus, making the operation more efficient. A slurry concentration of 10% was selected as a practical compromise between efficiency and completeness of sluicing.

Experiments were conducted using various gradations of rockfill sands to explore the relationship between coefficient of sluiceability, C_s, defined as $D_{10(gravel)}/d_{50(sand)}$, and the degree of sluicing achieved. Figure 5.7 shows a qualitative relationship developed between the mean rock diameter, D_{50}, C_s, and the resulting quality of sluicing. A coefficient of sluiceability of 65 to 70 was considered to be the minimum value where a good quality of sluicing could still be achieved.

Size, shape and orientation of the screened rock particles were all found to affect the quality of sluicing (High and Aswan Dams Authority, 1969). Figure 5.8 shows how the shape and the orientation of model grains may prevent complete sluicing from being accomplished in some instances when the sand is deposited through standing water. By jetting the sand slurry above the standing water level, all of the model voids were filled with sand.

Sand washed out of the surficial voids of the rockfill when gradients exceeded about 0.20 to 0.25. However, when the surface of the rockfill was protected by an inverted filter, gradients as high as 0.60 to 0.65 had no adverse effect even when applied for several months (High and Aswan Dams Authority, 1969).

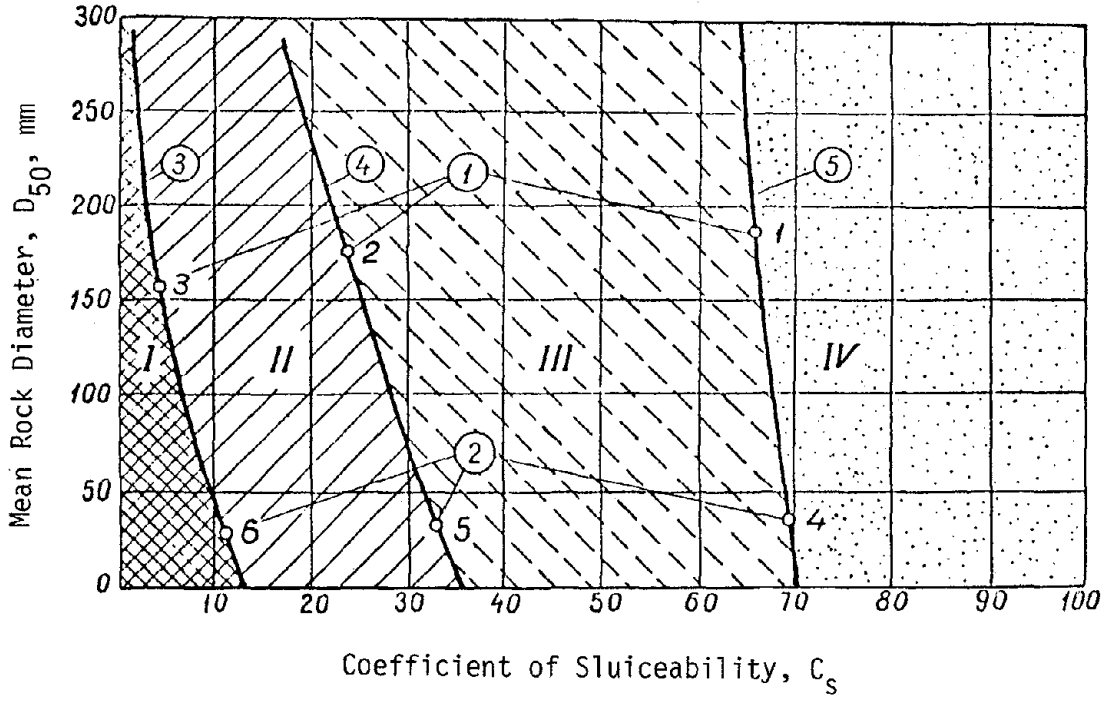

Zone: I - Essentially Unsluiceable

II - Difficult to Sluice

III - Satisfactorily Sluiced

IV - Well Sluiced

Figure 5.7 Relationship Between Mean Rock Diameter, Coefficient of Sluiceability and Quality of Sluicing (after High and Aswan Dams Authority, 1969)

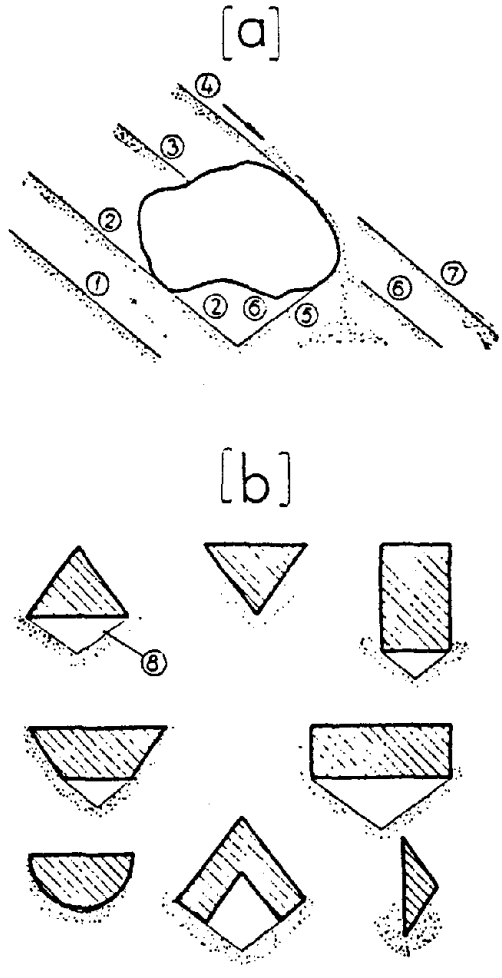

Figure 5.8 (a) Scheme of Under-Water Sluicing Around a Single 2-Dimensional Particle and (b) Effect of Particle Shape and Orientation on Sluicing Quality (after High and Aswan Dams Authority, 1969).

The density of the sand (and rockfill) was determined directly by performing large-scale density tests in pits excavated into the surface of the sluiced rock mass. Also, densities were determined indirectly by weighing the quantity of sand used for sluicing and comparing it to the calculated volume of rockfill voids.

The highest density of sluiced sand was achieved by above-water sluicing. All of the rockfill voids were visually well filled with sand when sluiced above water. When sluicing was performed through standing water, however, the rockfill voids were often poorly filled with sand. Table 5.2 summarizes the dry densities of the sand sluiced into the rockfill voids and the hydraulic conductivities of the sluiced rockfill mass for both laboratory and field sluicing applications.

Sand sluiced into the rockfill voids was compacted to a higher density than the value at which it was deposited by the development of a gradient through the rockfill. Dry densities were increased by about 4.5% under a downward gradient of about 1.

It may be seen from Table 5.2 that the coefficient of permeability of the sluiced rockfill mass was determined to be lower than that for sand deposited through water alone.

Laboratory Slucing Studies Performed in this Investigation

Experimental sluicing was performed as a preliminary part of this research in order to determine if gravel triaxial specimens could be sluiced with sand with satisfactory results. The purpose of this study was to achieve a degree of sluicing in the laboratory similar to that achieved in the Aswan High Dam. The general sluicing procedures and methods of evaluation used for the Aswan High Dam were used in this study. It was shown in Table 5.2 that sand sluiced into the dam below

Table 5.2 VARIATIONS IN SAND AND ROCKFILL PROPERTIES WITH DIFFERENT METHODS OF SAND DEPOSITION

Method of Depositing the Dune Sand	Dry Density of Dune Sand (pcf)	Hydraulic Conductivity of Sluiced Rockfill (cm/sec)
Deposited in Standing Water (not sluiced)	100	2×10^{-3} - 3.3×10^{-3}
Same as Above -Compacted	108	-
Sluiced in the Field -Above Water	85 - 88	2.5×10^{-3} - 8×10^{-3}
-Below Water	82 - 88	2.5×10^{-3} - 8×10^{-3}
Sluiced in the Laboratory -Above Water	97 - 103	2×10^{-2} - 4×10^{-3}
-Below Water	90 - 97	2×10^{-2} - 4×10^{-3}

(Abu-Wafa, Hanna Labib; 1970, 1971; Hassouna et al., 1970; High and Aswan Dams Authority, 1969)

the water level achieved an average dry density of 85 pcf which is only about 90% of the minimum dry density value. A degree of sluicing at least that good or better, as indicated by the dry density of the sand, was considered acceptable for sluiced triaxial test specimens.

Laboratory sluicing tests conducted for the Aswan High Dam indicated that the use of sands and rockfills with a high value of sluiceability coefficient, C_s, would typically result in achieving a satisfactory degree of sluicing. A high value of sluiceability coefficient may not be readily achieved in the triaxial test, however, since size constraints are placed on both the material forming the gravel specimen and the sand used for sluicing the specimen. Unlike the screened rock gradation used in the Aswan High Dam, maximum particle sizes of materials tested in the triaxial test are limited to about 1/6 to 1/8 the diameter of the triaxial specimen. It is not the maximum particle size, however, but D_{10} which is used to define C_s. In order to maximize D_{10} and thus maximize C_s in the triaxial test, two requirements were placed on the gravel gradations used to construct triaxial specimens: (1) The largest acceptable particle sizes were used for both 2.8 inch and 12 inch diameter specimens; and (2) Uniform grain size distributions were established for the gravel.

C_s could also be increased by using a finer sluicing sand having a low value of d_{50}. However, it seems reasonable that only sands should be used as a sluicing material. Finer materials might introduce errors into the undrained strength test if the hydraulic conductivity of the material was so low that it caused localized excess pore pressure development. Additionally, finer materials might contribute a cohesional strength component to the cyclic load resistance of the

gravelly specimen. Thus, soils no finer than fine sands were used as sluicing materials for the tests described in this study. The grain size distributions and the material properties for the sands and gravels used in this thesis will be described in the following chapter.

Trial sluicing tests were performed in a clear lucite cylinder, 12 inches in diameter and 24 inches tall. Three different gravel gradations and two sluicing sands were used to conduct these initial tests. Gravel was placed in the lucite cylinder by the same methods that would be used to construct the triaxial test specimens. The cylinder was next filled with water in order to simulate below-water sluicing in the Aswan High Dam, and sluicing sand was added slowly to the top surface of the specimen. The sand settled through the gravel voids and accumulated in the voids at the bottom of the specimen. As sand was continually added to the specimen and the voids in the bottom of the specimen were filled, the upper surface of the sand progressed from the bottom of the specimen to the top. Sluicing was considered to be completed and no more sand was added to the specimen once the progressing sand front reached the upper surface of the gravel specimen.

The effectiveness of the sluicing procedure was evaluated by quantitative and qualitative methods. The dry density of the sluicing sand was determined by using a known mass of sand and calculating the volume of the gravel voids. Figure 5.9 shows the effective dry density of the sand sluiced into the voids of three different gravels with four values of sluiceability coefficient ranging from 12.5 to 50. The effective dry density is defined as the mass of the sand used for sluicing divided by the total volume of all the specimen voids whether

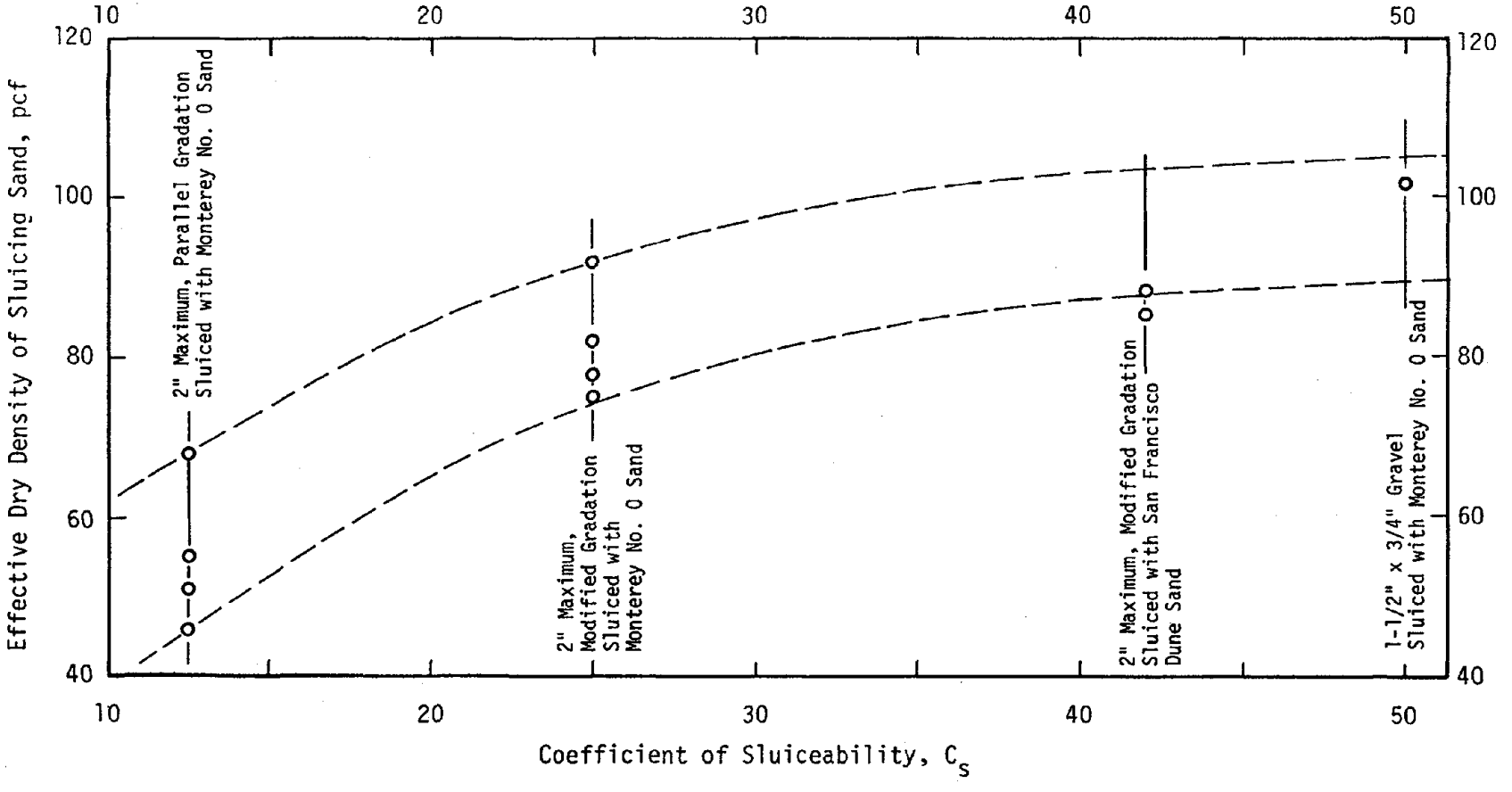

Figure 5.9 Results of Trial Sluicing Operations Showing the Relationship Between Effective Dry Density of Sluicing Sand and Coefficient of Sluiceability

or not they are completely filled with sand. It can be seen from this figure that by increasing the coefficient of sluiceability of the gravel/sand system, the quality of sluicing as assessed by the effective dry density is significantly improved. The average effective dry density of the sluicing sands varied with C_s as shown below:

C_s	Effective Dry Density, pcf
12.5	55
25	82
42	87
50	100

The minimum dry density of the Monterey No. 0 sand was determined to be about 89 pcf. Therefore, any value of effective dry density greater than about 81 pcf indicates that the gravel triaxial specimen is sluiced as thoroughly as the rockfill in the Aswan High Dam. Thus, it seems likely that any value of C_s greater than 25 should result in a satisfactory degree of sluicing being accomplished.

This study indicated that a laboratory triaxial specimen could be satisfactorily sluiced. The actual procedure followed in sluicing gravel triaxial specimens with sand will be described in the following chapter.

CHAPTER 6

TRIAXIAL TEST MATERIALS AND EQUIPMENT, AND SPECIMEN CONSTRUCTION PROCEDURES

Gravels

All of the gravels tested in this study were formed from a crushed granite obtained from Granite Rock Quarry of Watsonville, California. This material was actually derived from a hornblend gabbro-diorite deposit but it is generally called a granite at the Granite Rock Quarry (Bowen, 1986). Some of the gravel particles showed some slight evidence of hydrothermal alteration but all of the material was still hard and sound with a subangular shape. The specific gravity for this material was determined to be 2.78.

About 2000 pounds of crushed rock were obtained in assorted particle sizes and separated by sieving into discrete particle sizes ranging from 2 inch to #4, plus sand and fines. This material was stored in 55 gallon drums until such time as it was needed for triaxial testing. Gravel particles were taken from these drums in the appropriate sizes and quantities and mixed together in order to form the grain size distributions that were desired for testing.

Three different gravel grain size distributions were tested in 2.8 inch and 12 inch diameter triaxial specimens as listed below:

(1) A uniformly graded 3/8" x #4 gravel;

(2) A uniformly graded 1-1/2" x 3/4" gravel; and

(3) A 2" maximum, modified gradation gravel.

The grain size distribution curves for these gravels are shown as solid lines in Figures 6.1 & 6.2. The dashed line curves also shown in these figures indicate gravel gradations which were used only for maximum and

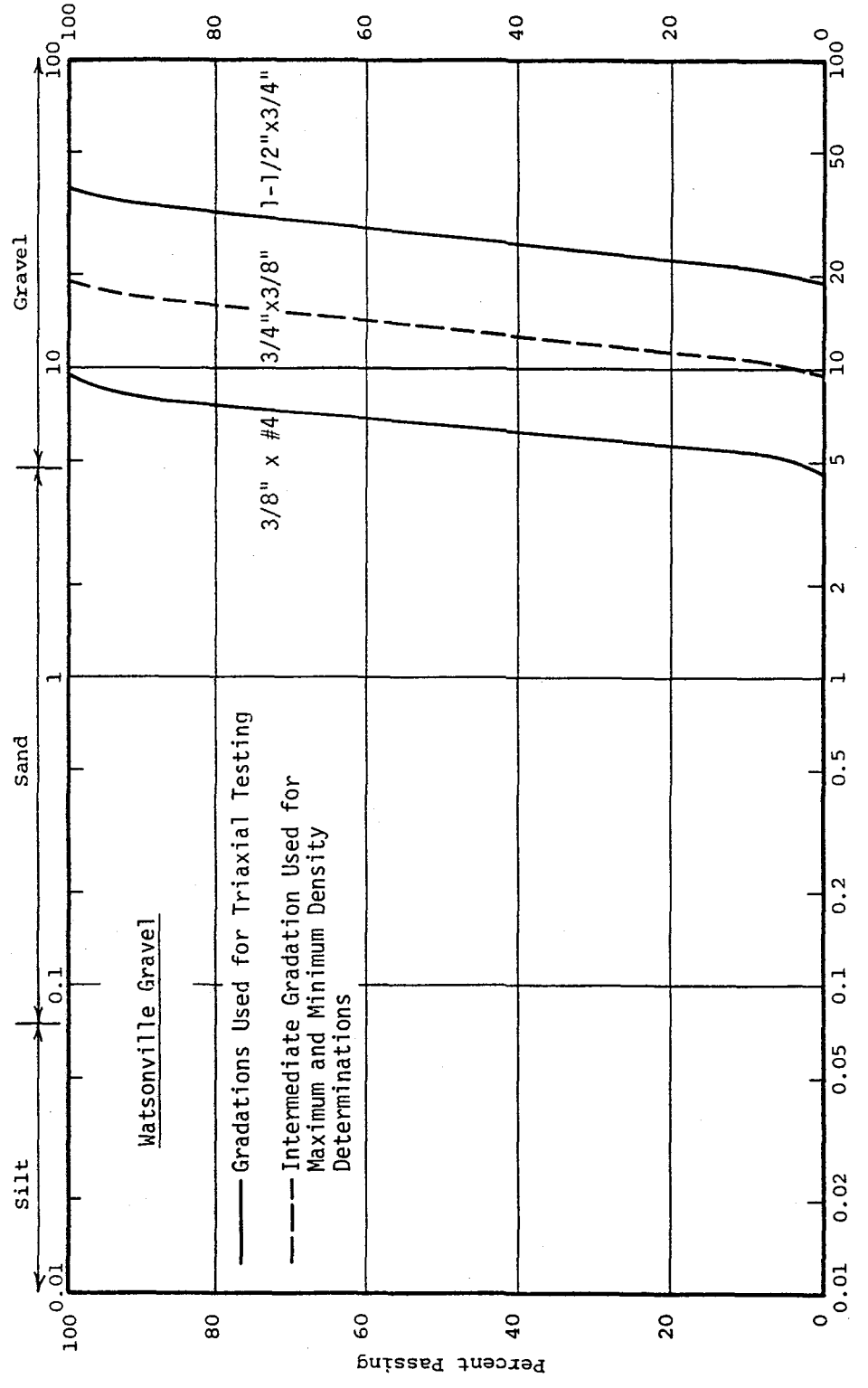

Figure 6.1 Grain Size Distributions for the Uniformly-Graded Gravels Tested in This Study

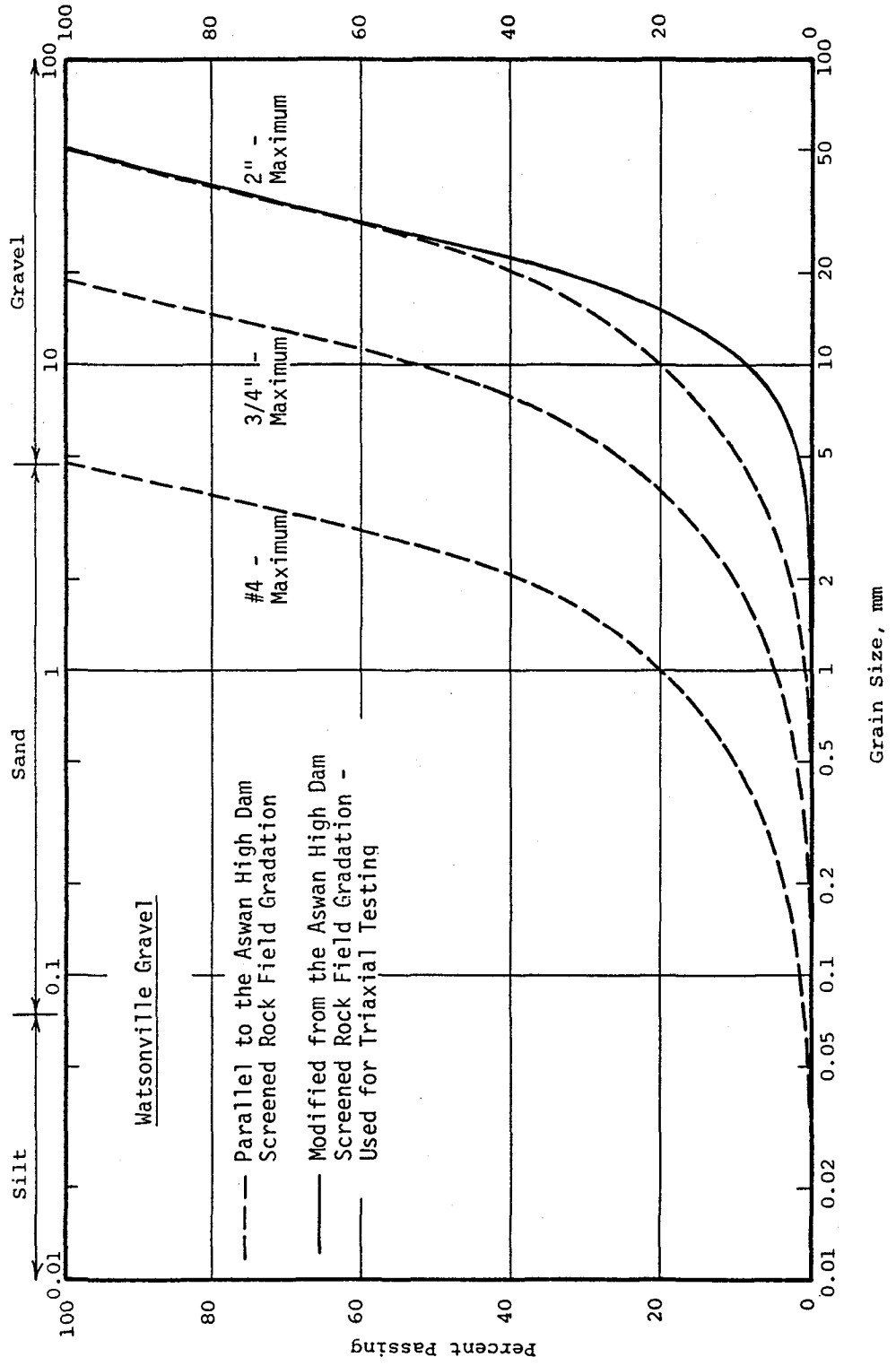

Figure 6.2 Grain Size Distributions for the Gravels Parallel to and Modified from the High Aswan Dam Screened Rock Gradation

minimum density determinations; no triaxial tests were performed on these materials. The 3/4" x 3/8" gradation material was used in order to define the maximum and minimum densities of the other two uniformly-graded gravels more precisely.

Originally, it was intended to use a 2" maximum particle size gradation that was parallel to the 40" maximum particle size Aswan High Dam field gradation for triaxial testing in this study. The grain size curves for this material and two parallel gradations are shown as dashed lines in Figure 6.2. This gradation was later modified, however, in order to increase the sluiceability coefficient of the gravel/sand system. This was accomplished by forming a new gravel gradation; the tail end of the original, parallel gradation curve was shifted to the right in order to form a more uniform material. This shift increased the value of D_{10} from about 5mm to 10mm and thus doubled C_s, thereby greatly improving the sluiceability of the gravel. The 2" maximum, modified gradation, shown as a solid curve in Figure 6.2, was used for the triaxial test program.

Maximum and minimum densities were determined for all of the various grain size distributions described above. The minimum density for all of these materials was determined by the lower result obtained from the two following methods:

(1) A quantity of material was placed in a tall cylinder of appropriate size, filling it no more than 1/3 to 1/2 full. The ratio of cylinder diameter to maximum particle size was at least eight. The cylinder was capped and then tumbled end over end and rolled along its length in order to thoroughly mix the material and achieve a very loose

state. The cylinder was then quickly yet carefully set upright and volume measurements were made to determine the dry density.

(2) Particles were carefully placed one or a few at a time into a cylindrical mold of known volume (0.5 ft^3 for the coarser gradation gravels containing particles greater than 3/4", and 0.1 ft^3 for the finer gradation gravels). The dry density was calculated when the cylinder was filled with soil level with the top of the mold.

The maximum density was determined using ASTM D-2049. The gravel specimens were vibrated both wet and dry in the appropriate size mold with various vibrating table amplitudes in order to determine the densest possible state. A second method used to determine the maximum density of the two coarser gravel gradations involved compacting material inside a 12 inch diameter triaxial specimen mold. A quantity of material that formed a lift about 4 inches high was deposited inside the mold. An 11 inch diameter circular vibrating plate was then lowered onto the surface of the material and the compactor was activated for about 3 minutes. Four to six additional lifts were compacted in the mold in the same manner before volume measurements were made and the dry density of the specimen was determined. This method typically resulted in higher maximum density values than those determined by ASTM D-2049. Grain size distributions were checked after these determinations to be sure that grain breakage was minimal.

The results of the maximum and minimum density determinations are plotted in Figures 6.3 & 6.4. Earlier studies (Becker et al., 1972) have shown that for parallel grain size distributions, lines defining the maximum and minimum density values are approximately parallel and the slope of these lines increases with increasing grain size. This

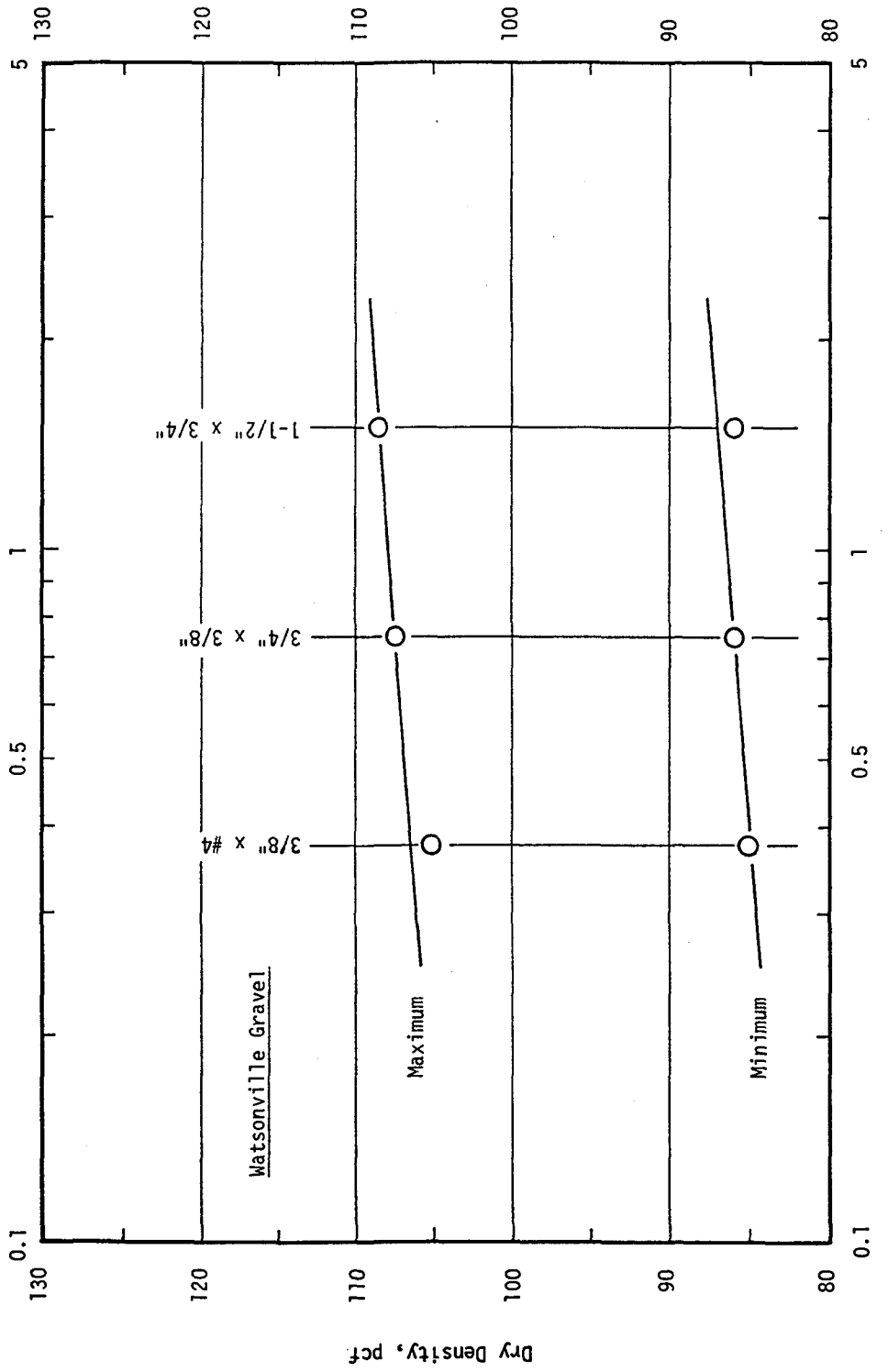

Figure 6.3 Relationship Between Maximum and Minimum Dry Densities and Maximum Grain Size for Three Uniformly-Graded Gravels

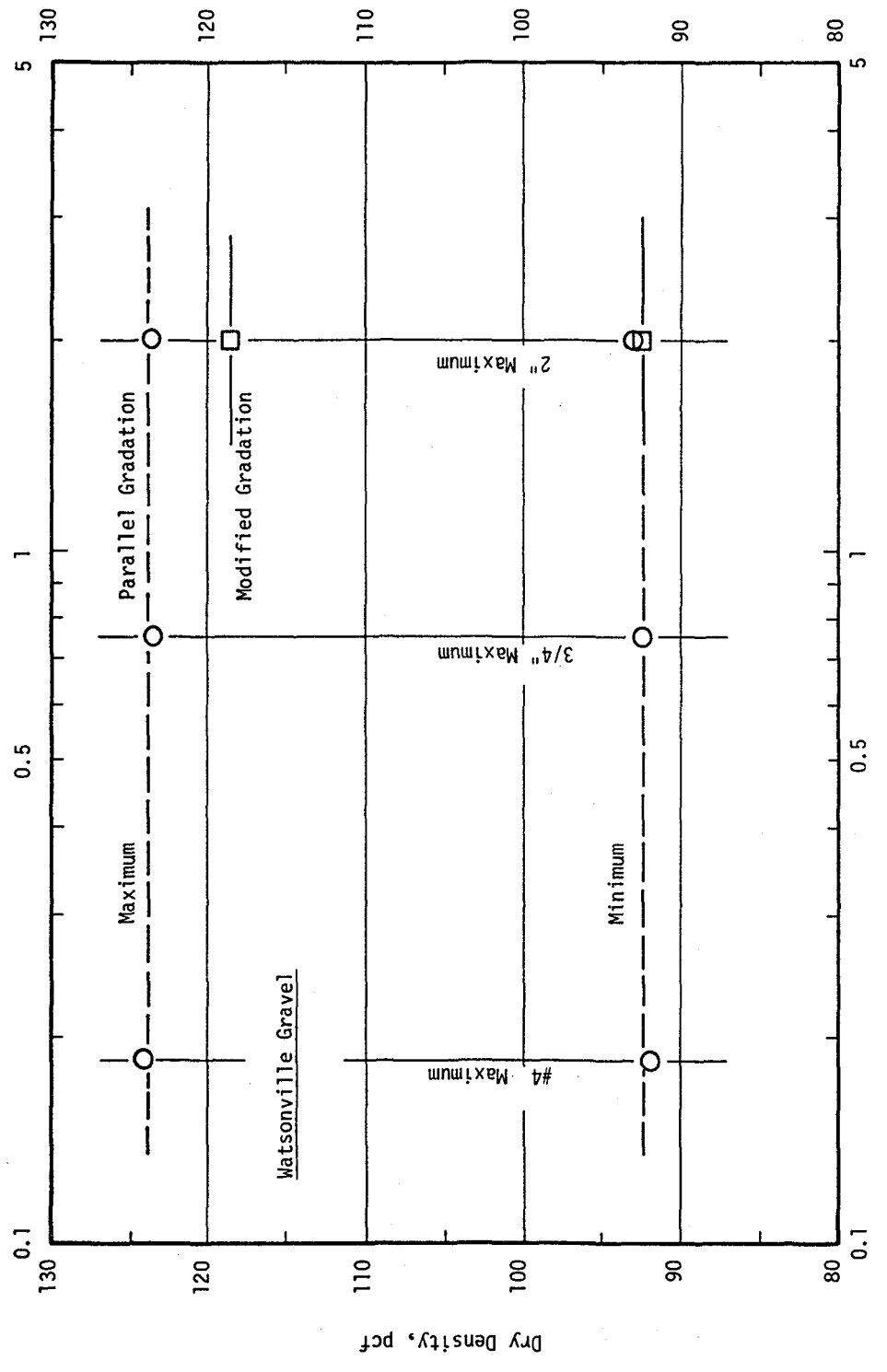

Figure 6.4 Relationship Between Maximum and Minimum Dry Densities and Maximum Grain Size for Three Parallel Gravels and the Modified Gradation Gravel

tendency was considered in defining the maximum and minimum densities used in this study.

The static strength envelope of the 3/8" x #4 grain size material was determined by a series of drained compression tests on 2.8 inch diameter specimens. The results of these tests are shown in Figures 6.5 and 6.6. The latter figure, after Leps (1970), shows the relationship between effective confining pressure and friction angle for various gravels compared to the 3/8" x #4 gravel used in this study. Gravel material properties are summarized in Table 6.1.

Sands

A number of different sands were used in this research including:

(1) Monterey No. 0 Sand;

(2) Monterey Fine Sand;

(3) San Francisco Dune Sand; and

(4) Banding Sand.

Grain size distributions and material properties for these sands are shown in Figure 6.7 and Table 6.2. The maximum and minimum density values presented in the table were determined using the same test procedures employed for the 3/8" x #4 gravel. Undrained, cyclic triaxial tests were performed on specimens of Monterey No. 0 sand (see Appendix A) in order to verify that various test parameters, such as rate of loading and sample size, did not significantly affect the cyclic loading resistance of the soil specimens. All of the other sands, along with Monterey No. 0 sand, were used only for sluicing gravel specimens.

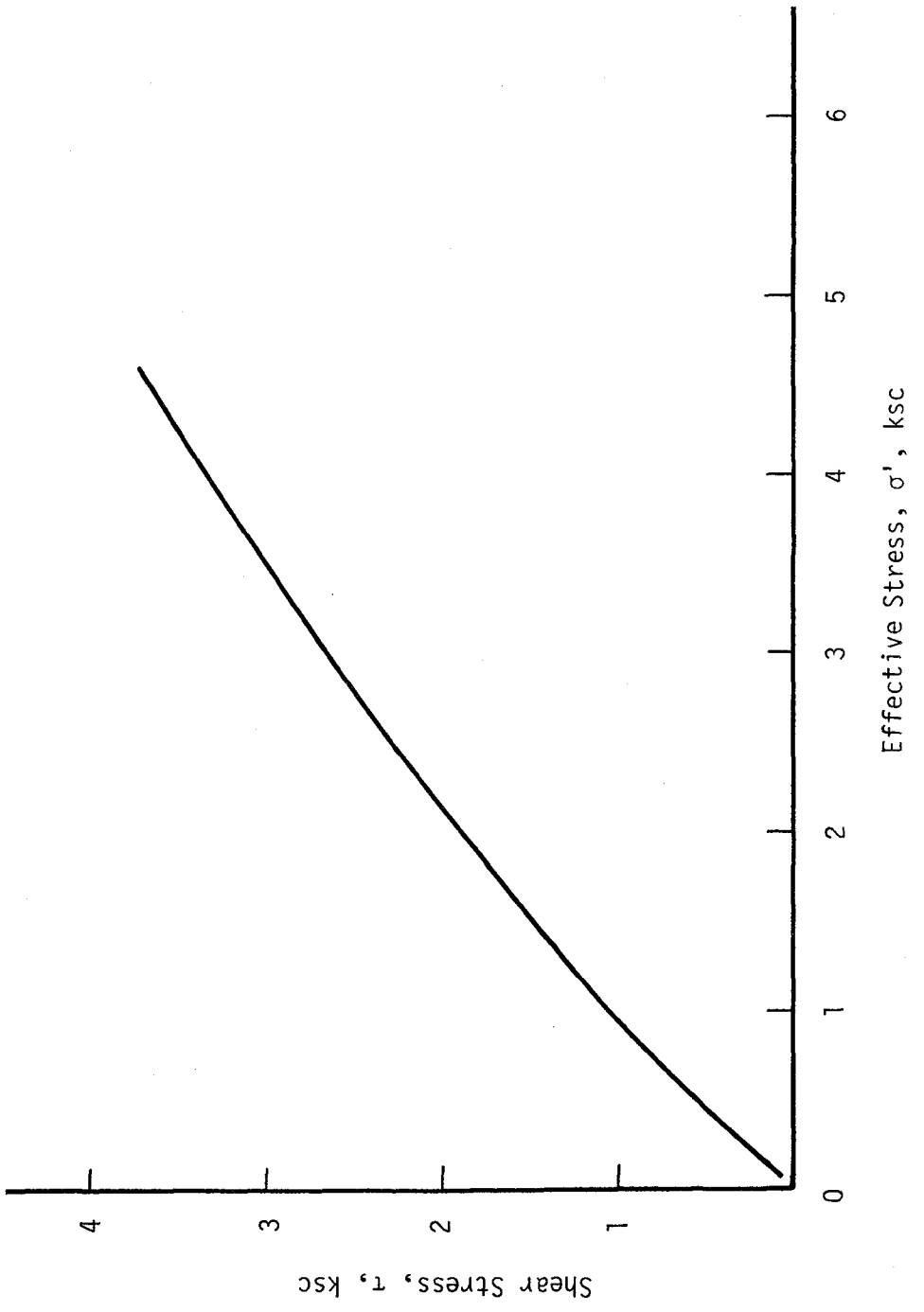

Figure 6.5 Static Failure Envelope for the 3/8" x #4 Watsonville Gravel

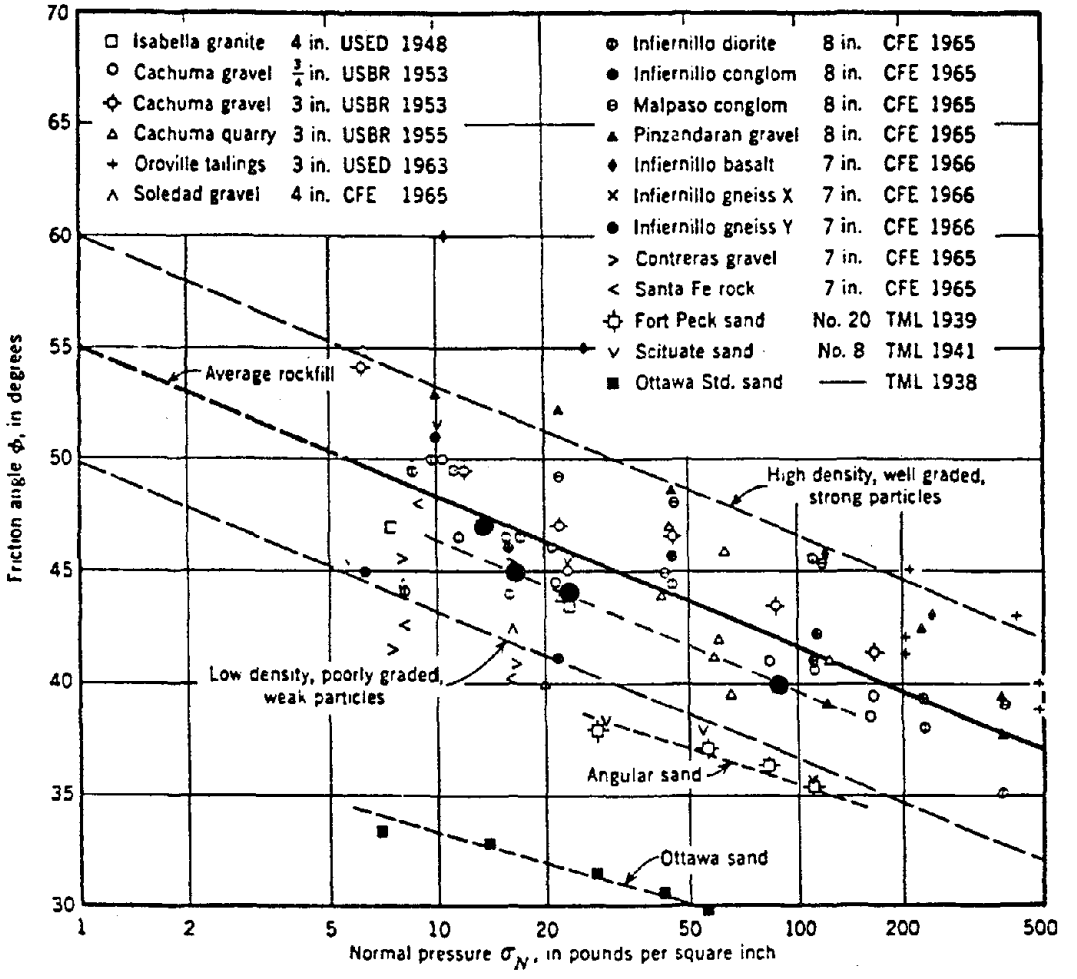

● - 3/8" x #4 Watsonville Gravel
2.8" Diameter Specimens

Figure 6.6 Relationship Between Effective Confining Pressure and Friction Angle for the 3/8" x #4 Watsonville Gravel Compared to Various Gravels (after Leps, 1970)

Table 6.1 Properties of the Gravels Used in this Study

WATSONVILLE GRAVEL

Material Description	D_{60}	D_{50} (mm)	D_{10}	G_s	γ_{max}	γ_{min} (pcf)	$\gamma_{max} - \gamma_{min}$	e_{max}	e_{min}	C_u
Uniform Gradation										
3/4" x 1-1/2"	28.0	27.0	21.0	2.78	108.5	87.0	21.5	0.992	0.597	1.3
3/8" x 3/4"	14.0	13.5	10.6	2.78	107.5	86.0	21.5	1.015	0.612	1.3
#4 x 3/8"	6.9	6.5	5.3	2.78	106.5	85.0	21.5	1.039	0.627	1.3
Modified Gradation										
2" Maximum	29.0	25.0	10.5	2.78	118.6	92.5	26.0	0.876	0.465	2.8
Parallel Gradation										
2" Maximum	29.0	25.0	5.0	2.78	124.0	92.5	31.5	0.876	0.400	5.8
3/4" Maximum	11.0	9.4	1.9	2.78	124.0	92.5	31.5	0.876	0.400	5.8
#4 Maximum	2.85	2.50	0.49	2.78	124.0	92.5	31.5	0.876	0.400	5.8

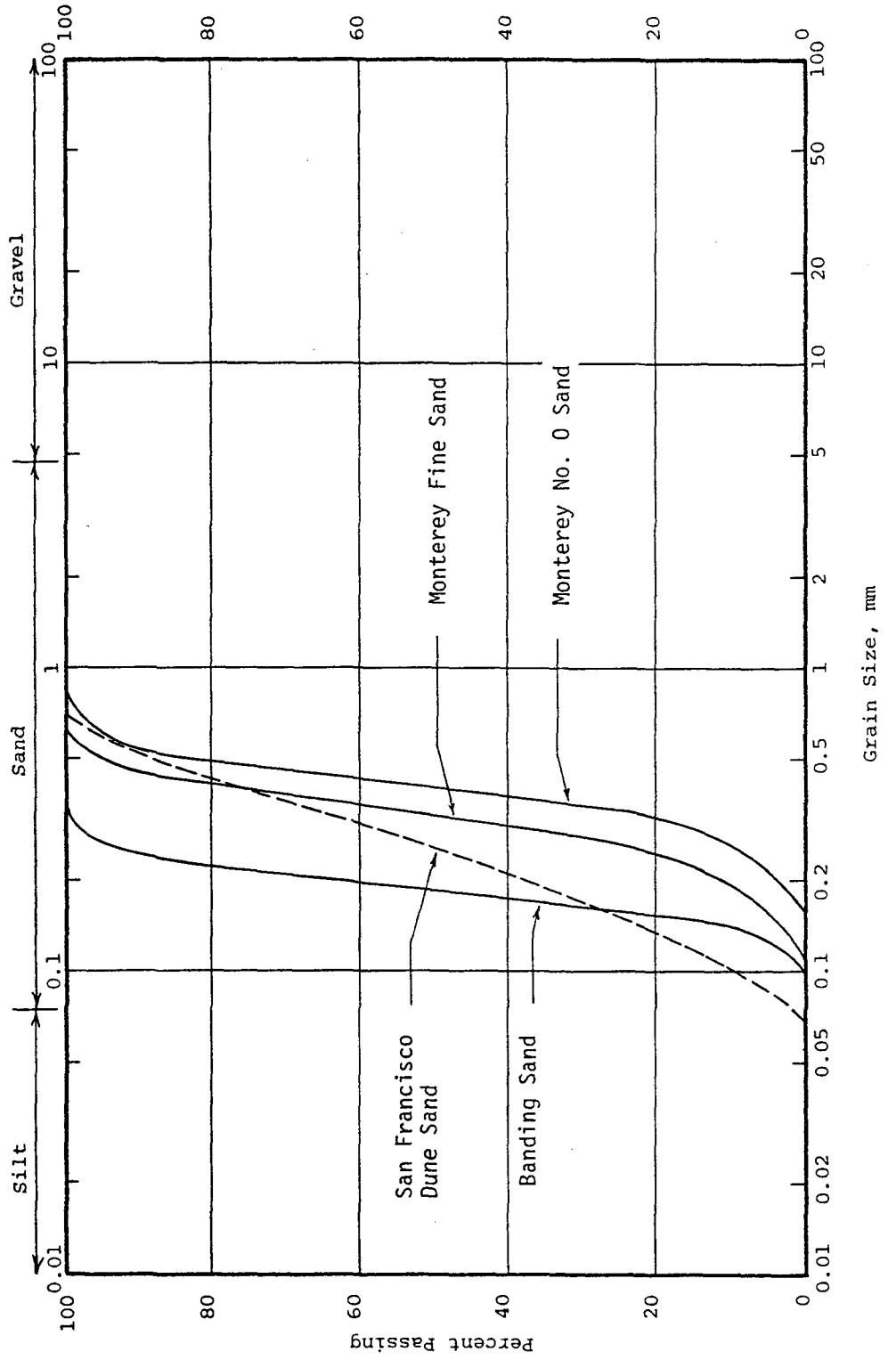

Figure 6.7 Grain Size Distributions for the Sands Used in This Study

Table 6.2 Properties of the Sands Used in this Study

SAND

Material Description	D_{60}	D_{50} (mm)	D_{10}	G_s	γ_{max}	γ_{min} (pcf)	$\gamma_{max} - \gamma_{min}$	e_{max}	e_{min}	C_u
San Francisco Dune	0.30	0.25	0.10	2.65*	115.0	92.4	22.5	0.790	0.439	3.0
Banding Sand	0.20	0.19	0.14	2.65*	112.0*	88.6	23.4	0.867	0.477	1.4
Monterey No. 0	0.44	0.41	0.26	2.65	108.0	89.0	19.0	0.859	0.532	1.7
Monterey Fine	0.35	0.32	0.20	2.65	-	-	-	-	-	1.8

* - indicates estimated values

Membranes

The properties of the membranes used in this study are obviously very significant since they influence the amount of membrane penetration volume change that occurs during consolidation. The subject of membrane penetration volume changes, together with membrane axial load corrections and a suggested membrane compliance correction based on volume changes, is presented in detail in Chapter 9.

The membranes used for testing the 2.8 inch diameter specimens were obtained from 3-D Polymers of Gardena, California. These were latex rubber membranes, 2.70 inches in diameter, 9 inches tall and 0.012 inches thick. Young's Modulus for this material is about 195 psi (Baldi and Nova, 1983).

The membranes used for testing the 12 inch diameter specimens were obtained from the American Rubber Manufacturing Co. of Emeryville, California. These membranes were constructed of black tire-tread stock and were about 0.1 inches thick, 36 in. tall and 12 in. in diameter. Young's Modulus for this material is about 500 psi (Banerjee et al, 1979).

Several 12 inch diameter test specimens were confined by two thin latex rubber membranes, about 0.025 inches thick, rather than the single, 0.10 inch thick tire-tread stock membrane. Differences in cyclic loading resistance for specimens confined by the two different membrane systems were small indicating that membrane compliance effects were not significantly influenced by variations in the membrane systems for the 12 inch diameter test specimens. Therefore, the single, thicker membrane was used for the majority of the 12 inch diameter tests that were performed. However, membrane penetration was more

easily observed in photographs taken using the lighter color, thinner membranes, thus, photographs of specimens confined by the two thinner membranes were shown previously in Figures 5.1 and 5.2.

Specimen Construction Procedures

Two basic types of gravel specimens, sluiced and unsluiced, were tested in this study, both with some minor variations during the testing program. Unsluiced specimens were set up in the manner typically used for sand or gravel specimens. The general procedure employed is outlined below:

(1) Install a rubber membrane on the lower end platen;

(2) Assemble a rigid sample mold around the membrane and attach the membrane to it;

(3) Evacuate the air between the mold and the membrane;

(4) Place the gravel material inside the membrane using one of several placement techniques which will be described in the following paragraphs;

(5) Level the top of the specimen and install a top platen;

(6) Fix the membrane to the top platen and apply a full or partial vacuum to the inside of the membrane; and finally,

(7) Remove the sample mold and assemble the triaxial cell for testing.

Most of the samples of the two uniformly graded materials (3/8" x #4 & 1-1/2" x 3/4"), both 2.8 and 12 inch diameter, were prepared by pluviating the gravel particles through air in order to achieve a low relative density. A tube which fit inside the sample mold and membrane was equipped with a series of baffle screens which acted to distribute the particles uniformly over the sample area and reduce the height of

fall of the particles (Mulilis et al., 1975, 1977). Gravel particles were poured into the top of the tube and allowed to rain through the tube and screens to form a specimen. The tube was raised as the sample grew in height in order to maintain a constant height of fall. This construction procedure resulted in samples of uniform density throughout their height. Sample density was varied from one sample to the next either by raising or lowering the tube and screen arrangement thereby changing the height of fall of the particles or by adjusting the rate of flow of the material into the tube. Densities were increased by increasing the height of fall of the particles or by decreasing the rate of flow of material through the tube. The opposite procedures resulted in specimens with lower densities. The method of pluviation described above was generally suitable for preparing samples in the range of 30% to 60% relative density. Other methods were required to construct either denser or looser specimens.

Some 12 inch diameter specimens of 1-1/2" x 3/4" gravel were prepared to 20% to 25% relative density. This was achieved by gently placing a few particles at a time into the sample mold using a small scoop.

Some 2.8 inch diameter specimens of 3/8" x #4 gravel were compacted to values over 60% relative density by placing the material in six individual lifts and tamping the surface of each lift until the desired density was achieved.

12 inch diameter samples of 2" maximum, modified gradation material were prepared by placing the material in six individual lifts. The material for each lift was placed into a special "bottom dump" bucket and thoroughly mixed by mechanically rotating the bucket for 3

minutes. The bucket was carefully set upright in order to minimize particle segregation and then lowered into the sample mold to the desired distance above the bottom platen or the top of the previous lift. The hinged bucket bottom was then tripped open thus allowing the material to fall into the specimen mold. By a trial and error procedure, a height of fall of 12 inches was determined to result in forming specimens with the desired relative density value of about 40%.

Specimen Sluicing Procedure

Samples which were going to be sluiced were prepared in exactly the same manner as unsluiced samples. The specimen forming mold was set-up and the gravel specimen was constructed using the method which resulted in specimens of the desired relative density. The procedure varied beyond this point, however, in that, before the top platen was installed, the gravel "skeleton" was sluiced with sand.

Sluicing was accomplished by first filling the gravel voids with water and then adding sluicing sand to the surface of the gravel sample. Provided that C_s (i.e.: D_{10}/d_{50}) is sufficiently large, the sand flows into the sample voids by gravity forces alone. This process was sometimes supplemented by opening the bottom drainage port and allowing a small gradient to develop. As sand accumulated in the specimen voids, however, the gradient was reduced to a very small value and consequently had negligible effect on compacting sand in the voids. Thus, it was not a routine part of the sluicing procedure. Sand was added to the top of the specimen until no more would be accepted into the sample. However, this does not necessarily mean that all of the gravel sample voids were filled, only that all of the accessible voids

were filled with sand. In fact, all of the skeletal voids were not filled as will be shown later in this chapter.

Since the objective of this study was to perform triaxial tests on gravel specimens, whether they were sluiced or unsluiced, care was taken so that no excess sand was added to the top of the specimen. A layer of sand over the topmost gravel particles, no matter how thin, was considered unacceptable. Sand was added to the point where it would just contact the top platen when it was put into place and the tops of the gravel particles were still visible in the sand.

Since the objective of sluicing the gravel specimen was to minimize membrane penetration, only the peripheral sample voids, those adjacent to the confining membrane, were required to be filled with sand. Filling of the interior sample voids occurs naturally as part of the sluicing process and is considered to have no influence on test results as will be discussed in later chapters. In order to aid in filling the peripheral sample voids, the outside of the sample mold was tapped lightly while adding the sand. For 12 inch diameter samples, a light rubber mallet was used, while for 2.8 inch diameter samples, a thin 6 inch long steel rod was used to tap the specimen mold. The height of the gravel skeleton was checked before and after sluicing on several samples to determine that the light tapping did not change the height of the sample and thus did not disrupt the gravel particle arrangement. It should be noted that the loosest gravel specimens had relative densities of about 25% and most were over 40%. The sand used for sluicing, on the other hand, was very near zero relative density because of the method of deposition. The sand was pluviated gently through water and followed a tortuous path through the gravel skeletal

voids resulting in a very loose structure. Consequently, even very light tapping helps to densify the sand in the peripheral voids while significantly harder tapping is required to change the density of the gravel skeleton.

Even with some special effort, it is not possible to fill all of the sample voids. However, it is convenient to assume that the voids are filled when evaluating the quality of the sluicing effort for a series of test specimens. By dividing the mass of the sluicing sand by the total volume of the gravel skeletal voids, one can compute the effective density of the sand. Figures 6.8 & 6.9 show the resulting effective dry density of the Monterey Fine sluicing sand sluiced into specimens of 3/8" x #4 gravel, and San Francisco Dune sand sluiced into specimens of 2" maximum, modified gradation gravel respectively. It may be seen from these figures that, in general, the sand achieves a higher effective dry density in the gravel specimens with a looser structure because the voids here are more open and continuous throughout the specimen. For gravel specimens with a denser structure, the void spaces are less open and continuous, and the sluicing sand achieves a lower effective dry density. These figures indicate that a true measure of sluiceability should consider not only particle size ratios (i.e.: $C_s=D_{10}/d_{50}$), but also the degree of compaction of the gravel skeleton.

Gravel Specimens with an Annular Sand Shell

In the initial phase of this study, it was decided to investigate the effects of a thin annular sand shell constructed around the outside of the confining membrane for the gravel specimen. It was believed that the presence of this shell might serve to prevent the penetrated

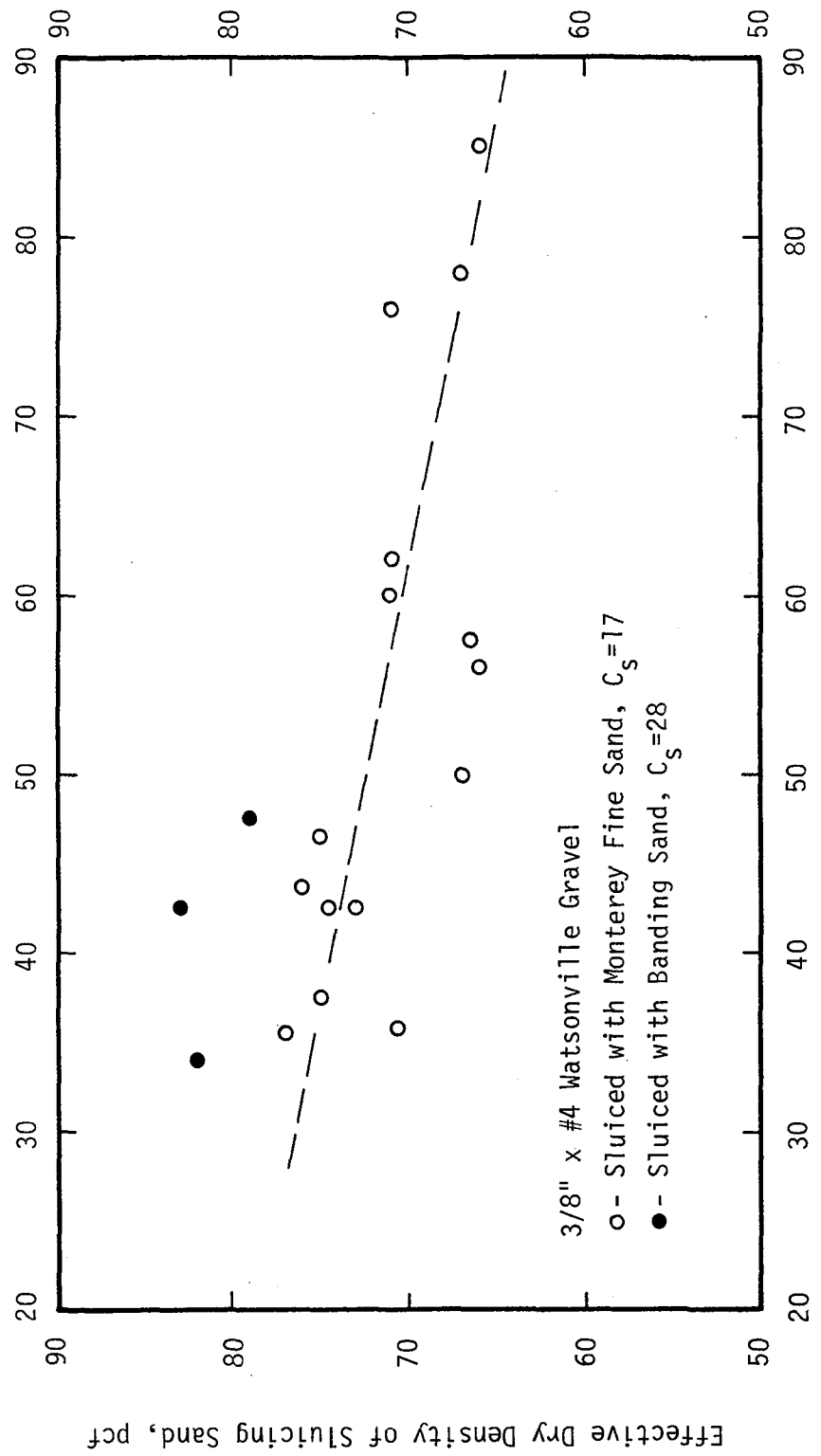

Figure 6.8 Relationship Between Effective Dry Density of the Sluicing Sand and Gravel Relative Density for 2.8" Diameter Specimens

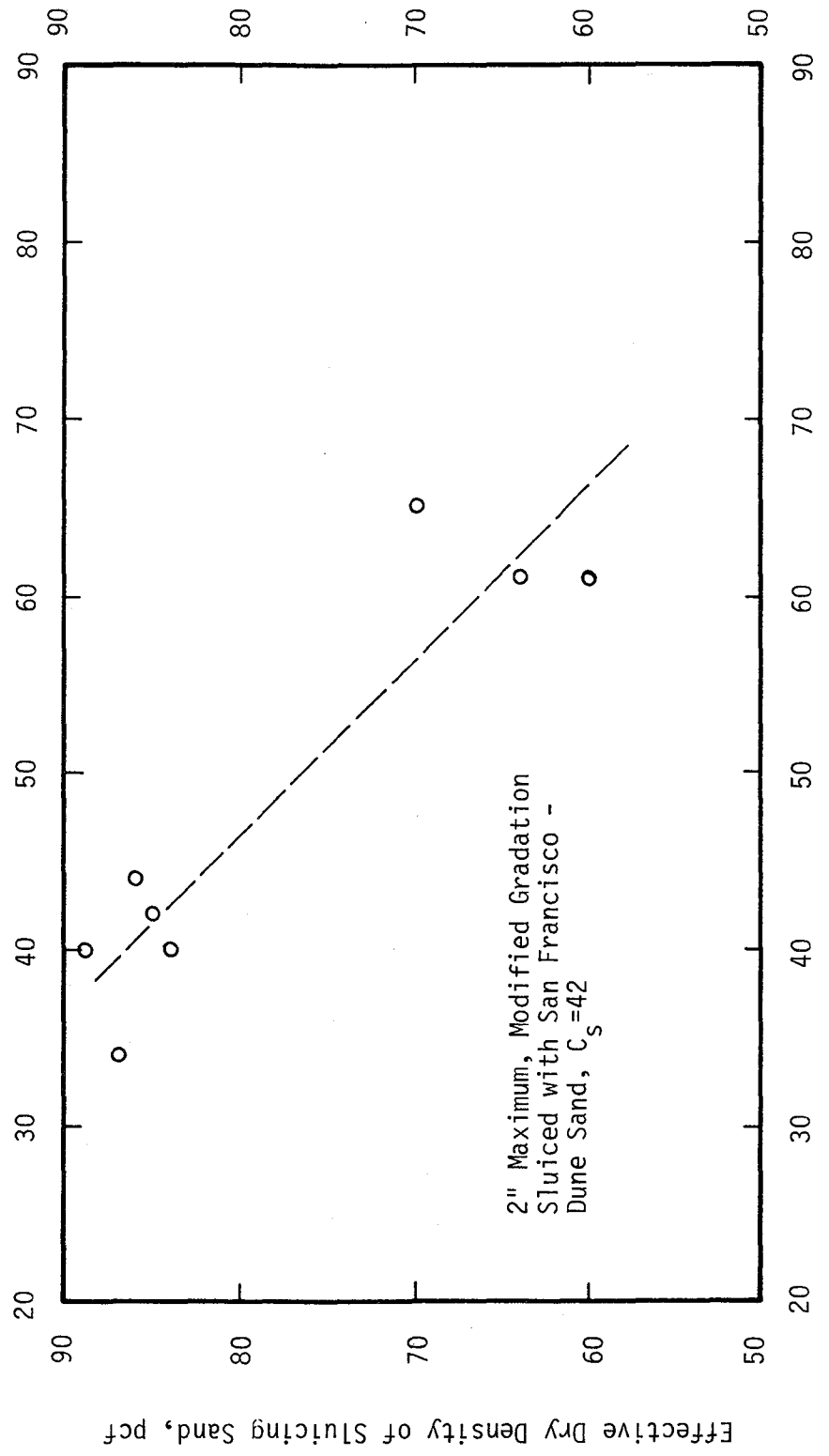

Figure 6.9 Relationship Between Effective Dry Density of the Sluicing Sand and Gravel Relative Density for 12" Diameter Specimens

membrane from rebounding during undrained cyclic loading. Such specimens were constructed as follows:

(1) The gravel specimen was constructed to the structure and state desired for testing, the top end platen was installed and attached to the membrane, and a full vacuum was applied to the specimen drainage line. As a result of the applied confining pressure, the membrane penetrated into the surficial specimen voids.

(2) A second membrane, about 0.025 inches thick, was installed around the outside of the 12 inch diameter specimen and sealed to the lower end platen. A 13 inch diameter forming mold was then constructed around the outer membrane and attached to the top of the membrane.

(3) The 1/2 inch thick annular space between the two membranes was filled with water in order to keep the space open, and then Monterey No. 0 sand was poured into the annulus through the opening in the top of the mold. When construction of the shell was completed, the top of the outer membrane was attached to the upper end platen, a partial vacuum was applied to the shell drainage line, and the forming mold was removed.

A cross-section of the gravel specimen and sand shell is shown schematically in Figure 6.10. Both the specimen and shell had separate drainage lines so that the effective pressure of both components could be independently controlled. All specimens were initially consolidated under an effective confining pressure of 2.00 ksc and then cyclically loaded in an undrained condition. As excess pore pressure was generated in the specimen, the effective confining pressure was reduced from its initial value to a value that approached zero at initial liquefaction. However, the effective confining pressure of the sand

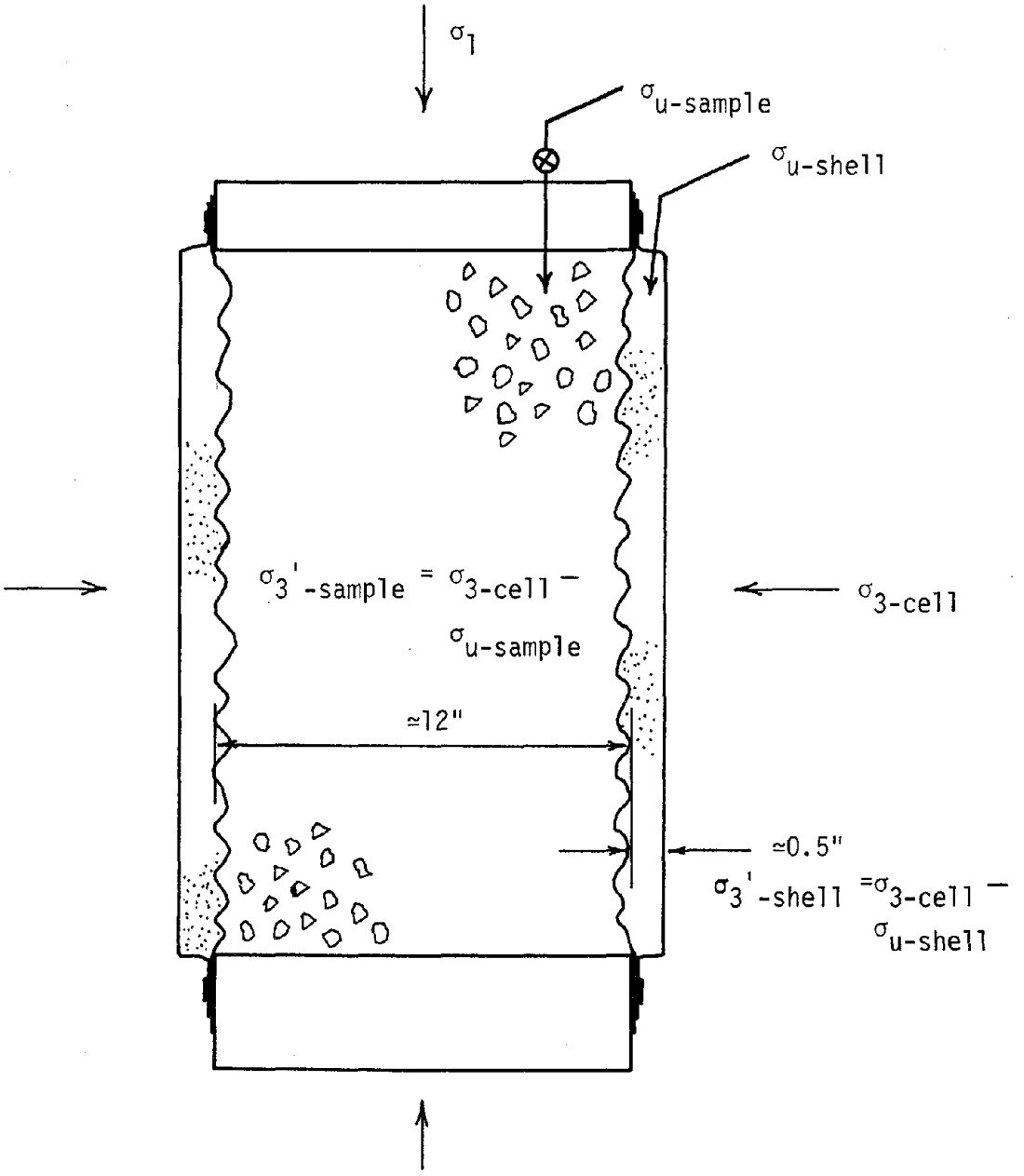

Figure 6.10 Schematic Diagram of a Gravel Specimen with an Annular Sand Shell Constructed Around the Perimeter

shell was maintained at a constant value of 0.25 ksc during the entire test.

Undrained, cyclic load tests were performed in the usual manner on gravel specimens with sand shells constructed as described above. A correction to the results of these tests was applied to account for the portion of the applied cyclic load that was carried by the sand shell. Such corrections were made by assuming that the strength of the sand was fully mobilized during each load cycle with an effective friction angle, ϕ', equal to 33^{o} (Lade, 1972). The stress state of the shell was calculated by using the following formula:

$$\sin \phi' = (\sigma_1' - \sigma_3')/(\sigma_1' + \sigma_3').$$

For $\phi' = 33^{o}$ and $\sigma_3' = 0.25$ ksc, the axial stress in the sand shell, $\sigma_{1'shell}$, was calculated to be equal to 12.05 psi. The average cross-sectional area of the sand shells was about 18 square inches. Thus, the portion of the applied cyclic load that was carried by the sand shell, L_S, was computed as:

$$L_S = 18 \text{ in}^2 \times 12.05 \text{ psi} = 217 \text{ pounds}$$

(i.e., about 12% to 16% of the total applied axial load).

The load value calculated above was subtracted from the measured value of the total applied axial load so that the corrected cyclic stress ratio felt by the gravel specimen, $\sigma_d/2\sigma_{3c}$, was calculated as:

$$\sigma_d/2\sigma_{3c} = [(L_A - L_S)/A_G]/2\sigma_{3c}$$

where L_A is the applied load as measured by the load cell,

L_S is the load carried by the sand shell as computed above, and

A_G is the cross-sectional area of the gravel specimen.

TRIAXIAL TESTING EQUIPMENT

Laboratory Equipment

The geotechnical engineering laboratory on the campus of the University of California at Berkeley is maintained at a constant temperature at all times to prevent temperature change which may affect soil-water interaction in test specimens, or general laboratory and electronic equipment used in long-term tests. The laboratory is served by a house air compressor which is capable of providing a steady pressure supply of approximately 6.5 kilograms per square centimeter (ksc). A house vacuum pump is capable of providing a steady vacuum supply of about 0.75 ksc and a portable vacuum pump was also available which was capable of developing a vacuum pressure of about 0.95 ksc. A de-aired water reservoir, filled by spraying a fine mist of water through a cylinder under house vacuum and maintained under vacuum, provides de-aired water for general laboratory use. Supplemental de-airing was accomplished with the use of the portable vacuum pump before the water was used to saturate specimens. The laboratory also contains standard laboratory support equipment such as drying ovens and scales in addition to the more specialized triaxial test equipment that is described below.

2.8 Inch Diameter Triaxial Testing Equipment

General

All 2.8 inch diameter triaxial tests performed in this study were performed using an automated version of the CKC electro-pneumatic (e/p) loading system (Chan, 1981; Li et al., 1986). Testing with this system requires that the operator set up the specimen, choose the

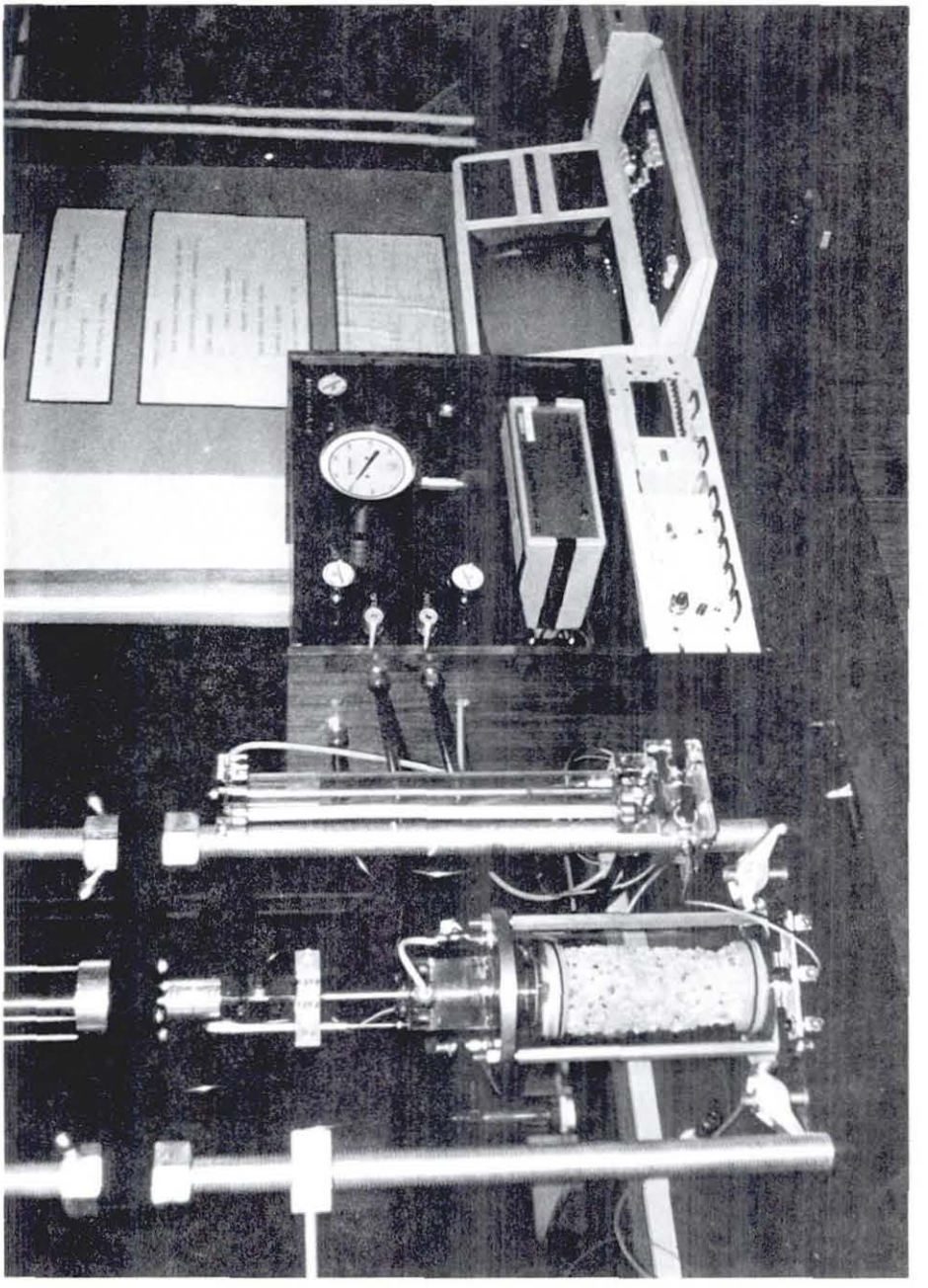

Figure 6.11 Photograph of the CKC Automated Triaxial System

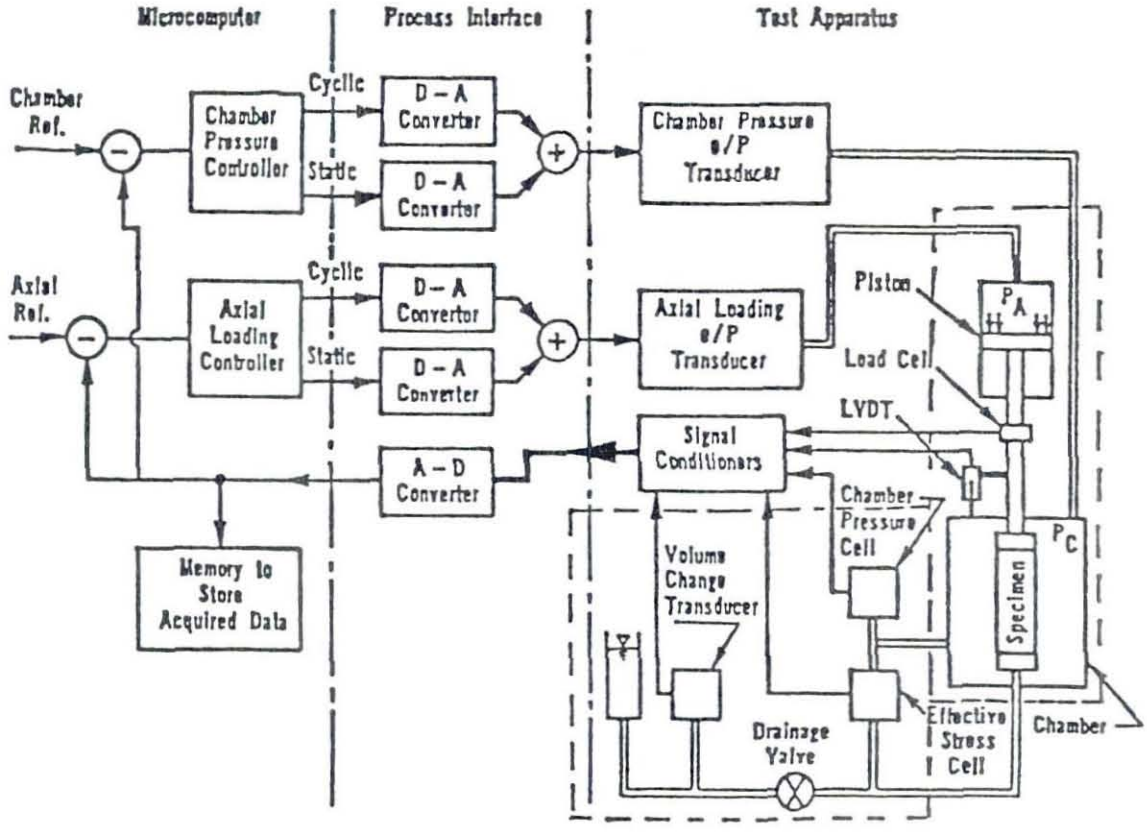

Figure 6.12 Schematic Diagram of the Automated Triaxial System (after Li et al., 1986)

desired mode of testing, answer the prompts, and then start the test with the computer. The computer automatically controls and runs the test, collects and stores the data, and calculates and plots the results. A photograph and a schematic diagram of the automated system are shown in Figures 6.11 and 6.12, respectively.

The system is capable of performing either stress or strain controlled loading, or various types of stress-path loading under both drained and undrained conditions. Both static and dynamic loading tests may also be performed. The tests are controlled by a microcomputer which determines the magnitude and frequency of the electronic signals that are generated and sent to the e/p transducers which, in turn, control pneumatic amplifiers for the application of lateral or axial loads. All but one of the available modes of loading is controlled by a closed-loop feedback scheme. The cyclic, stress-controlled loading mode used in this study was not controlled by a closed-loop feedback scheme since it was desired to apply sinusoidal loadings at a rate up to one cycle per second. This loading rate was too fast for the computer to control precisely with a closed-loop scheme, thus the desired loading piston pressures were predetermined by the computer and then applied via the e/p transducers. Load cell output data was collected during the test in order to verify that the desired cyclic loads were actually applied.

Controller

The automated triaxial system has two independent feedback loops for control of the axial and lateral e/p transducers which may be operated individually or in a synchronized manner. A block diagram of the axial feedback loop is shown in Figure 6.13. It may be seen from

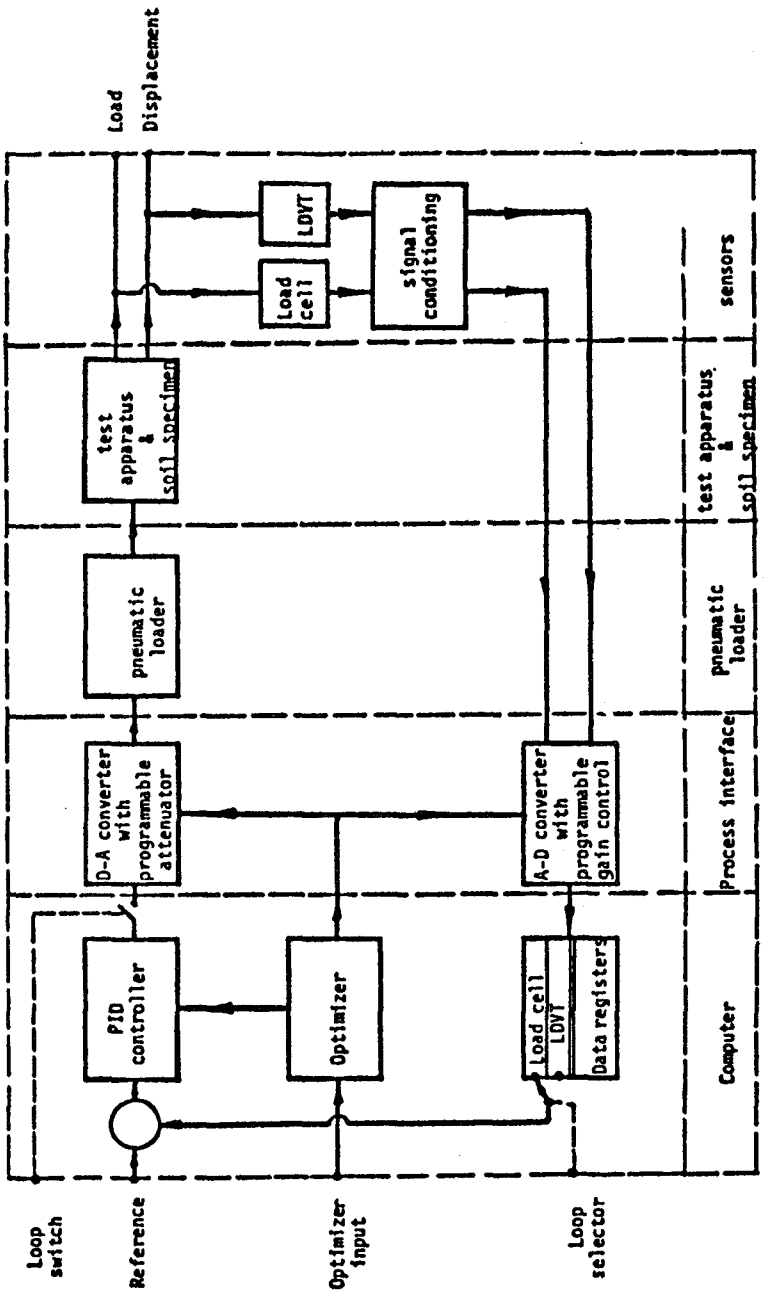

Figure 6.13 Block Diagram of the Loading System (after Li et al., 1986)

this figure that four control parameters are needed to specify the operation of the loop: (1) The Loop Switch either turns the feedback path on or off; (2) The Loop Selector determines whether load or displacement control will be used; (3) The Reference specifies the expected value of the selected control mode; and (4) The Optimizer adjusts the dynamic range of the analog to digital (A-D) converter. A high degree of testing flexibility can be achieved by properly selecting the parameters for each control loop. The major parts of the control loop are shown in Figure 6.13 and comprise a computer, a process interface unit, a pneumatic loader, the testing chamber, and various electronic sensors. A description of each of these various units is given below.

Computer and Software

A Radio Shack TRS 80 Model 4 microcomputer with two disk drives controls the automated system. It receives and stores the real-time data in its memory and sends electronic control signals to regulate the testing process. Through the keyboard and the display screen, the computer provides the means for effective interaction between the operator and the testing system. The computer also performs other functions such as data reduction, data processing, etc. An Epson FX-80 printer is used to record the output from the system. It prints out hard copies of test results in tabular and/or graphic form.

A software package has been developed by Li et al. specifically for use with the automated testing system. The programs are interactive, providing prompts which guide the operator through each phase of the test. Programs are available for controlling the following test operations:

- Back Pressure Saturation and B-Value Check;

- Consolidation - Isotropic, Anisotropic, and K_o;

- Shear Loading - Stress or Strain-Controlled,
  - Drained or Undrained;

- Stress Path Loading;

- Cyclic Loading - Stress or Strain-Controlled,
  - Loading Rates up to 1 Hz,
  - Sinusoidal or Triangular Wave Forms;

- Customized Loading;

- Data Retrieval and Plotting.

The software package is organized into three main function blocks: Calibration, Test, and Plot. The Calibration program may be used to update the input values of the calibration coefficients of the five sensors. Any minor changes in the sensitivities of these instruments may be determined by periodic calibration and then may be input into the computer by using this program. The Test control block is organized into three subgroups as follows: (1) Test management, system optimization, and load control; (2) Data acquisition and storage; and (3) Real-time data display via a digitized, multichannel display or, for most test modes, a high resolution graphics display. The Plot program loads test data, converts the data to any one of 20 quantities commonly used for plotting geotechnical engineering data, and generates X-Y plots of the desired quantities for viewing on the display. Display plots may then be sent to the dot-matrix plotter, if desired. Both logarithmic and linear scales are available using either automatic scaling or user specified scaling. Also, data may be conditioned using three levels of smoothing, and specific portions of the data may be enlarged for viewing in greater detail.

Process Interface Unit

The process interface forms the communication link between the computer and the loading system. The unit consists of a 16-channel, 12 bit, high speed A-D converter, an 8-channel, 12 bit, high speed D-A converter and a 24-channel digital input/output port. The D-A converter channels can also be configured as gain controllers to suit specific purposes of a designed system.

Seven channels of the A-D converter are used in the automated triaxial testing system - five channels are used to monitor the signals from the five sensors provided with the system; one is used to indicate whether the test conditions are drained or undrained; and the other is grounded as a zero reference to minimize the zero shift of the system. The digital input/output port is not used in this system.

Loading System

The dual channel e/p system is used to convert the computer-generated command electronic signal to pneumatic pressure, which then applies the axial load and the lateral pressure. The entire loading system is shown schematically in Figure 6.14. The e/p transducer operates essentially by balancing the force on the torque bar caused by the pressure at the end of a nozzle acting against the electronically controlled moving coil. The back-up pressure is then amplified by a pneumatic relay and a volume booster in order to perform the desired loading. A test gage is used to monitor the pressures being generated by the e/p transducers (i.e., the cyclic and lateral pressures), or controlled by the regulators (i.e., the steady and back pressures). A supply of clean, dry compressed air is required to operate the system.

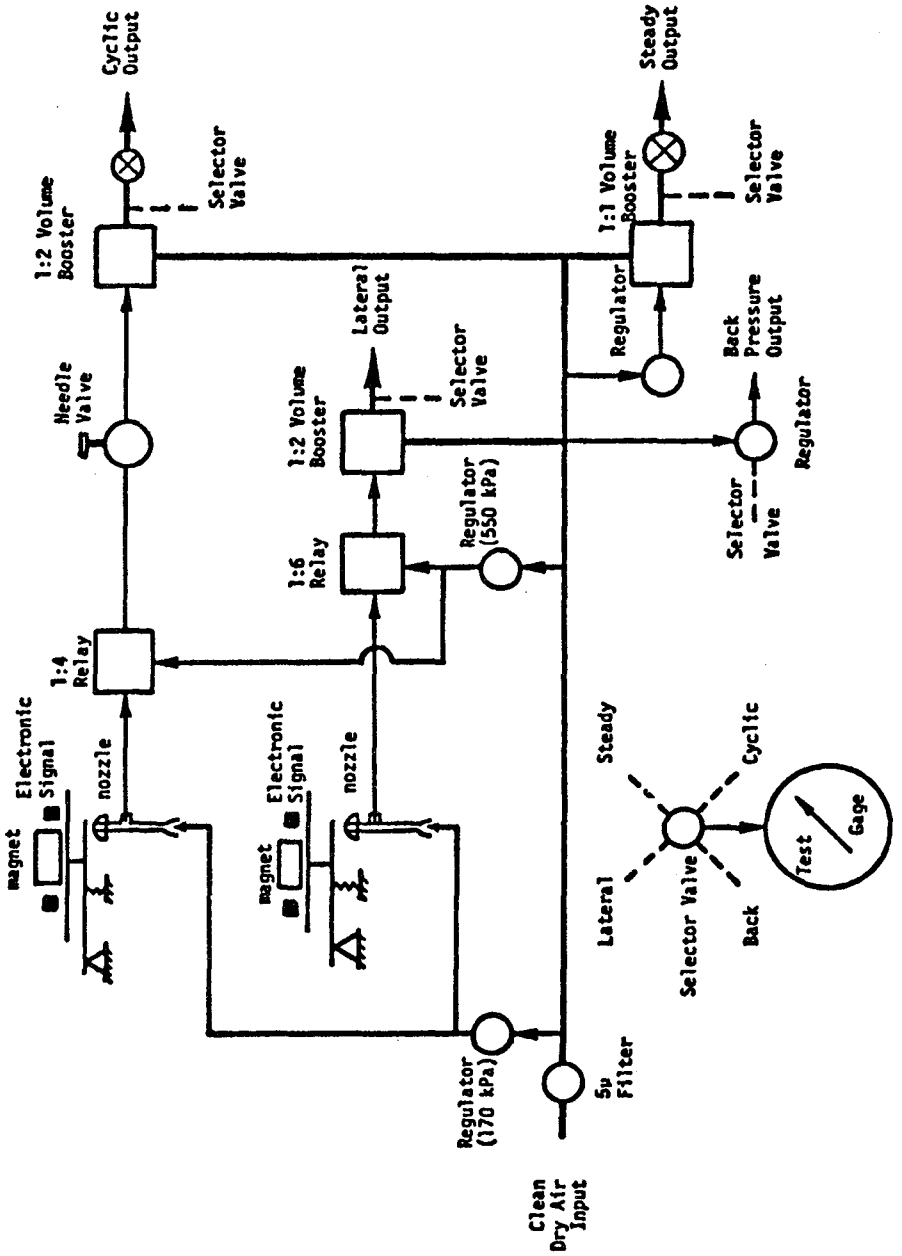

Figure 6.14 Schematic Diagram of the Loading System (after Li et al., 1986)

The load frame consists of two 1-1/2 inch diameter posts with an adjustable height crossbar and a flat base plate. The double acting (push/pull) pneumatic loader may be a bellofram type or similar low friction seal system on the piston and the rod. An oil filled loader may also be used for strain controlled testing of strain softening specimens. The actuator that was used for the tests described in this study was a low friction and low mass pneumatic loader designed specifically for use in stress-controlled dynamic testing of weak specimens. A rather flexible coupling device is used to connect the guided loading rod and the guided triaxial rod to allow for minor misalignment of the system. Hold down clamps for the triaxial cell are threaded into the base plate.

Triaxial Chamber

The triaxial cell used in this study is capable of testing 1.4 and 2.8 inch diameter specimens up to a chamber pressure of 100 psi with a clear acrylic chamber or 200 psi, if an optional aluminum chamber is used. The cell was built by the Civil Engineering machine shop at the University of California, Berkeley with the latest low-friction piston rod seals, three external tie rods, and straight through-tube fittings on all pore fluid lines.

This cell was designed to allow drainage (or pore pressure measurement) at the top and/or bottom of the sample during sample saturation, consolidation, and testing. During this investigation, drainage from the top of the sample was always used to aid in specimen saturation. The walls of the chamber consisted of a 1/4 inch thick, clear lucite cylinder.

The loading piston guide provides a low friction seal with accurate alignment by using two sets of Thompson ball bushings and a Teflon ring seal on the top and a close-fitting diffusion control seal on the bottom. Piston friction was measured to be approximately equal to the weight of the piston/top cap assembly.

Conventional, non-lubricated lucite caps and bases were used. Since the investigation was concerned with the initiation of liquefaction, which is known to occur at very low strain values, the effects of cap and base restraint on the stress conditions within the sample were considered to be very small in the strain range of primary interest.

Transducers and Signal Conditioning

A total of five sensors are used in the system - a load cell to monitor the axial load, a linear variable differential transformer (LVDT) to measure the vertical displacement, and three pressure transducers to measure the chamber pressure, the effective pressure, and the volume changes. The output signals of these sensors are conditioned and then received by the process interface unit.

The signal conditioning unit made by Validyne can accommodate ten channels for various transducers. A total of five channels are available for the five sensors (the load cell, the three pressure transducers, and the LVDT).

Included in the front panel of this unit is a 4-1/2 inch digital panel meter which may be used to monitor transducer output during testing or to calibrate the transducers prior to testing. Each channel may be switched for viewing on the panel meter. The output from this unit ranges from -10.0 to +10.0 volts DC.

An Interface SSM-3000 load cell which has a 3000 pound capacity in either tension or compression, was used to measure axial loads with the automated loading system. The shape of the load cell was selected so that the LVDT could be mounted as close to the center of the specimen as possible in order to give reliable low strain readings.

Axial deformation was measured with a G. L. Collins Corp. LMB-114E55 linear motion transformer (such devices are typically called LVDTs). The LVDT exhibited essentially linear response over a total range of about ±1.5 inches. The case size of the LVDT was selected in order to minimize the inertia loading on the sample and allow closer mounting to the center of the specimen.

Two of the three differential pressure transducers were Validyne DP-215-52, wet to wet type with diaphragms of the required flexibility for measuring pore pressures and chamber pressures. These transducers have a rated differential pressure range of about 200 psi. Full scale rated differential pressure causes deflection of the internal diaphragm which results in a volume change of only 0.0003 cubic inch. Effective stresses were measured directly by connecting one port of the transducer to the triaxial cell chamber while the other port was connected to the sample drainage line. The transducer could then measure the effective confining pressure as the difference between the pressure on the outside of the sample and the pressure on the inside of the sample.

Volume changes were measured during consolidation using a special volume change device designed by C.K. Chan of the University of California, Berkeley. This volume change device allows specimen drainage to be switched to any of three volume-calibrated tubes, each

of which has a different diameter. The back pressure is applied at the air/water interface at the top of the tubes. The pore pressure transducer is connected to the volume change device in such a way that, by closing a valve, drainage of the sample is prevented and pore pressure measurements can be made. The transducer used for this purpose was a Validyne DP-215 with a specially machined diaphragm which has a maximum differential pressure range of about 1.25 psi. Thus, by selecting a volume change measuring tube of the appropriate diameter, accurate measurements of very small volume changes can be obtained.

12 Inch Diameter Triaxial Testing Equipment

The 12 inch diameter cyclic testing equipment set-up used in this study consisted of an MTS Model 90308, described in detail by Wong (1971) and Banerjee (1979). Thus, only a brief description of this equipment is included in this report.

The testing apparatus, located at the University of California Richmond Field Station, is capable of applying static or dynamic loads in either a displacement-controlled mode or a stress-controlled mode through its two channel electro-hydraulic system. Axial loads are applied to the specimen with a 16 inch diameter hydraulic piston system connected to a 12 inch diameter load ram. The bottom platen is attached to this load ram, and thus, axial loads are applied to the bottom of the specimen. A steel chamber, 58 inches tall, 18 inches inside diameter, and with a 1 inch thick wall, provides the necessary load reaction. The specimen top cap is bolted to the top of the chamber and the base of the chamber is locked onto the load-ram flange. A 500 kip load cell is incorporated inside the top of the chamber for load measurement.

Axial displacements up to 12 inches or ±6 inches can be applied in static and dynamic loading modes, respectively. Deformations were measured by using an LVDT installed inside the MTS loading system. Cyclic loads were programmed via a Data Trak programmer on which a sinusoidal loading path had been inscribed. Cell pressures and effective pressures were measured using Validyne wet to wet differential pressure transducers as described previously. A Sanborn four channel recorder was used to monitor axial loads, axial deformations, effective pressures, and cell pressures. A schematic of the MTS loading and instrumentation system is shown in Figure 6.15 (after Banerjee et al., 1979); the components shown in this figure are noted in Table 6.3.

The frequency of cyclic loading for 2.8 inch diameter samples of the modeled material was 1 cycle per second which is considered to be a good simulation of normal earthquakes. This frequency, however, was not achievable with the MTS testing equipment used for the 12 inch diameter specimens. Instead, a frequency of 1 cycle per minute was used for all of the large scale tests performed in this study. Previous investigations, as well as tests conducted on sand specimens as part of this study (see Appendix A), have shown that the frequency of cyclic loading has no significant influence on the cyclic loading resistance of granular materials within the normal test loading range (Peacock and Seed, 1968; Lee and Fitton, 1969; Wong et al. 1974). Thus, the use of this frequency of cyclic loading (as compared to the frequency of actual earthquakes) was considered to be acceptable.

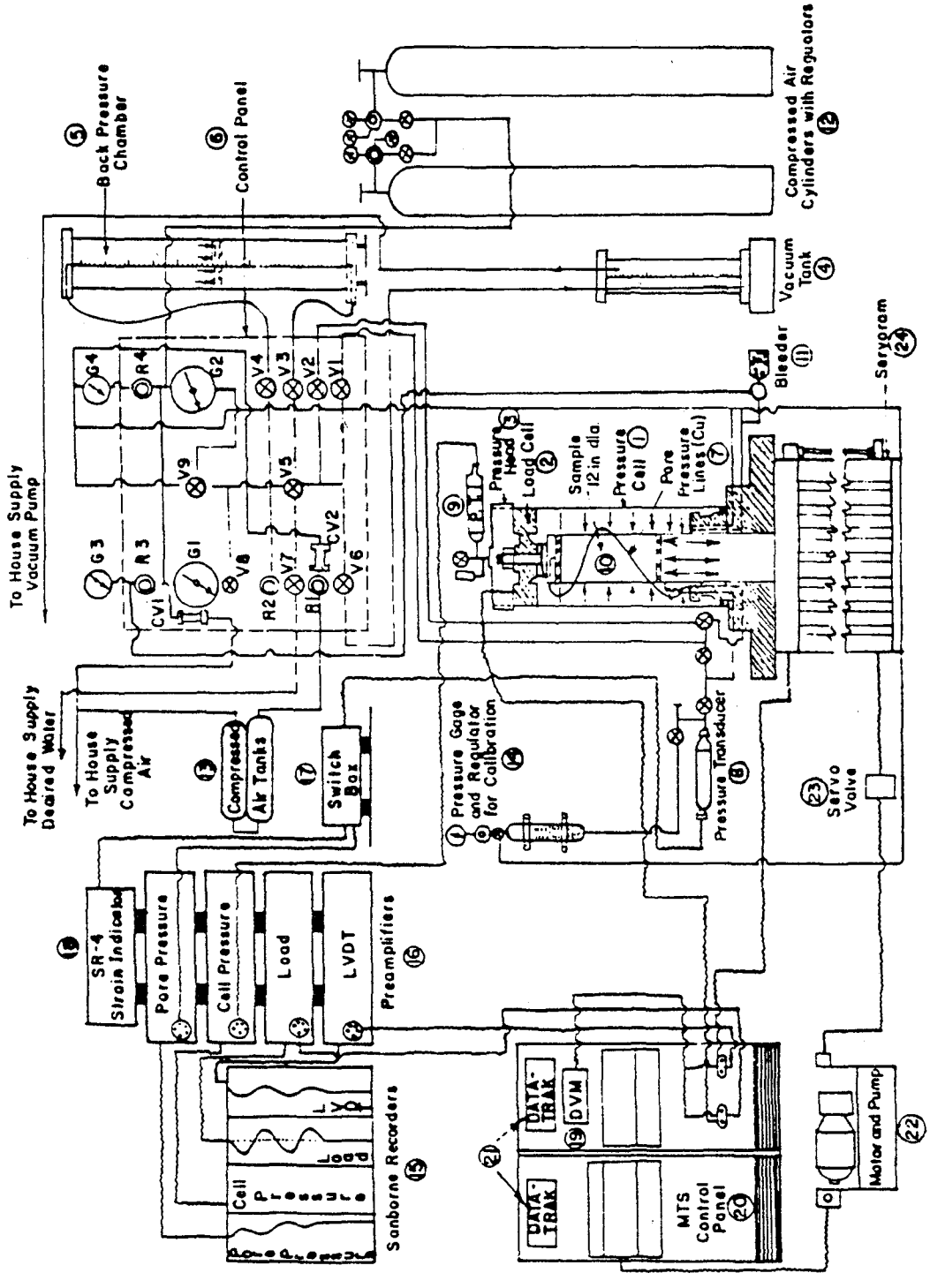

Figure 6.15 Schematic Diagram of the 12" Diameter Triaxial Testing System (after Banerjee et al., 1979)

Table 6.3 Identification of Principal Components in Figure 6.15 (after Banerjee et al., 1979)

1	Pressure Cell
2	Load Cell, 600 Kips Capacity
3	Pressure Head
4	Acrylic Vacuum Tank
5	Back Pressure Chamber
6	Control Panel
7	Pore Pressure Lines (copper)
8	Pressure Transducer
9	Pressure Transducer
10	Test Specimen (12 inch diameter)
11	Bleeder Valve
12	Compressed Air Cylinder (High Pressure)
13	Compressed Air Tank (Low Pressure)
14	Gage and Regulator for Calibration
15	Sanborn Recorders
16	Sanborn Preamplifiers
17	Multiple Channel Switch Box
18	Strain Recorder (SR-4)
19	Digital Voltmeter (DVM)
20	MTS Control Panel
21	Data Trak Programmer
22	Motor and Pump
23	Servo Valve
24	Servoram, 16 inch Bore, 12 inch Ram
V1-V9	Precision Valves
G1-G2	Precision Heise Gages
G3-G4	Gages
R1-R4	Pressure Regulators
CV1-CV2	Check Valves

CHAPTER 7

RESULTS OF TRIAXIAL TESTS PERFORMED ON 12 INCH DIAMETER SPECIMENS

Introduction

Over one hundred 2.8 inch and 12 inch diameter undrained cyclic triaxial tests were performed as part of this research program. The results of tests performed on 12 inch diameter specimens are presented in this chapter and the results of tests performed on 2.8 inch diameter specimens are presented in Chapter 8. Analyses and comparison of the test data will follow presentation of the test results in each section.

The test data presented in this chapter are divided into two sections according to the grain size distributions of the gravels used to construct the test specimens as follows:

Section (1) - 2" Maximum, Modified Gradation Watsonville Gravel

Section (2) - 1-1/2" x 3/4" Watsonville Gravel

Each of these sections are subdivided into a number of test groups to distinguish between different test conditions that were investigated within that particular section. The tests within each group are related by common factors such as specimen diameter, relative density, method of sample construction, type of sluicing sand, K_c, and several other factors which will be described.

The organization of a typical section is shown schematically in Figure 7.1. Each section is represented by the following generalized tables and figures:

(a) A Section Summary Table which summarizes the different test groups investigated; and for each test group:

(b) A Group Summary Table;

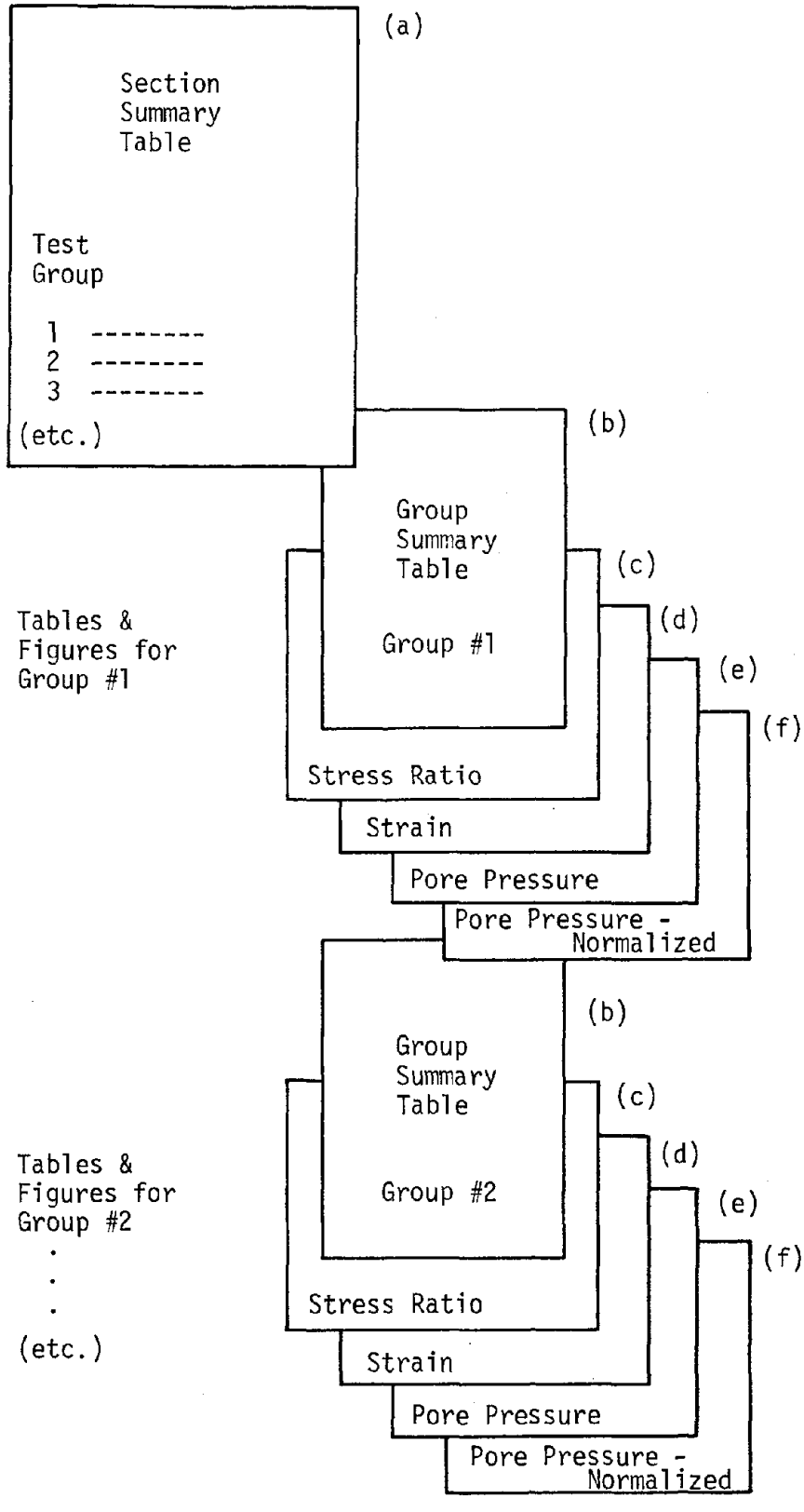

Figure 7.1 Organization of Tables and Figures for Each Test Section

(c) Cyclic Stress Ratio vs. N_c Plot;

(d) Double Amplitude Strain vs. N_c Plot;

(e) Residual Pore Pressure Ratio vs. N_c Plot;

and (f) Residual Pore Pressure Ratio vs. N_c/N_ℓ Plot.

where N_c is the number of applied stress cycles and N_ℓ is the number of stress cycles to 100% residual pore pressure ratio.

Data plots are numbered in the form; Figure 7.X.Y.Z, where "7" indicates the chapter number, "X" indicates the section number, "Y" indicates the test group number within that particular section, and "Z" indicates the figure number. Tables are numbered in a similar manner. Each of these tables and figures is described in the following sections.

(a) Section Summary Table

A typical section summary table is shown in Figure 7.2. This table contains information such as the gravel gradation used to construct the test specimens, the test group designation numbers, the condition of the test specimens within each group, the sluicing sand used (if any), the resulting sluiceability coefficient, and the general testing procedure, together with any particular test variations that were investigated in each group of specimens.

(b) Group Summary Table

A typical group summary table is shown in Figure 7.3. This table contains a listing of the reference numbers of each of the cyclic tests performed within each group, the condition of the test specimens, the condition of the sluicing sand (if any), the applied cyclic stress ratio, and the number of stress cycles required to cause failure by

Table Summary of Undrained Cyclic Triaxial Tests Performed on 2" Maximum, Modified Gradation - Watsonville Gravel

Test Group	Sluicing Sand	Gravel Relative Density, %	C_s	Comments*
1	none	42	-	
2	San Francisco Dune	42	42	
3	San Francisco Dune	62	42	

* - All test specimens are 12" diameter, dumped in 6 layers, one 0.1" membrane, $\sigma_3' = 2.0$ ksc, and $K_c=1$ except as noted.

Figure 7.2 Typical Section Summary Table

Table Material Properties and Test Conditions Causing Failure During Undrained Cyclic Loading

GRAVEL: 2" Maximum, Modified Gradation - Watsonville
SLUICING SAND: San Francisco Dune
C_S=42

Test No.	Gravel				Sand	
	Dry Density (pcf)	Void Ratio	Porosity	Relative Density (%)	Dry Density (pcf)	Void Ratio
7	101.7	0.707	0.414	41.1	84.4	0.997
9	101.5	0.710	0.415	40.3	89.4	0.885
10	102.6	0.692	0.409	44.7	86.1	0.958
11	100.4	0.729	0.422	35.8	87.1	0.935

Test No.	Cyclic Stress Ratio, $\sigma_d/2\sigma_{3c}$	Number of Cycles Causing...				
		80% Pore	100% Pressure Ratio	2% Peak	5% to Peak	10% Strain
7	0.238	-	1.0	1.6	2.5	3.8
9	0.180	-	6.2	7.0	8.8	11.0
10	0.150	-	23.0	25.0	29.0	-
11	0.170	-	11.0	12.0	13.5	15.0

* - All test specimens are 12" diameter, dumped in 6 layers, one 0.1" membrane, σ_3'= 2.0 ksc, and K_c=1.

Figure 7.3 Typical Group Summary Table

various pore pressure and strain criteria as obtained from the group data plots. Finally, each table contains a section of notes describing the particular test conditions or specimen construction procedures employed in that group.

(c) Cyclic Stress Ratio vs. N_c Plot

A typical figure of this type is shown in Figure 7.4. These figures show the relationship that was determined to exist between cyclic stress ratio and the number of stress cycles causing 5% double amplitude strain. Each data point appearing on these curves is the result of an individual undrained, cyclic compression triaxial test. Appearing above each data point is shown the test number for reference back to the group summary table, and the specimen relative density expressed as a percent. Although specimen densities may vary slightly within a group of tests, a smooth curve representative of the "average" relative density of all the test specimens is drawn by interpolating between points of higher or lower relative density. The average value, noted in the legend included in the figure, is not a true statistical average since the curve was not intended to intercept all of the data points. Rather, judgment was used to fit a curve to the data which would account for variations in relative density and a representative average value of the relative density was determined for the curve as drawn.

Curves such as the one described above are often drawn for various failure criteria such as 100% pore pressure ratio, 2%, 5%, or 10% double amplitude strain (The concept of double amplitude strain will be illustrated in Figure 7.9). It was decided that one failure criterion, 5% double amplitude strain, should be used consistently to

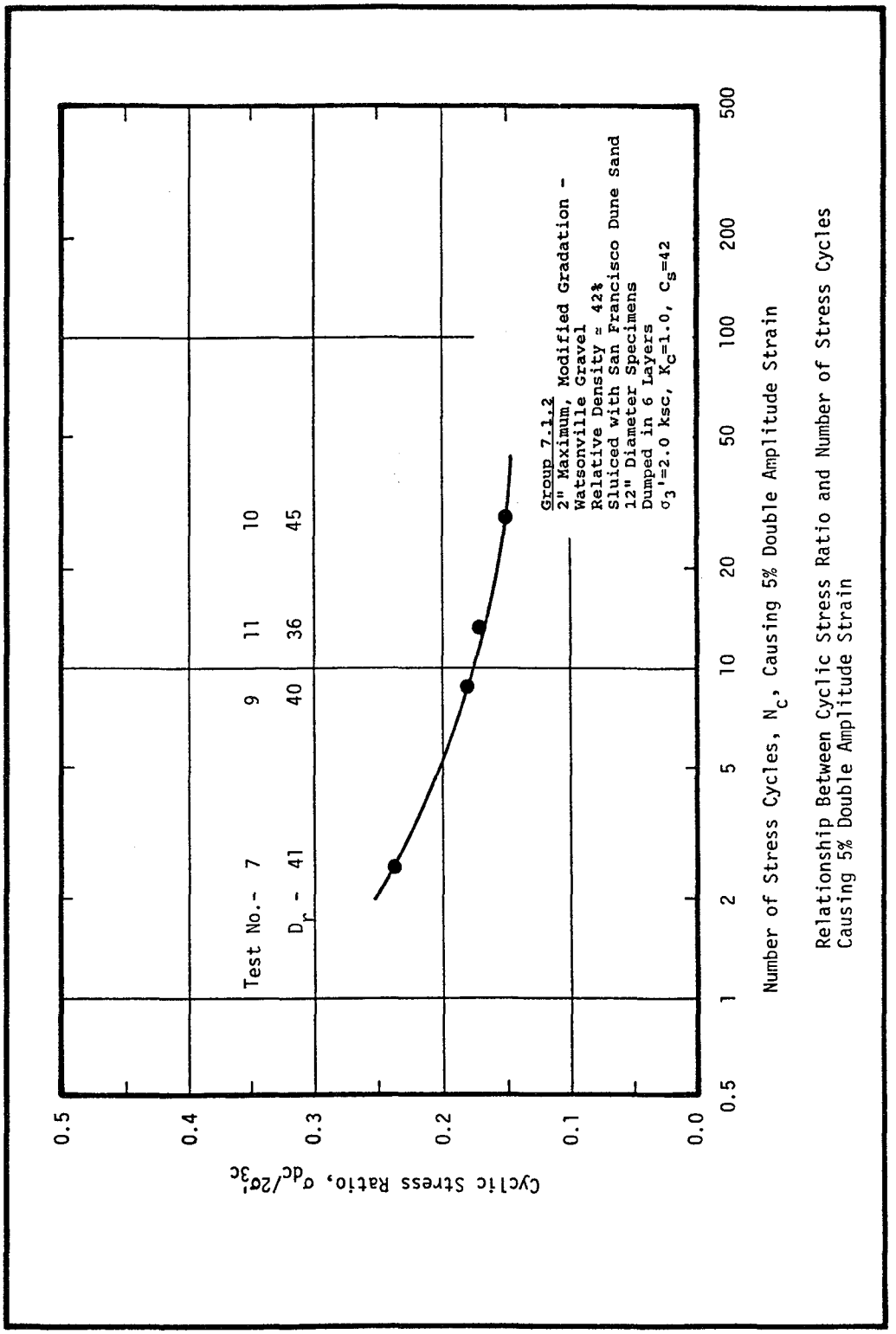

Figure 7.4 Typical Group Cyclic Stress Ratio vs. N_C Plot Showing the Relationship Between Cyclic Stress Ratio and Number of Stress Cycles Causing 5% Double Amplitude Strain

compare the cyclic loading resistance of the sluiced and the unsluiced gravel specimens. The 100% pore pressure ratio was also used as a failure criterion in addition to the strain criterion, in several cases. The 5% double amplitude strain criterion was chosen for use in comparing the cyclic stress ratio values reported in this report for the following reasons:

(1) Several investigators have shown that the development of 100% pore pressure ratio in an undrained test specimen usually occurs in approximately the same number of stress cycles as that required to cause about 5% double amplitude strain (Banerjee et al., 1979). Figures 7.5, 7.6, and 7.7 show relationships between cyclic stress ratio and the number of cycles required to cause different values of pore pressure ratio and different levels of strain in test specimens of Monterey No. 0 Sand (see Appendix A), sluiced 3/8" x #4 gravel, and unsluiced 3/8" x #4 gravel, respectively. It may be noted from these figures that the sand and sluiced gravel specimens did indeed develop a value of 100% pore pressure ratio in the range of 2% to 5% double amplitude strain. For the unsluiced gravel specimens, however, a somewhat higher value of strain was required before initial liquefaction (100% pore pressure ratio) occurred. The development of excess pore pressures was inhibited in the unsluiced specimens due to the effects of membrane compliance. Furthermore, it was considered reasonable to expect that strain and pore pressure would develop in a consistent pattern in any specimen tested in a noncompliant system, whether the test materials were sands or gravels. Therefore, the same failure criterion of 5% double amplitude strain was used for both sluiced and unsluiced specimens in order to maintain consistency when

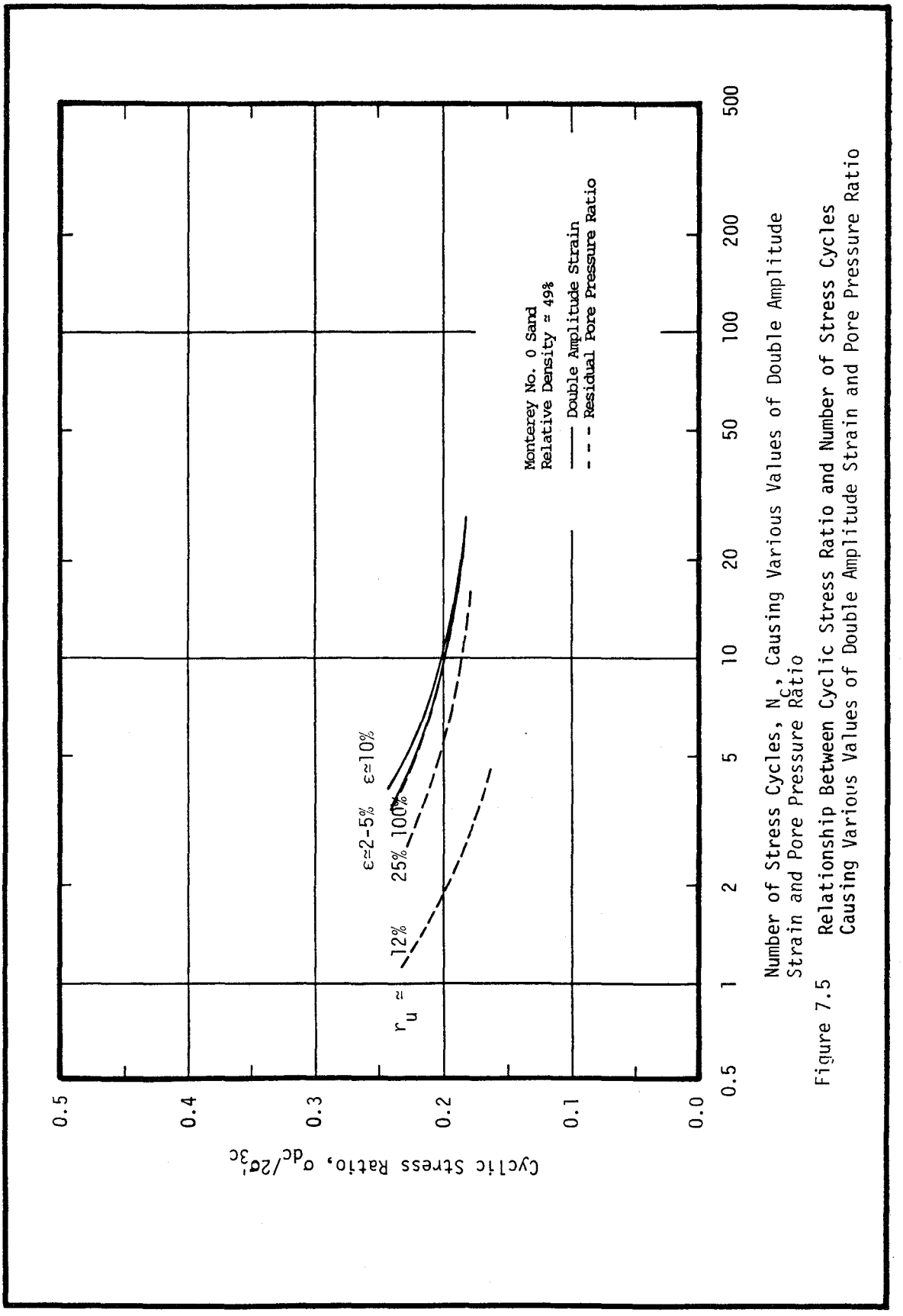

Figure 7.5 Relationship Between Cyclic Stress Ratio and Number of Stress Cycles Causing Various Values of Double Amplitude Strain and Pore Pressure Ratio

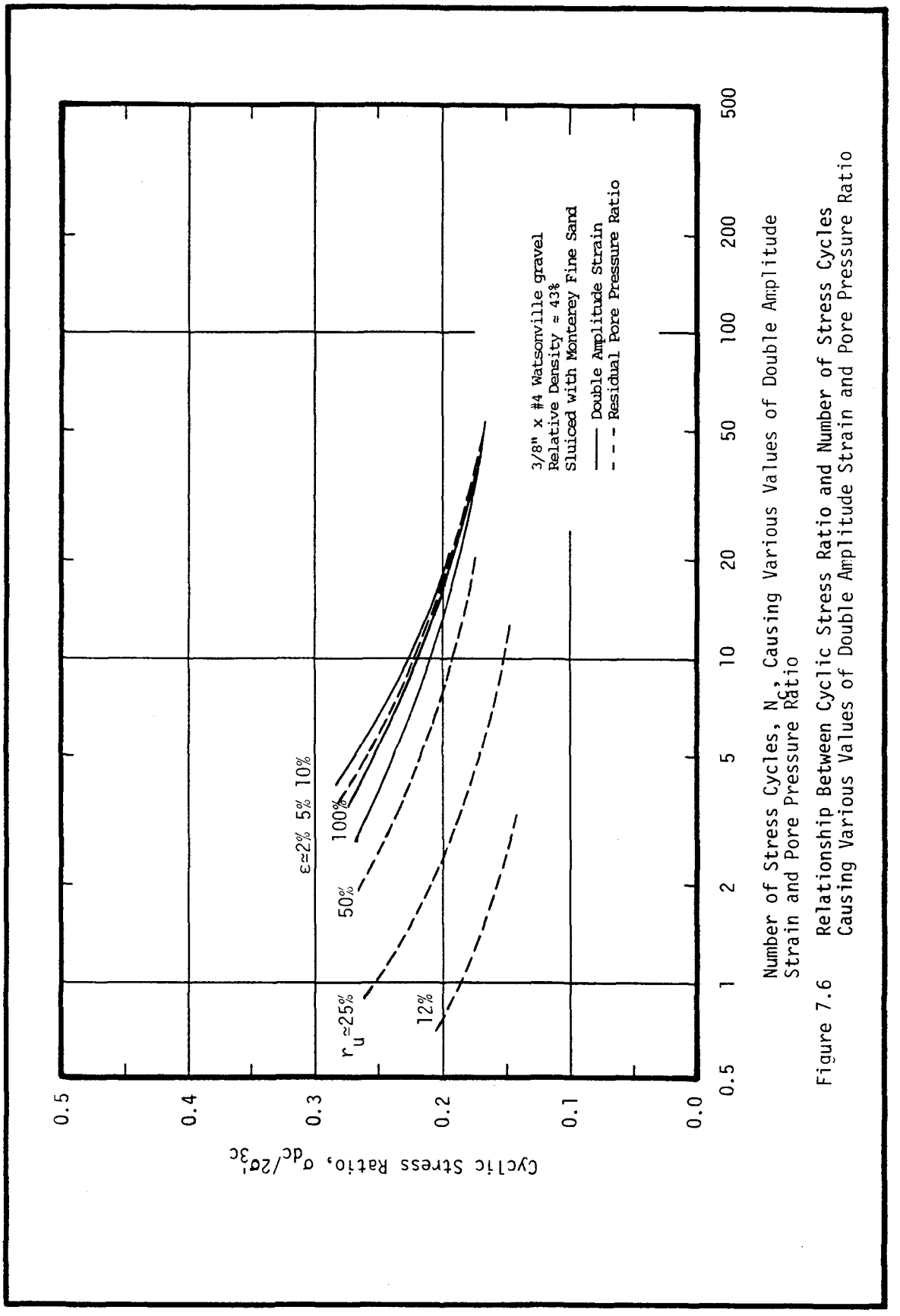

Figure 7.6 Relationship Between Cyclic Stress Ratio and Number of Stress Cycles Causing Various Values of Double Amplitude Strain and Pore Pressure Ratio

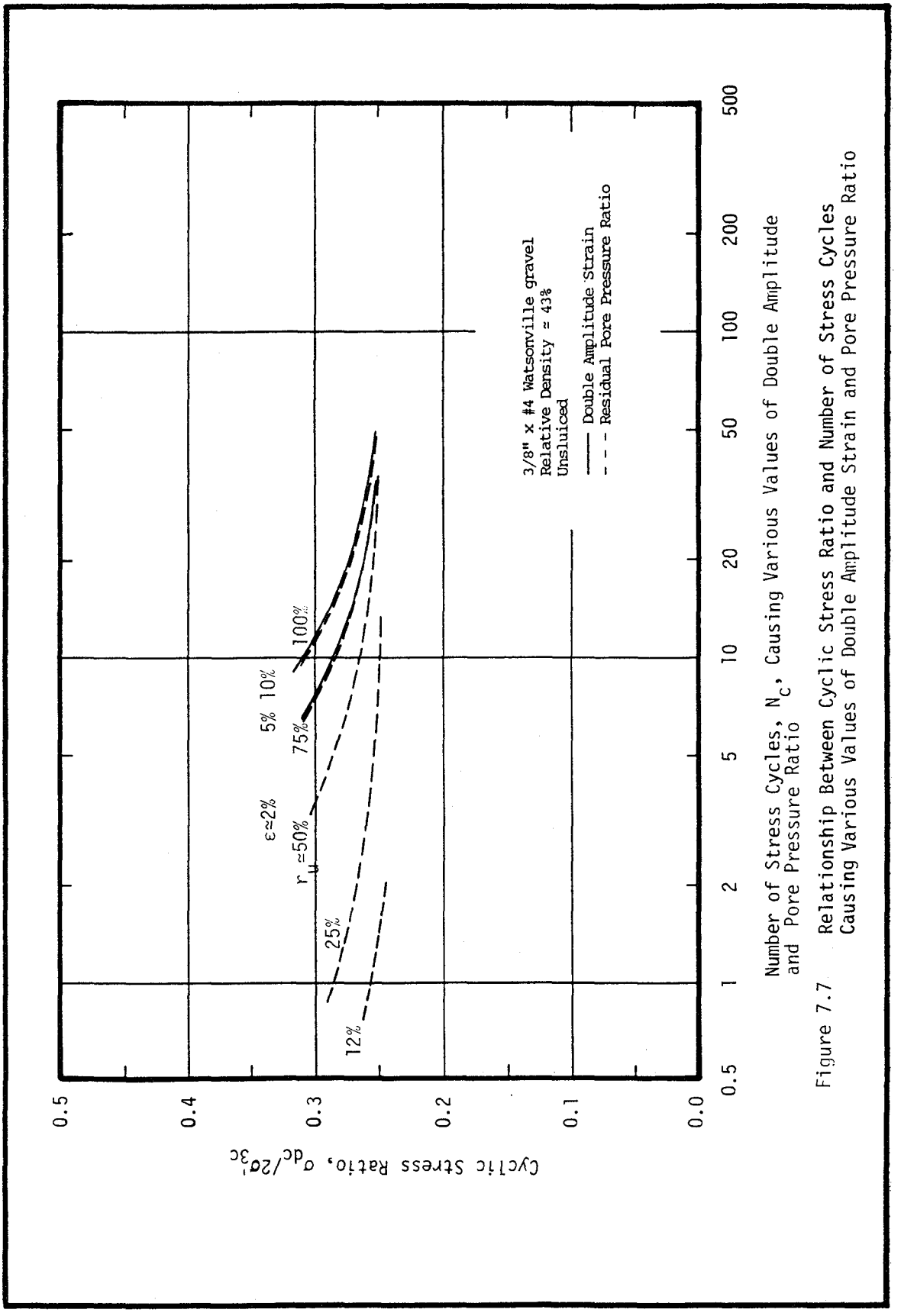

Figure 7.7 Relationship Between Cyclic Stress Ratio and Number of Stress Cycles Causing Various Values of Double Amplitude Strain and Pore Pressure Ratio and Pore Pressure Ratio

comparing the cyclic loading resistance. By specifying that the 5% double amplitude strain criterion be used, in effect, two criteria are expressed for noncompliant systems - 5% strain and 100% pore pressure ratio.

(2) Neither sluiced nor unsluiced specimens consistently developed pore pressure ratios of 100%. In fact, unsluiced 2.8 inch diameter gravel specimens typically developed no greater than 75% to 80% pore pressure ratio even though double amplitude strains in excess of 15% were developed. Consequently, it would have been impractical to make strength comparisons based on the development of 100% pore pressure ratio in unsluiced specimens. The 100% pore pressure ratios reported in this study are generally extrapolated values, as will be described in the section labeled: (e) Residual Pore Pressure Ratio vs. N_c Plot.

(3) A low value of strain was specified as the failure criterion in order to avoid complications of sand/gravel particle interaction that might occur in sluiced samples at high values of strain. At a strain value of ±2.5%, about 0.3 inches of peak to peak axial deformation would occur in typical 2.8 inch diameter specimens, and it was considered that such small deformations would cause little or no sand/gravel particle interaction. Even if some particle interaction did occur, it would seem likely to result in a higher cyclic loading resistance than would result if no interaction occurred. The sand in the sluiced specimens is occupying a position where only water, or some other pore fluid, would otherwise have been, as described previously in Chapter 5. Since even very loose, saturated sand, such as occurs in sluiced specimens, has a greater shear strength than water, it may well

contribute to the cyclic loading resistance of the gravel specimen. Any such contribution is considered to be slight, however, as compared to the effect that the sluicing sand has in reducing membrane penetration and thus reducing the cyclic loading resistance of the specimen as measured in the cyclic triaxial test.

The value of the cyclic stress ratio that causes failure in 10 stress cycles is used for comparison of the cyclic loading resistance of the specimens tested in this report. Ten cycles of stress were chosen because this number of significant stress cycles, at a frequency of 1 Hz, is generally representative of the effects of a 6.5 magnitude earthquake (Seed et al., 1975, Seed and Idriss, 1982). This value represents a typical earthquake magnitude which may be incorporated into an engineering design criteria for a seismic area, and thus it was considered to be a reasonable reference point for developing comparisons of the cyclic resistances of the test specimens. Similar comparisons may be derived over the range of about 3 to 26 cycles representative of earthquakes of magnitude 5.25 to 8.50 respectively.

(d) Double Amplitude Strain vs. N_c Plot

A typical figure of this type is shown in Figure 7.8. Such figures show the relationship that was determined to exist between double amplitude strain and number of stress cycles. These curves were developed by measuring the maximum peak to peak strain that developed in the test specimens during each complete stress cycle as shown in Figure 7.9. This procedure was followed for each load cycle and a smooth curve was drawn through the resulting data points. The number of stress cycles that occurred up to the development of the failure criterion of 5% double amplitude strain may be read from these curves.

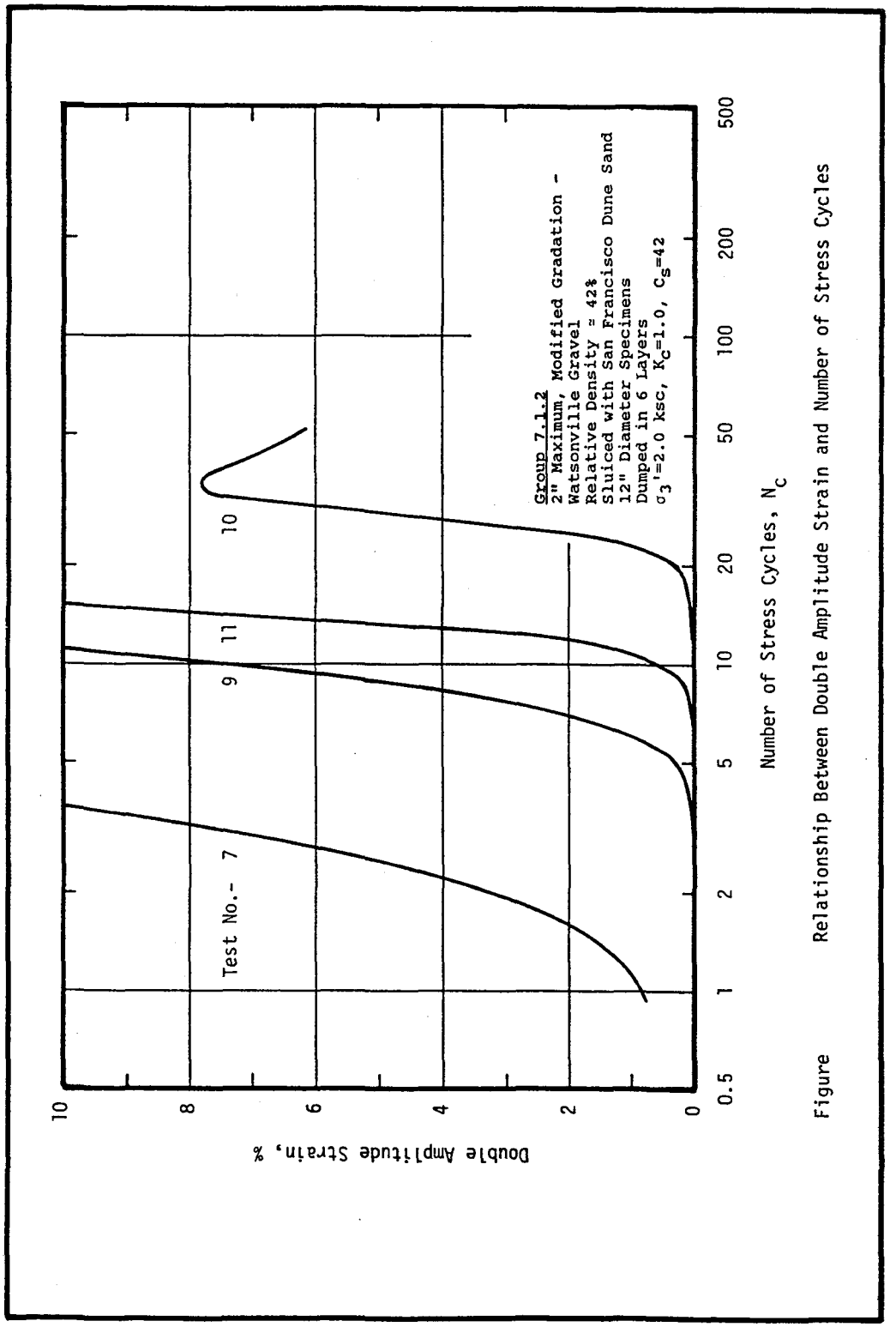

Figure Relationship Between Double Amplitude Strain and Number of Stress Cycles

Figure 7.8 Typical Group Double Amplitude Strain vs. N_c Plot Showing the Relationship Between Double Amplitude Strain and Number of Stress Cycles

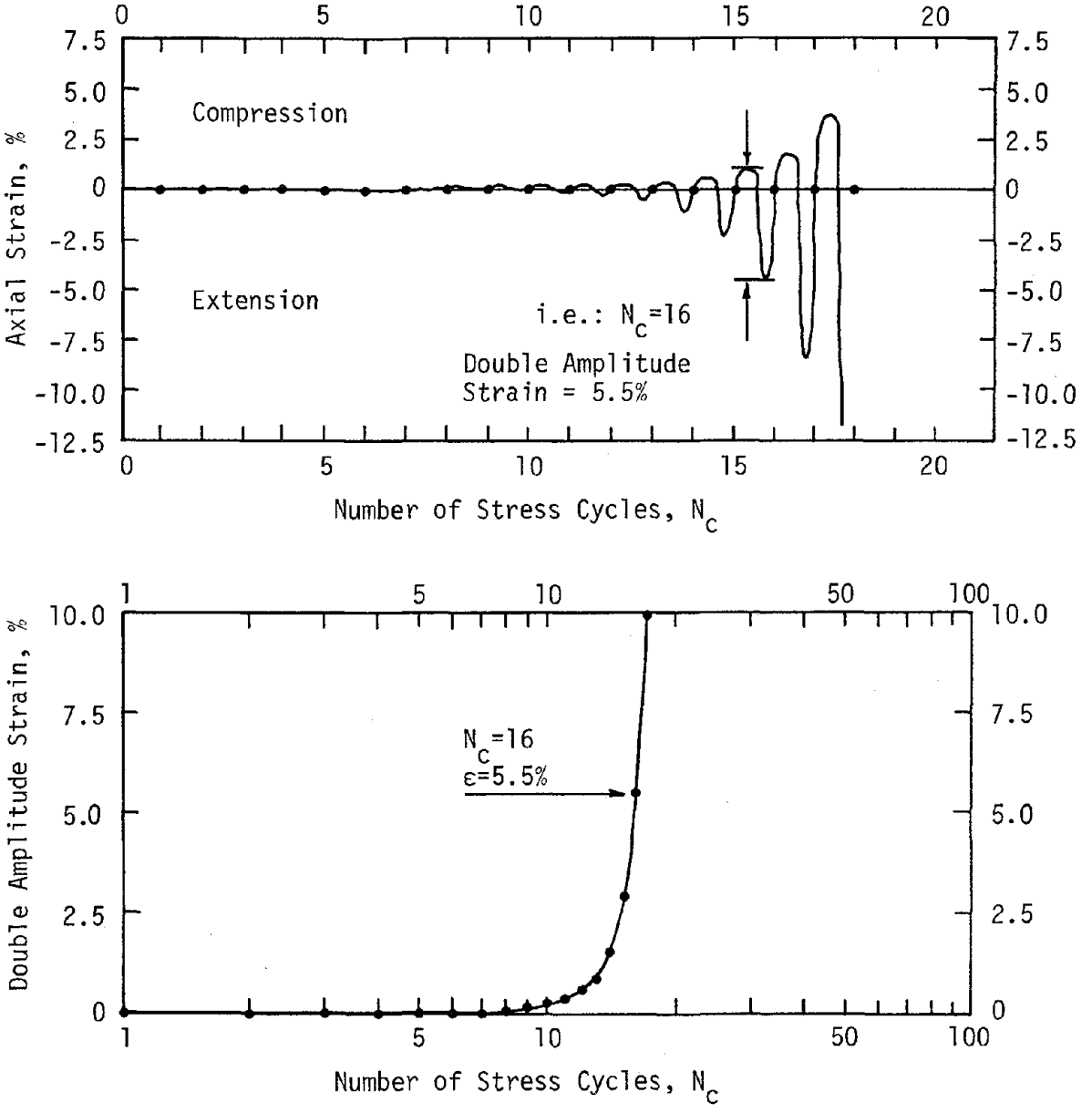

Figure 7.9 Construction of Double Amplitude Strain vs. N_c Plot

Clearly, any other failure criteria up to a value of 10% double amplitude strain may also be read from these curves in order to develop cyclic strength comparison curves for other values of strain.

Isotropically consolidated cyclic triaxial tests (K_c=1) typically developed approximately symmetric deformations about their original height as shown in Figure 7.10. Anisotropically consolidated specimens, on the other hand, often developed large compressive deformations with very low corresponding values of peak to peak deformation. In tests where peak compressive strains exceeded double amplitude strains in any cycle, compressive strain values were used to develop the plots of strain vs. number of stress cycles. The test numbers beside such curves are marked with an asterisk (*) and an explanatory note is included in the figure.

(e) Residual Pore Pressure Ratio vs. N_c Plot

A typical figure of this form is shown in Figure 7.11. Such figures show the relationship that was determined to exist between residual pore pressure ratio and number of stress cycles. These curves were developed by plotting the excess pore pressure ratio that existed at the end of each stress cycle vs. the corresponding cycle number as shown in Figure 7.12. A smooth solid curve was drawn through each of these points. A dashed line was drawn from the tops of these curves in order to extrapolate to 80% or 100% pore pressure ratio when such values were not reached during the test. These dashed lines are extensions of the pore pressure development trend that existed before some limiting pore pressure value was reached and the residual pore pressure stabilized to an approximately constant value.

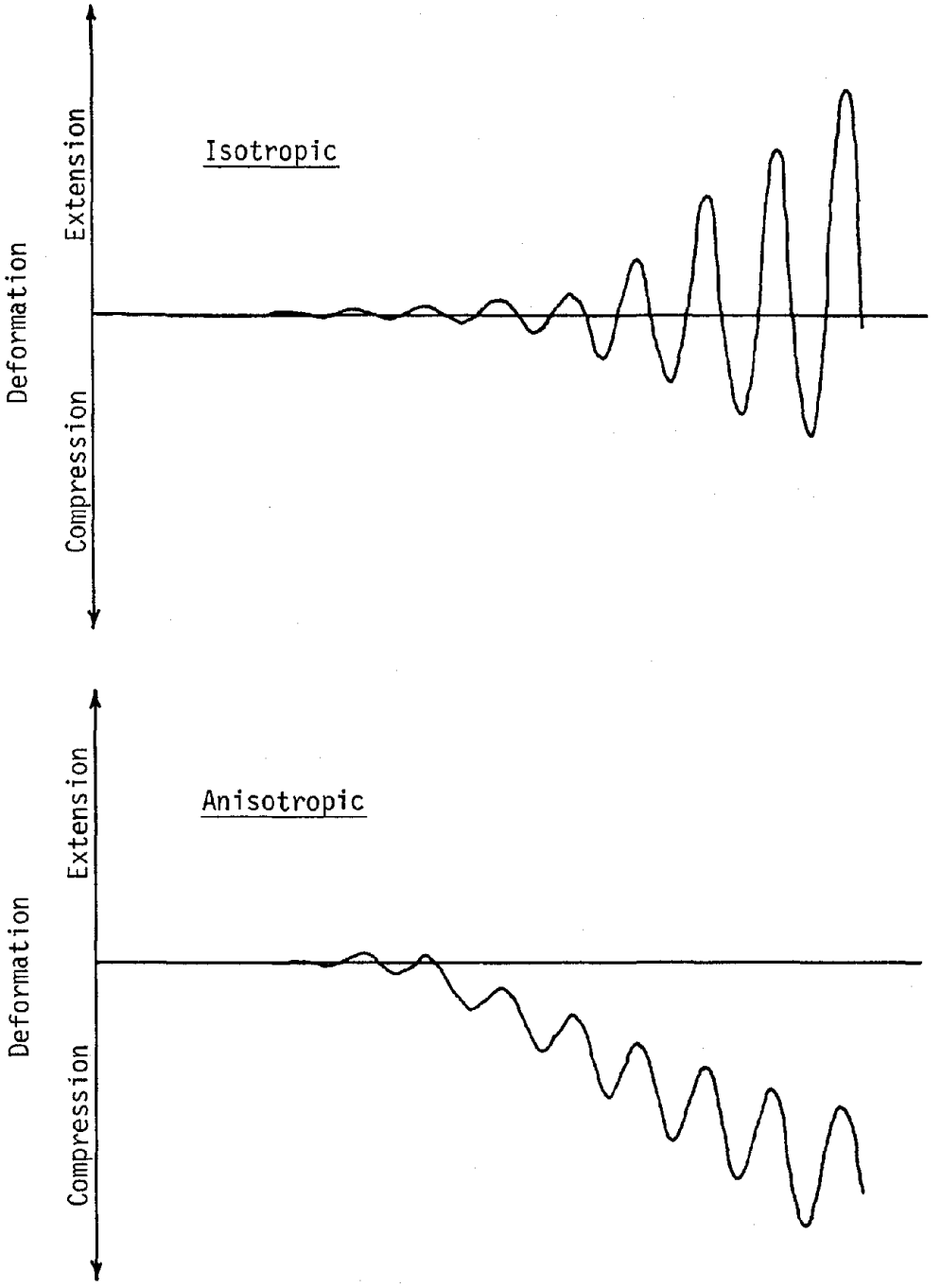

Figure 7.10 Typical Deformation Patterns for Isotropically and Anisotropically Consolidated Specimens

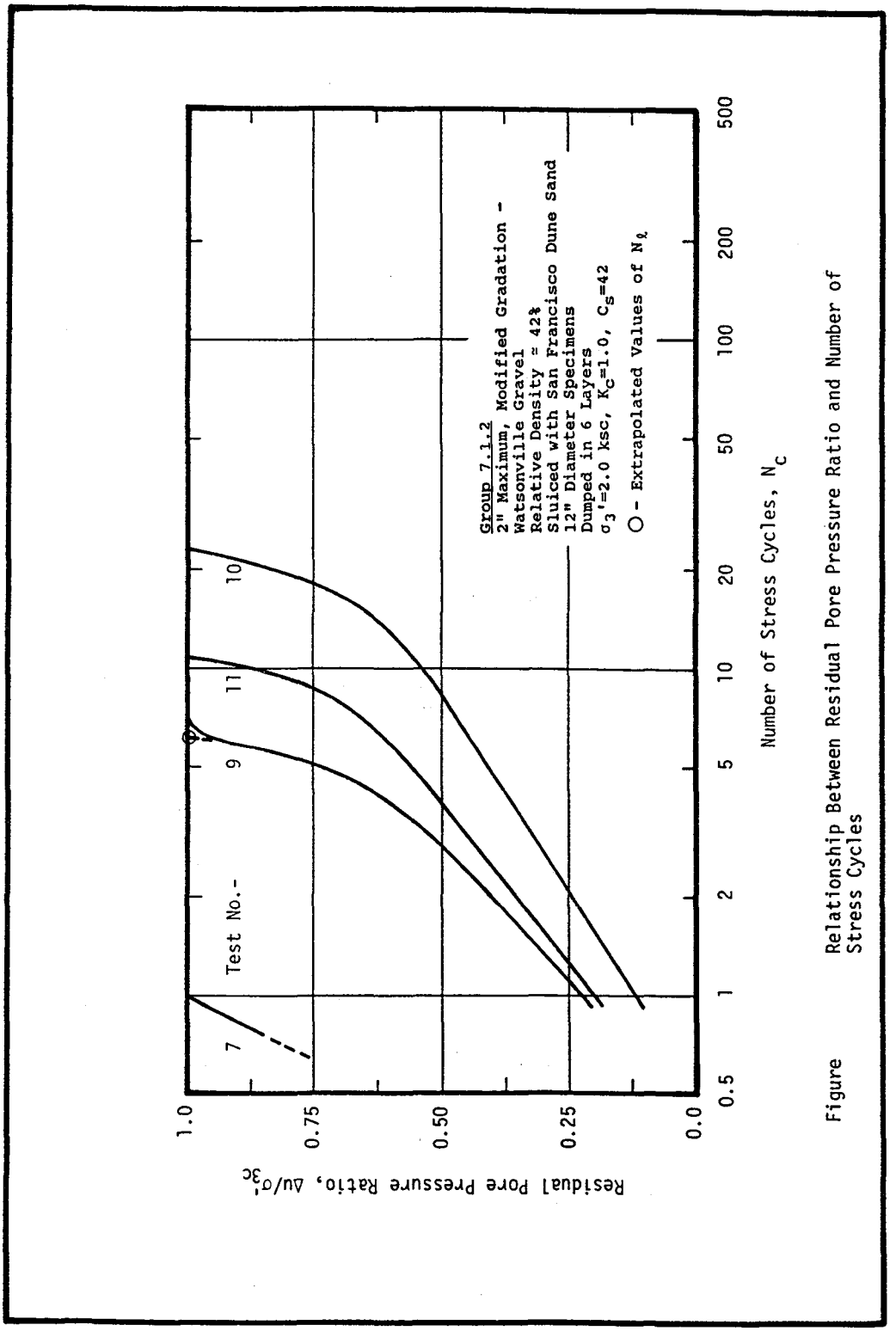

Figure Relationship Between Residual Pore Pressure Ratio and Number of Stress Cycles

Figure 7.11 Typical Group Residual Pore Pressure Ratio vs. N_c Plot Showing the Relationship Between Residual Pore Pressure Ratio and Number of Stress Cycles

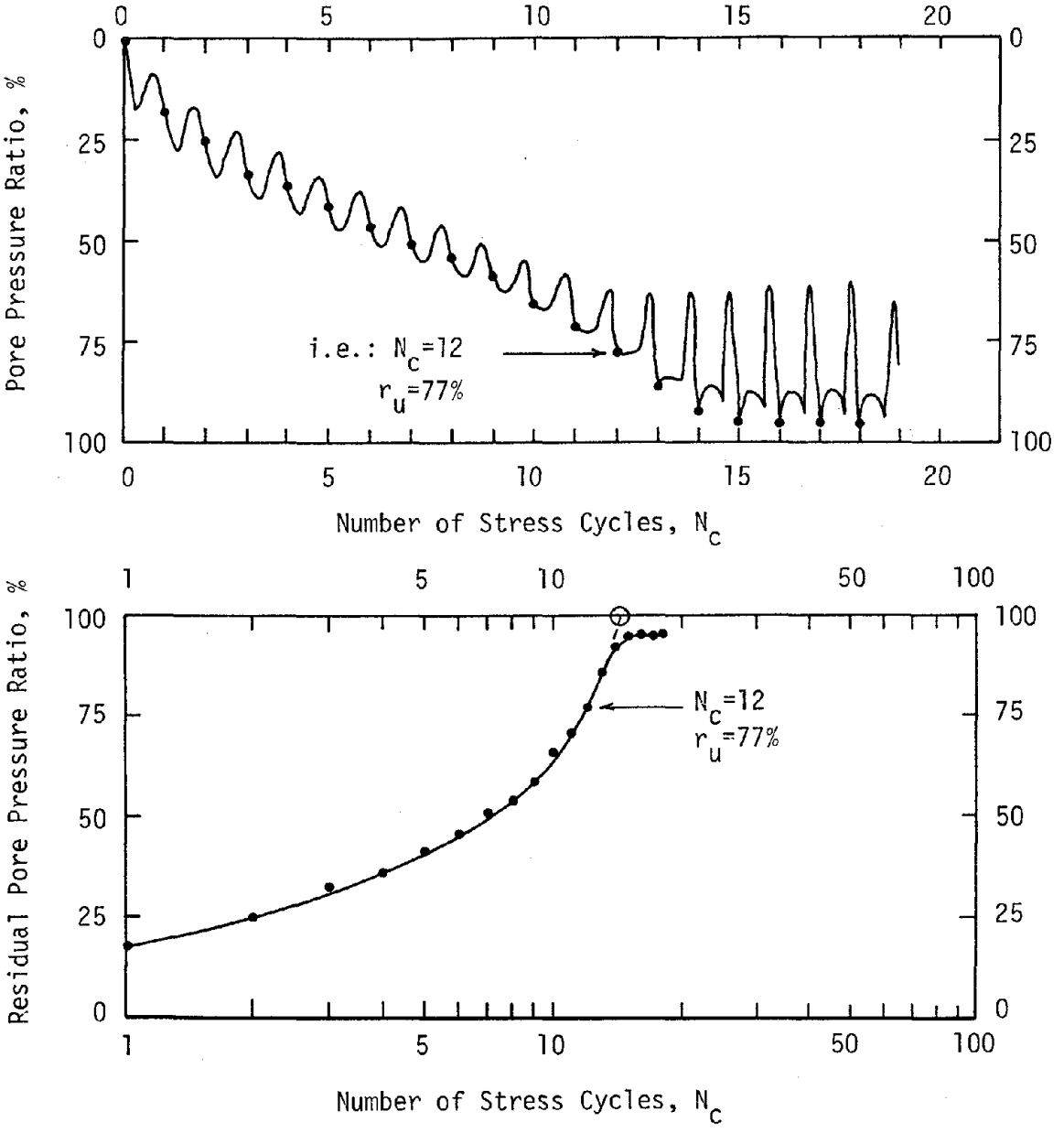

Figure 7.12 Construction of Residual Pore Pressure Ratio vs. N_c Plot

It is believed that this leveling off is mainly the result of membrane compliance effects. Without the effects of membrane compliance, it was considered that the pore pressure ratio would have continued to develop to a value of 100%. Undrained, cyclic load tests performed on specimens of Monterey No. 0 sand reached 100% pore pressure ratios during the application of only a few stress cycles after a value of 30% to 50% pore pressure ratio was surpassed (see Appendix A). Similar tests performed on specimens of 3/8" x #4 gravel also developed pore pressures more rapidly after 30% to 50% pore pressure ratio but only reached a peak residual pore pressure ratio of about 75%. It is argued that this difference is a direct result of the effects of membrane compliance and that, if this phenomenon could be eliminated, the gravel specimens would develop peak residual pore pressure ratios which would be similar to those developed in sand specimens. It was apparent from the tests that pore pressure build-up occurred more rapidly and to a greater extent in non-compliant systems or in systems with low compliance, than in tests with high degrees of compliance. The effects of membrane compliance, however, become greater at higher levels of pore pressure development. It was considered reasonable, therefore, to extrapolate the early portions of the pore pressure development curves when it was desired to estimate the behavior of samples in the absence of any membrane compliance effects. Extrapolated data is shown by dashed lines and special symbols on the figures. Open triangles, only used in a few figures, represent extrapolated values of 80% pore pressure ratio while the open circles represent extrapolated values of 100% pore pressure ratio.

(f) Residual Pore Pressure Ratio vs. N_c/N_ℓ Plot

A typical figure of this type is shown in Figure 7.13. Such figures show the relationship between the measured residual pore pressure ratio and the normalized number of stress cycles. These curves were developed by plotting the residual pore pressure ratio vs. the quantity N_c/N_ℓ, where N_ℓ is the number of cycles required to reach the actual or extrapolated value of 100% pore pressure ratio as previously discussed. Several test groups developed residual pore pressure ratios which were no greater than about 75%. It was reasoned that extrapolation to 100% may be judged to be excessive without first providing a basis for such extreme extrapolations at lower values of pore pressure ratio. Thus, similar curves designated 7.X.Y.5 were first developed with the quantity $N_c/N_{80\%}$ since extrapolation to 80% pore pressure ratio was considered to be reasonable. Comparison of both sets of curves generated using $N_{80\%}$ and N_ℓ indicates that similar trends exist in both sets of curves and that extrapolation to 100% may not be unreasonable. These curves will be used to compare pore pressure developments in sluiced and unsluiced gravel specimens later in this chapter.

The remainder of this chapter (as well as Chapter 8) is organized as follows: (1) All of the test data tables and figures are presented together, in the order listed in the section summary tables, for each of the gravel gradations; and (2) Analyses of the test results follow presentation of the test data. In the analysis sections, data curves are shown for comparison without their corresponding data points. Such curves are clearly labelled so that the reader may easily locate the

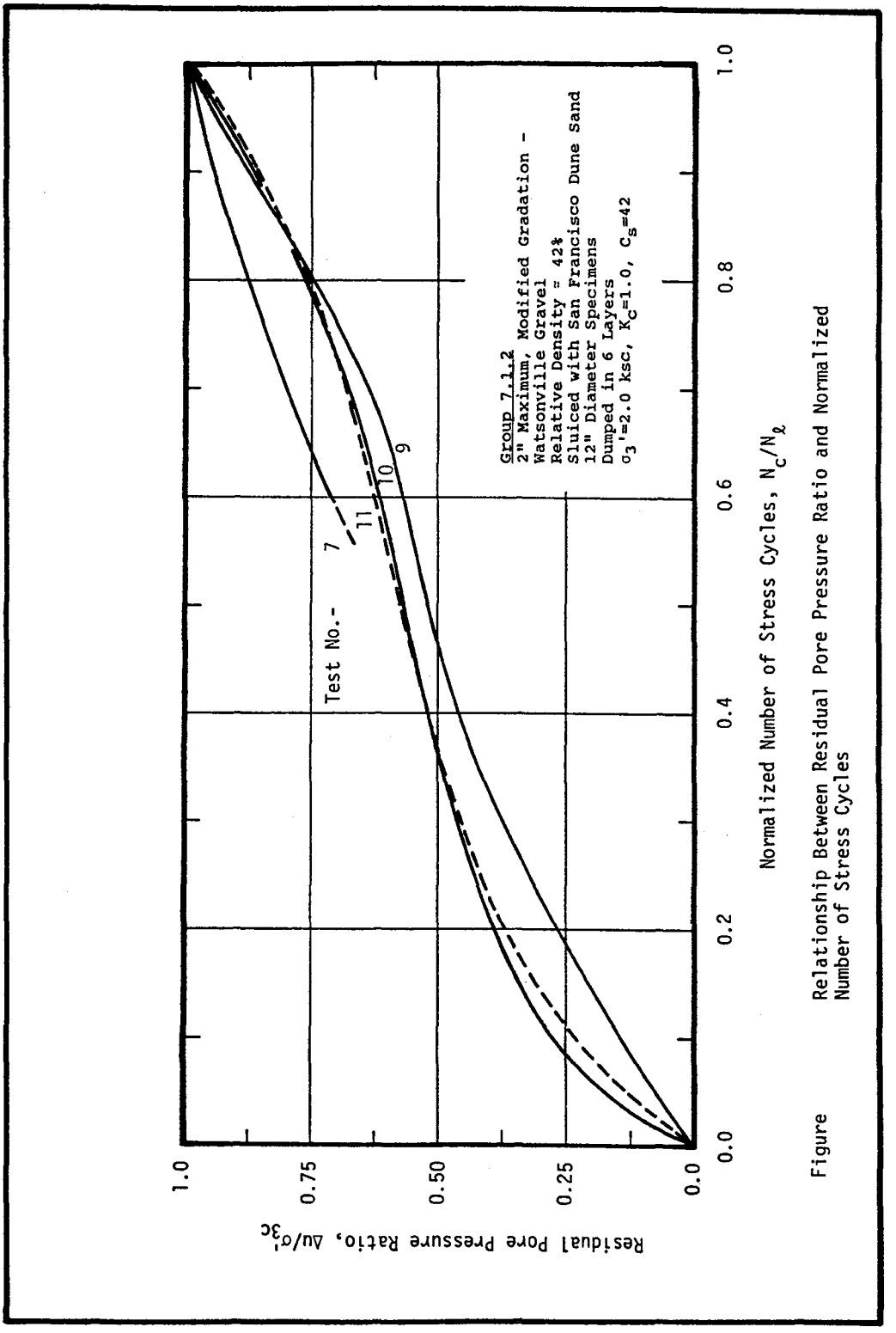

Figure 7.13 Typical Group Residual Pore Pressure Ratio vs. N_c/N_ℓ Plot Showing the Relationship Between Residual Pore Pressure Ratio and Normalized Number of Stress Cycles

pertinent figures containing the test data, if desired, and refer to them for clarification.

Tests Performed on 2" Maximum, Modified Gradation - Watsonville Gravel Specimens

Test Data Presentation

Three groups of undrained, cyclic triaxial tests were performed on 12 inch diameter specimens of modified gradation Watsonville gravel with 2" maximum size particles as summarized in Table 7.1.0 (found on page 192 following Figure 7.14). All specimens were constructed in six equal layers by dumping the lift material from a constant height of fall, using a special mixing and dumping bucket. The specimens of one test group, at a relative density of 42%, were unsluiced. The specimens of the other two groups, at relative densities of 42% and 62%, were sluiced with San Francisco dune sand which resulted in a value of C_s=42. Tables 7.1.1, 7.1.2, and 7.1.3 summarize the relevant test data for these groups of tests. Figures 7.1.1.1 through 7.1.3.4 are included along with these tables and contain the test data for this material as described earlier in this chapter.

Data Analyses

A comparison of the curves relating the cyclic stress ratio to the number of stress cycles causing 5% double amplitude strain, for sluiced and unsluiced specimens at a relative density of 42%, is shown in Figure 7.14. It may be seen from this figure that the value of cyclic stress ratio causing 5% double amplitude strain for the sluiced specimens in 10 stress cycles was only about 65% of the value required to cause the same level of strain for the unsluiced specimens. The

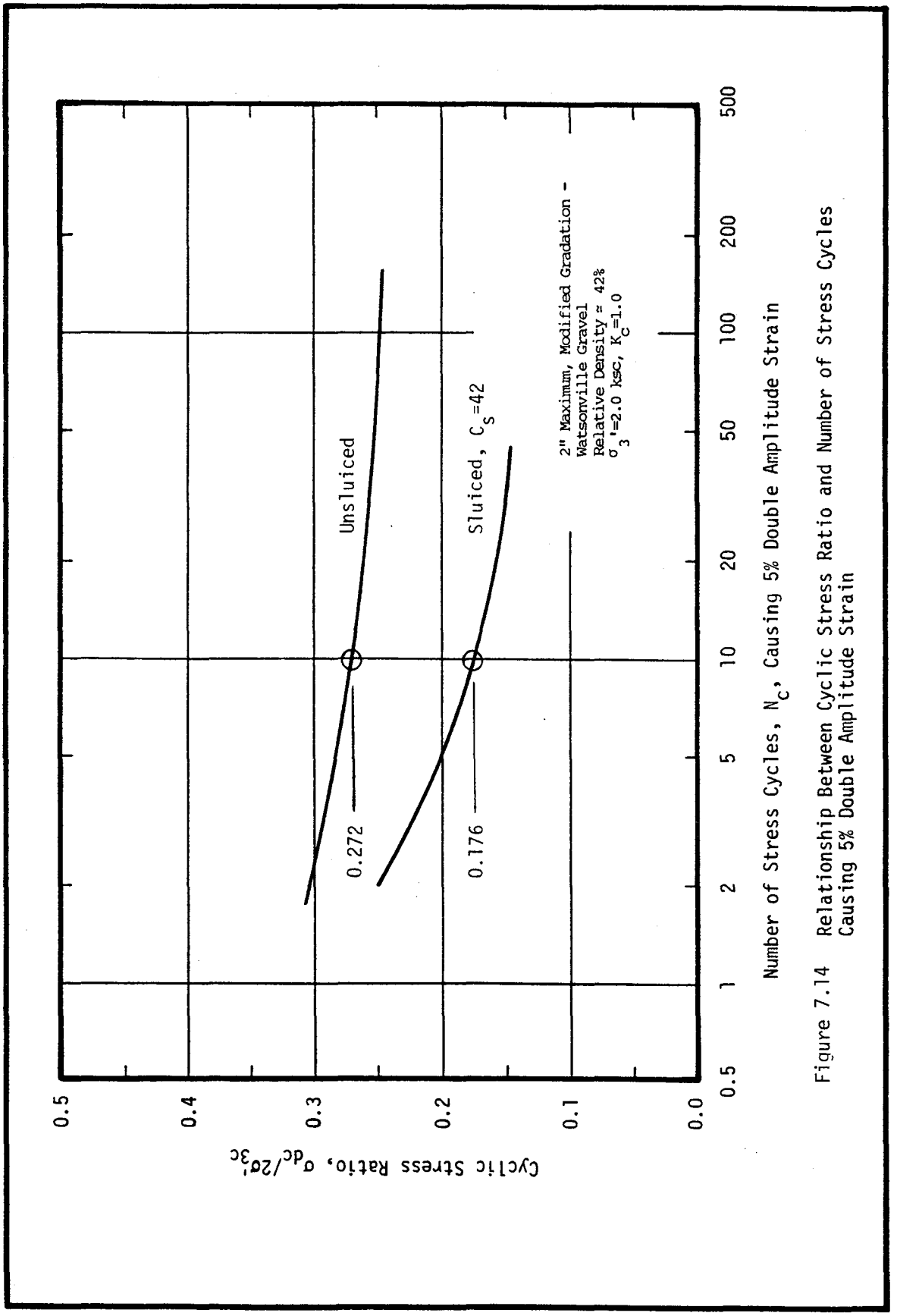

Figure 7.14 Relationship Between Cyclic Stress Ratio and Number of Stress Cycles Causing 5% Double Amplitude Strain

Table 7.1.0 Summary of Undrained Cyclic Triaxial Tests Performed on 2" Maximum, Modified Gradation - Watsonville Gravel

Test Group	Sluicing Sand	Gravel Relative Density, %	C_s	Comments*
1	none	42	-	
2	San Francisco Dune	42	42	
3	San Francisco Dune	62	42	

* - All test specimens are 12" diameter, dumped in 6 layers, one 0.1" membrane, $\sigma_3' = 2.0$ ksc, and $K_c = 1$ except as noted.

Table 7.1.1 Material Properties and Test Conditions Causing Failure During Undrained Cyclic Loading

GRAVEL: 2" Maximum, Modified Gradation - Watsonville
SLUICING SAND: none
C_s= -

Test No.	Gravel				Sand	
	Dry Density (pcf)	Void Ratio	Porosity	Relative Density (%)	Dry Density (pcf)	Void Ratio
2	101.6	0.708	0.415	40.7	-	-
3	100.9	0.720	0.419	37.8	-	-
4	103.0	0.685	0.407	46.3	-	-
5	102.7	0.690	0.408	45.1	-	-
6	102.5	0.693	0.409	44.3	-	-

Test No.	Cyclic Stress Ratio, $\sigma_d/2\sigma_{3c}$	Number of Cycles Causing...				
		80% Pore Pressure Ratio	100% Pore Pressure Ratio	2% Peak to Peak Strain	5% Peak to Peak Strain	10% Peak to Peak Strain
2	0.236	-	100	84	92	-
3	0.270	-	-	2.8	4.8	15.0
4	0.303	-	7.8	5.5	8.1	18.0
5	0.345	-	1.4	0.70	1.2	1.9
6	0.307	-	1.9	0.85	1.5	2.6

* - All test specimens are 12" diameter, dumped in 6 layers, one 0.1" membrane, σ_3'= 2.0 ksc, and K_c=1.

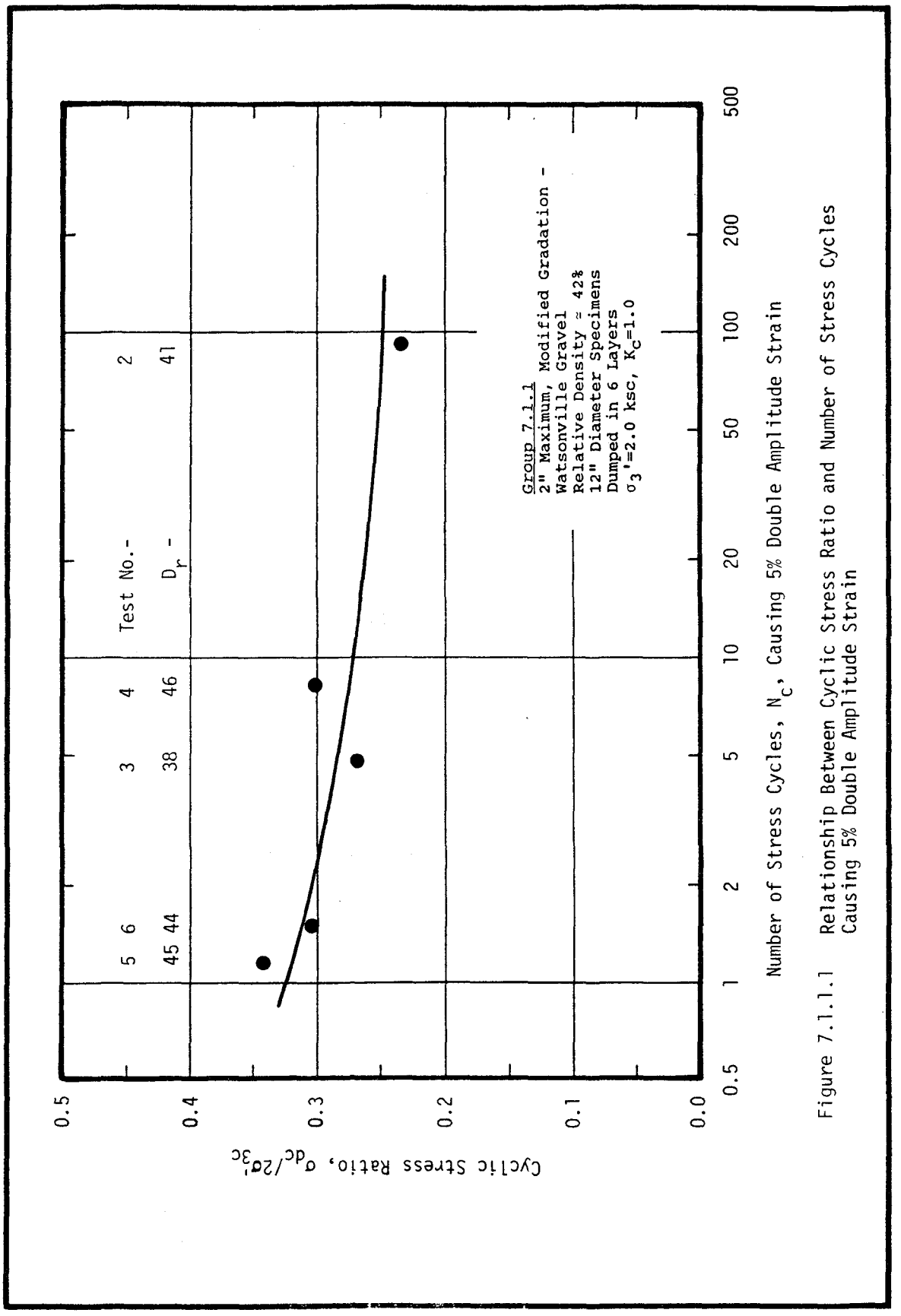

Figure 7.1.1.1 Relationship Between Cyclic Stress Ratio and Number of Stress Cycles Causing 5% Double Amplitude Strain

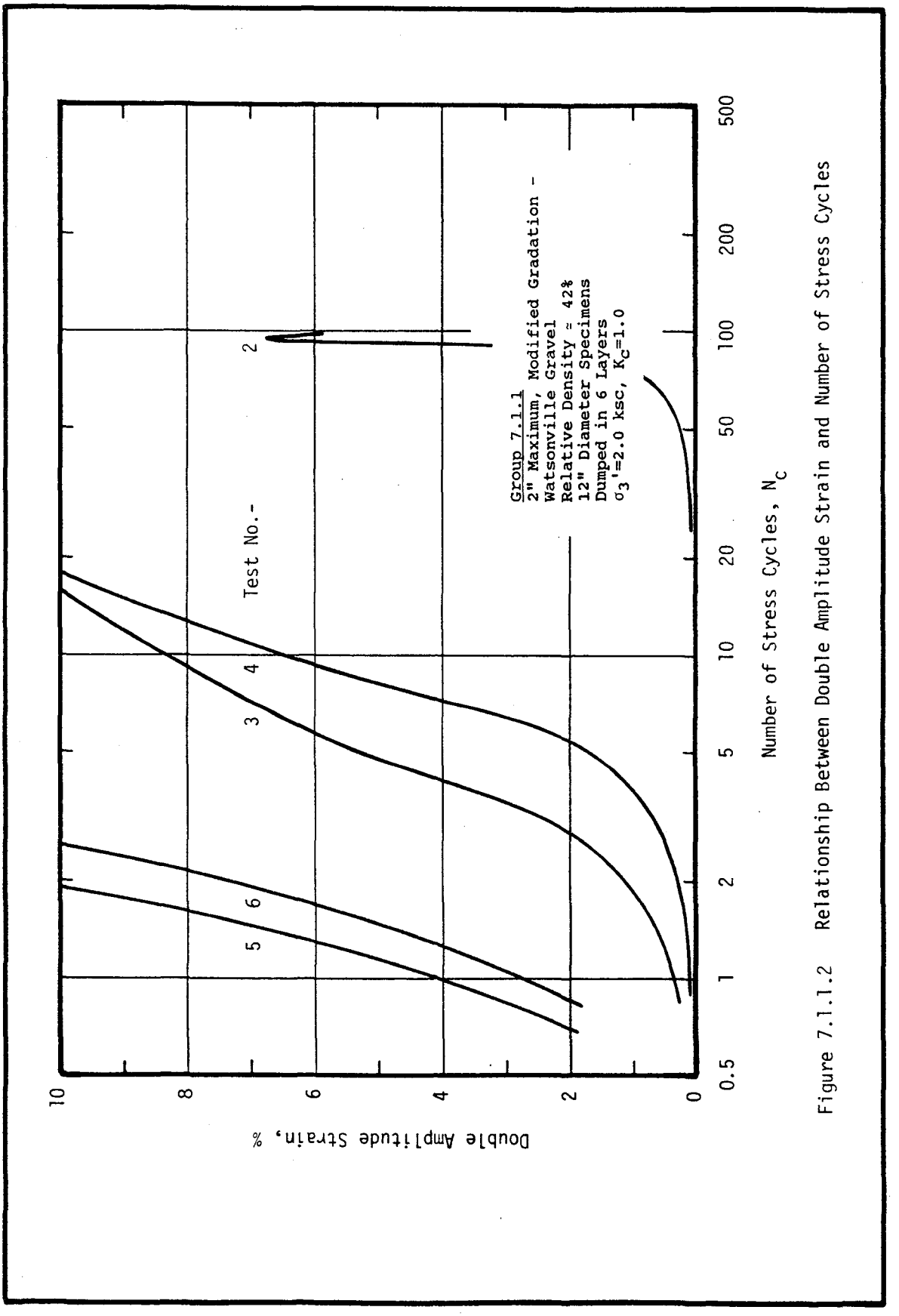

Figure 7.1.1.2 Relationship Between Double Amplitude Strain and Number of Stress Cycles

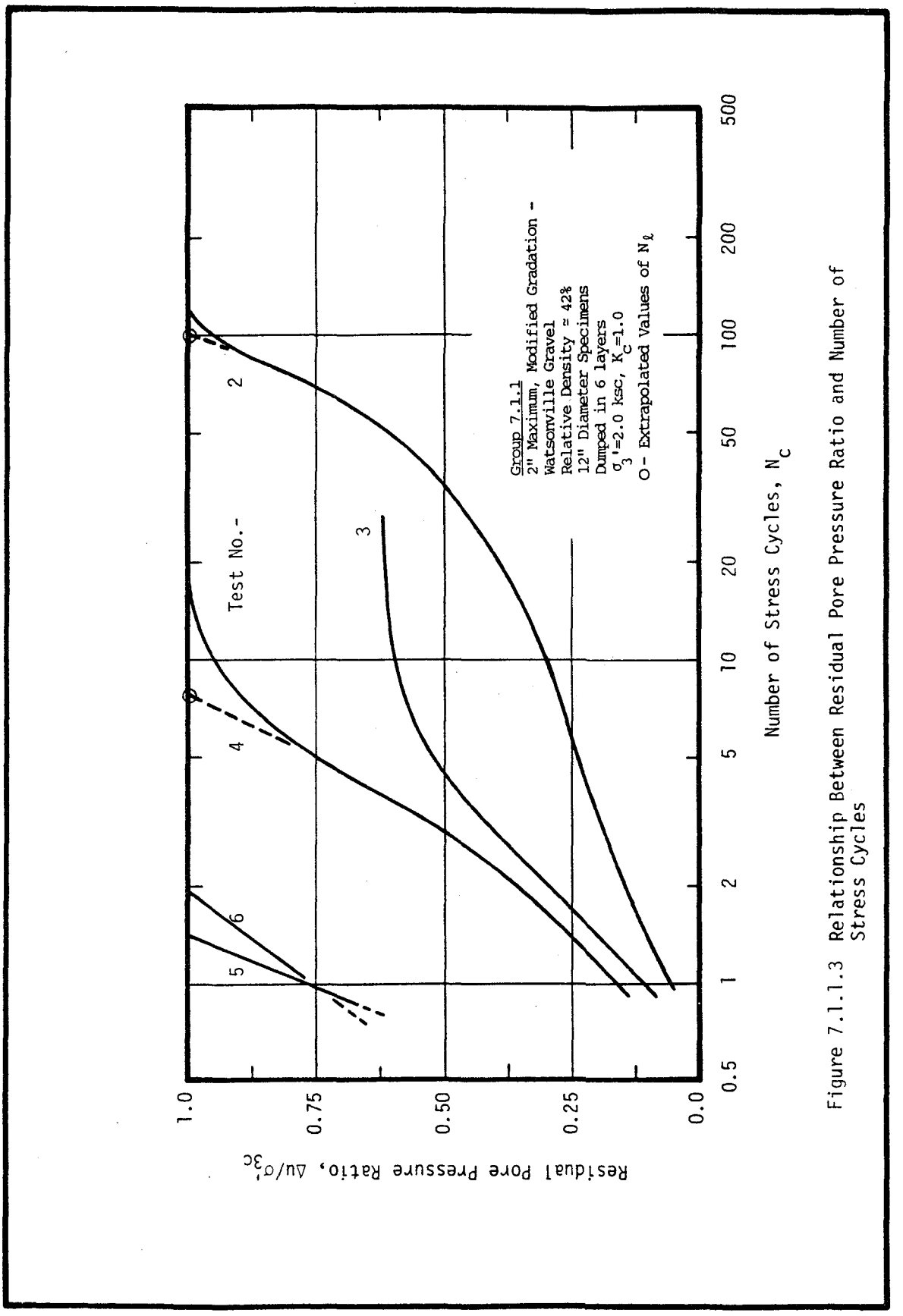

Figure 7.1.1.3 Relationship Between Residual Pore Pressure Ratio and Number of Stress Cycles

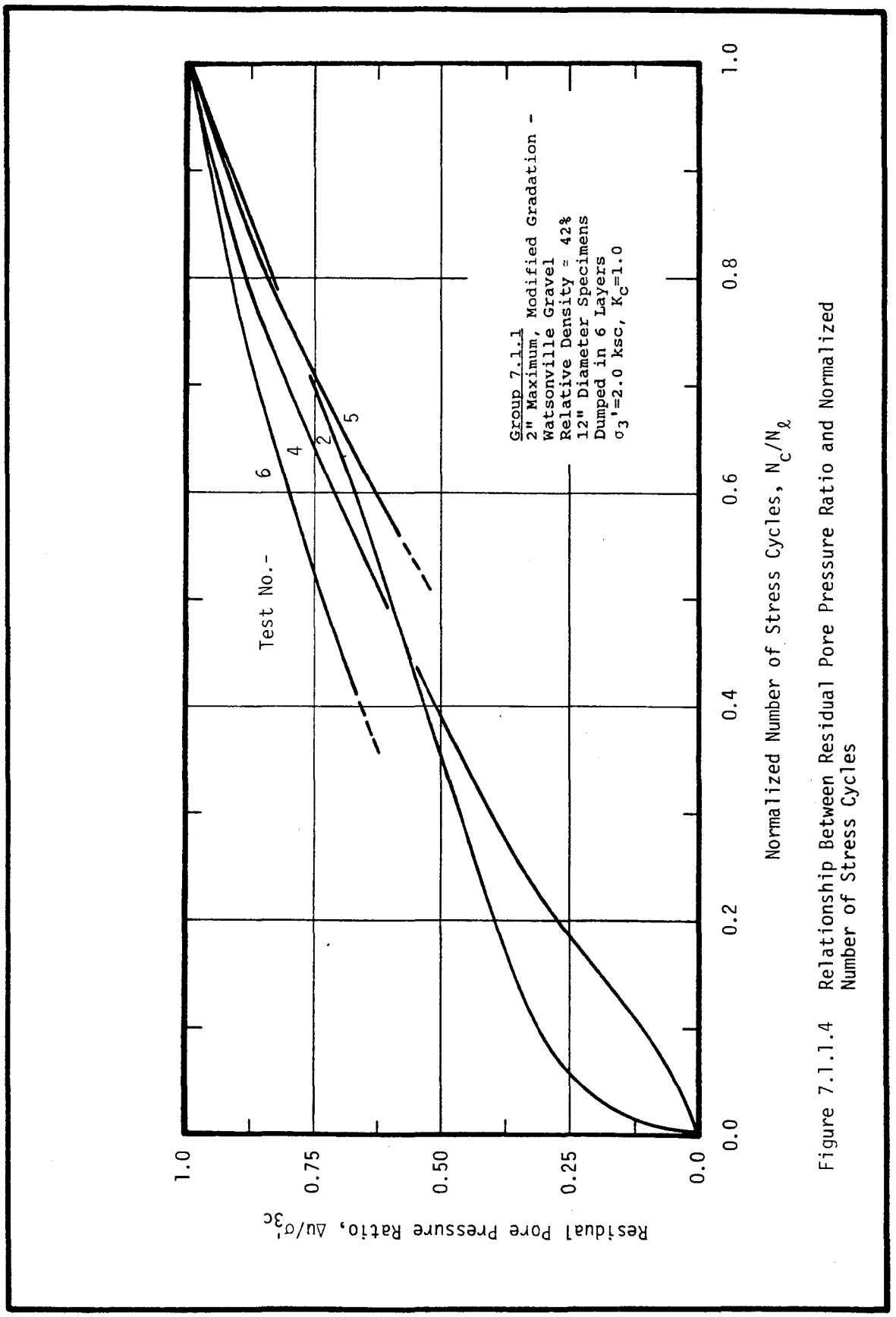

Figure 7.1.1.4 Relationship Between Residual Pore Pressure Ratio and Normalized Number of Stress Cycles

Table 7.1.2 Material Properties and Test Conditions Causing Failure During Undrained Cyclic Loading

GRAVEL: 2" Maximum, Modified Gradation - Watsonville
SLUICING SAND: San Francisco Dune
C_s=42

Test No.	Gravel				Sand	
	Dry Density (pcf)	Void Ratio	Porosity	Relative Density (%)	Dry Density (pcf)	Void Ratio
7	101.7	0.707	0.414	41.1	84.4	0.997
9	101.5	0.710	0.415	40.3	89.4	0.885
10	102.6	0.692	0.409	44.7	86.1	0.958
11	100.4	0.729	0.422	35.8	87.1	0.935

Test No.	Cyclic Stress Ratio, $\sigma_d/2\sigma_{3c}$	Number of Cycles Causing...				
		80% Pore Pressure Ratio	100% Pore Pressure Ratio	2% Peak to Peak Strain	5% Peak to Peak Strain	10% Peak to Peak Strain
7	0.238	-	1.0	1.6	2.5	3.8
9	0.180	-	6.2	7.0	8.8	11.0
10	0.150	-	23.0	25.0	29.0	-
11	0.170	-	11.0	12.0	13.5	15.0

* - All test specimens are 12" diameter, dumped in 6 layers, one 0.1" membrane, σ_3'= 2.0 ksc, and K_c=1.

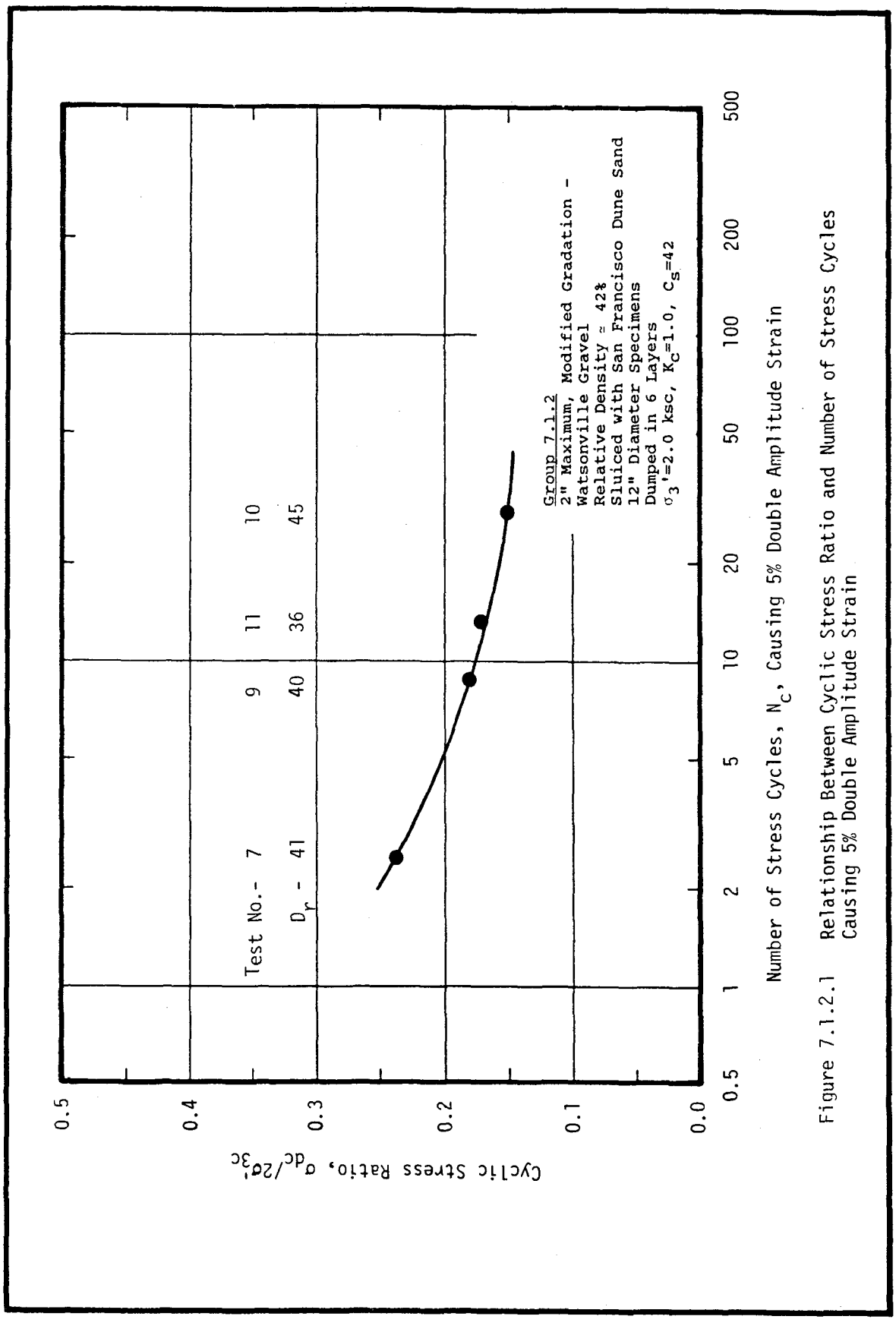

Figure 7.1.2.1 Relationship Between Cyclic Stress Ratio and Number of Stress Cycles Causing 5% Double Amplitude Strain

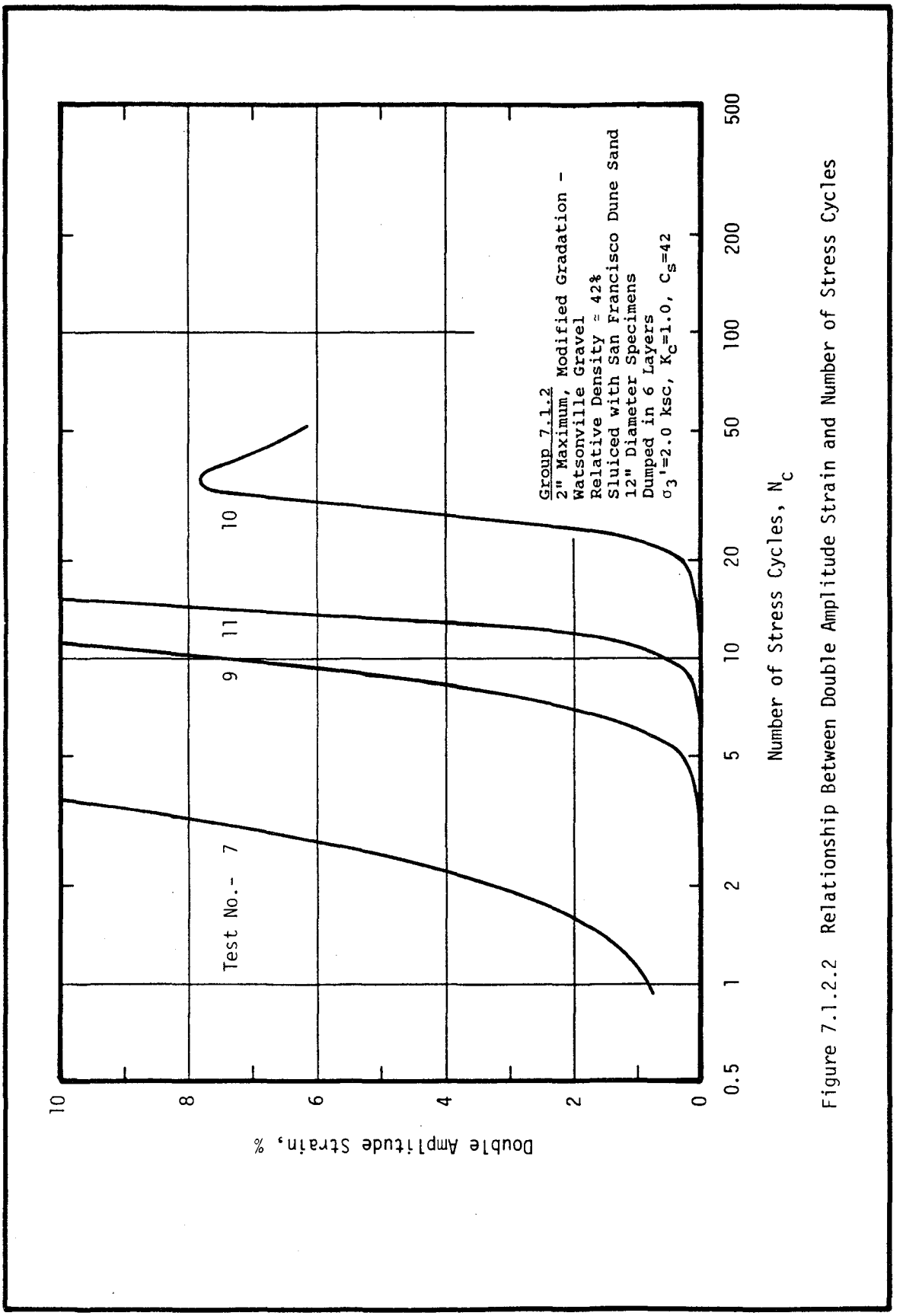

Figure 7.1.2.2 Relationship Between Double Amplitude Strain and Number of Stress Cycles

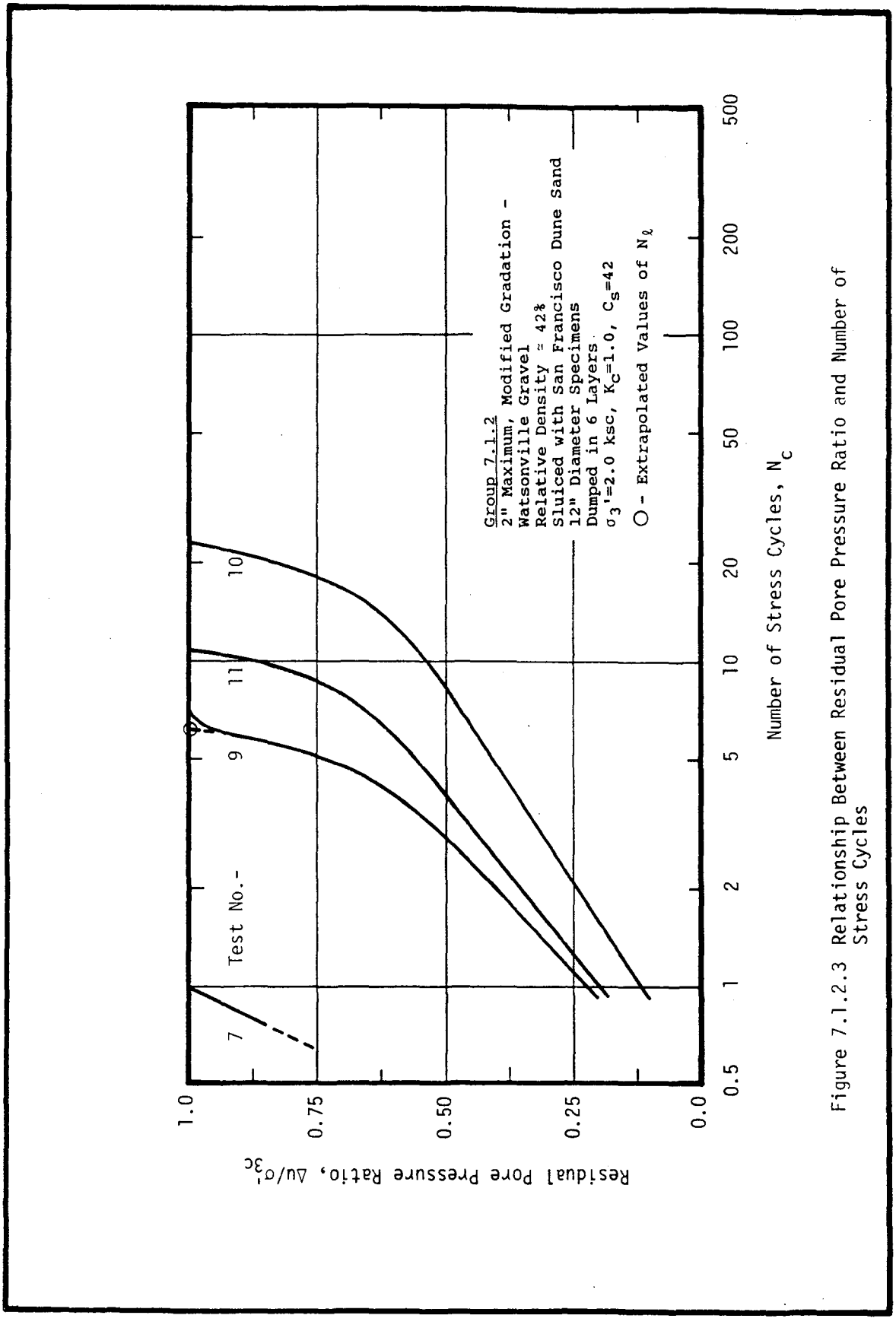

Figure 7.1.2.3 Relationship Between Residual Pore Pressure Ratio and Number of Stress Cycles

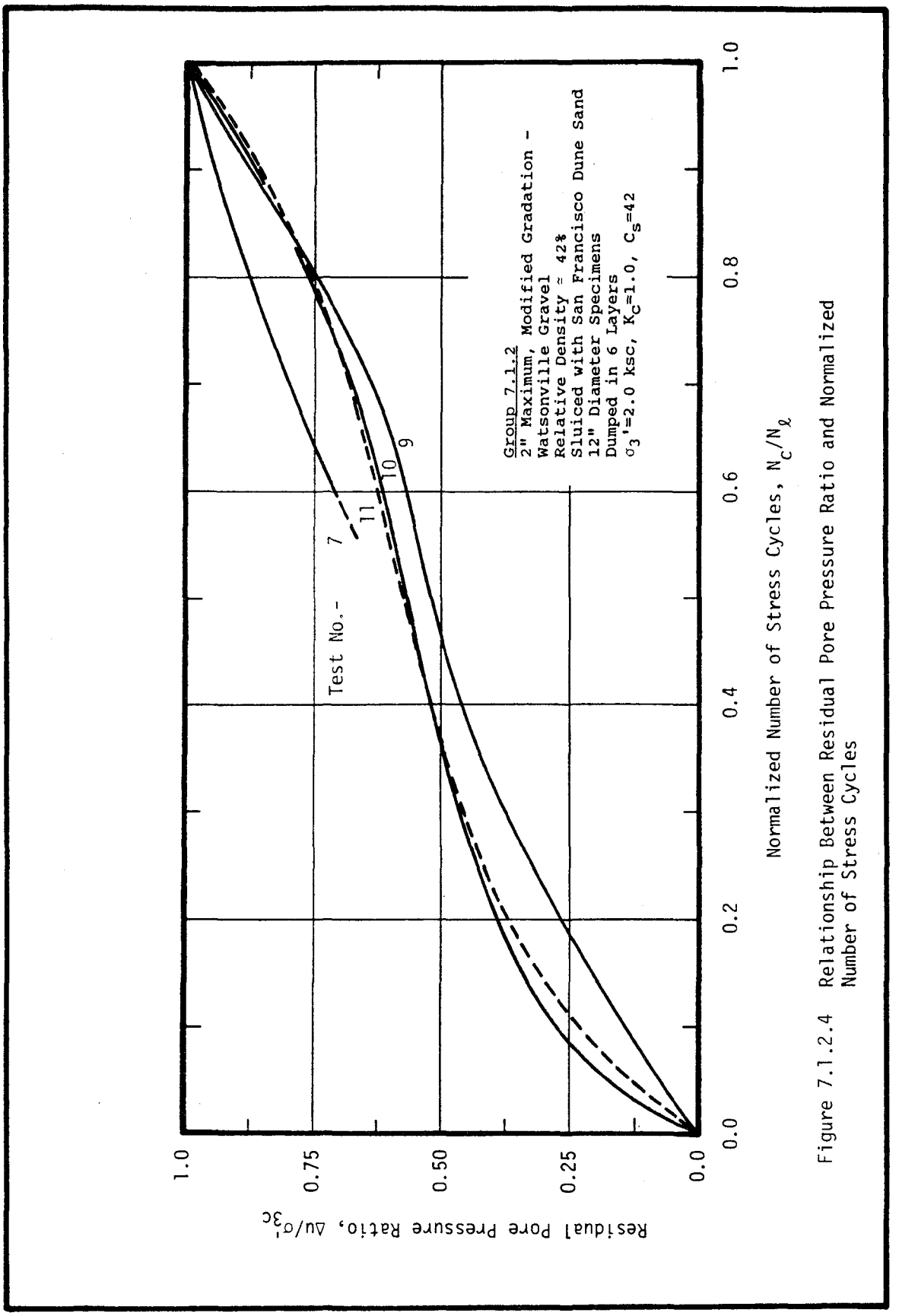

Figure 7.1.2.4 Relationship Between Residual Pore Pressure Ratio and Normalized Number of Stress Cycles

Table 7.1.3 Material Properties and Test Conditions Causing Failure During Undrained Cyclic Loading

GRAVEL: 2" Maximum, Modified Gradation - Watsonville
SLUICING SAND: San Francisco Dune
C_s=42

Test No.	Gravel				Sand	
	Dry Density (pcf)	Void Ratio	Porosity	Relative Density (%)	Dry Density (pcf)	Void Ratio
12	107.9	0.608	0.378	64.9	70.0	1.408
13	106.9	0.624	0.384	61.2	64.2	1.626
14	107.2	0.619	0.382	62.3	59.5	1.833

Test No.	Cyclic Stress Ratio, $\sigma_d/2\sigma_{3c}$	Number of Cycles Causing...				
		80% Pore Pressure Ratio	100% Pore Pressure Ratio	2% Peak to Peak Strain	5% Peak to Peak Strain	10% Peak to Peak Strain
12	0.210	-	11.0	12.0	15.0	20.0
13	0.220	-	3.3	3.3	4.1	5.0
14	0.223	-	6.8	6.5	7.8	9.0

* - All test specimens are 12" diameter, dumped in 6 layers, one 0.1" membrane, σ_3'= 2.0 ksc, and K_c=1.

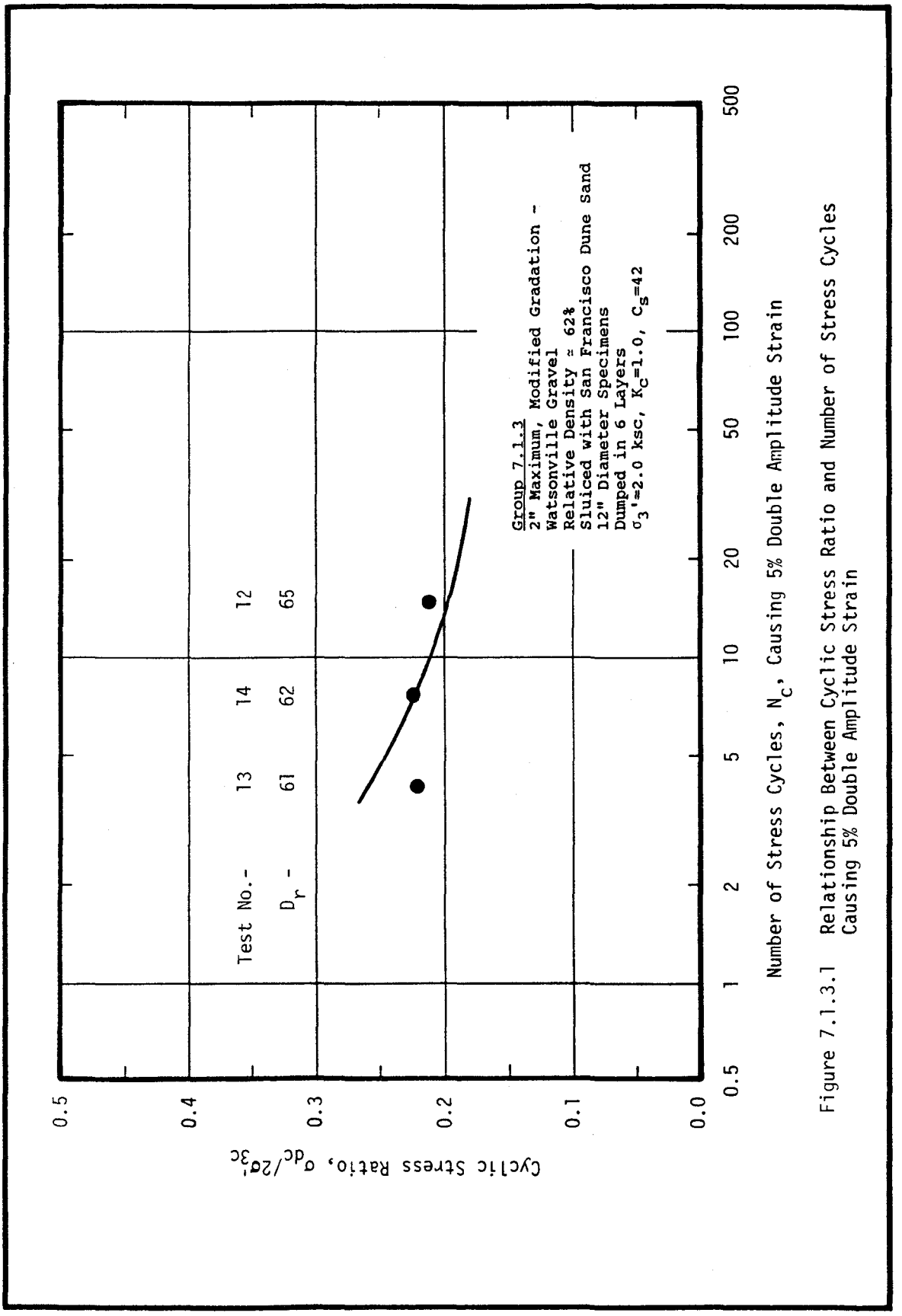

Figure 7.1.3.1 Relationship Between Cyclic Stress Ratio and Number of Stress Cycles Causing 5% Double Amplitude Strain

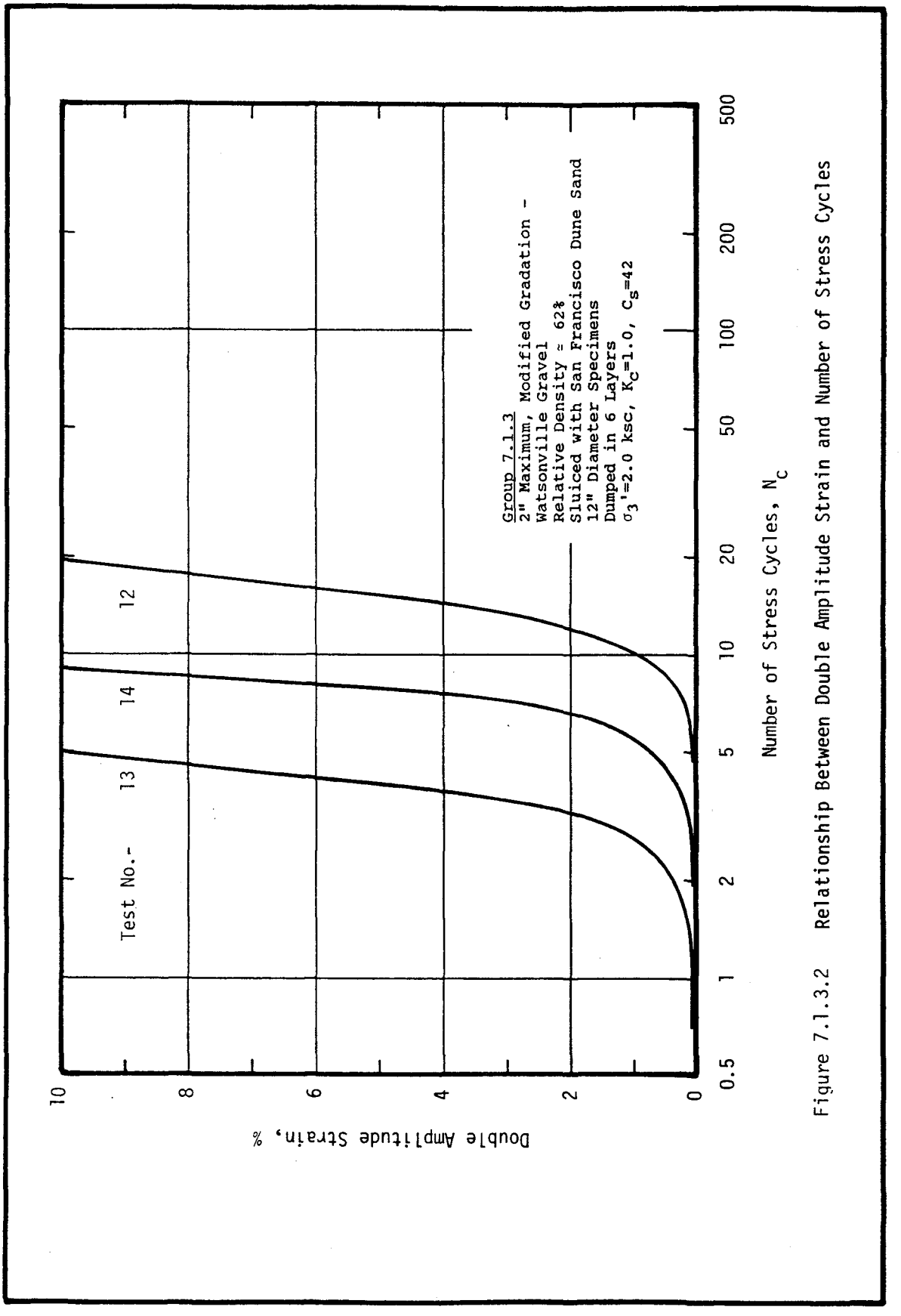

Figure 7.1.3.2 Relationship Between Double Amplitude Strain and Number of Stress Cycles

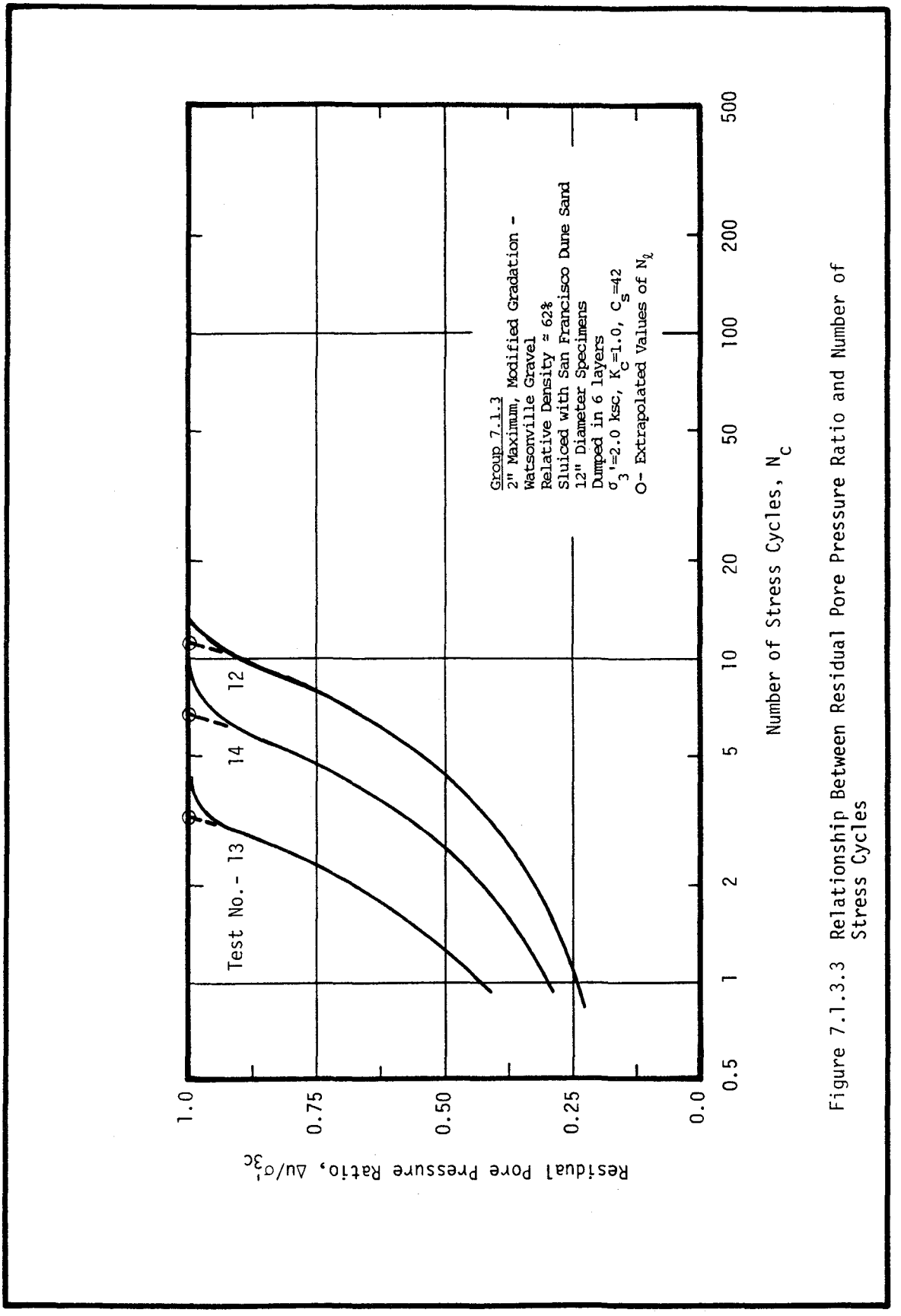

Figure 7.1.3.3 Relationship Between Residual Pore Pressure Ratio and Number of Stress Cycles

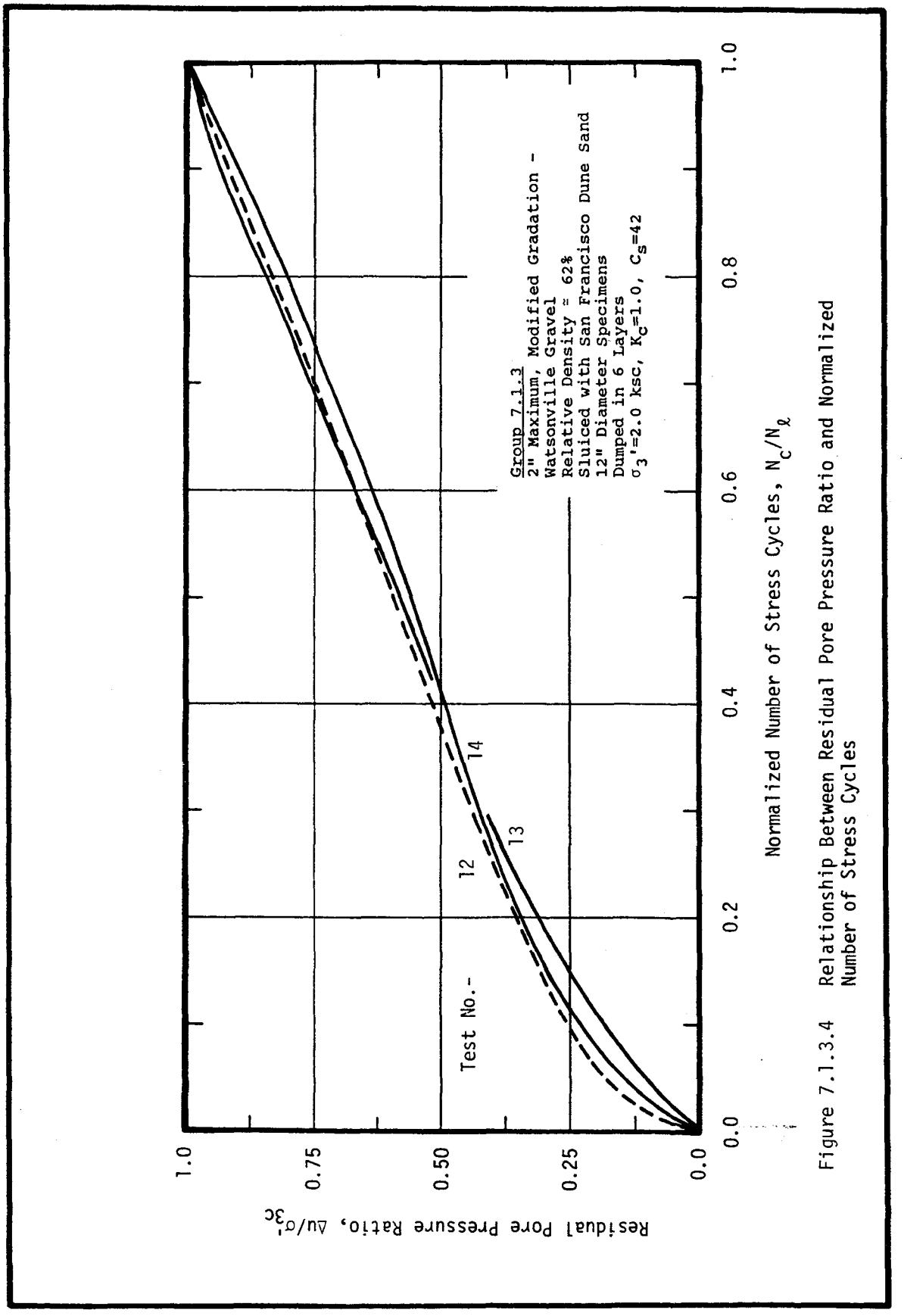

Figure 7.1.3.4 Relationship Between Residual Pore Pressure Ratio and Normalized Number of Stress Cycles

effect of membrane compliance in the unsluiced specimens is believed to be the major cause of the difference in the cyclic loading resistance of these two materials. Sluicing the gravel specimens with sand significantly reduced the effect of membrane compliance on the results of the undrained, cyclic triaxial tests. The resulting cyclic strength of the sluiced specimens would seem to be more representative of the true, undrained cyclic strength of the gravel which would be expected to occur in the field. The results from tests performed on unsluiced, compliant specimens of this particular gravel may then overestimate the true, noncompliant cyclic strength of the gravel by about 55%.

Figure 7.15 presents a comparison of the cyclic loading resistance of the sluiced gravel specimens at relative densities of 42% and 62% with the cyclic loading resistance of 12 inch diameter specimens of 2" x #200 very well-graded Oroville gravel ($C_u \simeq 40$) at a relative density of 60% determined by Wong et al. (1974). The effect of membrane compliance on the cyclic loading resistance of specimens of the well-graded Oroville gravel, or any other well-graded material, is expected to be very small because such materials produce specimens with very small surficial voids, and thus very little membrane penetration volume change will occur during consolidation. These two materials, the sluiced gravel and the very well-graded gravel both at relative densities of about 60%, would then be expected to have generally similar values of cyclic loading resistance since membrane compliance effects are minimized in both systems. It may be seen from Figure 7.15 that both gravels do have similar levels of cyclic loading resistance and the small difference in strength that does exist may easily be

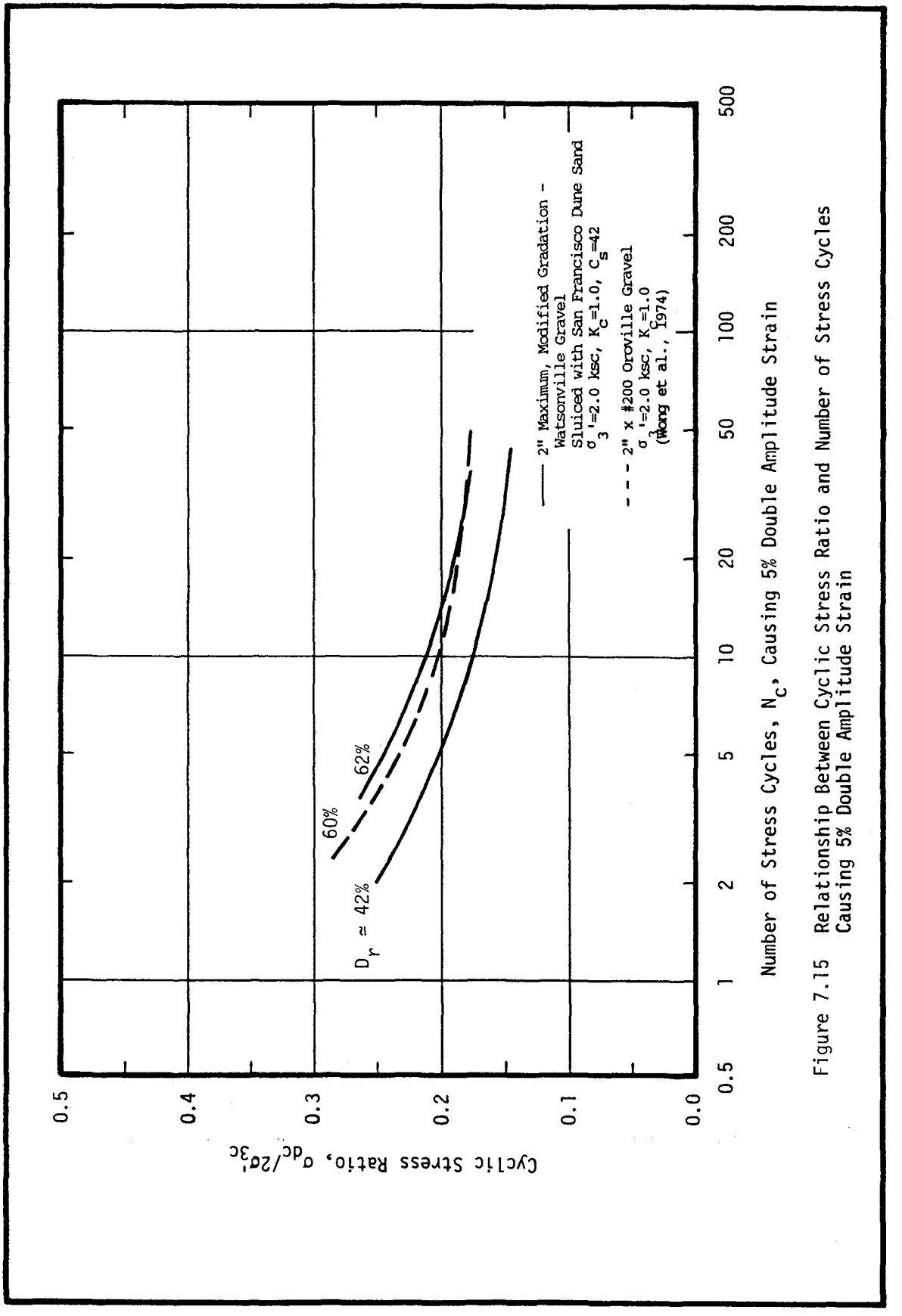

Figure 7.15 Relationship Between Cyclic Stress Ratio and Number of Stress Cycles Causing 5% Double Amplitude Strain

explained by differences in material properties and specimen construction procedures.

Combinations of cyclic stress ratio and numbers of stress cycles producing different levels of residual pore pressure ratio for sluiced and unsluiced gravel specimens at a relative density of 42% are shown in Figure 7.16. It may be noted that the 100% pore pressure ratio relationships for the sluiced gravel approximately coincides with the 12% pore pressure relationship for the unsluiced gravel. These relationships indicate that the value of cyclic stress ratio which causes a pore pressure ratio of 100% for the 2" maximum, modified gradation Watsonville gravel in a noncompliant test system, may be determined from cyclic compression tests performed on unsluiced gravel specimens, provided that the value of cyclic stress ratio which causes 12% pore pressure ratio is used as the failure load. In other words, according to these results, the stress ratio required to cause 12% pore pressure ratio in 10 stress cycles in the compliant system, is representative of the stress ratio which would be expected to cause a pore pressure ratio of 100% (or approximately 5% double amplitude strain) in an undrained, noncompliant testing system.

These data illustrate the potential magnitude of the effect of membrane compliance on the results of cyclic triaxial tests performed on gravel specimens when membrane penetration volume changes occur prior to and during undrained testing. If little membrane penetration occurs, in very well-graded gravel specimens for example, the compliance effect may be small. On the other hand, the effect of compliance is considerable when a significant amount of membrane penetration occurs during consolidation of coarse, uniform gravel

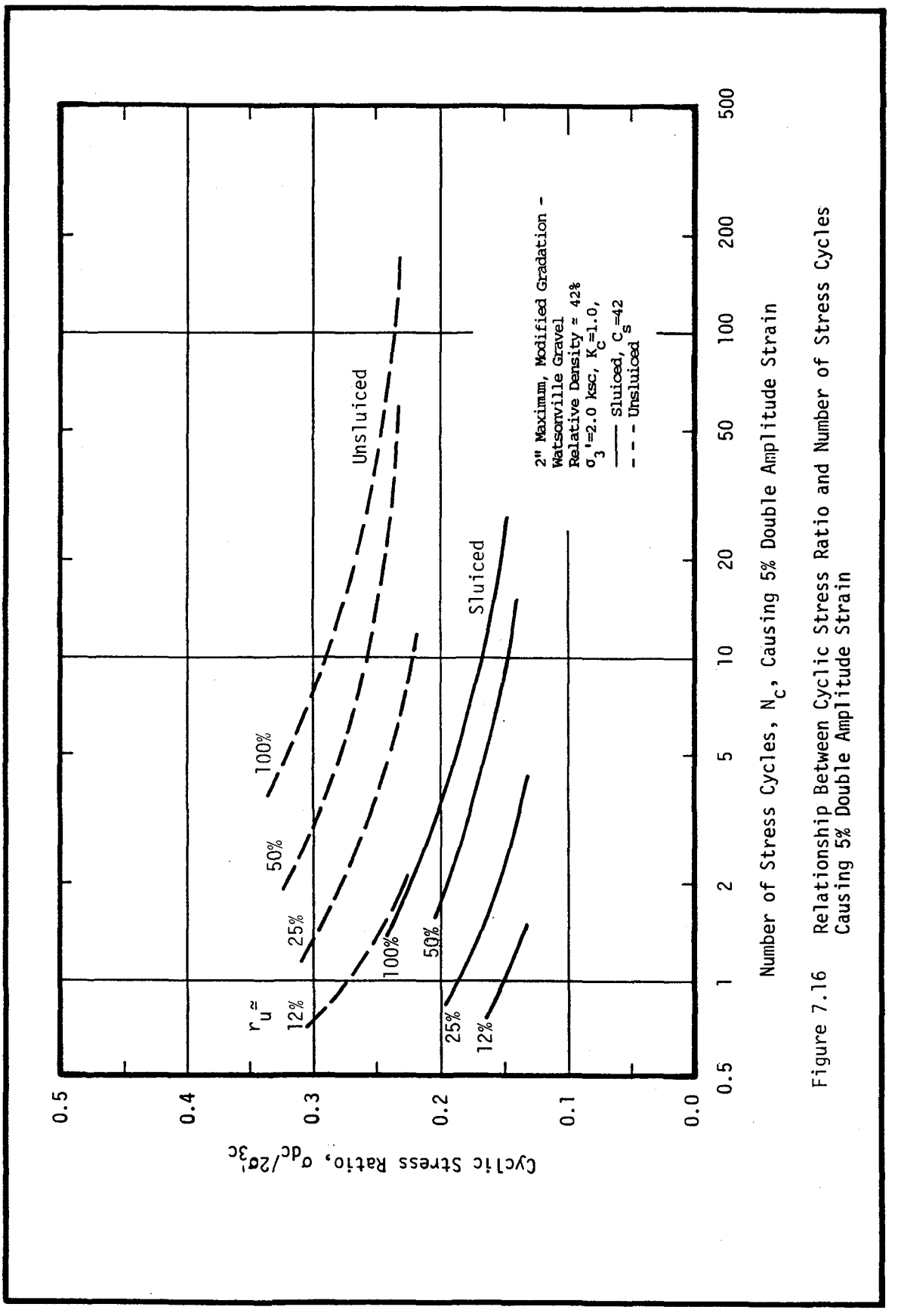

Figure 7.16 Relationship Between Cyclic Stress Ratio and Number of Stress Cycles Causing 5% Double Amplitude Strain

specimens. It is clearly not meant to imply by these results that only 60% to 65% of the cyclic strength of the gravel, as determined by triaxial testing, should be used as a design criterion in all cases. Rather, the results are intended only to illustrate the significance of the effect of membrane compliance that can occur when performing undrained, cyclic load triaxial tests on specimens of gravels and gravelly soils.

Tests Performed on 1-1/2" x 3/4" Watsonville Gravel Specimens

Test Data Presentation

Four groups of undrained, cyclic triaxial tests were performed on 12 inch diameter specimens of 1-1/2" x 3/4" Watsonville gravel as summarized in Table 7.2.0. Most specimens were constructed by gently placing the gravel particles into the specimen mold, a few at a time, in order to create a loose structure ($D_r \simeq 22\%$ to 25%). The specimens in one group were constructed by pluviating the material through air with a fixed height of fall in order to created a structure of moderate density ($D_r \simeq 50\%$). Two groups were sluiced with Monterey No. 0 sand resulting in a value of $C_s = 50$. Test group no. 4 was performed on specimens which had a thin sand shell constructed around the outside of the gravel confining membrane as described in Chapter 6. Tables 7.2.1, 7.2.2, 7.2.3, and 7.2.4 summarize the relevant test data for these test groups. Figures 7.2.1.1 through 7.2.4.4 are included along with these tables and contain the test data as described earlier in this chapter.

Table 7.2.0 Summary of Undrained Cyclic Triaxial Tests Performed on 1-1/2" x 3/4" Watsonville Gravel

Test Group	Sluicing Sand	Gravel Relative Density, %	C_s	Comments*
1	none	22	-	
2	Monterey No.0	22	50	
3	none	50	-	pluviated
4	none	25	-	(1)
	Monterey No. 0	25	50	(1)

* - All test specimens are 12" diameter, particles hand placed, one 0.1" membranes, $\sigma_3' = 2.0$ ksc, and $K_c=1$ except as noted.

(1) A thin sand shell was constructed around the outside of the membrane for all specimens.

Table 7.2.1 Material Properties and Test Conditions Causing Failure During Undrained Cyclic Loading

GRAVEL: 1-1/2" x 3/4" Watsonville Gravel
SLUICING SAND: none
C_s = -

Test No.	Gravel				Sand	
	Dry Density (pcf)	Void Ratio	Porosity	Relative Density (%)	Dry Density (pcf)	Void Ratio
A	90.59	0.916	0.478	23.3	-	-
B	89.88	0.931	0.482	19.6	-	-

Test No.	Cyclic Stress Ratio, $\sigma_d/2\sigma_{3c}$	Number of Cycles Causing...				
		80% Pore Pressure Ratio	100% Pore Pressure Ratio	2% Peak to Peak Strain	5% Peak to Peak Strain	10% Peak to Peak Strain
A	0.223	-	8.8	7.4	8.4	9.8
B	0.198	-	26.0	22.0	24.0	27.0

* - All test specimens are 12" diameter, particles hand placed, one 0.1" membrane, σ_3'= 2.0 ksc, and K_c=1.

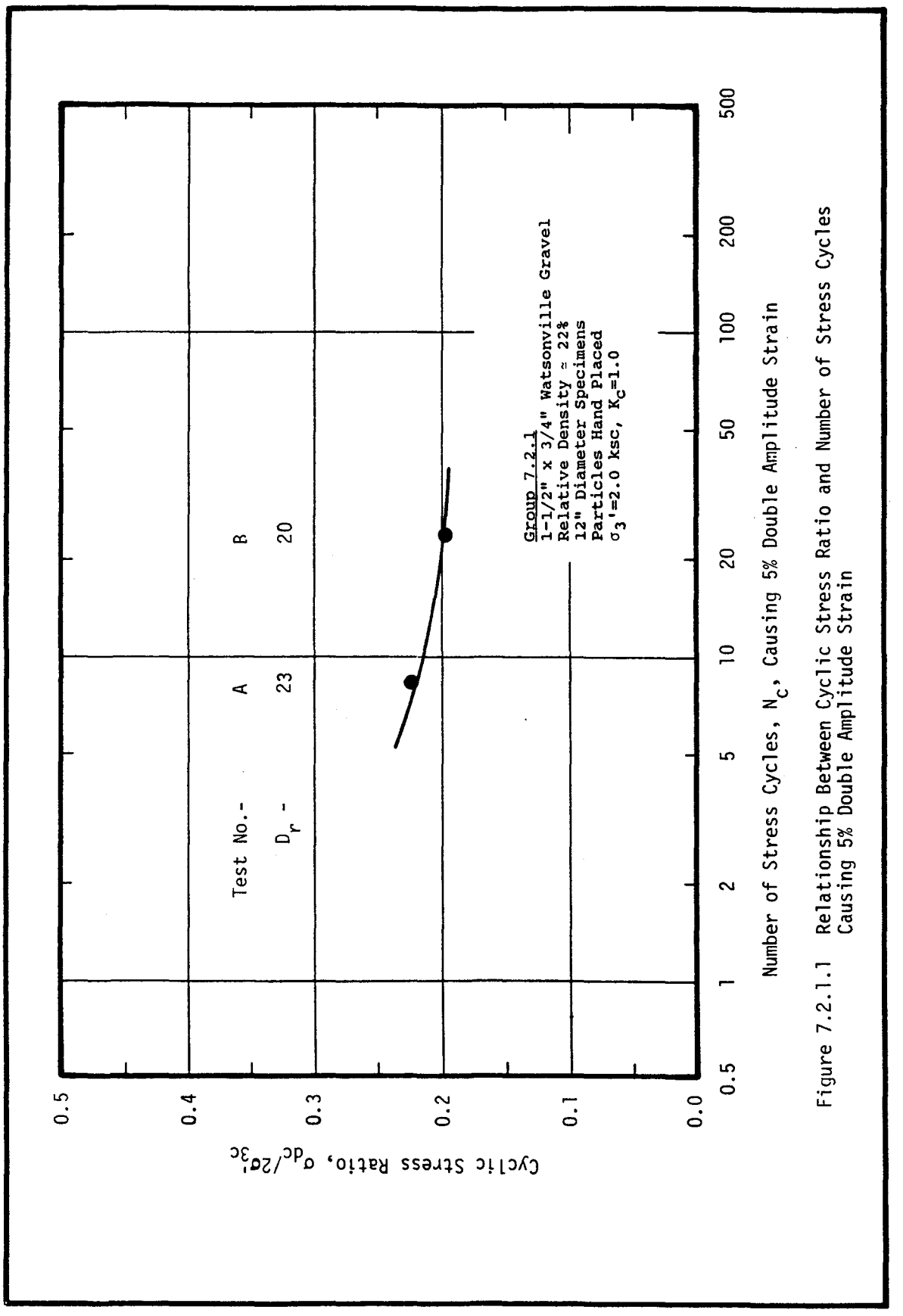

Figure 7.2.1.1 Relationship Between Cyclic Stress Ratio and Number of Stress Cycles Causing 5% Double Amplitude Strain

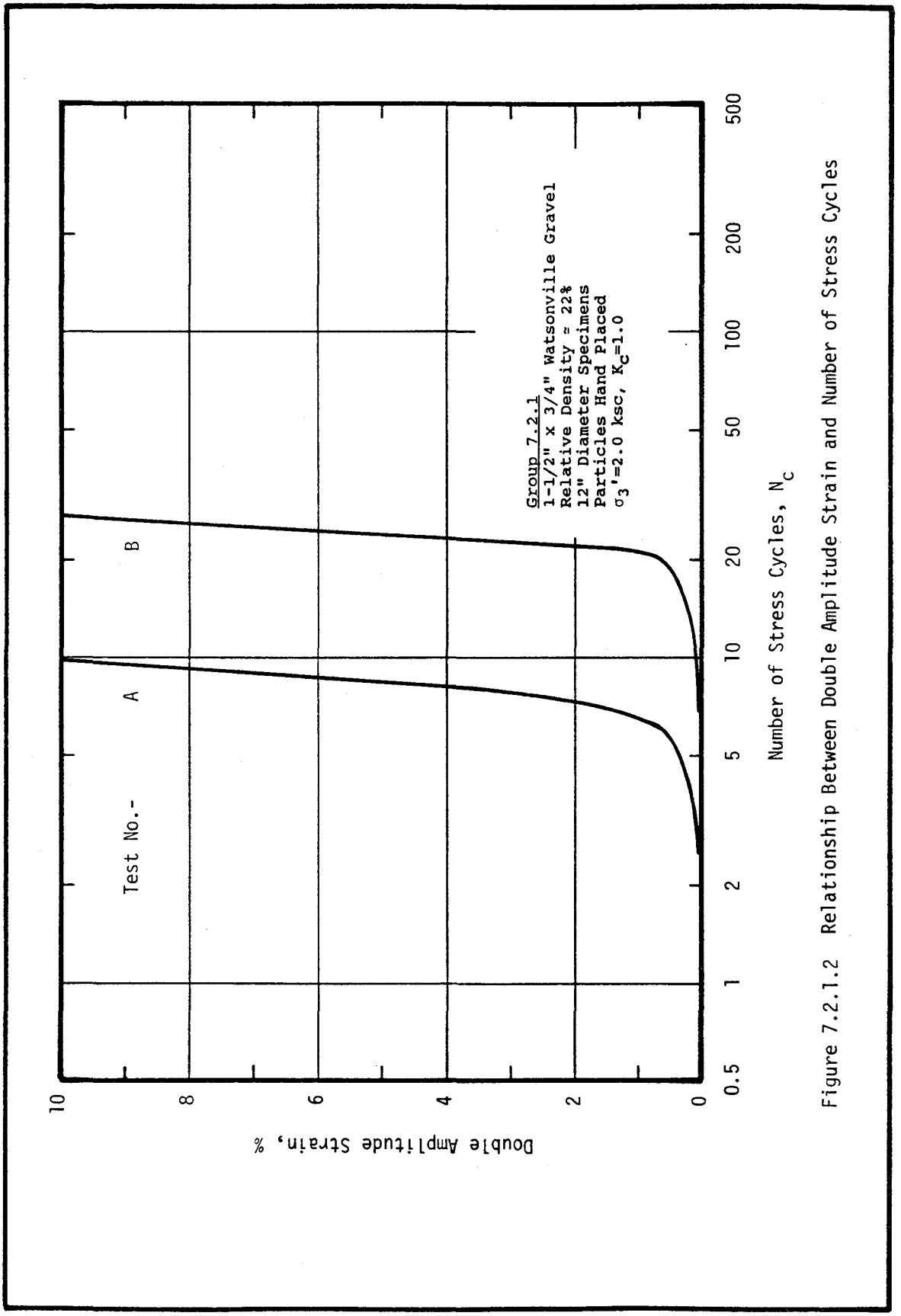

Figure 7.2.1.2 Relationship Between Double Amplitude Strain and Number of Stress Cycles

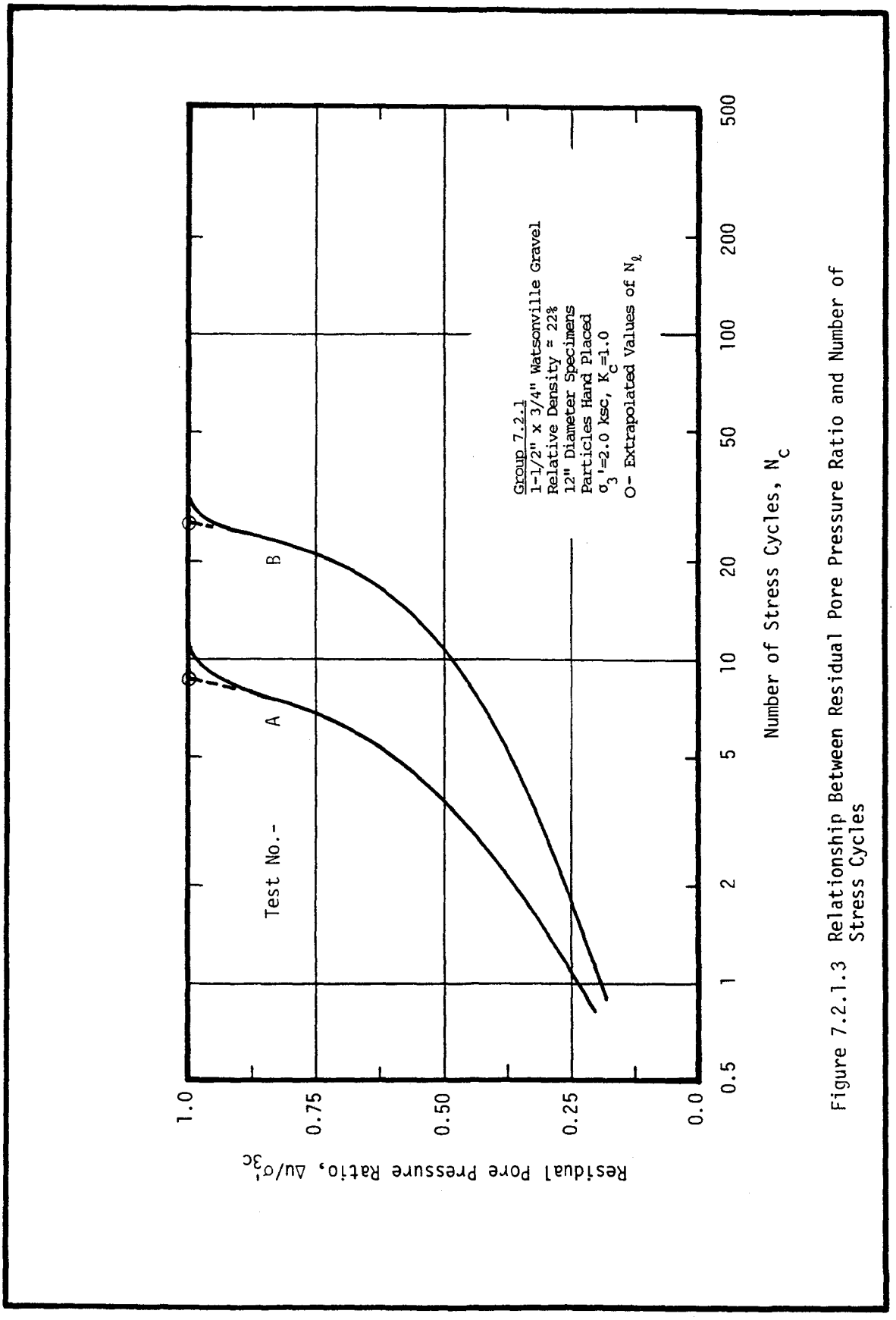

Figure 7.2.1.3 Relationship Between Residual Pore Pressure Ratio and Number of Stress Cycles

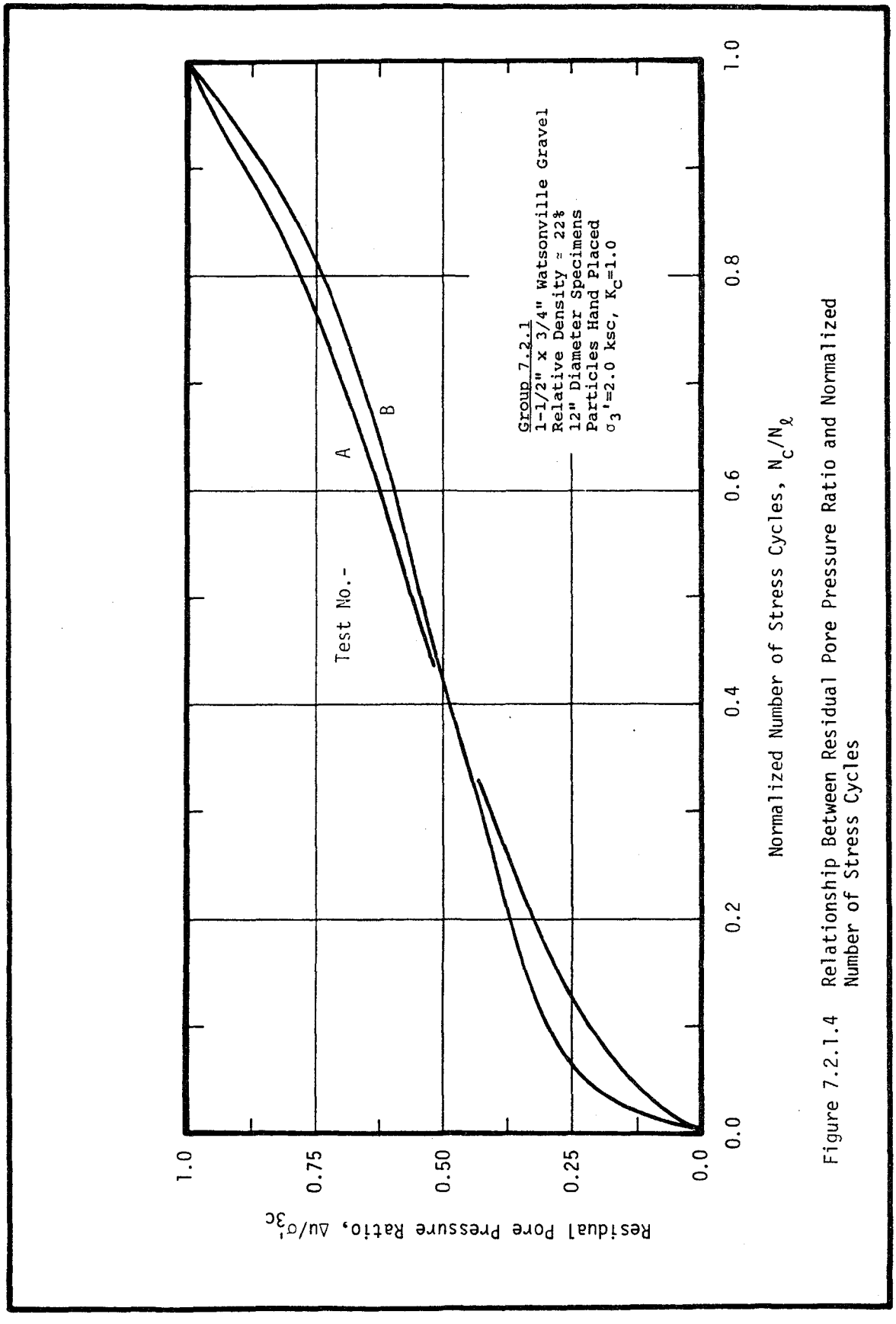

Figure 7.2.1.4 Relationship Between Residual Pore Pressure Ratio and Normalized Number of Stress Cycles

Table 7.2.2 Material Properties and Test Conditions Causing Failure During Undrained Cyclic Loading

GRAVEL: 1-1/2" x 3/4" Watsonville Gravel
SLUICING SAND: Monterey No. 0
C_s=50

Test No.	Gravel				Sand	
	Dry Density (pcf)	Void Ratio	Porosity	Relative Density (%)	Dry Density (pcf)	Void Ratio
13	90.30	0.922	0.480	21.8	87.4	0.886
14	89.89	0.931	0.482	19.7	86.3	0.910
15	89.69	0.935	0.483	18.6	87.8	0.877

Test No.	Cyclic Stress Ratio, $\sigma_d/2\sigma_{3c}$	Number of Cycles Causing...				
		80% Pore Pressure Ratio	100% Pore Pressure Ratio	2% Peak to Peak Strain	5% Peak to Peak Strain	10% Peak to Peak Strain
13	0.136	-	11.4	12.2	13.8	-
14	0.171	-	4.2	4.2	4.9	6.1
15	0.120	-	35.0	35.0	37.0	-

* - All test specimens are 12" diameter, particles hand placed, one 0.1" membrane, σ_3'= 2.0 ksc, and K_c=1.

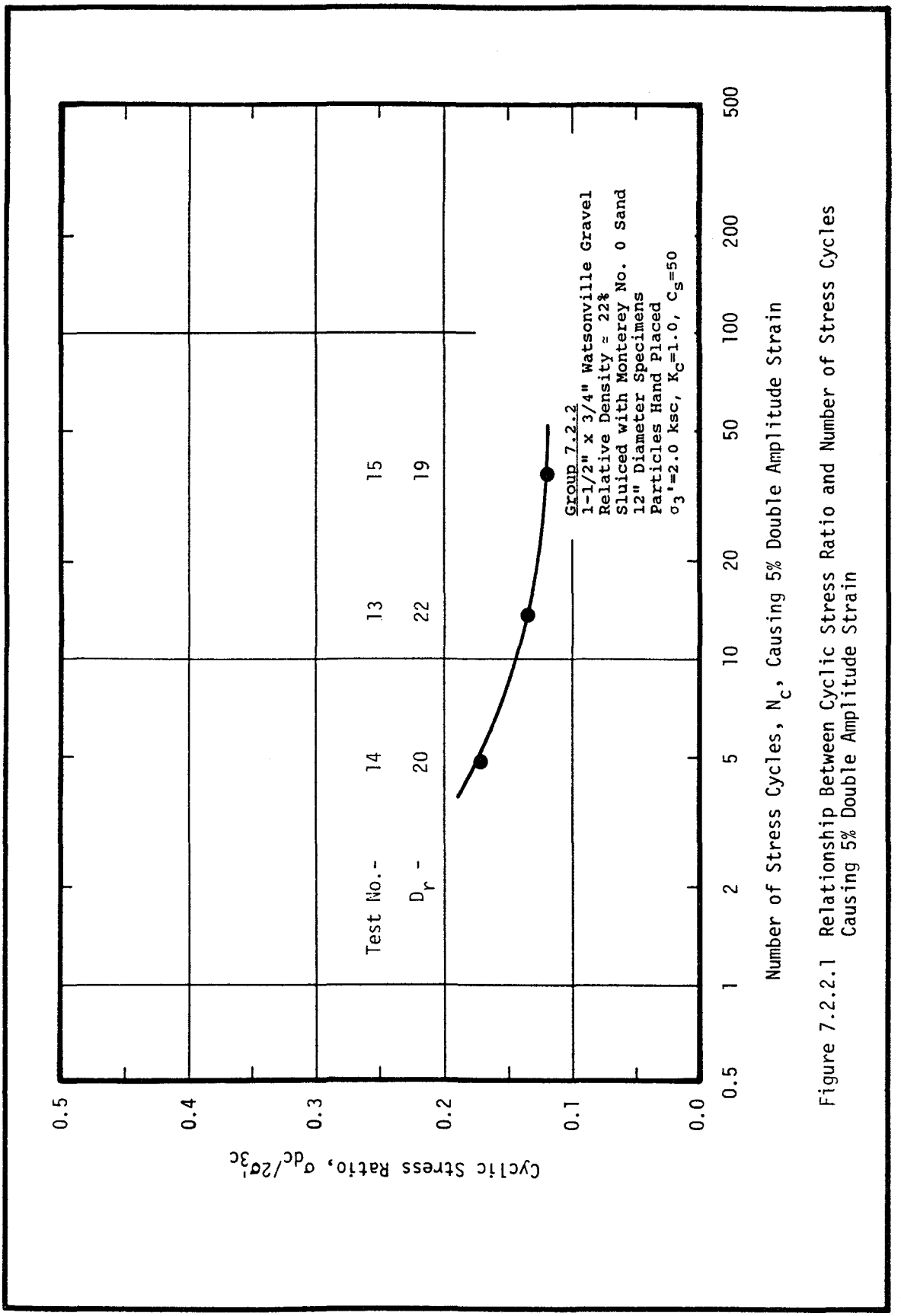

Figure 7.2.2.1 Relationship Between Cyclic Stress Ratio and Number of Stress Cycles Causing 5% Double Amplitude Strain

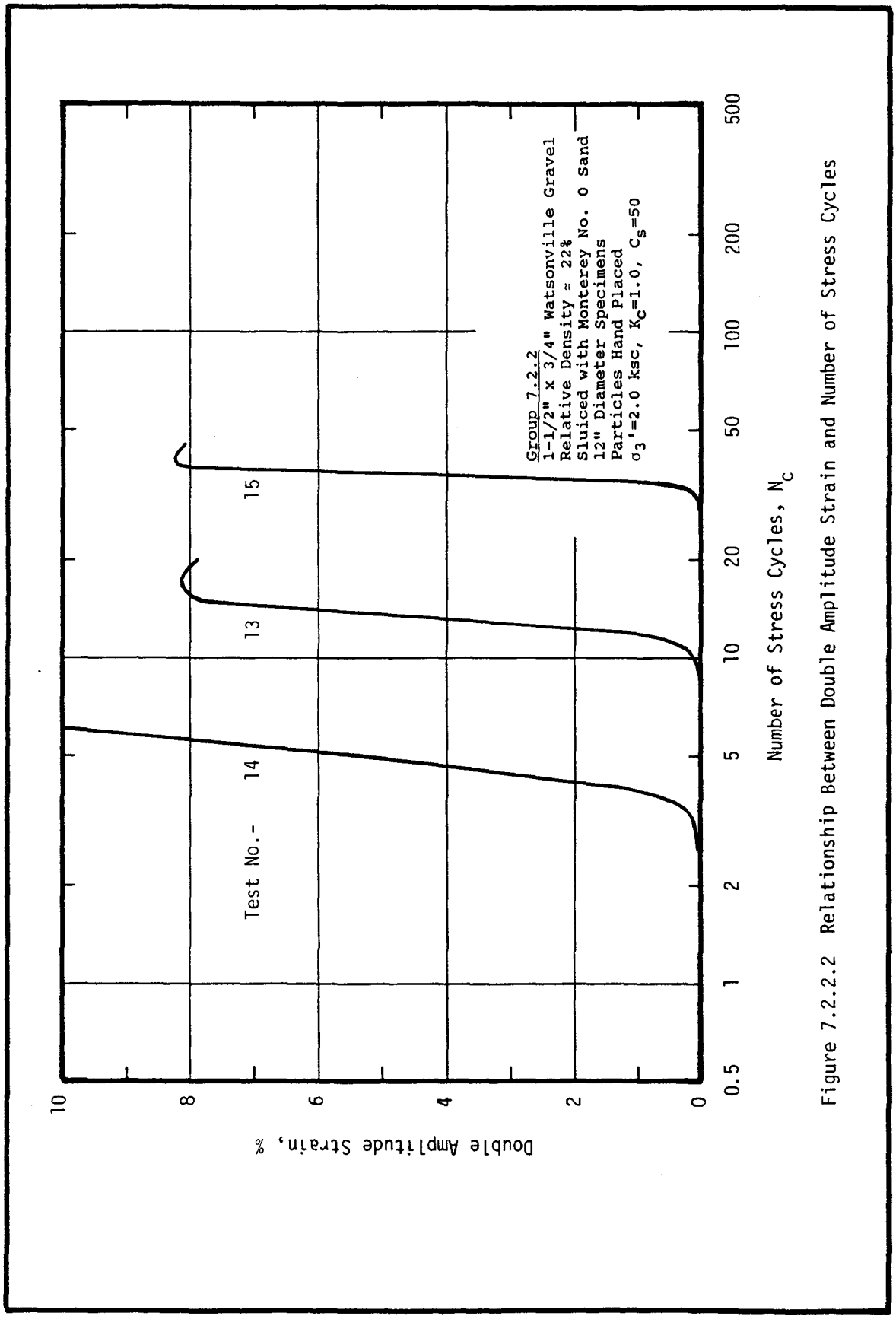

Figure 7.2.2.2 Relationship Between Double Amplitude Strain and Number of Stress Cycles

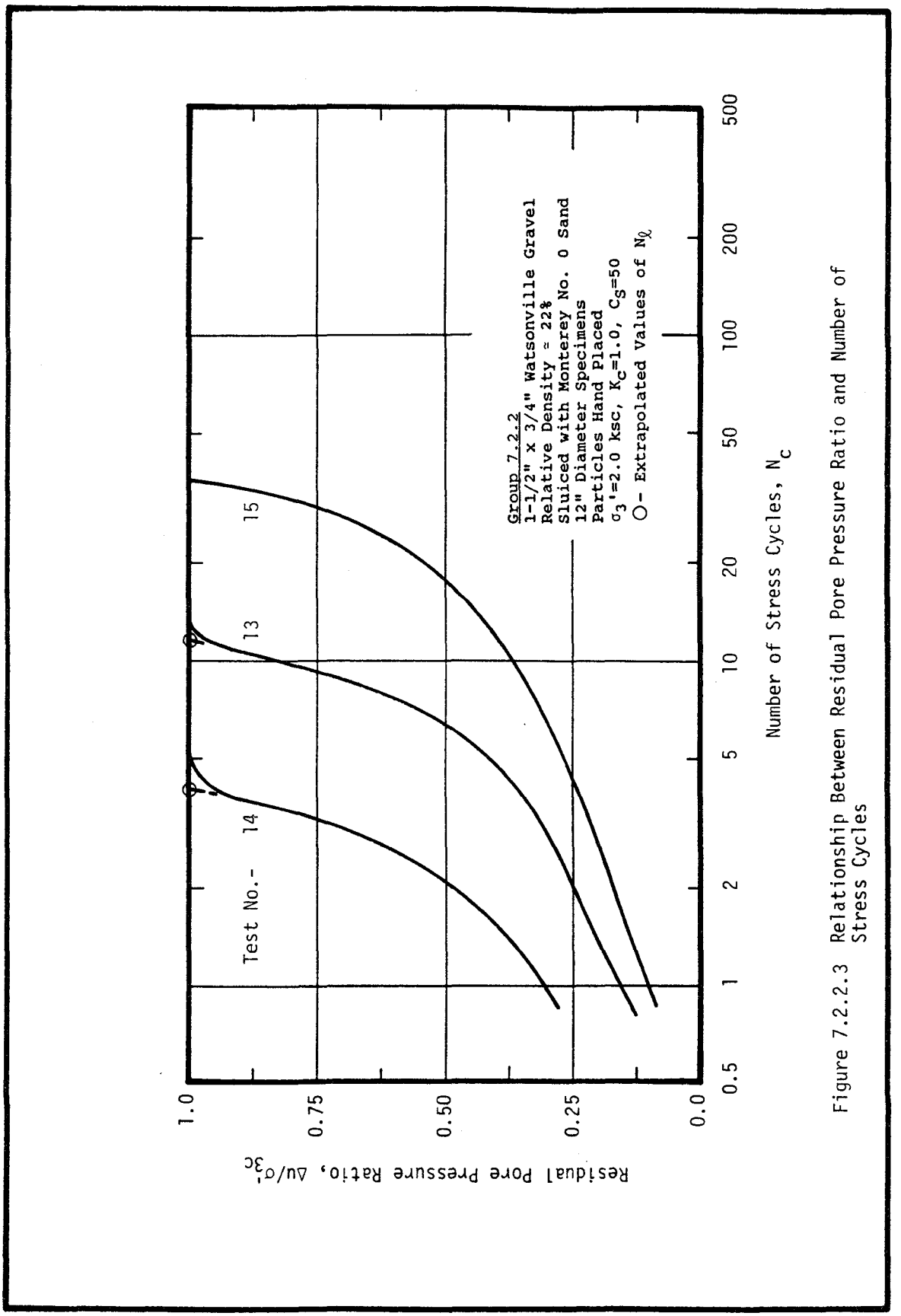

Figure 7.2.2.3 Relationship Between Residual Pore Pressure Ratio and Number of Stress Cycles

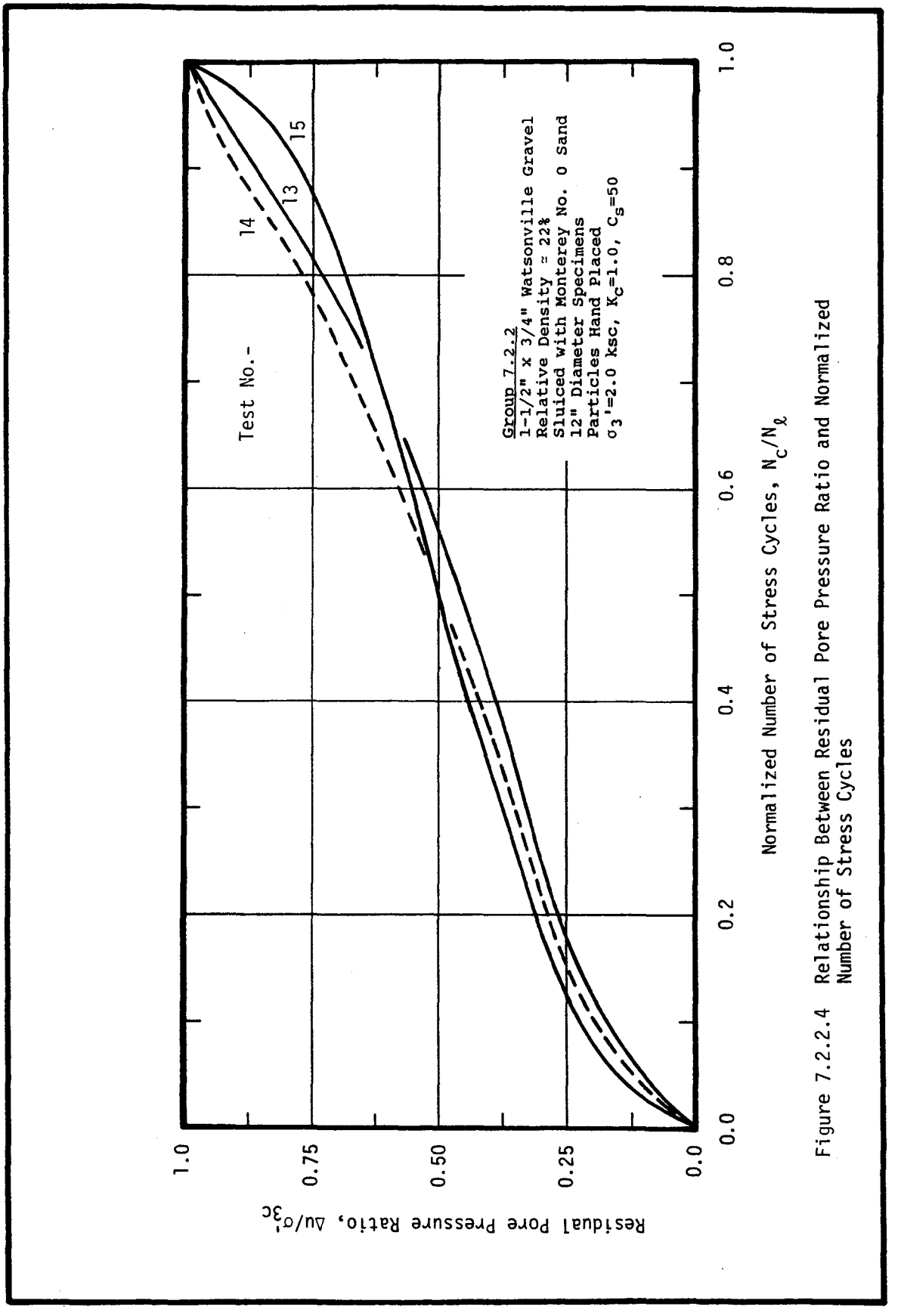

Figure 7.2.2.4 Relationship Between Residual Pore Pressure Ratio and Normalized Number of Stress Cycles

Table 7.2.3 Material Properties and Test Conditions Causing Failure During Undrained Cyclic Loading

GRAVEL: 1-1/2" x 3/4" Watsonville Gravel
SLUICING SAND: none
C_s = -

Test No.	Gravel				Sand	
	Dry Density (pcf)	Void Ratio	Porosity	Relative Density (%)	Dry Density (pcf)	Void Ratio
3	96.88	0.791	0.442	53.8	-	-
4	94.92	0.828	0.453	44.7	-	-
5	95.94	0.809	0.447	49.5	-	-
6	96.37	0.801	0.445	51.4	-	-
C (1)	94.50	0.837	0.456	42.7	-	-

Test No.	Cyclic Stress Ratio, $\sigma_d/2\sigma_{3c}$	Number of Cycles Causing...				
		80% Pore Pressure Ratio	100% Pore Pressure Ratio	2% Peak to Peak Strain	5% Peak to Peak Strain	10% Peak to Peak Strain
3	0.201	-	300(2)	250(2)	300(2)	-
4	0.239	-	24.0	18.0	22.0	25.0
5	0.266	-	10.0	5.9	8.4	11.5
6	0.300	-	3.9	1.6	3.3	5.2
C(1)	0.230	-	17.0	14.3	17.0	22.0

* - All test specimens are 12" diameter, pluviated structure, one 0.1" membrane, σ_3'= 2.0 ksc, and K_c=1 except as noted.

(1)Test C hand placed. (2)Extrapolated values.

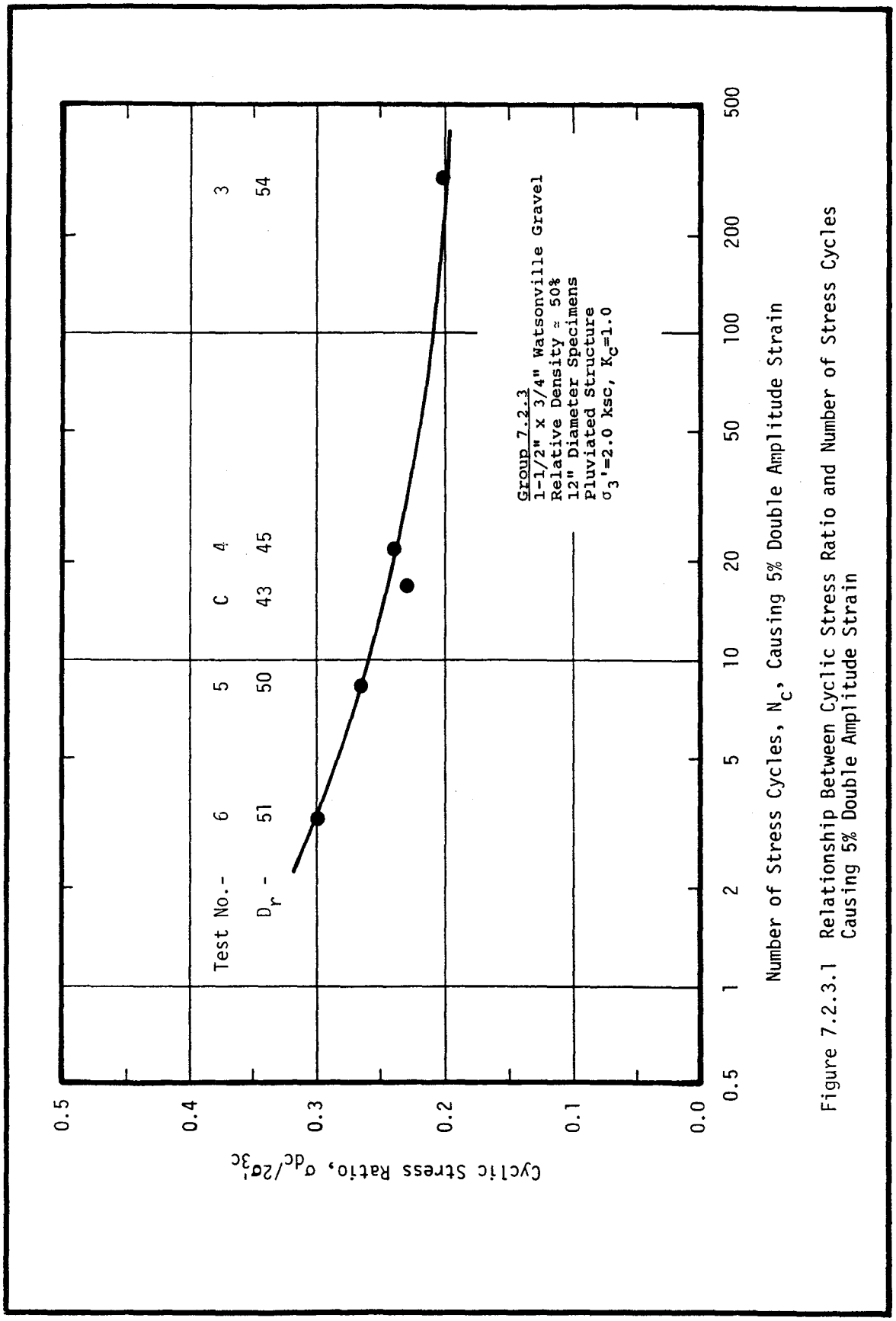

Figure 7.2.3.1 Relationship Between Cyclic Stress Ratio and Number of Stress Cycles Causing 5% Double Amplitude Strain

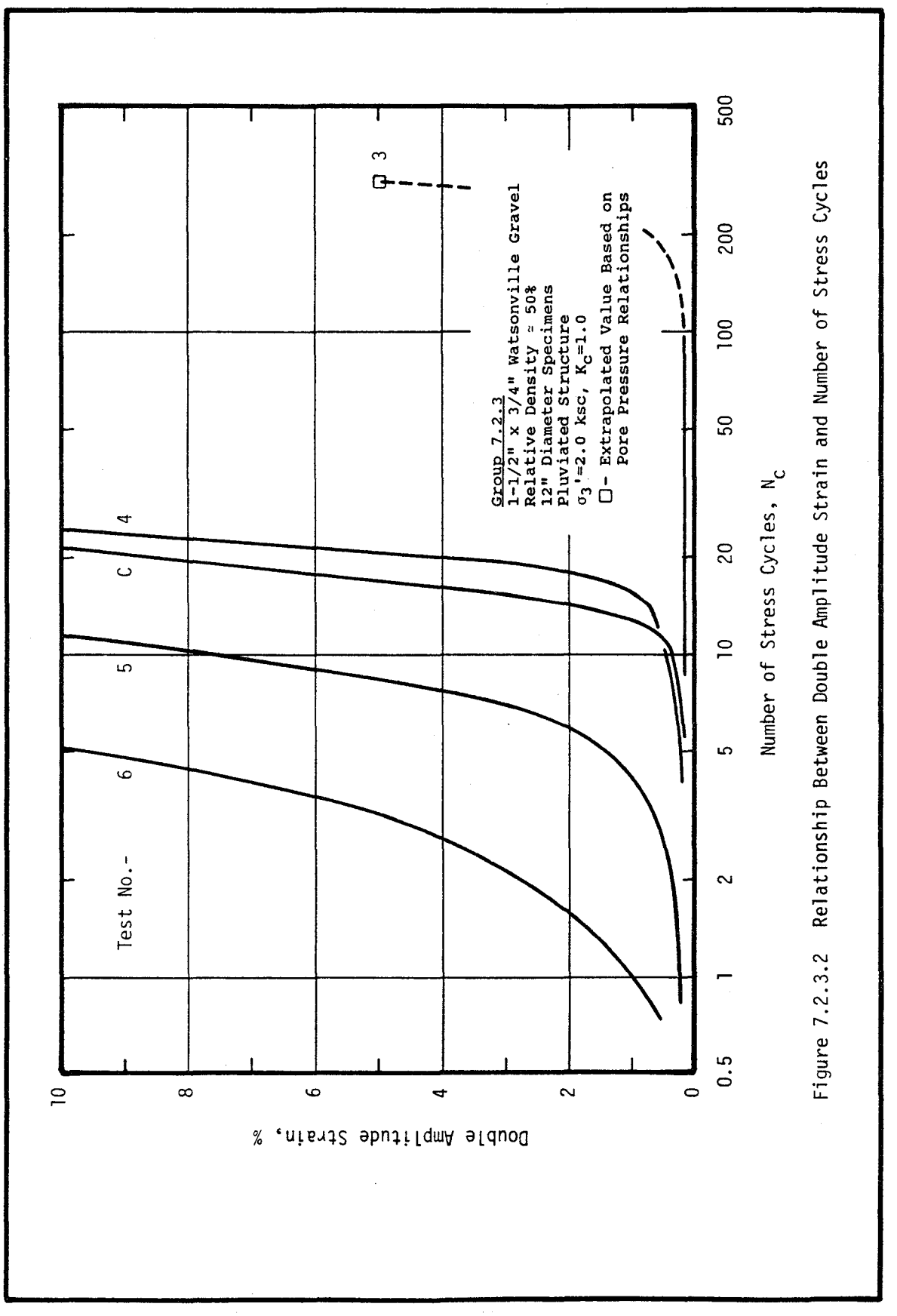

Figure 7.2.3.2 Relationship Between Double Amplitude Strain and Number of Stress Cycles

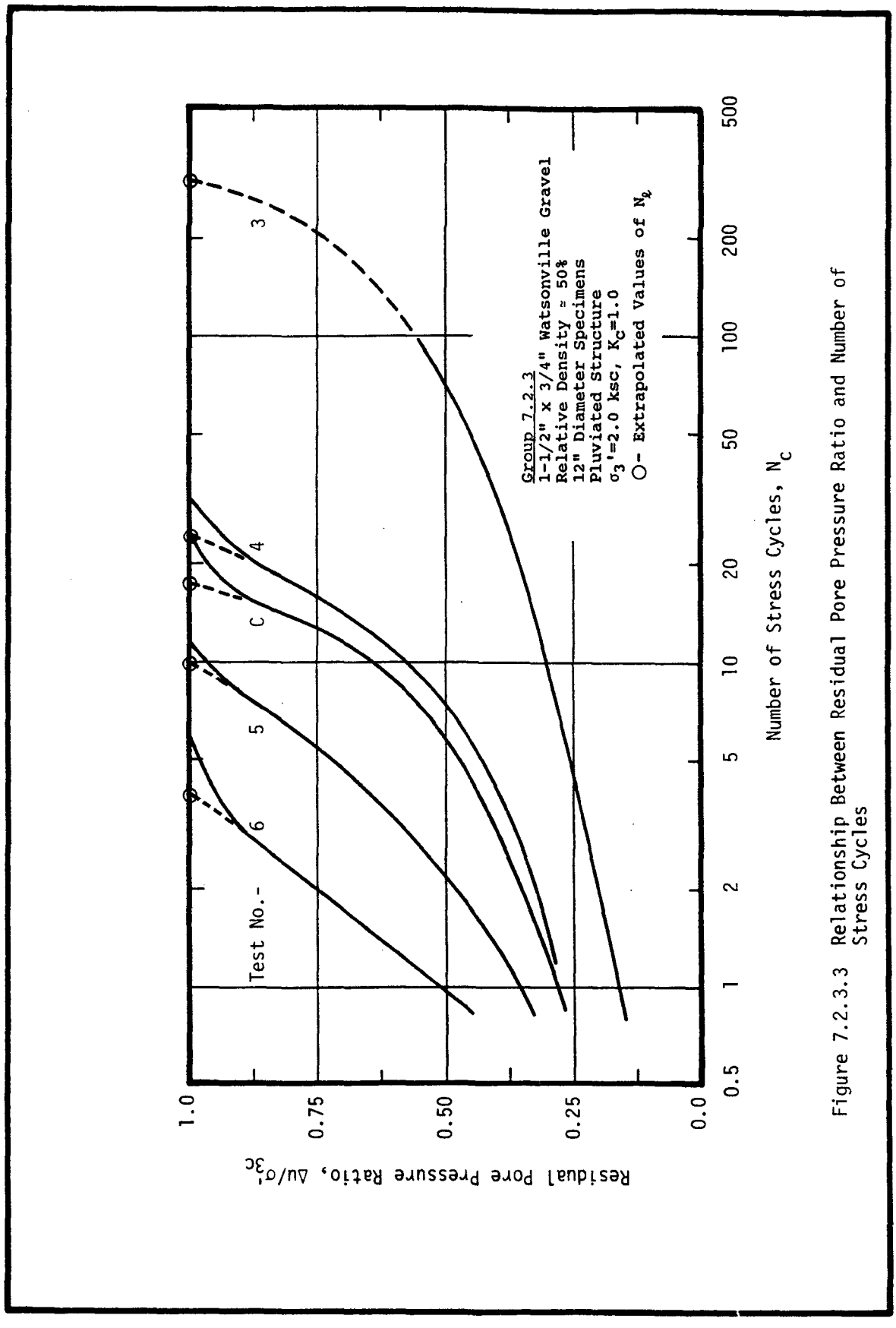

Figure 7.2.3.3 Relationship Between Residual Pore Pressure Ratio and Number of Stress Cycles

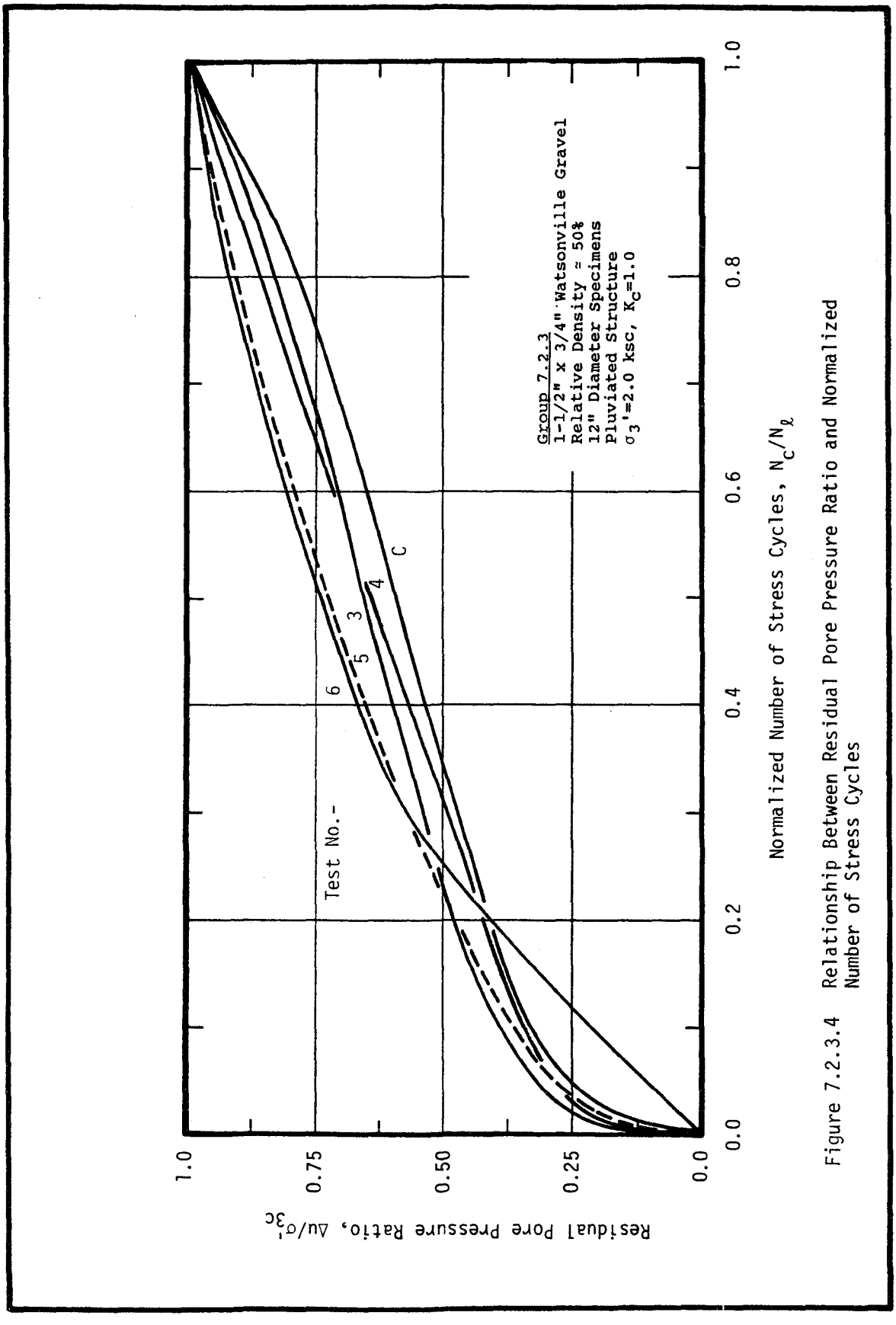

Figure 7.2.3.4 Relationship Between Residual Pore Pressure Ratio and Normalized Number of Stress Cycles

Table 7.2.4 Material Properties and Test Conditions Causing Failure During Undrained Cyclic Loading

GRAVEL: 1-1/2" x 3/4" Watsonville Gravel(2)
SLUICING SAND: Monterey No.0(1)
Cs=50(1)

Test No.	Gravel				Sand	
	Dry Density (pcf)	Void Ratio	Porosity	Relative Density (%)	Dry Density (pcf)	Void Ratio
8	95.80	0.812	0.448	48.8	-	-
9	91.03	0.907	0.475	25.6	-	-
10	92.38	0.879	0.468	32.4	-	-
11	90.86	0.910	0.477	24.7	-	-
12(1)	90.96	0.908	0.476	25.2	88.93	0.853

Test No.	Cyclic Stress Ratio,(3) $\sigma_d/2\sigma_{3c}$	Number of Cycles Causing...				
		80% Pore Pressure Ratio	100% Pore Pressure Ratio	2% Peak to Peak Strain	5% Peak to Peak Strain	10% Peak to Peak Strain
8	0.243	-	89	90	99	118
9	0.292	-	4.4	3.9	4.9	6.6
10	0.253	-	5.7	5.4	6.8	8.9
11	0.202	-	75	72	75	80
12(1)	0.225	-	2.0	1.8	2.6	4.5

Test No.	Cyclic Stress Ratio,(4) $\sigma_d/2\sigma_{3c}$
8	0.204
9	0.254
10	0.217
11	0.164
12	0.180

* - All test specimens are 12" diameter, particles hand placed, one 0.1" membrane, $\sigma_3' = 2.0$ ksc, and $K_c=1$.
(1) Only test no. 12 was sluiced.
(2) A thin sand shell was constructed around the specimen membrane for all tests. $\sigma_{3'shell} = 0.25$ ksc.
(3) Not corrected for shell strength.
(4) Corrected for shell strength.

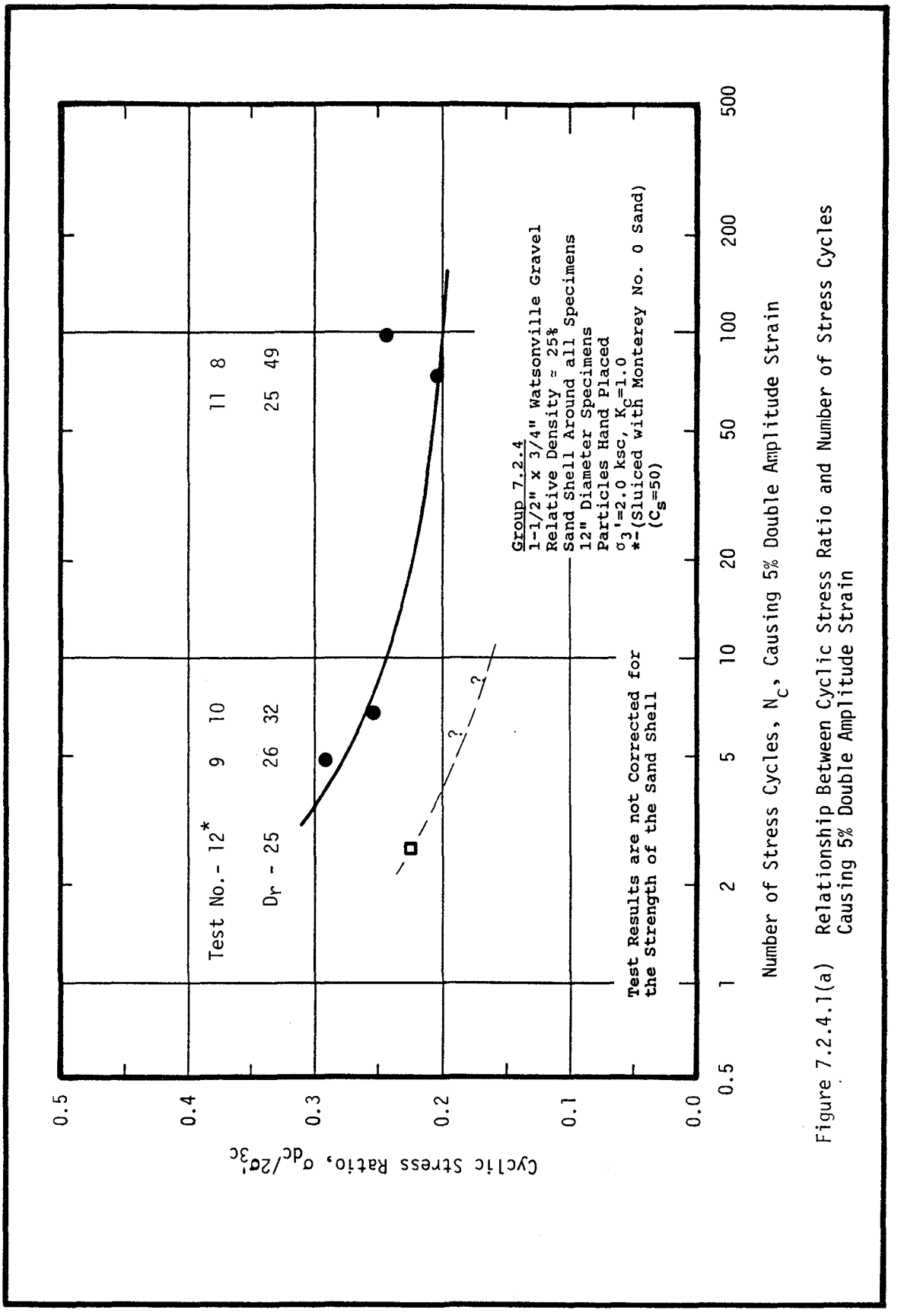

Figure 7.2.4.1(a) Relationship Between Cyclic Stress Ratio and Number of Stress Cycles Causing 5% Double Amplitude Strain

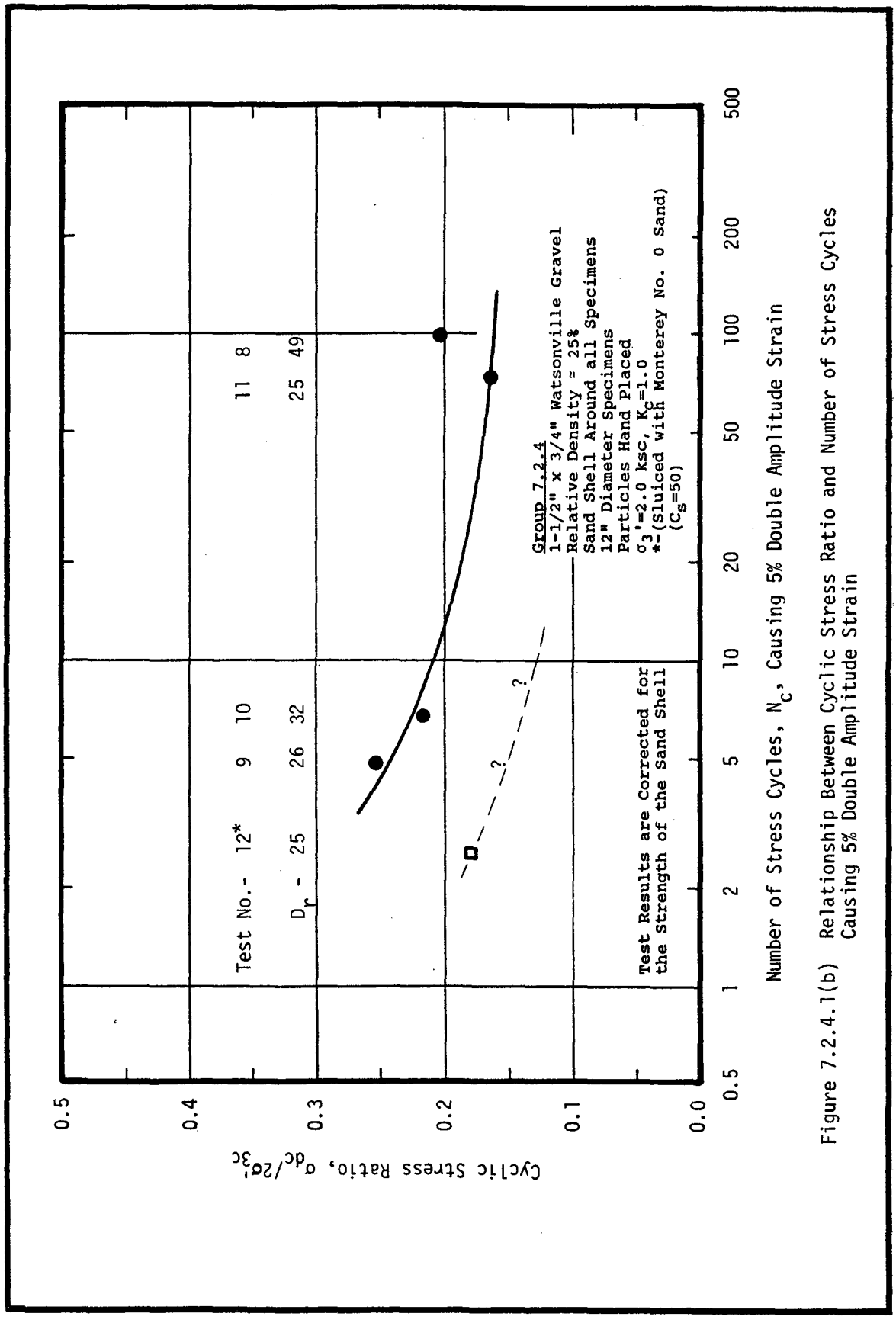

Figure 7.2.4.1(b) Relationship Between Cyclic Stress Ratio and Number of Stress Cycles Causing 5% Double Amplitude Strain

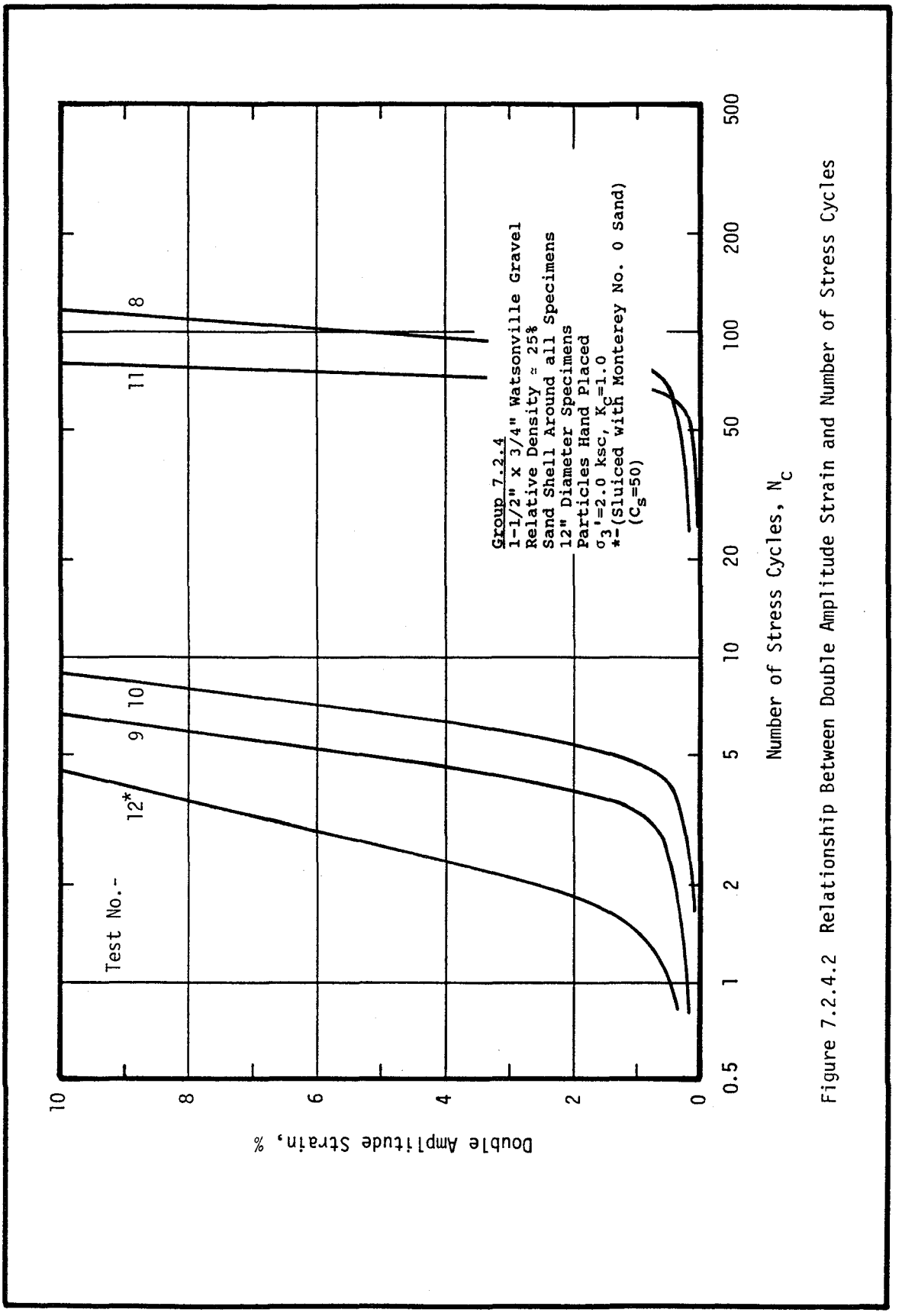

Figure 7.2.4.2 Relationship Between Double Amplitude Strain and Number of Stress Cycles

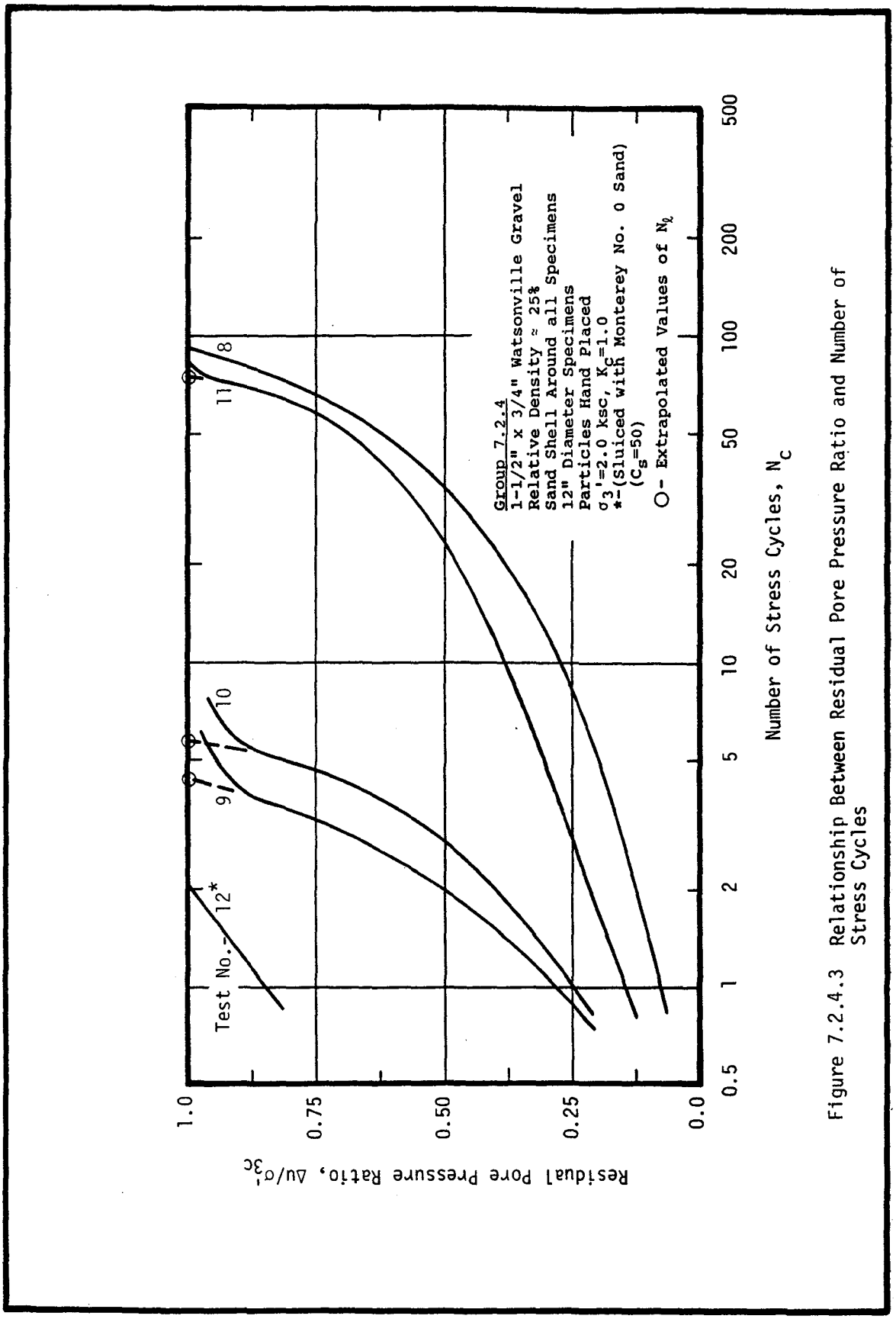

Figure 7.2.4.3 Relationship Between Residual Pore Pressure Ratio and Number of Stress Cycles

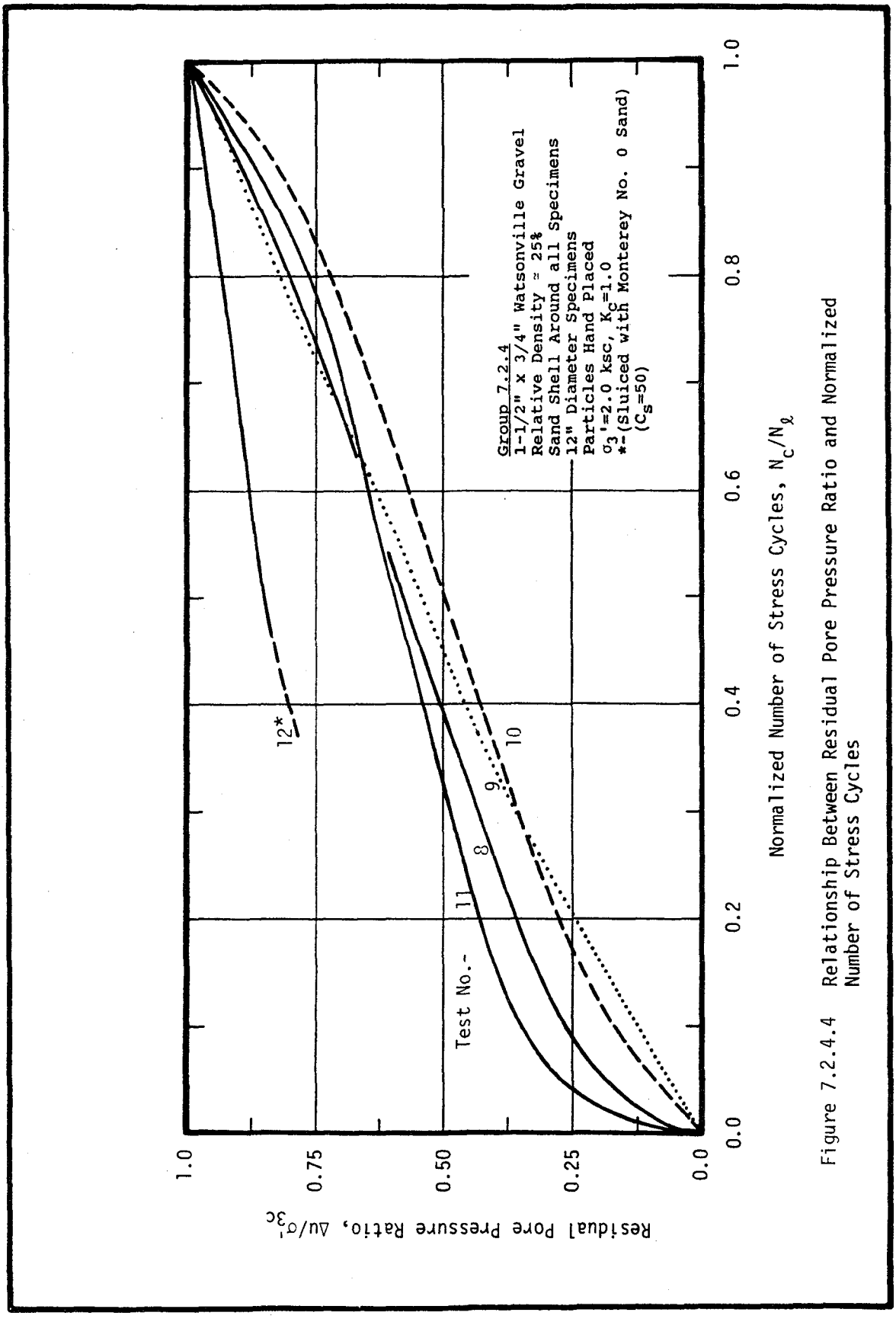

Figure 7.2.4.4 Relationship Between Residual Pore Pressure Ratio and Normalized Number of Stress Cycles

Data Analyses

A comparison of the values of cyclic stress ratio required to cause 5% double amplitude strain in 10 stress cycles for sluiced and unsluiced gravel specimens at a relative density of about 22% is shown in Figure 7.17. It may be seen from this figure that, again, only about 65% of the cyclic stress ratio which caused 5% double amplitude strain for the unsluiced specimens was required to cause a similar level of strain for the sluiced specimens due to the reduced effects of membrane compliance in the sluiced specimens. Again, if it is assumed that the results for the sluiced specimens are reasonably representative of the true, noncompliant cyclic loading resistance of the soil, the effect of membrane compliance on the triaxial test results is to overestimate the cyclic strength of the soil by about 55%.

Figure 7.18 presents a comparison of the cyclic loading resistance of the unsluiced gravel specimens at a relative density of 50% with the cyclic strength of 12 inch diameter specimens of 1-1/2" x 3/4" Oroville gravel at relative densities of 40% and 60% determined by Wong et al. (1974). It may be noted that the results from tests performed on these two materials compare reasonably well with the 50% relative density curve from this study falling approximately mid-way between the 40% and 60% relative density curves from Wong et al. in the area of 10 stress cycles. This would seem to indicate that the cyclic loading resistance of two different materials may be approximately the same for similar densities, grain size distributions and structures. Actually, the 50% relative density curve in this figure should probably be shifted upward relative to the other two curves to account for

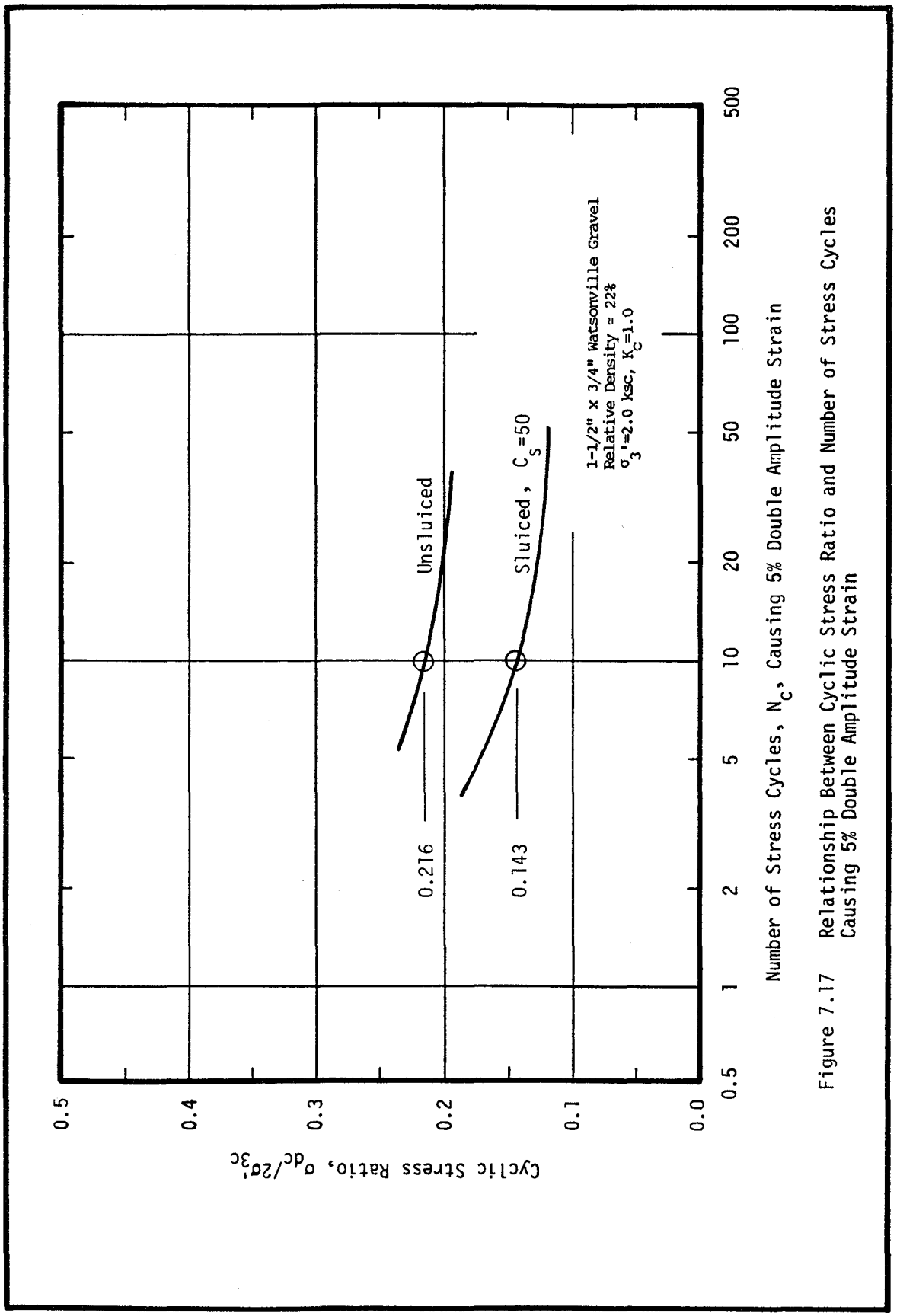

Figure 7.17 Relationship Between Cyclic Stress Ratio and Number of Stress Cycles Causing 5% Double Amplitude Strain

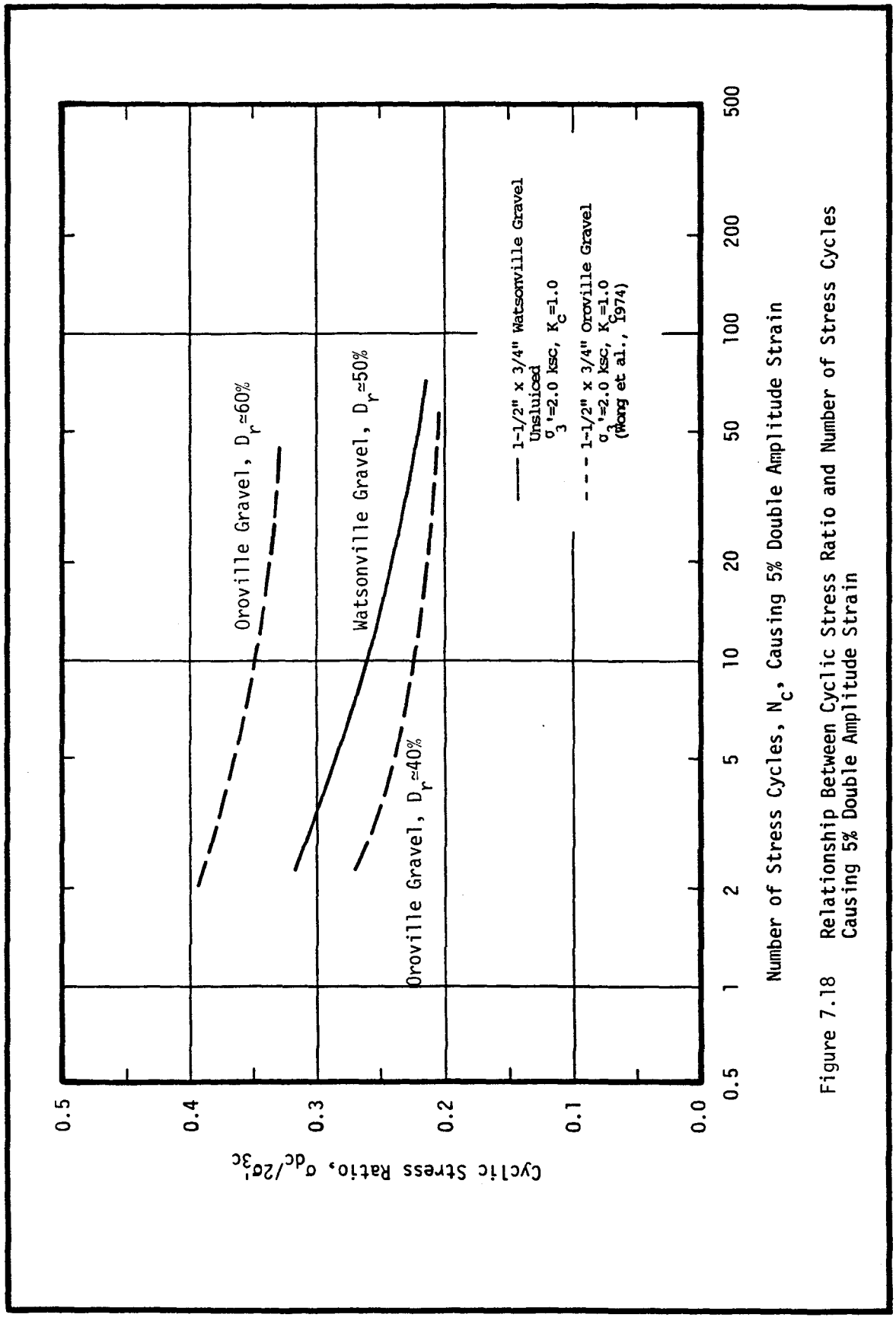

Figure 7.18 Relationship Between Cyclic Stress Ratio and Number of Stress Cycles Causing 5% Double Amplitude Strain

differences in structure between the specimens used in the two studies. The data from Wong et al. are from specimens constructed by compacting the soil in 10 equal layers and the specimens in this study were constructed by pluviation. Previous investigations (Mulilis et al., 1975, 1977) have shown that specimens constructed by compaction in layers result in somewhat higher cyclic loading resistance than those constructed by pluviation, as shown in Figure 7.19. Thus, the data from the two studies agree quite well when the differences in structure are considered.

Combinations of cyclic stress ratio and numbers of stress cycles producing different levels of residual pore pressure ratio for sluiced and unsluiced gravel specimens, at a relative density of 22%, determined in this study are shown in Figure 7.20. In this case, a pore pressure ratio of about 25% in the unsluiced specimens appears to correspond reasonably well with a 100% pore pressure ratio in the sluiced specimens. Thus, assuming that the results from the sluiced specimens are reasonably representative of the true, noncompliant cyclic loading resistance of the material, the stress ratio required to cause a pore pressure ratio of 100% in a noncompliant system may be estimated by determining the stress ratio which causes about 25% pore pressure ratio in a compliant system. It should be noted that this relationship is not necessarily applicable to all soils susceptible to membrane compliance effects. The relationship is likely to be affected by changes in a number of factors including: material gradation, density and structure; specimen size; membrane thickness and modulus; and initial consolidation pressure. However, it might reasonably be expected that this material gradation represents the coarsest and most

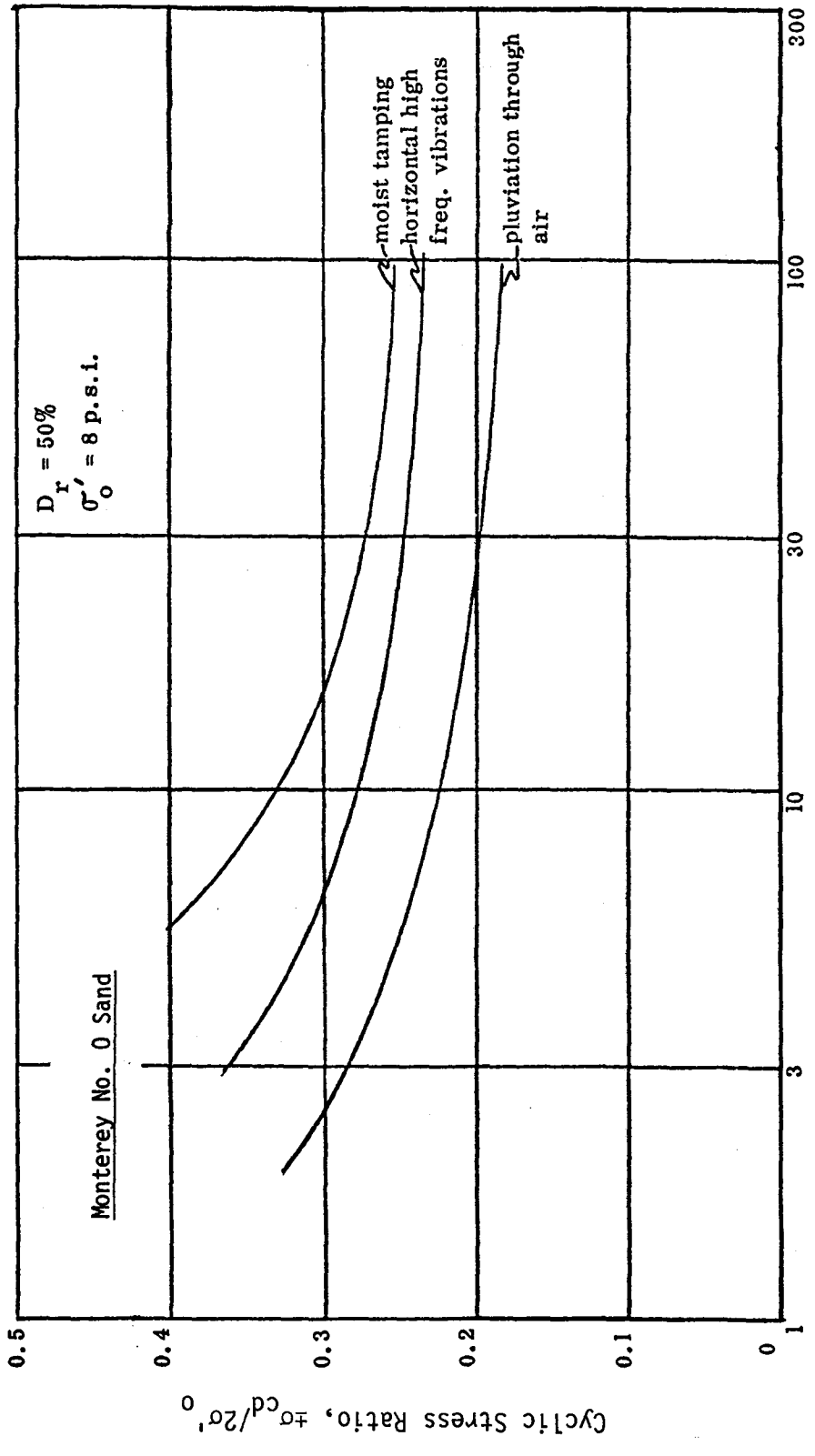

Figure 7.19 Relationship Between Cyclic Stress Ratio and Number of Stress Cycles Causing 5% Double Amplitude Strain for Specimens of Monterey No. 0 Sand Prepared by Three Different Construction Methods (after Mulilis et al., 1975)

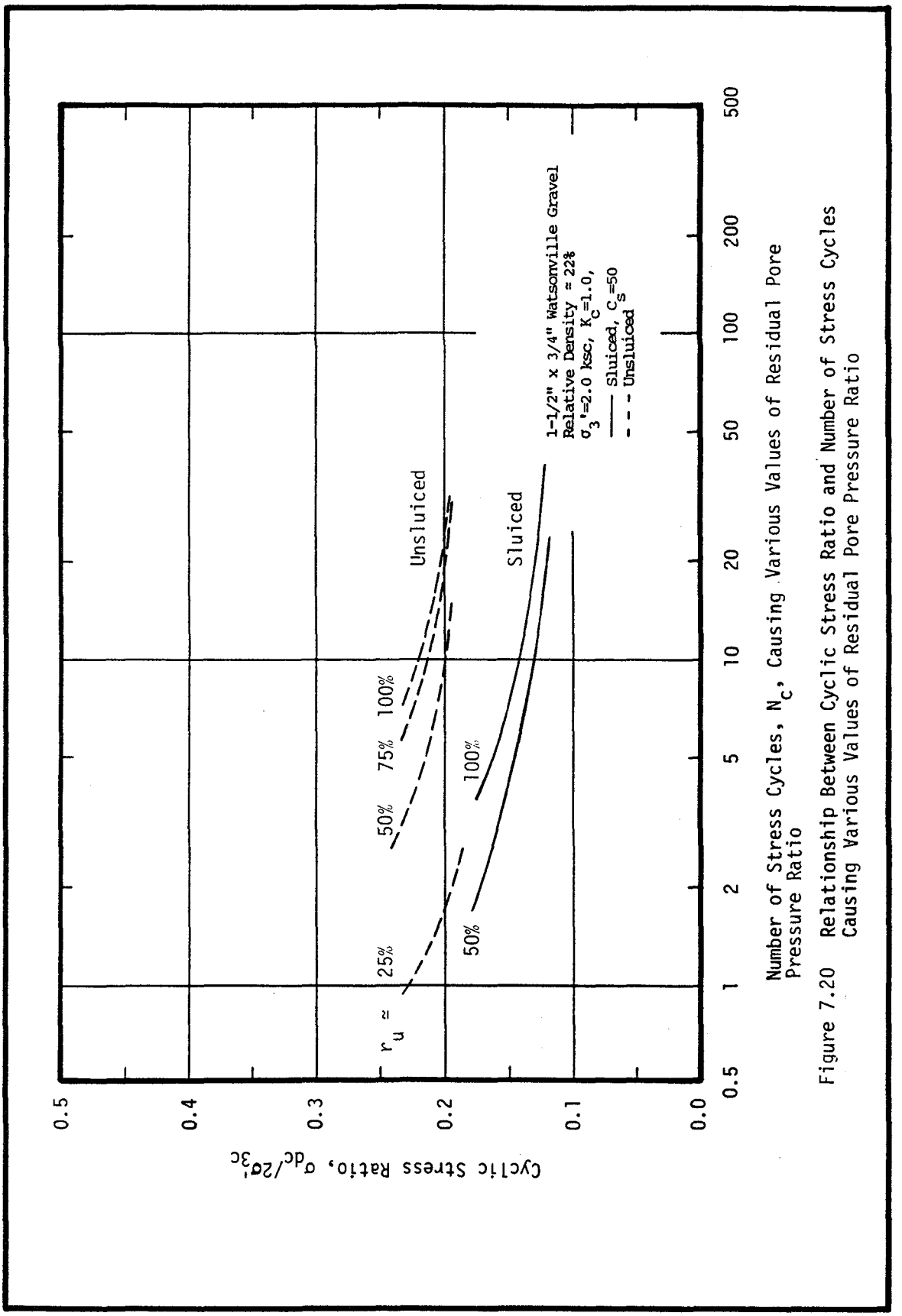

Figure 7.20 Relationship Between Cyclic Stress Ratio and Number of Stress Cycles Causing Various Values of Residual Pore Pressure Ratio

uniformly-graded material that is likely to be tested in a 12 inch diameter cyclic triaxial test and, other factors remaining equal, such a material would be expected to experience the largest volume change due to membrane penetration that is likely to occur in this size specimen over the same range of confining pressures. Thus, the magnitude of the effect of membrane compliance on the results of the tests on this gravel are likely to represent an approximate upper-bound of membrane compliance effects for 12 inch diameter specimens consolidated to 2.0 ksc.

Several gravel specimens were tested with a thin sand shell constructed around the outside of the specimen confining membrane as described in Chapter 6. A comparison of the cyclic loading resistance of the unsluiced specimens of 1-1/2" x 3/4" Watsonville gravel with and without a sand shell is shown in Figure 7.21. It may be seen that the cyclic loading resistance of the gravel is not greatly affected by the presence of the sand shell provided that a correction is made to account for the strength of the sand shell as described in Chapter 6. Thus, the use of a sand shell does not appear to reduce the effect of membrane compliance significantly. A similar comparison is made in Figure 7.22 for gravel specimens at relative densities of 50%, tested with and without a sand shell. In this figure, it may again be seen that the sand shell has little or no effect in reducing membrane compliance effects in tests on these unsluiced specimens.

Since it had been shown that a sand shell had no significant effect on the cyclic loading resistance of the unsluiced gravel specimens, it seemed reasonable to assume that the sand shell would likewise have no effect on the cyclic strengths of sluiced gravel

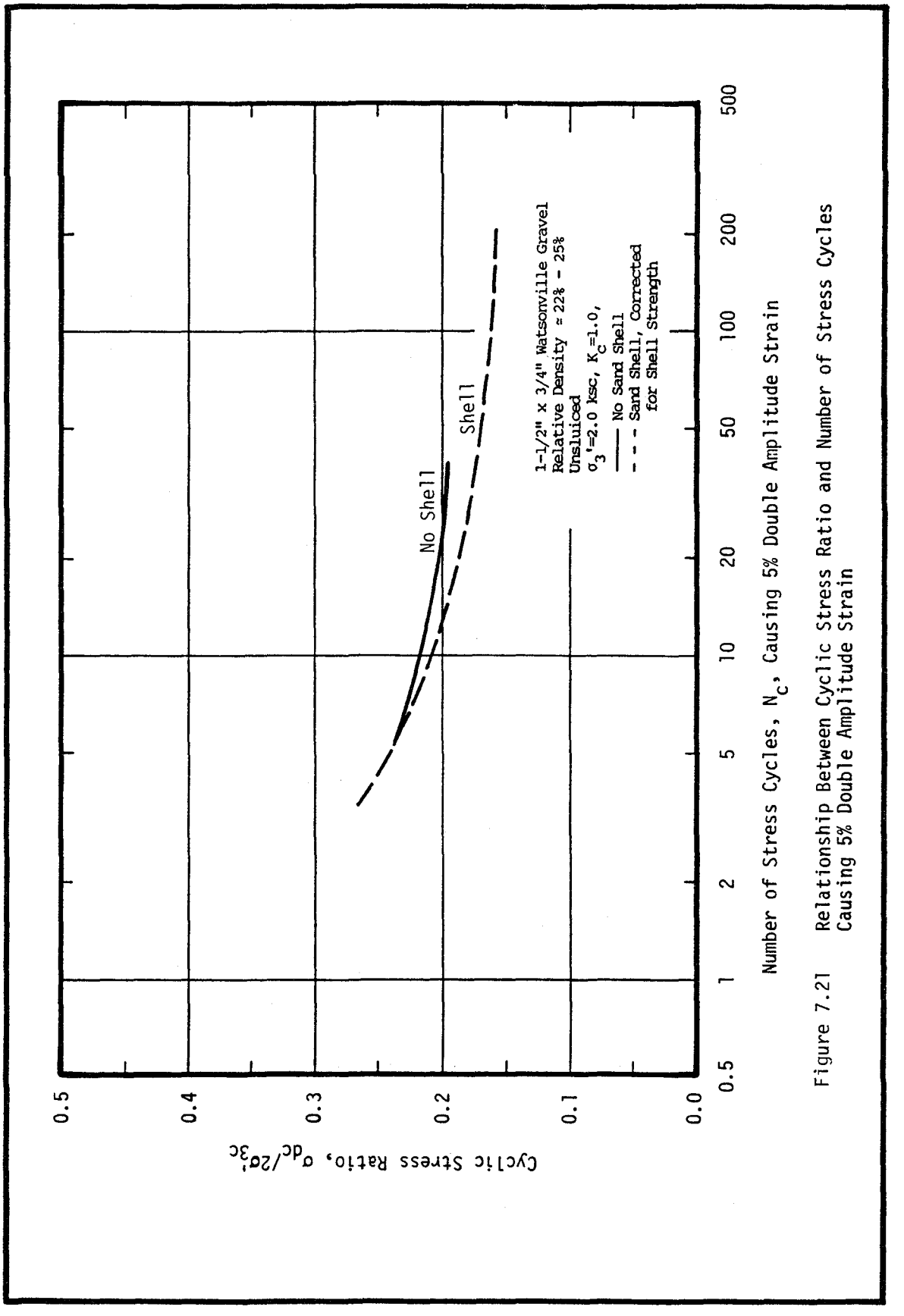

Figure 7.21 Relationship Between Cyclic Stress Ratio and Number of Stress Cycles Causing 5% Double Amplitude Strain

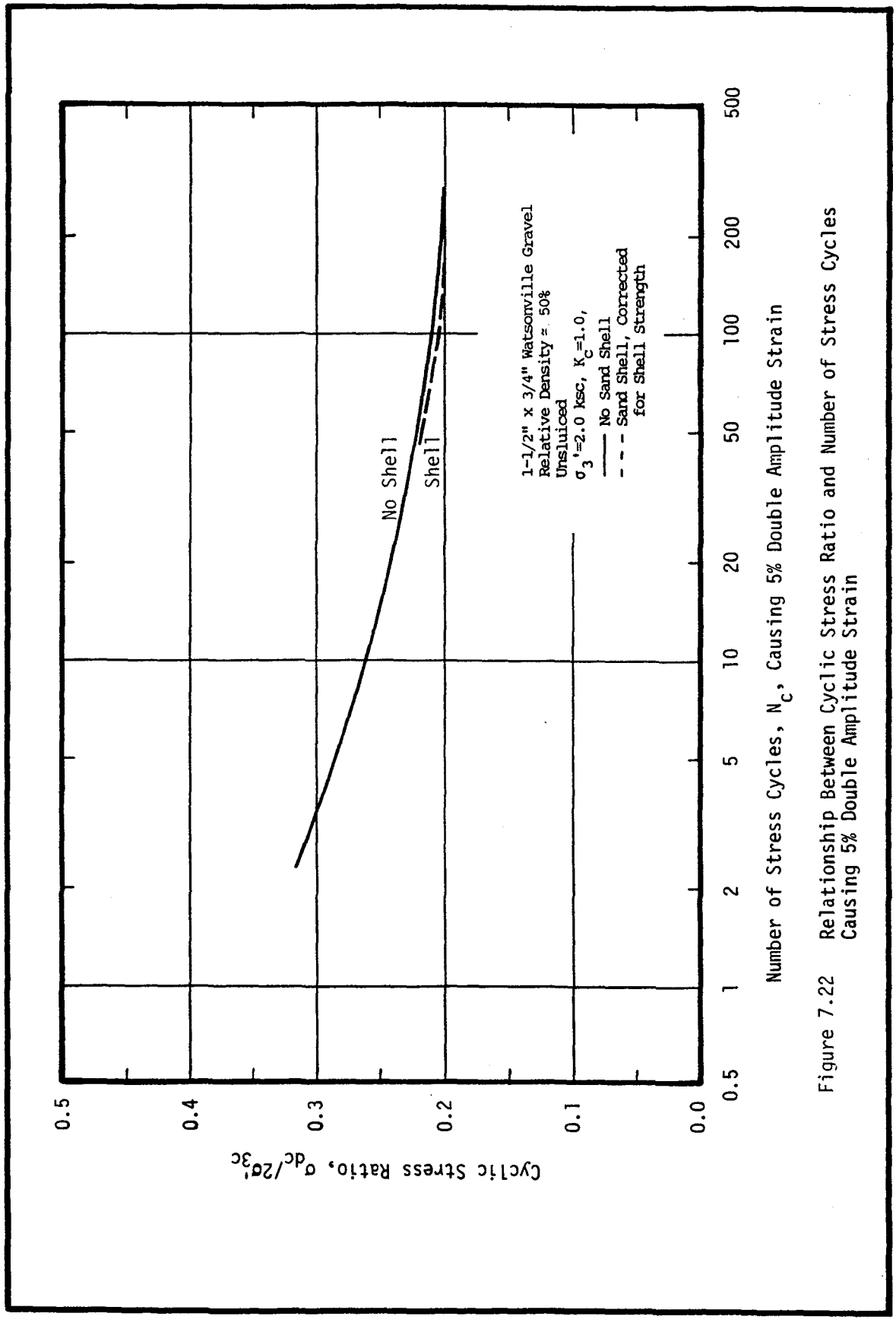

Figure 7.22 Relationship Between Cyclic Stress Ratio and Number of Stress Cycles Causing 5% Double Amplitude Strain

specimens. In order to test this assumption, a single cyclic test was performed on a sluiced gravel specimen around which had been constructed a sand shell. This specimen was constructed of 1-1/2" x 3/4" Watsonville gravel at a relative density of 25% and was sluiced with Monterey No. 0 sand. The result from this test is shown in Figure 7.23 together with the results of tests on sluiced specimens without sand shells. Although it provides only a single data point, it is interesting to note that there is little difference between the results of tests performed using these two procedures. Since this result was expected, no additional tests were performed to determine the effect of a sand shell on other sluiced specimens. Thus it was concluded that a sand shell constructed around the perimeter of a gravel specimen did not appear to significantly reduce the effects of membrane compliance.

Normalized pore pressure ratio curves for the 1-1/2" x 3/4" gravel and the 2" maximum size gravel specimens which reach failure in about 10 stress cycles are shown in Figure 7.24 and 7.25, respectively. It may be seen that the form of these curves is very similar to that previously observed in tests on sands (Lee and Albeisa, 1974; DeAlba, et al, 1975).

The magnitude of the apparent error due to membrane compliance in cyclic stress ratio causing 5% double amplitude strain in 10 stress cycles for tests performed on unsluiced specimens is compared in Figure 7.26 with the errors in cyclic stress ratio causing initial liquefaction in 30 cycles suggested by Martin et al. (1978). It may be noted that the error in cyclic stress ratio due to membrane compliance, determined in this study, is approximately twice the predicted error using the line for 12 inch diameter samples shown in Figure 7.26.

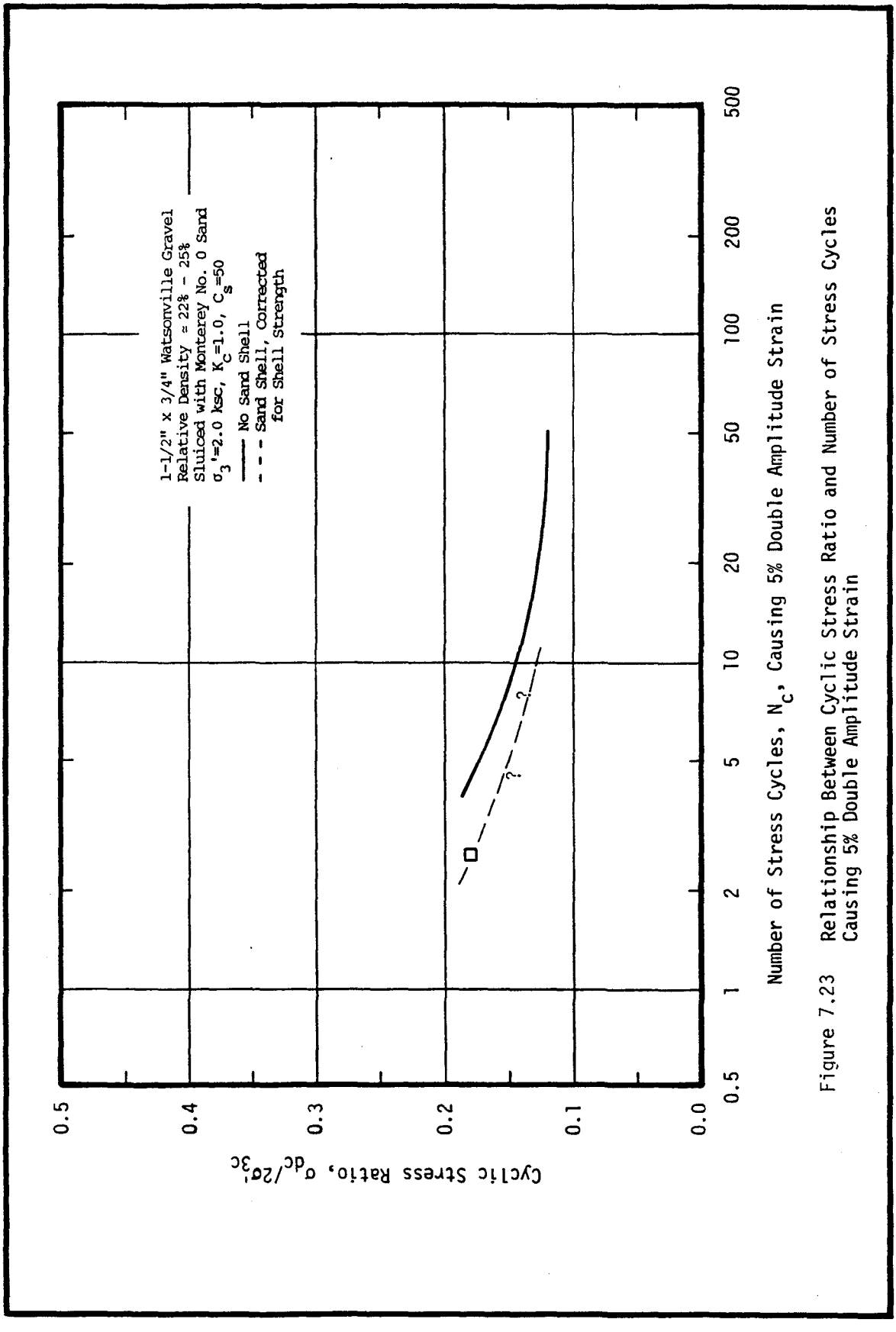

Figure 7.23 Relationship Between Cyclic Stress Ratio and Number of Stress Cycles Causing 5% Double Amplitude Strain

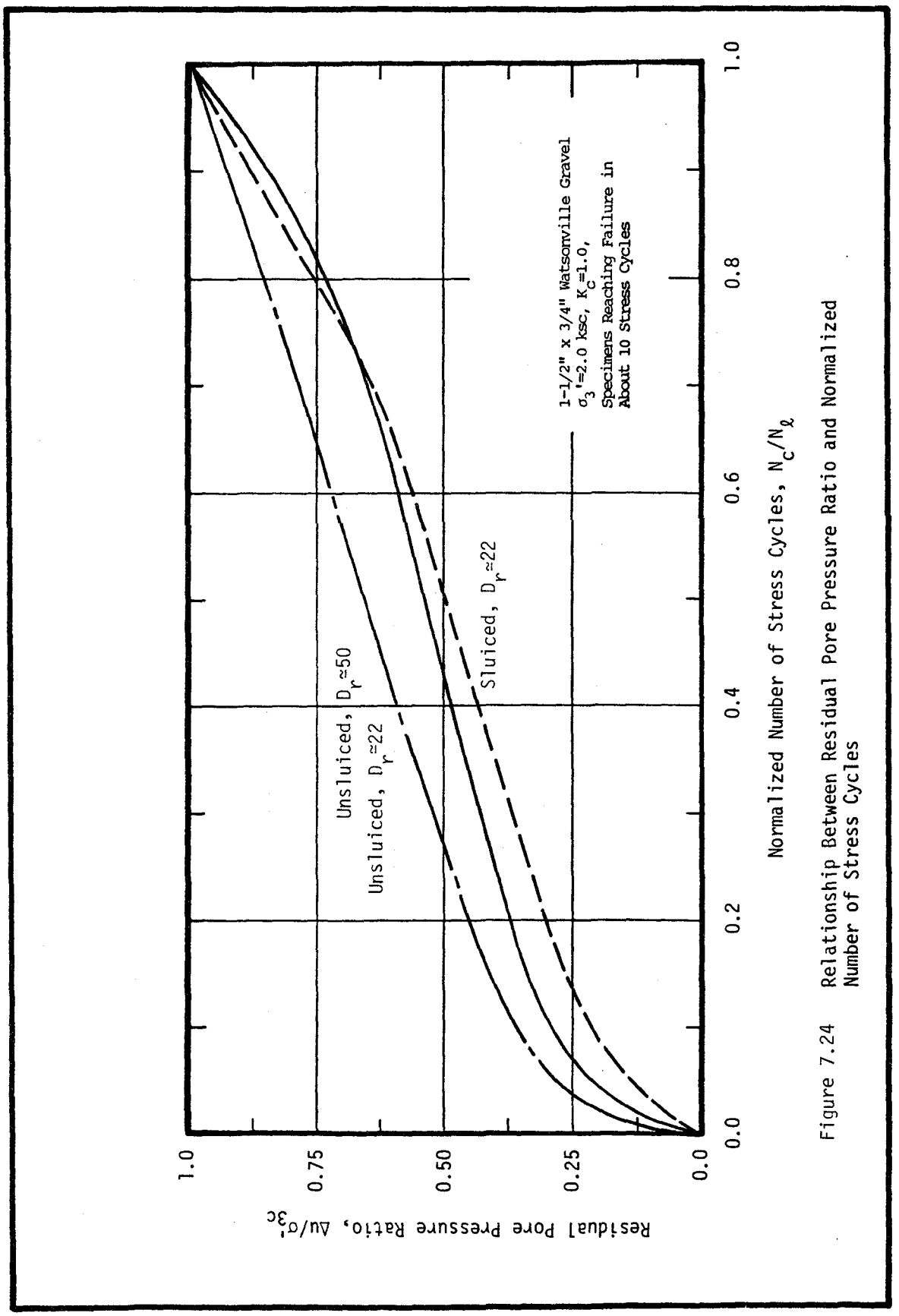

Figure 7.24 Relationship Between Residual Pore Pressure Ratio and Normalized Number of Stress Cycles

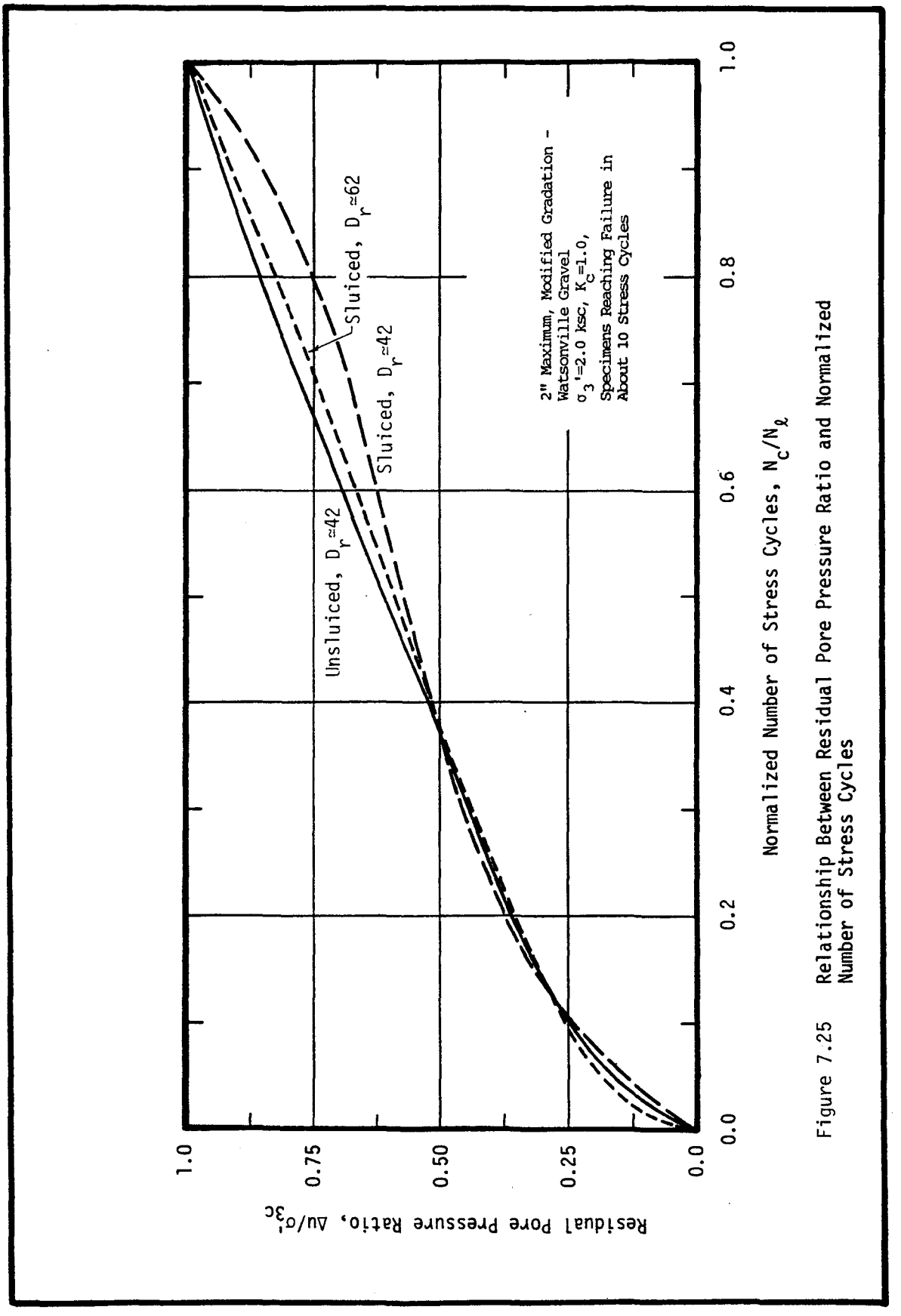

Figure 7.25 Relationship Between Residual Pore Pressure Ratio and Normalized Number of Stress Cycles

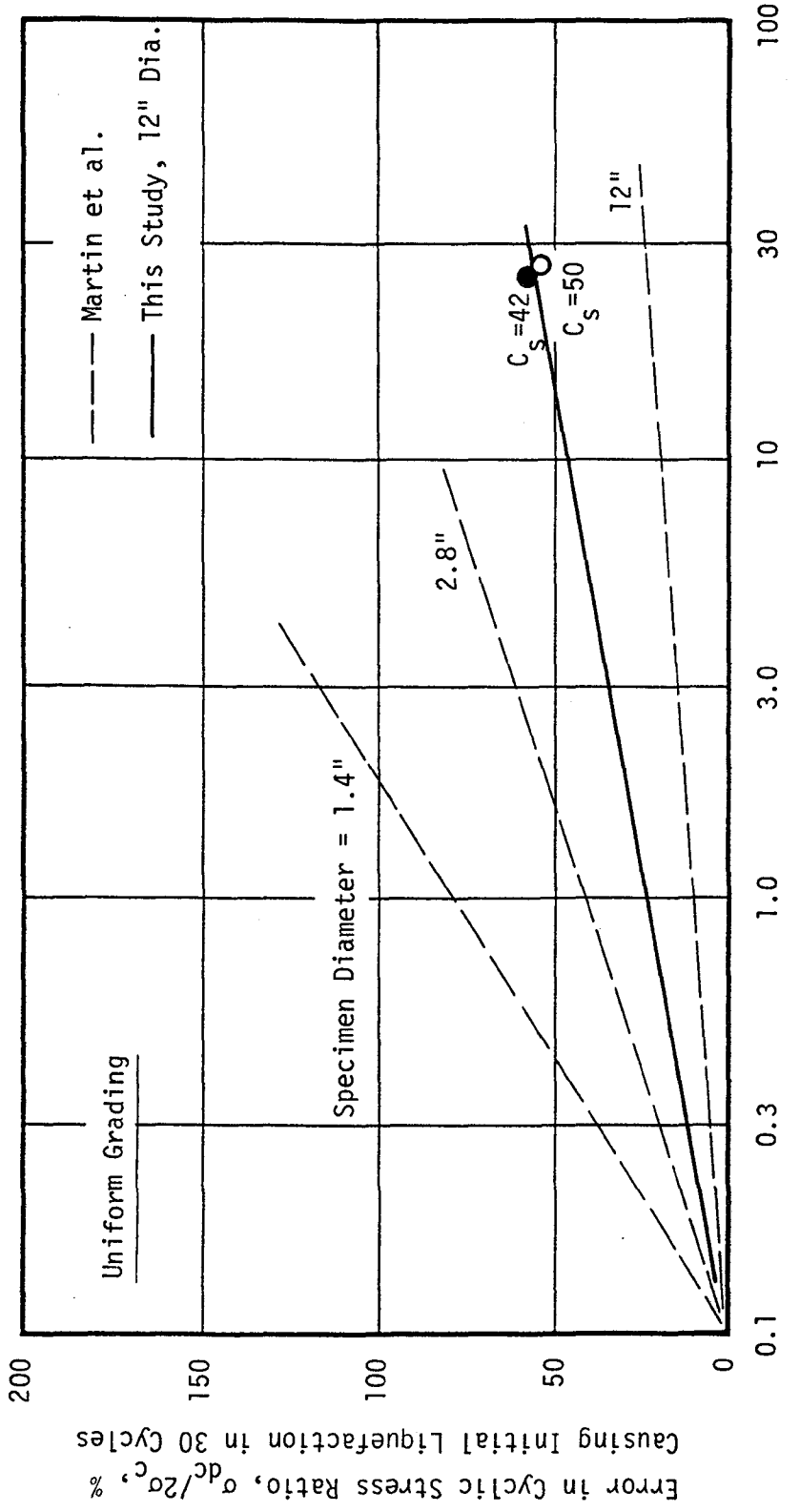

Figure 7.26 Error in Cyclic Stress Ratio Due to Membrane Compliance vs. Mean Grain Diameter for Various Specimen Diameters (after Martin et al., 1978)

CHAPTER 8

RESULTS OF TRIAXIAL TESTS PERFORMED ON 2.8 INCH DIAMETER SPECIMENS

Tests Performed on 3/8" x #4 Watsonville Gravel Specimens

Test Data Presentation

Ten groups of undrained, cyclic triaxial tests were performed on 2.8 inch diameter specimens of 3/8" x #4 Watsonville gravel in order to further investigate the effects of membrane compliance on the results of cyclic triaxial tests. Test specimens in these groups were constructed according to the following general guidelines:

(1) Specimens were constructed to about 43% or 58% relative density by pluviating the sample material through air.

(2) Monterey Fine sand was used for sluicing, resulting in a value of C_s=17.

(3) Two membranes were used to confine the specimens.

(4) Specimens were isotropically consolidated to an effective confining pressure of 2.0 ksc.

Variations from these guidelines were made in several test groups in order to investigate the effect of special test conditions as follows:

(a) Specimens in one group were constructed to a relative density of about 80% by compacting the gravel in six equal layers.

(b) Banding sand was used to sluice the specimens of another group, resulting in a value of C_s=28.

(c) Specimens in three test groups were anisotropically consolidated to values of K_c equal to 1.25, 1.50, 1.75, and

2.00 with the lateral consolidation pressure equal to 2.0 ksc in all cases.

(d) Four membranes were used to confine the test specimens in one group of tests.

Test data figures and tables for each test group are organized and presented as described in Chapter 7. Specific details of the testing conditions for each of the test groups are summarized in Table 8.0 (found on page 254 following Figure 8.3). Test data for the ten groups of tests are presented in Tables 8.1 through 8.10, and the relevant test data are shown in Figures 8.1.1 through 8.10.4.

Data Analyses

(1) Effects of Sluicing on Isotropically Consolidated Test Specimens

Figure 8.1 shows an unsluiced 2.8 inch diameter specimen of 3/8" x #4 Watsonville gravel confined with a single membrane and subjected to full vacuum pressure. The extremely high degree of membrane penetration that may occur in coarse gravel specimens, and is the cause of inaccurate cyclic loading resistance determinations, is clearly visible in this photograph. Figure 8.2 shows a comparable gravel specimen which had been sluiced with Banding sand. It may be seen that membrane penetration has been essentially eliminated from the specimen in this photograph and thus, it was considered that membrane compliance effects on the cyclic loading resistance of the specimen would be negligible.

A comparison of the cyclic loading resistance of the sluiced and unsluiced 3/8" x #4 Watsonville gravel specimens is shown in Figure 8.3. In this figure, three curves are shown representing the cyclic

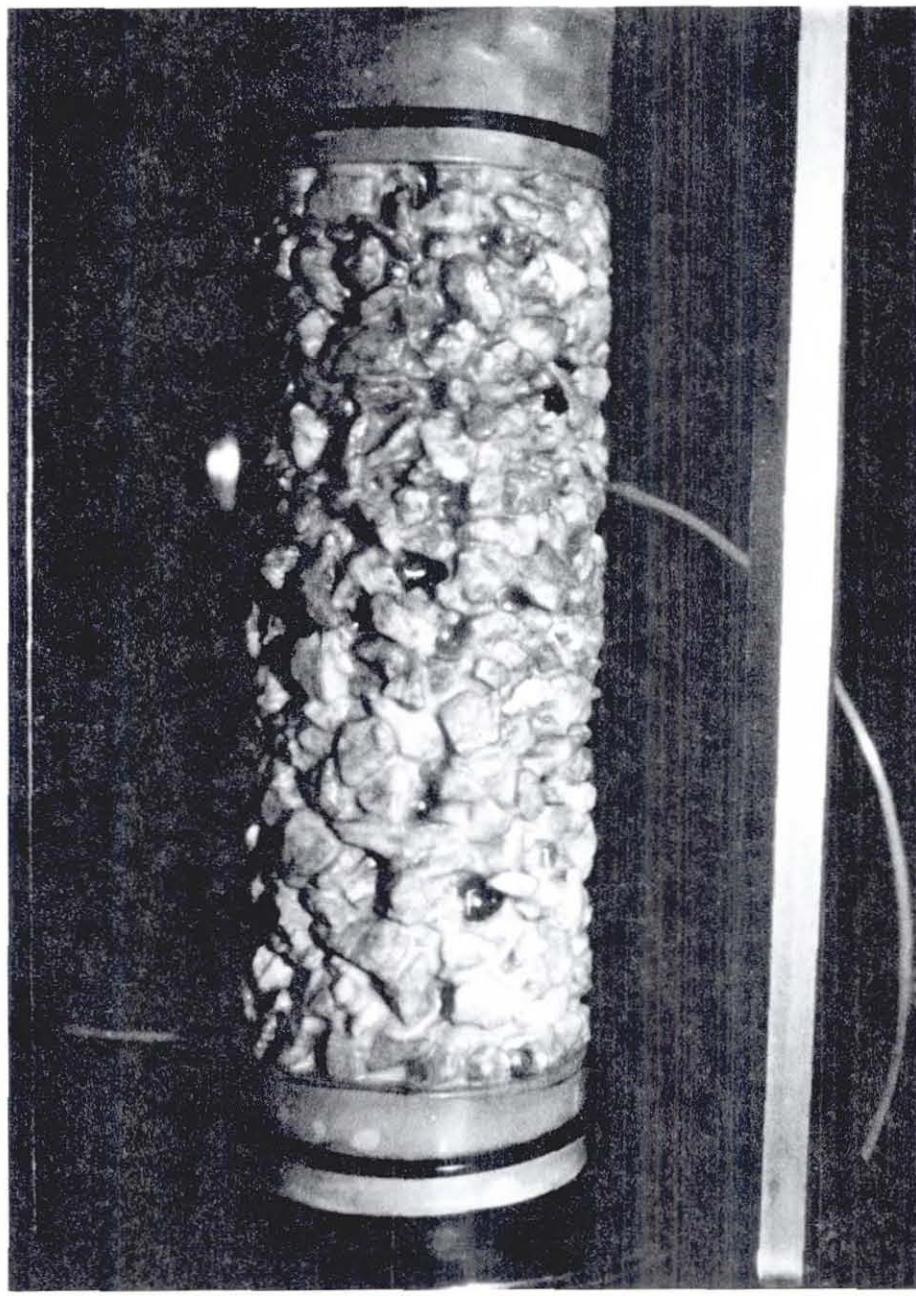

Figure 8.1 Photograph of a 2.8 Inch Diameter, Unsluiced Gravel Specimen

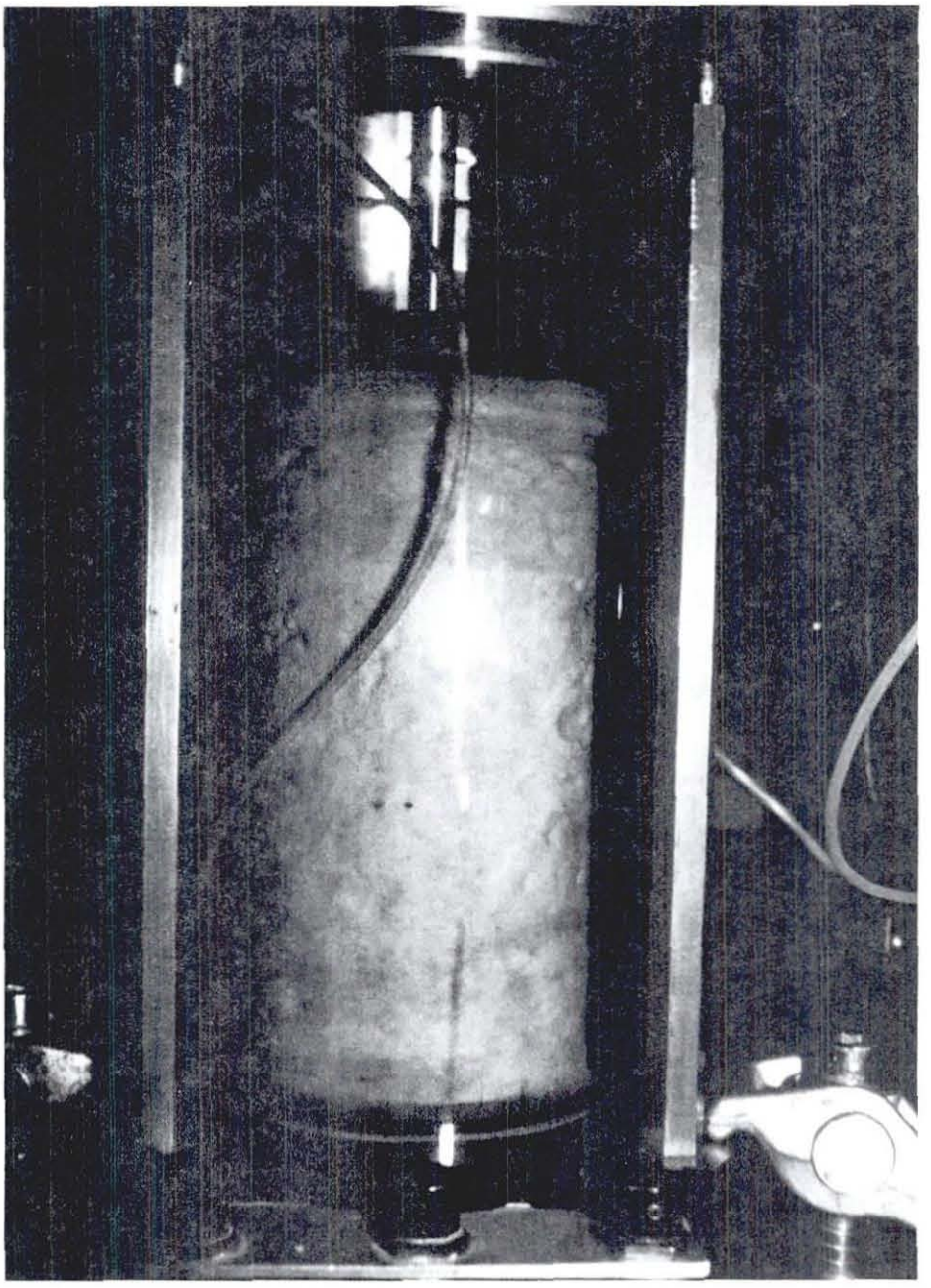

Figure 8.2 Photograph of a 2.8 Inch Diameter, Sluiced Gravel Specimen

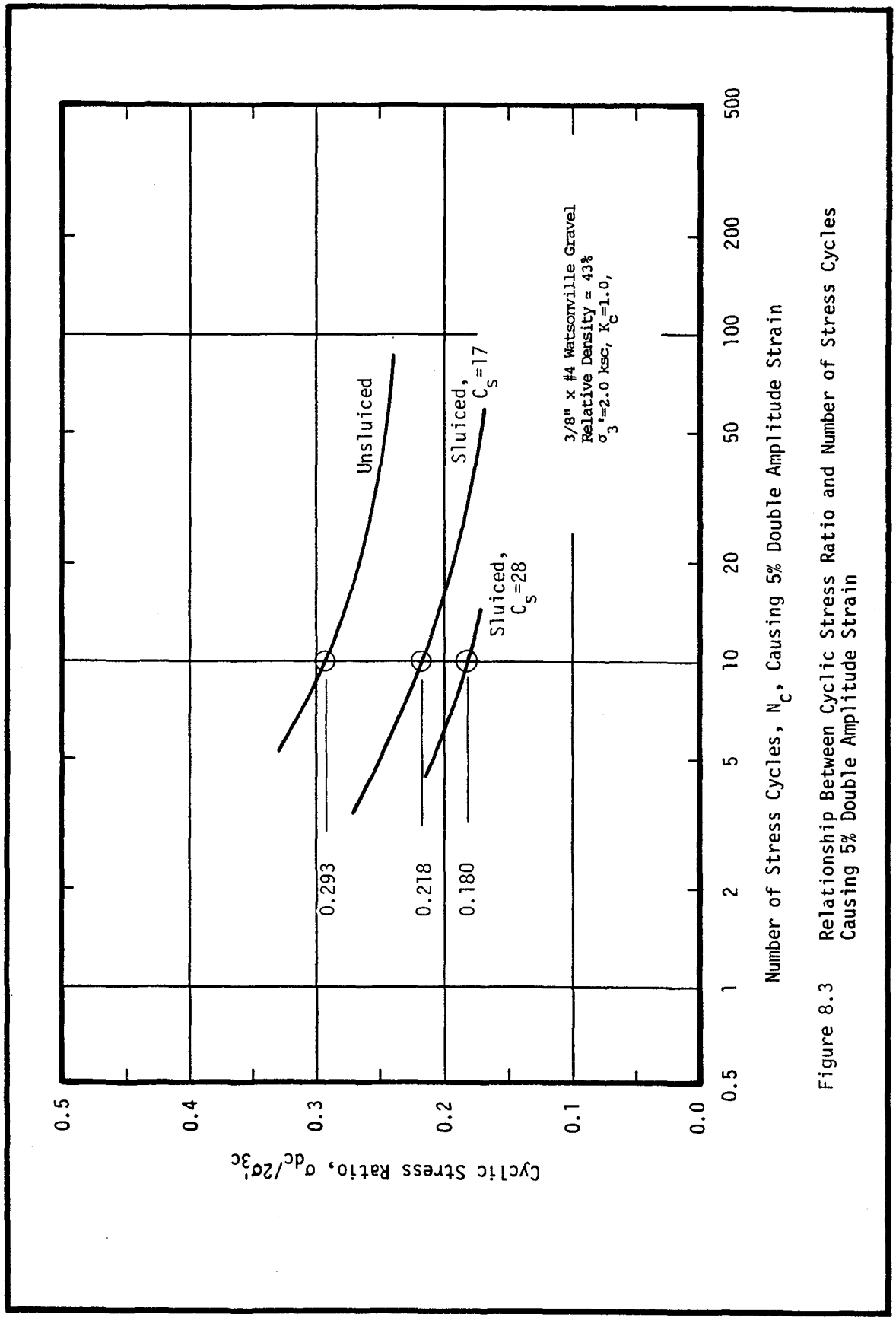

Figure 8.3 Relationship Between Cyclic Stress Ratio and Number of Stress Cycles Causing 5% Double Amplitude Strain

Table 8.0 Summary of Undrained Cyclic Triaxial Tests Performed on 3/8" x #4 Watsonville Gravel

Test Group	Sluicing Sand	Gravel Relative Density, %	C_s	Comments*
1	none	43	-	
2	Monterey Fine	43	17	
3	Banding	43	28	
4	none	43	-	4 membranes
5	none	58	-	
6	Monterey Fine	58	17	
7	Monterey Fine	80	17	tamped in 6 layers
8	none	43	-	K_c=2
9	Monterey Fine	43	17	K_c=2
10	Monterey Fine	45	17	K_c=1.25, 1.5, & 1.75

* - All test specimens are 2.8" diameter, pluviated structure, two membranes, σ_3'= 2.0 ksc, and K_c=1 except as noted.

Table 8.1 Material Properties and Test Conditions Causing Failure During Undrained Cyclic Loading

GRAVEL: 3/8" x #4 Watsonville Gravel
SLUICING SAND: none
C_s = -

Test No.	Gravel: Dry Density (pcf)	Gravel: Void Ratio	Gravel: Porosity	Gravel: Relative Density (%)	Sand: Dry Density (pcf)	Sand: Void Ratio
43	95.26	0.822	0.451	53.4	-	-
44	93.49	0.856	0.461	45.0	-	-
45	92.49	0.876	0.467	40.1	-	-
47	92.95	0.867	0.464	42.4	-	-
48	92.71	0.872	0.466	41.2	-	-
49	92.30	0.880	0.468	39.2	-	-

Test No.	Cyclic Stress Ratio, $\sigma_{d/2}\sigma_{3c}$	Number of Cycles Causing...: 80% Pore Pressure	100% Pore Pressure Ratio	2% Double Ampl.	5% Ampl.	10% Strain
43	0.290	-	-	11.5	20.0	-
44	0.255	36.0	38.0	33.0	42.0	-
45	0.293	9.0	12.5	1.6	7.9	-
47	0.265	19.0	24.0	14.0	21.0	-
48	0.292	4.4	7.4	0.45	3.3	5.9
49	0.282	12.5	16.0	7.3	11.6	14.9

* - All test specimens are 2.8" diameter, pluviated structure, two membranes, σ_3'= 2.0 ksc, and K_c=1.

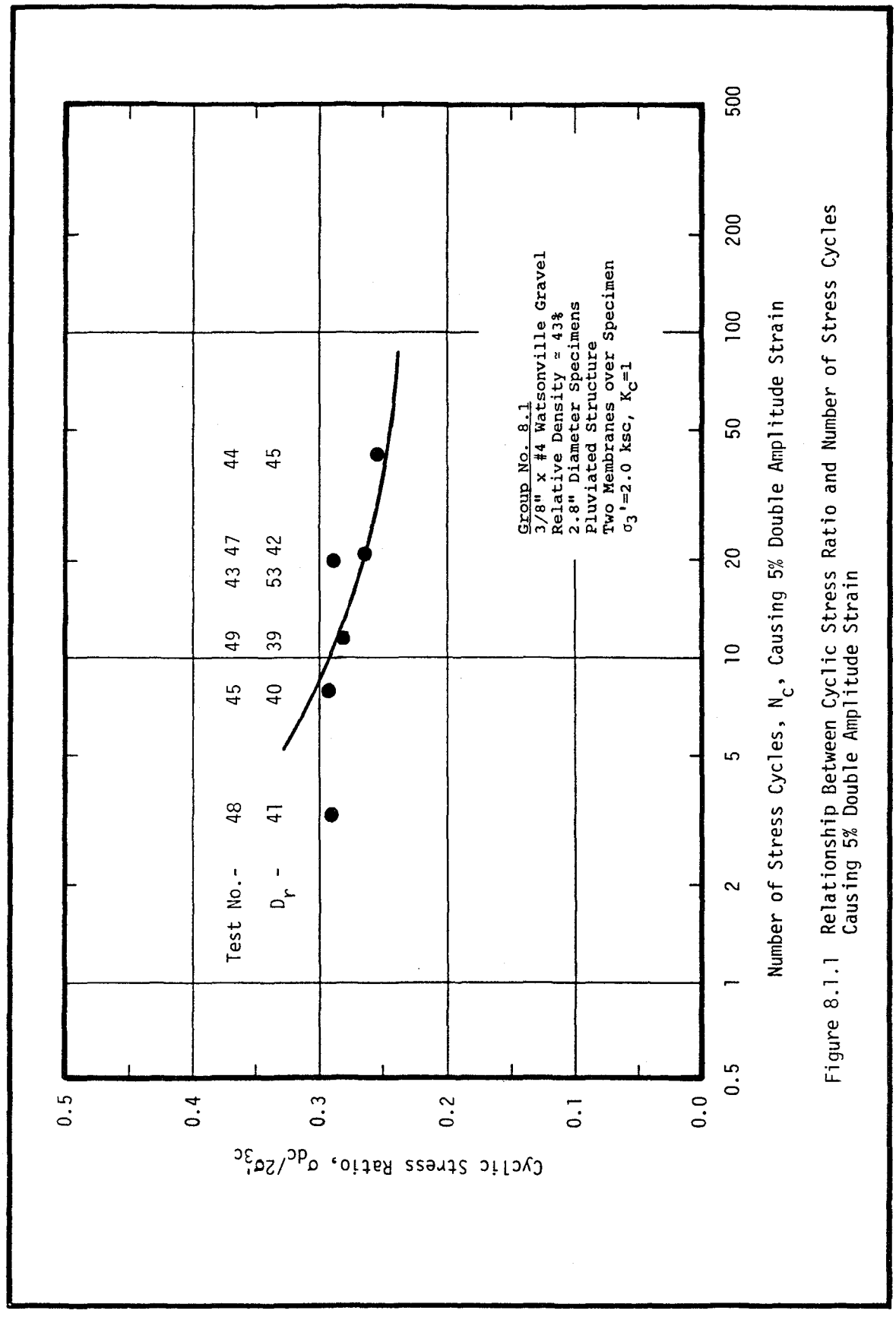

Figure 8.1.1 Relationship Between Cyclic Stress Ratio and Number of Stress Cycles Causing 5% Double Amplitude Strain

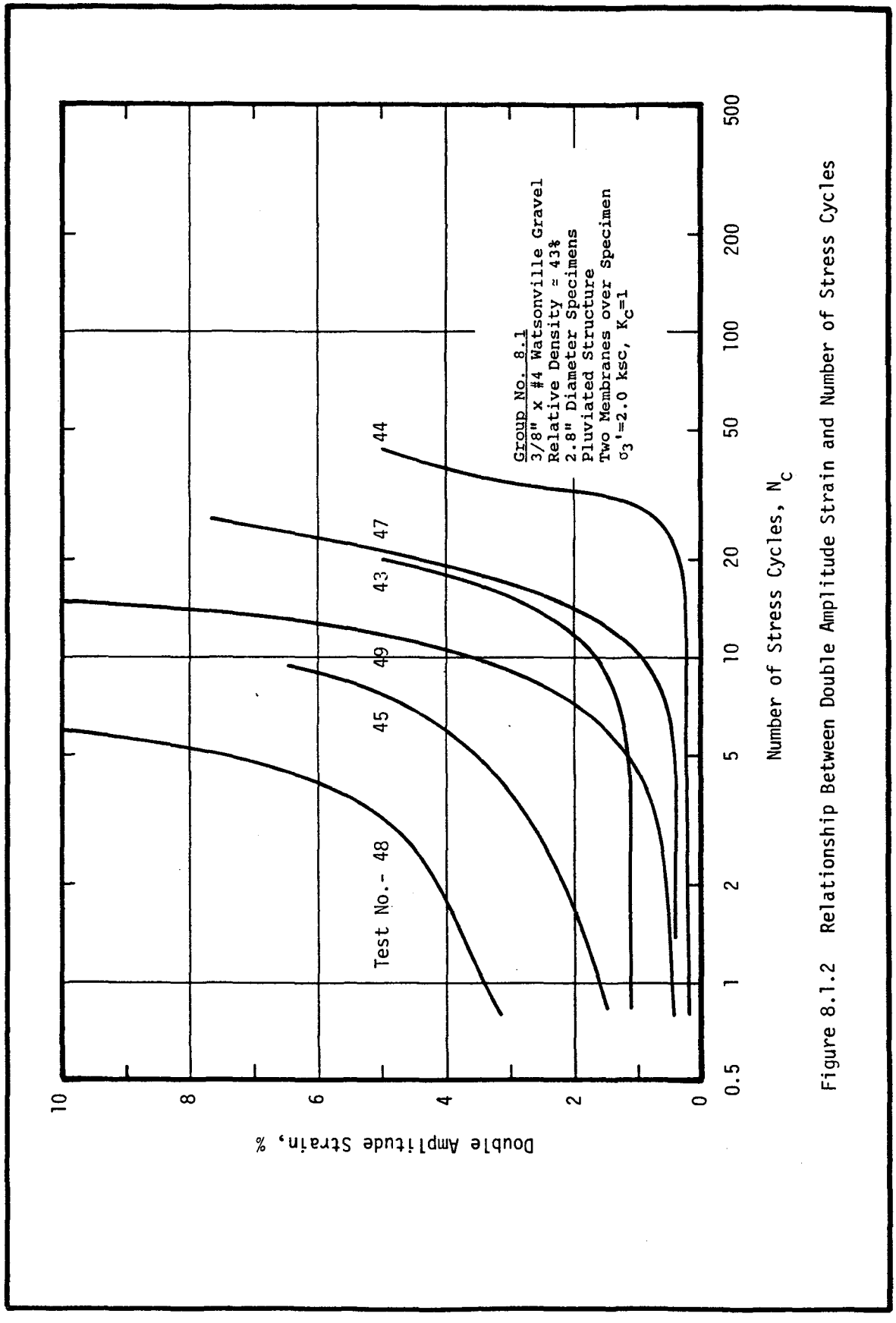

Figure 8.1.2 Relationship Between Double Amplitude Strain and Number of Stress Cycles

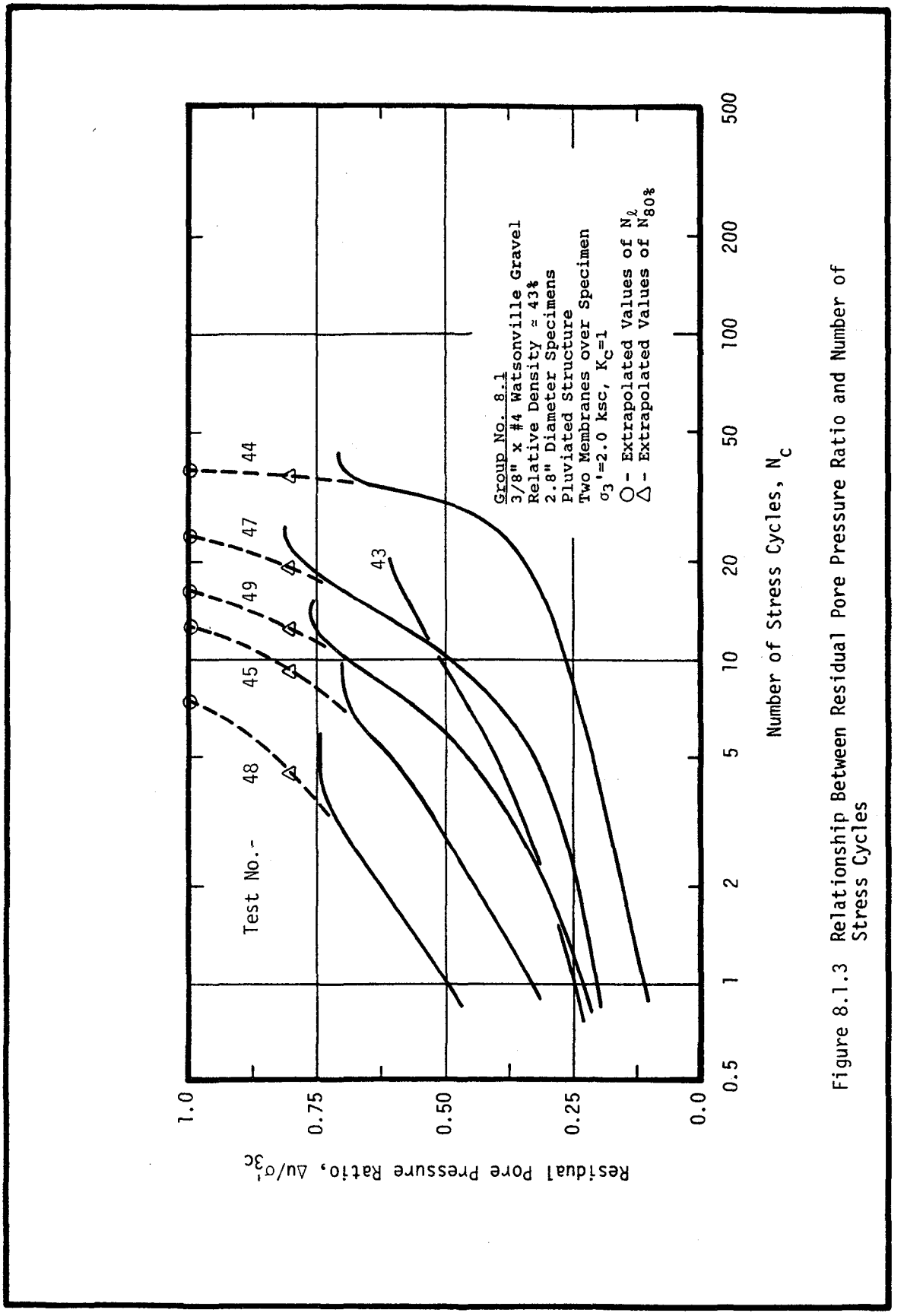

Figure 8.1.3 Relationship Between Residual Pore Pressure Ratio and Number of Stress Cycles

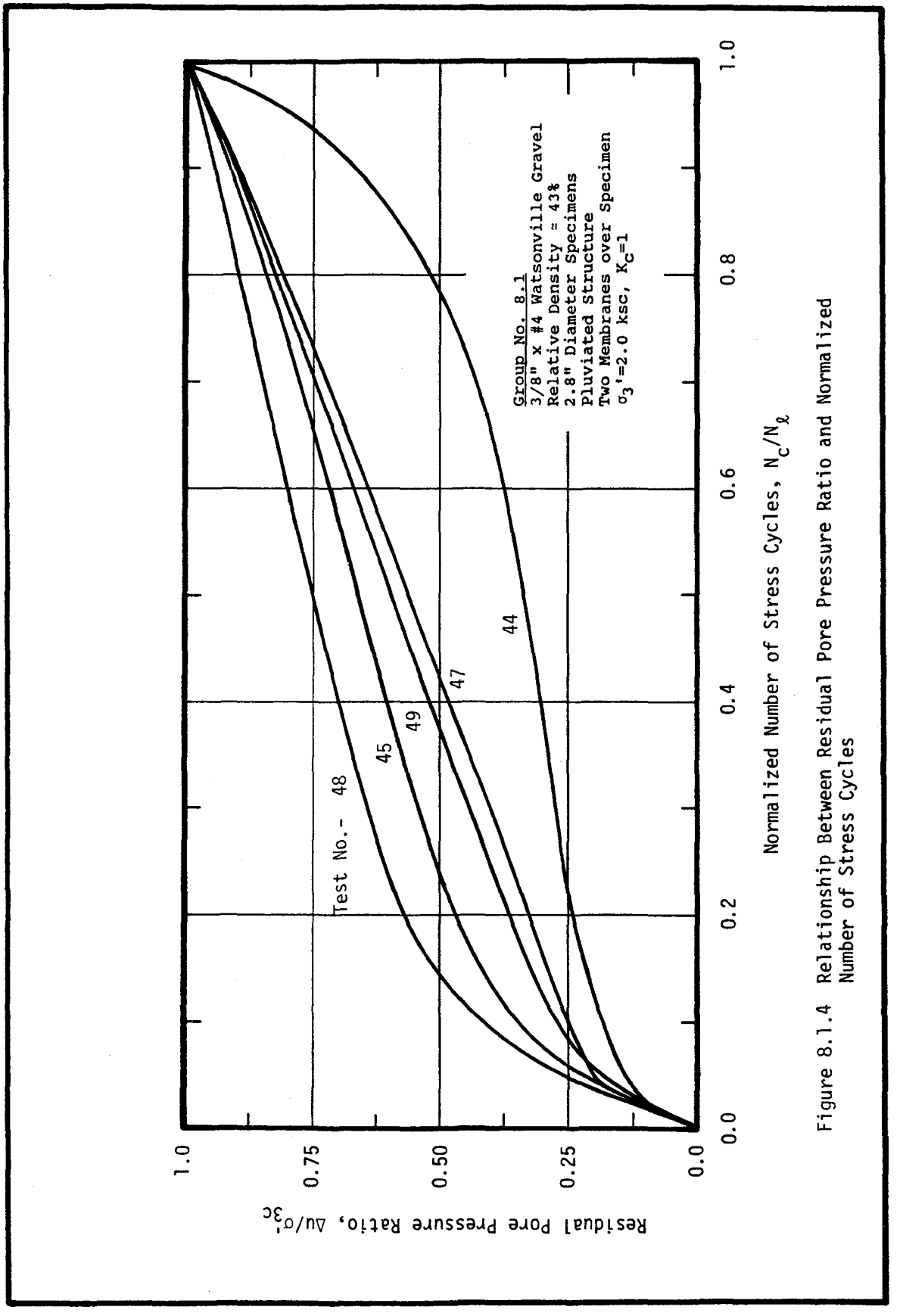

Figure 8.1.4 Relationship Between Residual Pore Pressure Ratio and Normalized Number of Stress Cycles

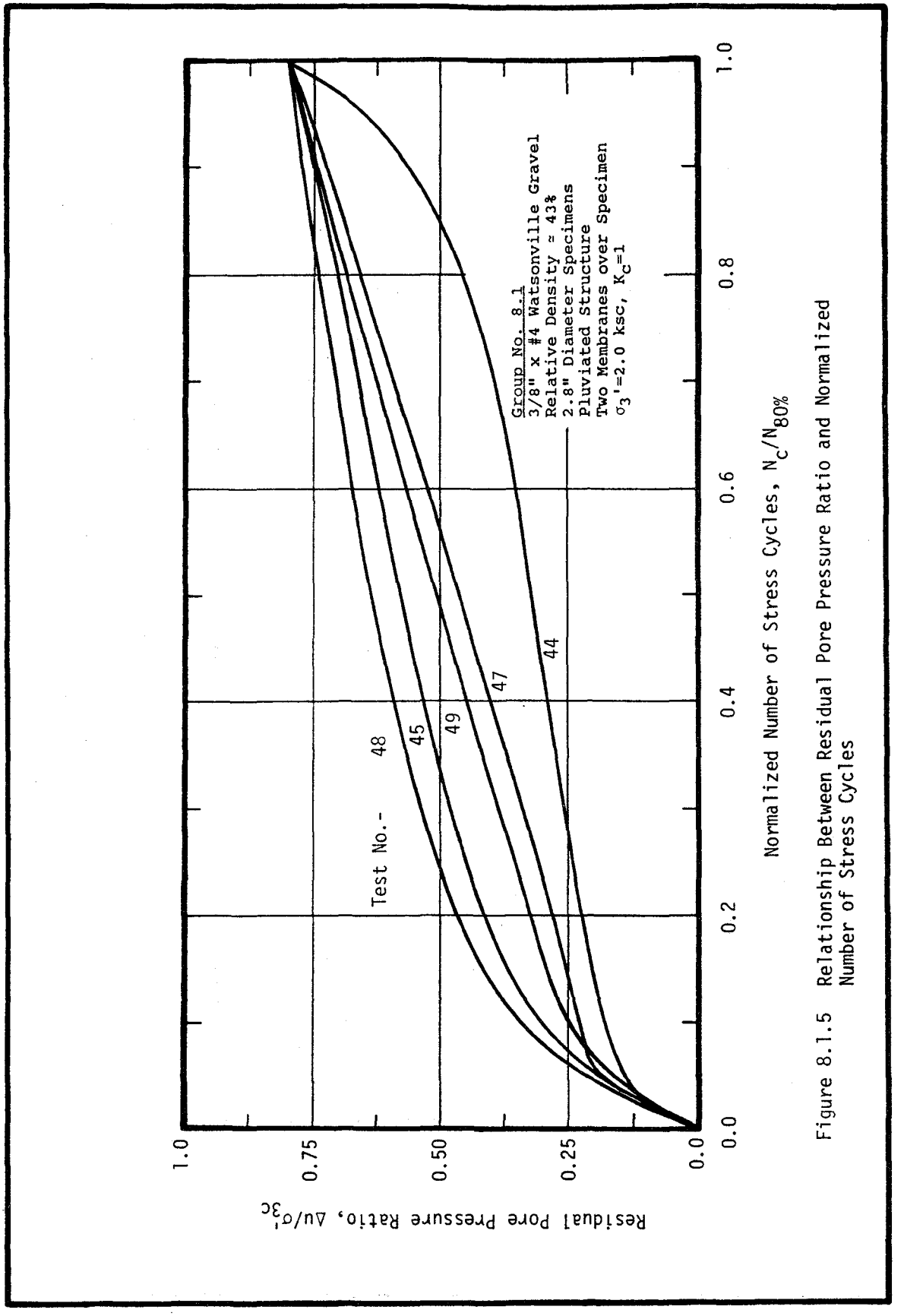

Figure 8.1.5 Relationship Between Residual Pore Pressure Ratio and Normalized Number of Stress Cycles

Table 8.2 Material Properties and Test Conditions Causing Failure During Undrained Cyclic Loading

GRAVEL: 3/8" x #4 Watsonville Gravel
SLUICING SAND: Monterey Fine
C_s=17

Test No.	Gravel				Sand	
	Dry Density (pcf)	Void Ratio	Porosity	Relative Density (%)	Dry Density (pcf)	Void Ratio
51	92.04	0.886	0.470	37.9	70.6	1.324
52	92.40	0.878	0.468	39.7	74.9	1.206
53	93.66	0.853	0.460	45.8	76.0	1.169
54	93.42	0.858	0.462	44.6	72.8	1.264
55	94.34	0.840	0.456	49.0	75.1	1.195
56	91.97	0.887	0.470	37.5	76.9	1.143
57	93.46	0.857	0.461	44.8	74.5	1.212

Test No.	Cyclic Stress Ratio, $\sigma_d/2\sigma_{3c}$	Number of Cycles Causing...				
		80% Pore	100% Pressure Ratio	2% Double	5% Ampl.	10% Strain
51	0.190	-	23.0	21.3	22.5	24.0
52	0.213	-	8.5	7.9	9.4	11.0
53	0.182	-	28.0	27.3	30.0	31.0
54	0.245	-	5.8	4.5	6.1	7.3
55	0.202	-	16.0	14.7	16.8	19.0
56	0.255	-	7.5	3.2	4.5	5.5
57	0.160	-	38.0	38.0	41.0	42.0

Test No.	Cyclic Stress Ratio, $\Delta\tau_{ff}/\sigma_{fc}$
51	0.137
52	0.155
53	0.131
54	0.176
55	0.144
56	0.183
57	0.115

* - All test specimens are 2.8" diameter, pluviated structure, two membranes, σ_3'= 2.0 ksc, and K_c=1.

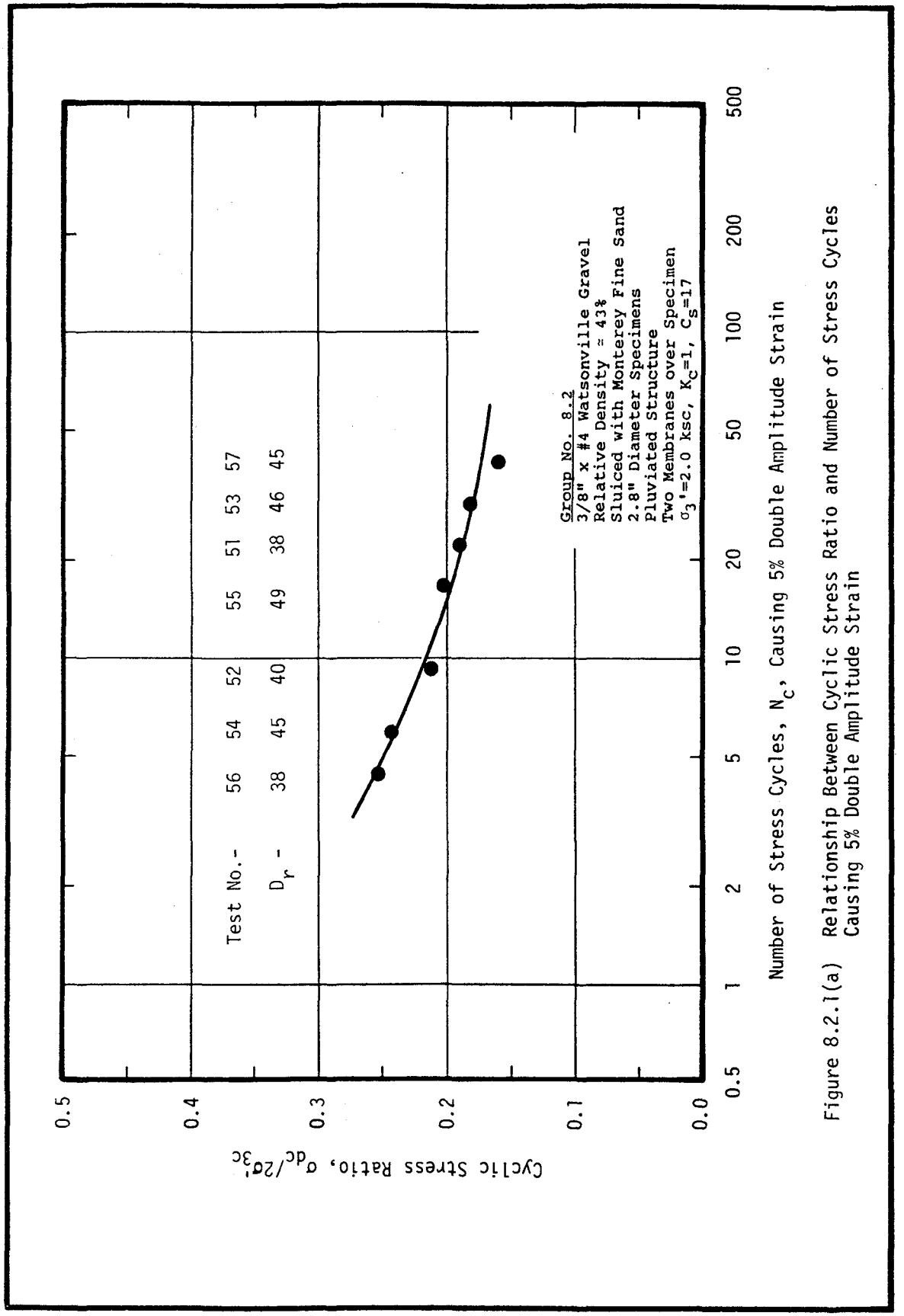

Figure 8.2.1(a) Relationship Between Cyclic Stress Ratio and Number of Stress Cycles Causing 5% Double Amplitude Strain

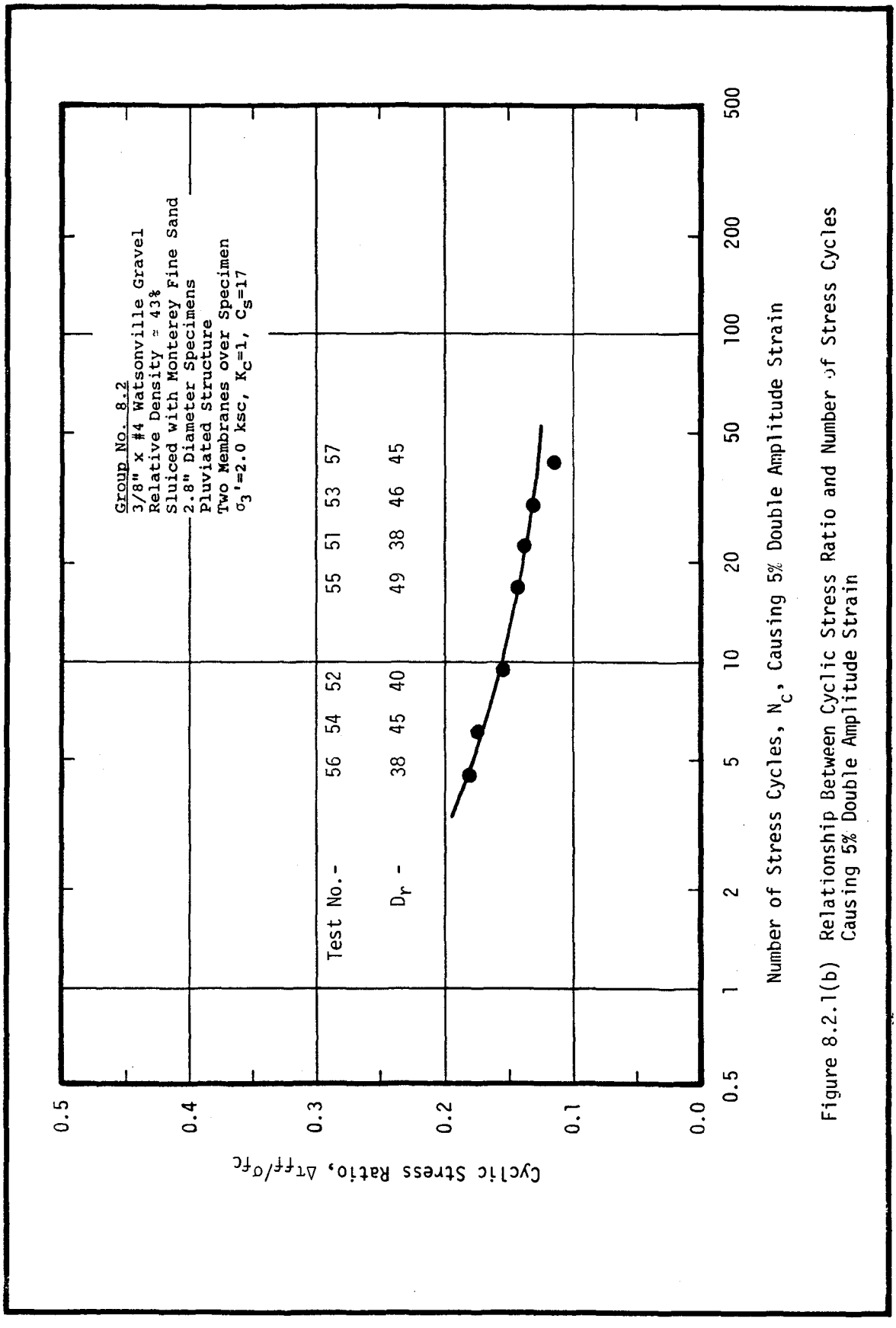

Figure 8.2.1(b) Relationship Between Cyclic Stress Ratio and Number of Stress Cycles Causing 5% Double Amplitude Strain

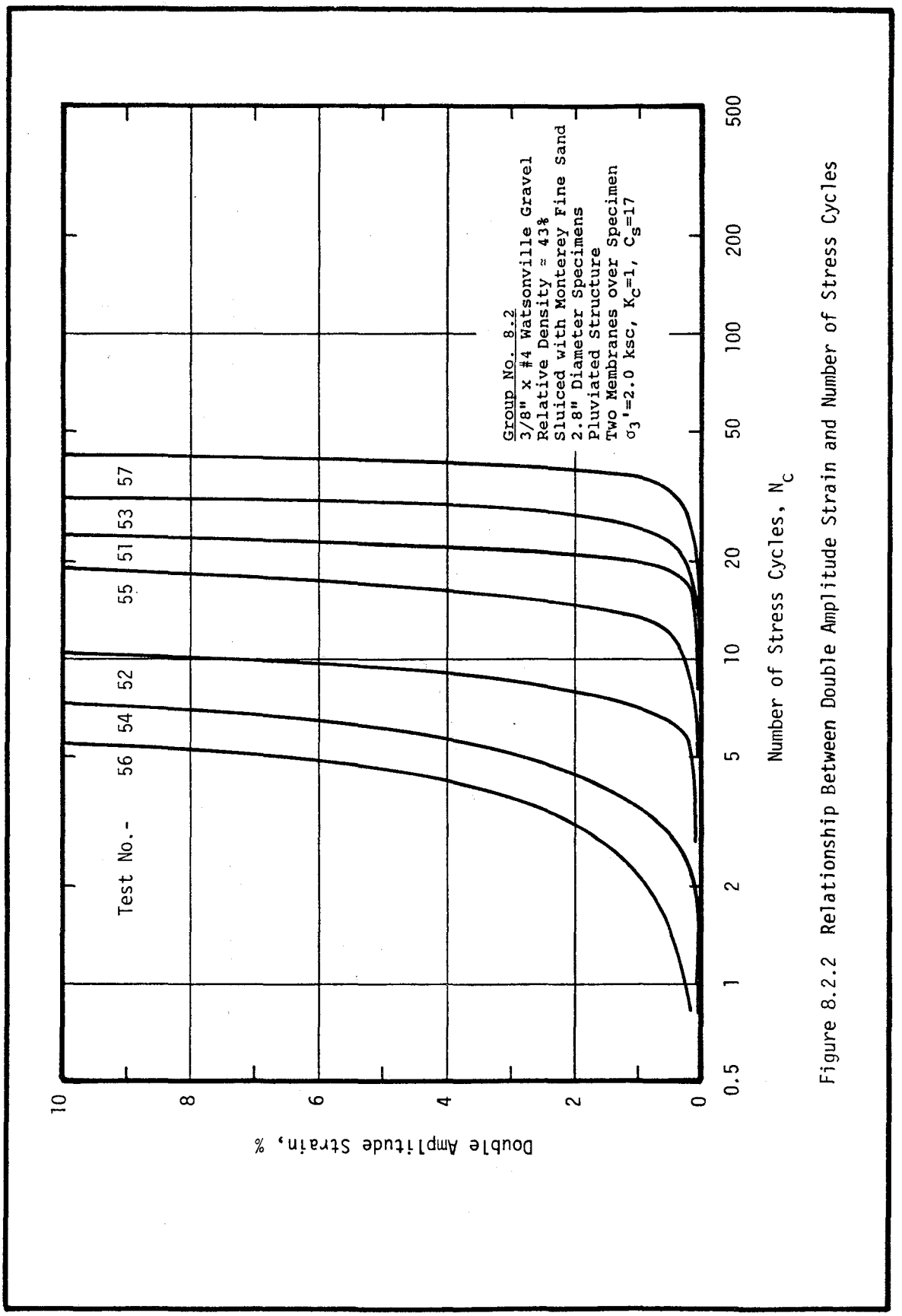

Figure 8.2.2 Relationship Between Double Amplitude Strain and Number of Stress Cycles

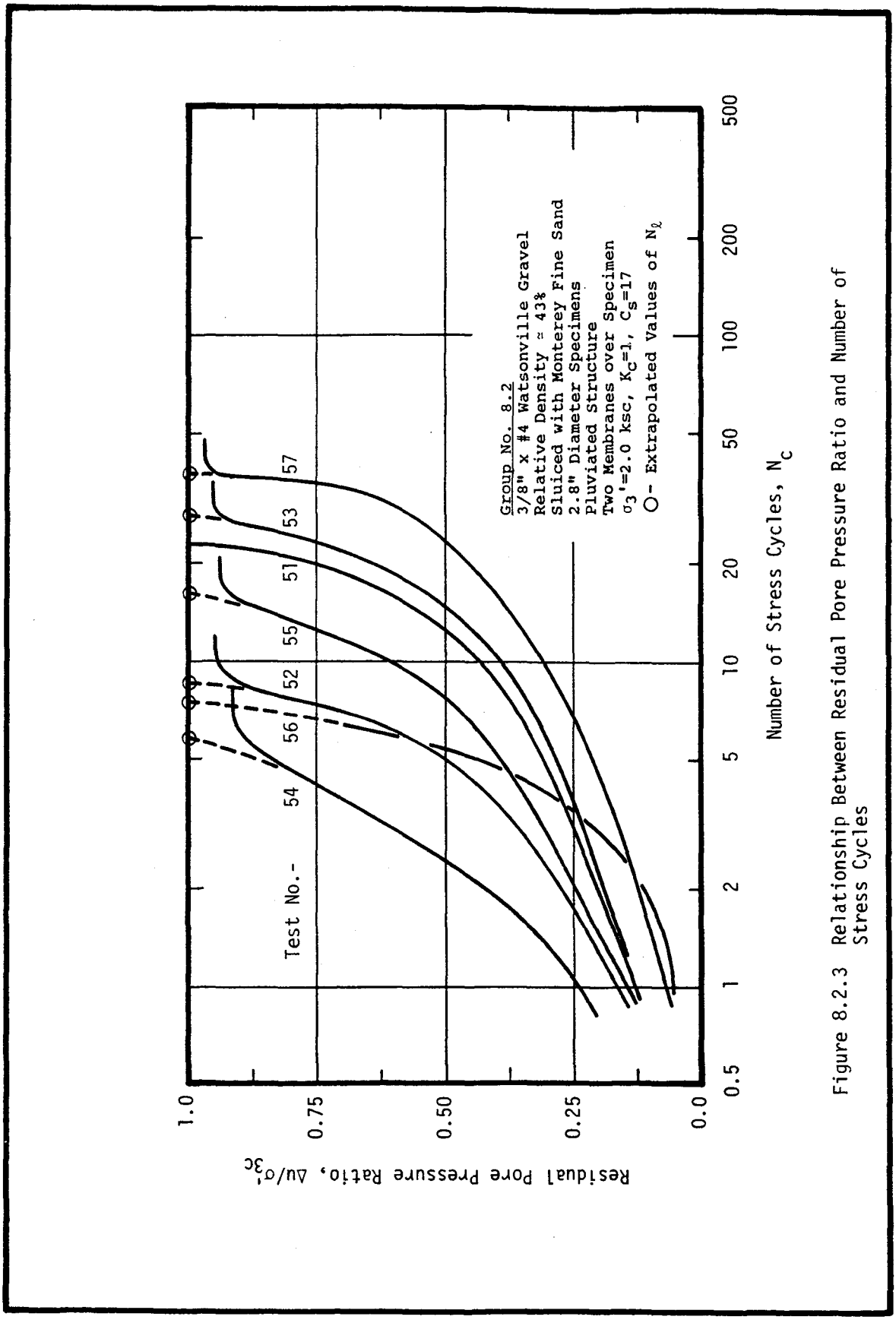

Figure 8.2.3 Relationship Between Residual Pore Pressure Ratio and Number of Stress Cycles

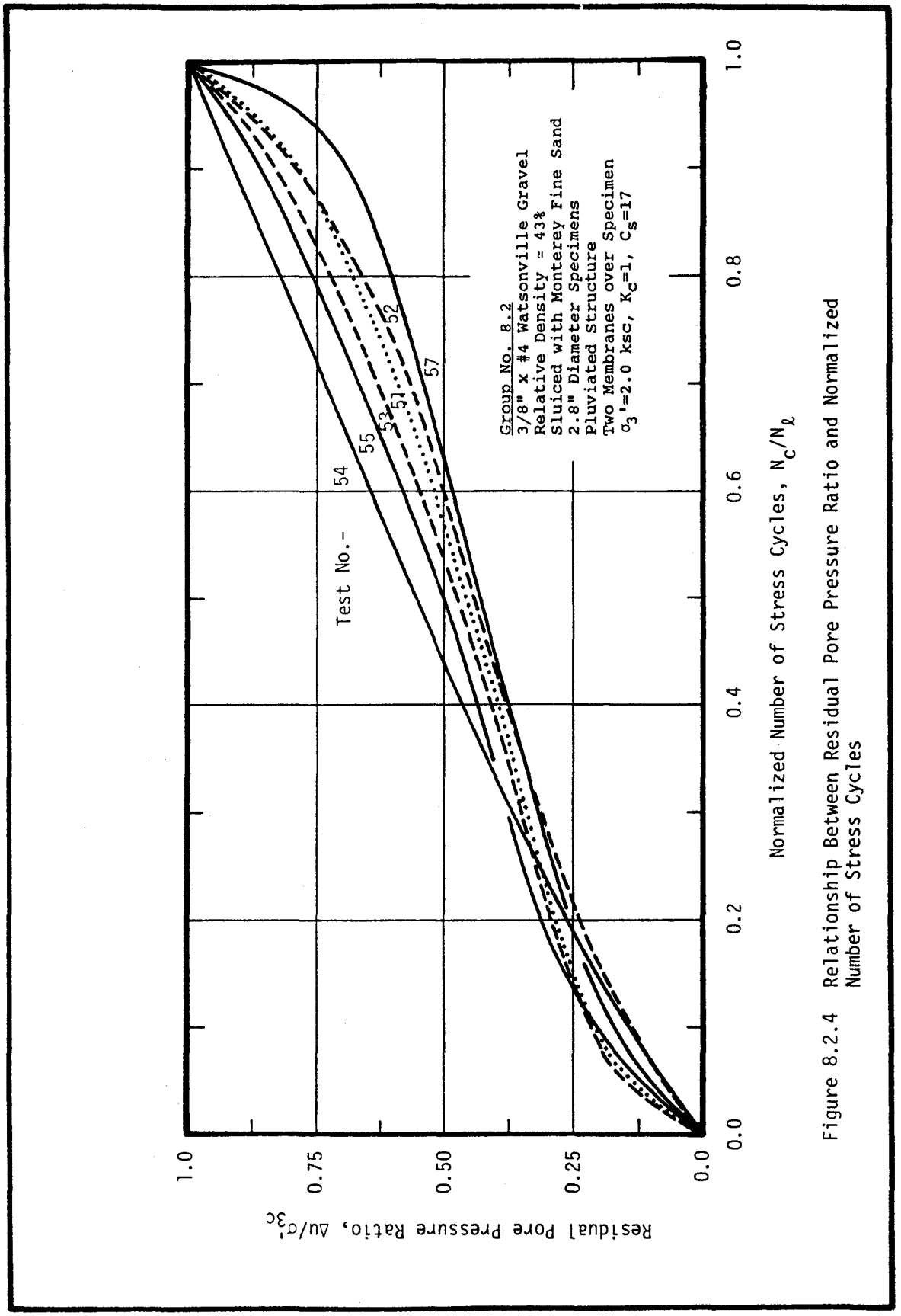

Figure 8.2.4 Relationship Between Residual Pore Pressure Ratio and Normalized Number of Stress Cycles

Table 8.3 Material Properties and Test Conditions Causing Failure During Undrained Cyclic Loading

GRAVEL: 3/8" x #4 Watsonville Gravel
SLUICING SAND: Banding
C_s=28

Test No.	Gravel				Sand	
	Dry Density (pcf)	Void Ratio	Porosity	Relative Density (%)	Dry Density (pcf)	Void Ratio
76	94.48	0.837	0.456	49.7	79.2	1.089
77	93.46	0.857	0.461	44.8	82.8	0.998
78	91.70	0.893	0.472	36.2	81.6	1.030

Test No.	Cyclic Stress Ratio, $\sigma_d/2\sigma_{3c}$	Number of Cycles Causing...				
		80% Pore	100% Pressure Ratio	2% Double	5% Ampl.	10% Strain
76	0.213	-	7.0	7.4	9.0	10.2
77	0.204	-	4.5	4.8	5.9	6.9
78	0.182	-	5.8	6.2	7.6	8.9

* - All test specimens are 2.8" diameter, pluviated structure, two membranes, σ_3'= 2.0 ksc, and K_c=1.

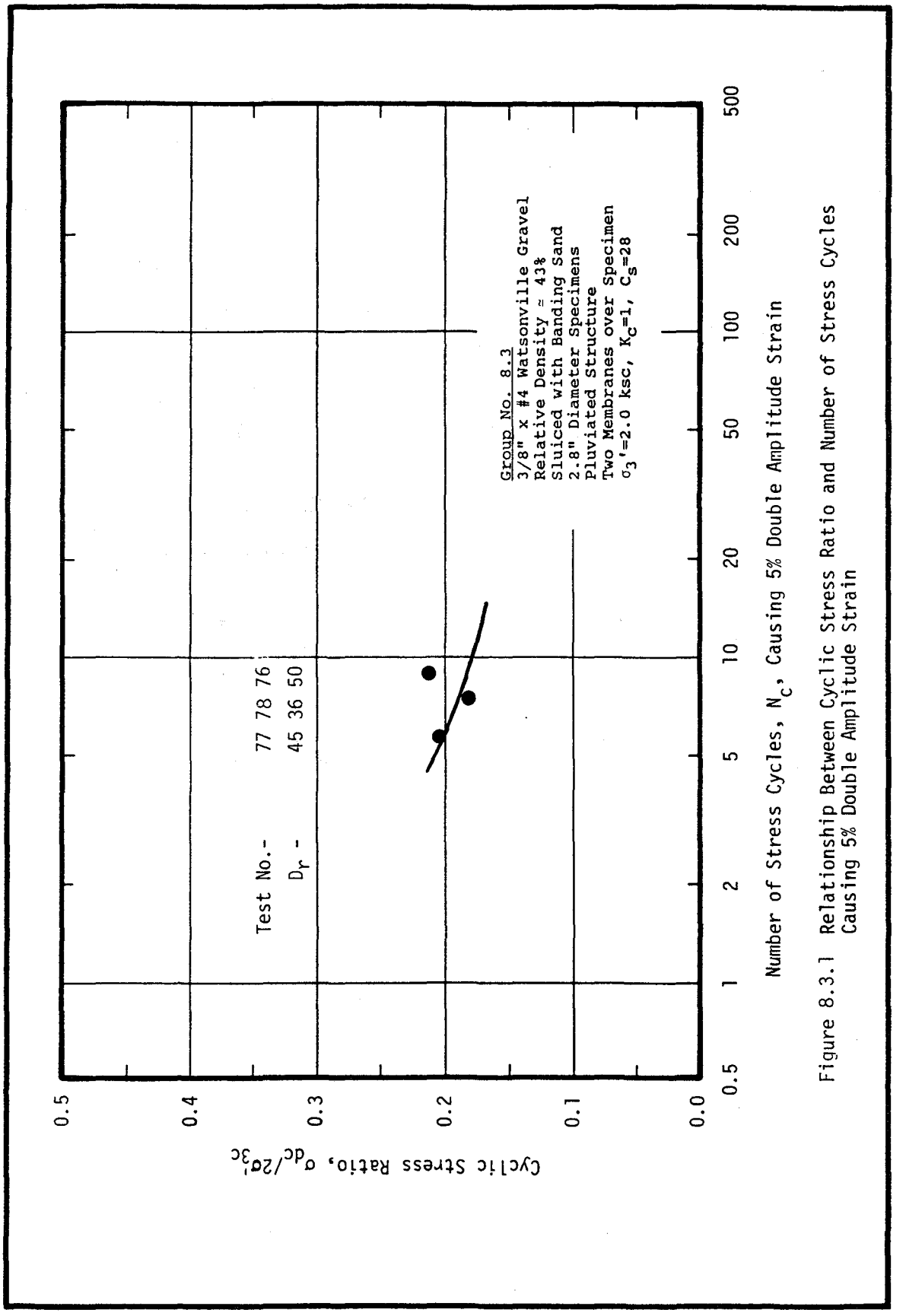

Figure 8.3.1 Relationship Between Cyclic Stress Ratio and Number of Stress Cycles Causing 5% Double Amplitude Strain

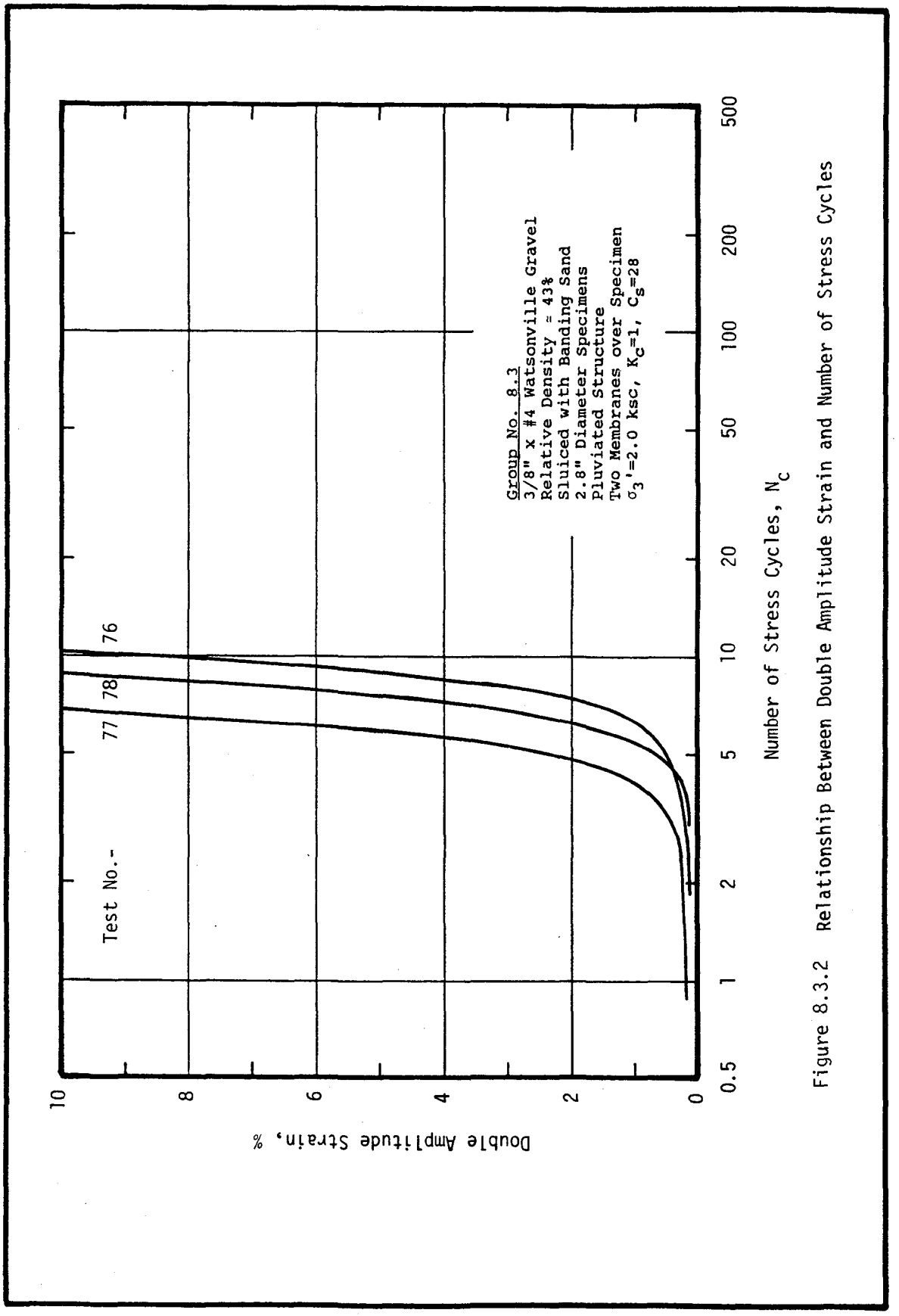

Figure 8.3.2 Relationship Between Double Amplitude Strain and Number of Stress Cycles

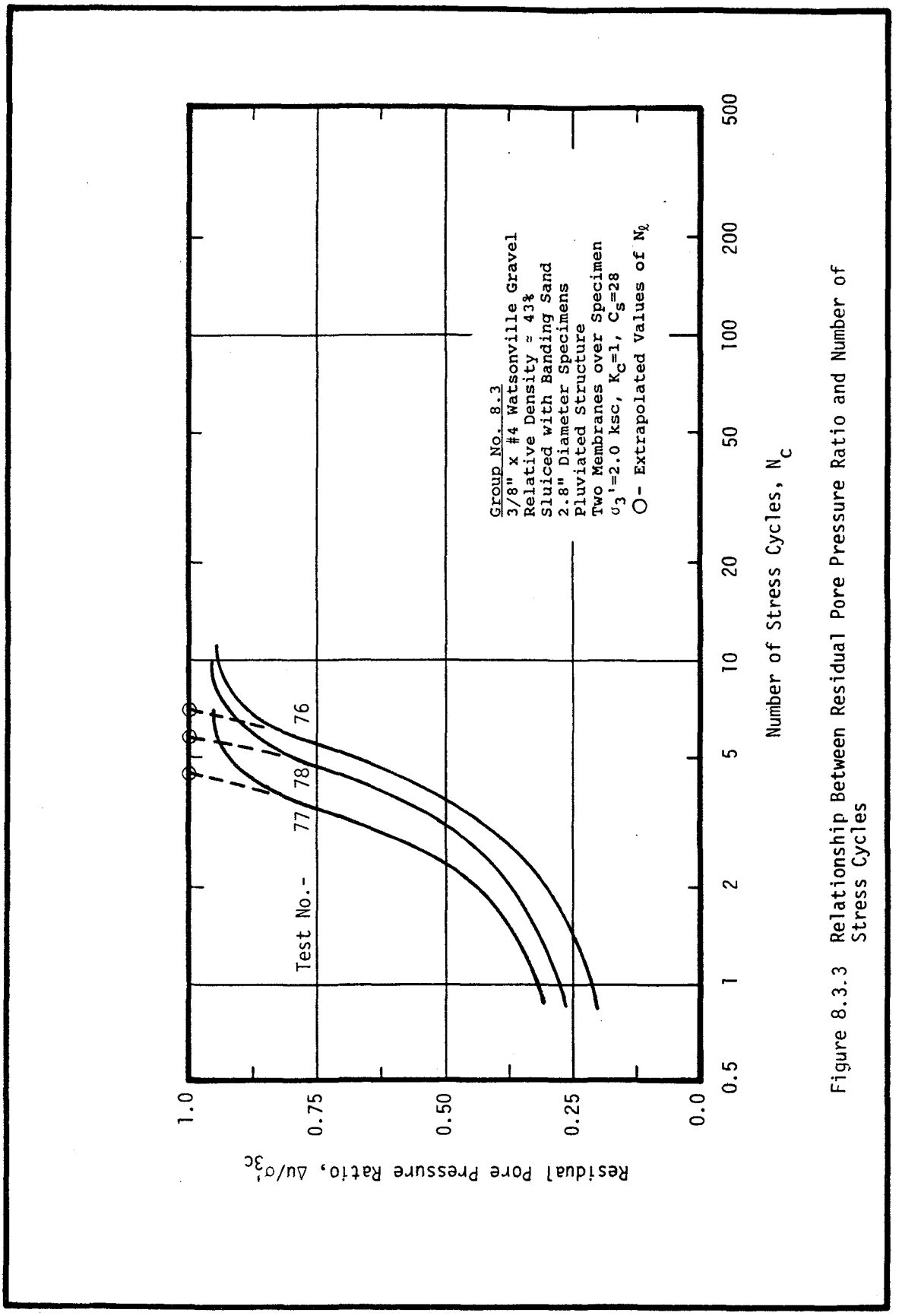

Figure 8.3.3 Relationship Between Residual Pore Pressure Ratio and Number of Stress Cycles

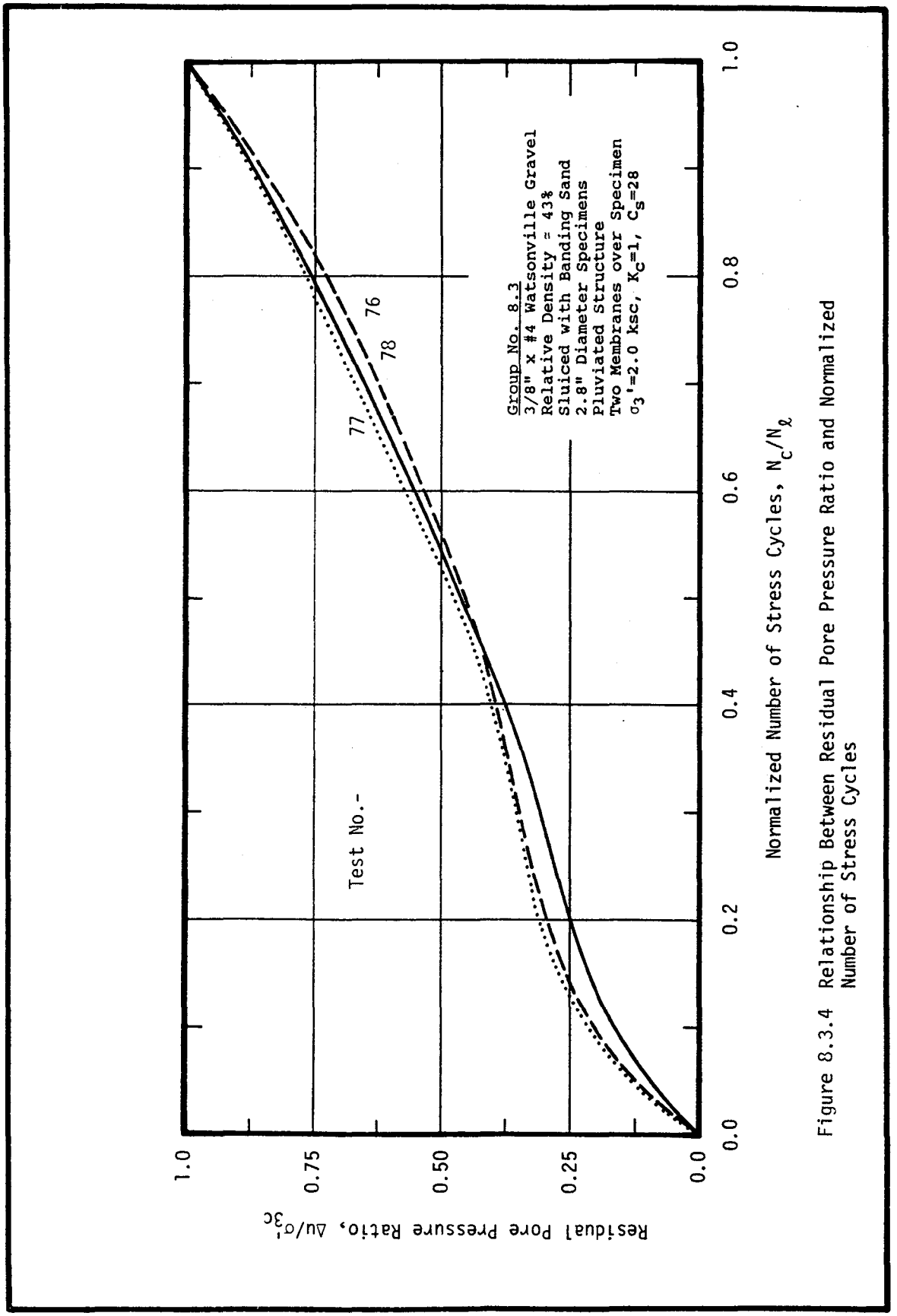

Figure 8.3.4 Relationship Between Residual Pore Pressure Ratio and Normalized Number of Stress Cycles

Table 8.4 Material Properties and Test Conditions Causing Failure During Undrained Cyclic Loading

GRAVEL: 3/8" x #4 Watsonville Gravel
SLUICING SAND: none
C_s = -

Test No.	Gravel: Dry Density (pcf)	Gravel: Void Ratio	Gravel: Porosity	Gravel: Relative Density (%)	Sand: Dry Density (pcf)	Sand: Void Ratio
58	92.77	0.871	0.465	41.5	-	-
59	91.47	0.897	0.473	35.0	-	-
60	92.96	0.867	0.464	42.3	-	-
61	90.70	0.914	0.477	31.1	-	-
62	93.59	0.854	0.461	45.5	-	-

Test No.	Cyclic Stress Ratio, $\sigma_d/2\sigma_{3c}$	Number of Cycles Causing...: 80% Pore Pressure Ratio	100% Pore Pressure Ratio	2% Double Ampl. Strain	5% Double Ampl. Strain	10% Double Ampl. Strain
58	0.296	7.9	14.5	3.3	9.1	16.0
59	0.270	15.0	20.0	9.6	16.5	26.0
60	0.251	165	180	158	175	190
61	0.303	4.5	8.7	1.2	4.0	11.0
62	0.294	16.0	21.0	14.2	22.0	32.0

* - All test specimens are 2.8" diameter, pluviated structure, four membranes, σ_3' = 2.0 ksc, and K_c=1.

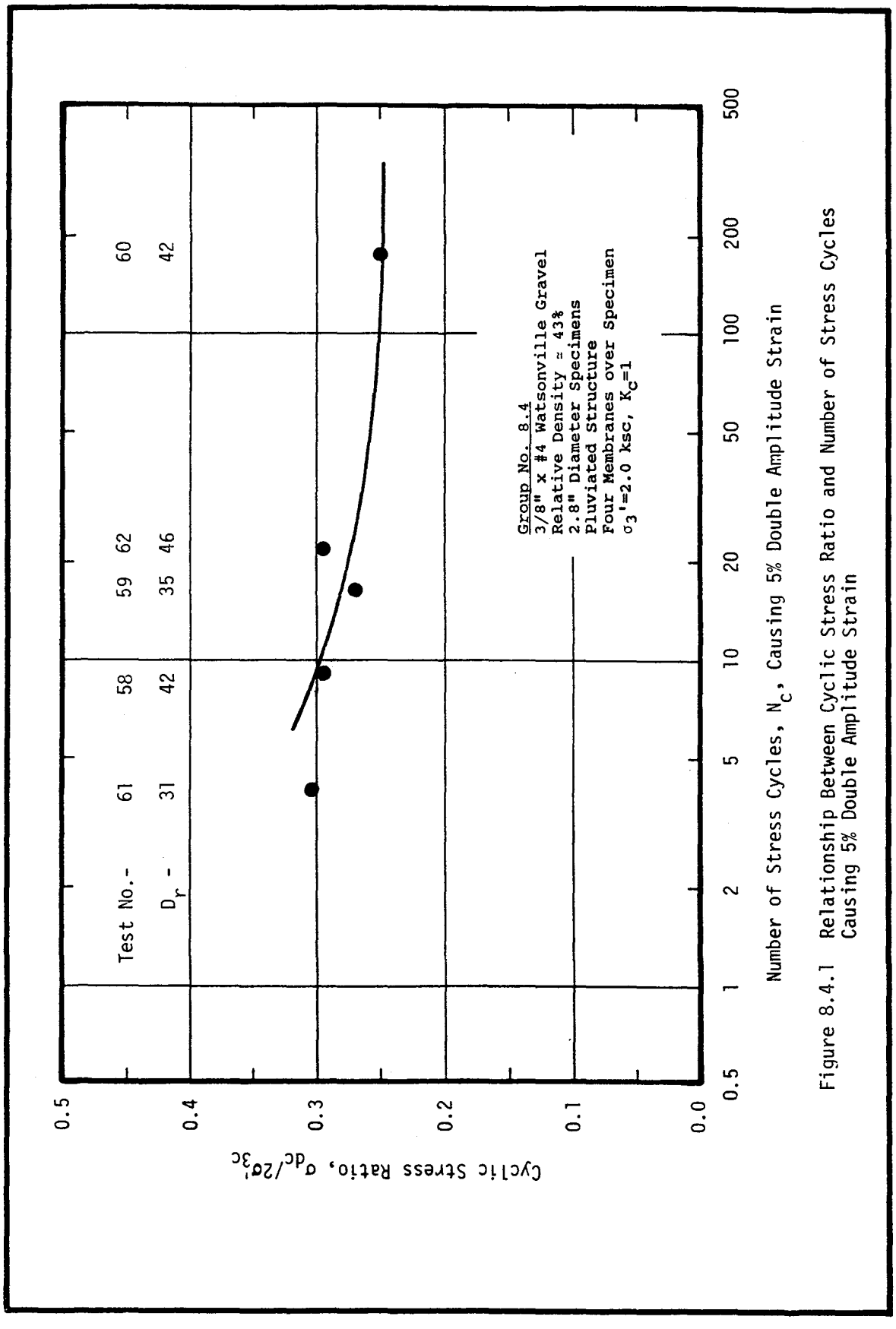

Figure 8.4.1 Relationship Between Cyclic Stress Ratio and Number of Stress Cycles Causing 5% Double Amplitude Strain

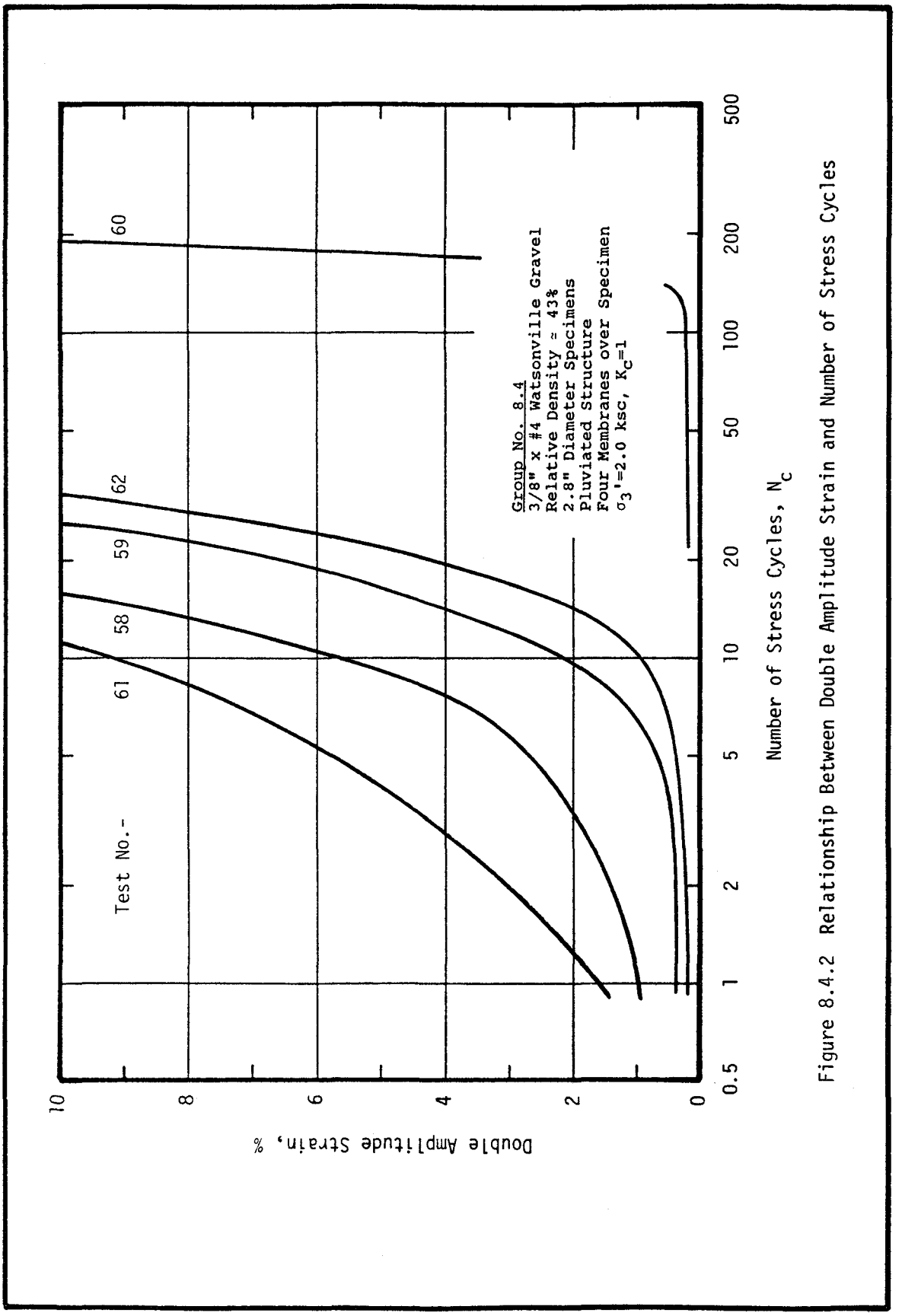

Figure 8.4.2 Relationship Between Double Amplitude Strain and Number of Stress Cycles

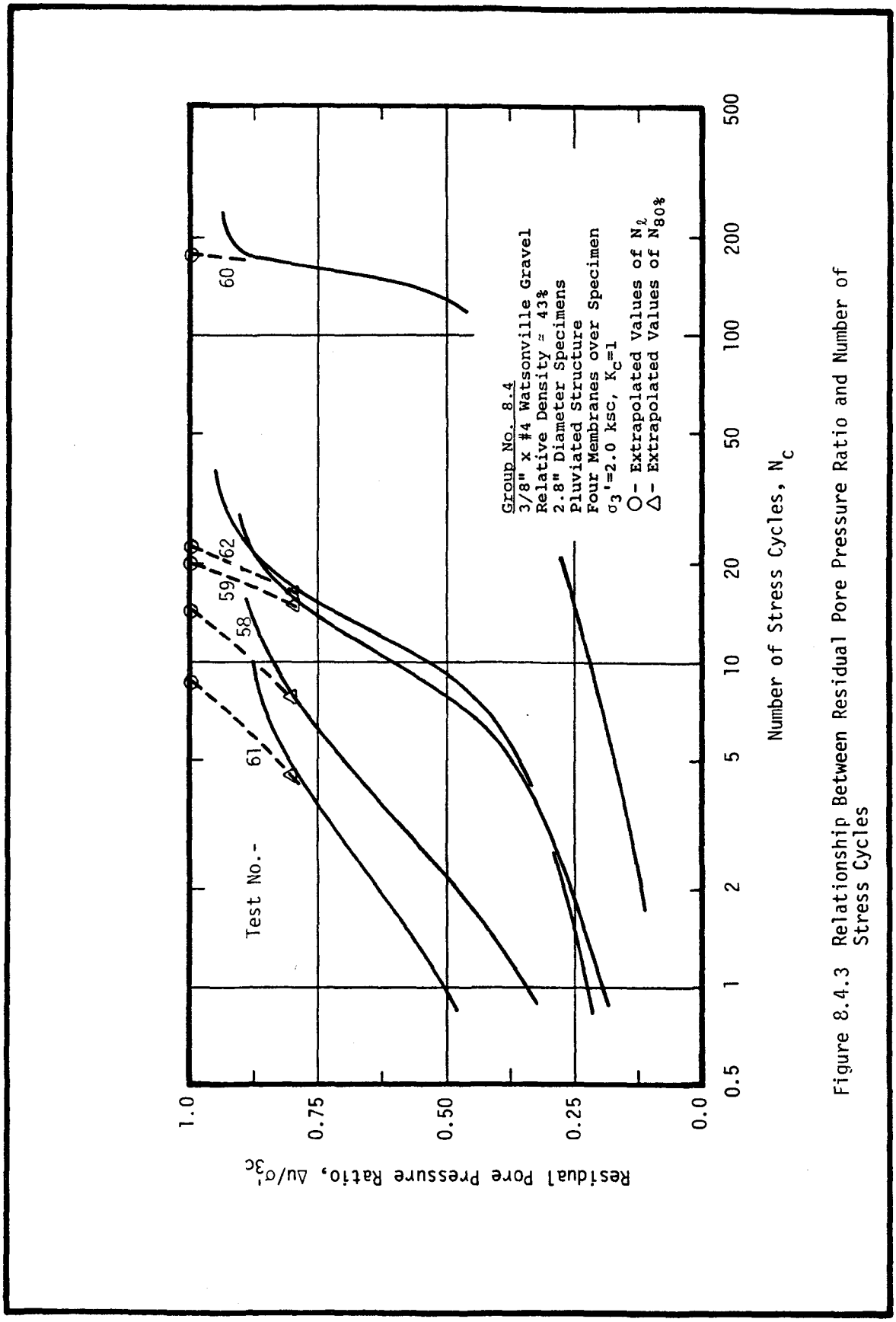

Figure 8.4.3 Relationship Between Residual Pore Pressure Ratio and Number of Stress Cycles

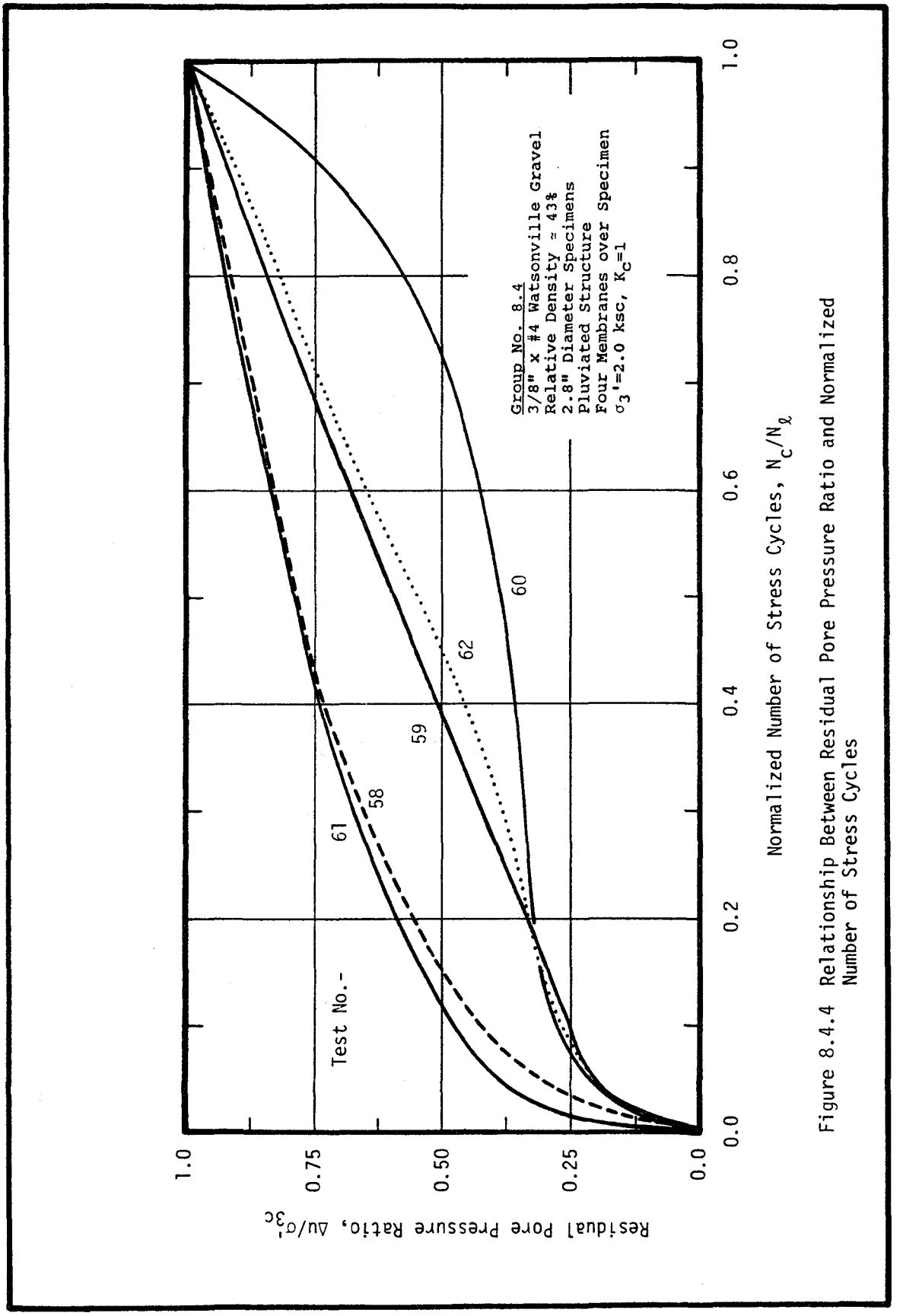

Figure 8.4.4 Relationship Between Residual Pore Pressure Ratio and Normalized Number of Stress Cycles

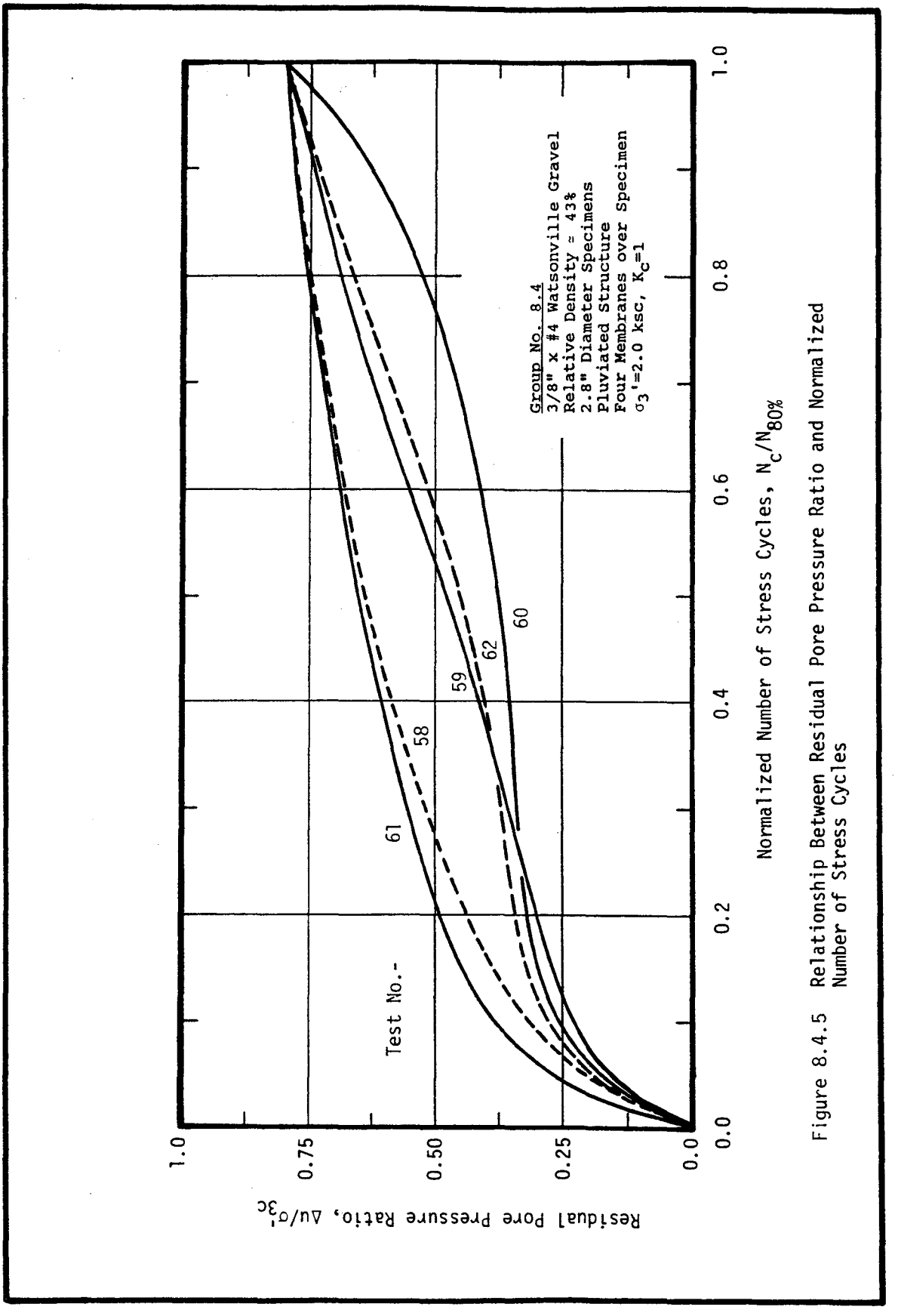

Figure 8.4.5 Relationship Between Residual Pore Pressure Ratio and Normalized Number of Stress Cycles

Table 8.5 Material Properties and Test Conditions Causing Failure During Undrained Cyclic Loading

GRAVEL: 3/8" x #4 Watsonville Gravel
SLUICING SAND: none
C_s = -

Test No.	Gravel				Sand	
	Dry Density (pcf)	Void Ratio	Porosity	Relative Density (%)	Dry Density (pcf)	Void Ratio
43	95.26	0.822	0.451	53.4	-	-
64	95.74	0.813	0.448	55.6	-	-
65	95.16	0.824	0.452	52.9	-	-
66	96.39	0.801	0.445	58.5	-	-
67	96.31	0.802	0.445	58.2	-	-
68	95.28	0.822	0.451	53.4	-	-
69	95.92	0.809	0.447	56.4	-	-

Test No.	Cyclic Stress Ratio, $\sigma_d/2\sigma_{3c}$	Number of Cycles Causing...				
		75% Pore	100% Pressure Ratio	2% Double	5% Ampl.	10% Strain
43	0.290	-	-	11.8	20	-
64	0.349	7.9	-	2.2	8.6	-
65	0.291	16.2	-	12.0	26	-
66	0.314	26.5	-	19.0	28	-
67	0.277	108	-	102	110	-
68	0.319	22.2	-	15.5	28	-
69	0.385	4.2	-	-	3.8	-

* - All test specimens are 2.8" diameter, pluviated structure, two membranes, $\sigma_3' = 2.0$ ksc, and $K_c = 1$.

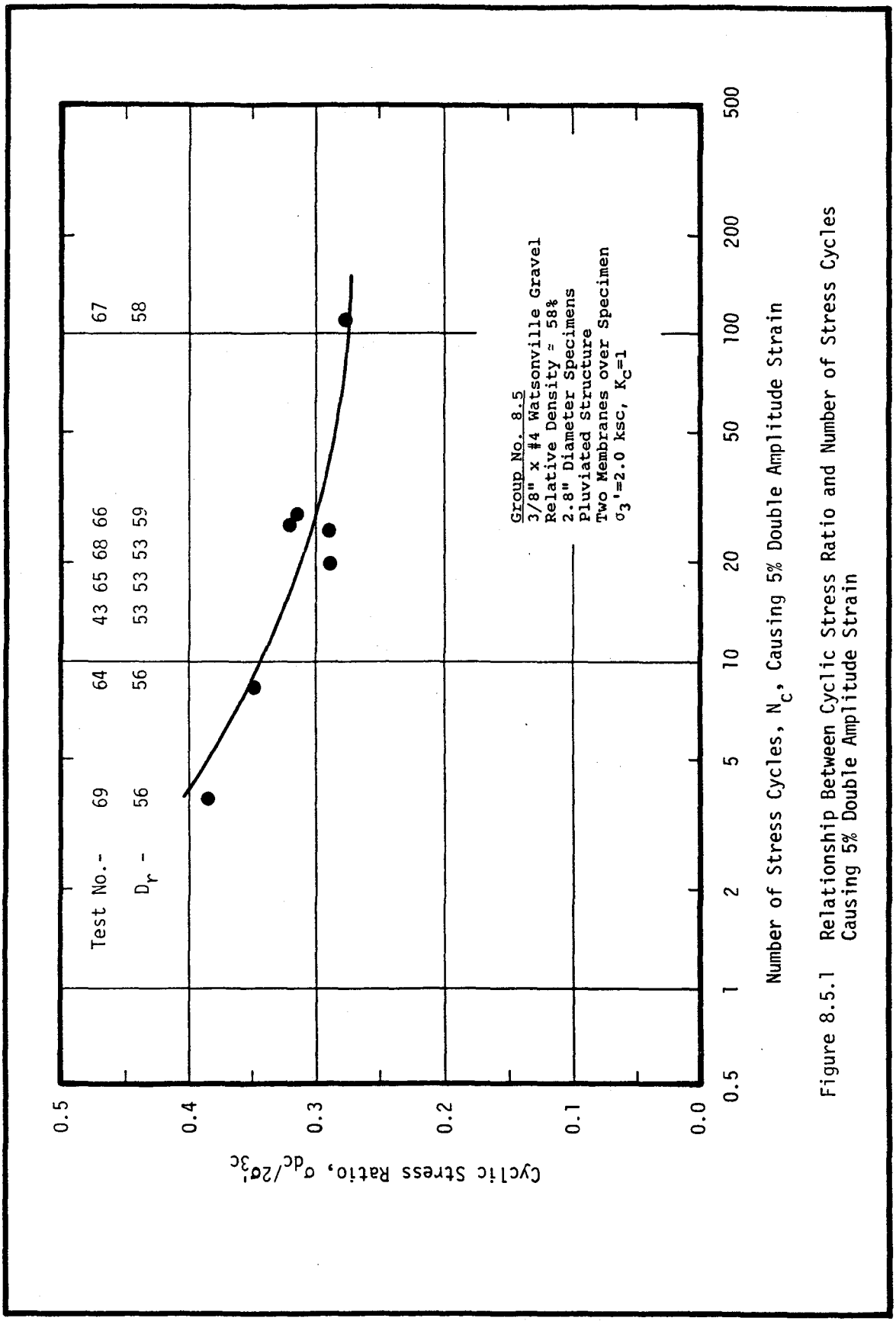

Figure 8.5.1 Relationship Between Cyclic Stress Ratio and Number of Stress Cycles Causing 5% Double Amplitude Strain

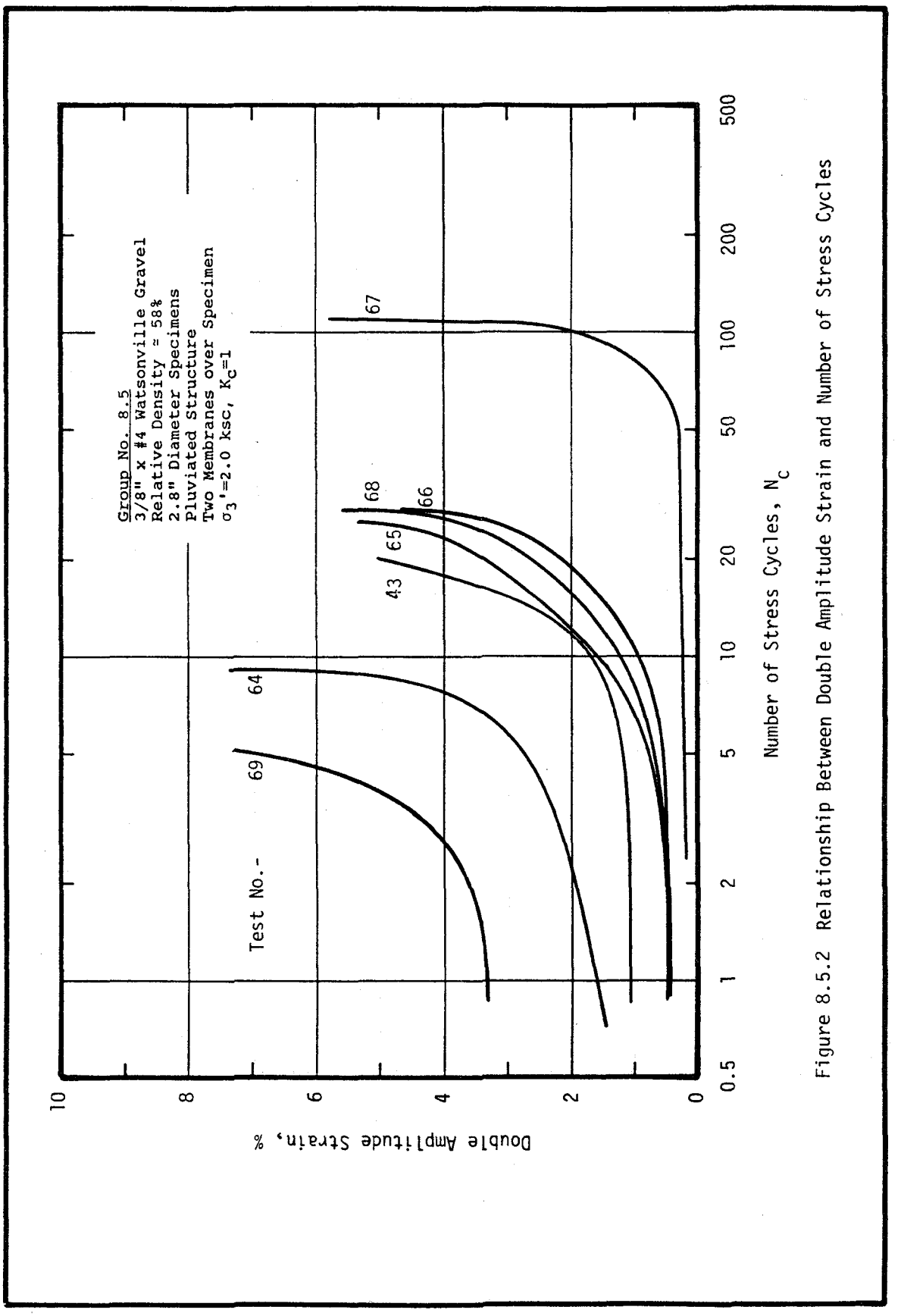

Figure 8.5.2 Relationship Between Double Amplitude Strain and Number of Stress Cycles

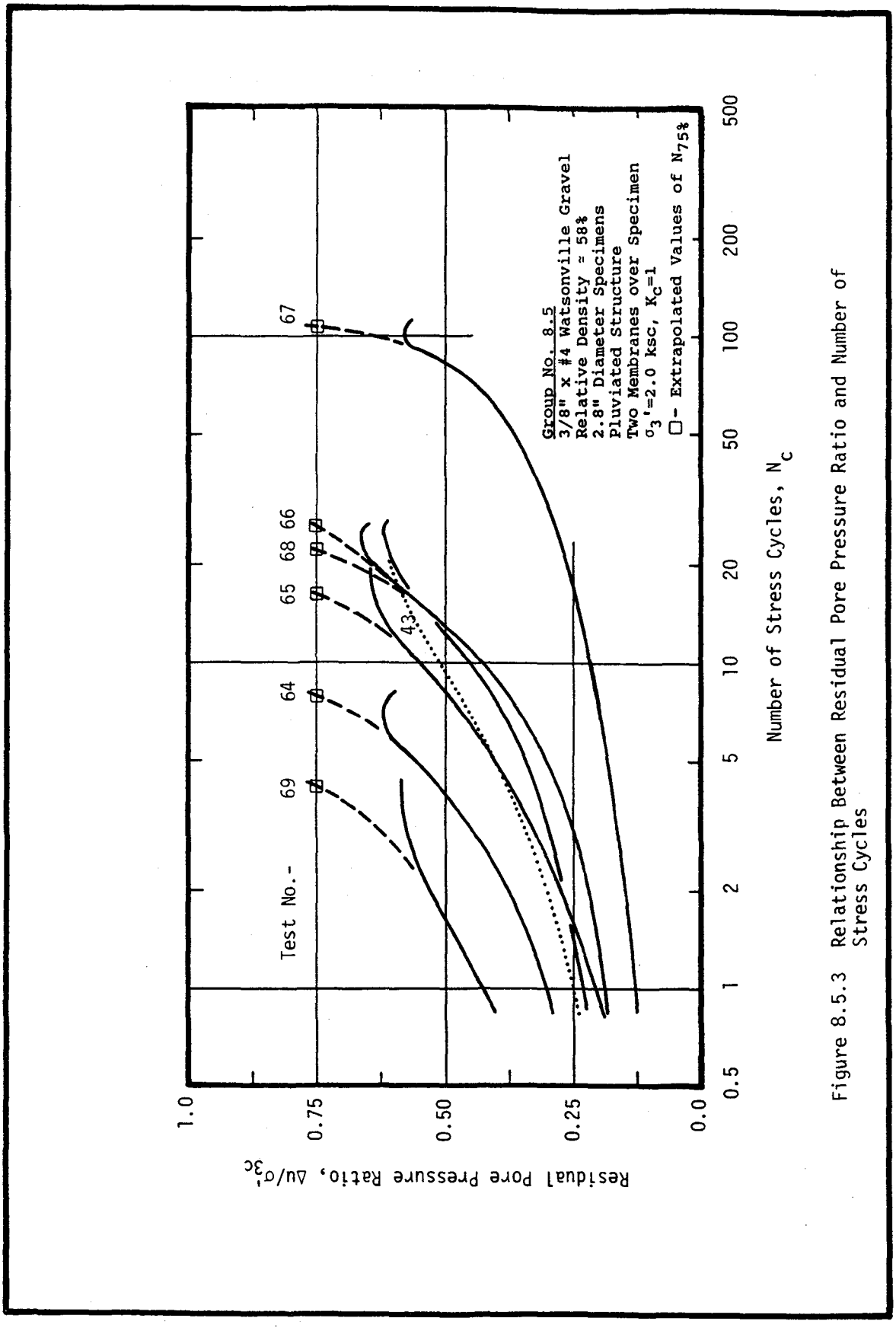

Figure 8.5.3 Relationship Between Residual Pore Pressure Ratio and Number of Stress Cycles

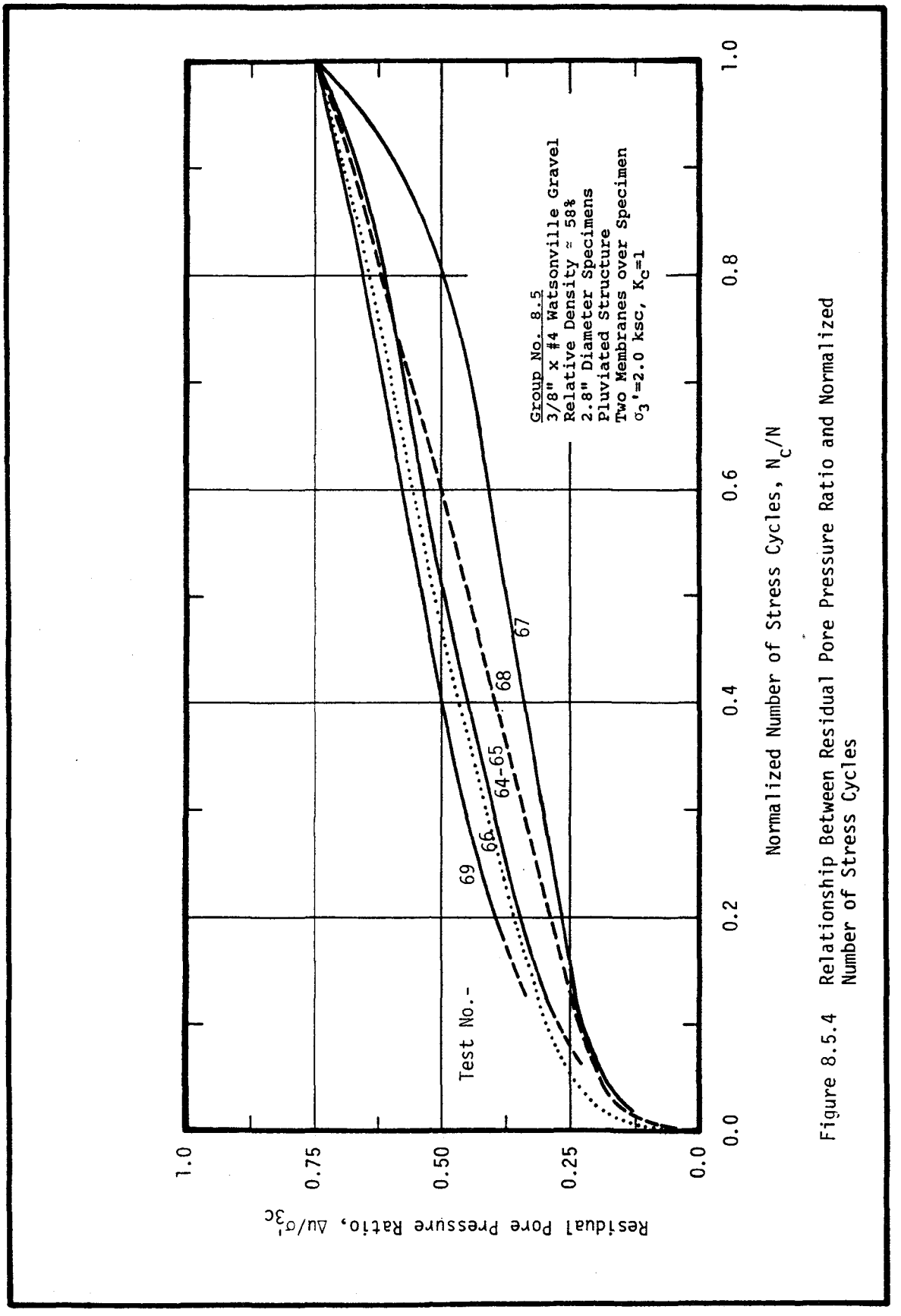

Figure 8.5.4 Relationship Between Residual Pore Pressure Ratio and Normalized Number of Stress Cycles

Table 8.6 Material Properties and Test Conditions Causing Failure During Undrained Cyclic Loading

GRAVEL: 3/8" x #4 Watsonville Gravel
SLUICING SAND: Monterey Fine
C_s=17

Test No.	Gravel				Sand	
	Dry Density (pcf)	Void Ratio	Porosity	Relative Density (%)	Dry Density (pcf)	Void Ratio
70	96.30	0.802	0.445	58.1	66.39	1.49
71	95.04	0.826	0.452	52.3	66.51	1.49
73	97.68	0.777	0.437	64.3	71.18	1.32
74	97.20	0.786	0.440	62.2	71.09	1.33
75	96.66	0.796	0.443	59.8	66.50	1.49

Test No.	Cyclic Stress Ratio, $\sigma_d/2\,\sigma_{3c}$	Number of Cycles Causing...				
		80% Pore	100% Pressure	2% Double	5% Ampl.	10% Strain
70	0.275	-	3.8	3.3	5.2	6.8
71	0.201	-	15.8	15.5	17.2	19.0
73	0.225	-	19.0	17.0	19.8	22.6
74	0.268	-	5.2	5.2	7.1	8.8
75	0.230	-	17.3	18.5	20	22.6

* - All test specimens are 2.8" diameter, pluviated structure, two membranes, σ_3'= 2.0 ksc, and K_c=1.

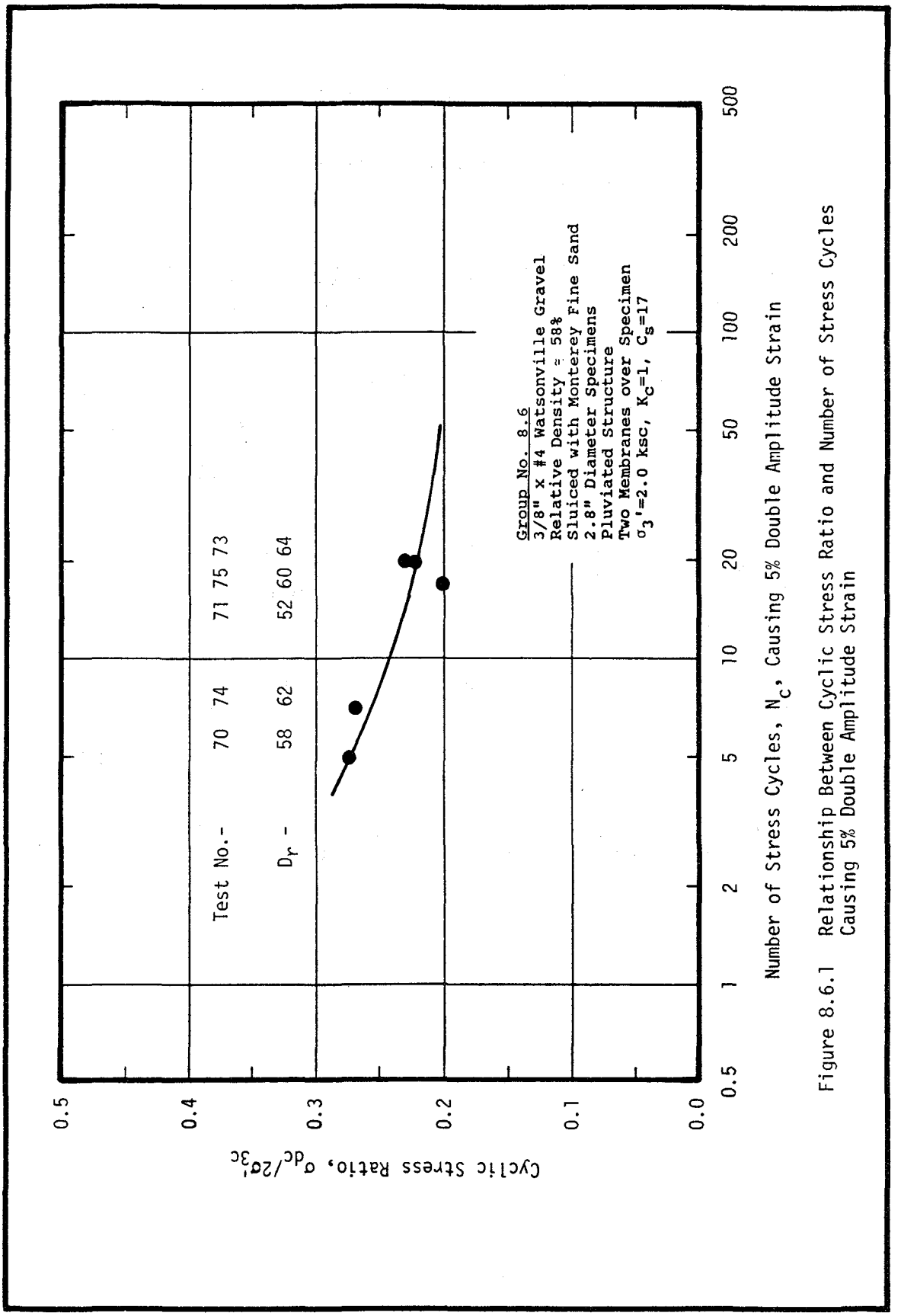

Figure 8.6.1 Relationship Between Cyclic Stress Ratio and Number of Stress Cycles Causing 5% Double Amplitude Strain

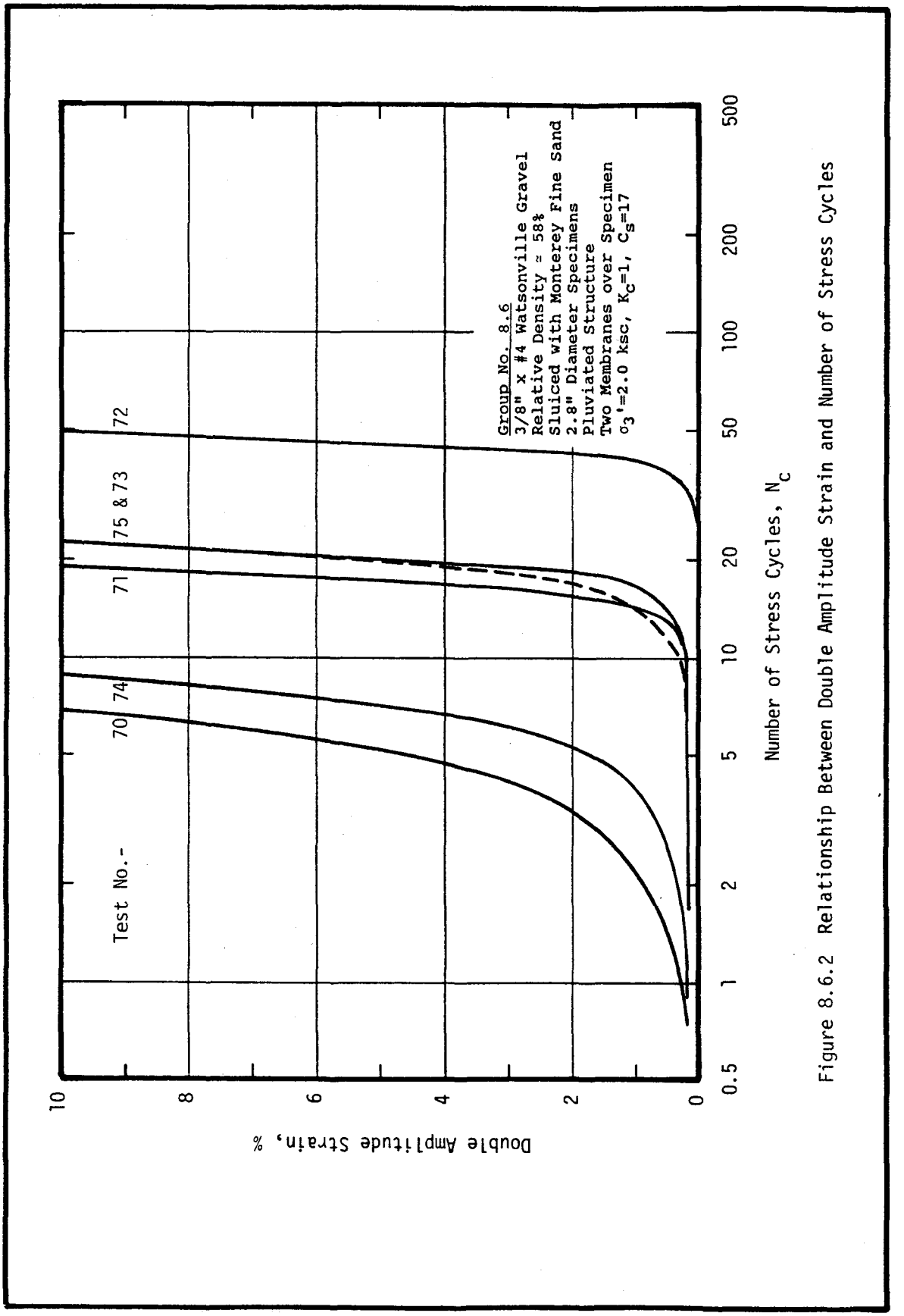

Figure 8.6.2 Relationship Between Double Amplitude Strain and Number of Stress Cycles

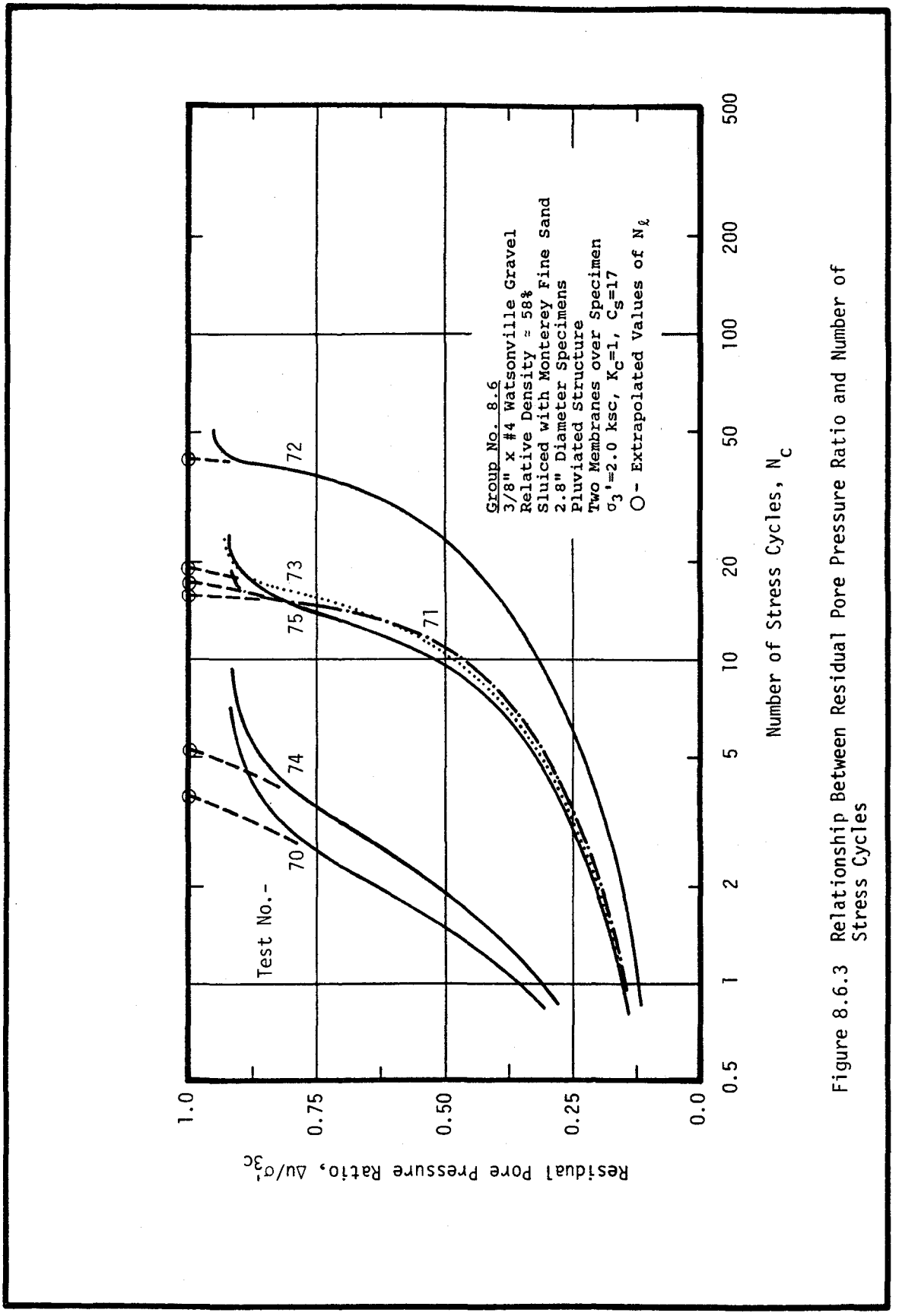

Figure 8.6.3 Relationship Between Residual Pore Pressure Ratio and Number of Stress Cycles

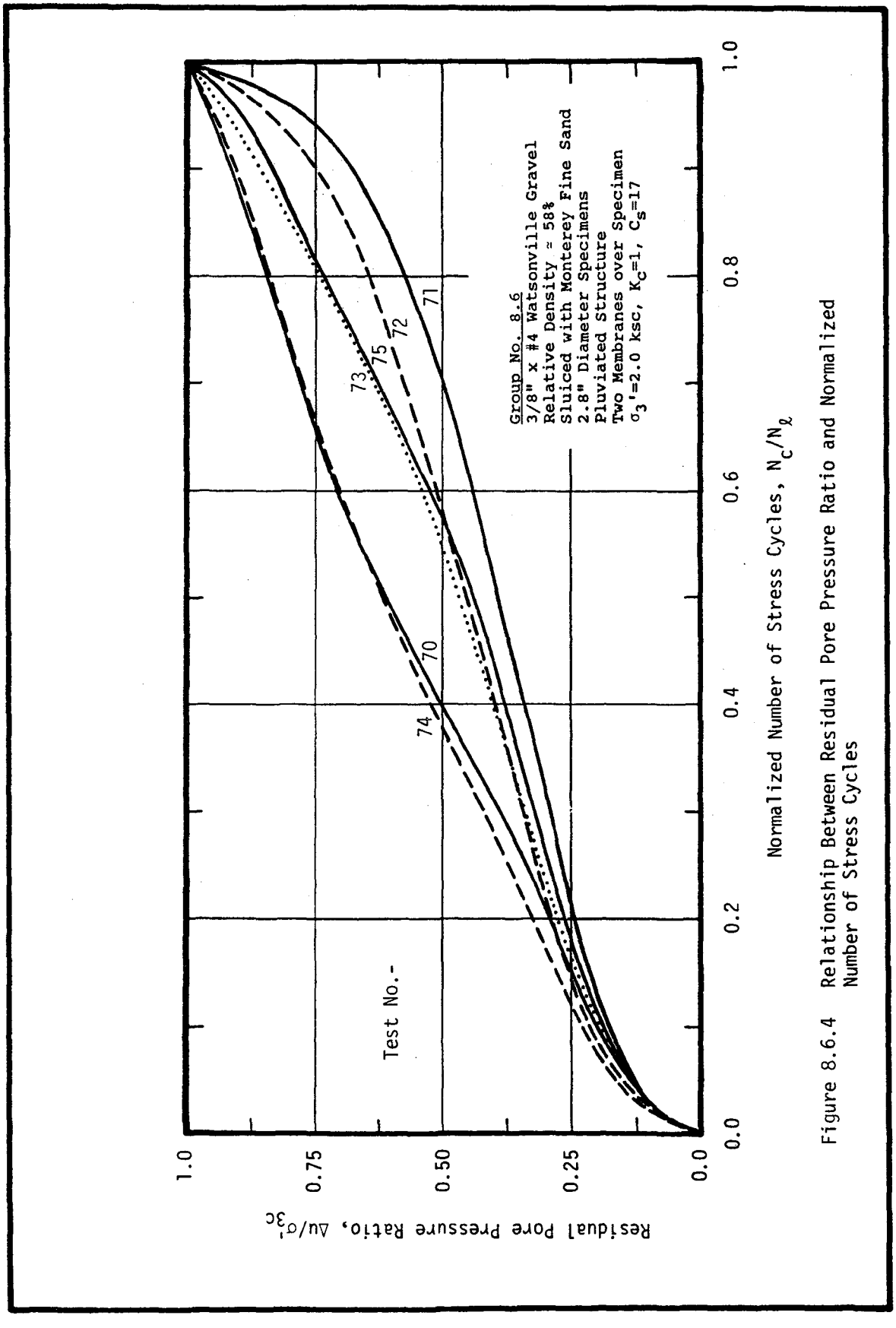

Figure 8.6.4 Relationship Between Residual Pore Pressure Ratio and Normalized Number of Stress Cycles

Table 8.7 Material Properties and Test Conditions Causing Failure During Undrained Cyclic Loading

GRAVEL: 3/8" x #4 Watsonville Gravel
SLUICING SAND: Monterey Fine
C_s=17

Test No.	Gravel				Sand	
	Dry Density (pcf)	Void Ratio	Porosity	Relative Density (%)	Dry Density (pcf)	Void Ratio
79	100.00	0.736	0.424	74.3	52.9	2.13
80	101.61	0.708	0.415	81.0	67.0	1.47
81	103.14	0.683	0.406	87.1	65.7	1.52
82	100.95	0.719	0.418	78.3	70.9	1.33

Test No.	Cyclic Stress Ratio, $\sigma_d/2\,\sigma_{3c}$	Number of Cycles Causing...				
		80% Pore	100% Pressure Ratio	2% Double	5% Ampl.	10% Strain
79	0.295	-	67	65	65	-
80	0.362	-	7.5	6.1	10.3	-
81	0.365	-	11.9	12	21.5	-
82	0.340	-	5.6	4.3	7.3	13.0

* - All test specimens are 2.8" diameter, tamped in six layers, two membranes, σ_3'= 2.0 ksc, and K_c=1.

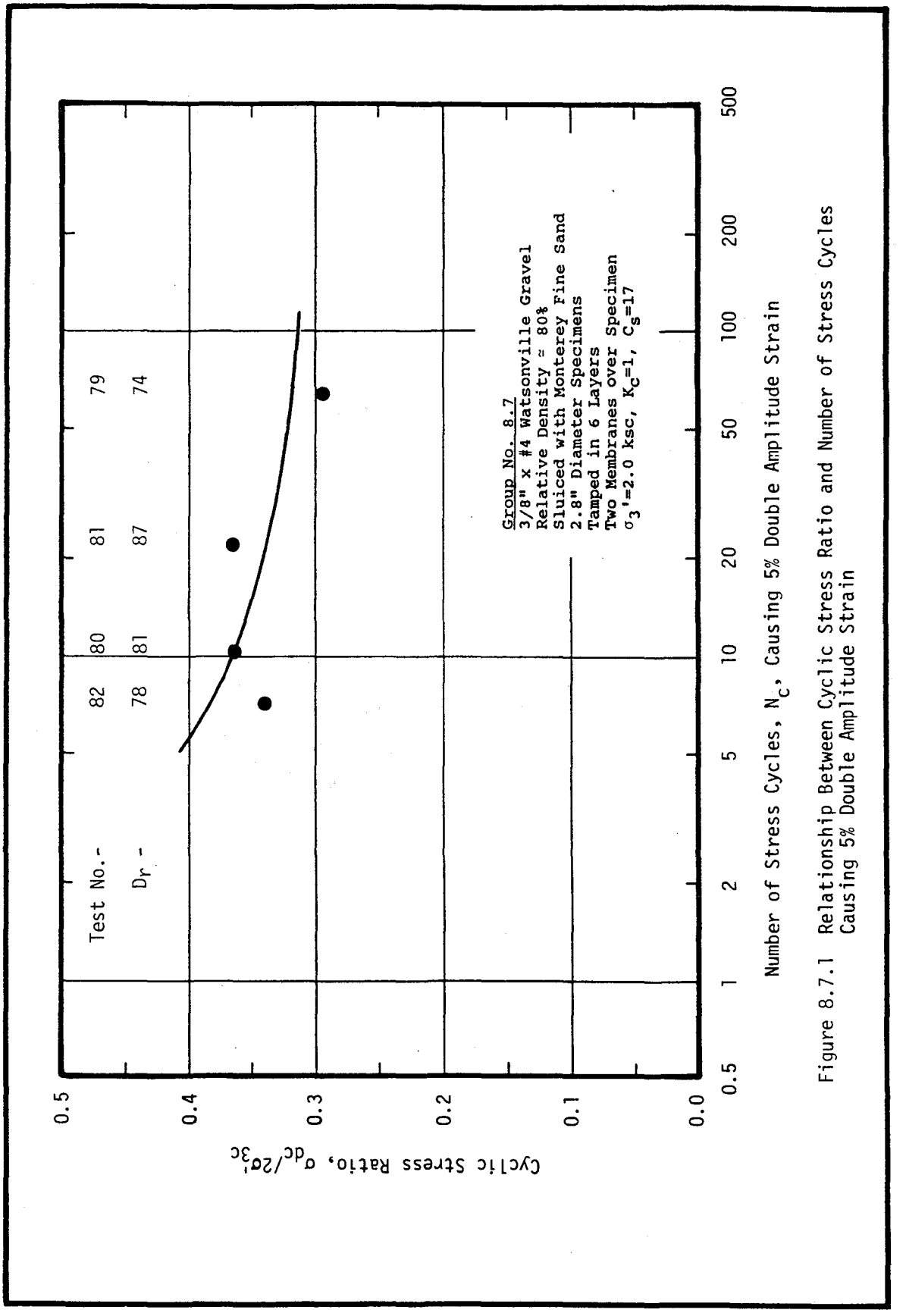

Figure 8.7.1 Relationship Between Cyclic Stress Ratio and Number of Stress Cycles Causing 5% Double Amplitude Strain

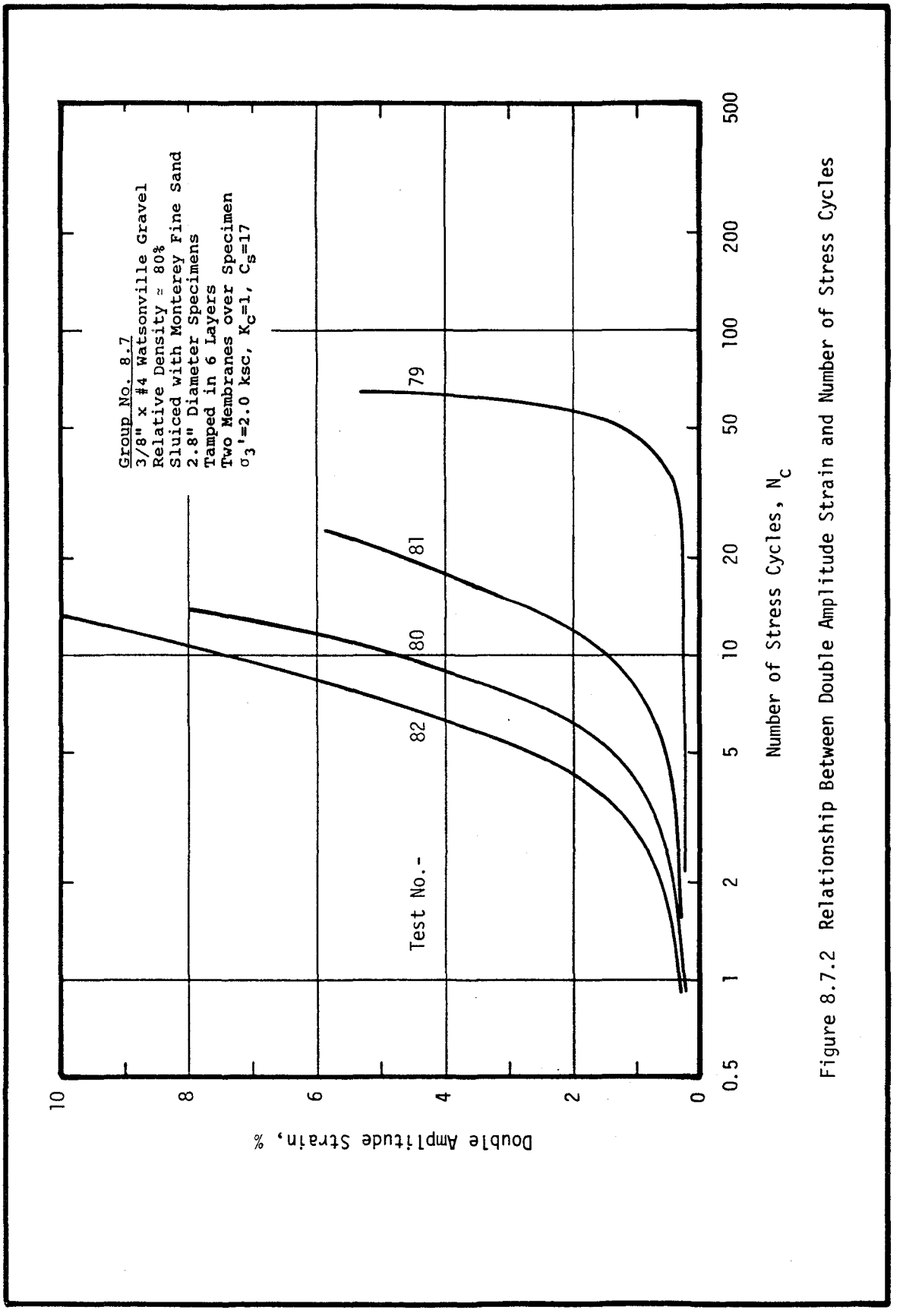

Figure 8.7.2 Relationship Between Double Amplitude Strain and Number of Stress Cycles

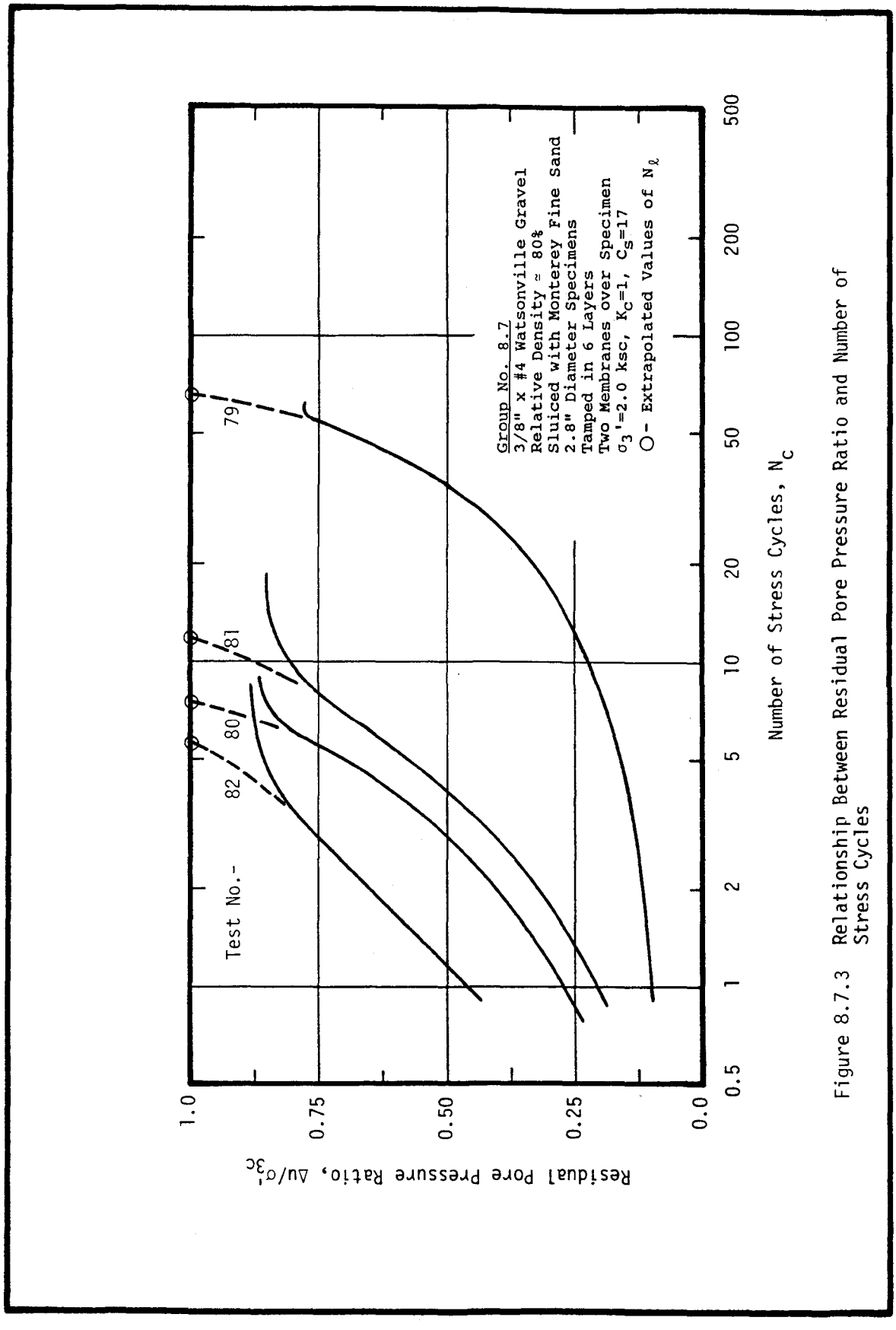

Figure 8.7.3 Relationship Between Residual Pore Pressure Ratio and Number of Stress Cycles

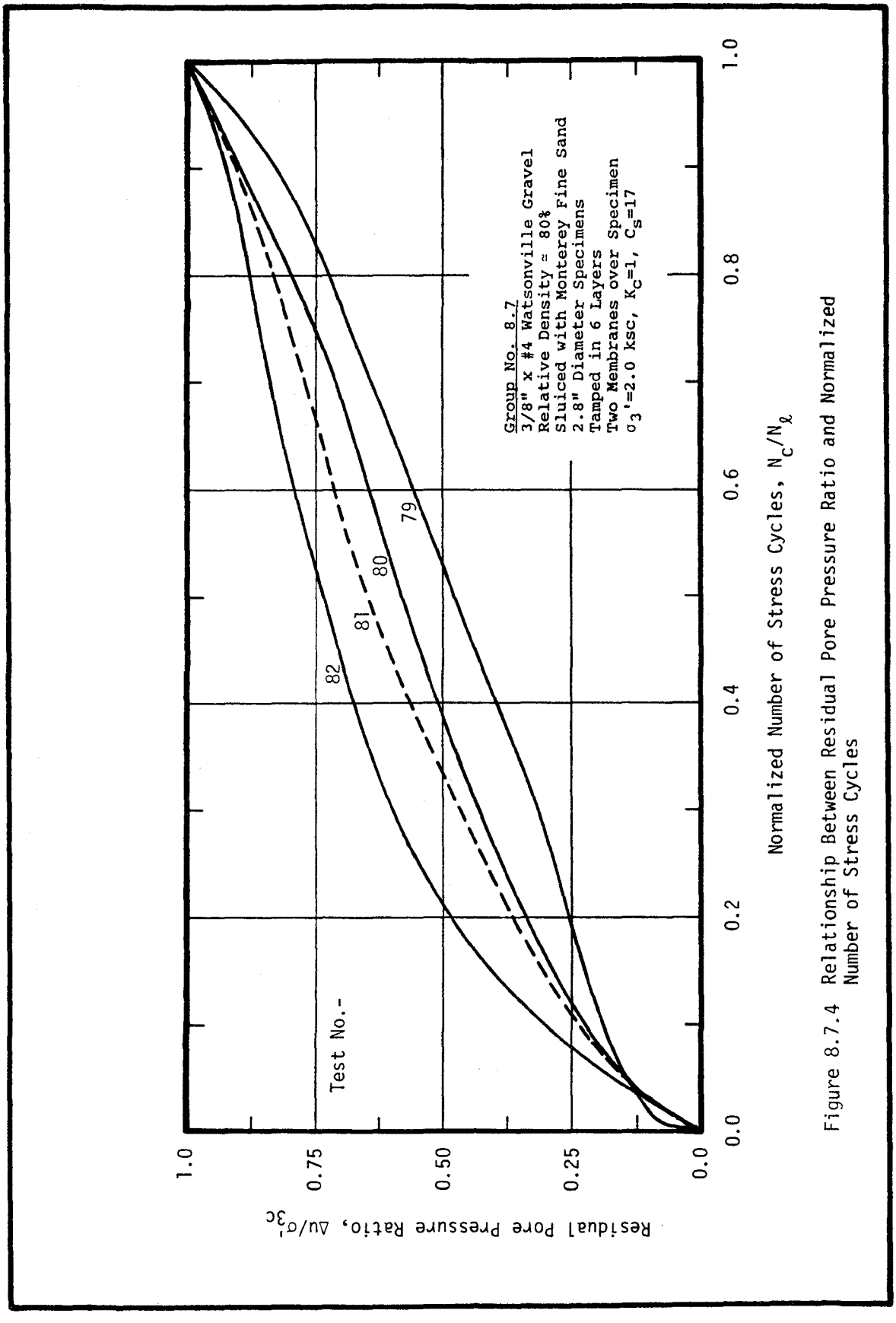

Figure 8.7.4 Relationship Between Residual Pore Pressure Ratio and Normalized Number of Stress Cycles

Table 8.8 Material Properties and Test Conditions Causing Failure During Undrained Cyclic Loading

GRAVEL: 3/8" x #4 Watsonville Gravel
SLUICING SAND: none
C_s = -

Test No.	Gravel				Sand	
	Dry Density (pcf)	Void Ratio	Porosity	Relative Density (%)	Dry Density (pcf)	Void Ratio
87	93.69	0.852	0.460	45.9	-	-
91	94.27	0.841	0.457	48.7	-	-
92	93.38	0.859	0.462	44.5	-	-
93	92.62	0.874	0.466	40.8	-	-
94	95.13	0.824	0.452	52.7	-	-

Test No.	Cyclic Stress Ratio, $\Delta\tau_{ff}/\sigma_{fc}$	Number of Cycles Causing...				
		80% Pore Pressure	100% Pore Pressure	2% Double Ampl. Ratio	5% Ampl. Strain	10% Strain
87	0.358	-	640	520	540	-
91	0.435	2.9	5.0	0.9	2.3	5.0
92	0.398	6.0	10.0	2.75	5.3	10.0
93	0.364	-	78	47	55	-
94	0.385	-	700	570	610	-

Test No.	Number of Cycles Causing... Peak Compressive Strain		
	2%	5%	10%
87	70	480	540
91	-	3.9	8.6
92	-	3.6	8.6
93	0.8	30	54
94	18.0	550	590

* - All test specimens are 2.8" diameter, pluviated structure, two membranes, σ_3' = 2.0 ksc, and K_c=2.

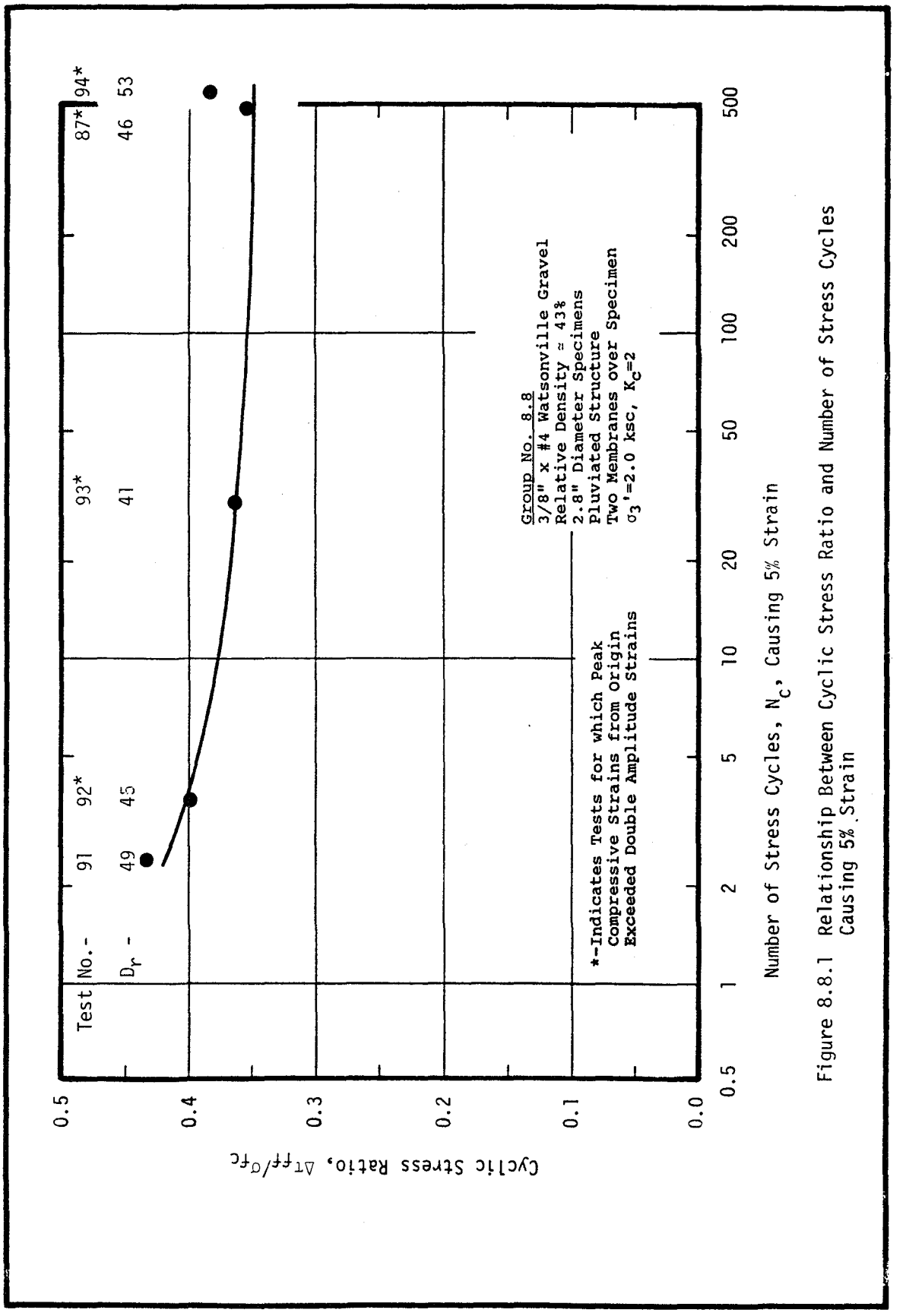

Figure 8.8.1 Relationship Between Cyclic Stress Ratio and Number of Stress Cycles Causing 5% Strain

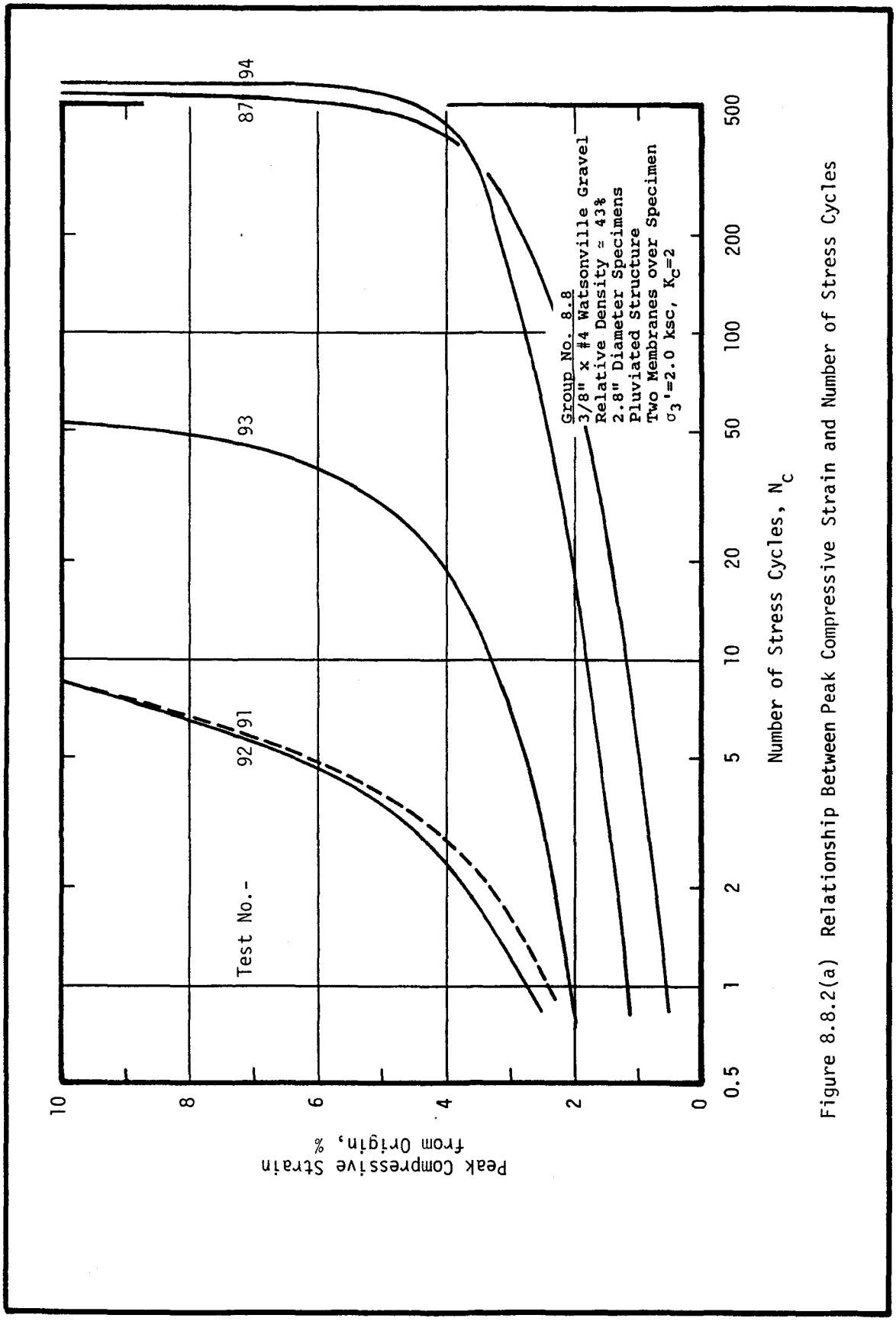

Figure 8.8.2(a) Relationship Between Peak Compressive Strain and Number of Stress Cycles

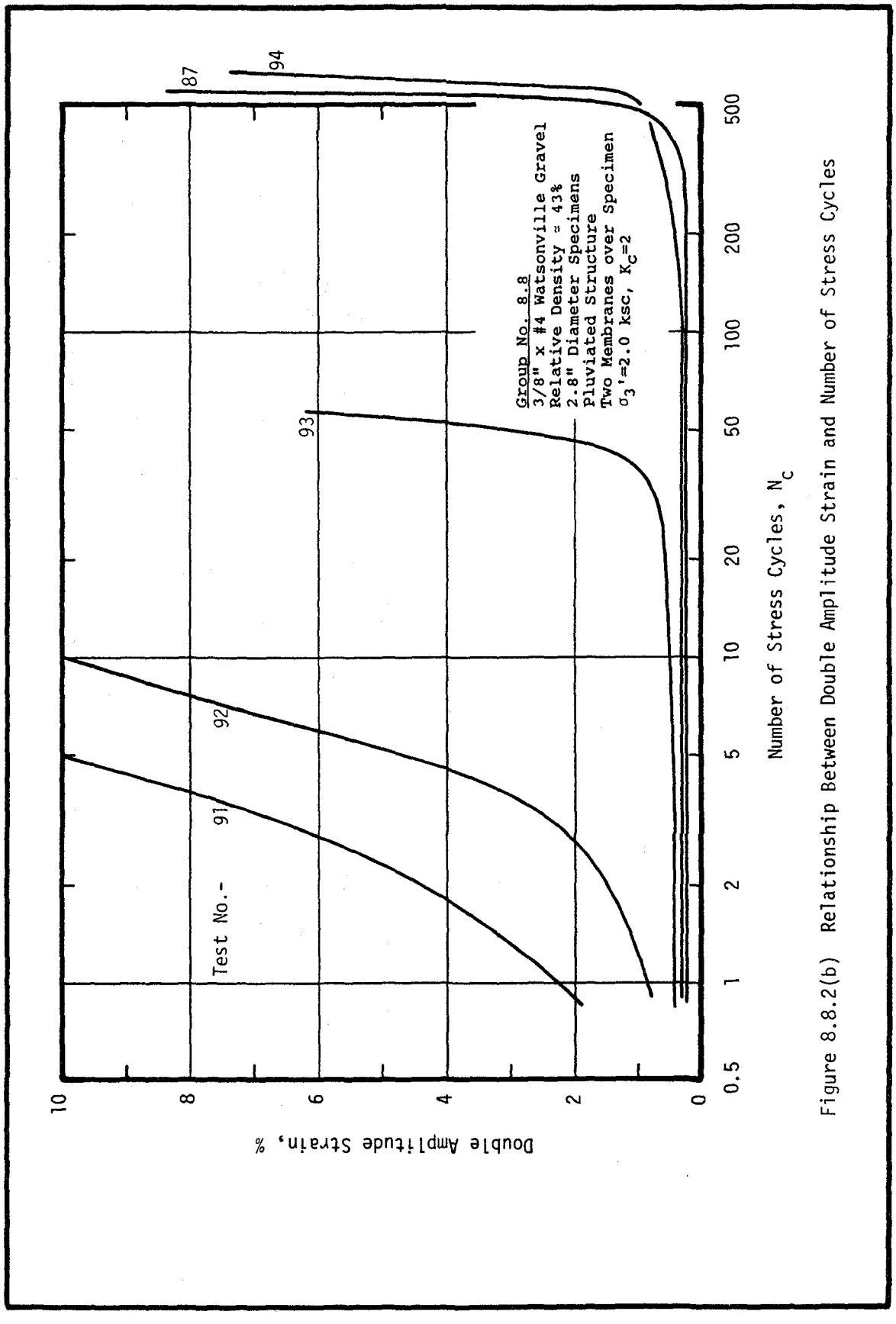

Figure 8.8.2(b) Relationship Between Double Amplitude Strain and Number of Stress Cycles

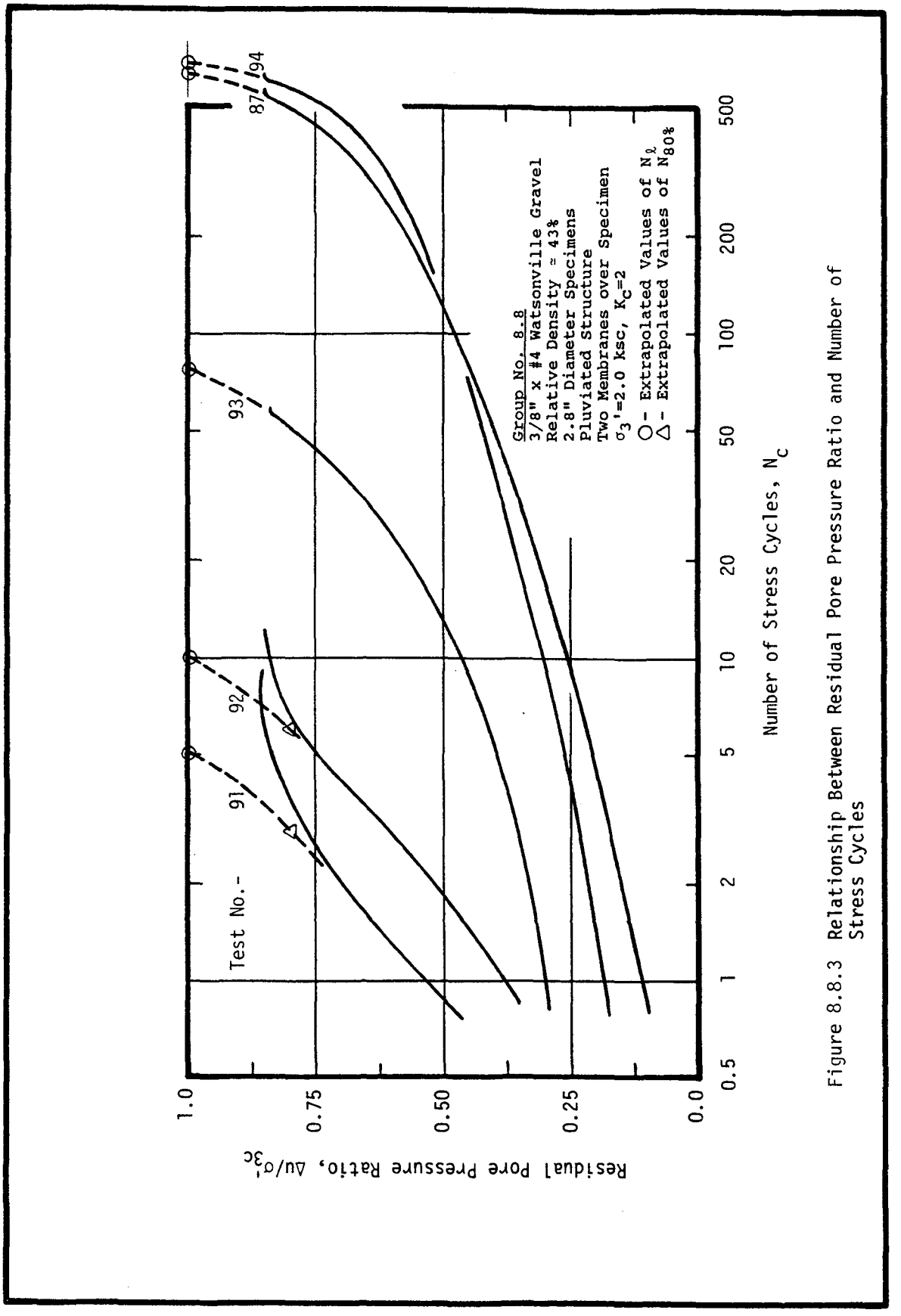

Figure 8.8.3 Relationship Between Residual Pore Pressure Ratio and Number of Stress Cycles

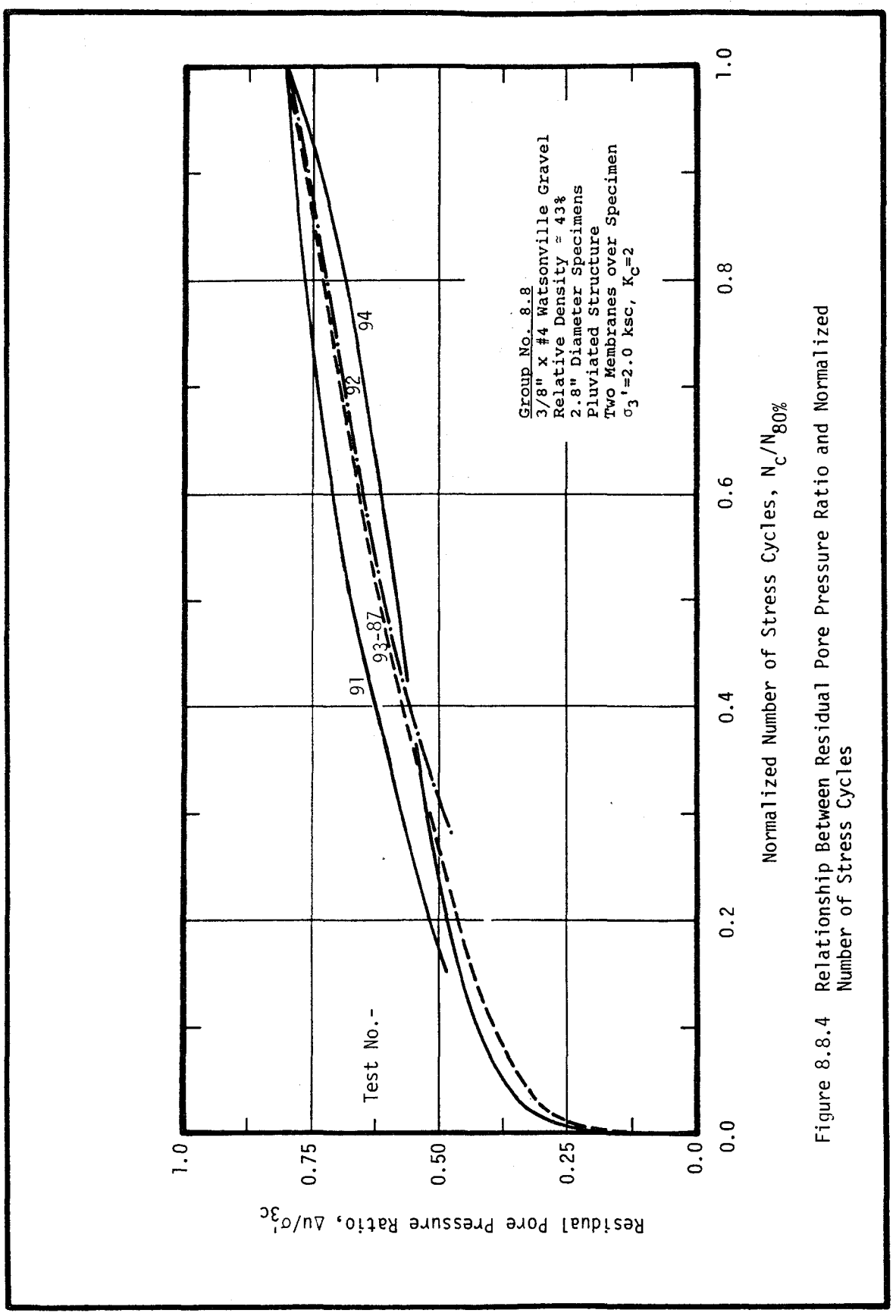

Figure 8.8.4 Relationship Between Residual Pore Pressure Ratio and Normalized Number of Stress Cycles

Table 8.9 Material Properties and Test Conditions Causing Failure During Undrained Cyclic Loading

GRAVEL: 3/8" x #4 Watsonville Gravel
SLUICING SAND: Monterey Fine
C_s=17

Test No.	Gravel				Sand	
	Dry Density (pcf)	Void Ratio	Porosity	Relative Density (%)	Dry Density (pcf)	Void Ratio
95	92.67	0.873	0.466	41.0	71.5	1.31
96	93.62	0.854	0.461	45.6	71.4	1.31
97	92.66	0.873	0.466	40.9	71.7	1.30
98	93.68	0.853	0.460	45.9	75.5	1.18

Test No.	Cyclic Stress Ratio, $\Delta\tau_{ff}/\sigma_{fc}$	Number of Cycles Causing...				
		80% Pore Pressure Ratio	100%	2% Double Ampl.	5%	10% Strain
95	0.245	150	-	-	-	-
96	0.315	6.5	-	31	50	-
97	0.349	4.0	-	7.2	9.9	13.0
98	0.378	0.6	-	1.25	2.2	3.4

Test No.	Number of Cycles Causing...		
	2%	5%	10%
	Peak Compressive Strain		
95	25	175	-
96	6.4	20	33
97	3.2	8.2	11.3
98	1.3	3.2	4.5

* - All test specimens are 2.8" diameter, pluviated structure, two membranes, σ_3'= 2.0 ksc, and K_c=2.

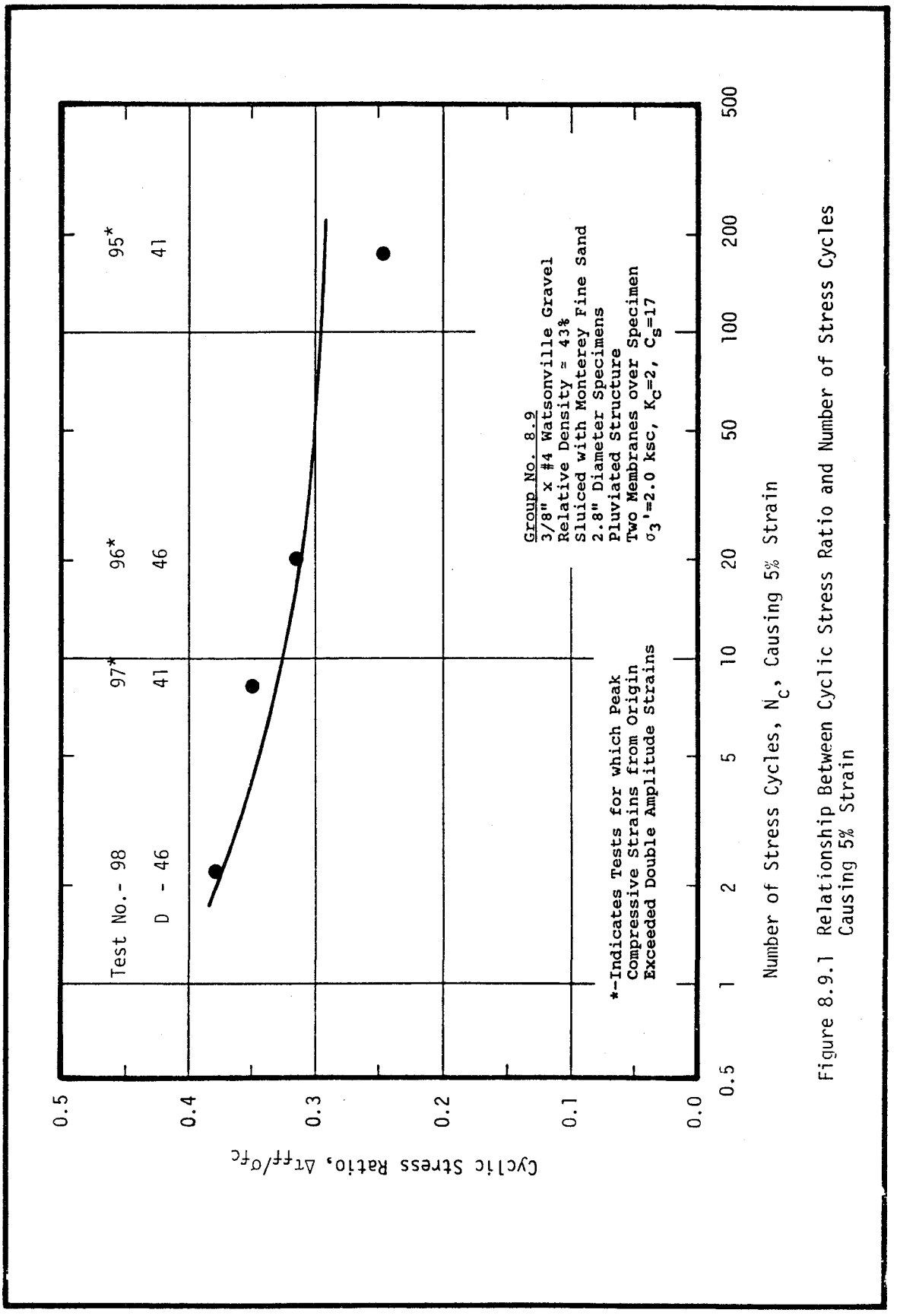

Figure 8.9.1 Relationship Between Cyclic Stress Ratio and Number of Stress Cycles Causing 5% Strain

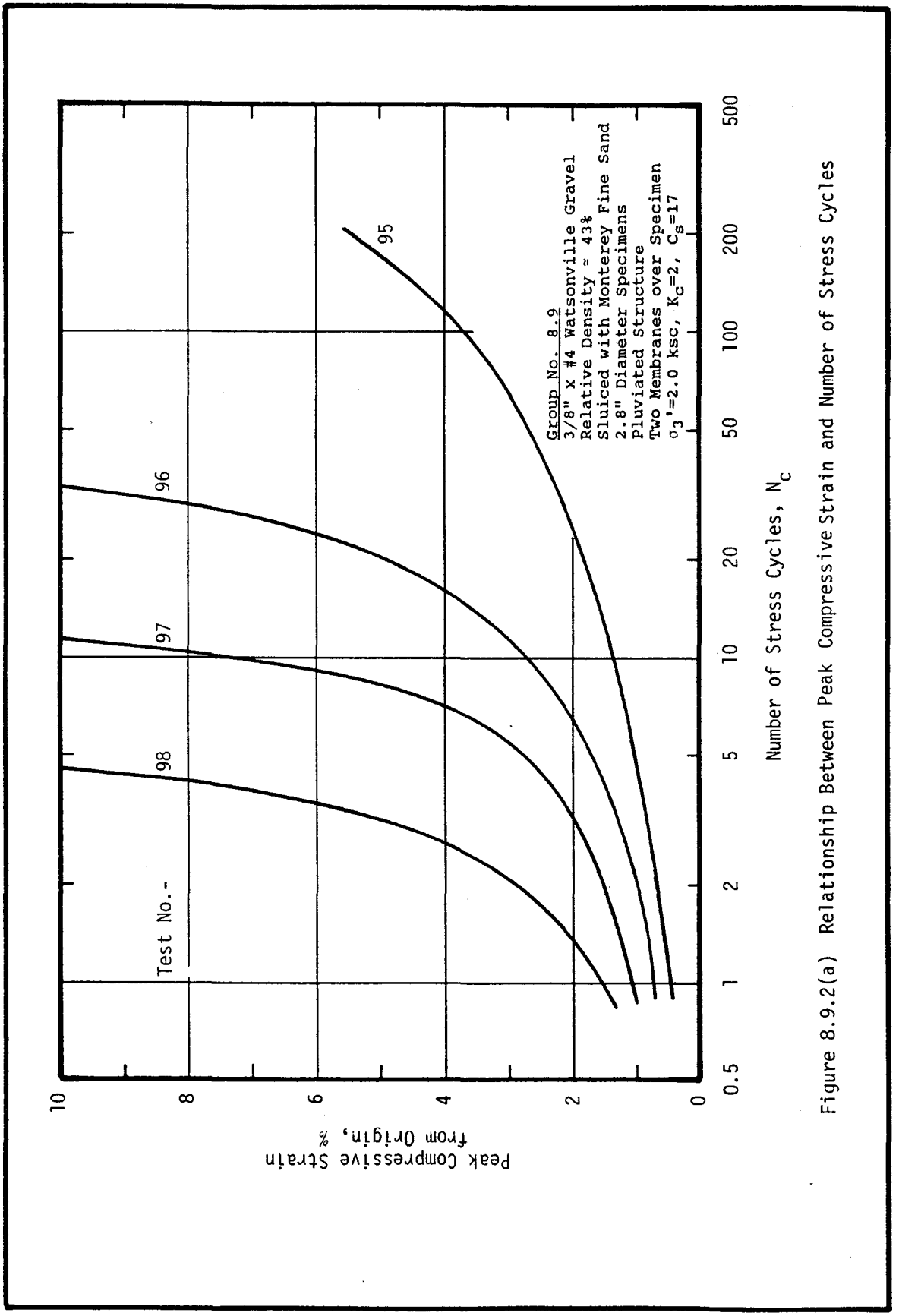

Figure 8.9.2(a) Relationship Between Peak Compressive Strain and Number of Stress Cycles

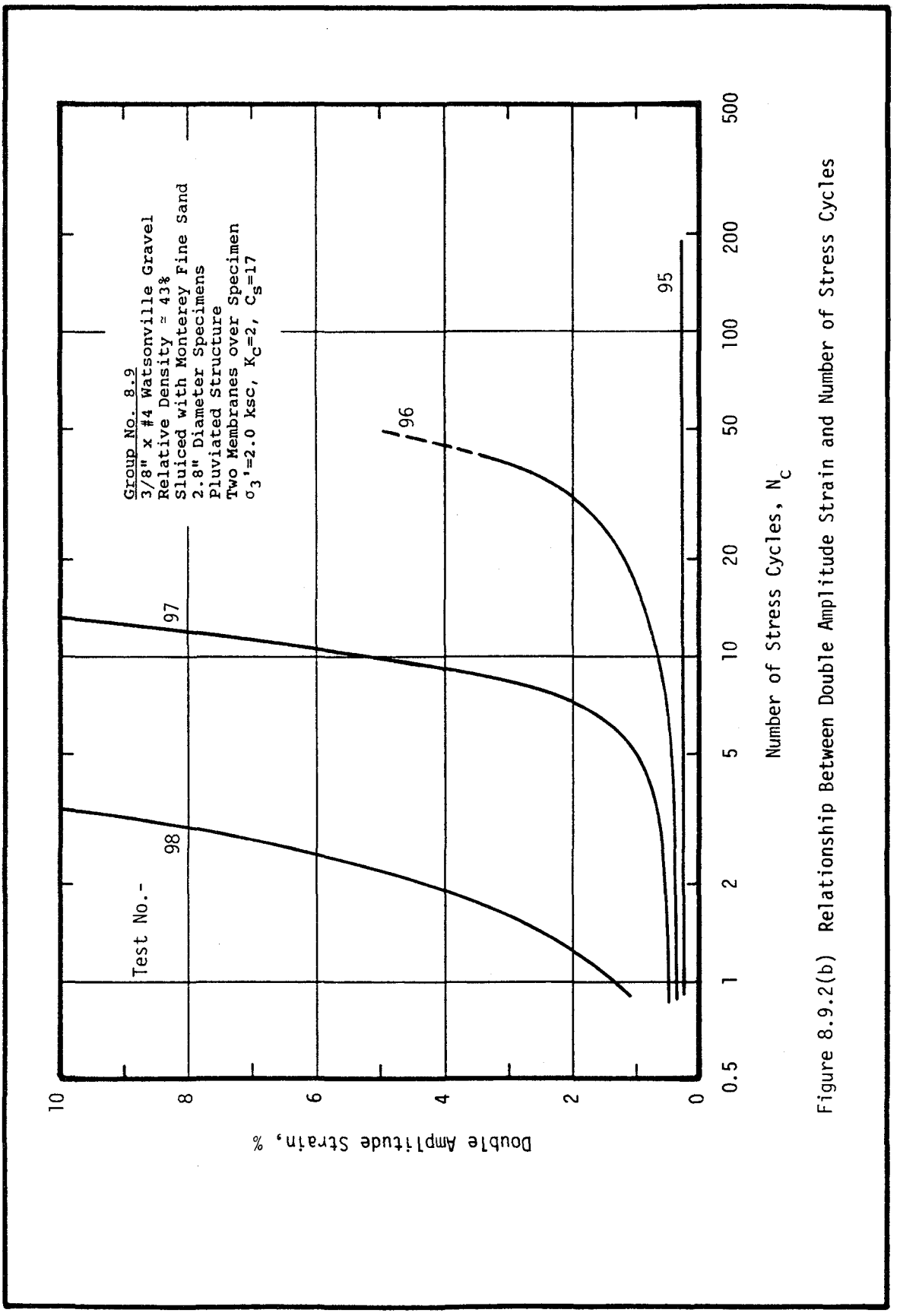

Figure 8.9.2(b) Relationship Between Double Amplitude Strain and Number of Stress Cycles

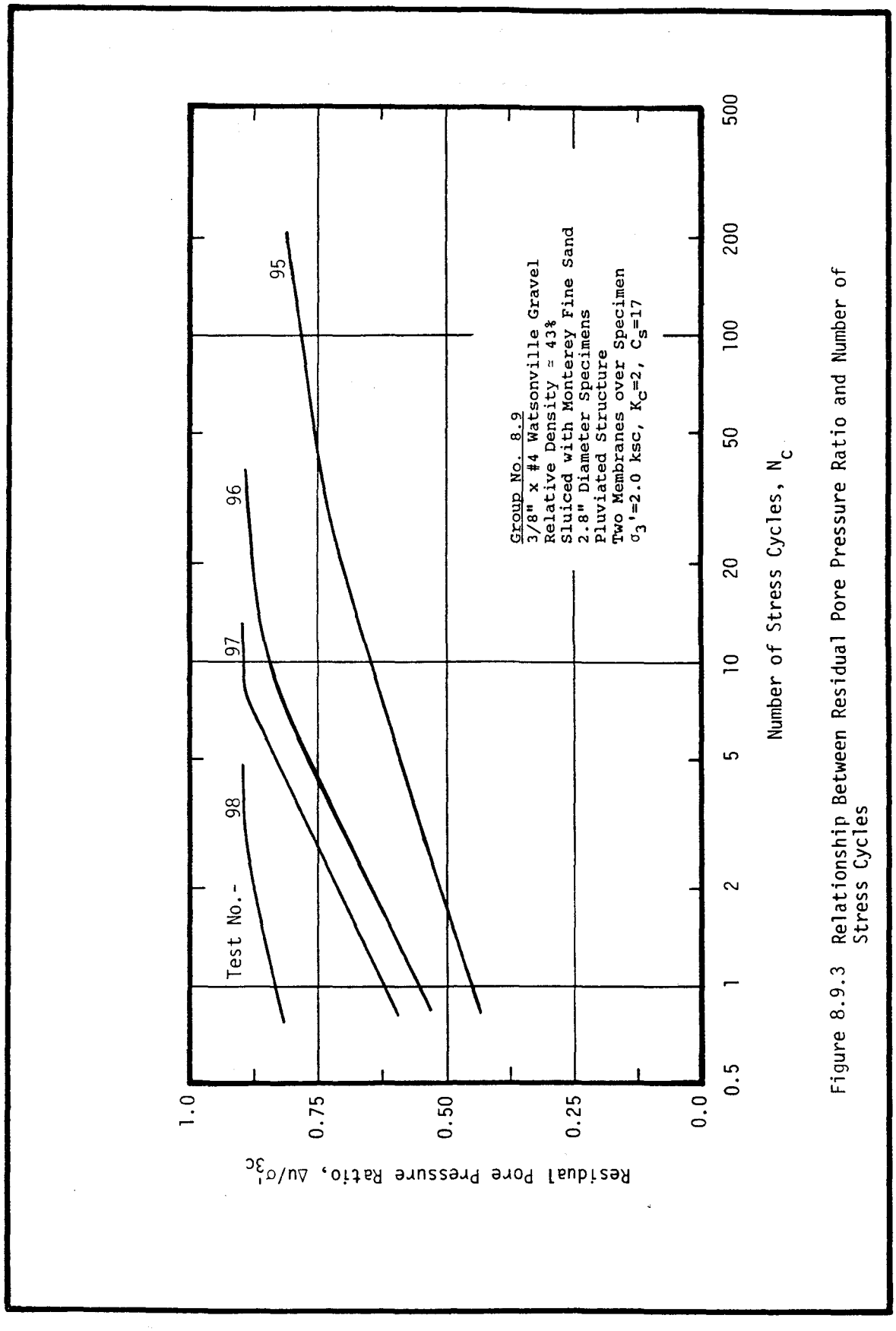

Figure 8.9.3 Relationship Between Residual Pore Pressure Ratio and Number of Stress Cycles

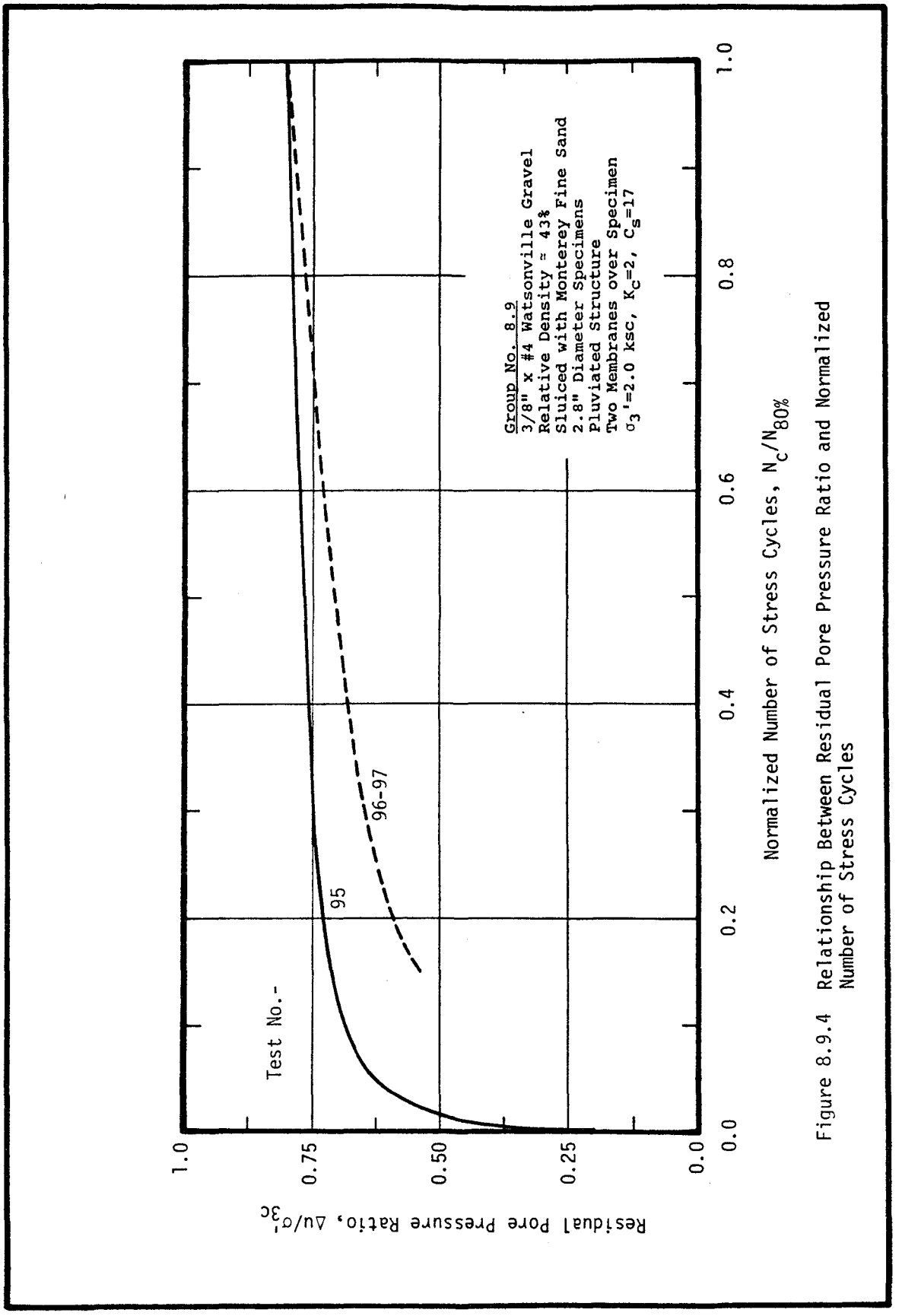

Figure 8.9.4 Relationship Between Residual Pore Pressure Ratio and Normalized Number of Stress Cycles

Table 8.10 Material Properties and Test Conditions Causing Failure During Undrained Cyclic Loading

GRAVEL: 3/8" x #4 Watsonville Gravel
SLUICING SAND: Monterey Fine
C_s=17

Test No.	Gravel				Sand	
	Dry Density (pcf)	Void Ratio	Porosity	Relative Density (%)	Dry Density (pcf)	Void Ratio
99	93.25	0.861	0.463	43.8	75.8	1.173
100	93.46	0.857	0.461	44.8	72.6	1.270
101	94.05	0.845	0.458	47.7	77.3	1.130

Test No.	Cyclic Stress Ratio, $\Delta\tau_{ff}/\sigma_{fc}$	Number of Cycles Causing...				
		80% Pore	100% Pressure	2% Double	5% Ampl.	10% Strain
99	0.215(1)	-	15.2	14.6	16.2	17.0
100	0.277(2)	-	5.7	6.2	7.5	8.0
101	0.302(3)	-	9.5	9.9	13.6	16.0

* - All test specimens are 2.8" diameter, pluviated structure, two membranes, and σ_3'= 2.0 ksc.

(1) K_c=1.25, (2) K_c=1.50, (3) K_c=1.75.

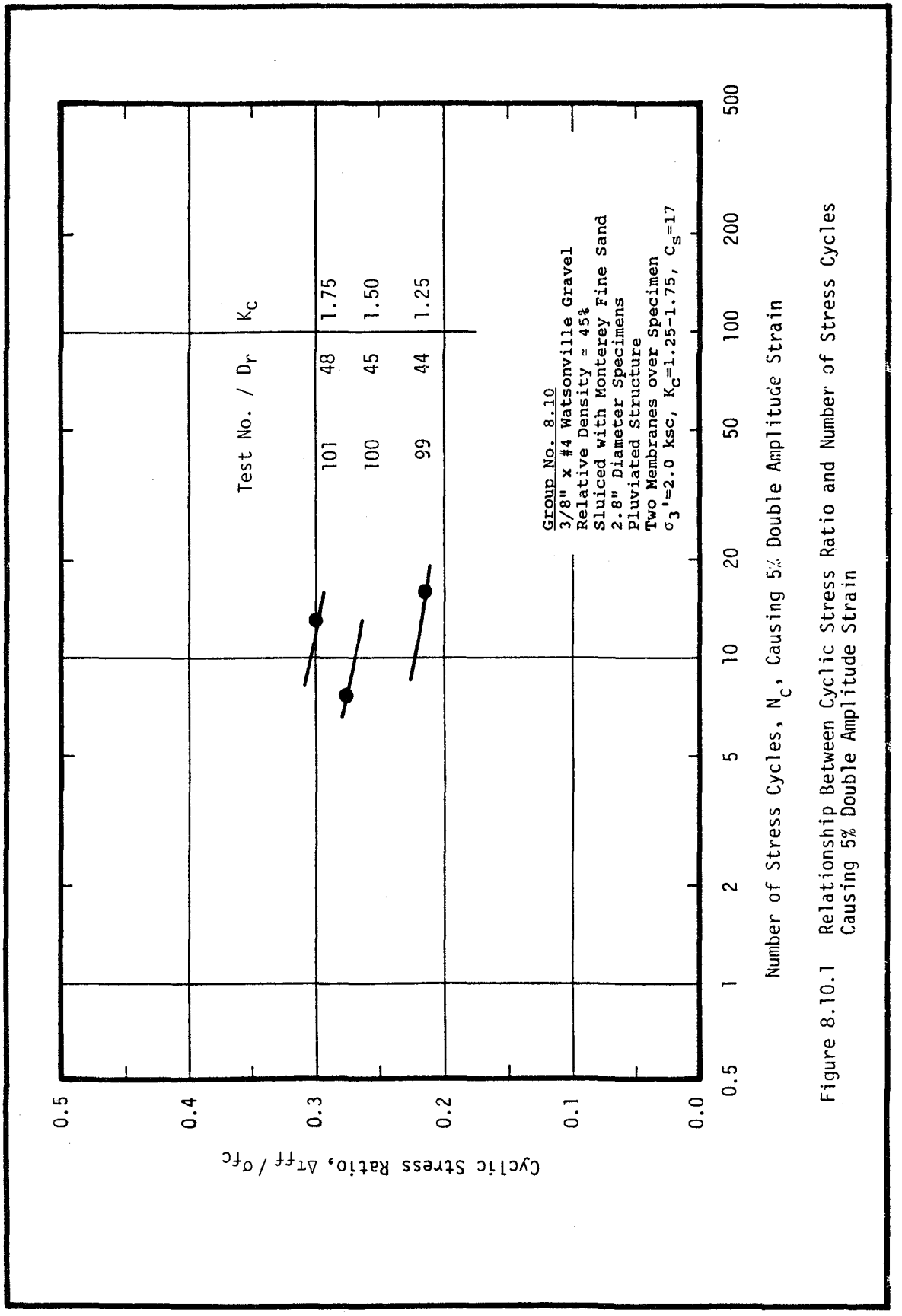

Figure 8.10.1 Relationship Between Cyclic Stress Ratio and Number of Stress Cycles Causing 5% Double Amplitude Strain

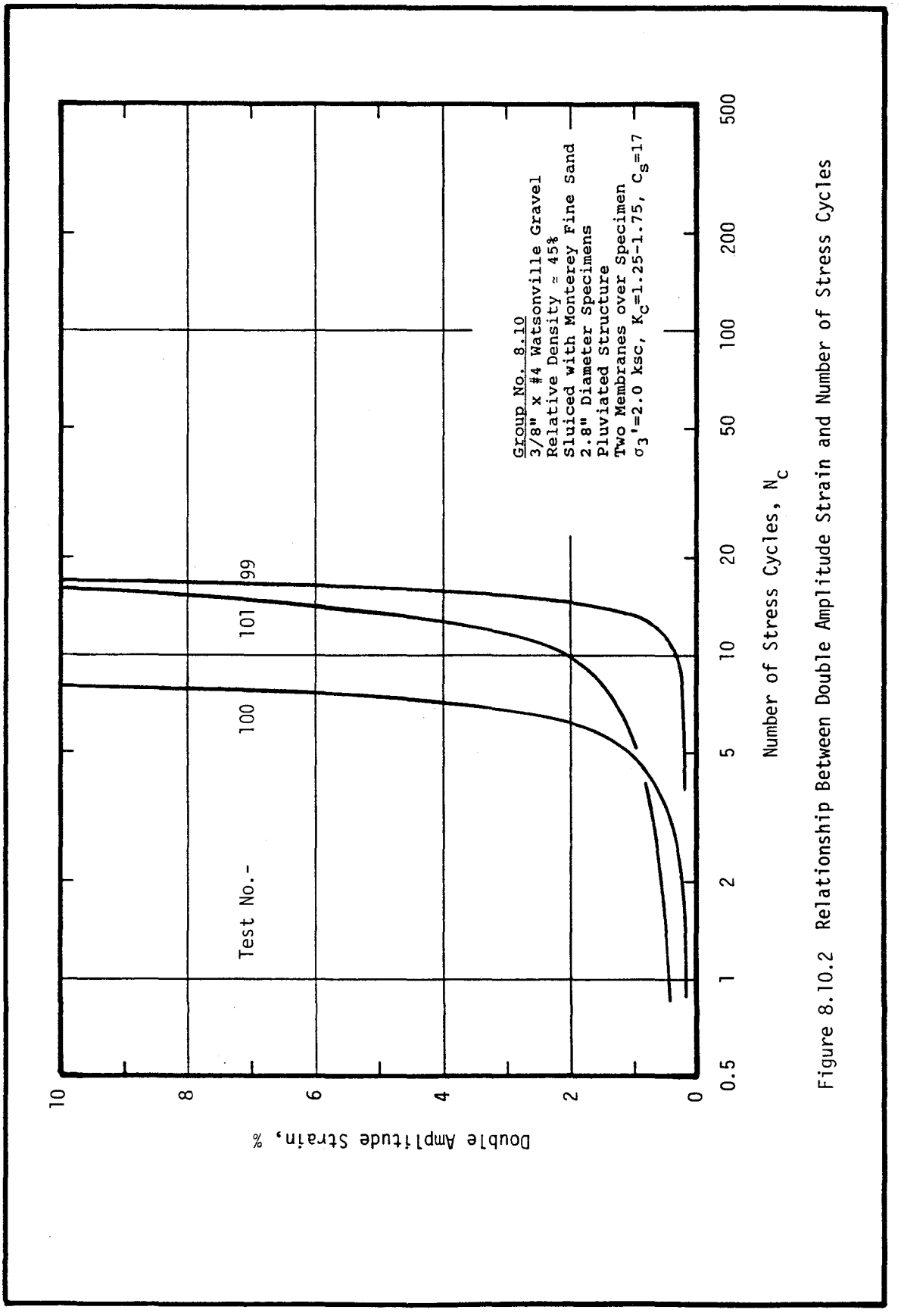

Figure 8.10.2 Relationship Between Double Amplitude Strain and Number of Stress Cycles

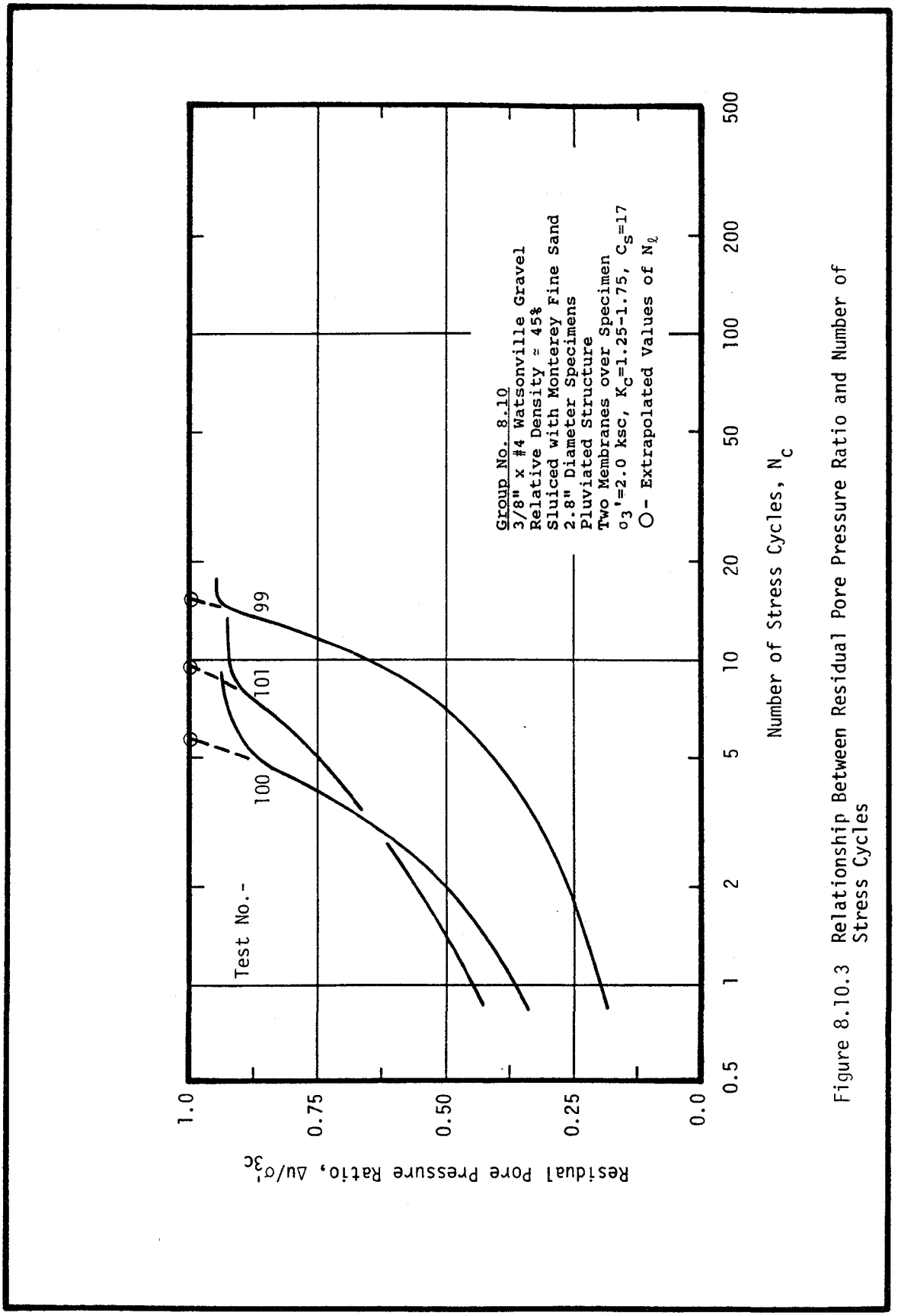

Figure 8.10.3 Relationship Between Residual Pore Pressure Ratio and Number of Stress Cycles

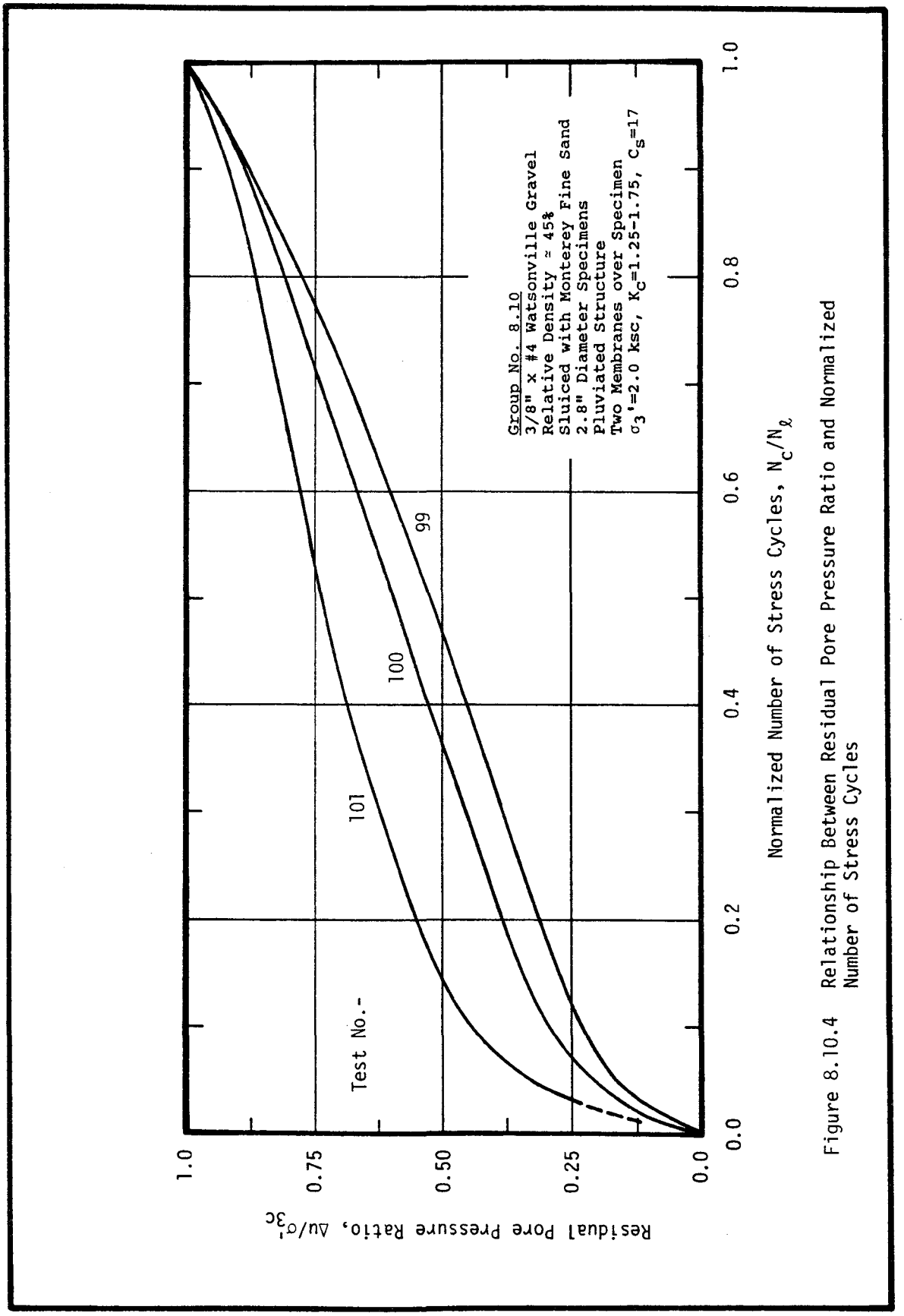

Figure 8.10.4 Relationship Between Residual Pore Pressure Ratio and Normalized Number of Stress Cycles

loading resistance curves of specimens of unsluiced gravel, sluiced gravel with C_s=17, and sluiced gravel with C_s=28, from top to bottom respectively. Each curve shown represents test data for a relative density of the gravel of about 43%. It may be noted from this figure that the cyclic stress ratio resulting in 5% double amplitude strain for specimens sluiced with sand for which C_s=17, is only about 74% of that causing corresponding strains in the unsluiced specimens. The value of cyclic stress ratio causing 5% double amplitude strain was further reduced to 61% of the unsluiced cyclic loading resistance for tests on sluiced specimens with a higher value of C_s=28. This figure serves to illustrate that: (1) The effects of membrane compliance can lead to an unconservative determination of the cyclic loading resistance of a gravel specimen as shown previously; and (2) It is important to achieve a suitable value of the sluiceability ratio in order to significantly reduce the effects of membrane compliance in sluiced gravel specimens. Membrane compliance effects were reduced considerably when a low value of the sluiceability ratio, C_s=17, was used. However, increasing the value of the sluiceability ratio to C_s=28, reduced the effects of membrane compliance on cyclic loading resistance by an additional 16%. It was not possible to further increase the value of C_s in these test specimens for the reasons noted in Chapter 6. However, it was concluded from the test data that the cyclic loading resistances of the sluiced materials would not be further reduced to any significant extent even if a higher value of C_s could have been used in the tests.

Evidence in support of this conclusion is shown in Figure 8.4. In this figure, curves of cyclic loading resistance determined for both

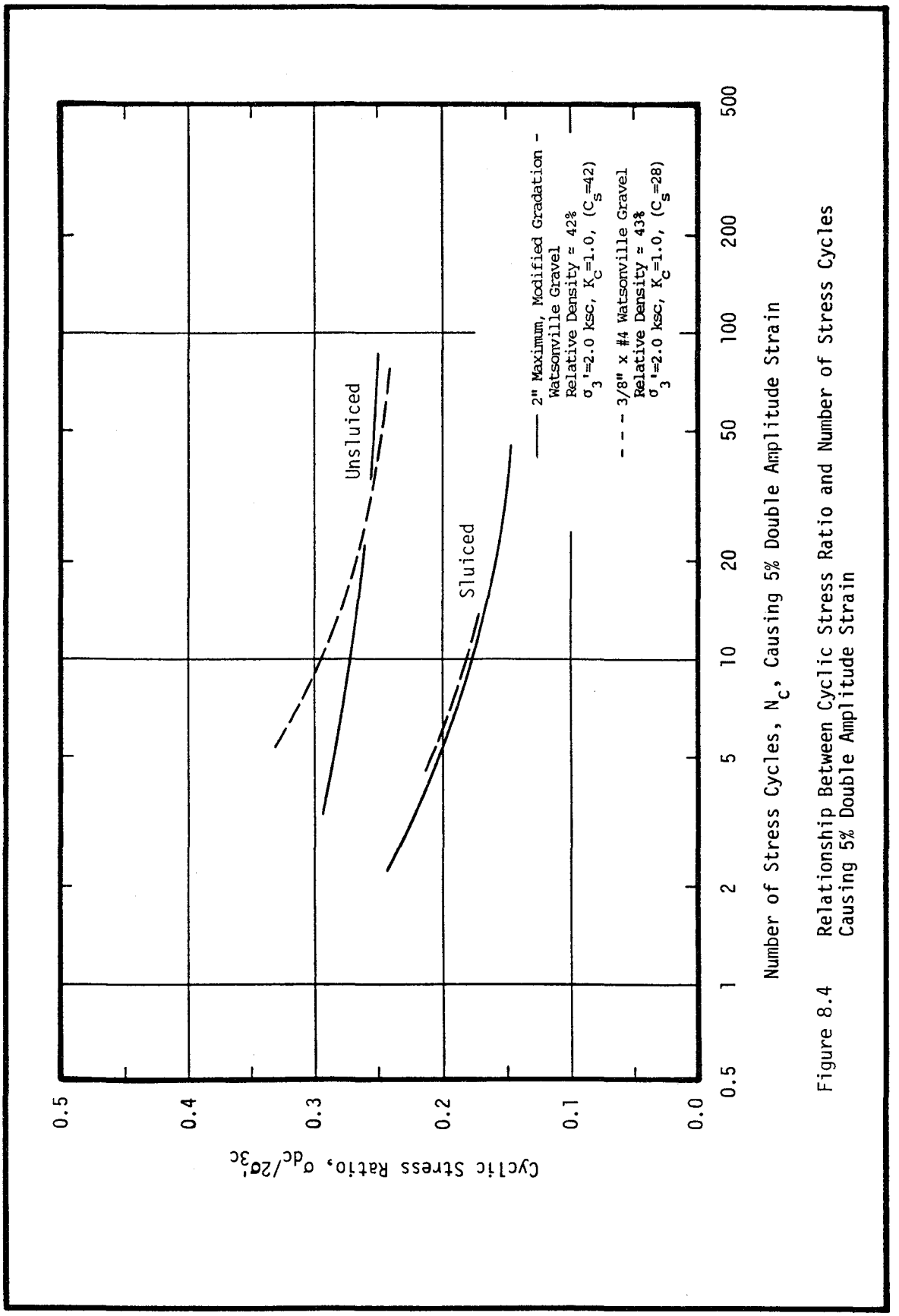

Figure 8.4 Relationship Between Cyclic Stress Ratio and Number of Stress Cycles Causing 5% Double Amplitude Strain

sluiced (C_s=28) and unsluiced specimens of 3/8" x #4 gravel at 43% relative density are shown together with the corresponding curves for sluiced (C_s=42) and unsluiced specimens of 2" maximum, modified gradation gravel at 42% relative density. It may be noted that the cyclic loading resistance of the 3/8" x #4 unsluiced gravel is somewhat higher than that of the 2" maximum unsluiced gravel in the range of 10 stress cycles because of the increased effects of membrane compliance in the smaller, 2.8 inch diameter test specimens. However, the values of cyclic loading resistance for the sluiced materials were nearly identical for both test materials. This may be the result of the fact that the effects of membrane compliance have been nearly eliminated by sluicing for both materials.

Tests performed on specimens of Monterey No. 0 sand in this study (see Appendix A), have shown that there is no significant difference in the cyclic loading resistance of a material determined by testing either 2.8 inch diameter or 12 inch diameter specimens. Thus, specimen size should not affect the cyclic loading resistance of a gravel specimen when membrane compliance effects are insignificant. If it is assumed that the effects of membrane compliance have been essentially eliminated in the sluiced 3/8" x #4 gravel specimens (C_s=28) and the sluiced 2" maximum gravel specimens (C_s=42), then it would appear from the results presented in Figure 8.4 that two uniformly graded materials with similar structure and relative density (pluviated structure and $D_r \simeq 42\%$ in this case) have nearly identical values of cyclic loading resistance regardless of the mean grain size of the material. If the above supposition is true, then a uniformly graded sand with a pluviated structure and relative density of about 42% would also be

expected to have approximately the same value of cyclic loading resistance. Figure 8.5 shows the cyclic loading resistance of Monterey No. 0 sand at a relative density of 49%, determined in this study, compared with the cyclic loading resistance of the sluiced gravels at 42% and 43% relative density from Figure 8.4. It may be noted that the cyclic loading resistance of the sand is not significantly different from values determined from the sluiced gravel specimens, indicating that gravels and sands at the same relative density and structure would indeed have approximately the same cyclic loading resistance if the effects of membrane compliance were substantially reduced or eliminated from the test results.

A comparison of the relationships showing residual pore pressure ratio vs. number of stress cycles for both sluiced (shown as solid lines) and unsluiced gravel specimens (shown as dashed lines) at 43% relative density is shown in Figure 8.6. It may be noted that, on average, the unsluiced gravel specimens developed maximum residual pore pressure ratios of about 73% and the sluiced gravel specimens developed maximum values of about 95%. These pore pressure ratio values were not exceeded even when double amplitude strains greater than 15% were achieved. This comparison serves to illustrate that: (1) The effect of membrane compliance is considerable in inhibiting the development of pore pressures that would otherwise have developed in a noncompliant system; and (2) By sluicing the gravel specimens with sand, the effects of membrane compliance may be significantly reduced, but probably not eliminated. However, there was no discernible difference between the residual pore pressure ratios developed for the two sluiced specimen groups with values of C_s equal to 17 and 28. Additional evidence of

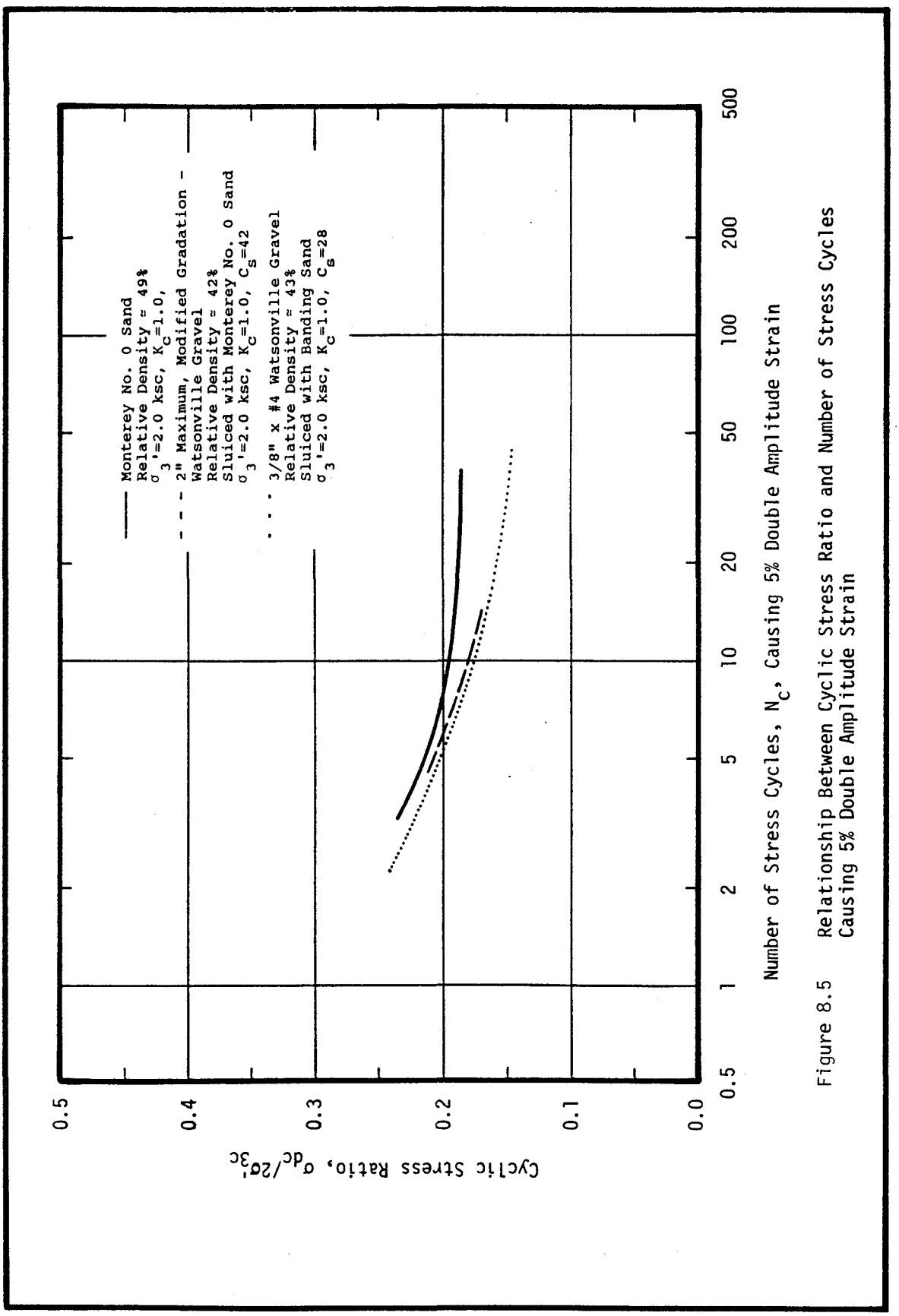

Figure 8.5 Relationship Between Cyclic Stress Ratio and Number of Stress Cycles Causing 5% Double Amplitude Strain

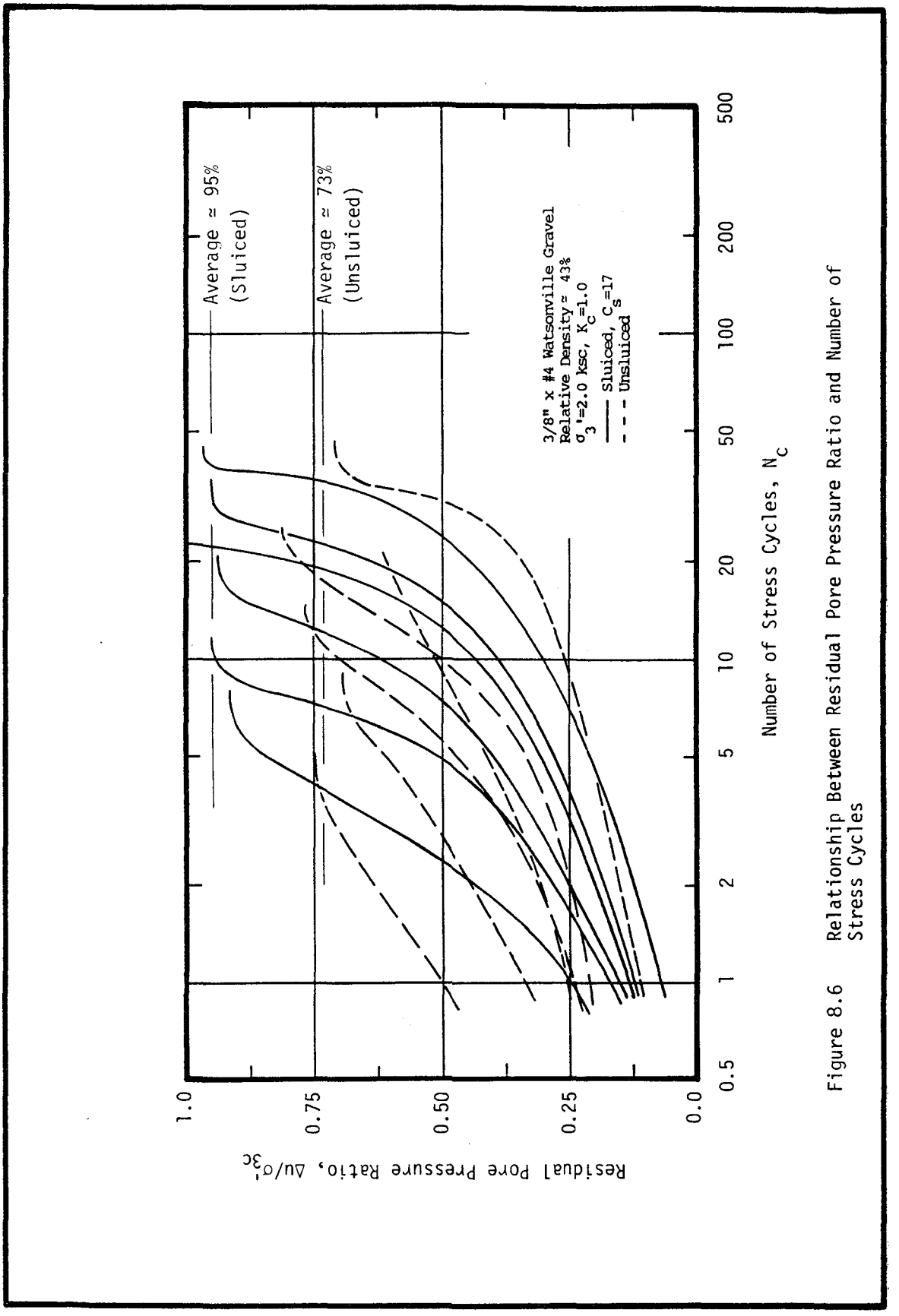

Figure 8.6 Relationship Between Residual Pore Pressure Ratio and Number of Stress Cycles

the effects of membrane compliance on pore pressure development and volume changes will be presented in Chapter 9.

Curves showing the cyclic stress ratios resulting in residual pore pressure ratios of 12%, 25%, 50%, and 100% in tests on specimens of unsluiced gravel at a relative density of 43%, are compared with the cyclic loading resistances (for 100% residual pore pressure ratio) determined for the two groups of sluiced gravel specimens, with values of C_s equal to 17 and 28, in Figure 8.7. It may be noted from this figure that the value of cyclic stress ratio which induced a residual pore pressure ratio of about 12% in specimens of unsluiced gravel, in ten stress cycles, would develop 100% pore pressure ratio in sluiced specimens (C_s=17) subjected to the same number of load cycles. Thus, as noted from the analyses of the 2" maximum and 1-1/2" x 3/4" gravels, identical values of cyclic stress ratio cause much higher pore pressures to develop in tests on sluiced specimens than would develop in tests on unsluiced specimens because of the differences in effects of membrane compliance in these specimens. When the gravel specimens are sluiced more effectively, as is likely to occur with a higher value of C_s, a lower value of stress ratio would cause 100% pore pressure ratio to develop. This is shown in Figure 8.7 where it may be noted that values of 100% pore pressure ratio were developed in sluiced specimens, with C_s=28, at the same value of cyclic stress ratio which would induce considerably less than 12% pore pressure ratio in unsluiced gravel specimens. A stress ratio correction factor, C_m, may be developed from the data in this figure by comparing the values of cyclic stress ratio, at ten cycles, for 100% pore pressure development in the unsluiced gravel specimens, with the corresponding values for

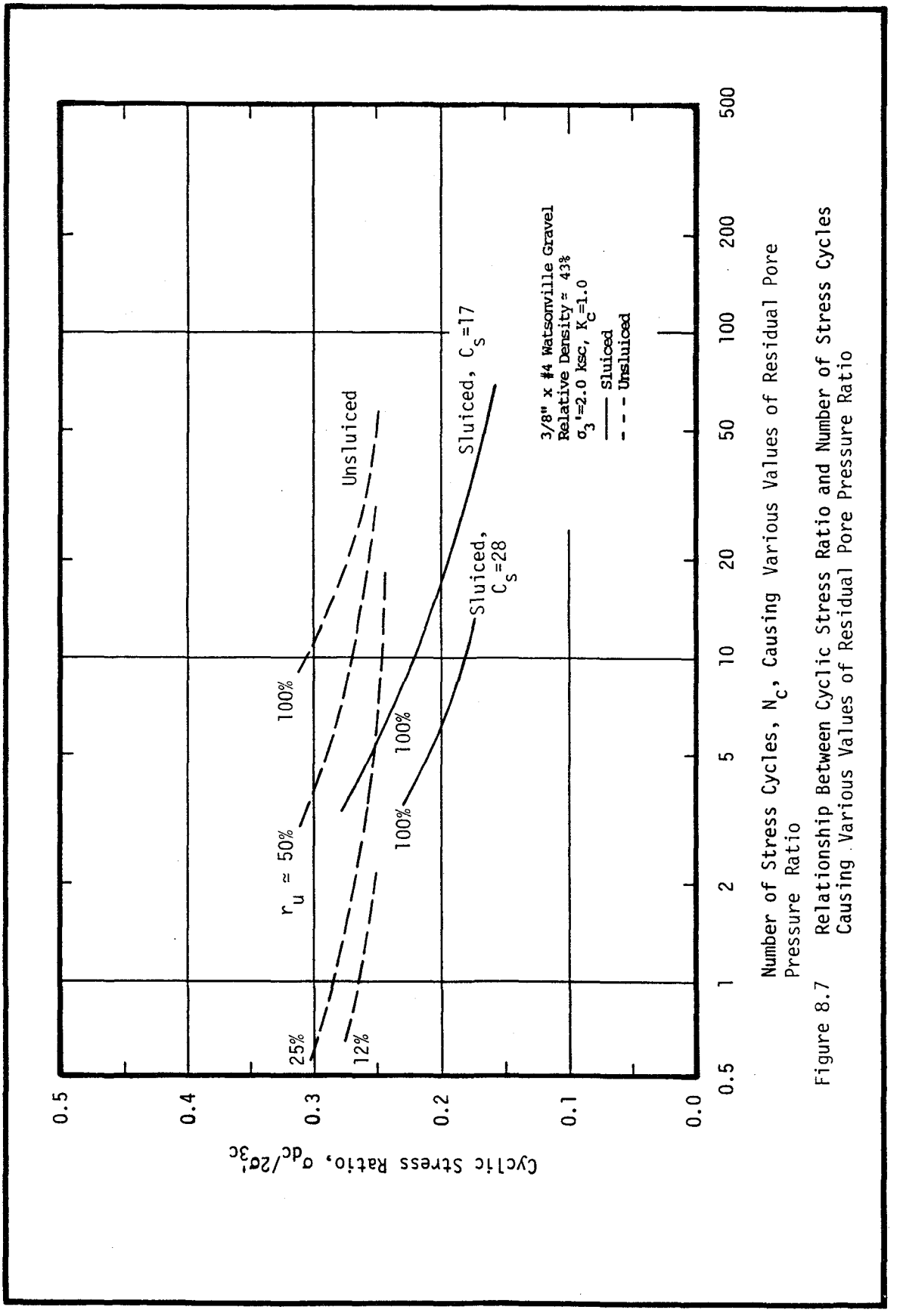

Figure 8.7 Relationship Between Cyclic Stress Ratio and Number of Stress Cycles Causing Various Values of Residual Pore Pressure Ratio

the two sluiced specimen curves. Values of C_m were determined to be equal to 0.71 and 0.59 from tests performed on sluiced specimens with C_s=17 and C_s=28, respectively.

A similar pore pressure ratio comparison is shown in Figure 8.8 for sluiced (C_s=17) and unsluiced gravel specimens at a relative density of 58%. Again, it may be noted that a value of stress ratio which causes about 12% pore pressure ratio to develop in ten stress cycles in the unsluiced gravel specimens, would produce a pore pressure ratio, r_u, of 100% in the sluiced gravel specimens. A stress ratio correction factor was not developed from these data because the unsluiced specimens developed maximum residual pore pressure ratios of only about 60% to 65%. The sluiced gravel specimens, on the other hand, developed maximum pore pressure ratios ranging from 90% to 95%. Thus, the unsluiced gravel specimens are clearly more resistant to cyclic loading and this fact is believed to be due to the effects of membrane compliance in these specimens.

A comparison of the cyclic loading resistances for specimens of unsluiced 3/8" x #4 gravel confined with either two or four membranes is shown in Figure 8.9. It may be seen that these two groups of specimens have essentially the same cyclic loading resistance. Thus, the addition of two extra membranes did not significantly reduce the effects of membrane compliance in these test specimens. Axial loads carried by these membranes were determined to be very small, and the procedure used to determine these loads, together with the results for a typical test, are included in Chapter 9.

A comparison of the cyclic loading resistances of the sluiced (C_s=17) and unsluiced 3/8" x #4 gravel specimens at a relative density

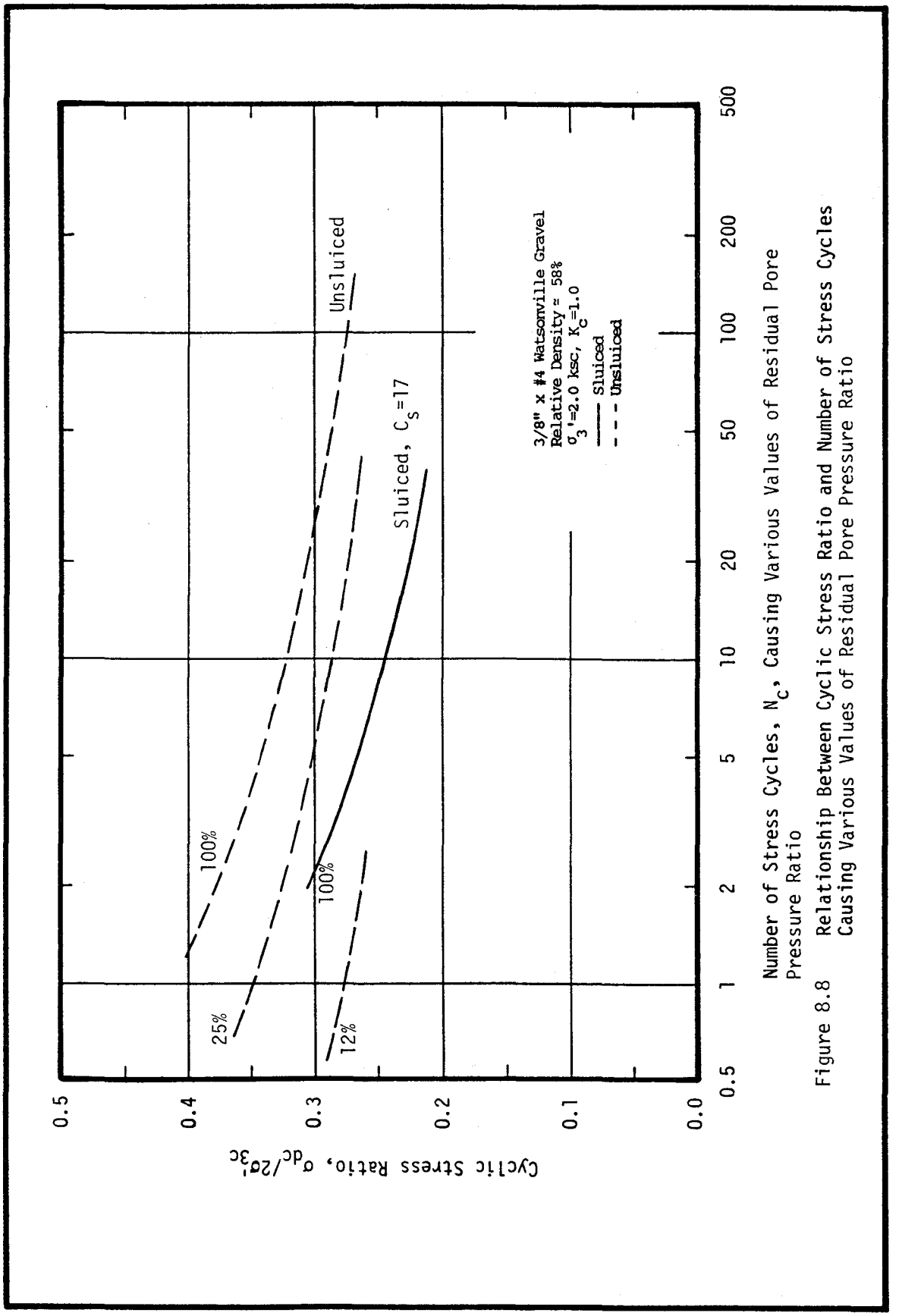

Figure 8.8 Relationship Between Cyclic Stress Ratio and Number of Stress Cycles Causing Various Values of Residual Pore Pressure Ratio

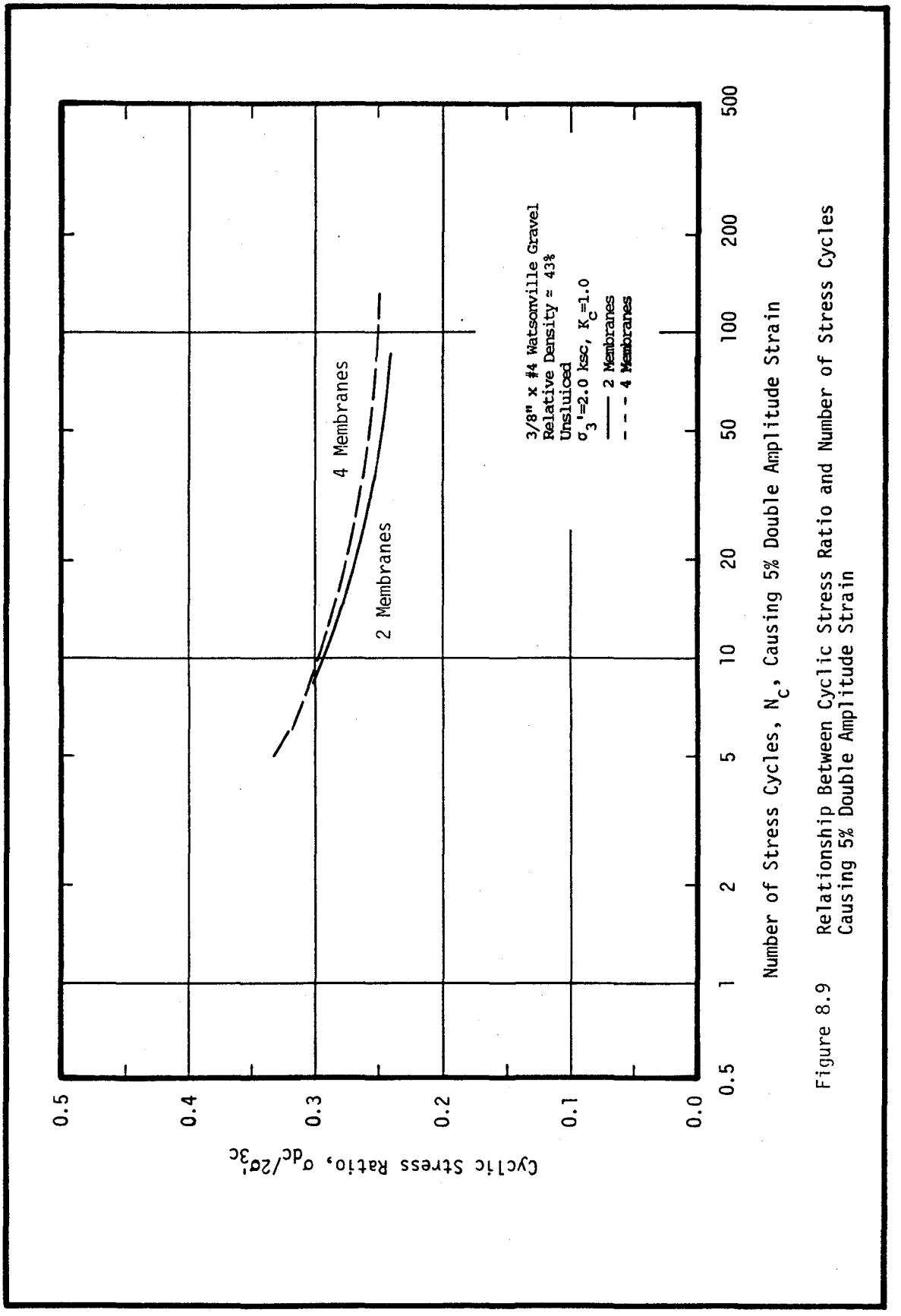

Figure 8.9 Relationship Between Cyclic Stress Ratio and Number of Stress Cycles Causing 5% Double Amplitude Strain

of 58% is shown in Figure 8.10. Again, it may be seen that the cyclic loading resistance of the sluiced gravel is considerably lower than that for the unsluiced gravel. In fact, the sluiced specimens had only 70% of the cyclic loading resistance of the unsluiced specimens. Thus, in order to account for the effects of membrane compliance in such specimens, only 70% of the cyclic loading resistance determined by laboratory testing should be used as a basis for evaluating prototype performance.

The cyclic loading resistance of unsluiced gravel at 43% and 58% relative density is compared with that for Monterey No. 0 Sand at 35% and 49% relative density in Figure 8.11. It would appear from this figure that the cyclic loading resistance of the gravel specimens is about 1.5 to 2.0 times greater than that of a sand with the same structure and relative density. However, the increased loading resistance of the gravel specimens is due essentially to the effects of membrane compliance in these specimens. If these effects are eliminated or significantly reduced, the cyclic loading resistance of both the gravel and the sand would be expected to be approximately equal.

A comparison of the cyclic loading resistance curves for samples of the sluiced gravel and samples of Monterey No. 0 sand is shown in Figure 8.12. Cyclic loading resistance curves are shown for sluiced gravel and sand specimens; (1) sluiced gravel with D_r=58%, C_s=17; (2) sluiced gravel with D_r=43%, C_s=28; and (3) sand with D_r=37% and D_r=49%. It may be seen from this figure that the values of cyclic loading resistance for the sand and the sluiced gravel specimens appear to form a consistent pattern. Thus, the relationship for the sluiced gravel at

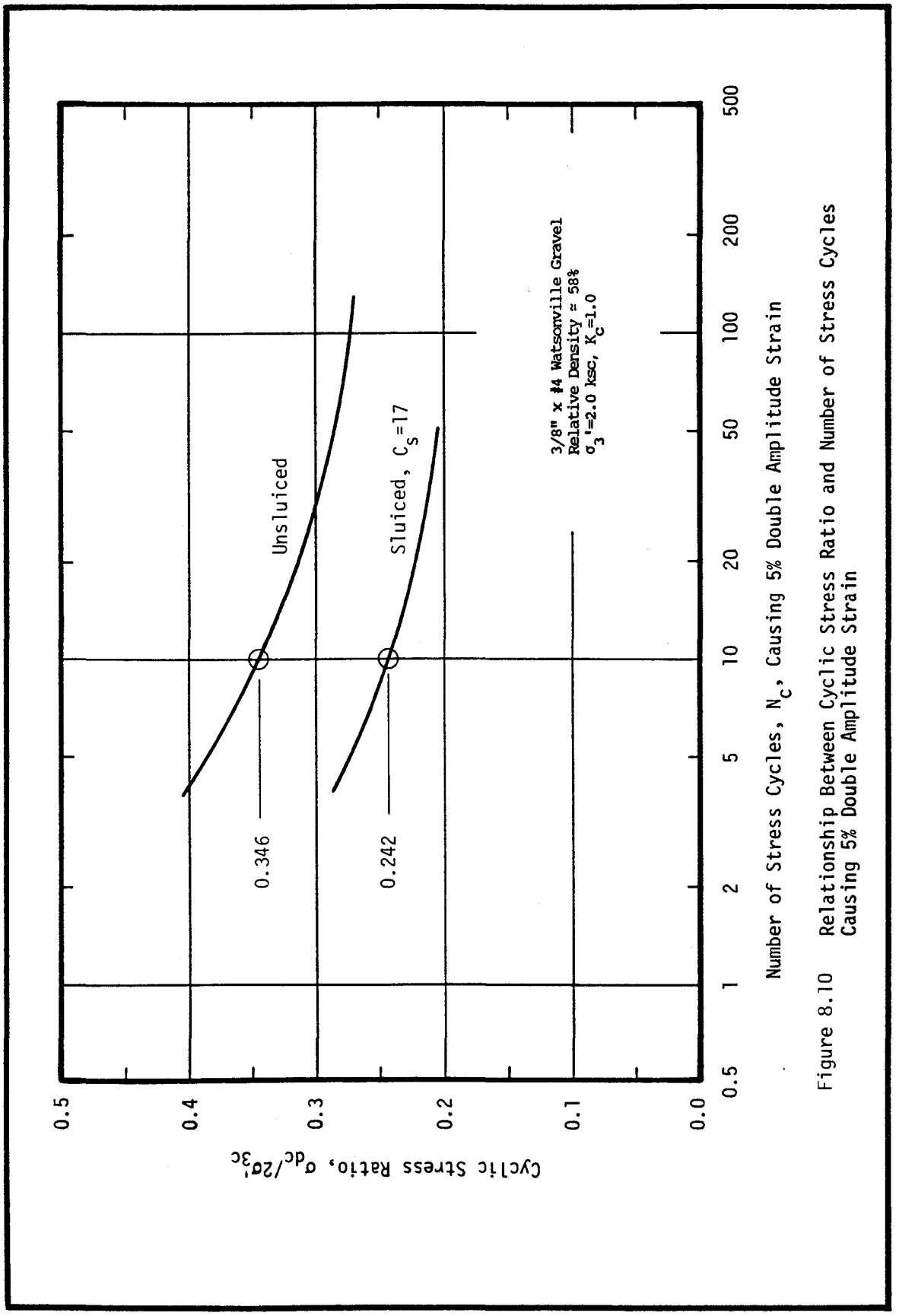

Figure 8.10 Relationship Between Cyclic Stress Ratio and Number of Stress Cycles Causing 5% Double Amplitude Strain

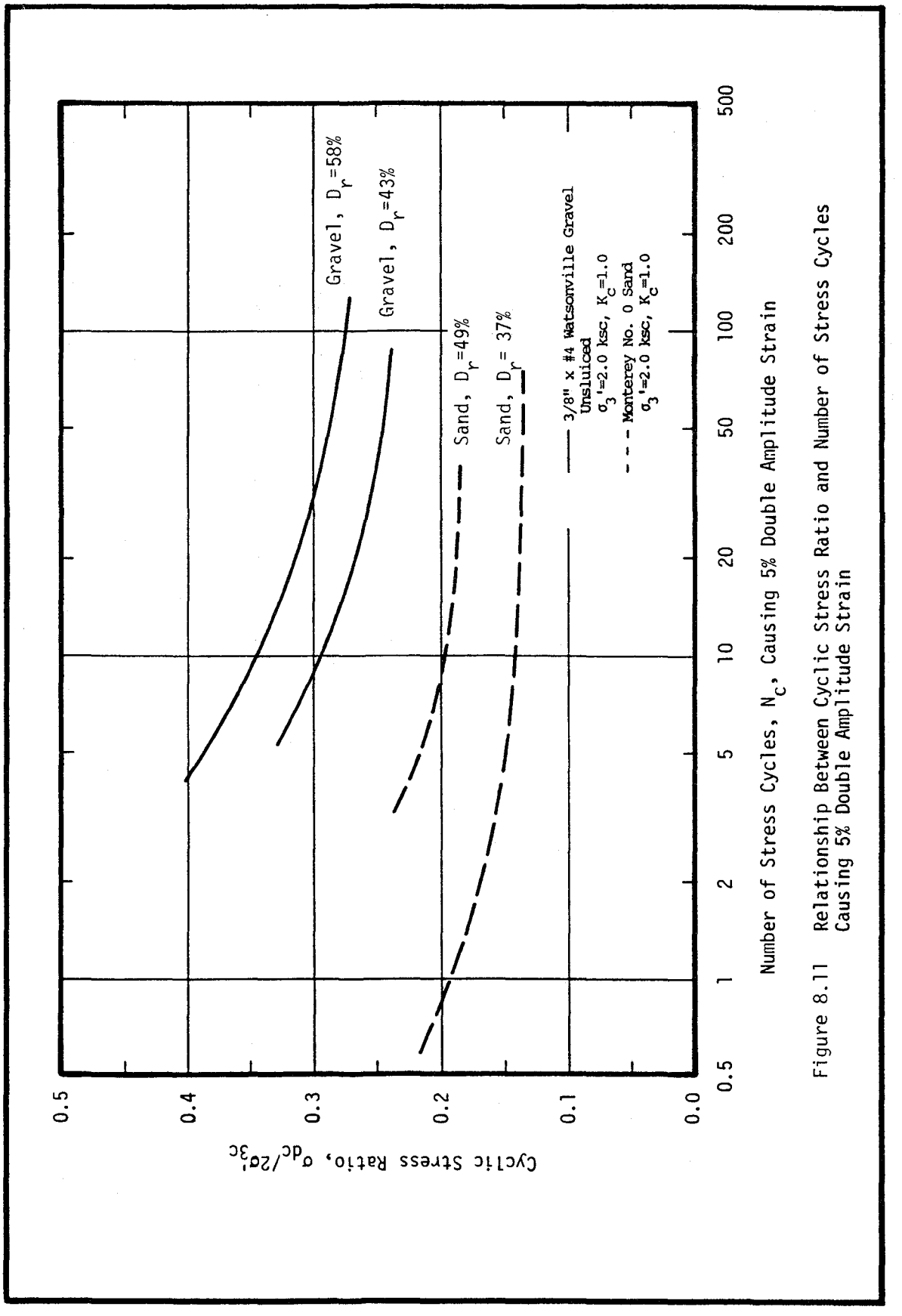

Figure 8.11 Relationship Between Cyclic Stress Ratio and Number of Stress Cycles Causing 5% Double Amplitude Strain

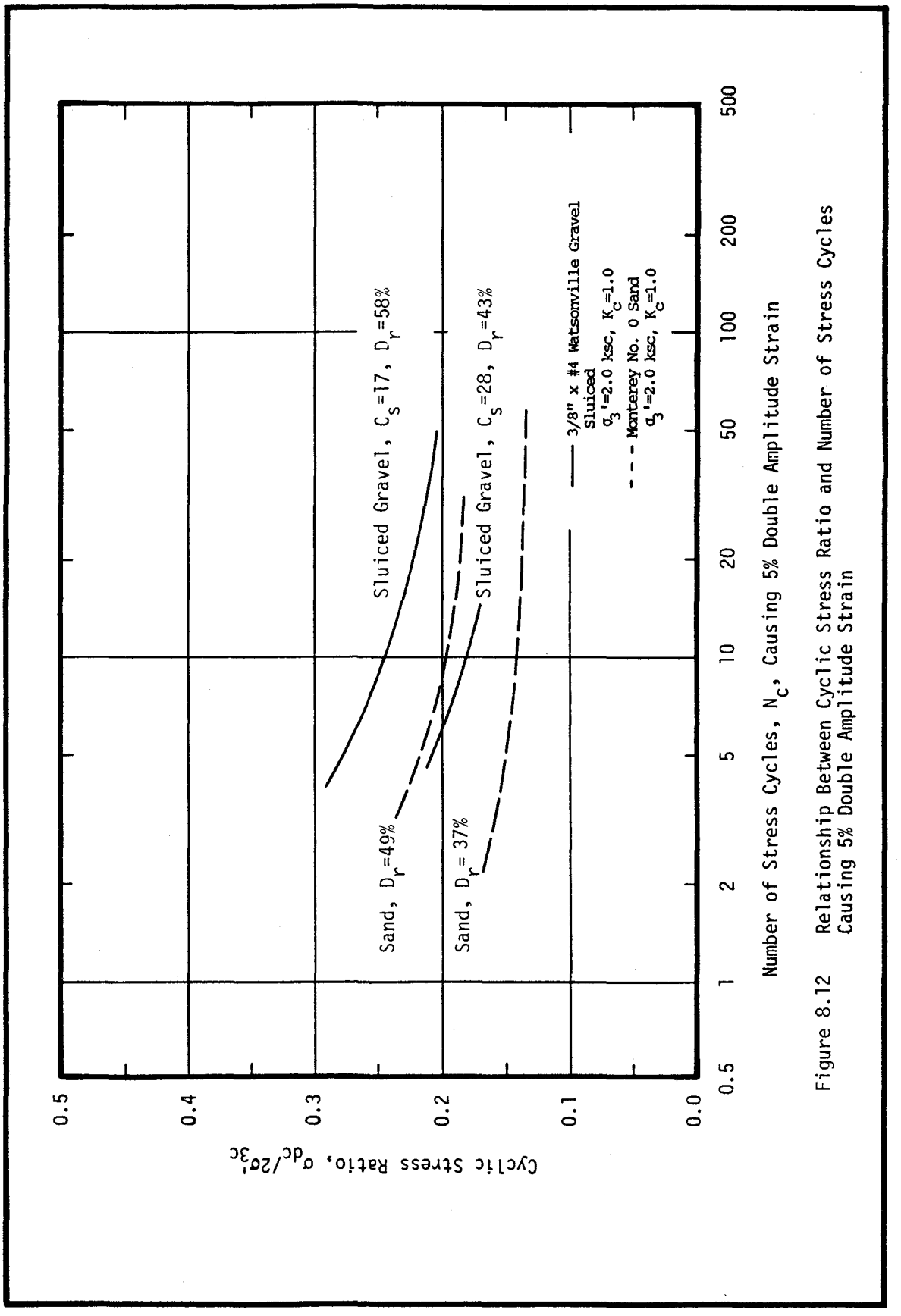

Figure 8.12 Relationship Between Cyclic Stress Ratio and Number of Stress Cycles Causing 5% Double Amplitude Strain

43% relative density with C_s=28 falls about midway between the sand curves at relative densities of 37% and 49%. Also, the cyclic loading resistance curve for the sluiced gravel at 58% relative density is about 20% greater than the cyclic loading resistance of the sand at 49% relative density. These values agree with previous observations indicating that the cyclic loading resistance of a sand at 60% relative density is about 60/50 or 1.20 times greater than the cyclic loading resistance of the same sand at 50% relative density. Thus, given that the effects of membrane compliance are essentially eliminated in the sluiced specimens and that the sluicing sand does not interfere with the gravel particle interaction during cyclic loading (see Chapter 10), the cyclic loading resistance of a sand and a gravel with similar structures and similar relative densities would appear to be essentially the same.

The relationships between residual pore ratio and number of stress cycles for specimens of sluiced gravel and specimens of Monterey No. 0 sand at about 40% relative density are shown in Figure 8.13. It may be seen that excess pore pressure is developed in the sand at a much faster rate than is developed in the gravel specimens after about 30% to 50% pore pressure ratio is reached, especially when the number of cycles to failure is low. Also, the sluiced gravel specimens reach a maximum value of residual pore pressure of only about 95% as compared with 100% for the sand specimens. These differences may be due to the fact that the effects of membrane compliance were not completely eliminated in the sluiced specimens, or to some difference in material properties (such as friction angle) between these two materials. It is not certain why these differences occur; however, two observations may

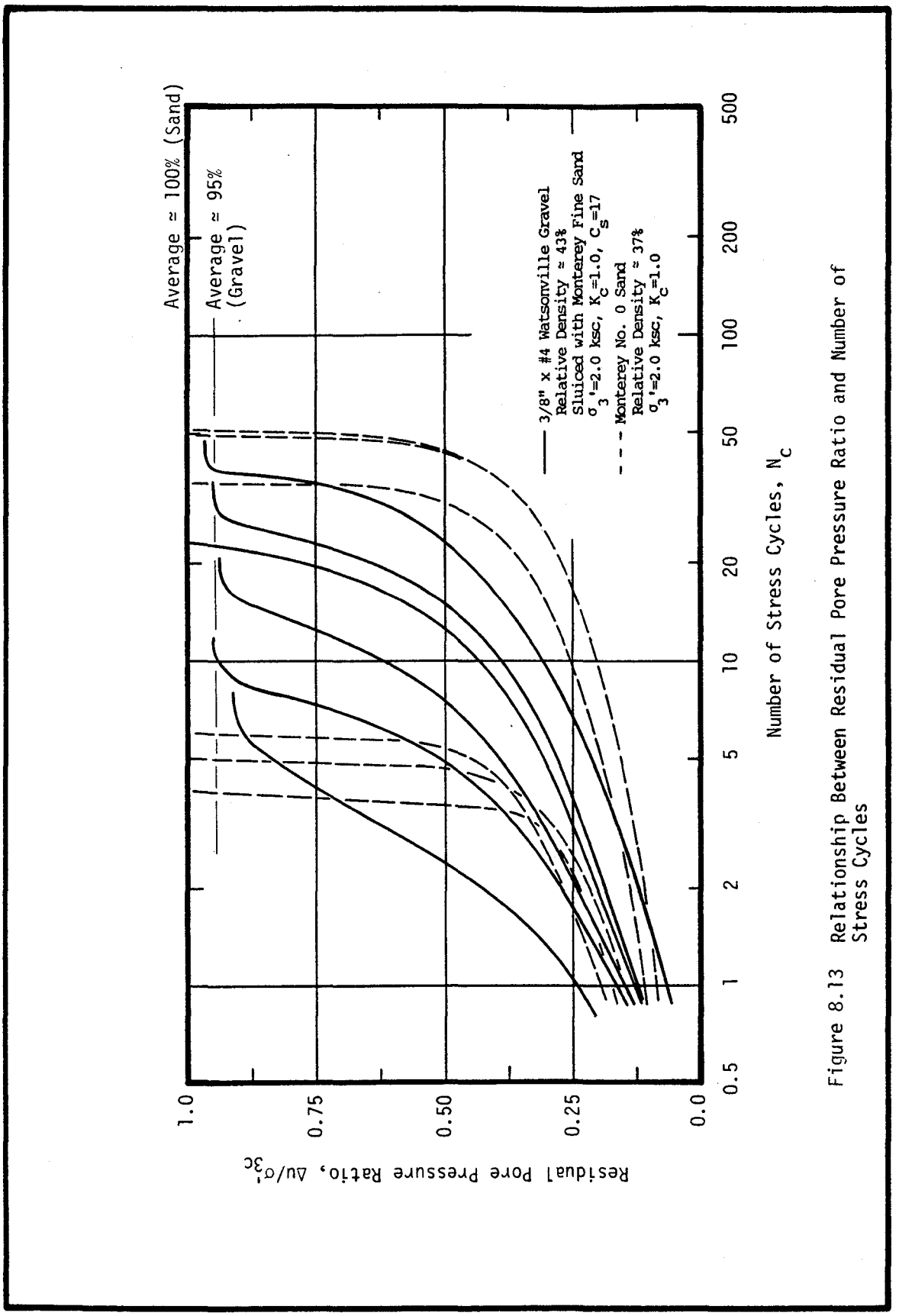

Figure 8.13 Relationship Between Residual Pore Pressure Ratio and Number of Stress Cycles

be made: (1) The differences noted in pore pressure developments did not seem to significantly affect the development of axial strains in the specimens; and (2) Pore pressure development curves for the sluiced gravel specimens much more closely approximate the curves for sand specimens than do those for the unsluiced gravel specimens.

One group of sluiced gravel specimens was constructed to about 80% relative density by tamping the gravel in six equal layers before sluicing. Specimens of this density and structure were constructed in order to determine whether a specimen which would be expected to have a high value of cyclic loading resistance, even after the effects of membrane compliance were accounted for, would still have a relatively high value of cyclic loading resistance after being sluiced. Figure 8.14 shows the results of tests performed on sluiced gravel specimens at 80% relative density compared to the cyclic loading resistance of sluiced gravel specimens at relative densities of 43% and 58%. It may be seen that these three relationships appear to be in good agreement since the curve representative of the 80% relative density gravel would be expected to have about twice the cyclic loading resistance of the material at about 40% relative density. Thus, it would appear that the gravel particle structure is the primary contributor to the cyclic loading resistance of the specimen, and that sluicing yields consistent and reasonable results while reducing the effects of membrane compliance in gravel specimens.

(2) Comparison of Observed and Theoretical Effects of Membrane Compliance

Figure 8.15 shows the error in cyclic stress ratio determined for 2.8 inch diameter gravel specimens in this study, compared with the

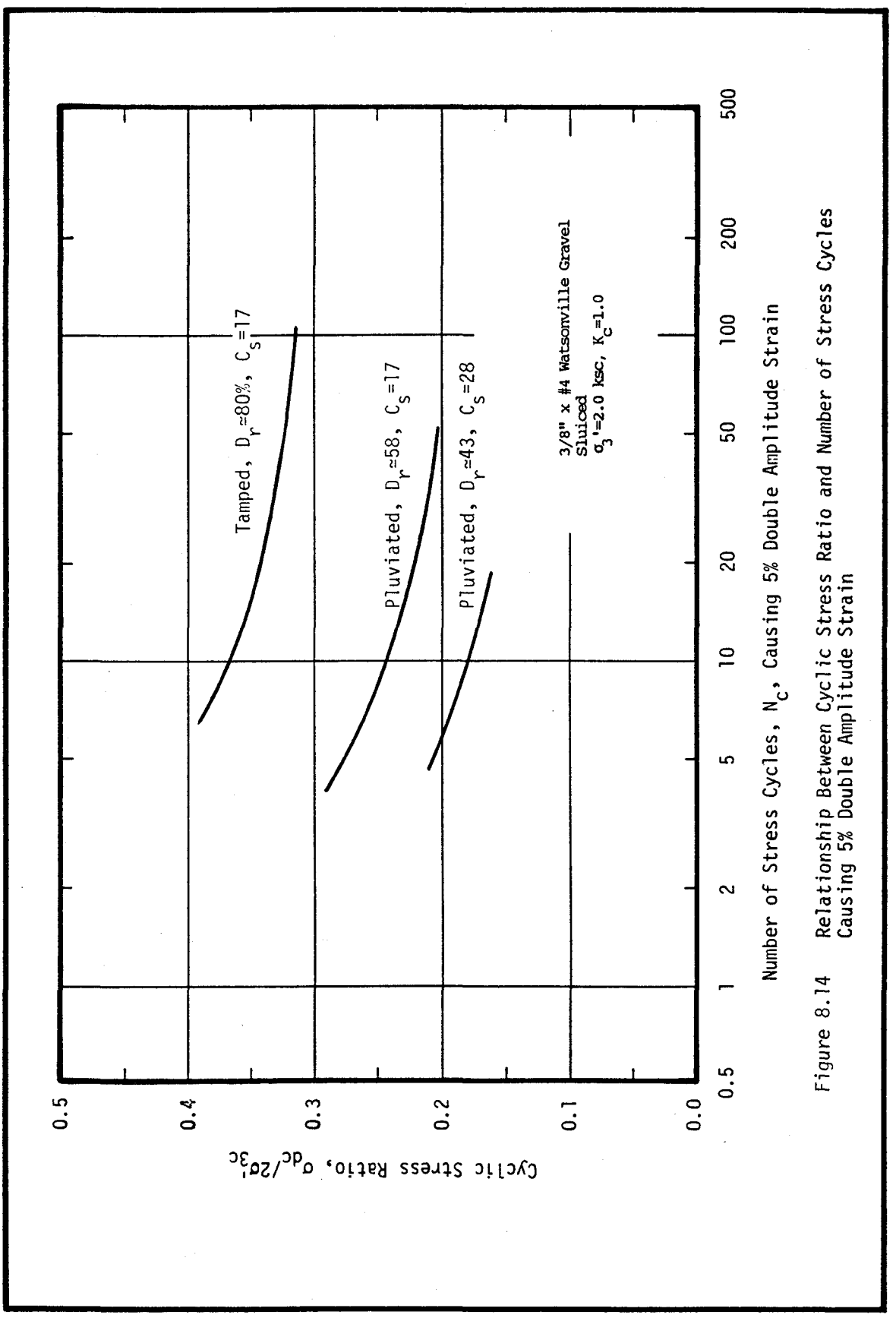

Figure 8.14 Relationship Between Cyclic Stress Ratio and Number of Stress Cycles Causing 5% Double Amplitude Strain

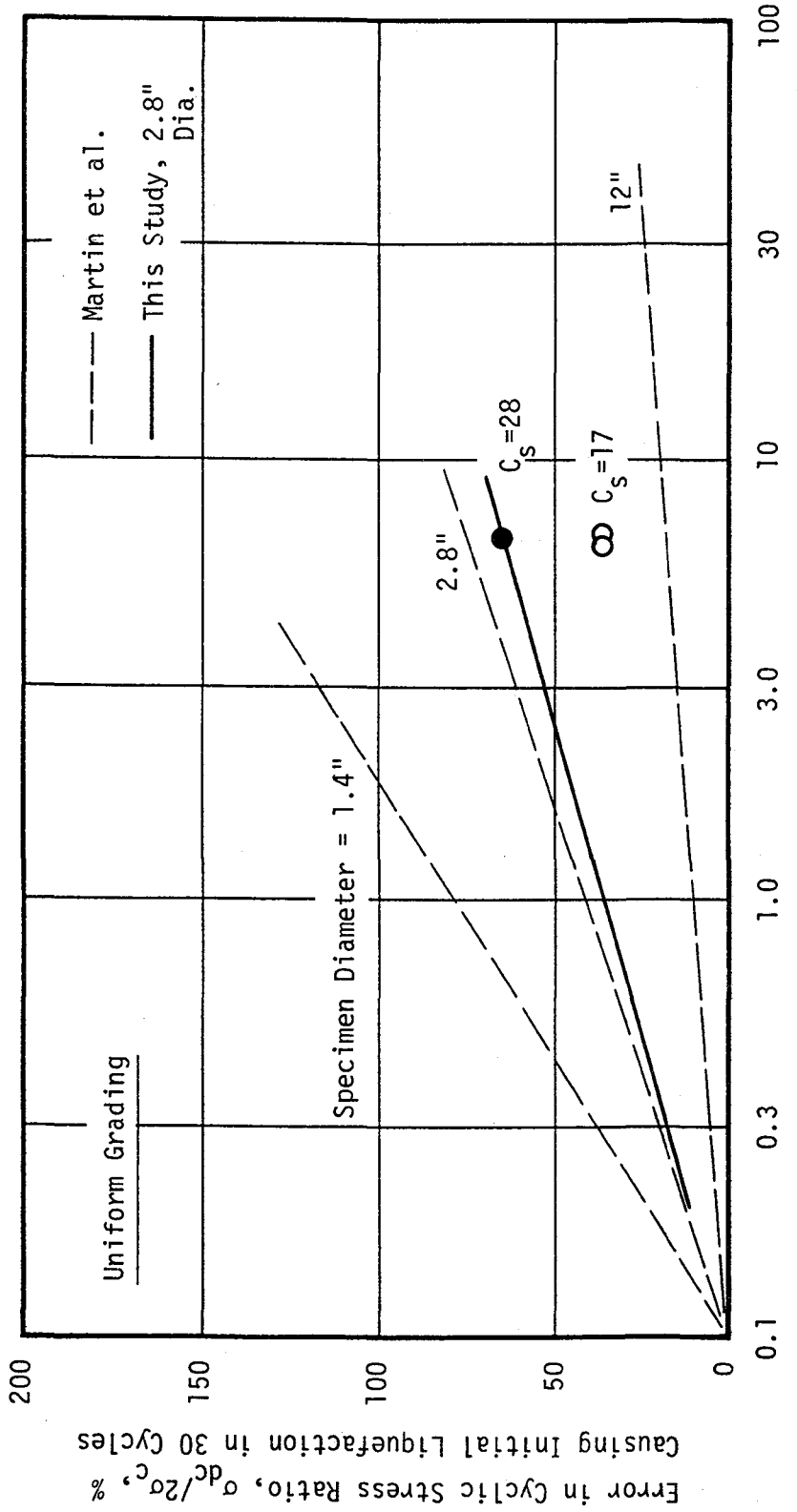

Figure 8.15 Error in Cyclic Stress Ratio Due to Membrane Compliance vs. Mean Grain Diameter for Various Specimen Diameters (after Martin et al., 1978)

relationships developed by Martin et al. (1978). It may be noted that the errors determined by this study, for two separate determinations (at $D_r \simeq 43\%$ and 58%) with $C_s=17$, are only about one-half the error values suggested by Martin et al. However, it seems likely that a value of C_s equal to 17 will not completely eliminate membrane compliance effects and thus, a higher correction might be required as discussed previously. On the other hand, the error in cyclic stress ratio determined from specimens for which $C_s=28$ may be seen to fall only slightly below the value suggested by Martin et al. Thus, it would seem that the relationship suggested by Martin et al., in Figure 8.15, might well provide a good indication of the error in cyclic stress ratio that would occur in 2.8 inch diameter specimens due to the effects of membrane compliance.

(3) Effects of Sluicing on Anisotropically Consolidated Test Specimens

Several test groups were anisotropically consolidated with values of K_c ranging from 1.25 to 2.0, prior to cyclic loading. The results of tests performed on sluiced and unsluiced specimens at a relative density of about 45% and $K_c=2.0$ are shown in Figure 8.16. Again, it may be seen that the cyclic loading resistance of the gravel specimens is reduced as a result of sluicing, presumably due to reduced membrane penetration effects. Only 86% of the unsluiced cyclic loading resistance was measured in the sluiced specimens as compared to 60% to 65% of the comparable values determined for isotropically consolidated specimens, even though the volume changes due to membrane penetration were about the same for both groups of specimens. Thus, it appears from this analysis that anisotropically consolidated specimens are less

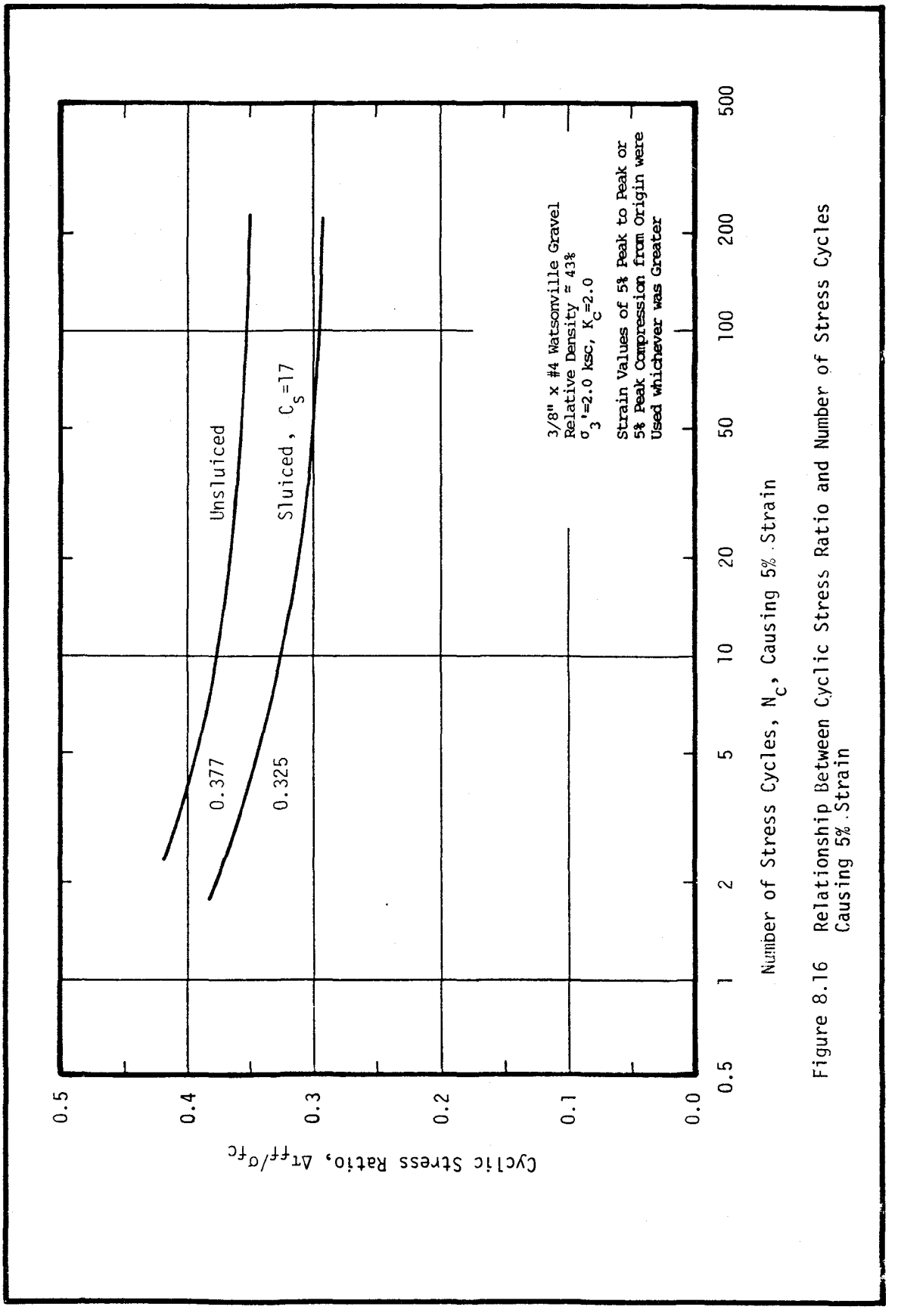

Figure 8.16 Relationship Between Cyclic Stress Ratio and Number of Stress Cycles Causing 5% Strain

affected by the effects of membrane compliance than are isotropically consolidated specimens. However, the value of cyclic stress ratio which resulted in 5% double amplitude strain in the sluiced gravel specimens (K_c=2.0) appears to be in good agreement with the value of cyclic stress ratio which resulted in about 12% pore pressure ratio in unsluiced gravel specimens (also with K_c=2.0) as shown in Figure 8.17. A similar relationship was found to occur in the previous analyses of test data for gravel specimens with K_c=1.0. Using these results as a basis for comparison, anisotropically consolidated specimens appear to be affected by membrane compliance to the same degree as are isotropically consolidated specimens.

It was observed that gravel particles in the unsluiced specimens with values of K_c=2.0 were being crushed during cyclic loading. Two grain size analyses were performed on the material from two of these specimens after testing was completed. The average result from these analyses is shown in Figure 8.18 along with the original grain size distribution. It may be noted that about 5% of the total sample weight was finer than the #4 sieve after the test, whereas no material was finer than the #4 sieve at the start of the test. The 5% quantity represents material that was created by breakage and crushing of particles during cyclic loading. It may be recalled from Chapter 3 that particle breakage is one of the reactions to cyclic loading that can lead to liquefaction. It was not determined whether this same degree of breakage also occurred in the sluiced specimens.

Figure 8.19 shows curves of cyclic loading resistance, expressed as $\Delta\tau_{ff}/\sigma_{fc}$ (the change in shear stress on the failure plane at failure divided by the normal stress on the failure plane during

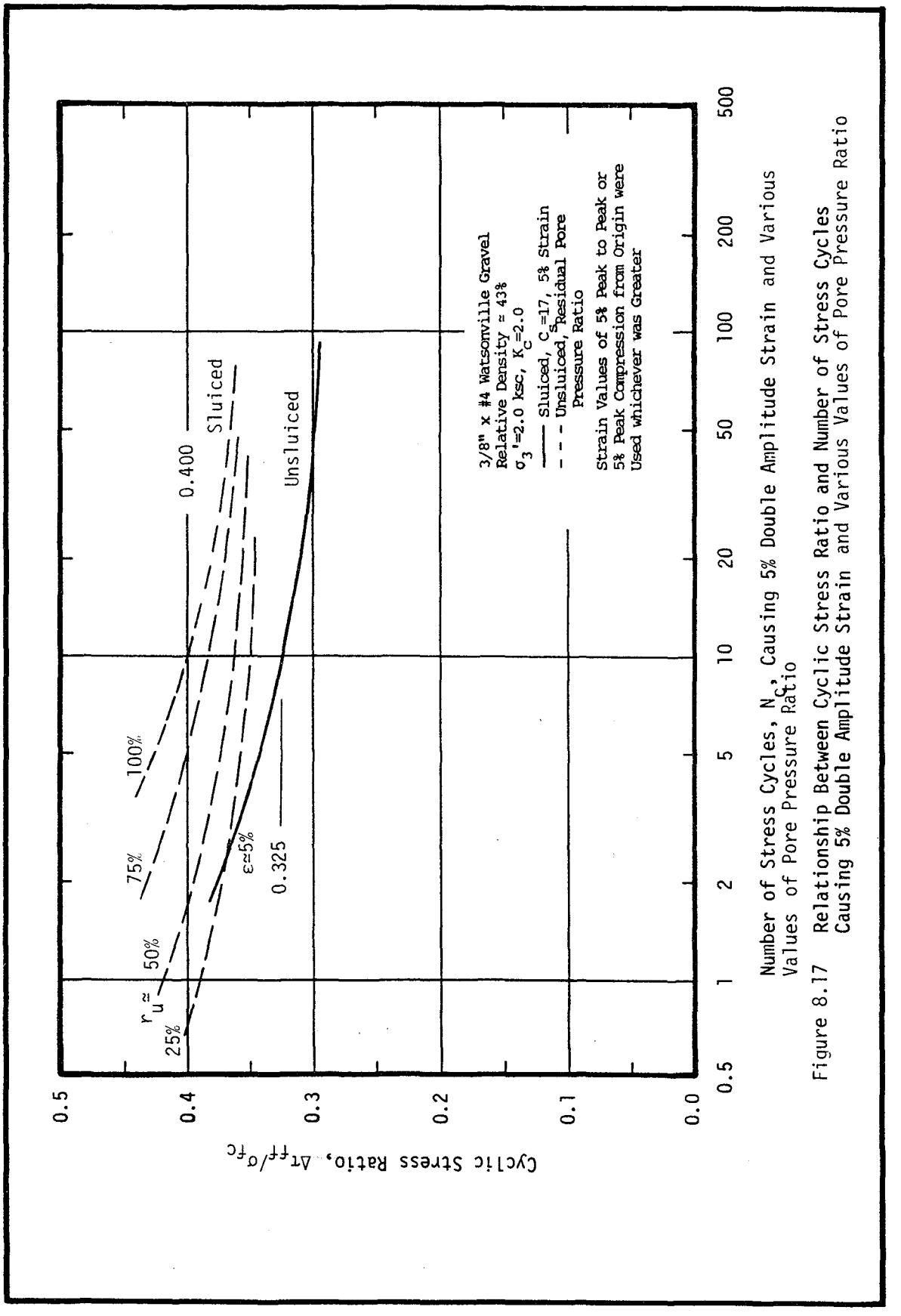

Figure 8.17 Relationship Between Cyclic Stress Ratio and Number of Stress Cycles Causing 5% Double Amplitude Strain and Various Values of Pore Pressure Ratio

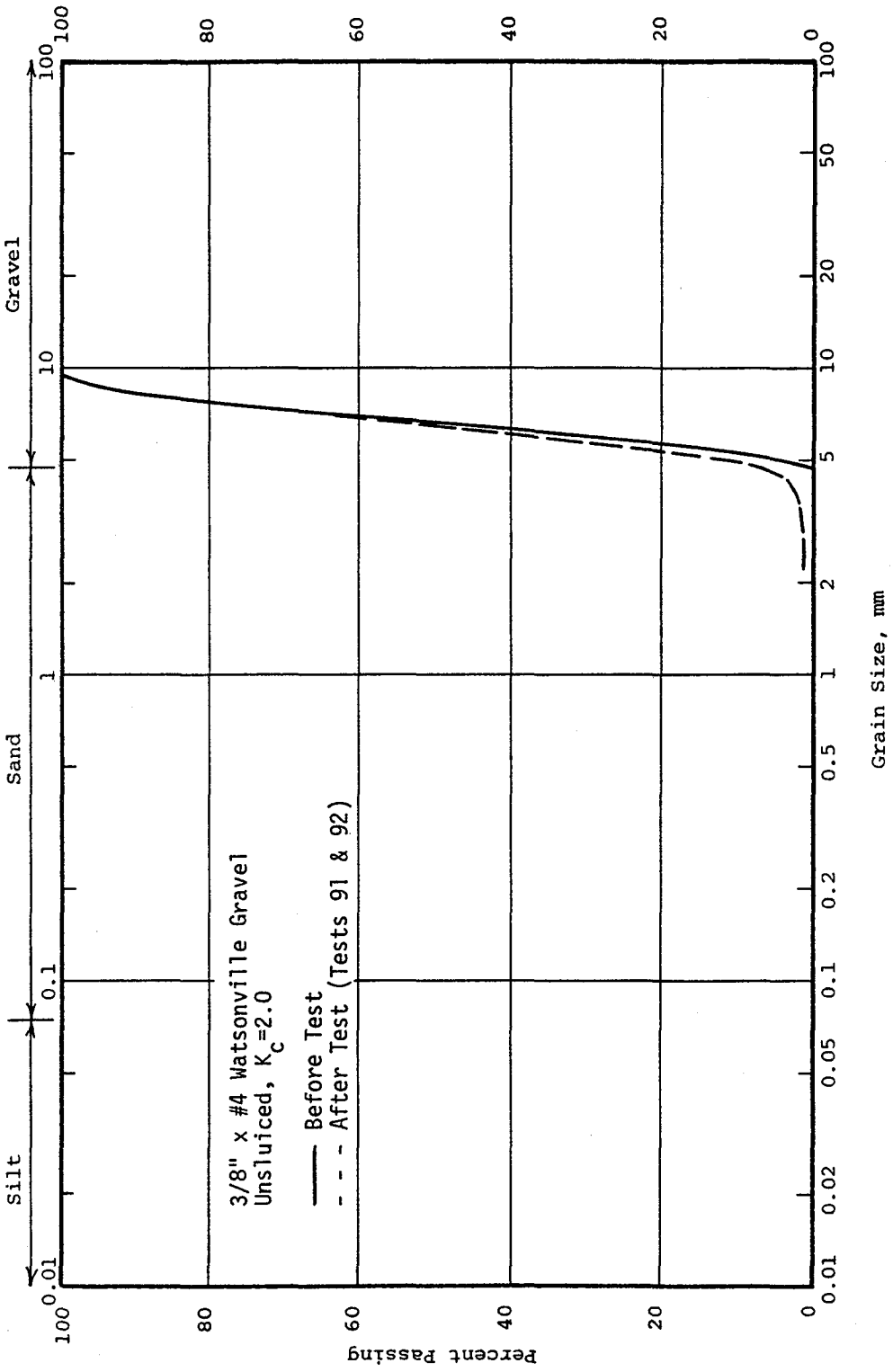

Figure 8.18 Grain Breakage Due to Cyclic Loading of Anisotropically Consolidated Specimens

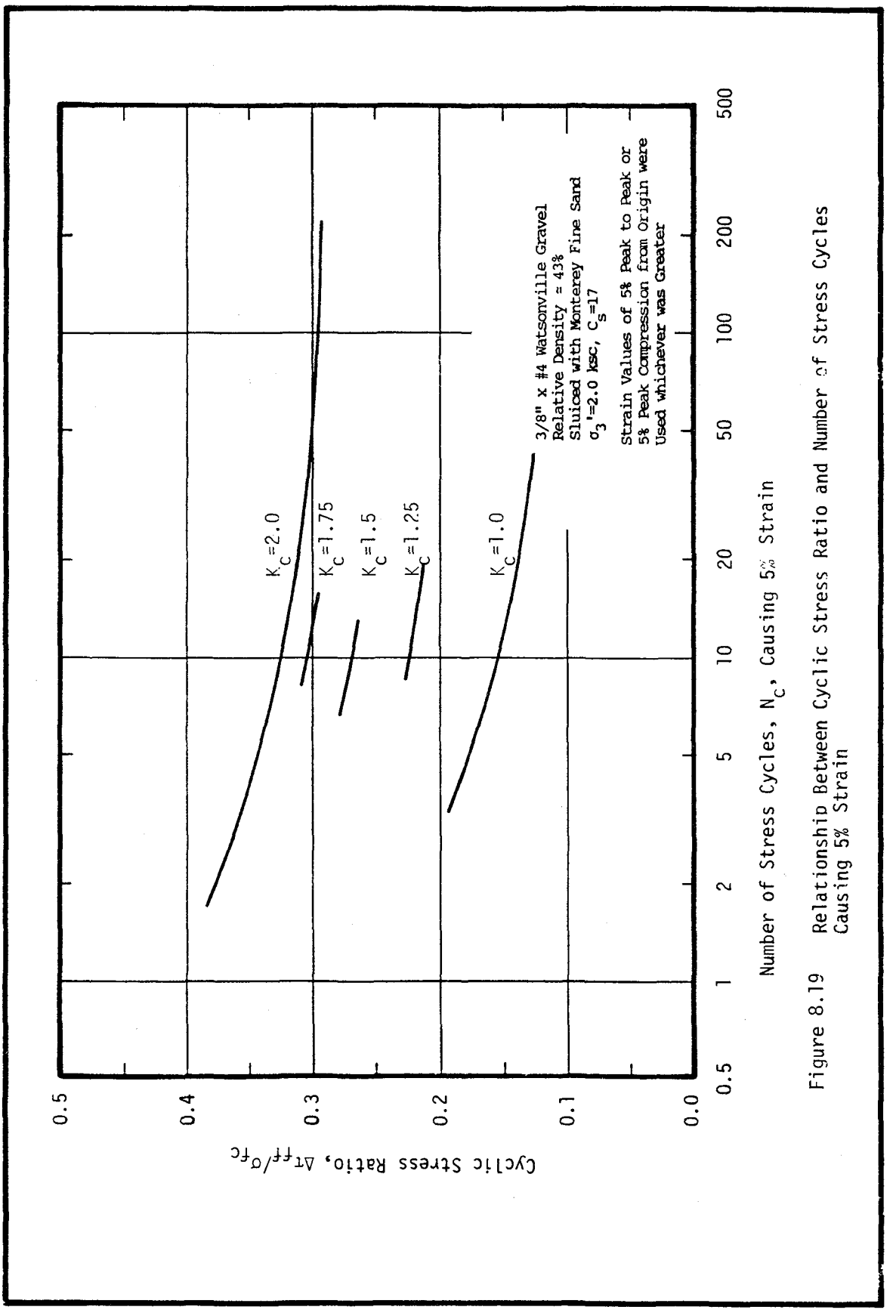

Figure 8.19 Relationship Between Cyclic Stress Ratio and Number of Stress Cycles Causing 5% Strain

consolidation), determined from three groups of sluiced gravel specimens at about 45% relative density and with five values of K_c ranging from 1.0 to 2.0. It may be seen that the cyclic loading resistance of the specimens increased significantly with increased values of K_c; the cyclic loading resistance of the sluiced specimens at K_c=2.0 (D_r=45%) is slightly more than double the cyclic loading resistance of the sluiced specimens with K_c=1.0 (D_r=45%).

(4) Summary of Sluicing Effects on Rate of Pore Pressure Generation

Relationships between residual pore pressure ratios and number of stress cycles for sluiced specimens at about 45% relative density and with values of K_c ranging from 1.0 to 2.0 are shown in Figure 8.20. These relationships are shown for specimens that reached failure in the range of about 5 to 15 stress cycles. It may be seen that excess residual pore pressures develop more rapidly in specimens with increasingly higher values of K_c. Figure 8.21 presents relationships between residual pore pressure ratios and normalized number of stress cycles for these same seven sluiced specimens. This figure also shows that excess pore pressures developed at a much faster rate in the first few cycles of loading with each successive increase in values of K_c. Specimens with lower values of K_c developed pore pressures much more gradually during the early stages of a test but then more rapidly as a pore pressure ratio of 100% was approached.

Figure 8.22 presents relationships between residual pore pressure ratio and normalized number of stress cycles for various sand and gravel specimens at K_c=1.0. Relationships are shown in this figure for: (1) Several sands at various confining pressures and number of

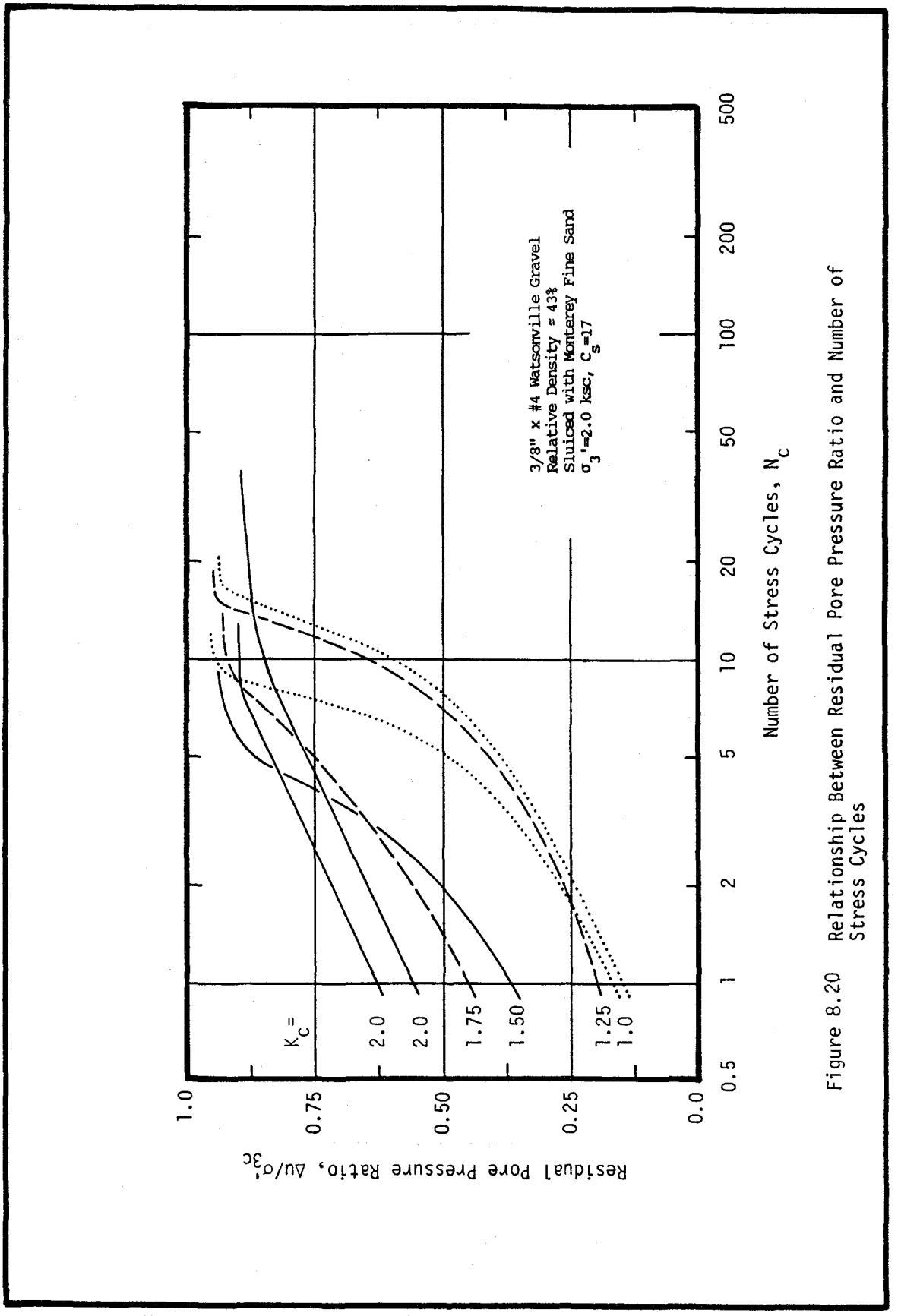

Figure 8.20 Relationship Between Residual Pore Pressure Ratio and Number of Stress Cycles

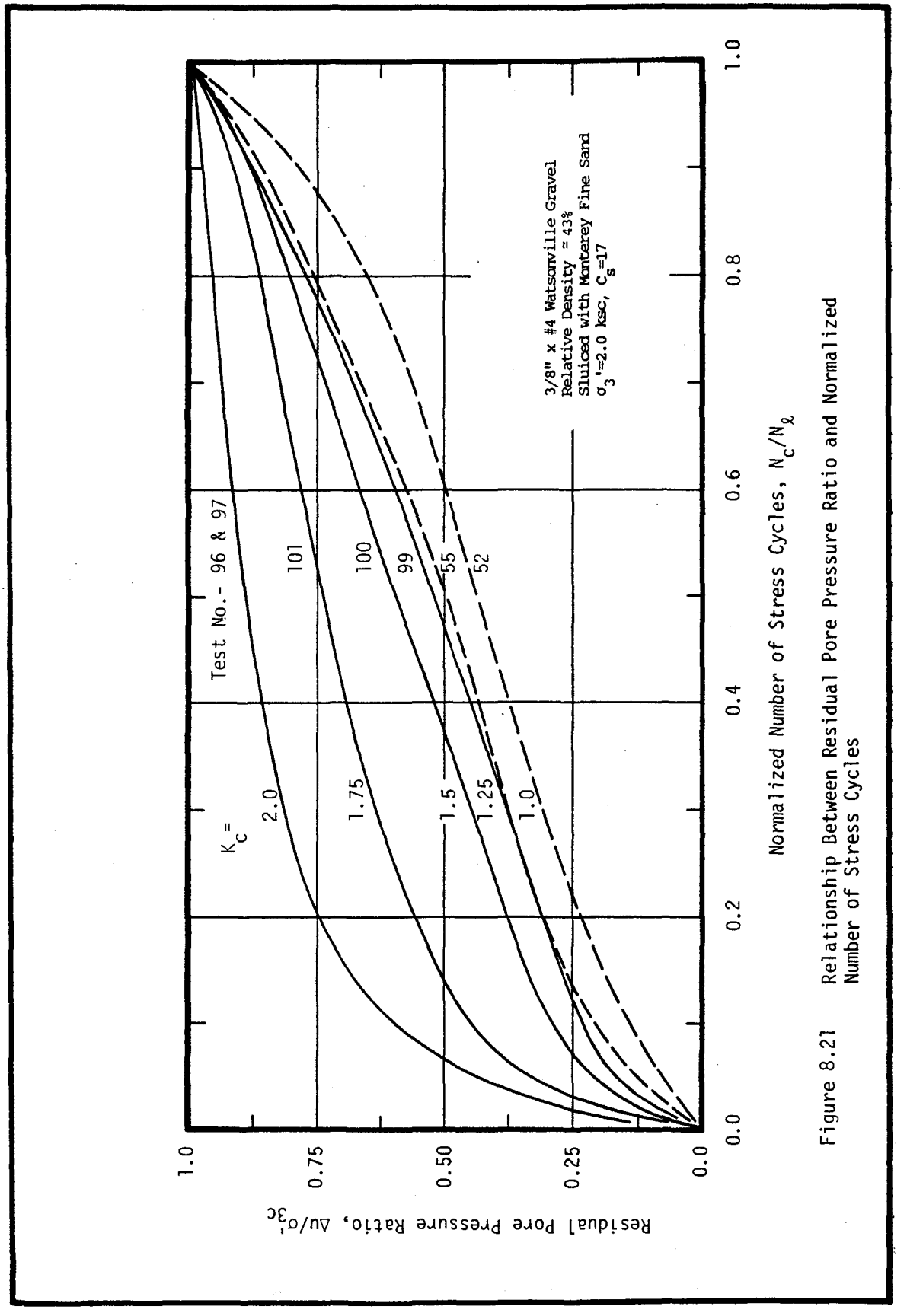

Figure 8.21 Relationship Between Residual Pore Pressure Ratio and Normalized Number of Stress Cycles

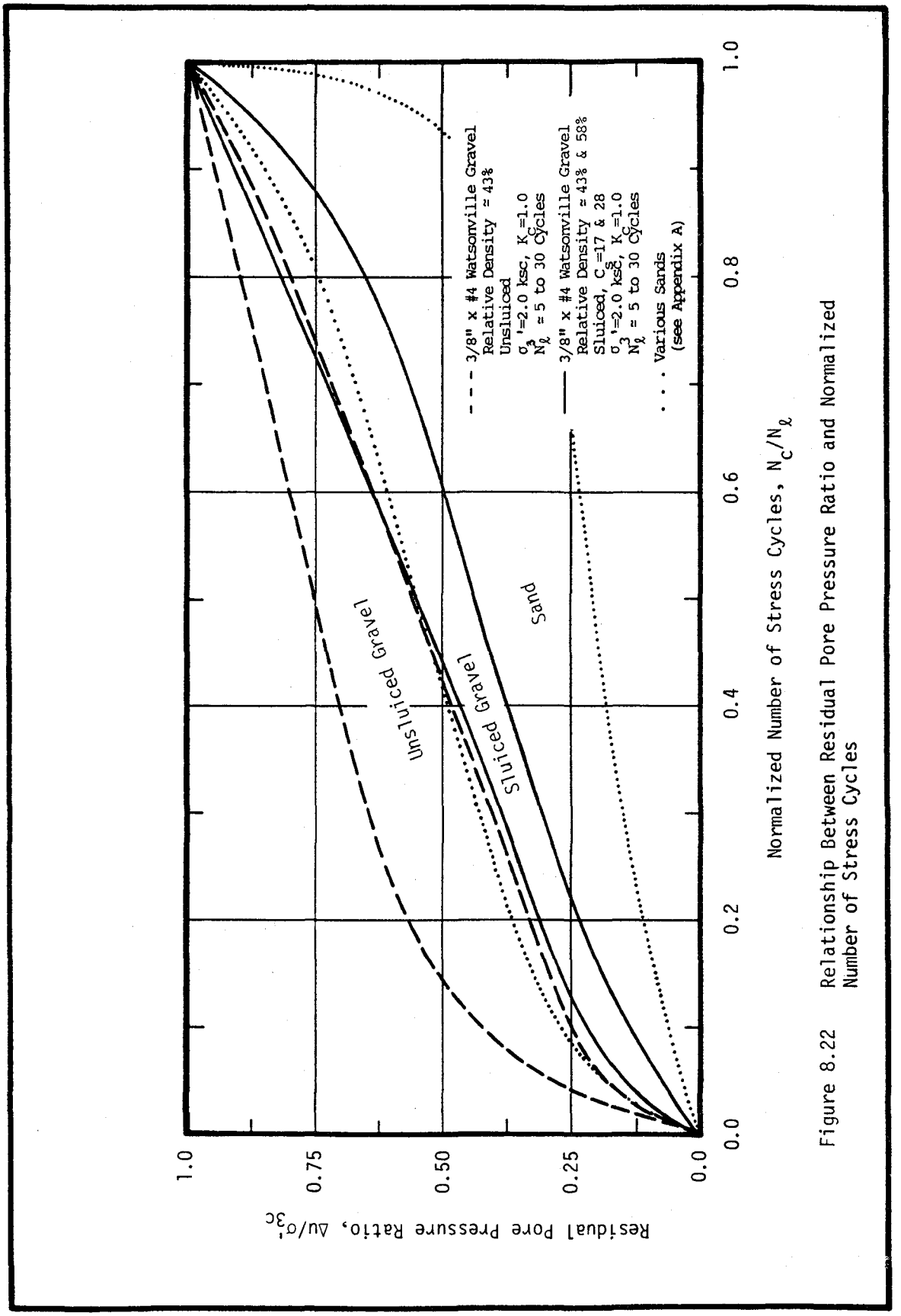

Figure 8.22 Relationship Between Residual Pore Pressure Ratio and Normalized Number of Stress Cycles

cycles to failure as presented in Appendix A; (2) Sluiced 3/8" x #4 gravel specimens at 43% and 58% relative density sluiced with both Banding sand (C_s=28) and Monterey Fine sand (C_s=17); and (3) Unsluiced gravel specimens at a relative density of 43%. Data for the gravel specimens are shown only for specimens reaching 5% double amplitude strain in a range of about 5 to 30 stress cycles. It may be seen that the sluiced gravel specimens developed residual pore pressure ratios that fall within the upper portion of the band for the sand specimens. The unsluiced gravel specimens, however, developed residual pore pressure ratios more rapidly than did either the sand or the sluiced gravel specimens.

The sand specimens tended to develop excess residual pore pressures very slowly in the early stages of the undrained, cyclic loading test but then went on to develop 100% pore pressure ratio at a very rapid rate after a value of about 50% pore pressure ratio was attained. Such behavior can lead to catastrophic soil failures, since the shearing resistance of the soil remains relatively high until near the end of the test and then decreases very rapidly to near zero.

Unsluiced gravel specimens, on the other hand, developed 50% pore pressure ratio very early in the test and thereafter the pore pressure ratio increased quite slowly to 100% during the remaining stress cycles of the test. Thus, because of the effects of membrane compliance, the unsluiced gravel specimens appeared to be more stable and approach failure very slowly and gradually during the latter part of the test. The high initial pore pressure build-up is due largely to the high value of cyclic stress ratio that is required to cause failure in these specimens.

It had been shown previously that the cyclic stress ratios required to cause failure in the unsluiced gravel specimens are about 55% greater than the cyclic stress ratios required to cause failure in the sand specimens. In spite of these increased values of applied cyclic stress ratio, the unsluiced specimens still approached a failure condition gradually due to the effects of membrane compliance. It may be recalled that, as pore pressures increase in an undrained, compliant system, membrane penetration into peripheral specimen voids is reversed. This process is most pronounced at lower confining pressures, thus, as a value of 100% pore pressure ratio is approached, the effects of membrane compliance become more significant and a slower, more gradual pore pressure build-up is likely to occur after 50% pore pressure ratio is reached. Thus, as a result of membrane compliance effects, a soil that possesses a low value of cyclic loading resistance and that tends to fail at a rapid rate as r_u=100% is approached, may be erroneously determined to possess a considerably higher value of cyclic loading resistance and to lose strength more gradually as failure is approached.

It might be expected that the relationship between residual pore pressure ratio and normalized number of stress cycles for the sluiced gravel specimens would be similar to corresponding relationships developed from sand specimens. However, the relationships developed from the sluiced gravel specimens fall somewhere between the curve for the sand specimens and the curve for the unsluiced gravel specimens. The difference between the curves for the sluiced gravel specimens and the sand specimens is undoubtedly due in part to the effects of membrane compliance which were not completely eliminated by sluicing.

It is not certain, however, if the curves for these two materials would be identical even in the event that membrane compliance effects were completely eliminated. Some of the differences between these two curves may still remain due to differences in the properties of the sands and gravels that were tested. However, the sluiced gravel specimens clearly developed excess pore pressures and strains which would seem to more closely approximate the values which may be obtained in a system with very little compliance effects.

CHAPTER 9

MEMBRANE CHARACTERISTICS AND CORRECTIONS

Load Correction

The portion of the applied axial load that was carried by the rubber confining membrane was determined for both the 2.8 inch and 12 inch diameter specimens. The simplified method used to determine these corrections was that developed by Duncan and Seed (1967) and is based on the equation:

$$\Delta\tau_{am} = -C_{am} \times (2/3) \times E_m \times 4t_{om}/D_{os}$$

where $\Delta\tau_{am}$ is the correction to be applied to the axial stress due to the load carried by the membrane,

C_{am} is a correction factor which may be determined graphically by using Figure 9.1,

E_m is Young's Modulus of the membrane,

t_{om} is the original membrane thickness,

and D_{os} is the original specimen diameter.

The characteristics of the membranes used in the tests were as follows:

D_{om} (in.)	t_{om} (in.)	E_m (psi)
2.70	0.012	195 - (Baldi and Nova, 1983)
12.0	0.10	500 - (Banerjee et al., 1979)

It may be noted from Figure 9.1 that C_{am} varies with axial strain. Thus, membrane load corrections determined for cyclic loading tests, in which the axial strains vary with each new stress cycle, should be based on the average value of strain developed during each

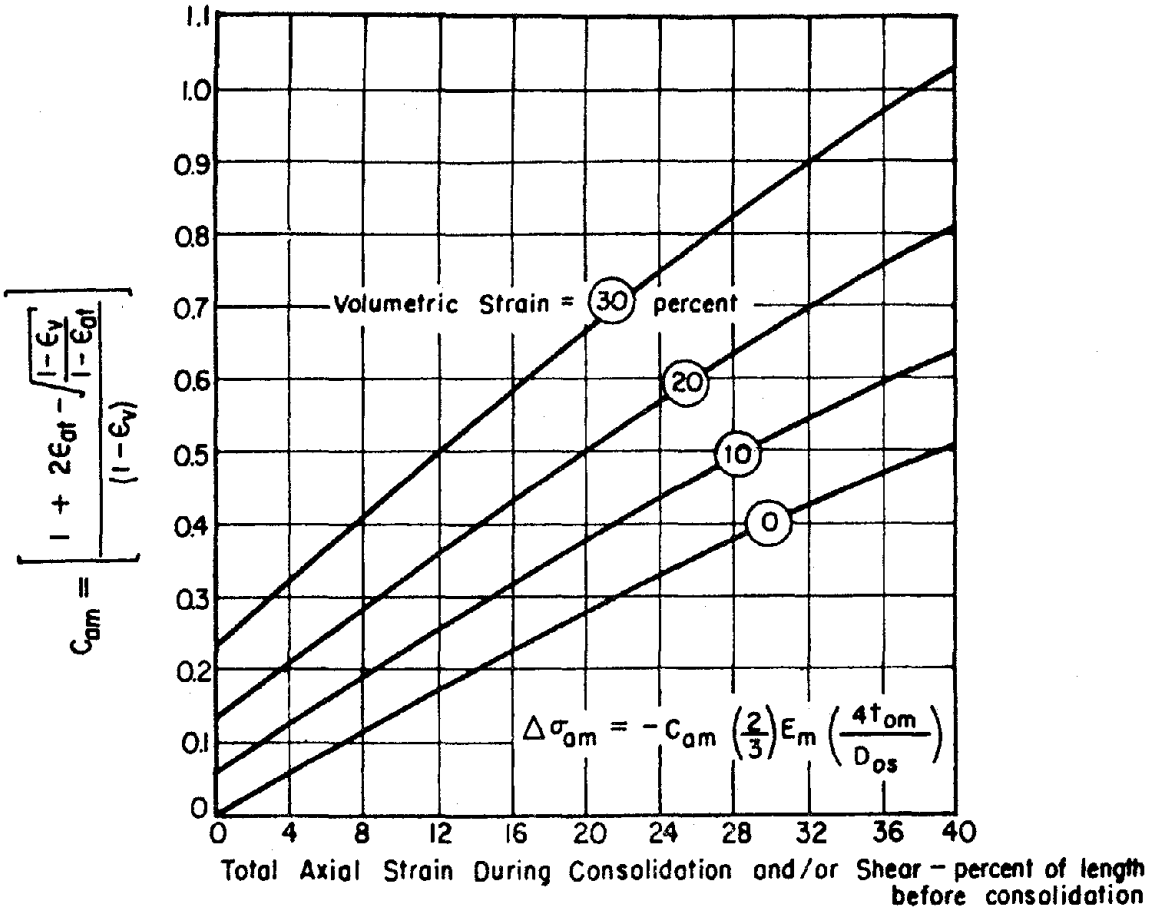

Figure 9.1 Correction Factor, C_{am}, for Corrections to Axial Stress for Membrane Strength (after Duncan and Seed, 1967)

cycle up to the point of failure. For example, it may be seen from either Figure 7.8 or 7.1.2.2 showing the relationship between double amplitude strain and number of stress cycles for Test No. 9 performed on 12 inch diameter specimens of 2" maximum, modified gradation Watsonville gravel, that double amplitude strains developed in this representative specimen with each stress cycle as follows:

TEST NO. 9

Cycle No.	Double Amplitude Strain, %
1	0
2	0
3	0
4	0
5	0.3
6	1.1
7	2.1
8	3.4
9	5.0

Average = 11.9/9 = 1.32%/cycle

Thus, the average value of double amplitude strain developed during each cycle was determined to be about 1.3%. However, since load corrections should be computed based on single amplitude strains, the appropriate average strain value in this case is about 0.65% for each cycle. Referring again to Figure 9.1, it may be seen that for zero volumetric strain (total volumetric strains for 12 inch diameter specimens during consolidation were actually in the range of 1% to 2%) the value of C_{am} is determined to be about 0.01. Therefore, the stress correction may be computed as follows:

$$\Delta\tau_{am} = -0.01 \times (2/3) \times 500 \times 4 \times (0.10/12)$$

$$= 0.11 \text{ psi} \quad (0.0075 \text{ ksc}).$$

The resulting stress ratio correction may also be computed for Test No. 9 as:

$$-\Delta\tau_{am}/2\sigma_{3c} = -0.0075/4 = -0.002.$$

And the corrected cyclic stress ratio for this test would thus be:

$$0.180 - 0.002 \simeq 0.178.$$

Corrections of this magnitude are clearly negligible.

Samples failing in a greater number of cycles would have a smaller error in stress ratio due to membrane load since the axial strains would develop over a greater number of cycles and, conversely, samples failing in fewer cycles would require that a slightly greater stress ratio correction be applied. However, the load correction was determined for specimens failing in about 10 stress cycles since this value was used for comparison of the cyclic loading resistances of the test specimens presented in the preceding chapters. Load corrections for a 2.8 inch diameter specimen confined with 2 thin membranes which developed strains similar to the values from Test No. 9 may be computed as follows:

$$-\Delta\tau_{am} = -0.01 \times (2/3) \times 195 \times 4 \times (2 \times (0.012/2.7))$$

$$= 0.0116 \text{ psi}$$

$$= 0.0008 \text{ ksc}$$

Again this value is negligibly small. It is apparent that any errors in cyclic loading resistance due to membrane load for the specimens tested in this study are extremely small, and it was thus considered that no practical benefit would be gained from making such corrections. Furthermore, the majority of the studies involved comparisons between the cyclic loading resistances of sluiced and unsluiced specimens having the same diameters and confined by similar membrane systems.

Therefore, even if the load corrections were more significant, the comparative relationships between sluiced and unsluiced specimens would be essentially unchanged. For these reasons, no correction for membrane axial load was applied to the data presented in this report.

Volume Changes Due to Membrane Penetration

Hydrostatic compression and rebound tests were performed on a number of sluiced and unsluiced 2.8 inch diameter gravel specimens in order to determine the amount of volume change that would occur due to membrane penetration. All specimens were constructed of 3/8" x #4 gravel at a relative density of about 50%, prepared by dry pluviation and confined by two thin membranes. The membranes, obtained from 3-D Polymers of Gardena, California, were all 2.70 inches in diameter, 9 inches tall, and 0.012 inches thick. Young's modulus for such material is typically about 195 psi (Baldi and Nova, 1983).

Height and total volume change measurements were recorded during hydrostatic compression and rebound. The specimens were assumed to behave isotropically, thus, the skeletal volumetric strain was computed to be equal to three times the axial strain. Volumetric strain due to membrane penetration, ε_{vm}, may be determined by subtracting the skeletal volumetric strain, ε_{vs}, from the total measured volumetric strain, ε_{vt}, in accordance with the equation:

$$\varepsilon_{vm} = \varepsilon_{vt} - \varepsilon_{vs}.$$

Figure 9.2 shows compression and rebound curves for total and skeletal volumetric strains measured in sluiced and unsluiced gravel specimens confined with two thin membranes. It may be noted from these curves that the skeletal volumetric strain is a very small percentage of the total volumetric strain measured in the unsluiced specimens.

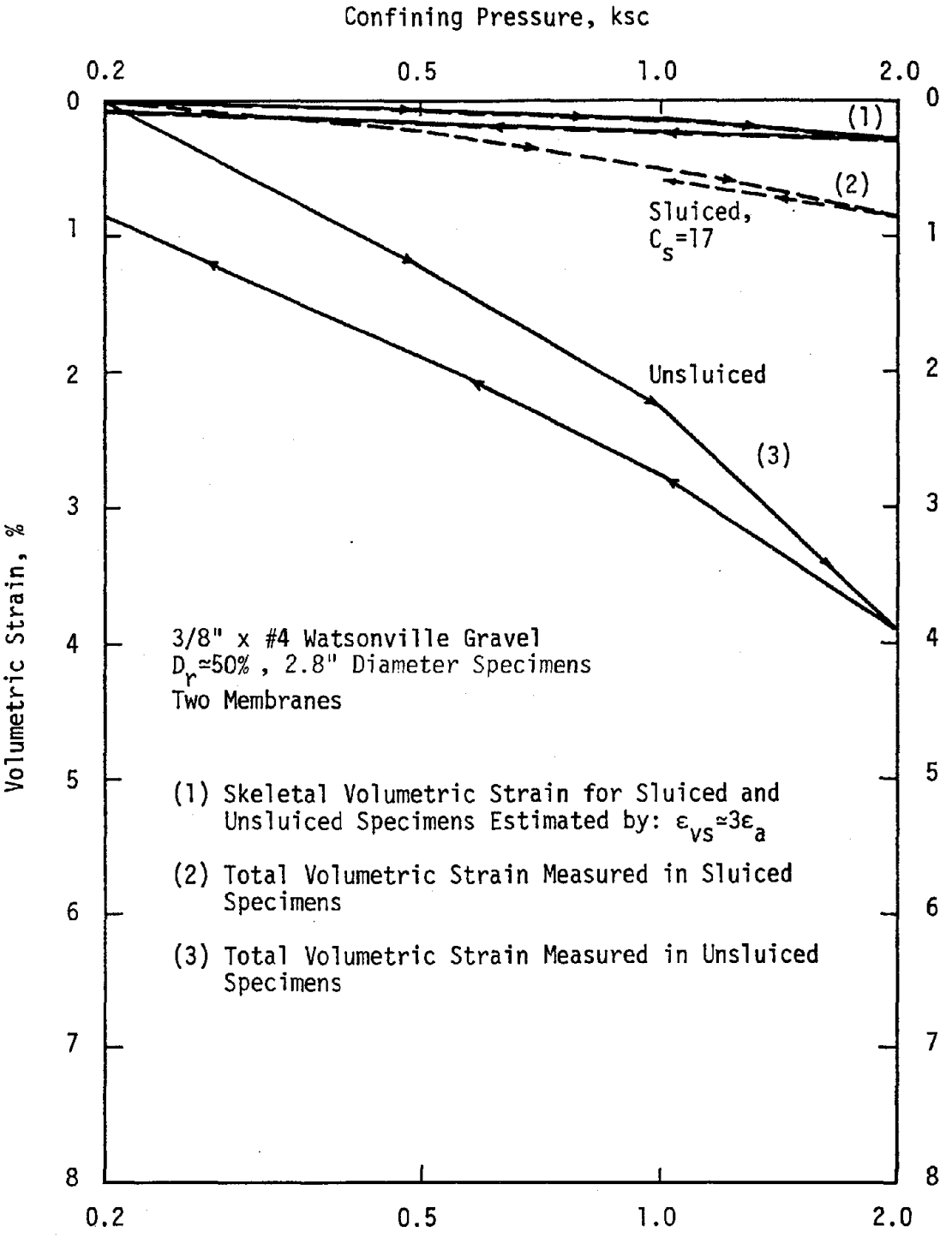

Figure 9.2 Total and Skeletal Volumetric Strains Measured in Sluiced and Unsluiced 2.8 Inch Diameter Specimens

Consequently, even if the assumption of isotropic deformation is incorrect, a more precise determination of skeletal volume change would have a very small effect on the value of volumetric strain that is determined to be due to membrane penetration. Thus, it would seem reasonable to consider that for this material, or for other such materials where membrane penetration volume changes are a high proportion of the total measured volume changes, the assumption of isotropic compression and rebound will introduce very small errors in interpretation of the results. Well-graded gravels, on the other hand, will have much smaller volume changes due to membrane penetration and thus a more precise determination of the skeletal volumetric strain may be required. For such materials, skeletal volumetric strains should be determined using radial strains which may be measured by using one of several methods such as the use of girth gages as proposed by Chan (1978) and Banerjee et al. (1979).

The assumption of isotropic behavior may also be more appropriate than it first appears. Vaid and Negussey (1984) suggested that most soils deform isotropically during hydrostatic rebound as described in Chapter 4. Thus, if the specimen was first consolidated and then total volumetric strains were measured during hydrostatic rebound, the assumption of isotropic specimen deformations may be entirely valid.

Also shown in Figure 9.2 are values of computed skeletal volumetric strains, for both sluiced and unsluiced specimens, based on measured axial strains. It may be noted from this figure that there is no significant difference between the values of skeletal strains computed for either sluiced or unsluiced specimens. Thus, the sluicing sand does not appear to influence compression of the gravel structure

during hydrostatic consolidation. It may also be noted that only about 0.55% volumetric strain due to membrane penetration occurred in the sluiced specimens over the range of confining pressures indicated. For the unsluiced specimens, however, about 3.6% volumetric strain occurred due to membrane penetration over the same range of confining pressures. Thus, about 85% of the membrane penetration volume change that occurred in the unsluiced specimens was eliminated by sluicing the gravel specimen with sand (C_s=17). This reduction in membrane penetration volume change resulted in a corresponding reduction in membrane compliance effects and consequently, the sluiced specimens were determined to have lower values of cyclic loading resistance.

Rebound curves should also be used to determine membrane penetration volume changes in order to account for any temporary plastic deformation of the membrane that may occur. It may be noted from Figure 9.2 that a residual value of about 0.1% skeletal strain remained after hydrostatic rebound from 2.0 to 0.20 ksc, whereas a residual value of about 0.8% total volumetric strain was not recovered during rebound. The latter value represents about 21% of the total volume change that occurred during consolidation from 0.2 ksc to 2.0 ksc in the unsluiced specimens. Thus, 21% of the total volumetric strain was not recovered during rebound due to plastic deformation of the membranes. Plastic deformation will prevent the membrane from assuming its original cylindrical shape after the effective confining pressure is decreased to zero.

Such membrane deformations seemed to be particularly pronounced when using systems composed of multiple membranes and are apparently the result of adhesion that develops between two membranes after they

deform due to the applied confining pressure. Once this adhesion develops, the membranes are prevented from sliding along their contact surfaces. The membrane system seemed to behave as if it were a group of flexible beams which have been bent into some irregular shape and then clamped together in order to prevent them from regaining their original shape. Vacuum grease applied to the interface seemed to have no effect in reducing the adhesion that developed between the membranes. After being removed from the gravel specimens, the multiple membrane systems retained the irregular shape of the gravel specimen and each of the membranes had to be peeled apart from the others. Only then did they revert back to their original, cylindrical shape.

The adhesion that may develop between two membranes is considered to have a positive influence in reducing the effects of membrane compliance. The amount of volume change due to membrane penetration that is measured during hydrostatic rebound would be less than that for consolidation because of the residual penetration which is not recoverable. Thus, rebound curves should be used when attempting to quantify the amount of membrane penetration volume change that may occur due to membrane penetration rebound during undrained cyclic loading.

The effect of multiple membranes on total measured volumetric strain is significant. The amount of volumetric strain measured in single membrane systems was approximately double that measured in two or four membrane systems as shown in Figure 9.3. However, there is very little difference between two or four membrane systems either in measured volumetric strain or in measured cyclic loading resistance as shown earlier. This would seem to indicate that there is probably some

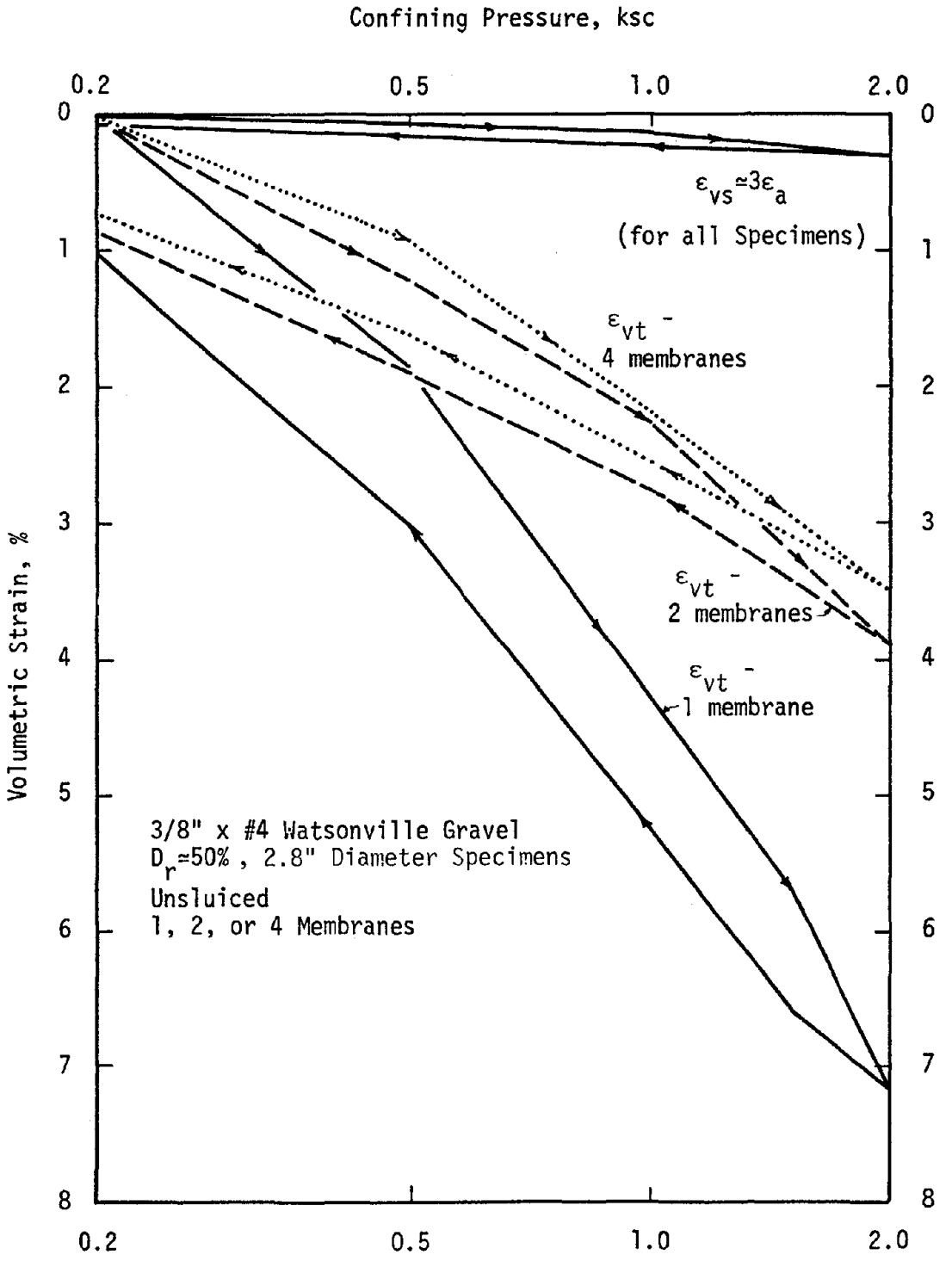

Figure 9.3 Total and Skeletal Volumetric Strains Measured in Unsluiced 2.8 Inch Diameter Specimens Confined with 1, 2, or 4 Membranes

optimal number of membranes where both membrane compliance and membrane thickness (and thus membrane axial loads) are minimized. It may also be noted from Figure 9.3 that about 14% of the total volumetric strain that occurred in the single membrane system was not recovered after rebound, while about 20% was not recovered in the two and four membrane systems, again indicating the effects of multiple membranes in reducing membrane penetration volume changes during rebound.

Correction for Membrane Compliance Based on Volume Changes

Drained hydrostatic compression and rebound tests were performed on several unsluiced 3/8" x #4 gravel specimens that were confined with two membranes and ranged in relative density from nearly zero to about 50%. Volume changes were determined from rebound curves, similar to the curve shown in Figure 9.2, for changes in effective pressure which would correspond to pore pressure ratios of 50%, 75%, and 90% in an undrained system. For example, hydrostatic rebound from 2.0 ksc to 0.50 ksc would result in a drained membrane penetration volume change that would correspond to the membrane penetration volume change that would occur in an undrained system with an induced pore pressure ratio of 75%. The results from these tests are shown in Figure 9.4 where a range of volume changes is noted for changes in confining pressure that are representative of various pore pressure ratios. The values of membrane penetration volume change may be used to compute skeletal density changes that occur during cyclic loading as a result of pore water redistribution. The basis for such a correction was described in Chapter 3 and is summarized by the following three points: (1) Recovered membrane penetration that occurred during undrained cyclic loading would result in a redistribution of water content within the

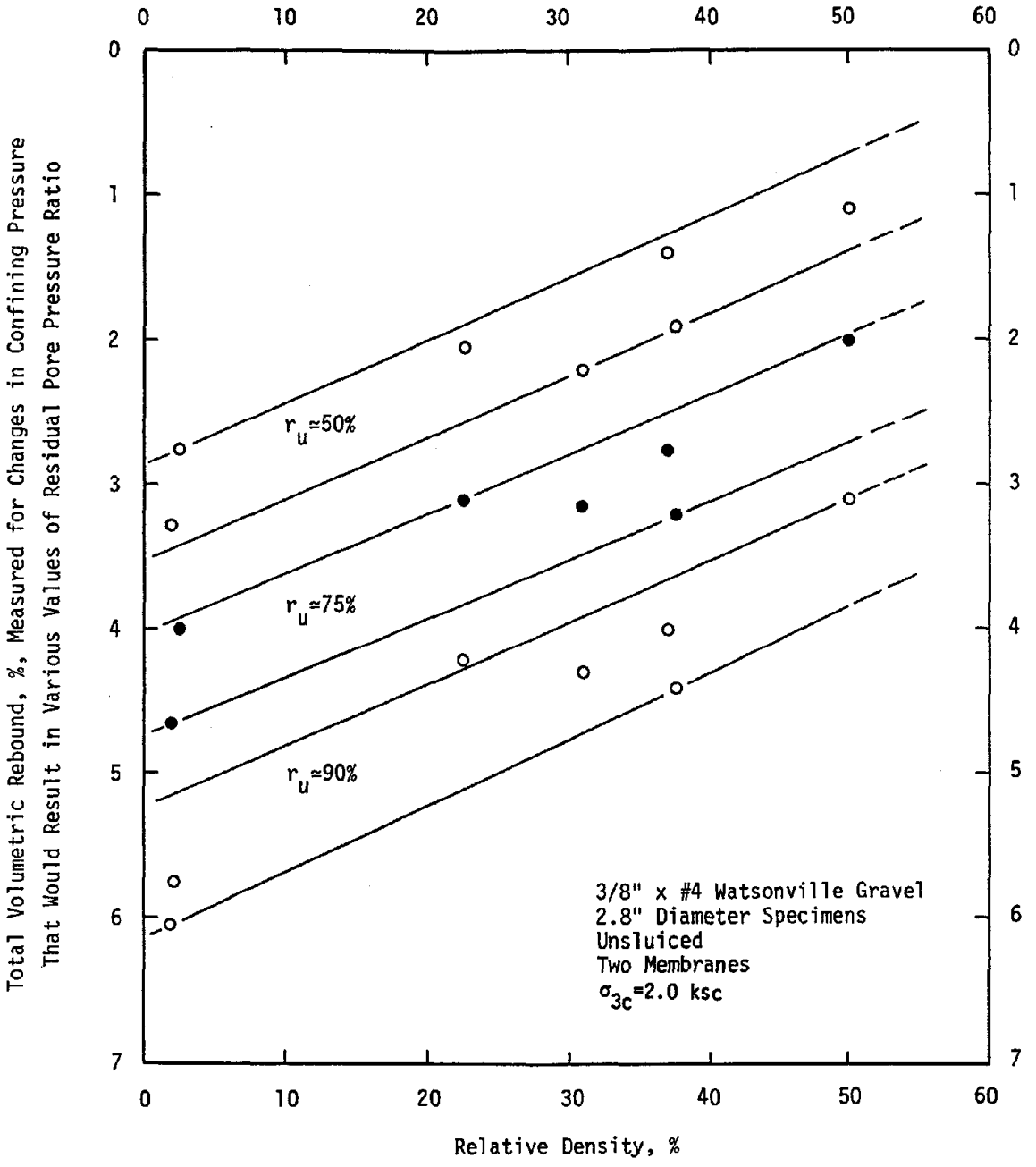

Figure 9.4 Measured Volumetric Rebound for Changes in Confining Pressure That Would Result in Various Values of Pore Pressure Ratio in an Undrained Specimen

confines of the confining membranes; (2) Water migrates from within the specimen voids to zones at the perimeter of the specimen where membrane penetration rebound has occurred; and (3) This water content redistribution results in the gravel particle structure becoming more densely packed so that, by the time failure occurs, the sample density is higher than at the start of the test.

In order to compute the corrected specimen density, data such as that presented in Figure 9.5 is also required. Figure 9.5 shows the residual pore pressure ratio values that developed in unsluiced gravel specimens of various relative densities at 5% double amplitude strain. It may be seen from this figure that the induced residual pore pressures at 5% double amplitude strain decreased with increasing specimen relative density for specimens confined with two membranes.

With the aid of this information, the change in specimen density that occurs due to membrane compliance may be computed as described in the following example:

(1) Assume that a 3/8" x #4 gravel specimen at a relative density of about 43% (93.1 pcf) and confined with two membranes is to be tested.

(2) It may be seen from Figure 9.5 that such specimens would develop about 75% pore pressure ratio at 5% double amplitude strain.

(3) The value of membrane penetration volume change that occurs for $r_u \simeq 75\%$ may then be determined from Figure 9.4. For a specimen at 43% relative density and $r_u \simeq 75\%$, a volumetric strain due to membrane compliance of about 2.75% may be noted.

(4) The gravel is thus expected to densify by 2.75% resulting in a final density of 93.1 pcf x 1.0275 = 95.7 pcf. This corresponds, for

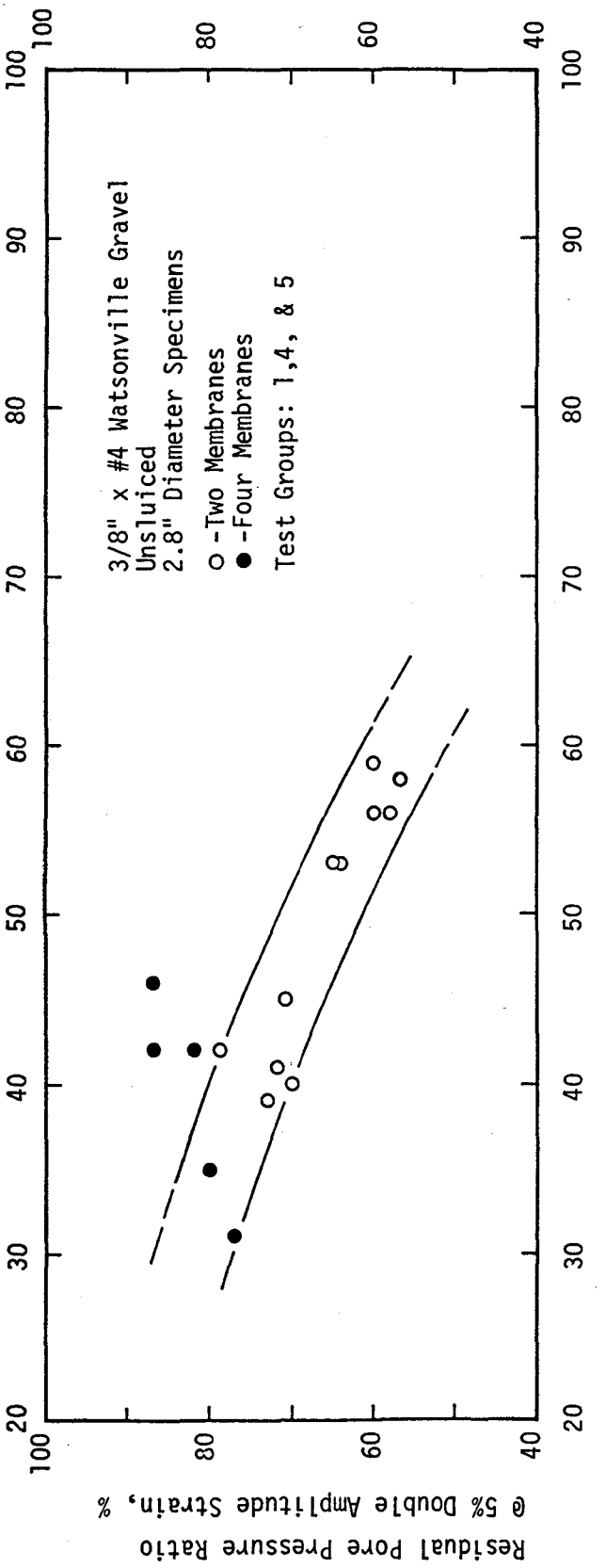

Figure 9.5 Residual Pore Pressure Ratios Developed in Unsluiced Specimens at 5% Peak to Peak Strain

the 3/8" x #4 gravel used in this testing program, to an increased relative density of about 55%.

It was originally considered that volumetric strains due to membrane rebound might be used to account for the effects of membrane compliance in the undrained cyclic triaxial test. By testing a specimen with the appropriate lower initial density, which may be determined from data such as that presented in Figures 9.4 and 9.5, the noncompliant cyclic loading resistance of the resulting higher density specimen may be determined. If this approach were valid, then the unsluiced cyclic loading resistance of the 43% relative density unsluiced gravel specimens, determined in this study, would approximately predict the value of cyclic loading resistance for the sluiced, 58% relative density gravel specimens. It may be seen from Figure 9.6 that the 43% relative density unsluiced (compliant) gravel specimens would overestimate the cyclic loading resistance of the 58% relative density sluiced (noncompliant) gravel specimens. Thus, this approach does not appear to provide a valid method for evaluating the effects of membrane compliance, at least not in its present, simplified form.

There is, however, a considerable amount of information concerning the effects of membrane compliance to be gained from the data presented in the preceding figures. A loose, 25% relative density (89.5 pcf) gravel specimen, for example, may develop a residual pore pressure ratio of up to 90% at failure as shown in Figure 9.5. This value of induced pore pressure ratio translates into a volumetric strain due to membrane penetration rebound and pore water redistribution of about 4.75% as shown in Figure 9.4. Thus, at failure

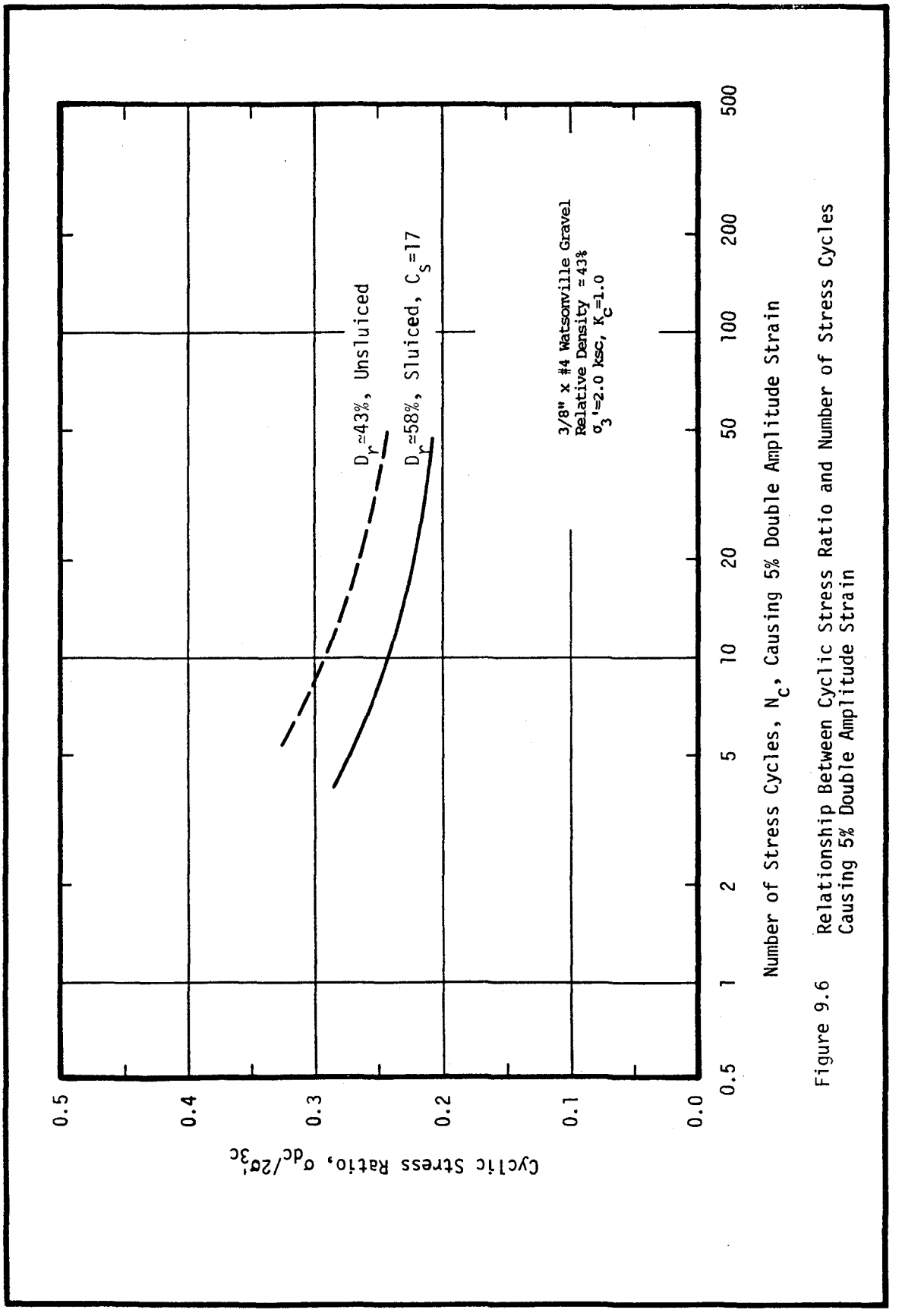

Figure 9.6 Relationship Between Cyclic Stress Ratio and Number of Stress Cycles Causing 5% Double Amplitude Strain

the specimen relative density would have increased from 25% to a value of about 46% (i.e.: 89.5 pcf x 1.0475 = 93.8 pcf). With this extreme amount of specimen densification taking place during testing, it should be readily apparent that the effects of membrane compliance on the cyclic loading resistance of such specimens are considerable and should be taken into account.

The effects of membrane compliance are also shown in Figure 9.5 where it may be seen that unsluiced specimens confined with two membranes, in the range of about 30% to 60% relative density, developed an average residual pore pressure ratio at 5% double amplitude strain that ranged from about 55% to 82%. Over the same range of relative densities, sluiced specimens developed average residual pore pressure ratios of about 90% to 96% as shown in Figure 9.7. Thus, although they were not eliminated, the effects of membrane compliance were reduced considerably by sluicing the gravel specimens with sand.

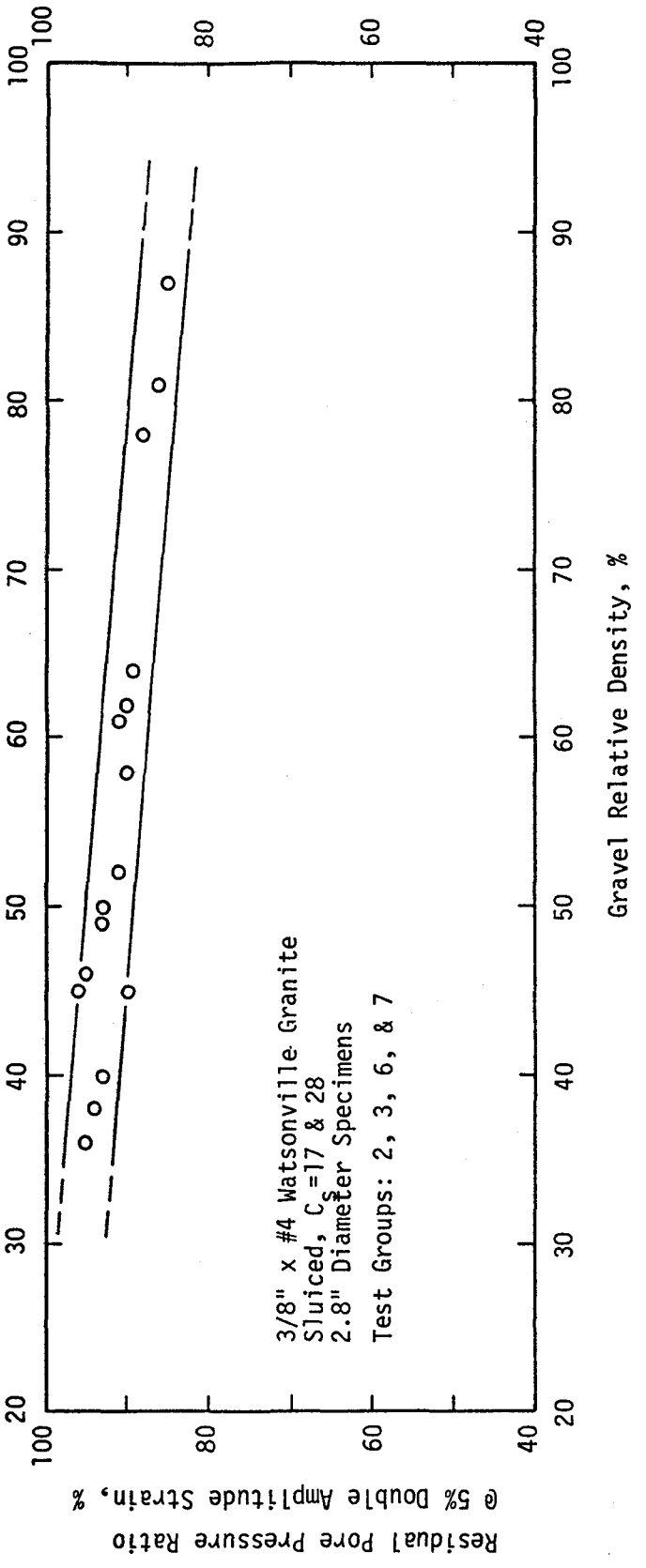

Figure 9.7 Residual Pore Pressure Ratios Developed in Sluiced Specimens at 5% Peak to Peak Strain

CHAPTER 10

SUMMARY AND CONCLUSIONS

Summary of Investigation

Membrane compliance effects can substantially increase the cyclic loading resistance of granular soils, particularly gravels, as determined by the undrained, cyclic triaxial test. However, previous investigations have focused mainly on the effects of membrane compliance on the results of tests performed on sand specimens, while the effects of the phenomenon on gravel specimens have been largely ignored. Clearly, the effects of membrane compliance on the cyclic loading resistance of gravel specimens would be expected to be more significant than the effects for sand specimens since greater membrane penetration volume changes would typically occur during consolidation of the gravel specimens. Several expressions based on these considerations have been developed by previous investigators relating membrane compliance effects to the mean particle diameter of the test material. Such relationships have, in many cases, been assumed to apply to gravel-sized particles, even though the relationships were developed from the results of tests performed on sands. Consequently, it appeared that there was a need to investigate the magnitude of the effect of membrane compliance on the cyclic loading resistance of gravels and to determine if relationships developed from studies performed on sand specimens may be used to accurately account for the effects of membrane compliance in gravel specimens.

In order to investigate the effects of membrane compliance on the results of tests performed on gravel specimens, a comparative study was made between the results of tests performed on gravel specimens tested

in a conventional, compliant system and comparable gravel specimens tested in a specially prepared, noncompliant or low-compliance system. The noncompliant system was achieved by washing sand into the voids of the gravel specimens, thus filling the peripheral specimen voids thereby limiting the amount of membrane penetration that occurred during consolidation. Undrained, cyclic triaxial loading tests were performed on sluiced and unsluiced 2.8 inch and 12 inch diameter specimens composed of three uniformly-graded gravels at various relative densities. These gravels represented the coarsest gradations, having the highest values of D_{50}, that could reasonably be tested in specimens of these diameters. Various sands were used to sluice the gravel specimens resulting in values of sluiceability coefficient, C_s ($D_{10\text{-gravel}}/d_{50\text{-sand}}$), ranging from 17 to 50. Special test conditions were also imposed on several test groups in order to investigate the effects of the conditions on the results of the relationships between the cyclic loading resistance curves and the pore pressure ratio curves for sluiced and unsluiced gravel specimens. The conditions that were investigated included isotropic and anisotropic consolidation, the use of various numbers and thicknesses of confining membranes, and construction of a thin annular sand shell around the outside of the gravel specimens.

Justification for Sluicing Gravel Specimens with Sand

In interpreting the results of this investigation it was considered that the only significant effect of the sluicing sand in the voids of a gravel specimen was to reduce membrane penetration volume changes that occurred during consolidation and thus reduce membrane

compliance effects during undrained, cyclic loading. Arguments and observations supporting such a consideration are outlined below:

(1) If at the start of a cyclic triaxial test there is no significant degree of membrane penetration, then there is no strong reason to believe that any membrane compliance effects could develop during the test.

(2) The gravel skeletal structures were essentially identical for all specimens whether they were sluiced or unsluiced. Both of these specimen groups were constructed in the same manner, the only difference being that the water in the voids of the sluiced specimens was replaced with a loosely deposited sand. Since the loose sand in the voids of the sluiced specimens should have a higher shearing resistance than the water in the voids of the unsluiced specimens, it seems reasonable to believe that the only direct effect of the sand in the voids, if any, would be to increase the strength of the gravel specimen. In this case, the sluicing sand indirectly reduces the cyclic loading resistance of the gravel specimen by reducing membrane compliance effects, and it may directly increase the cyclic loading resistance as described above. However, it was noted that the overall effect of sluicing was to significantly reduce the cyclic loading resistance of the gravel specimens, thus indicating that any contribution of the sand to the cyclic loading resistance of the specimen was likely to be very small.

(3) If the sand did contribute directly to a reduction in the cyclic loading resistance of the sluiced specimens, it is considered that this would be a secondary effect at best. A comparison of the cyclic loading resistances of sluiced specimens at 43%, 58%, and 80%

relative density is shown in Figure 8.14. It may be seen that the cyclic loading resistance curves for both of the higher relative density specimen groups are proportionally higher (based on relative density ratios) than the corresponding curve for the 43% relative density specimens. Thus it appears that the cyclic loading resistance of the sluiced specimens is primarily dependent on the relative density of the gravel skeleton as might be expected. Additionally, the average values of effective dry density of the sand in the voids of these specimens ranged from about 68 pcf for the D_r=80% specimens to 75 pcf for the D_r=43% specimens as shown in Figure 6.8. Thus, if the sluicing sand had an effect on cyclic loading resistance, it would be expected that it would have been greater for the lower relative density specimens and less for the higher relative density specimens, thus tending to make the cyclic loading resistance curves for the three groups of specimens closer together; there is no indication that this did in fact occur.

(4) The cyclic loading resistance of the anisotropically consolidated gravel specimens was not reduced as significantly by sluicing as were the test results for the groups of isotropically consolidated specimens. It may be recalled that the cyclic loading resistances of the sluiced, isotropically consolidated specimens were only about 60% to 65% of the corresponding values for the unsluiced, isotropically consolidated specimens. However, the cyclic loading resistance of the sluiced, anisotropically consolidated specimens was about 85% of the corresponding value for unsluiced, anisotropically consolidated specimens. Thus, the additional contraction of the gravel skeleton during anisotropic consolidation may have moved the gravel

particles into greater contact with the loose sand and it appears that the result was to increase the cyclic loading resistance of the anisotropically consolidated, sluiced gravel specimens.

(5) Skeletal volumetric strains during hydrostatic compression and rebound were found to be essentially identical for both sluiced and unsluiced gravel specimens (see Figure 9.2). Thus, the sluicing sand would seem to have no significant influence on the gravel particle structure at the end of consolidation and at the start of cyclic loading.

(6) The results of this investigation for 2.8 inch diameter specimens indicated similar values of error in cyclic loading resistance due to the effects of membrane compliance as did the earlier, theoretical study conducted by Martin et al. (1978). If it is considered that the potential errors in cyclic loading resistance proposed by Martin et al. are reasonably reliable, then it may again be concluded that the presence of the sluicing sand does not contribute to the reduction in cyclic loading resistance observed in this study, other than by reducing membrane compliance effects.

Despite these arguments, it cannot be conclusively proved that the change in structure of the soil due to sluicing did not have some effect on the cyclic loading resistance of the samples.

Summary of Test Results for 12 Inch Diameter Specimens

The results of tests performed on 12 inch diameter specimens of both the 2" maximum and the 1-1/2" x 3/4" gravels indicated that the cyclic loading resistance of sluiced specimens was only about 65% of that for the unsluiced specimens. The reduction in cyclic loading resistance for the sluiced specimens is considered to be the direct

result of the practical elimination of the effects of membrane compliance. Pore pressure ratios of 100% were developed in sluiced specimens for the same values of cyclic stress ratio and number of stress cycles that caused only about 12% pore pressure ratio to develop in the unsluiced specimens, again indicating that the unsluiced, compliant specimens are much more resistant to undrained cyclic loading due to the effects of membrane compliance. It is considered that the sluiced specimens provide a more accurate assessment of the cyclic loading resistance of the noncompliant, in-situ material. There was no significant difference in these results for gravel specimens having either 22% or 42% relative density, or with the use of thinner, more flexible membranes.

An annular sand shell was constructed around the confining membrane of several sluiced and unsluiced specimens to determine if membrane compliance effects could be reduced by this method. The effect on the cyclic loading resistance of specimens confined with such shells was negligible after an axial load correction was made to account for the strength of the sand shell.

A comparison was also made between the cyclic loading resistance of the sluiced specimens and specimens composed of a very well-graded gravel determined by an earlier investigation, both at the same relative density. These two materials were found to have substantially the same values of cyclic loading resistance. The specimens from both studies had a similar structure and relative density, and membrane compliance effects were negligibly small since the specimens from this study were sluiced and the specimens from the previous study were composed of a very well-graded material. Thus, it was observed that

there is no apparent difference between the cyclic loading resistances of two gravels composed of very different grain size distributions provided that the relative density and structure of the specimens are similar and that membrane compliance effects are taken into account.

Summary of Test Results for 2.8 Inch Diameter Specimens

The cyclic loading resistance of sluiced 2.8 inch diameter specimens of 3/8" x #4 gravel was reduced to between 60% and 75% of the cyclic loading resistance of unsluiced specimens for values of the sluiceability coefficient, C_s, ranging from 17 to 28. It was considered that the cyclic loading resistance of the specimens with the higher value of C_s is more representative of the actual, noncompliant cyclic loading resistance of the gravel in-situ since higher values of C_s result in better sluicing, filling more of the peripheral voids, and thus membrane penetration volume changes are reduced to a negligibly small value. Values of cyclic stress ratio causing only about 12% pore pressure ratio in unsluiced specimens after 10 stress cycles caused 100% pore pressure ratios in the same number of cycles in tests on sluiced specimens, a result very similar to the relationship that was found for tests on 12 inch diameter specimens. The average value of maximum residual pore pressure ratio that was developed in the sluiced specimens was about 95% while the corresponding value developed in tests on unsluiced specimens was only about 73%. These results were observed for isotropically consolidated specimens with relative density values between 43% and 58%, and they were not significantly different for either two or four membrane systems. These results clearly indicate the significance of the effects of membrane compliance on the cyclic loading resistance of gravel specimens.

Comparisons were made between the cyclic loading resistances of (1) sluiced gravel specimens and Monterey No. 0 sand specimens, and (2) sluiced gravel specimens and very well-graded (unsluiced) gravel specimens; the values of cyclic loading resistance were comparable for specimens with similar structure and relative density. Thus, the results of this investigation indicate that there is no apparent difference between the cyclic loading resistances of a sand or a gravel specimen at the same relative density, structure, and stress conditions, provided that membrane compliance effects are eliminated in the gravel specimens.

Relationships between residual pore pressure ratio and normalized number of stress cycles indicated that the sluiced gravel specimens developed pore pressures in a pattern similar to those developed by sand specimens. The unsluiced gravel specimens, on the other hand, appeared to develop higher values of residual pore pressures in the early stages of the test and then show a greatly reduced rate of pore pressure change during the remaining stress cycles of the test. This result is undoubtedly due, in part, to the higher values of cyclic stress ratio that are required to induce failure in the unsluiced (compliant) gravel specimens.

Anisotropically consolidated test specimens were apparently less affected by membrane compliance. The cyclic loading resistance of sluiced, anisotropically consolidated specimens was about 85% of the value determined for comparable unsluiced specimens at 10 stress cycles. However, values of cyclic stress ratio causing 100% pore pressure ratio in the sluiced specimens resulted in only about 12% pore pressure ratio in the unsluiced specimens as observed in tests on

isotropically-consolidated specimens. Thus, this comparison indicates that there is indeed a significant effect of membrane compliance in anisotropically consolidated test specimens.

Conclusions

(1) It appears that sluicing provides a viable means for significantly reducing or eliminating the effects of membrane compliance from the results of undrained, cyclic triaxial tests performed on gravel specimens. Reasonable results may be obtained when a value of sluiceability coefficient, C_s, of about 20 or greater is used.

(2) It was considered that the gravels tested in this study were subjected to the greatest degree of membrane compliance effects that would be expected in specimens of the same diameter because the maximum allowable particle sizes were used and the gravels were very uniformly-graded. Thus, the membrane compliance corrections developed using these materials should be considered to represent upper-bound levels of membrane compliance effects for materials tested under similar conditions. Either finer-grained or more well-graded gravels would be less severely affected by membrane compliance.

(3) The results of this investigation indicate that a reasonably accurate assessment of the noncompliant cyclic loading resistance of the gravels tested in this study may be determined by any of the following methods:

(a) Testing sluiced specimens;

(b) Testing unsluiced specimens and using only 60% to 65% of the value of cyclic loading resistance determined for isotropically consolidated specimens or 80% to 85% of the

cyclic loading resistance determined for anisotropically consolidated specimens; or

(c) Testing unsluiced specimens and using the value of cyclic stress ratio that causes about 12% residual pore pressure ratio to develop in 10 stress cycles.

(4) The relationships between the error in cyclic loading resistance due to membrane compliance effects and mean particle size, D_{50}, presented by Martin et al. (1978) are shown in Figure 10.1 together with the results from the present investigation. The results from the earlier study agree reasonably well with the results from this investigation for 2.8 inch diameter specimens. However, for 12 inch diameter samples, the results from this investigation indicated errors which were about double the correction values presented in the earlier study. Thus, although the theoretical relationships provide an excellent basis for determining membrane compliance effects in 2.8 inch diameter specimens of sand or gravel, the effects are apparently underestimated for 12 inch diameter specimens. The relationship developed in this investigation may be used to assess the error in the cyclic loading resistance caused by membrane compliance effects in 2.8 inch and 12 inch diameter specimens of sand or gravel.

(5) The results of this study may be applied to other gravels if judgment is used to determine the proper value of membrane compliance correction. Membrane penetration volume changes during hydrostatic rebound seem to be the key to determining the severity of the effects of membrane compliance that may occur. Although insufficient testing was performed to verify the following conclusion, it is tentatively suggested that an estimate of the effects of membrane compliance may be

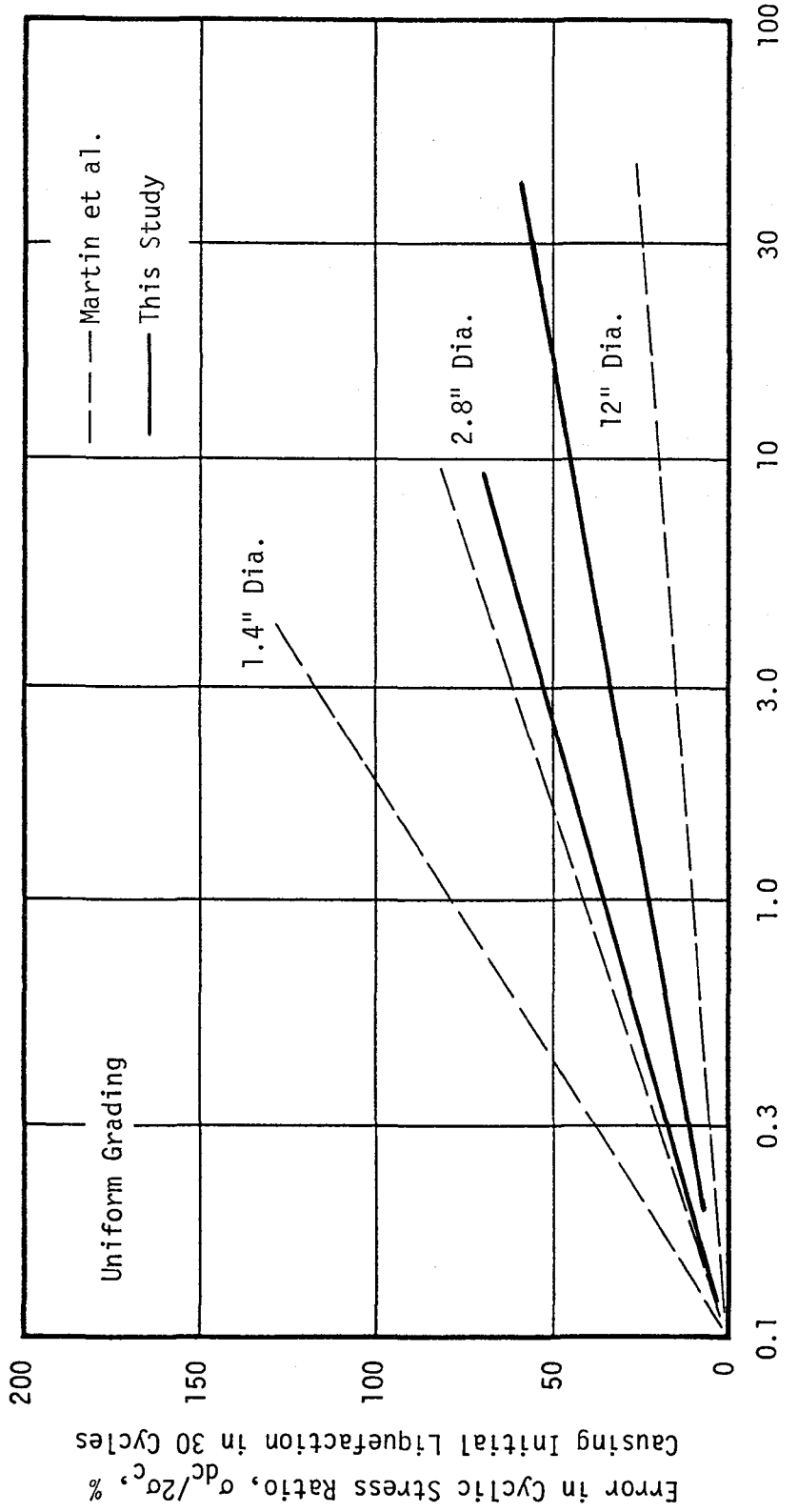

Figure 10.1 Error in Cyclic Stress Ratio Due to Membrane Compliance vs. Mean Grain Diameter for Various Specimen Diameters (after Martin et al., 1978)

determined by comparing membrane penetration volume changes to the values measured in this study and computing a proportional value of membrane compliance correction. For example, if only half of the membrane penetration volume changes recorded in this study were measured, then half of the cyclic loading resistance correction would be used. Further investigation is required to substantiate the use of such relationships.

(6) For a given set of test conditions, the cyclic loading resistance of a well-graded gravel specimen, a uniformly-graded gravel specimen and a sand specimen were all found to be approximately equal, provided that the effects of membrane compliance were eliminated and all of the specimens had the same relative density and structure.

REFERENCES

Abu-Wafa, Taher; Hanna Labib, Aziz (1970) "New Techniques Applied To The Design And Construction of The High Aswan Dam," Proceedings of the Tenth Congress on Large Dams; Montreal, Canada, June, 1970.

Abu-Wafa, Taher; Hanna Labib, Aziz (1971) "Aswan High Dam: Rockfill built under water," Civil Engineering Magazine, ASCE; August, 1971.

Andrus, R.D., Youd, T.L., and Carter, R.R. (1986) "Geotechnical Evaluation of a Liquefaction Induced Lateral Spread, Thousand Springs Valley Idaho," Proceedings of the Twenty-Second Annual Symposium on Engineering Geology and Soils Engineering, Boise, ID, February, 1986.

Baldi, G. and Nova, R. (1983) Membrane Penetration Effects in Triaxial Testing, Istituto Sperimentale Modelli e Strutture S.P.A., Italy, August, 1983.

Banerjee, N. (1979) Measurement of System Compliance, Appendix 2, PhD Dissertation, University of California (U.C.), Berkeley, 1979.

Banerjee, N.G., Seed, H.B., Chan, C.K. (1979) "Cyclic Behavior of Dense Coarse-Grained Materials in Relation to the Seismic Stability of Dams," Earthquake Engineering Research Center (EERC), U.C. Berkeley, Report No. UCB/EERC-79/13, June, 1979.

Becker, E., Chan C.K., and Seed, H.B. (1972) "Strength and Deformation Characteristics of Rockfill Materials in Plain Strain and Triaxial Compression Tests", Report No. TE 72-3, U.C. Berkeley, 1972.

Bowen, Oliver (1986) geologist for Granite Rock Quarry, Personal discussion, July, 1986.

Casagrande, A. (1975) "Liquefaction and Cyclic Deformation of Sands, A Critical Review," Proceedings of the Fifth Pan-American Conference on Soil Mechanics and Foundation Engineering, Buenos Aires, Argentina, 1975

Castro, G. (1969) "Liquefaction of Sands," Harvard Soil Mechanics Series No. 81, Harvard University, Cambridge, Mass.,January, 1969.

Castro, G. (1975) "Liquefaction and Cyclic Mobility of Saturated Sands," Journal of the Geotechnical Engineering Division (JGED), ASCE, Vol. 101, No. GT6, June, 1975.

Chan, C.K. (1972) Membrane for Rockfill Triaxial Testing, Technical Note, Journal of the Soil Mechanics and Foundations Division (JSMFD), ASCE, Volume 98, Number SM8, August 1972.

Chan, C.K. (1978) Unpublished data on girth gage measurements, Personal discussion, September 1985.

Chan, C.K. (1981) "An Electropneumatic Cyclic Loading System," Geotechnical Testing Journal, GTJODJ, Vol. 4, No. 4, Dec., 1981.

Chan, C.K. (1982) Unpublished data on polyurethane coated membranes, Personal discussion, September 1985.

Coulter, H.W., Migliaccio, R.R. (1966) "Effects of the Earthquake of March 27, 1964 at Valdez, Alaska," U.S. Geologic Survey Professional Paper 542-C, U.S. Department of the Interior, 1966.

DeAlba, P., Chan, C.K., and Seed, H.B. (1975) Determination of Soil Liquefaction Characteristics by Large-Scale Laboratory Tests, Chapter IV, Stress Ratio Correction for Compliance, Report Number EERC 75-14, EERC, U.C. Berkeley, 1975.

DeAlba, P., Seed, H.B., and Chan, C.K. (1976) "Sand Liquefaction in Large-Scale Simple Shear Tests," JGED, ASCE, Vol. 102, No. GT9, September, 1976.

Donaghe, R.T., and Townsend, F.C. (1976) "Scalping and Replacement Effects on the Compaction Characteristics of Earth-Rock Mixtures," Soil Specimen Preparation for Laboratory Testing, ASTM STP 599, 1976.

Duncan, J.M. and Seed, H.B. (1967) "Corrections for Strength Test Data," JSMFD, ASCE, No. SM5, September, 1967.

El-Sohby, M. (1964) The Behavior of Particulate Materials Under Stress, PhD Thesis, University of Manchester, Manchester, England, 1964.

El-Sohby, M.A. (1969) "Elastic Behavior of Sand," JSMFD, ASCE, Vol. 95, No. SM6, Proc. Paper 6916, Nov., 1969.

El-Sohby, M.A., and Andrawes, K.Z. (1972) "Deformation Characteristics of Granular Materials Under Hydrostatic Compression," Canadian Geotechnical Journal, Volume 9, June 1972.

Frydman, S., Zeitlen, J.G., and Alpan, I. (1973) The Membrane Effect in Triaxial Testing of Granular Soils, Journal of Testing and Evaluation, Volume 1, 1973.

Harder, L.F., Seed, H.B. (1986) "Determination of Penetration Resistance for Coarse-Grained Soils Using the Becker Hammer Drill," EERC, U.C. Berkeley, Report No. UCB/EERC-86/06, May, 1986.

Hassouna, Mohamed E.; Shenouda, William K.; Nashed, Kamal (1970) "New Technique Of Sluicing Screened Stones With Sand And Loam As Performed In The Aswan High Dam," Proceedings of the Tenth Congress on Large Dams, Montreal, Canada, June, 1970.

High and Aswan Dams Authority (1969) Materials for Engineering Report on Construction, Bulletin No. 9, 1969.

Holtz, W.G., and Gibbs, H.J. (1956) "Triaxial Shear Tests on Pervious Gravelly Soils," JSMFD, ASCE, Vol. 82, No. SM1, January, 1956.

Holubec, I.(1966) The Yielding of Cohesionless Soils, PhD Thesis, University of Waterloo, Toronto, Canada, 1966.

Ishihara, K. (1985) "Stability of Natural Deposits During Earthquakes," Proceedings of the Eleventh International Conference on Soil Mechanics and Foundation Engineering, A.A. Balkema Publishers, Rotterdam, Netherlands, 1985.

Kiekbusch, M., and Schuppener, B. (1977) "Membrane Penetration and its Effect on Pore Pressures," JGED, ASCE, Vol. 103, No. GT11, November, 1977.

Lade, P.V. (1972) "The Stress-Strain and Strength Characteristics of Cohesionless Soils," Ph.D. Dissertation, U.C. Berkeley, California, September, 1972.

Lade, P.V., and Hernandez, S.B. (1977) "Membrane Penetration Effects in Undrained Tests," JGED, ASCE, Volume 103, GT2, February 1977.

Lee, K.L. and Albeisa, A. (1974) "Earthquake Induced Settlements in Saturated Sands," JSMFD, ASCE, Volume 100, No. GT4, April, 1974.

Lee, K. L. and Fitton, J. A., (1969) "Factors Affecting the Dynamic Strength of Soil," Vibration Effects of Earthquakes on Soils and Foundations, ASTM, STP 450, 1969.

Lee, K.L., Seed, H.B. (1967) "Cyclic Stresses Causing Liquefaction of Sand," JSMFD, ASCE, Vol. 93, No. SM1, January, 1967.

Leps, T. (1970) "Review of Shearing Strength of Rockfill," JSMFD, ASCE, Vol. 96, No. SM4, July, 1970.

Leslie, D.D. (1963) "Large Scale Triaxial Tests on Gravelly Soils," Proceedings of the Second Pan-American Conference on Soil Mechanics and Foundation Engineering, Vol. I, 1963.

Li, X.S., Chan, C.K., and Shen, C.K. (1986) "An Automated Triaxial Testing System," Prepared for the ASTM Symposium on Advanced Triaxial Testing of Soil and Rock, Louisville, Kentucky, June, 1986.

Martin, G.R., Finn, W.O.L., and Seed, H.B. (1975) "Fundamentals of Liquefaction under Cyclic Loading," JGED, ASCE, Volume 101, No. GT5, May, 1975.

Martin, G.R., Finn, W.O.L., and Seed, H.B. (1978) "Effects of System Compliance on Liquefaction Tests," JGED, ASCE, Volume 104, GT4, April, 1978.

Mori, K., Seed, H.B., and Chan, C.K. (1977) "Influence of Sample Disturbance on Sand Response to Cyclic Loading," EERC, U.C. Berkeley, Report No. UCB/EERC-77/03, 1977.

Mulilis, J.P., Chan C.K., and Seed, H.B. (1975) "The Effects of Method of Sample Preparation on the Cyclic Stress-Strain Behavior of Sands," EERC, U.C. Berkeley, Report No. UCB/EERC-75/18, 1975.

Mulilis, J.P., Seed, H.B., Chan, C.K., Mitchell, J.K., and Arulanandan, K. (1977) "Effects of Sample Preparation on Sand Liquefaction," JGED, ASCE, Vol. 103, No. GT2, February, 1977.

Newland, P.L., and Allely, B.H. (1957) "Volume Changes During Drained Triaxial Tests on Granular Materials," Geotechnique, Volume 7:17-34, 1957.

Newland, P.L., and Allely, B.H. (1959) "Volume Changes During Undrained Triaxial Tests on Saturated Dilatent Granular Materials," Geotechnique, Volume 9, Number 4, December 1959.

Park, Allen S. (1939) "A Peruvian Dam of Unusual Design;" Compressed Air Magazine, July, 1939.

Peacock, W.H. and Seed, H.B. (1968) "Sand Liquefaction Under Cyclic Loading Simple Shear Conditions," JSMFD, ASCE, Vol. 94, No. SM3, March, 1968.

Pickering, D.J. (1973) "Drained Liquefaction Testing in Simple Shear," JSMFD, ASCE, Volume 99, SM12, December 1973.

Raju, V.S. and Sadasivan, S.K. (1974) "Membrane Penetration in Triaxial Tests on Sand," Technical Note, JGED, ASCE, Volume 100, GT4, April 1974.

Raju, V.S., and Venkataramana, K. (1980) "Undrained Triaxial Tests to Assess Liquefaction Potential of Sands - Effect of Membrane Penetration," Proceedings of the International Symposium on Soils Under Cyclic and Transient Loading, Volume 2, Pande and Zienkiewicz, editors, A. A. Balkema, January 1980.

Ramana, K.V., and Raju, V.S. (1981) "Constant-Volume Triaxial Tests to Study the Effects of Membrane Penetration," ASTM Geotechnical Journal, Volume 4, Number 3, September 1981.

Ramana, K.V., and Raju, V.S. (1982) "Membrane Penetration in Triaxial Tests," Technical Note, JGED, ASCE, Volume 108, GT2, February 1982.

Roscoe, K.H., Schofield, A.N., and Thurairajah, A. (1963) "A Critical Review of Test Data for Selecting a Yield Criterion for Soils," Cambridge University, England, advanced copy, Laboratory Shear Testing of Soils Symposium, ASTM, Ottawa, Canada, September 1963.

Seed, H.B. (1979) "Soil Liquefaction and Cyclic Mobility Evaluation for Level Ground During Earthquakes," JGED, ASCE, Vol. 105, No. GT2, Proceedings Paper 14380, February, 1979.

Seed, H.B., Arango, I., and Chan, C.K. (1975) "Evaluation of Soil Liquefaction Potential during Earthquakes," EERC, U.C. Berkeley, Report No. UCB/EERC-75/28, 1975.

Seed, H.B., and Idriss, I.M. (1971) "Simplified Procedure for Evaluating Soil Liquefaction Potential," JSMFD, ASCE, Vol. 97, No. SM9, September, 1971.

Seed, H.B., and Idriss, I.M. (1982) "Ground motions and soil Liquefaction During Earthquakes," monograph series, Earthquake Engineering Research Institute, Berkeley, California, 1982.

Seed, H.B., Idriss, I.M., and Arango, I. (1983) "Evaluation of Liquefaction Potential Using Field Performance Data," JGED, ASCE, Vol. 109, No. GT3, March, 1983.

Seed, H.B., Lee, K.L. (1966) "Liquefaction of Saturated Sand During Cyclic Loading," JSMFD, ASCE, Vol. 92, No. SM6, Proceedings Paper 4972, November, 1966.

Seed, H.B., Martin, P.P., and Lysmer, J. (1976) "Pore Water Pressure Changes During Soil Liquefaction," JGED, ASCE, Vol. 102, No. GT4, April, 1976.

Seed, H.B., Mori, K., and Chan, C.K. (1977) "Influence of Seismic History on Liquefaction of Sands," JGED, ASCE, Vol. 102, No. GT4, April, 1977.

Seed, H.B., Peacock, W.H. (1971) "Test Procedures for Measuring Soil Liquefaction Characteristics," JSMFD, ASCE, Vol. 97, No. SM8, August, 1971.

Seed, H.B., Tokimatsu, K., Harder, L.F., and Chung, R.M. (1984) "The Influence of SPT Procedures in Soil Liquefaction Resistance Evaluations," EERC, U.C. Berkeley, Report No. UCB/EERC-84/15, October, 1984.

Siddiqi, F.H., "Strength Evaluation of Cohesionless Soils with Oversize Particles," Ph. D. Dissertation, U.C. Davis, November, 1984.

Singh, S., Seed, H.B., and Chan, C.K. (1982) "Undisturbed Sampling of Saturated Sands by Freezing," JGED, ASCE, Vol. 108, No. GT2, February, 1982.

Singh, S., Seed, H.B., and Chan, C.K. (1979) "Undisturbed Sampling and Cyclic Load Testing of Sands," EERC, U.C. Berkeley, Report No. UCB/EERC-79/33, December, 1979.

Steinbach, J. (1967) "Volume Change Due to Membrane Penetration in Triaxial Tests on Granular Material," MS Thesis, Cornell University, 1967.

Tamura, C., Lin, G. (1983) "Damage to Dams During Earthquakes in China and Japan," from "Report of Japan-China Cooperative Research on Engineering Lessons from Recent Chinese Earthquakes Including the 1976 Tangshan Earthquake (Part I)", Edited by Tamura, C., Katayama, T., and Tatsuoka, F., University of Tokyo, November, 1983.

Torres, L.P. (1983) "Membrane Penetration in Cyclic Triaxial Test," Unpublished report, CE299, U.C. Berkeley, December 1983.

Vaid, Y.P., and Negussey, D. (1984) "A Critical Assessment of Membrane Penetration in the Triaxial Test," Geotechnical Testing Journal, Volume 7, Number 2, June 1984.

Wang, W. (1984) "Earthquake Damages to Earth Dams and Levees in Relation to Soil Liquefaction," Proceedings of the International Conference on Case Histories on Geotechnical Engineering, 1984.

Wong, R.T. (1971) "Deformation Characteristics of Gravels and Gravelly Soils Under Cyclic Loading Conditions," Ph.D Thesis, University of California, Berkeley, 1971.

Wong, R.T., Seed, H.B., and Chan, C.K. (1974) "Liquefaction of Gravelly Soils under Cyclic Loading Conditions," EERC, U.C. Berkeley, Report No. UCB/EERC-74/11, June, 1974.

Wong, R., Seed, H.B., and Chan, C.K. (1975) "Cyclic Loading Liquefaction of Gravelly Soils," JGED, ASCE, Volume 101, GT6, June 1975.

Wu, H.C., and Chang, G.S. (1982) "Stress Analysis of Dummy Rod Method for Sand Specimens," JGED, ASCE, Volume 108, GT9, September 1982.

Yoshimi, Y., and Tokimatsu, K. (1983) "SPT Practice Survey and Comparative Tests," Soils and Foundations, Vol. 23, No. 3, September, 1983.

Youd, T.L., Harp, E.L., Keefer, D.K., and Wilson, R.C. (1985) "The Borah Peak, Idaho Earthquake of October 28, 1983 - Liquefaction," Earthquake Spectra, Earthquake Engineering Research Institute, Vol. 2, No. 1, November, 1985.

APPENDIX A

RESULTS OF TRIAXIAL TESTS PERFORMED ON MONTEREY NO. 0 SAND SPECIMENS

Test Data Presentation

Three groups of tests were performed on specimens of Monterey No. 0 Sand. One group of tests was performed on 12 inch diameter specimens at a relative density of about 35%. The other two groups were performed on 2.8 inch diameter specimens at relative densities of about 37% and 49%. All test specimens were constructed by pluviation and were isotropically consolidated under an effective confining pressure of 2.0 ksc. Test data for the three groups are presented in Tables A.1 through A.3 and the relevant test data is shown in Figure A.1.1 through A.3.4.

Data Analyses

A comparison of the cyclic loading resistances of specimens of Monterey No. 0 sand at a relative density of about 36% for 2.8 inch diameter and 12 inch diameter test specimens is shown in Figure A.1 (on page following the test data). It may be noted that the cyclic loading resistances of the specimens for both sample sizes are in good agreement, indicating that specimen diameter does not significantly influence cyclic test results for this material. Wong et al. (1974) performed a similar study on specimens of Monterey No. 0 sand and found that the cyclic loading resistance of the 2.8 inch diameter specimens was about 10% higher than that for the 12 inch diameter specimens. These investigators concluded that the difference was due mainly to the effects of membrane compliance in the smaller diameter test specimens.

Table A.1 Material Properties and Test Conditions Causing Failure During Undrained Cyclic Loading

SAND: Monterey No.0

Test No.	Sand			
	Dry Density (pcf)	Void Ratio	Porosity	Relative Density (%)
16	96.3	0.718	0.418	43.1
17	94.5	0.751	0.429	33.1
18	95.2	0.738	0.425	37.0
19	94.9	0.743	0.426	35.3

Test No.	Cyclic Stress Ratio, $\sigma_d/2\sigma_{3c}$	Number of Cycles Causing...				
		80% Pore Pressure Ratio	100% Pore Pressure Ratio	2% Peak to Peak Strain	5% Peak to Peak Strain	10% Peak to Peak Strain
16	0.160	-	99	98	99	101
17	0.170	-	2.0	1.4	1.7	2.1
18	0.160	-	2.1	2.2	2.5	3.2
19	0.120	-	46	46	47	47

* - All test specimens are 12" diameter, pluviated through water, one 0.1" membrane, $\sigma_3' = 2.0$ ksc, and $K_c=1$. Results corrected for membrane load.

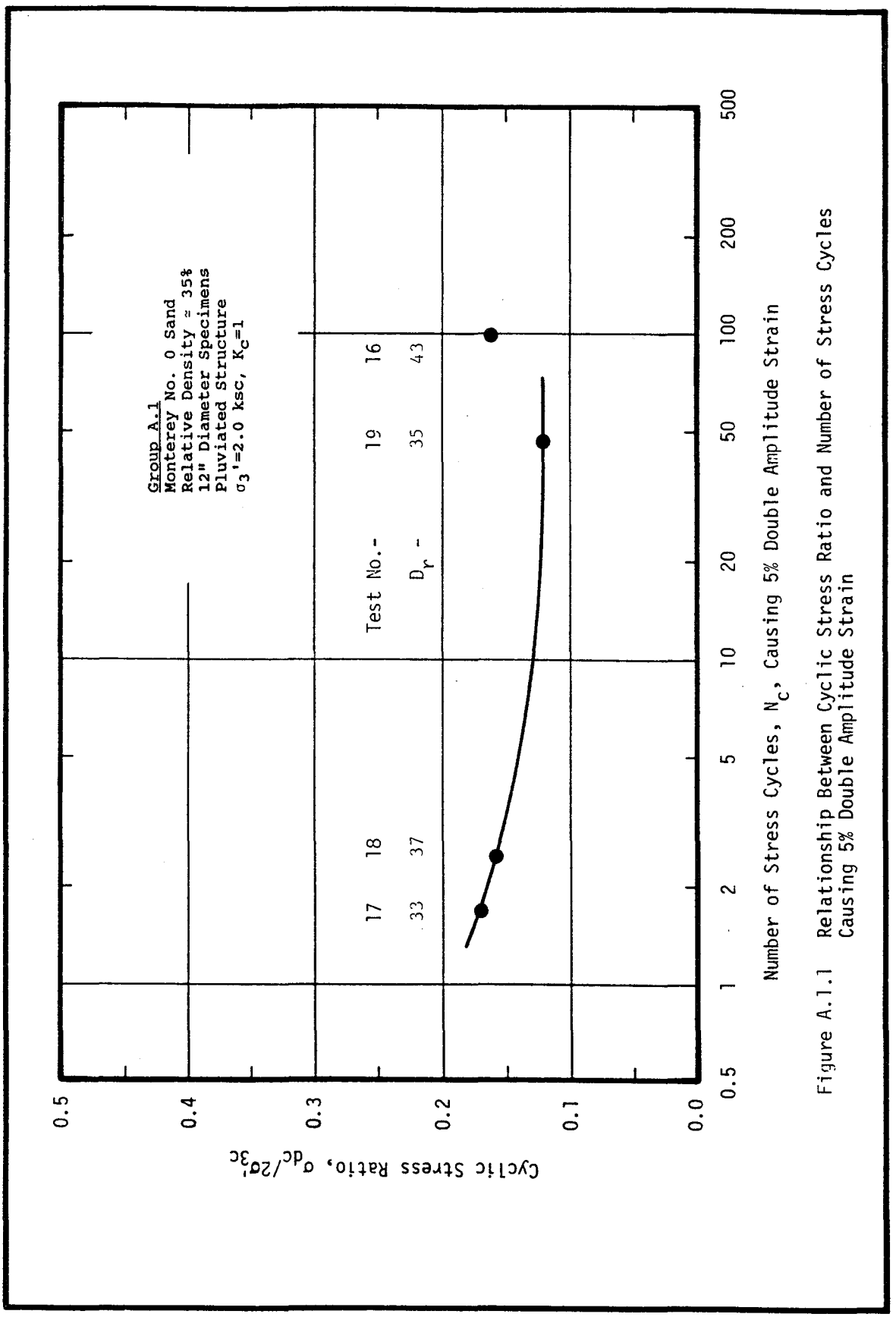

Figure A.1.1 Relationship Between Cyclic Stress Ratio and Number of Stress Cycles Causing 5% Double Amplitude Strain

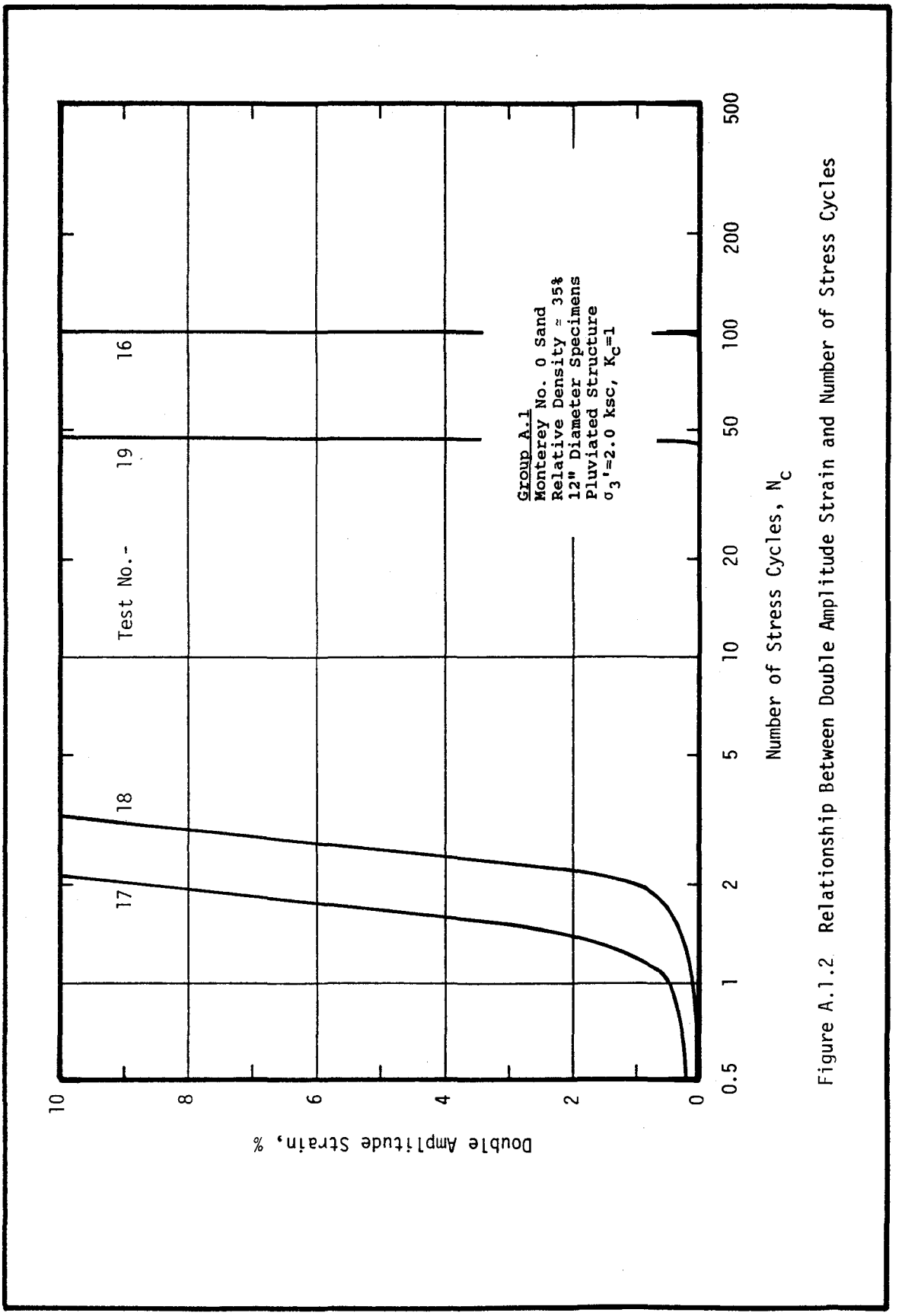

Figure A.1.2 Relationship Between Double Amplitude Strain and Number of Stress Cycles

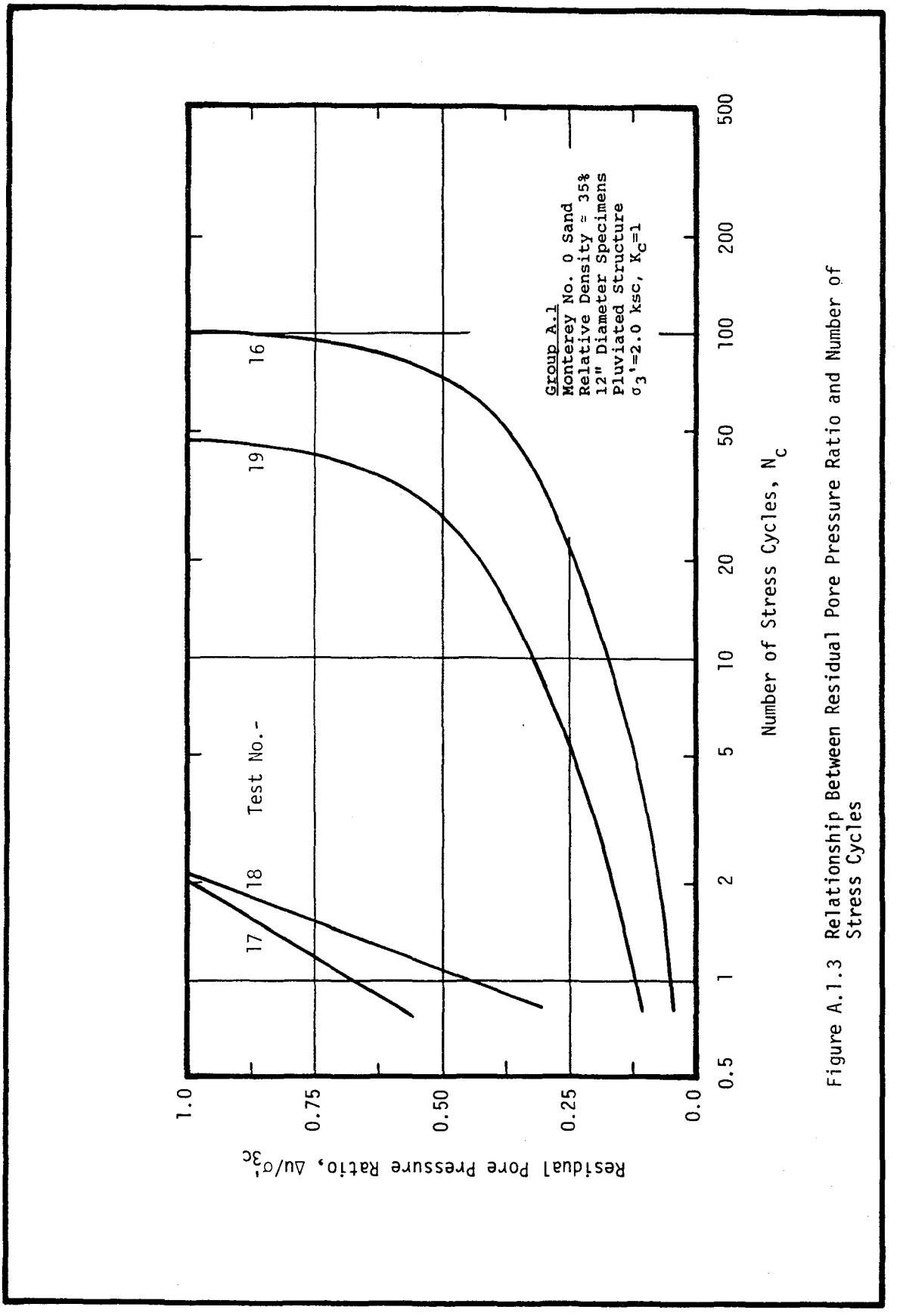

Figure A.1.3 Relationship Between Residual Pore Pressure Ratio and Number of Stress Cycles

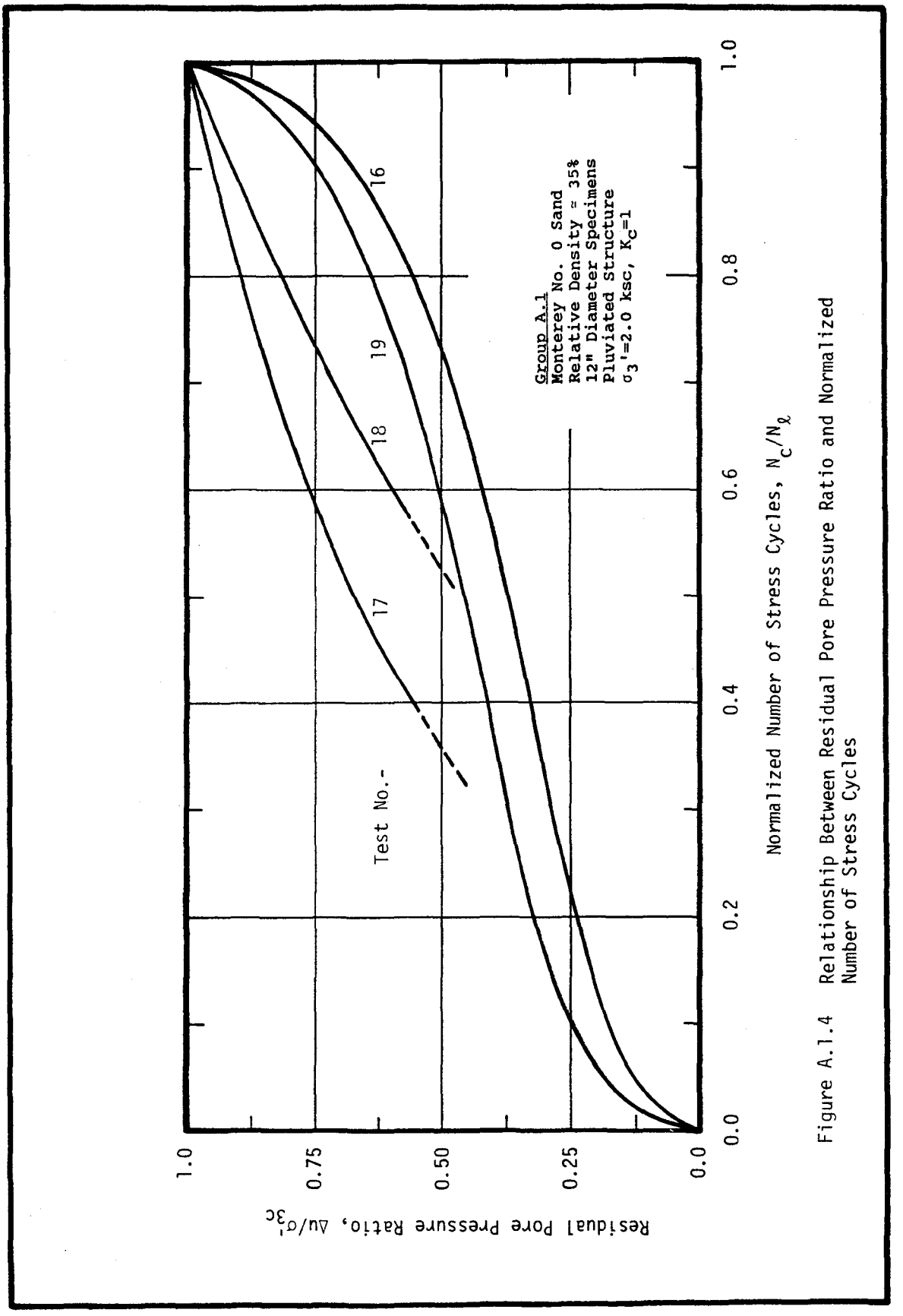

Figure A.1.4 Relationship Between Residual Pore Pressure Ratio and Normalized Number of Stress Cycles

Table A.2 Material Properties and Test Conditions Causing Failure During Undrained Cyclic Loading

SAND: Monterey No.0

Test No.	Sand: Dry Density (pcf)	Void Ratio	Porosity	Relative Density (%)
20	95.3	0.736	0.424	37.6
21	94.9	0.743	0.426	35.3
22	94.7	0.747	0.427	34.2
23	95.0	0.742	0.426	35.9
24	95.0	0.742	0.426	35.9
25	95.4	0.735	0.423	38.1
26	95.5	0.733	0.423	38.7
30	95.7	0.730	0.421	39.8

Test No.	Cyclic Stress Ratio, $\sigma_d/2\sigma_{3c}$	Number of Cycles Causing... 80% Pore Pressure Ratio	100% Pore Pressure Ratio	2% Peak to Peak Strain	5% Peak to Peak Strain	10% Peak to Peak Strain
20	0.156	-	6.0	5.2	5.8	6.3
21	0.128	-	48	45	46	47
22	0.134	-	35	33	34	34
23	0.144	-	4.0	3.3	3.6	4.0
24	0.140	-	50	47	48	49
25	0.140	-	5	4.5	4.7	4.9
26	0.213	-	1.0	0.5	0.7	0.9
30	0.207	-	1.0	0.2	0.5	0.9

* - All test specimens are 2.8" diameter, pluviated through water, one thin membrane, $\sigma_3' = 2.0$ ksc, and $K_c=1$.

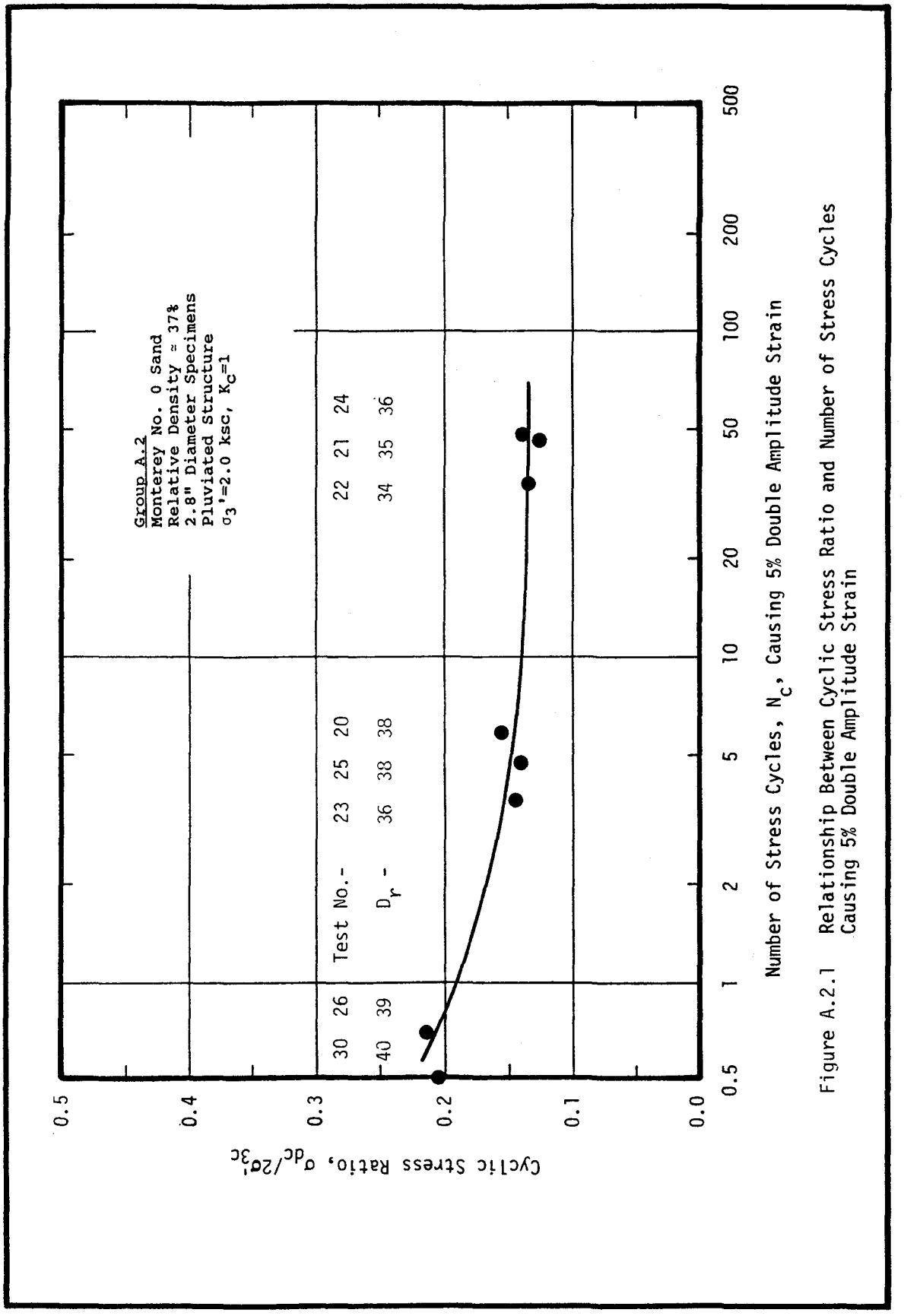

Figure A.2.1 Relationship Between Cyclic Stress Ratio and Number of Stress Cycles Causing 5% Double Amplitude Strain

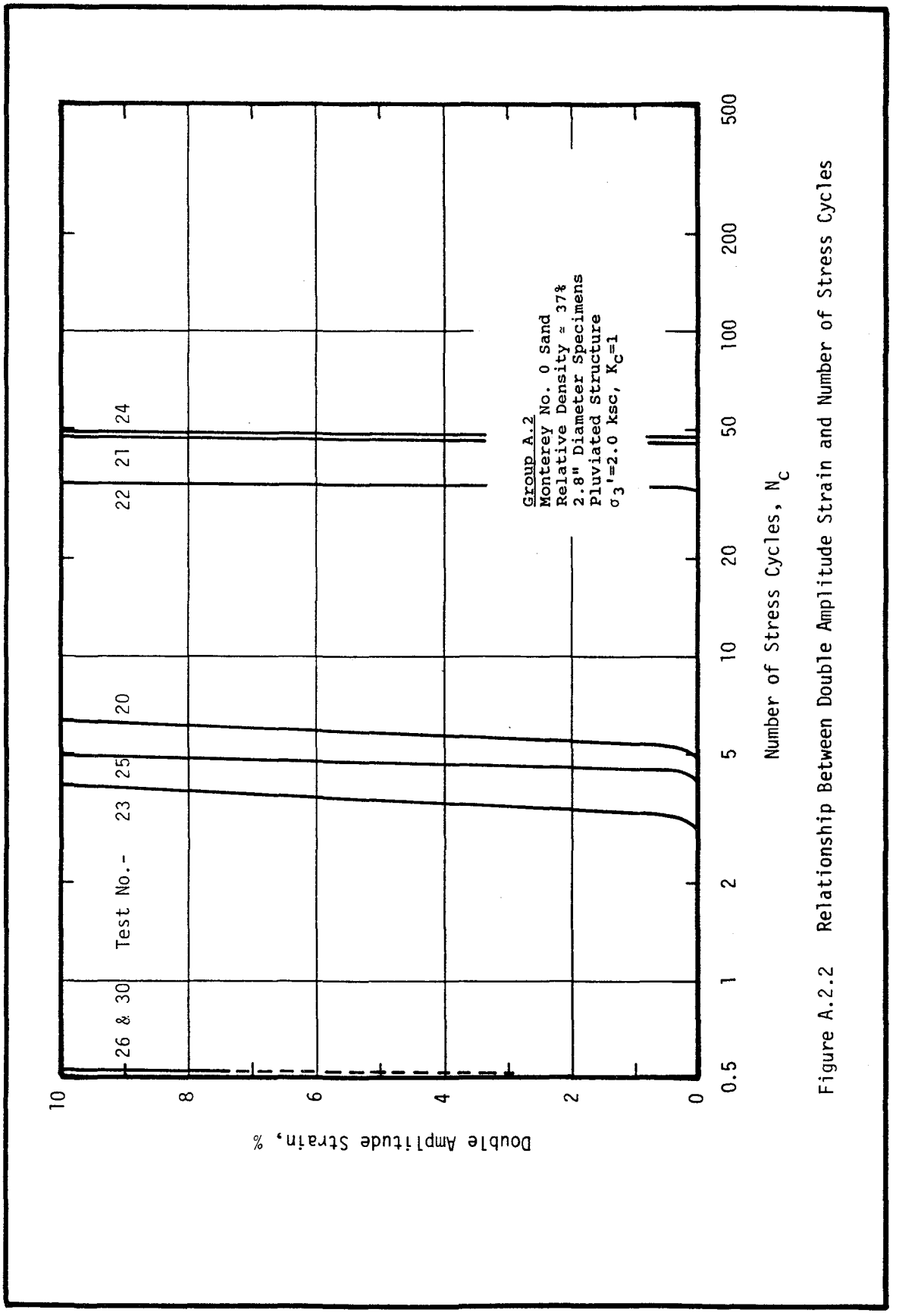

Figure A.2.2 Relationship Between Double Amplitude Strain and Number of Stress Cycles

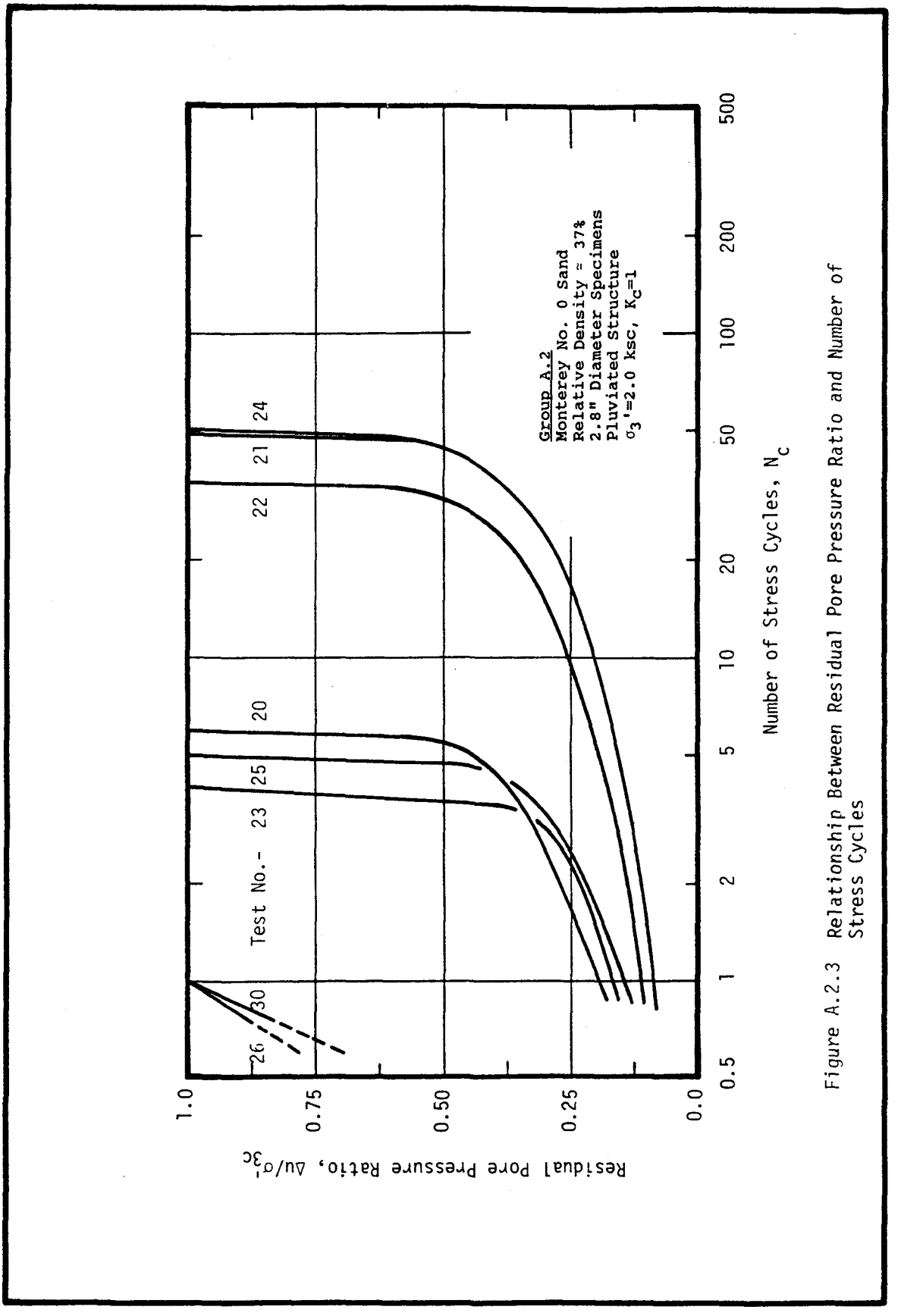

Figure A.2.3 Relationship Between Residual Pore Pressure Ratio and Number of Stress Cycles

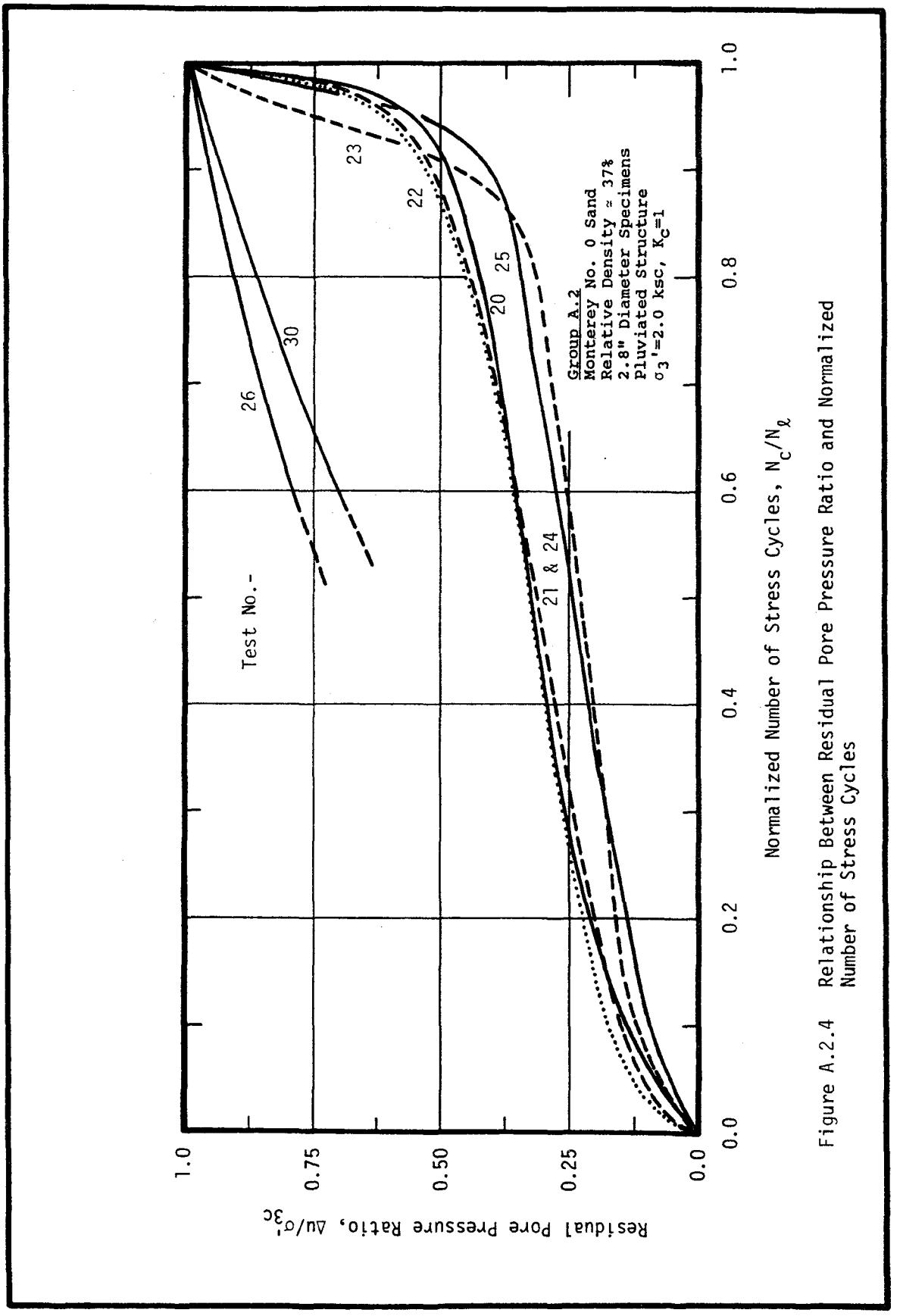

Figure A.2.4 Relationship Between Residual Pore Pressure Ratio and Normalized Number of Stress Cycles

Table A.3 Material Properties and Test Conditions Causing Failure During Undrained Cyclic Loading

SAND: Monterey No.0

Test No.	Sand			
	Dry Density (pcf)	Void Ratio	Porosity	Relative Density (%)
27	97.6	0.695	0.410	50.0
28	97.5	0.697	0.411	49.6
29	97.2	0.702	0.412	48.0

Test No.	Cyclic Stress Ratio, $\sigma_d/2\sigma_{3c}$	Number of Cycles Causing...				
		80% Pore	100% Pressure Ratio	2% Peak to	5% Peak	10% Strain
27	0.213	-	6.0	5.8	6.2	7.0
28	0.188	-	4.0	3.6	4.0	4.8
29	0.185	-	23.0	23.0	23.0	24.0

* - All test specimens are 2.8" diameter, pluviated through water, one thin membrane, $\sigma_3' = 2.0$ ksc, and $K_c = 1$.

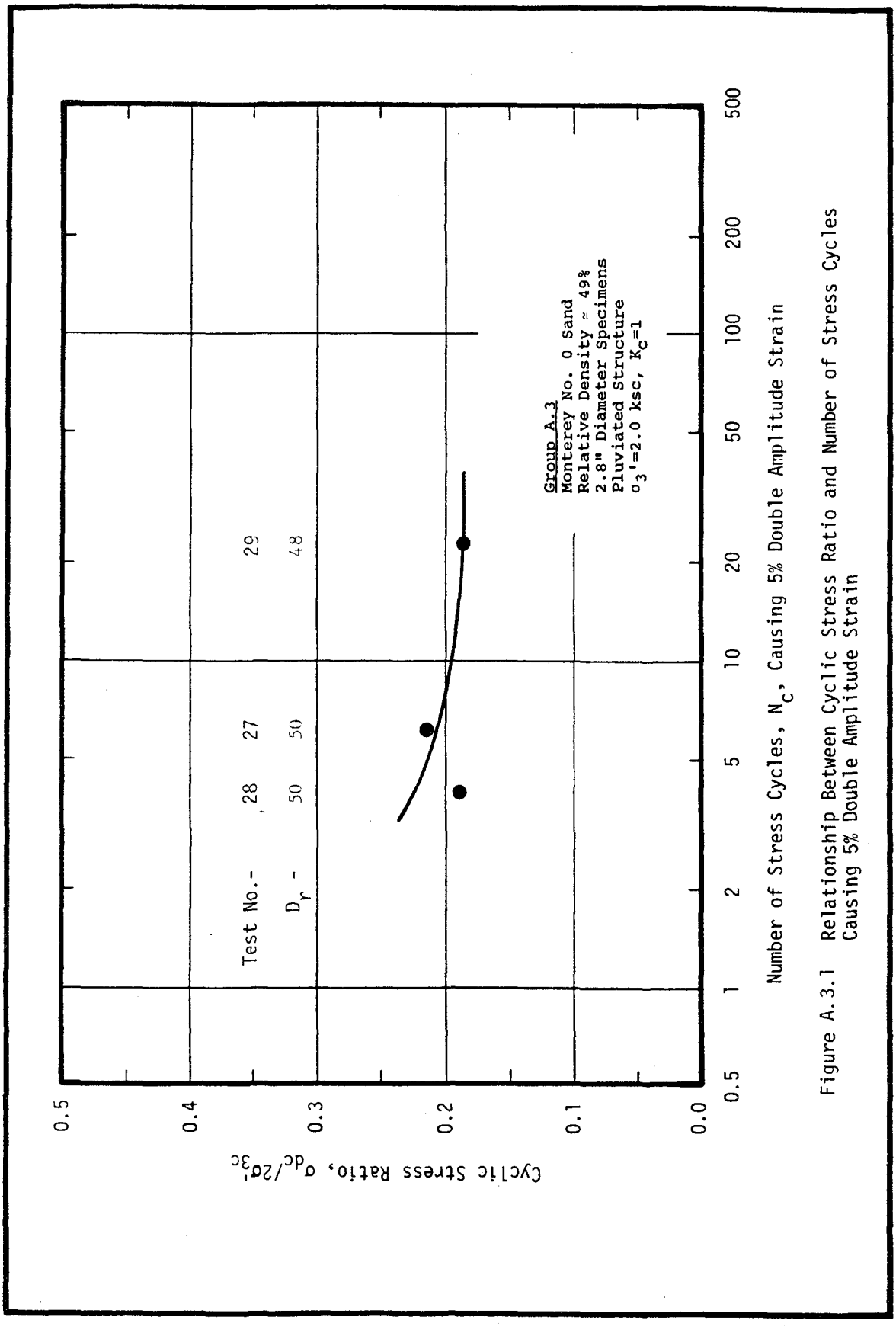

Figure A.3.1 Relationship Between Cyclic Stress Ratio and Number of Stress Cycles Causing 5% Double Amplitude Strain

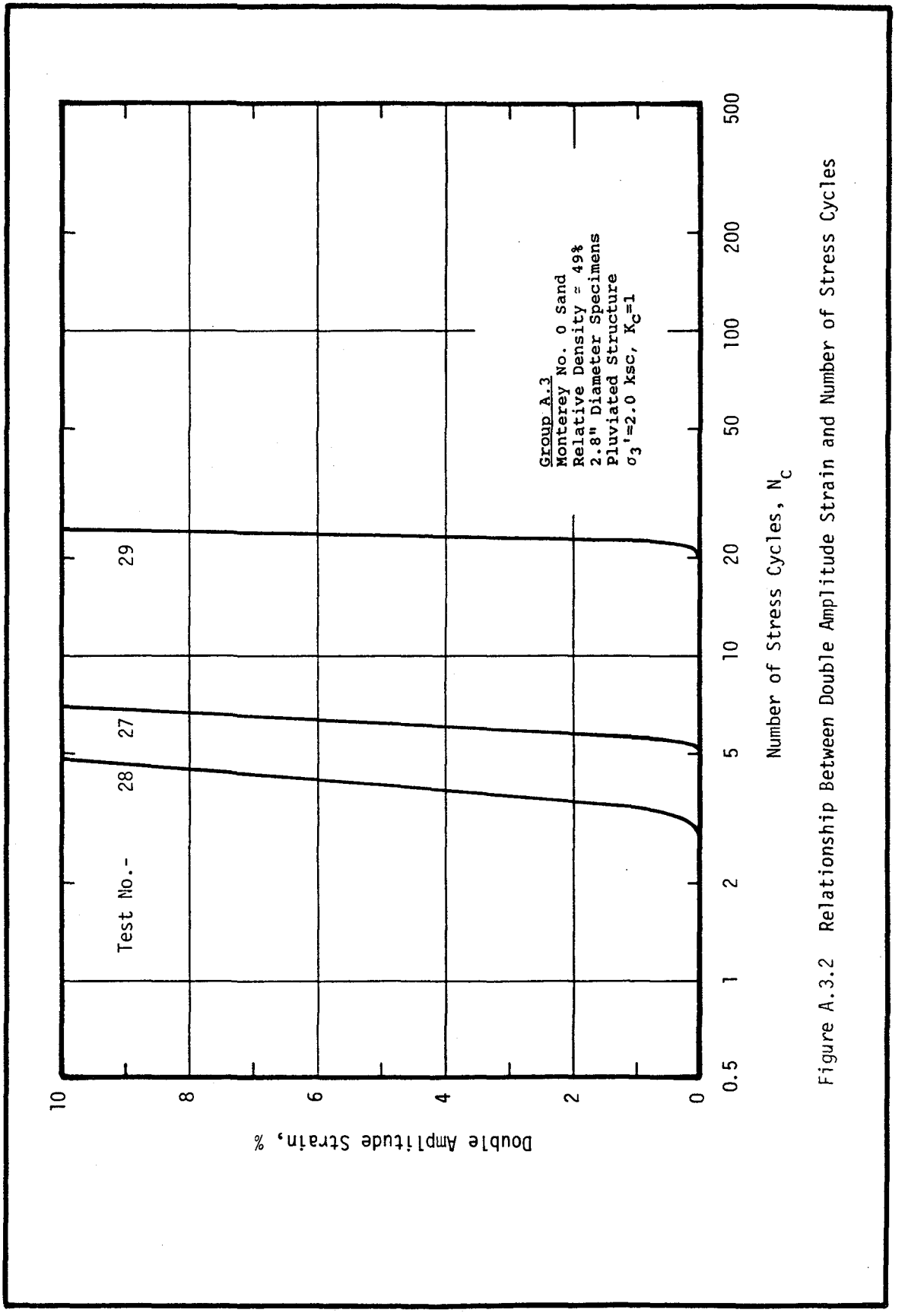

Figure A.3.2 Relationship Between Double Amplitude Strain and Number of Stress Cycles

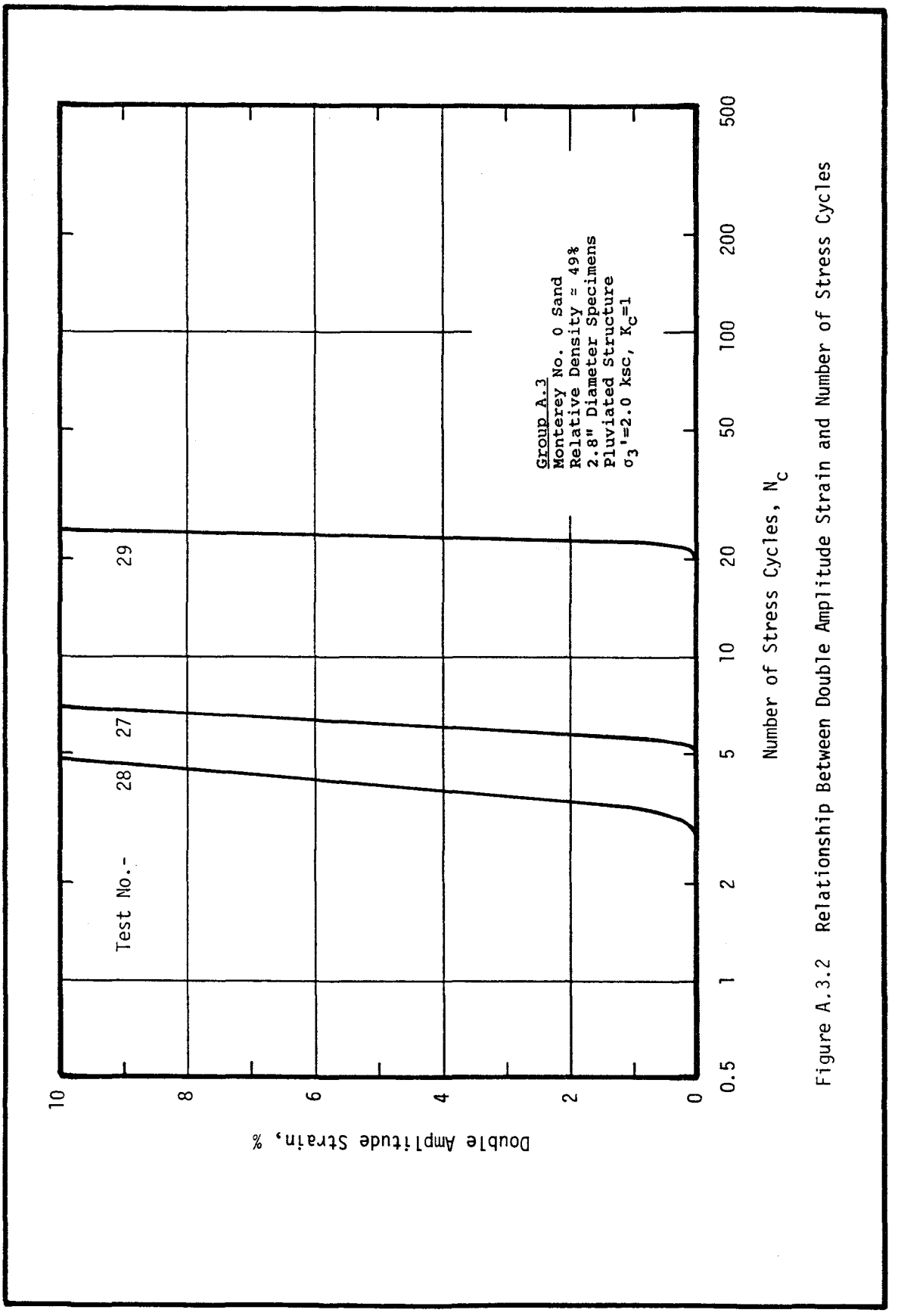

Figure A.3.2 Relationship Between Double Amplitude Strain and Number of Stress Cycles

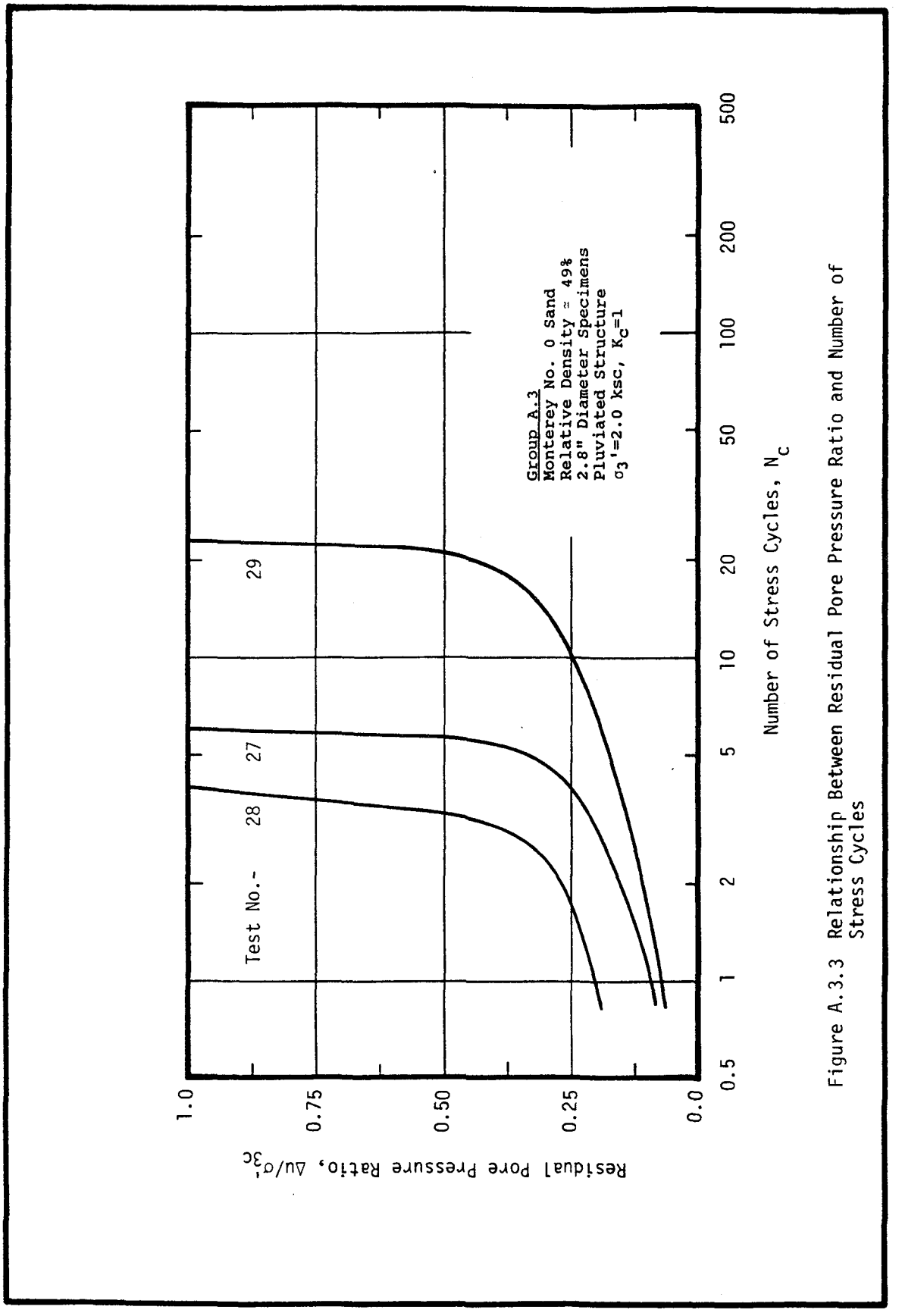

Figure A.3.3 Relationship Between Residual Pore Pressure Ratio and Number of Stress Cycles

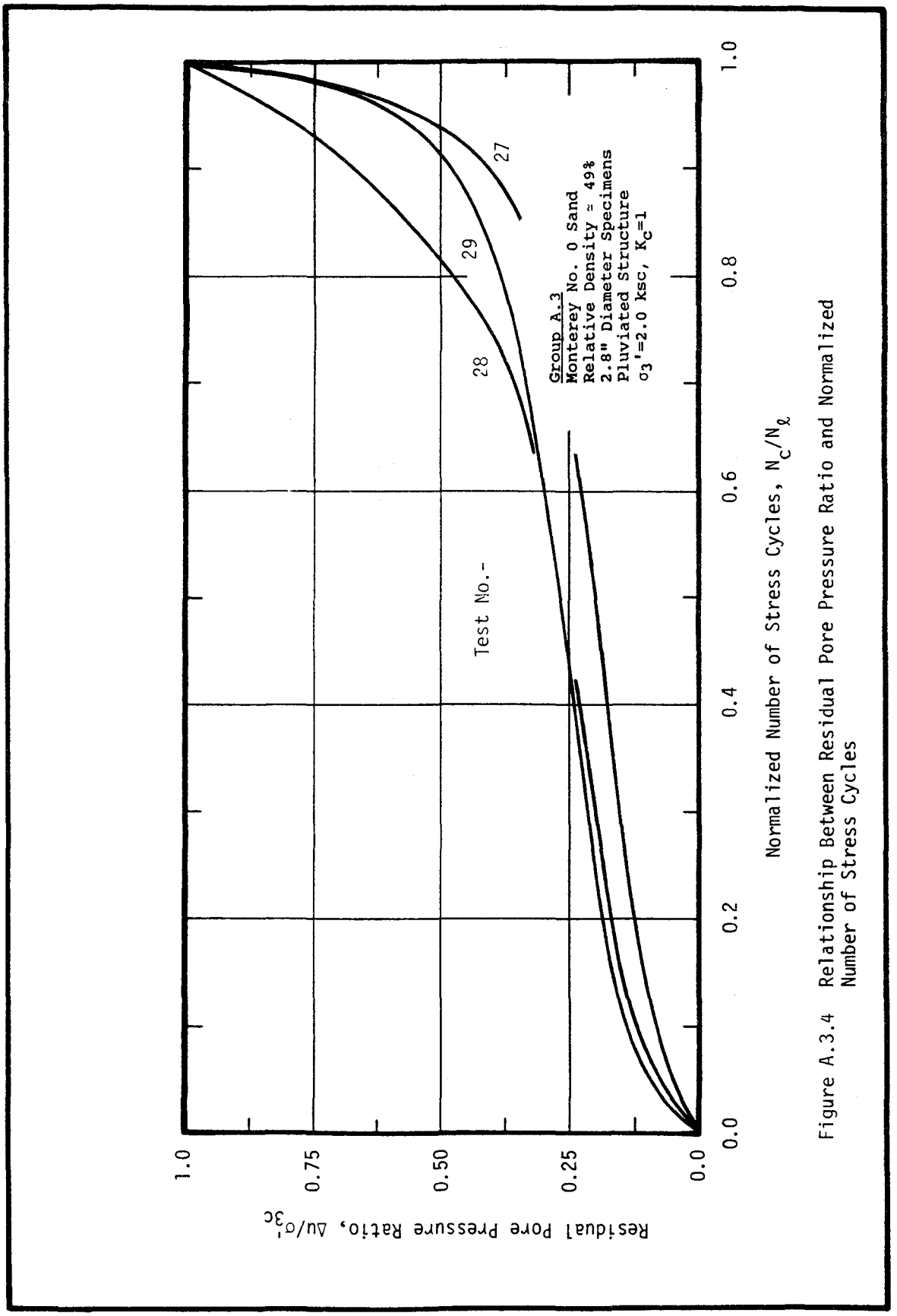

Figure A.3.4 Relationship Between Residual Pore Pressure Ratio and Normalized Number of Stress Cycles

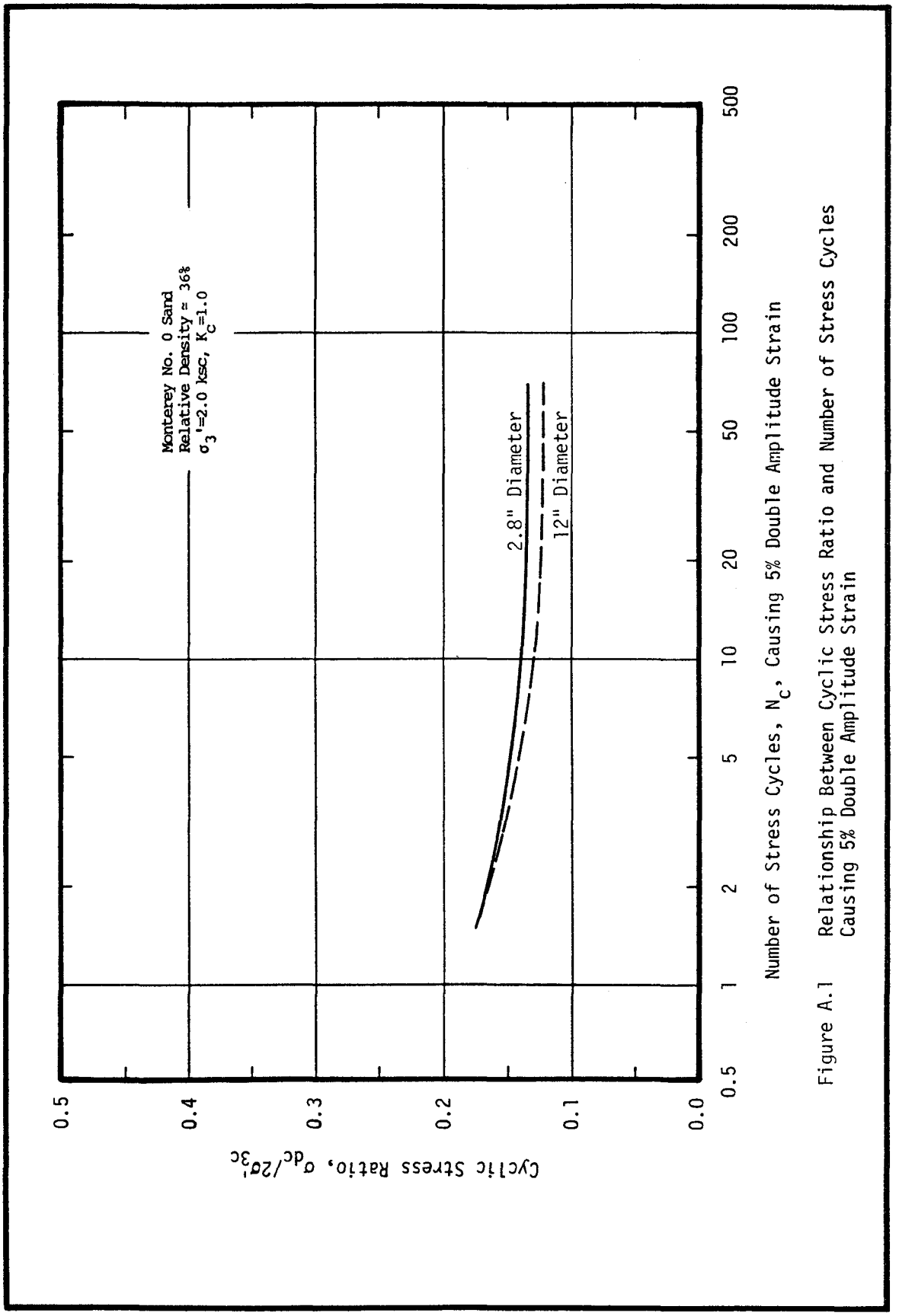

Figure A.1 Relationship Between Cyclic Stress Ratio and Number of Stress Cycles Causing 5% Double Amplitude Strain

Thus, it was considered that specimen size would not significantly affect the cyclic loading resistance of the gravels tested in this study, once the effects of membrane compliance were accounted for.

A comparison of the cyclic loading resistance of the two 2.8 inch diameter specimen groups at relative densities of 37% and 49% is shown in Figure A.2. It may be noted that the cyclic loading resistance of the 49% relative density specimen is about (49/37) or 1.32 times greater than the cyclic loading resistance of the 37% relative density specimens. Such relationships have been shown to exist for sands by other investigators (DeAlba, 1975) and it was considered that these relationships would also apply to the gravels tested in this study.

Figure A.3 shows the relationship relating residual pore pressure ratio to normalized number of stress cycles for 2.8 inch diameter and 12 inch diameter specimens. It may be noted that the smaller diameter test specimens develop excess pore pressures much more rapidly toward the end of the test than did the 12 inch diameter specimens. This probably occurred as a result of differences in the loading systems. The 12 inch diameter specimens were cyclically loaded at a rate of 1 cycle per minute while the 2.8 inch diameter specimens were cyclically loaded at a rate of 1 cycle per second. Although it has been shown that such differences in loading rates do not significantly affect the number of stress cycles required to cause 100% pore pressure or 2% to 10% double amplitude strain (Peacock and Seed, 1968; Lee and Fitton, 1969; Wong et al., 1974)), it might nevertheless account for the differences in the relationships shown in Figure A.3.

Figures A.4, A.5, and A.6 show similar relationships between residual pore pressure ratio and normalized number of stress cycles for

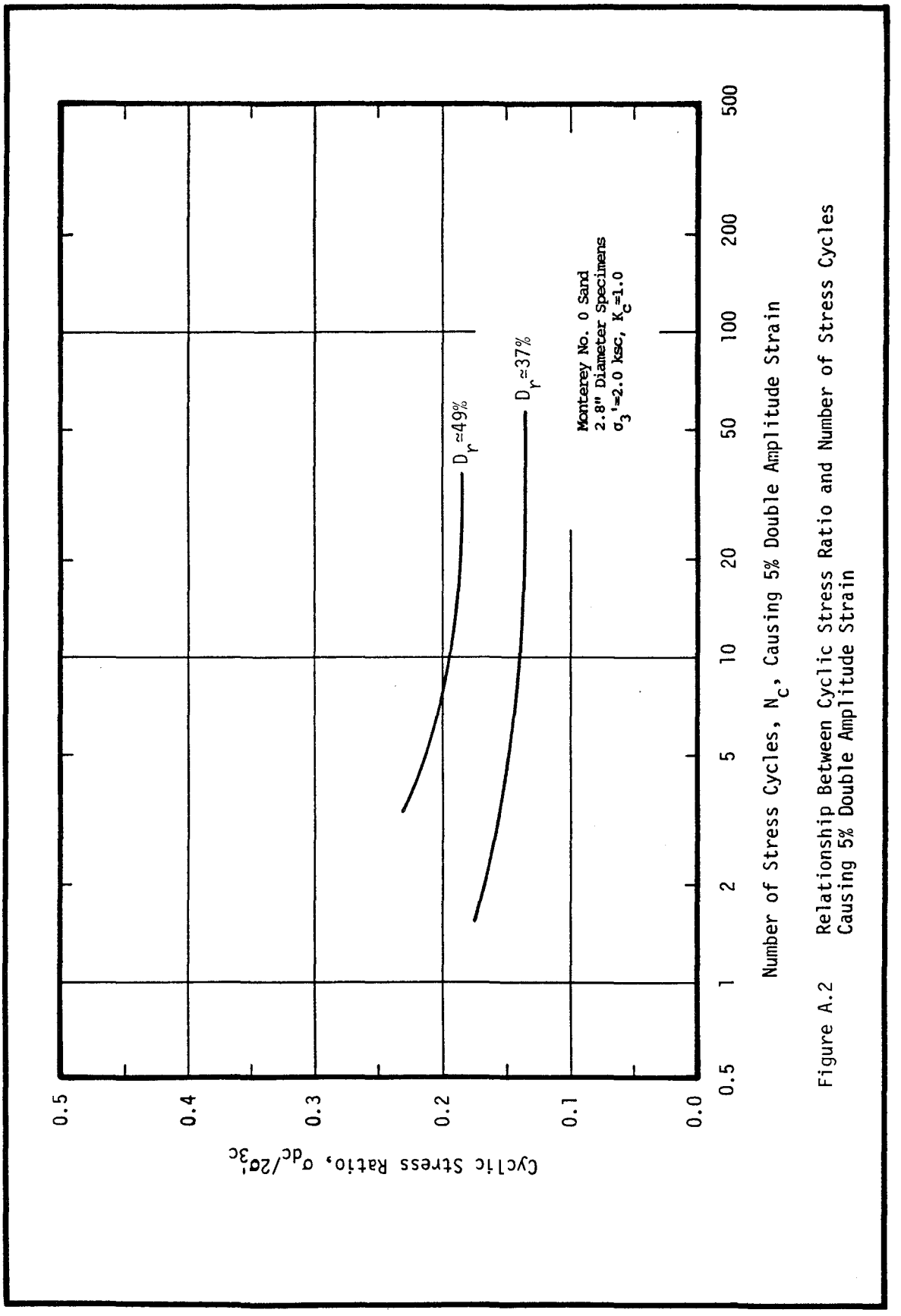

Figure A.2 Relationship Between Cyclic Stress Ratio and Number of Stress Cycles Causing 5% Double Amplitude Strain

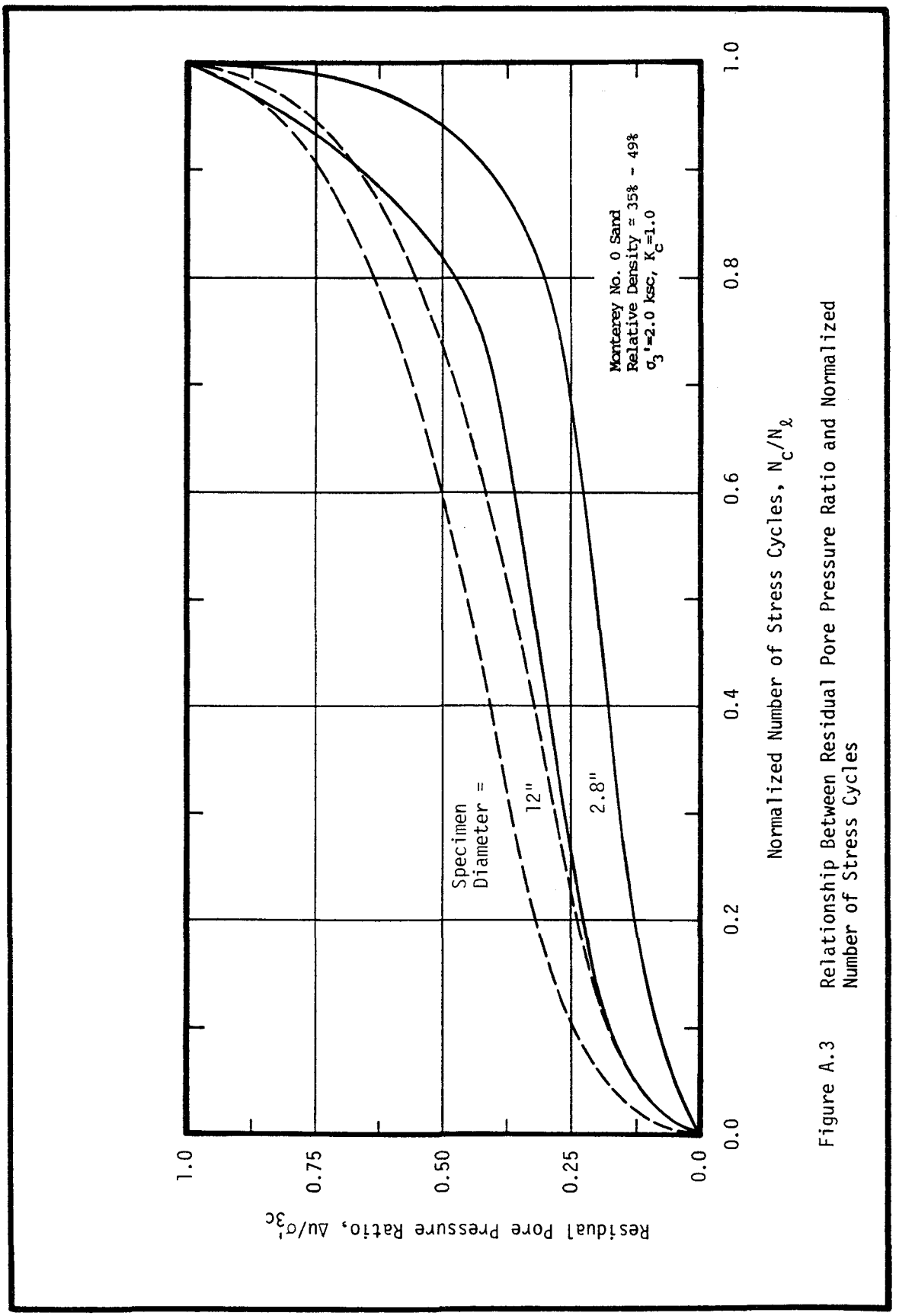

Figure A.3 Relationship Between Residual Pore Pressure Ratio and Normalized Number of Stress Cycles

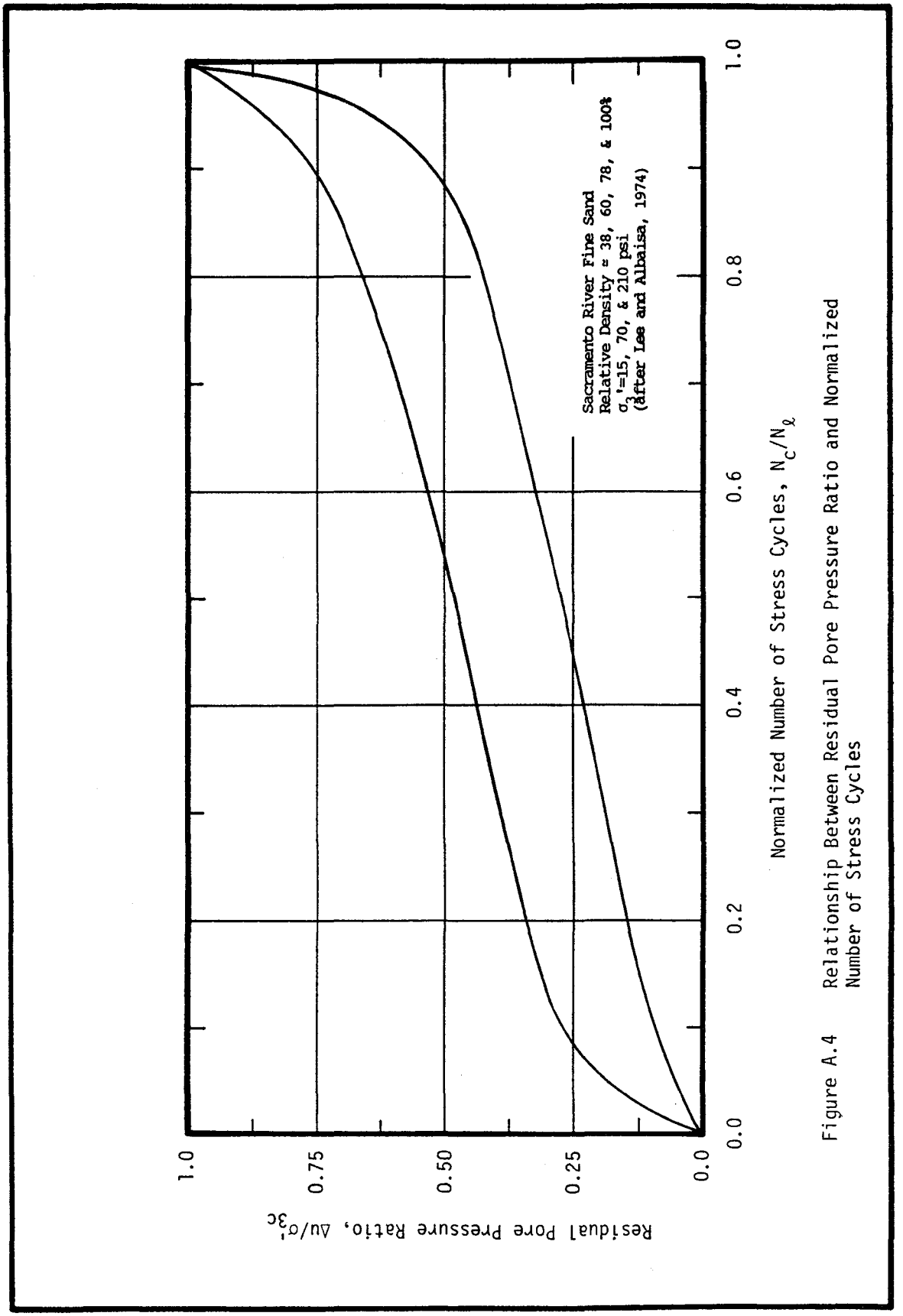

Figure A.4 Relationship Between Residual Pore Pressure Ratio and Normalized Number of Stress Cycles

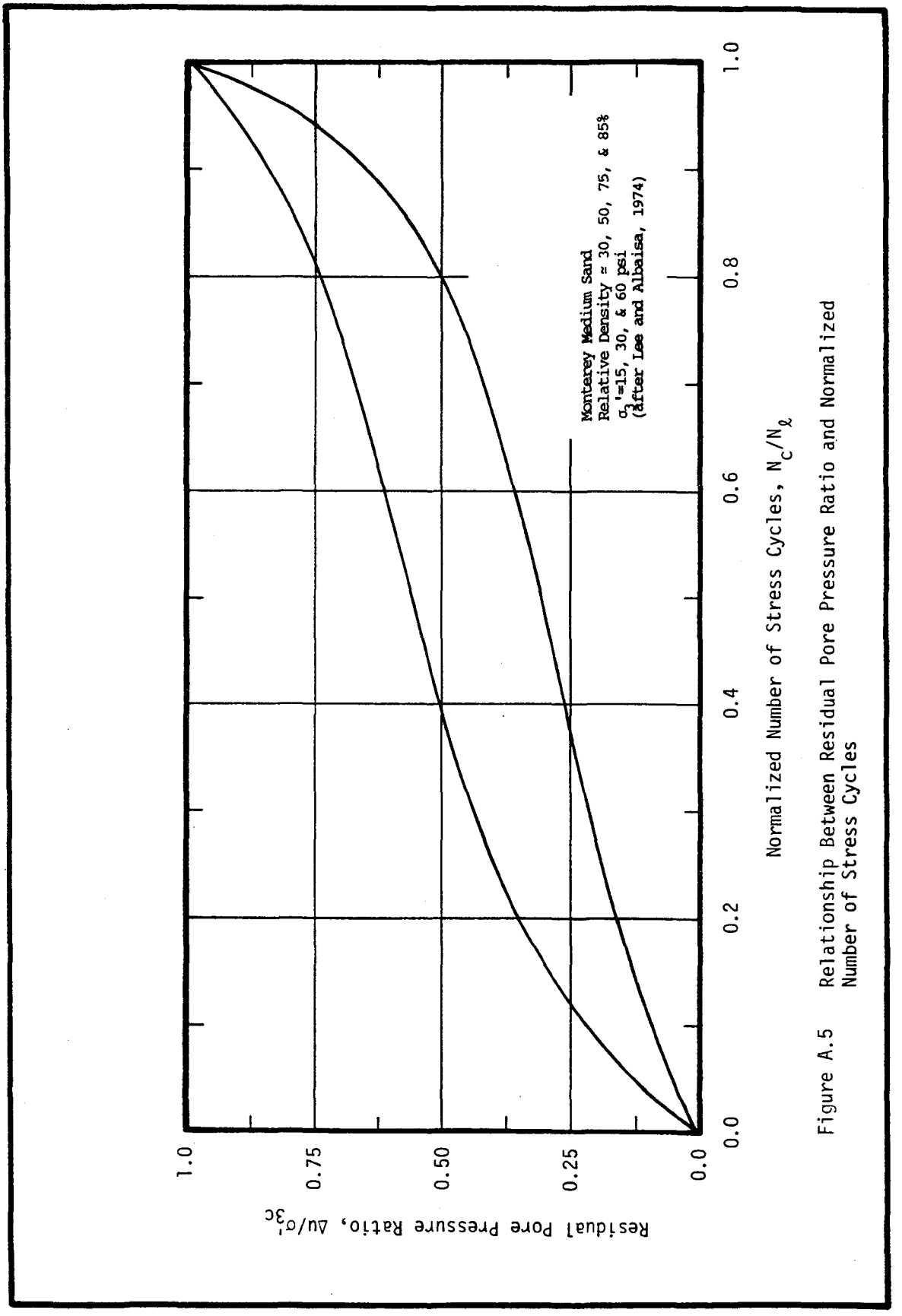

Figure A.5 Relationship Between Residual Pore Pressure Ratio and Normalized Number of Stress Cycles

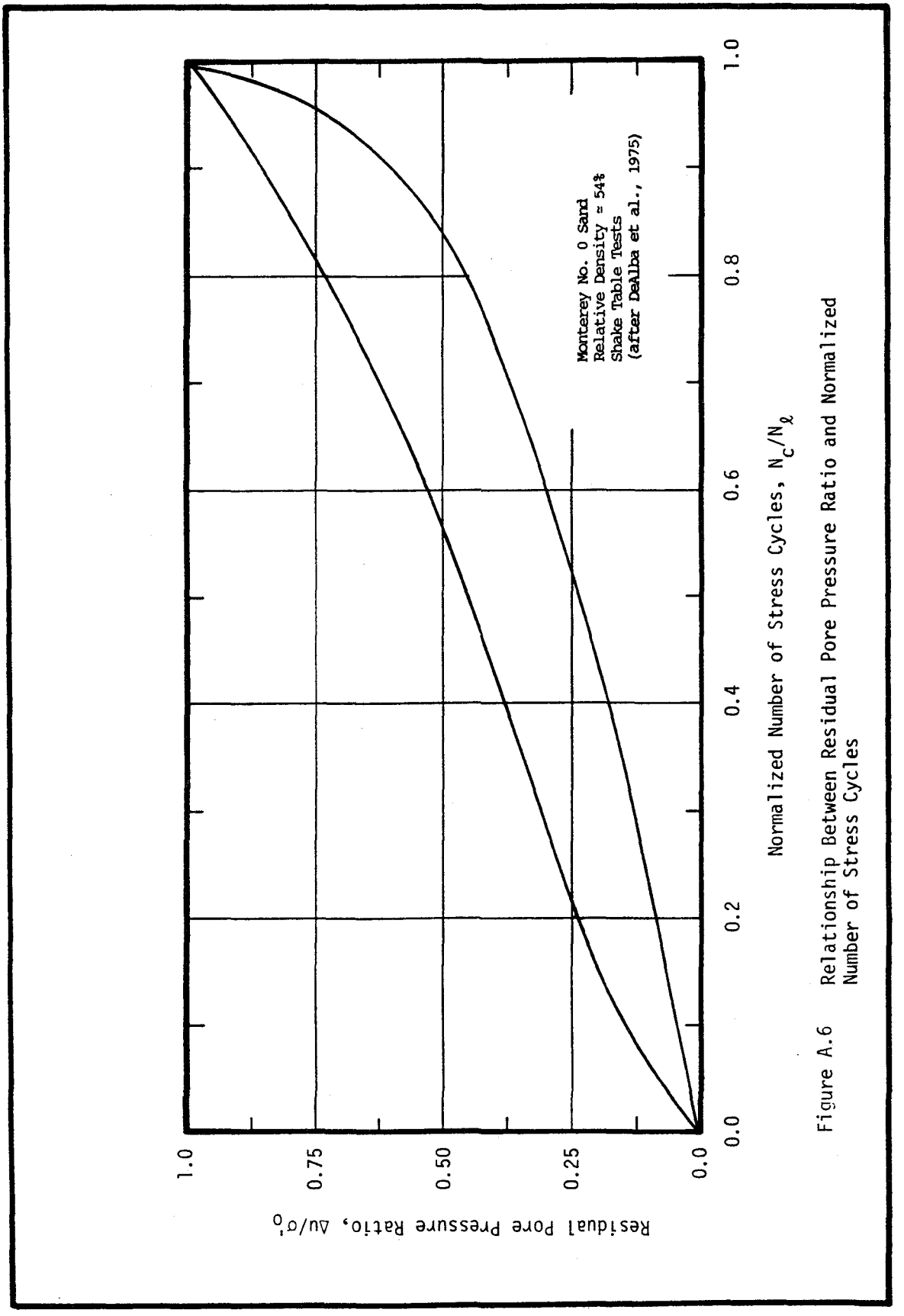

Figure A.6 Relationship Between Residual Pore Pressure Ratio and Normalized Number of Stress Cycles

Sacramento River Fine Sand (Lee and Albeisa, 1974), Monterey Medium Sand (Lee and Albeisa, 1974), and Monterey No. 0 Sand (DeAlba et al., 1975), respectively. It may be seen that the data from these earlier studies are in good agreement with the data presented in this study even though data for a wide range of relative densities and confining pressures is presented from the earlier studies. These data were used for comparison with similar data generated from sluiced and unsluiced gravel specimens presented in Chapter 8.

EARTHQUAKE ENGINEERING RESEARCH CENTER REPORT SERIES

EERC reports are available from the National Information Service for Earthquake Engineering(NISEE) and from the National Technical Information Service(NTIS). Numbers in parentheses are Accession Numbers assigned by the National Technical Information Service; these are followed by a price code. Contact NTIS, 5285 Port Royal Road, Springfield Virginia, 22161 for more information. Reports without Accession Numbers were not available from NTIS at the time of printing. For a current complete list of EERC reports (from EERC 67-1) and availablity information, please contact University of California, EERC, NISEE, 1301 South 46th Street, Richmond, California 94804.

UCB/EERC-80/01 "Earthquake Response of Concrete Gravity Dams Including Hydrodynamic and Foundation Interaction Effects," by Chopra, A.K., Chakrabarti, P. and Gupta, S., January 1980, (AD-A087297)A10.

UCB/EERC-80/02 "Rocking Response of Rigid Blocks to Earthquakes," by Yim, C.S., Chopra, A.K. and Penzien, J., January 1980, (PB80 166 002)A04.

UCB/EERC-80/03 "Optimum Inelastic Design of Seismic-Resistant Reinforced Concrete Frame Structures," by Zagajeski, S.W. and Bertero, V.V., January 1980, (PB80 164 635)A06.

UCB/EERC-80/04 "Effects of Amount and Arrangement of Wall-Panel Reinforcement on Hysteretic Behavior of Reinforced Concrete Walls," by Iliya, R. and Bertero, V.V., February 1980, (PB81 122 525)A09.

UCB/EERC-80/05 "Shaking Table Research on Concrete Dam Models," by Niwa, A. and Clough, R.W., September 1980, (PB81 122 368)A06.

UCB/EERC-80/06 "The Design of Steel Energy-Absorbing Restrainers and their Incorporation into Nuclear Power Plants for Enhanced Safety (Vol 1a): Piping with Energy Absorbing Restrainers: Parameter Study on Small Systems," by Powell, G.H., Oughourlian, C. and Simons, J., June 1980.

UCB/EERC-80/07 "Inelastic Torsional Response of Structures Subjected to Earthquake Ground Motions," by Yamazaki, Y., April 1980, (PB81 122 327)A08.

UCB/EERC-80/08 "Study of X-Braced Steel Frame Structures under Earthquake Simulation," by Ghanaat, Y., April 1980, (PB81 122 335)A11.

UCB/EERC-80/09 "Hybrid Modelling of Soil-Structure Interaction," by Gupta, S., Lin, T.W. and Penzien, J., May 1980, (PB81 122 319)A07.

UCB/EERC-80/10 "General Applicability of a Nonlinear Model of a One Story Steel Frame," by Sveinsson, B.I. and McNiven, H.D., May 1980, (PB81 124 877)A06.

UCB/EERC-80/11 "A Green-Function Method for Wave Interaction with a Submerged Body," by Kioka, W., April 1980, (PB81 122 269)A07.

UCB/EERC-80/12 "Hydrodynamic Pressure and Added Mass for Axisymmetric Bodies.," by Nilrat, F., May 1980, (PB81 122 343)A08.

UCB/EERC-80/13 "Treatment of Non-Linear Drag Forces Acting on Offshore Platforms," by Dao, B.V. and Penzien, J., May 1980, (PB81 153 413)A07.

UCB/EERC-80/14 "2D Plane/Axisymmetric Solid Element (Type 3-Elastic or Elastic-Perfectly Plastic) for the ANSR-II Program," by Mondkar, D.P. and Powell, G.H., July 1980, (PB81 122 350)A03.

UCB/EERC-80/15 "A Response Spectrum Method for Random Vibrations," by Der Kiureghian, A., June 1981, (PB81 122 301)A03.

UCB/EERC-80/16 "Cyclic Inelastic Buckling of Tubular Steel Braces," by Zayas, V.A., Popov, E.P. and Martin, S.A., June 1981, (PB81 124 885)A10.

UCB/EERC-80/17 "Dynamic Response of Simple Arch Dams Including Hydrodynamic Interaction," by Porter, C.S. and Chopra, A.K., July 1981, (PB81 124 000)A13.

UCB/EERC-80/18 "Experimental Testing of a Friction Damped Aseismic Base Isolation System with Fail-Safe Characteristics," by Kelly, J.M., Beucke, K.E. and Skinner, M.S., July 1980, (PB81 148 595)A04.

UCB/EERC-80/19 "The Design of Steel Emergy-Absorbing Restrainers and their Incorporation into Nuclear Power Plants for Enhanced Safety (Vol.1B): Stochastic Seismic Analyses of Nuclear Power Plant Structures and Piping Systems Subjected to Multiple Supported Excitations," by Lee, M.C. and Penzien, J., June 1980, (PB82 201 872)A08.

UCB/EERC-80/20 "The Design of Steel Energy-Absorbing Restrainers and their Incorporation into Nuclear Power Plants for Enhanced Safety (Vol 1C): Numerical Method for Dynamic Substructure Analysis," by Dickens, J.M. and Wilson, E.L., June 1980.

UCB/EERC-80/21 "The Design of Steel Energy-Absorbing Restrainers and their Incorporation into Nuclear Power Plants for Enhanced Safety (Vol 2): Development and Testing of Restraints for Nuclear Piping Systems," by Kelly, J.M. and Skinner, M.S., June 1980.

UCB/EERC-80/22 "3D Solid Element (Type 4-Elastic or Elastic-Perfectly-Plastic) for the ANSR-II Program," by Mondkar, D.P. and Powell, G.H., July 1980, (PB81 123 242)A03.

UCB/EERC-80/23 "Gap-Friction Element (Type 5) for the Ansr-II Program," by Mondkar, D.P. and Powell, G.H., July 1980, (PB81 122 285)A03.

UCB/EERC-80/24 "U-Bar Restraint Element (Type 11) for the ANSR-II Program," by Oughourlian, C. and Powell, G.H., July 1980, (PB81 122 293)A03.

UCB/EERC-80/25 "Testing of a Natural Rubber Base Isolation System by an Explosively Simulated Earthquake," by Kelly, J.M., August 1980, (PB81 201 360)A04.

UCB/EERC-80/26 "Input Identification from Structural Vibrational Response," by Hu, Y., August 1980, (PB81 152 308)A05.

UCB/EERC-80/27 "Cyclic Inelastic Behavior of Steel Offshore Structures," by Zayas, V.A., Mahin, S.A. and Popov, E.P., August 1980, (PB81 196 180)A15.

UCB/EERC-80/28 "Shaking Table Testing of a Reinforced Concrete Frame with Biaxial Response," by Oliva, M.G., October 1980, (PB81 154 304)A10.

UCB/EERC-80/29 "Dynamic Properties of a Twelve-Story Prefabricated Panel Building," by Bouwkamp, J.G., Kollegger, J.P. and Stephen, R.M., October 1980, (PB82 138 777)A07.

UCB/EERC-80/30 "Dynamic Properties of an Eight-Story Prefabricated Panel Building," by Bouwkamp, J.G., Kollegger, J.P. and Stephen, R.M., October 1980, (PB81 200 313)A05.

UCB/EERC-80/31 "Predictive Dynamic Response of Panel Type Structures under Earthquakes," by Kollegger, J.P. and Bouwkamp, J.G., October 1980, (PB81 152 316)A04.

UCB/EERC-80/32 "The Design of Steel Energy-Absorbing Restrainers and their Incorporation into Nuclear Power Plants for Enhanced Safety (Vol 3): Testing of Commercial Steels in Low-Cycle Torsional Fatique," by Spanner, P., Parker, E.R., Jongewaard, E. and Dory, M., 1980.

UCB/EERC-80/33 "The Design of Steel Energy-Absorbing Restrainers and their Incorporation into Nuclear Power Plants for Enhanced Safety (Vol 4): Shaking Table Tests of Piping Systems with Energy-Absorbing Restrainers," by Stiemer, S.F. and Godden, W.G., September 1980, (PB82 201 880)A05.

UCB/EERC-80/34 "The Design of Steel Energy-Absorbing Restrainers and their Incorporation into Nuclear Power Plants for Enhanced Safety (Vol 5): Summary Report," by Spencer, P., 1980.

UCB/EERC-80/35 "Experimental Testing of an Energy-Absorbing Base Isolation System," by Kelly, J.M., Skinner, M.S. and Beucke, K.E., October 1980, (PB81 154 072)A04.

UCB/EERC-80/36 "Simulating and Analyzing Artificial Non-Stationary Earth Ground Motions," by Nau, R.F., Oliver, R.M. and Pister, K.S., October 1980, (PB81 153 397)A04.

UCB/EERC-80/37 "Earthquake Engineering at Berkeley - 1980," by , September 1980, (PB81 205 674)A09.

UCB/EERC-80/38 "Inelastic Seismic Analysis of Large Panel Buildings," by Schricker, V. and Powell, G.H., September 1980, (PB81 154 338)A13.

UCB/EERC-80/39 "Dynamic Response of Embankment, Concrete-Gavity and Arch Dams Including Hydrodynamic Interation," by Hall, J.F. and Chopra, A.K., October 1980, (PB81 152 324)A11.

UCB/EERC-80/40 "Inelastic Buckling of Steel Struts under Cyclic Load Reversal.," by Black, R.G. , Wenger, W.A. and Popov, E.P., October 1980, (PB81 154 312)A08.

UCB/EERC-80/41 "Influence of Site Characteristics on Buildings Damage during the October 3,1974 Lima Earthquake," by Repetto, P., Arango, I. and Seed, H.B., September 1980, (PB81 161 739)A05.

UCB/EERC-80/42 "Evaluation of a Shaking Table Test Program on Response Behavior of a Two Story Reinforced Concrete Frame," by Blondet, J.M., Clough, R.W. and Mahin, S.A., December 1980, (PB82 196 544)A11.

UCB/EERC-80/43 "Modelling of Soil-Structure Interaction by Finite and Infinite Elements," by Medina, F., December 1980, (PB81 229 270)A04.

UCB/EERC-81/01 "Control of Seismic Response of Piping Systems and Other Structures by Base Isolation," by Kelly, J.M., January 1981, (PB81 200 735)A05.

UCB/EERC-81/02 "OPTNSR- An Interactive Software System for Optimal Design of Statically and Dynamically Loaded Structures with Nonlinear Response," by Bhatti, M.A., Ciampi, V. and Pister, K.S., January 1981, (PB81 218 851)A09.

UCB/EERC-81/03 "Analysis of Local Variations in Free Field Seismic Ground Motions," by Chen, J.-C., Lysmer, J. and Seed, H.B., January 1981, (AD-A099508)A13.

UCB/EERC-81/04 "Inelastic Structural Modeling of Braced Offshore Platforms for Seismic Loading. ," by Zayas, V.A., Shing, P.-S.B., Mahin, S.A. and Popov, E.P., January 1981, (PB82 138 777)A07.

UCB/EERC-81/05 "Dynamic Response of Light Equipment in Structures," by Der Kiureghian, A., Sackman, J.L. and Nour-Omid, B., April 1981, (PB81 218 497)A04.

UCB/EERC-81/06 "Preliminary Experimental Investigation of a Broad Base Liquid Storage Tank," by Bouwkamp, J.G., Kollegger, J.P. and Stephen, R.M., May 1981, (PB82 140 385)A03.

UCB/EERC-81/07 "The Seismic Resistant Design of Reinforced Concrete Coupled Structural Walls," by Aktan, A.E. and Bertero, V.V., June 1981, (PB82 113 358)A11.

UCB/EERC-81/08 "Unassigned," by Unassigned, 1981.

UCB/EERC-81/09 "Experimental Behavior of a Spatial Piping System with Steel Energy Absorbers Subjected to a Simulated Differential Seismic Input," by Stiemer, S.F., Godden, W.G. and Kelly, J.M., July 1981, (PB82 201 898)A04.

UCB/EERC-81/10 "Evaluation of Seismic Design Provisions for Masonry in the United States," by Sveinsson, B.I., Mayes, R.L. and McNiven, H.D., August 1981, (PB82 166 075)A08.

UCB/EERC-81/11 "Two-Dimensional Hybrid Modelling of Soil-Structure Interaction," by Tzong, T.-J., Gupta, S. and Penzien, J., August 1981, (PB82 142 118)A04.

UCB/EERC-81/12 "Studies on Effects of Infills in Seismic Resistant R/C Construction," by Brokken, S. and Bertero, V.V., October 1981, (PB82 166 190)A09.

UCB/EERC-81/13 "Linear Models to Predict the Nonlinear Seismic Behavior of a One-Story Steel Frame," by Valdimarsson, H., Shah, A.H. and McNiven, H.D., September 1981, (PB82 138 793)A07.

UCB/EERC-81/14 "TLUSH: A Computer Program for the Three-Dimensional Dynamic Analysis of Earth Dams," by Kagawa, T., Mejia, L.H., Seed, H.B. and Lysmer, J., September 1981, (PB82 139 940)A06.

UCB/EERC-81/15 "Three Dimensional Dynamic Response Analysis of Earth Dams," by Mejia, L.H. and Seed, H.B., September 1981, (PB82 137 274)A12.

UCB/EERC-81/16 "Experimental Study of Lead and Elastomeric Dampers for Base Isolation Systems," by Kelly, J.M. and Hodder, S.B., October 1981, (PB82 166 182)A05.

UCB/EERC-81/17 "The Influence of Base Isolation on the Seismic Response of Light Secondary Equipment," by Kelly, J.M., April 1981, (PB82 255 266)A04.

UCB/EERC-81/18 "Studies on Evaluation of Shaking Table Response Analysis Procedures," by Blondet, J. Marcial, November 1981, (PB82 197 278)A10.

UCB/EERC-81/19 "DELIGHT.STRUCT: A Computer-Aided Design Environment for Structural Engineering. ," by Balling, R.J., Pister, K.S. and Polak, E., December 1981, (PB82 218 496)A07.

UCB/EERC-81/20 "Optimal Design of Seismic-Resistant Planar Steel Frames," by Balling, R.J., Ciampi, V. and Pister, K.S., December 1981, (PB82 220 179)A07.

UCB/EERC-82/01 "Dynamic Behavior of Ground for Seismic Analysis of Lifeline Systems," by Sato, T. and Der Kiureghian, A., January 1982, (PB82 218 926)A05.

UCB/EERC-82/02 "Shaking Table Tests of a Tubular Steel Frame Model," by Ghanaat, Y. and Clough, R.W., January 1982, (PB82 220 161)A07.

UCB/EERC-82/03 "Behavior of a Piping System under Seismic Excitation: Experimental Investigations of a Spatial Piping System supported by Mechanical Shock Arrestors," by Schneider, S., Lee, H.-M. and Godden, W. G., May 1982, (PB83 172 544)A09.

UCB/EERC-82/04 "New Approaches for the Dynamic Analysis of Large Structural Systems," by Wilson, E.L., June 1982, (PB83 148 080)A05.

UCB/EERC-82/05 "Model Study of Effects of Damage on the Vibration Properties of Steel Offshore Platforms," by Shahrivar, F. and Bouwkamp, J.G., June 1982, (PB83 148 742)A10.

UCB/EERC-82/06 "States of the Art and Pratice in the Optimum Seismic Design and Analytical Response Prediction of R/C Frame Wall Structures," by Aktan, A.E. and Bertero, V.V., July 1982, (PB83 147 736)A05.

UCB/EERC-82/07 "Further Study of the Earthquake Response of a Broad Cylindrical Liquid-Storage Tank Model," by Manos, G.C. and Clough, R.W., July 1982, (PB83 147 744)A11.

UCB/EERC-82/08 "An Evaluation of the Design and Analytical Seismic Response of a Seven Story Reinforced Concrete Frame," by Charney, F.A. and Bertero, V.V., July 1982, (PB83 157 628)A09.

UCB/EERC-82/09 "Fluid-Structure Interactions: Added Mass Computations for Incompressible Fluid. ," by Kuo, J.S.-H., August 1982, (PB83 156 281)A07.

UCB/EERC-82/10 "Joint-Opening Nonlinear Mechanism: Interface Smeared Crack Model," by Kuo, J.S.-H., August 1982, (PB83 149 195)A05.

UCB/EERC-82/11 "Dynamic Response Analysis of Techi Dam," by Clough, R.W., Stephen, R.M. and Kuo, J.S.-H., August 1982, (PB83 147 496)A06.

UCB/EERC-82/12 "Prediction of the Seismic Response of R/C Frame-Coupled Wall Structures," by Aktan, A.E., Bertero, V.V. and Piazzo, M., August 1982, (PB83 149 203)A09.

UCB/EERC-82/13 "Preliminary Report on the Smart 1 Strong Motion Array in Taiwan," by Bolt, B.A. , Loh, C.H., Penzien, J. and Tsai, Y.B., August 1982, (PB83 159 400)A10.

UCB/EERC-82/14 "Shaking-Table Studies of an Eccentrically X-Braced Steel Structure," by Yang, M.S., September 1982, (PB83 260 778)A12.

UCB/EERC-82/15 "The Performance of Stairways in Earthquakes," by Roha, C., Axley, J.W. and Bertero, V.V., September 1982, (PB83 157 693)A07.

UCB/EERC-82/16 "The Behavior of Submerged Multiple Bodies in Earthquakes," by Liao, W.-G., September 1982, (PB83 158 709)A07.

UCB/EERC-82/17 "Effects of Concrete Types and Loading Conditions on Local Bond-Slip Relationships," by Cowell, A.D., Popov, E.P. and Bertero, V.V., September 1982, (PB83 153 577)A04.

UCB/EERC-82/18 "Mechanical Behavior of Shear Wall Vertical Boundary Members: An Experimental Investigation," by Wagner, M.T. and Bertero, V.V., October 1982, (PB83 159 764)A05.

UCB/EERC-82/19 "Experimental Studies of Multi-support Seismic Loading on Piping Systems," by Kelly, J.M. and Cowell, A.D., November 1982.

UCB/EERC-82/20 "Generalized Plastic Hinge Concepts for 3D Beam-Column Elements," by Chen, P. F.-S. and Powell, G.H., November 1982, (PB83 247 981)A13.

UCB/EERC-82/21 "ANSR-II: General Computer Program for Nonlinear Structural Analysis," by Oughourlian, C.V. and Powell, G.H., November 1982, (PB83 251 330)A12.

UCB/EERC-82/22 "Solution Strategies for Statically Loaded Nonlinear Structures," by Simons, J.W. and Powell, G.H., November 1982, (PB83 197 970)A06.

UCB/EERC-82/23 "Analytical Model of Deformed Bar Anchorages under Generalized Excitations," by Ciampi, V., Eligehausen, R., Bertero, V.V. and Popov, E.P., November 1982, (PB83 169 532)A06.

UCB/EERC-82/24 "A Mathematical Model for the Response of Masonry Walls to Dynamic Excitations," by Sucuoglu, H., Mengi, Y. and McNiven, H.D., November 1982, (PB83 169 011)A07.

UCB/EERC-82/25 "Earthquake Response Considerations of Broad Liquid Storage Tanks," by Cambra, F.J., November 1982, (PB83 251 215)A09.

UCB/EERC-82/26 "Computational Models for Cyclic Plasticity, Rate Dependence and Creep," by Mosaddad, B. and Powell, G.H., November 1982, (PB83 245 829)A08.

UCB/EERC-82/27 "Inelastic Analysis of Piping and Tubular Structures," by Mahasuverachai, M. and Powell, G.H., November 1982, (PB83 249 987)A07.

UCB/EERC-83/01 "The Economic Feasibility of Seismic Rehabilitation of Buildings by Base Isolation," by Kelly, J.M., January 1983, (PB83 197 988)A05.

UCB/EERC-83/02 "Seismic Moment Connections for Moment-Resisting Steel Frames.," by Popov, E.P., January 1983, (PB83 195 412)A04.

UCB/EERC-83/03 "Design of Links and Beam-to-Column Connections for Eccentrically Braced Steel Frames," by Popov, E.P. and Malley, J.O., January 1983, (PB83 194 811)A04.

UCB/EERC-83/04 "Numerical Techniques for the Evaluation of Soil-Structure Interaction Effects in the Time Domain," by Bayo, E. and Wilson, E.L., February 1983, (PB83 245 605)A09.

UCB/EERC-83/05 "A Transducer for Measuring the Internal Forces in the Columns of a Frame-Wall Reinforced Concrete Structure," by Sause, R. and Bertero, V.V., May 1983, (PB84 119 494)A06.

UCB/EERC-83/06 "Dynamic Interactions Between Floating Ice and Offshore Structures," by Croteau, P., May 1983, (PB84 119 486)A16.

UCB/EERC-83/07 "Dynamic Analysis of Multiply Tuned and Arbitrarily Supported Secondary Systems. ," by Igusa, T. and Der Kiureghian, A., July 1983, (PB84 118 272)A11.

UCB/EERC-83/08 "A Laboratory Study of Submerged Multi-body Systems in Earthquakes," by Ansari, G.R., June 1983, (PB83 261 842)A17.

UCB/EERC-83/09 "Effects of Transient Foundation Uplift on Earthquake Response of Structures," by Yim, C.-S. and Chopra, A.K., June 1983, (PB83 261 396)A07.

UCB/EERC-83/10 "Optimal Design of Friction-Braced Frames under Seismic Loading," by Austin, M.A. and Pister, K.S., June 1983, (PB84 119 288)A06.

UCB/EERC-83/11 "Shaking Table Study of Single-Story Masonry Houses: Dynamic Performance under Three Component Seismic Input and Recommendations," by Manos, G.C., Clough, R.W. and Mayes, R.L., July 1983, (UCB/EERC-83/11)A08.

UCB/EERC-83/12 "Experimental Error Propagation in Pseudodynamic Testing," by Shiing, P.B. and Mahin, S.A., June 1983, (PB84 119 270)A09.

UCB/EERC-83/13 "Experimental and Analytical Predictions of the Mechanical Characteristics of a 1/5-scale Model of a 7-story R/C Frame-Wall Building Structure," by Aktan, A.E., Bertero, V.V., Chowdhury, A.A. and Nagashima, T., June 1983, (PB84 119 213)A07.

UCB/EERC-83/14 "Shaking Table Tests of Large-Panel Precast Concrete Building System Assemblages," by Oliva, M.G. and Clough, R.W., June 1983, (PB86 110 210/AS)A11.

UCB/EERC-83/15 "Seismic Behavior of Active Beam Links in Eccentrically Braced Frames," by Hjelmstad, K.D. and Popov, E.P., July 1983, (PB84 119 676)A09.

UCB/EERC-83/16 "System Identification of Structures with Joint Rotation," by Dimsdale, J.S., July 1983, (PB84 192 210)A06.

UCB/EERC-83/17 "Construction of Inelastic Response Spectra for Single-Degree-of-Freedom Systems," by Mahin, S. and Lin, J., June 1983, (PB84 208 834)A05.

UCB/EERC-83/18 "Interactive Computer Analysis Methods for Predicting the Inelastic Cyclic Behaviour of Structural Sections," by Kaba, S. and Mahin, S., July 1983, (PB84 192 012)A06.

UCB/EERC-83/19 "Effects of Bond Deterioration on Hysteretic Behavior of Reinforced Concrete Joints," by Filippou, F.C., Popov, E.P. and Bertero, V.V., August 1983, (PB84 192 020)A10.

UCB/EERC-83/20 "Analytical and Experimental Correlation of Large-Panel Precast Building System Performance," by Oliva, M.G., Clough, R.W., Velkov, M. and Gavrilovic, P., November 1983.

UCB/EERC-83/21 "Mechanical Characteristics of Materials Used in a 1/5 Scale Model of a 7-Story Reinforced Concrete Test Structure," by Bertero, V.V., Aktan, A.E., Harris, H.G. and Chowdhury, A.A., October 1983, (PB84 193 697)A05.

UCB/EERC-83/22 "Hybrid Modelling of Soil-Structure Interaction in Layered Media," by Tzong, T.-J. and Penzien, J., October 1983, (PB84 192 178)A08.

UCB/EERC-83/23 "Local Bond Stress-Slip Relationships of Deformed Bars under Generalized Excitations," by Eligehausen, R., Popov, E.P. and Bertero, V.V., October 1983, (PB84 192 848)A09.

UCB/EERC-83/24 "Design Considerations for Shear Links in Eccentrically Braced Frames," by Malley, J.O. and Popov, E.P., November 1983, (PB84 192 186)A07.

UCB/EERC-84/01 "Pseudodynamic Test Method for Seismic Performance Evaluation: Theory and Implementation," by Shing, P.-S. B. and Mahin, S.A., January 1984, (PB84 190 644)A08.

UCB/EERC-84/02 "Dynamic Response Behavior of Kiang Hong Dian Dam," by Clough, R.W., Chang, K.-T., Chen, H.-Q. and Stephen, R.M., April 1984, (PB84 209 402)A08.

UCB/EERC-84/03 "Refined Modelling of Reinforced Concrete Columns for Seismic Analysis," by Kaba, S.A. and Mahin, S.A., April 1984, (PB84 234 384)A06.

UCB/EERC-84/04 "A New Floor Response Spectrum Method for Seismic Analysis of Multiply Supported Secondary Systems," by Asfura, A. and Der Kiureghian, A., June 1984, (PB84 239 417)A06.

UCB/EERC-84/05 "Earthquake Simulation Tests and Associated Studies of a 1/5th-scale Model of a 7-Story R/C Frame-Wall Test Structure," by Bertero, V.V., Aktan, A.E., Charney, F.A. and Sause, R., June 1984, (PB84 239 409)A09.

UCB/EERC-84/06 "R/C Structural Walls: Seismic Design for Shear," by Aktan, A.E. and Bertero, V.V., 1984.

UCB/EERC-84/07 "Behavior of Interior and Exterior Flat-Plate Connections subjected to Inelastic Load Reversals," by Zee, H.L. and Moehle, J.P., August 1984, (PB86 117 629/AS)A07.

UCB/EERC-84/08 "Experimental Study of the Seismic Behavior of a Two-Story Flat-Plate Structure. ," by Moehle, J.P. and Diebold, J.W., August 1984, (PB86 122 553/AS)A12.

UCB/EERC-84/09 "Phenomenological Modeling of Steel Braces under Cyclic Loading," by Ikeda, K., Mahin, S.A. and Dermitzakis, S.N., May 1984, (PB86 132 198/AS)A08.

UCB/EERC-84/10 "Earthquake Analysis and Response of Concrete Gravity Dams," by Fenves, G. and Chopra, A.K., August 1984, (PB85 193 902/AS)A11.

UCB/EERC-84/11 "EAGD-84: A Computer Program for Earthquake Analysis of Concrete Gravity Dams," by Fenves, G. and Chopra, A.K., August 1984, (PB85 193 613/AS)A05.

UCB/EERC-84/12 "A Refined Physical Theory Model for Predicting the Seismic Behavior of Braced Steel Frames," by Ikeda, K. and Mahin, S.A., July 1984, (PB85 191 450/AS)A09.

UCB/EERC-84/13 "Earthquake Engineering Research at Berkeley - 1984," by , August 1984, (PB85 197 341/AS)A10.

UCB/EERC-84/14 "Moduli and Damping Factors for Dynamic Analyses of Cohesionless Soils," by Seed, H.B., Wong, R.T., Idriss, I.M. and Tokimatsu, K., September 1984, (PB85 191 468/AS)A04.

UCB/EERC-84/15 "The Influence of SPT Procedures in Soil Liquefaction Resistance Evaluations," by Seed, H.B., Tokimatsu, K., Harder, L.F. and Chung, R.M., October 1984, (PB85 191 732/AS)A04.

UCB/EERC-84/16 "Simplified Procedures for the Evaluation of Settlements in Sands Due to Earthquake Shaking," by Tokimatsu, K. and Seed, H.B., October 1984, (PB85 197 887/AS)A03.

UCB/EERC-84/17 "Evaluation of Energy Absorption Characteristics of Bridges under Seismic Conditions," by Imbsen, R.A. and Penzien, J., November 1984.

UCB/EERC-84/18 "Structure-Foundation Interactions under Dynamic Loads," by Liu, W.D. and Penzien, J., November 1984, (PB87 124 889/AS)A11.

UCB/EERC-84/19 "Seismic Modelling of Deep Foundations," by Chen, C.-H. and Penzien, J., November 1984, (PB87 124 798/AS)A07.

UCB/EERC-84/20 "Dynamic Response Behavior of Quan Shui Dam," by Clough, R.W., Chang, K.-T., Chen, H.-Q., Stephen, R.M., Ghanaat, Y. and Qi, J.-H., November 1984, (PB86 115177/AS)A07.

UCB/EERC-85/01 "Simplified Methods of Analysis for Earthquake Resistant Design of Buildings," by Cruz, E.F. and Chopra, A.K., February 1985, (PB86 112299/AS)A12.

UCB/EERC-85/02 "Estimation of Seismic Wave Coherency and Rupture Velocity using the SMART 1 Strong-Motion Array Recordings," by Abrahamson, N.A., March 1985, (PB86 214 343)A07.

UCB/EERC-85/03 "Dynamic Properties of a Thirty Story Condominium Tower Building," by Stephen, R.M., Wilson, E.L. and Stander, N., April 1985, (PB86 118965/AS)A06.

UCB/EERC-85/04 "Development of Substructuring Techniques for On-Line Computer Controlled Seismic Performance Testing," by Dermitzakis, S. and Mahin, S., February 1985, (PB86 132941/AS)A08.

UCB/EERC-85/05 "A Simple Model for Reinforcing Bar Anchorages under Cyclic Excitations," by Filippou, F.C., March 1985, (PB86 112 919/AS)A05.

UCB/EERC-85/06 "Racking Behavior of Wood-framed Gypsum Panels under Dynamic Load," by Oliva, M.G., June 1985.

UCB/EERC-85/07 "Earthquake Analysis and Response of Concrete Arch Dams," by Fok, K.-L. and Chopra, A.K., June 1985, (PB86 139672/AS)A10.

UCB/EERC-85/08 "Effect of Inelastic Behavior on the Analysis and Design of Earthquake Resistant Structures," by Lin, J.P. and Mahin, S.A., June 1985, (PB86 135340/AS)A08.

UCB/EERC-85/09 "Earthquake Simulator Testing of a Base-Isolated Bridge Deck," by Kelly, J.M., Buckle, I.G. and Tsai, H.-C., January 1986, (PB87 124 152/AS)A06.

UCB/EERC-85/10 "Simplified Analysis for Earthquake Resistant Design of Concrete Gravity Dams," by Fenves, G. and Chopra, A.K., June 1986, (PB87 124 160/AS)A08.

UCB/EERC-85/11 "Dynamic Interaction Effects in Arch Dams," by Clough, R.W., Chang, K.-T., Chen, H.-Q. and Ghanaat, Y., October 1985, (PB86 135027/AS)A05.

UCB/EERC-85/12 "Dynamic Response of Long Valley Dam in the Mammoth Lake Earthquake Series of May 25-27, 1980," by Lai, S. and Seed, H.B., November 1985, (PB86 142304/AS)A05.

UCB/EERC-85/13 "A Methodology for Computer-Aided Design of Earthquake-Resistant Steel Structures," by Austin, M.A., Pister, K.S. and Mahin, S.A., December 1985, (PB86 159480/AS)A10 .

UCB/EERC-85/14 "Response of Tension-Leg Platforms to Vertical Seismic Excitations," by Liou, G.-S., Penzien, J. and Yeung, R.W., December 1985, (PB87 124 871/AS)A08.

UCB/EERC-85/15 "Cyclic Loading Tests of Masonry Single Piers: Volume 4 - Additional Tests with Height to Width Ratio of 1," by Sveinsson, B., McNiven, H.D. and Sucuoglu, H., December 1985.

UCB/EERC-85/16 "An Experimental Program for Studying the Dynamic Response of a Steel Frame with a Variety of Infill Partitions," by Yanev, B. and McNiven, H.D., December 1985.

UCB/EERC-86/01 "A Study of Seismically Resistant Eccentrically Braced Steel Frame Systems," by Kasai, K. and Popov, E.P., January 1986, (PB87 124 178/AS)A14.

UCB/EERC-86/02 "Design Problems in Soil Liquefaction," by Seed, H.B., February 1986, (PB87 124 186/AS)A03.

UCB/EERC-86/03 "Implications of Recent Earthquakes and Research on Earthquake-Resistant Design and Construction of Buildings," by Bertero, V.V., March 1986, (PB87 124 194/AS)A05.

UCB/EERC-86/04 "The Use of Load Dependent Vectors for Dynamic and Earthquake Analyses," by Leger, P., Wilson, E.L. and Clough, R.W., March 1986, (PB87 124 202/AS)A12.

UCB/EERC-86/05 "Two Beam-To-Column Web Connections," by Tsai, K.-C. and Popov, E.P., April 1986 , (PB87 124 301/AS)A04.

UCB/EERC-86/06 "Determination of Penetration Resistance for Coarse-Grained Soils using the Becker Hammer Drill," by Harder, L.F. and Seed, H.B., May 1986, (PB87 124 210/AS)A07.

UCB/EERC-86/07 "A Mathematical Model for Predicting the Nonlinear Response of Unreinforced Masonry Walls to In-Plane Earthquake Excitations," by Mengi, Y. and McNiven, H.D., May 1986, (PB87 124 780/AS)A06.

UCB/EERC-86/08 "The 19 September 1985 Mexico Earthquake: Building Behavior," by Bertero, V.V., July 1986.

UCB/EERC-86/09 "EACD-3D: A Computer Program for Three-Dimensional Earthquake Analysis of Concrete Dams," by Fok, K.-L., Hall, J.F. and Chopra, A.K., July 1986, (PB87 124 228/AS)A08.

UCB/EERC-86/10 "Earthquake Simulation Tests and Associated Studies of a 0.3-Scale Model of a Six-Story Concentrically Braced Steel Structure," by Uang, C.-M. and Bertero, V.V., December 1986.

UCB/EERC-86/11 "Mechanical Characteristics of Base Isolation Bearings for a Bridge Deck Model Test," by Kelly, J.M., Buckle, I.G. and Koh, C.-G., 1987.

UCB/EERC-86/12 "Modelling of Dynamic Response of Elastomeric Isolation Bearings," by Koh, C.-G. and Kelly, J.M., 1987.

UCB/EERC-87/01 "FPS Earthquake Resisting System: Experimental Report," by Zayas, V.A., Low, S.S. and Mahin, S.A., June 1987.

UCB/EERC-87/02 "Earthquake Simulator Tests and Associated Studies of a 0.3-Scale Model of a Six-Story Eccentrically Braced Steel Structure," by Whittaker, A., Uang, C.-M. and Bertero, V.V., July 1987.

UCB/EERC-87/03 "A Displacement Control and Uplift Restraint Device for Base-Isolated Structures," by Kelly, J.M., Griffith, M.C. and Aiken, I.G., April 1987.

UCB/EERC-87/04 "Earthquake Simulator Testing of a Combined Sliding Bearing and Rubber Bearing Isolation System," by Kelly, J.M. and Chalhoub, M.S., 1987.

UCB/EERC-87/05 "Three-Dimensional Inelastic Analysis of Reinforced Concrete Frame-Wall Structures," by Moazzami, S. and Bertero, V.V., May 1987.

UCB/EERC-87/06 "Experimental Studies of Seismically Resistant Eccentrically Braced Steel Frames Having Composite Floors," by Ricles, J. and Popov, E., June 1987.

UCB/EERC-87/07 "Analytical Studies of Seismically Resistant Eccentrically Braced Steel Frames," by Ricles, J. and Popov, E., June 1987.

UCB/EERC-87/08 "Undrained Cyclic Triaxial Testing of Gravels-The Effect of Membrane Compliance, " by Evans, M.D. and Seed, H.B., July 1987.